

Advanced Combustion Engine Research and Development

2013

VEHICLE TECHNOLOGIES OFFICE

U.S. Department of Energy
1000 Independence Avenue, S.W.
Washington, D.C. 20585-0121

FY 2013 PROGRESS REPORT FOR ADVANCED COMBUSTION ENGINE RESEARCH AND DEVELOPMENT

Energy Efficiency and Renewable Energy
Vehicle Technologies Office

Approved by Gurpreet Singh
Program Manager, Advanced Combustion Engine R&D
Vehicle Technologies Office

December 2013

Acknowledgement

We would like to express our sincere appreciation to Alliance Technical Services, Inc. and Oak Ridge National Laboratory for their technical and artistic contributions in preparing and publishing this report.

In addition, we would like to thank all the participants for their contributions to the programs and all the authors who prepared the project abstracts that comprise this report.

Table of Contents

| | | |
|-------|---|--------|
| I. | Introduction | I-1 |
| I.1 | Subprogram Overview and Status | I-3 |
| I.2 | Project Highlights | I-10 |
| I.3 | Honors and Special Recognitions/Patents | I-23 |
| I.4 | Future Project Directions | I-25 |
| II. | Combustion Research | II-1 |
| II.1 | Sandia National Laboratories: Low-Temperature Automotive Diesel Combustion | II-3 |
| II.2 | Sandia National Laboratories: Heavy-Duty Low-Temperature Diesel Combustion and Heavy-Duty Combustion Modeling | II-9 |
| II.3 | Sandia National Laboratories: Spray Combustion Cross-Cut Engine Research | II-15 |
| II.4 | Sandia National Laboratories: HCCI and Stratified-Charge CI Engine Combustion Research | II-19 |
| II.5 | Sandia National Laboratories: Automotive Low-Temperature Gasoline Combustion Engine Research | II-26 |
| II.6 | Argonne National Laboratory: Spray and Combustion Modeling using High-Performance Computing Tools | II-30 |
| II.7 | Argonne National Laboratory: Fuel Injection and Spray Research Using X-Ray Diagnostics | II-36 |
| II.8 | Sandia National Laboratories: Large Eddy Simulation Applied to Advanced Engine Combustion Research | II-41 |
| II.9 | Argonne National Laboratory: Collaborative Combustion Research with Basic Energy Science | II-46 |
| II.10 | Lawrence Livermore National Laboratory: Chemical Kinetic Models for HCCI and Diesel Combustion | II-51 |
| II.11 | Lawrence Livermore National Laboratory: Computationally Efficient Modeling of High Efficiency Clean Combustion Engines | II-55 |
| II.12 | Lawrence Livermore National Laboratory: Improved Solvers for Advanced Combustion Engine Simulation | II-62 |
| II.13 | Los Alamos National Laboratory: KIVA Development | II-67 |
| II.14 | University of Michigan: University Consortium on Efficient and Clean High-Pressure Lean-Burn (HPLB) Engines | II-72 |
| II.15 | Michigan State University: Flex-Fuel Optimized SI and HCCI Engine | II-82 |
| II.16 | Oak Ridge National Laboratory: Engine Efficiency Fundamentals – Accelerating Predictive Simulation of Internal Combustion Engines with High Performance Computing | II-87 |
| II.17 | Argonne National Laboratory: Use of Low Cetane Fuel to Enable Low-Temperature Combustion | II-90 |
| II.18 | Argonne National Laboratory: High Efficiency GDI Engine Research | II-93 |
| II.19 | Oak Ridge National Laboratory: High Dilution Stoichiometric Gasoline Direct-Injection (GDI) Combustion Control Development | II-98 |
| II.20 | Oak Ridge National Laboratory: High Efficiency Clean Combustion in Light-Duty Multi-Cylinder Diesel Engines | II-102 |
| II.21 | Oak Ridge National Laboratory: Stretch Efficiency – Exploiting New Combustion Regimes | II-107 |
| II.22 | Sandia National Laboratories: Free-Piston Electric Generator (FPEG) | II-112 |
| II.23 | Oak Ridge National Laboratory: Variable Compression Ratio (VCR) Assessment to Enable Higher Efficiency in Gasoline Engines | II-117 |
| II.24 | Argonne National Laboratory: Engine Benchmarking CRADA Annual Report | II-122 |
| II.25 | Oak Ridge National Laboratory: Cummins-ORNL Combustion CRADA: Characterization and Reduction of Combustion Variations | II-124 |

Table of Contents

| | | |
|--------|---|--------|
| III. | Emission Control R&D | III-1 |
| III.1 | Oak Ridge National Laboratory: Cross-Cut Lean Exhaust Emission Reduction Simulation (CLEERS): Administrative Support | III-3 |
| III.2 | Oak Ridge National Laboratory: Cross-Cut Lean Exhaust Emissions Reduction Simulations (CLEERS): Joint Development of Benchmark Kinetics | III-8 |
| III.3 | Pacific Northwest National Laboratory: CLEERS Aftertreatment Modeling and Analysis | III-15 |
| III.4 | Pacific Northwest National Laboratory: Enhanced High- and Low-Temperature Performance of NO _x Reduction Catalyst Materials. | III-21 |
| III.5 | Pacific Northwest National Laboratory: Investigation of Mixed Oxide Catalysts for NO Oxidation. | III-28 |
| III.6 | Pacific Northwest National Laboratory: Integration of DPF and SCR Technologies for Combined Soot and NO _x After-Treatment | III-32 |
| III.7 | Oak Ridge National Laboratory: Low-Temperature Emissions Control. | III-37 |
| III.8 | Oak Ridge National Laboratory: Emissions Control for Lean-Gasoline Engines | III-43 |
| III.9 | Oak Ridge National Laboratory: Cummins-ORNL SmartCatalyst CRADA: NOx Control and Measurement Technology for Heavy-Duty Diesel Engines | III-48 |
| III.10 | University of Houston: Development of Optimal Catalyst Designs and Operating Strategies for Lean NO _x Reduction in Coupled LNT-SCR Systems | III-53 |
| III.11 | Oak Ridge National Laboratory: Neutron Imaging of Advanced Transportation Technologies | III-60 |
| III.12 | Argonne National Laboratory: Particulate Emissions Control by Advanced Filtration Systems for GDI Engines | III-66 |
| III.13 | Pacific Northwest National Laboratory: Fuel-Neutral Studies of PM Transportation Emissions | III-71 |
| III.14 | Health Effects Institute: The Advanced Collaborative Emissions Study (ACES) | III-77 |
| IV. | High Efficiency Engine Technologies | IV-1 |
| IV.1 | Cummins, Inc.: Technology and System Level Demonstration of Highly Efficient and Clean, Diesel Powered Class 8 Trucks. | IV-3 |
| IV.2 | Detroit Diesel: SuperTruck – Improving Transportation Efficiency through Integrated Vehicle, Engine, and Powertrain Research; Fiscal Year 2013 Engine Activities. | IV-8 |
| IV.3 | Volvo Technology of America: SuperTruck Initiative for Maximum Utilized Loading in the United States | IV-11 |
| IV.4 | Delphi Automotive Systems LLC: Gasoline Ultra-Efficient Vehicle with Advanced Low-Temperature Combustion | IV-15 |
| IV.5 | Ford Motor Company: Advanced Gasoline Turbocharged Direct Injection Engine Development | IV-19 |
| IV.6 | General Motors LLC: Lean Gasoline System Development for Fuel Efficient Small Cars | IV-26 |
| IV.7 | Cummins, Inc.: Cummins Next Generation Tier 2 Bin 2 Diesel | IV-29 |
| IV.8 | Robert Bosch: Advanced Combustion Controls—Enabling Systems and Solutions (ACCESS) | IV-32 |
| IV.9 | Chrysler Group LLC: Recovery Act – A MultiAir/MultiFuel Approach to Enhancing Engine System Efficiency | IV-38 |
| IV.10 | Filter Sensing Technologies, Inc.: Development of Radio Frequency Diesel Particulate Filter Sensor and Controls for Advanced Low-Pressure Drop Systems to Reduce Engine Fuel Consumption | IV-42 |
| IV.11 | General Motors LLC: The Application of High Energy Ignition and Boosting/Mixing Technology to Increase Fuel Economy in Spark Ignition Gasoline Engines by Increasing EGR Dilution Capability. | IV-48 |
| IV.12 | Eaton Innovation Center: Heavy-Duty Diesel Engines Waste Heat Recovery Using Roots Expander Organic Rankine Cycle System | IV-54 |
| IV.13 | MAHLE Powertain LLC: Next Generation Ultra-Lean Burn Powertrain | IV-59 |

| | | |
|-------|--|-------|
| IV. | High Efficiency Engine Technologies (Continued) | |
| IV.14 | Envera LLC: High Efficiency Variable Compression Ratio Engine with Variable Valve Actuation and New Supercharging Technology | IV-64 |
| IV.15 | Robert Bosch LLC: Recirculated Exhaust Gas Intake Sensor (REGIS) Enabling Cost-Effective Fuel Efficiency Improvement | IV-68 |
| IV.16 | Los Alamos National Laboratory: Robust Nitrogen Oxide/Ammonia Sensors for Vehicle Onboard Emissions Control | IV-72 |
| V. | Solid State Energy Conversion..... | V-1 |
| V.1 | Gentherm: Gentherm Thermoelectric Waste Heat Recovery Project for Passenger Vehicles | V-3 |
| V.2 | General Motors LLC: Improving Energy Efficiency by Developing Components for Distributed Cooling and Heating Based on Thermal Comfort Modeling | V-8 |
| V.3 | General Motors LLC: Development of Cost-Competitive Advanced Thermoelectric Generators for Direct Conversion of Vehicle Waste Heat into Useful Electrical Power | V-14 |
| V.4 | GMZ Energy Inc: Nanostructured High-Temperature Bulk Thermoelectric Energy Conversion for Efficient Automotive Waste Heat Recovery | V-19 |
| V.5 | Ohio State University: NSF/DOE Thermoelectrics Partnership Project SEEBECK: Saving Energy Effectively By Engaging in Collaborative research and Sharing Knowledge..... | V-23 |
| V.6 | Purdue University: NSF/DOE Thermoelectrics Partnership: Purdue – GM Partnership on Thermoelectrics for Automotive Waste Heat Recovery..... | V-28 |
| V.7 | Stanford University: Automotive Thermoelectric Modules with Scalable Thermomechanical and Electromechanical Interfaces..... | V-35 |
| V.8 | Stony Brook University: NSF/DOE Thermoelectrics Partnership: Integrated Design and Manufacturing of Cost-Effective and Industrial-Scalable TEG for Vehicle Applications | V-44 |
| V.9 | Texas A&M University: NSF/DOE Thermoelectrics Partnership: Inorganic-Organic Hybrid Thermoelectrics | V-48 |
| V.10 | University of California, Los Angeles: Integration of Advanced Materials, Interfaces, and Heat Transfer Augmentation Methods for Affordable and Durable Thermoelectric Devices | V-55 |
| V.11 | University of California, Santa Cruz: High-Performance Thermoelectric Waste Heat Recovery System Based on Zintl-Phase Materials with Embedded Nanoparticles | V-59 |
| V.12 | Virginia Tech: An Integrated Approach Towards Efficient, Scalable, and Low-Cost Thermoelectric Waste Heat Recovery Devices for Vehicles | V-64 |
| V.13 | University of Texas at Austin: High-Performance Thermoelectric Devices Based on Abundant Silicide Materials for Vehicle Waste Heat Recovery..... | V-68 |
| V.14 | Ford Motor Company: Thermoelectric HVAC and Thermal Comfort Enablers for Light-Duty Vehicle Applications | V-74 |
| VI. | Acronyms, Abbreviations and Definitions..... | VI-1 |
| VII. | Index of Primary Contacts | VII-1 |

I. INTRODUCTION

I.1 Program Overview and Status

DEVELOPING ADVANCED COMBUSTION ENGINE TECHNOLOGIES

On behalf of the Vehicle Technologies Office (VTO) of the U.S. Department of Energy (DOE), we are pleased to introduce the Fiscal Year (FY) 2013 Annual Progress Report for the Advanced Combustion Engine (ACE) Program. The mission of the VTO is to develop more energy-efficient and environmentally friendly highway transportation technologies that will enable the United States to use significantly less petroleum and reduce greenhouse gas and other regulated emissions while meeting or exceeding drivers' performance expectations. The ACE Program supports this mission by addressing critical technical barriers to commercializing higher efficiency, very low emissions, advanced combustion engines for passenger and commercial vehicles that meet future federal emissions regulations.

Dramatically improving the efficiency of internal combustion engines (ICEs) and enabling their introduction in conventional as well as hybrid-electric vehicles is one of the most promising and cost-effective approaches to increasing vehicle fuel economy over the next several decades. Already offering outstanding drivability and reliability to over 230 million highway transportation vehicles, ICEs have the potential to become substantially more efficient. Improvements in engine efficiency alone have the potential to increase passenger vehicle fuel economy by 35% to 50%, and commercial vehicle fuel economy by 30% with a concomitant reduction in greenhouse gas emissions, specifically, carbon dioxide emissions. These improvements are expected to be even greater when coupled with advanced hybrid electric powertrains. The Energy Information Administration Annual Energy Outlook 2013 reference case scenario forecasts that even by the year 2040, over 99% of all highway transportation vehicles sold will have ICEs.

The following are representative goals of the ACE Program that can contribute to meeting national energy security, environmental, and economic objectives:

- By 2015, increase the efficiency of ICEs for passenger vehicles resulting in fuel economy improvements of 25% for gasoline vehicles and 40% for diesel vehicles compared to baseline 2009 gasoline vehicles, and by 2020, achieve fuel economy improvements of 35% and 50% for gasoline and diesel vehicles, respectively.
- By 2015, increase the efficiency of ICEs for commercial vehicles from 42% (2009 baseline) to 50% (20% improvement) and by 2020, further improve engine efficiency to 55% (30% improvement) with demonstrations on commercial vehicle platforms.
- By 2015, increase the fuel economy of passenger vehicles by at least 5% with thermoelectric generators that convert energy from engine waste heat to electricity.

The passenger and commercial vehicle goals will be met while utilizing advanced fuel formulations that can incorporate a non-petroleum-based blending agent to enhance combustion efficiency and reduce petroleum dependence.

Two initiatives launched in FY 2010 to address the first two goals, namely the SuperTruck Initiative and the Advanced Technology Powertrains for Light-Duty Vehicles (ATP-LD) continued in FY 2013. Funding for these two initiatives includes more than \$100 million from the American Recovery and Reinvestment Act, and with a private cost share of 50%, supports nearly \$375 million in total research, development and demonstration projects across the country. Four projects under the SuperTruck Initiative focus on cost-effective measures to improve the freight efficiency of Class 8 long-haul trucks by 50%, 20% that will come from engine efficiency improvements alone. Projects under the ATP-LD Initiative focus on increasing the fuel economy of passenger vehicles by at least 25% using an engine/powertrain-only approach. From a FY 2012 solicitation, DOE awarded cost-shared (from 20% to 50%) contracts to six competitively selected teams of suppliers and vehicle manufacturers to develop and demonstrate innovations to achieve breakthrough engine and powertrain system efficiencies while meeting federal emission standards for passenger and commercial vehicles, including long-haul tractor trailers. These projects continued in FY 2013 to address the technical barriers inhibiting wider use of these advanced enabling engine technologies in the mass market.

Three projects initiated in FY 2011 to address the third goal continued in FY 2013. These projects are developing thermoelectric generators with cost-competitive advanced thermoelectric materials that will improve passenger vehicle fuel economy by at least 5% in FY 2015.

I. Introduction

This introduction outlines the nature, current focus, recent progress, and future directions of the ACE Program. The research activities of this Program are planned in conjunction with U.S.DRIVE (Driving Research and Innovation for Vehicle efficiency and Energy sustainability) and the 21st Century Truck partnerships, and are carried out in collaboration with industry, national laboratories, and universities. Because of the importance of clean fuels and advanced materials in achieving high efficiency and low emissions, R&D activities are closely coordinated with the relevant activities of the Fuel & Lubricant Technologies and Materials Technology Programs, also within VTO.

CURRENT TECHNICAL FOCUS AREAS AND OBJECTIVES

The ACE Program focuses on developing advanced ICE technologies for all highway transportation vehicles. Fuel efficiency improvement is the overarching focus of this activity, but resolving the interdependent emissions challenges is an integral requirement. The reduction of engine-out emissions is critical to managing the extra cost of exhaust aftertreatment devices that can be a barrier to market acceptance. Accordingly, the VTO ACE Program has been emphasizing the development of advanced engine combustion strategies that maximize engine efficiency and minimize the formation of emissions within the engine cylinders and developing cost-effective aftertreatment technologies that further reduce exhaust emissions. Research is focused on three major combustion strategies: a) Low-Temperature Combustion (LTC), including Homogeneous Charge Compression Ignition (HCCI), Pre-Mixed Charge Compression Ignition (PCCI), Reactivity Controlled Compression Ignition (RCCI); b) lean-burn (or dilute) gasoline combustion; and c) clean-diesel combustion. These combustion strategies will increase efficiency beyond current state-of-the-art engines and reduce engine-out emissions of nitrogen oxides (NOx) and particulate matter (PM) to near-zero levels. In parallel, research on emission control systems is underway to increase their efficiency and durability for overall emissions compliance at an acceptable cost and with reduced dependence on precious metals. Projects to stretch engine efficiency via innovative combustion methods and thermal energy recovery (such as compound cycles) are in progress as well. In response to the challenges of realizing and implementing higher efficiency engines, the ACE Program is working toward achieving the following objectives:

- Further the fundamental understanding of advanced combustion strategies that simultaneously exhibit high efficiency and very low emissions. A fuel-neutral approach is also being taken, with research addressing gasoline- and diesel-based advanced engines, including renewable fuels. The effects of fuel properties on combustion are addressed in the Fuel & Lubricant Technologies Program. Technology advances are expected to reduce the size and complexity of emission control hardware and minimize potential fuel efficiency penalties.
- Improve the effectiveness, efficiency, and durability of engine emission control devices as well as reduce their dependence on precious metals to enable increased penetration of advanced combustion engines in the light-duty market and maintain and/or expand application to heavy-duty vehicles.
- Extend robust engine operation and efficiency through the development and implementation of high-speed predictive models for improvements in combustion control and thermal management.
- Develop key enabling technologies for advanced engines such as sensors for control systems and engine diagnostics, and components for thermal energy recovery.
- Further the development of approaches to producing useful work from engine waste heat such as through incorporation of bottoming cycles. Advanced engine technologies such as turbo-machinery, flexible valve systems, advanced combustion systems, and fuel system components to achieve a reduction in parasitic losses and other losses to the environment to maximize engine efficiency.
- Improve the integration of advanced engine/emissions technologies with hybrid-electric systems for improved efficiency with lowest possible emissions.
- Identify that any potential health hazards associated with the use of new vehicle technologies being developed by VTO will not have adverse impacts on human health through exposure to toxic particles, gases, and other compounds generated by these new technologies.
- Develop thermoelectric generators that convert energy in the engine exhaust directly to electricity.

- Develop thermoelectric heating, ventilation and air-conditioning (HVAC) systems to maintain vehicle occupant comfort. This technology is particularly important for hybrid-electric and all-electric vehicles that have insufficient or no engine heat for occupant heating.

The ACE Program maintains close communication with industry through a number of working groups and teams, and utilizes these networks for setting goals, adjusting priorities of research, and tracking progress. These cooperative groups include the Advanced Combustion and Emission Control Tech Team of the U.S. DRIVE Partnership and the Engine Systems Team of the 21st Century Truck. Focused efforts are carried out under the Advanced Combustion Memorandum of Understanding (which includes auto manufacturers, engine companies, fuel suppliers, national laboratories, and universities) and the CLEERS (Cross-Cut Lean Exhaust Emission Reduction Simulation) activity for the Advanced Engine Cross-Cut Team.

TECHNOLOGY STATUS AND KEY BARRIERS

Significant advances in engine combustion, emission controls, fuel injection, turbo-machinery, and other advanced engine technologies continue to increase the thermal efficiency of ICEs with simultaneous reductions in emissions. With these advances, gasoline and diesel engines continue to be attractive engine options for conventional and hybrid-electric vehicles. These engines offer outstanding drivability, fuel economy, and reliability; they can readily use natural gas and biofuels such as ethanol and biodiesel, and can be integrated with hybrid and plug-in hybrid electric vehicle powertrains.

The majority of the U.S. light-duty vehicle fleet is powered by spark-ignition (SI) gasoline engines. Substantial progress in gasoline engine efficiency in recent years has been the result of advances in engine technologies including direct fuel injection, flexible valve systems, improved combustion chamber design, and reduced mechanical friction.

LTC strategies such as HCCI, PCCI, and RCCI exhibit high efficiency with significant reductions in NOx and PM formation such that engine-out emissions are at levels that remove or reduce the requirements for exhaust aftertreatment. Significant progress continues for LTC strategies and the operational range continues to be expanded to better cover the speed/load combinations consistent with light-duty and heavy-duty drive cycles. The major R&D challenges include fuel mixing, conditioning of intake air, combustion timing control, and expansion of the operational range. To meet these challenges, there has been significant R&D on allowing independent control of the intake/exhaust valves relative to piston motion and on improvements in air-handling and engine controls. Many of these technologies are transitioning to the vehicle market.

While all vehicular gasoline engines currently sold in the U.S. operate with stoichiometric combustion (needed for emission control by highly cost-effective three-way catalysts), other areas in the world with less stringent emissions regulations are seeing the introduction of higher efficiency lean-burn gasoline engines. Although these engines are characterized by higher efficiencies at part load, they will require more costly lean-NOx emission controls to meet more stringent U.S. emissions regulations. In addition, the direct injection technology utilized for most advanced gasoline engines produces particulate emissions that although smaller in mass than the diesel engine still represent significant emissions in terms of particulate number counts. Advances in lean-burn gasoline emission controls are critical for meeting U.S. regulations and ultimately the introduction of this efficiency technology in the U.S. market.

Attaining the high efficiency potential of lean-burn gasoline technology will require better understanding of the dynamics of fuel-air mixture preparation and other enabling technologies. Consistently creating combustible mixtures near the spark plug and away from walls in an overall lean environment is a challenge requiring improved understanding of fuel-air mixture preparation and modeling tools that embody the information. A comprehensive understanding of intake air flows and fuel sprays, as well as their interaction with chamber/piston geometry over a wide operating range is needed. Generating appropriate turbulence for enhancement of flame speed is a further complexity requiring attention. The wide range of potential intake systems, piston geometries, and injector designs makes the optimization of lean-burn systems dependent on the development of improved simulation tools. Furthermore, reliable ignition and combustion of lean (dilute) fuel-air mixtures remains a challenge. Lean and possibly boosted conditions require a more robust, high-energy ignition system that, along with proper mixture control, is needed to reduce combustion variability. Several new ignition systems have been proposed (high-energy plugs, plasma, corona, laser, etc.) and need to be investigated.

I. Introduction

Diesel engines are also well-suited for light-duty vehicle applications, delivering fuel economy considerably higher than comparable SI engines. Key developments in combustion and emission controls, plus low-sulfur fuel have enabled manufacturers to achieve the necessary emissions levels and introduce additional diesel-powered models to the U.S. market. DOE research contributed to all of these areas. Diesels in passenger cars have limited market penetration in the U.S. primarily due to the cost of the added components to reduce emissions and diesel fuel price. Hence reducing the cost of emission compliance continues to be addressed.

The heavy-duty diesel is the primary engine for commercial vehicles because of its high efficiency and outstanding durability. However, the implementation of increasingly stringent heavy-duty engine emission standards over the last decade held efficiency gains to a modest level. Current heavy-duty diesel engines have efficiencies in the 42-43% range. With stability in NOx and PM regulations in 2010, further gains in efficiency are now seen as achievable. Continued aggressive R&D to improve boosting, thermal management, and the reduction and/or recovery of rejected thermal energy are expected to enable efficiencies to reach 55%. Heavy-duty vehicles using diesel engines have significant potential to employ advanced combustion regimes and a wide range of waste heat recovery technologies that will improve engine efficiency and reduce fuel consumption.

Emissions of NOx and PM are a significant challenge for all lean-burn technologies including conventional and advanced diesel combustion strategies, both light-and heavy-duty, as well as lean-burn gasoline. Numerous technologies are being investigated to reduce vehicle NOx emissions while minimizing the fuel penalty associated with operating these devices. These technologies include advanced combustion strategies that make use of high levels of dilution to reduce in-cylinder NOx formation as well as post-combustion emission control devices.

The final guidance issued by the U.S. Environmental Protection Agency (EPA) in 2007 allowed the introduction of urea selective catalytic reduction (urea-SCR) technology for NOx control in Tier 2 light-duty vehicles, heavy-duty engines, and in other future diesel engine applications in the United States. Strategies to supply the urea-water solution (given the name “diesel exhaust fluid”) for vehicles have been developed and are being implemented. Using urea-SCR, light-duty manufacturers have been able to meet the Tier 2, Bin 5 emissions standard. Most heavy-duty diesel vehicle manufacturers are adopting urea-SCR since it has a broader temperature range of effectiveness than competing means of NOx reduction and allows the engine/emission control system to achieve higher fuel efficiency. Although urea-SCR is a relatively mature catalyst technology, more support research is needed to aid formulation optimization and minimize degradation effects such as hydrocarbon fouling.

Another technology being used to control NOx emissions from diesel engines and potentially lean-burn gasoline engines is lean-NOx traps (LNTs), which are also referred to as NOx adsorbers. Although LNTs have been commercialized for light-duty diesels, further advancement of the technology is needed to expand market penetration of light-duty diesels and to enable use of LNTs in lean-burn gasoline engine passenger car vehicles.

A primary limitation to further adoption of current light-duty diesels is cost. Complex engine and exhaust gas recirculation (EGR) systems, and the larger catalyst volumes associated with LNTs and diesel particulate filters (DPFs) result in higher overall costs in comparison to conventional gasoline vehicle systems. LNTs are particularly cost-sensitive because they require substantial quantities of platinum group metals, and the cost of these materials is high and volatile due to limited sources that are primarily mined in foreign countries. Improvements in the temperature range of operation for LNTs are also desired to reduce cost and enable success in the lean-gasoline engine application. Both LNTs and DPFs result in extra fuel use, or a “fuel penalty,” as they require fueling changes in the engine for regeneration processes. Aggressive research has substantially decreased the combined fuel penalty for both devices to approximately 4% of total fuel flow; further reduction would be beneficial. While LNTs have a larger impact on fuel consumption than urea-SCR, light-duty vehicle manufacturers appear to prefer LNTs since overall fuel efficiency is less of a concern and urea replenishment is more of a challenge for light-duty customers as compared to heavy-duty vehicle users. Another improvement being pursued for LNT technology is to pair them with SCR catalysts. The advantage is that the SCR catalyst uses the NH₃ produced by the LNT so no urea is needed. Formulation and system geometries are being researched to reduce the overall precious metal content of LNT+SCR systems that reduces cost and makes the systems more feasible for light-duty vehicles.

Advanced LTC strategies being pursued have lower engine-out emission levels thus reducing the requirements for exhaust aftertreatment. They exhibit high efficiency with significant reductions in NOx and

PM emissions. However, emissions of hydrocarbons (HCs) and carbon monoxide (CO) are often higher and require additional controls which are often a challenge with the low exhaust temperature characteristic of these combustion modes.

High dilution operation through advanced EGR has been a major contributor to meeting the 2010 EPA heavy-duty engine emission standards and is also applicable to light-duty diesel and gasoline engines. There are numerous advantages of advanced EGR compared to urea-SCR and LNT packages including lower vehicle weight, less maintenance, and lower operating cost. The disadvantages relative to post-combustion emission controls include increased heat rejection load on the engine and the potential for increased fuel consumption due to more frequent DPF active regeneration.

Complex and precise engine and emission controls require sophisticated feedback systems employing new types of sensors. A major advancement in this area for light-duty engines has been the introduction of in-cylinder pressure sensors integrated into the glow plug. Start-of-combustion sensors (other than the aforementioned pressure sensor) have been identified as a need, and several development projects have been completed. Sensors are also beneficial for the emission control system. NOx and PM sensors are under development and require additional advances to be cost-effective, accurate, and reliable. Upcoming regulations with increased requirements for onboard diagnostics will also challenge manufacturers trying to bring advanced fuel efficient solutions to market. The role of sensors and catalyst diagnostic approaches will be a key element of emission control research in the next few years.

Waste heat recovery approaches (e.g., bottoming cycles) are being implemented in heavy-duty diesel vehicles and explored for light-duty diesel and gasoline applications. Experiments have shown that waste heat recovery has the potential to improve vehicle fuel economy by as much as 10%.

Another form of waste heat recovery is a thermoelectric generator. In current gasoline production passenger vehicles, roughly over 70% of the fuel energy is lost as waste heat from an engine operating at full power. About 35% to 40% is lost in the exhaust gases and another 30% to 35% is lost to the engine coolant. Thermoelectric generators can directly convert energy in the engine's exhaust to electricity for operating auxiliary loads and accessories, thereby improving the vehicle's fuel economy. Vehicular thermoelectric generators are on a path to commercialization; several manufacturers intend to introduce thermoelectric generators in their cars later this decade in Europe and North America.

Use of thermoelectric devices for vehicle occupant comfort heating or cooling is also being pursued as a more fuel efficient alternative to the conventional mobile HVAC systems. In addition, the refrigerant gas R-134a used in conventional systems has a warming potential that is 1,300 times that of carbon dioxide, the primary greenhouse gas. Vehicle air conditioners could contribute as much as 11% CO₂ equivalent emissions (from the fuel needed to run the air conditioner and refrigerant leakage) compared to the total CO₂ produced by the engine. It is estimated that dispersed thermoelectric devices can maintain single occupant comfort conditioning with about one-sixth of the energy used by conventional systems that cool the entire driver and passenger cabin. Zonal (dispersed) thermoelectric HVAC systems have been designed and installed in passenger vehicle models for a ride-and-drive demonstration in FY 2013 and early FY 2014.

FUTURE DIRECTIONS

ICEs have a maximum theoretical fuel conversion efficiency that is considerably higher than the mid-40% peak values seen today. The primary limiting factors to approaching these theoretical limits of conversion efficiency start with the high irreversibility in traditional premixed or diffusion flames, but more practically the limits are imposed by heat losses during combustion/expansion, structural limits that constrain peak cylinder pressures, untapped exhaust energy, and mechanical friction. Emphasis must be placed on enabling the engine to operate near peak efficiency over a real-world driving cycle to improve vehicle fuel economy. For SI engines this means reducing the throttling losses with technologies such as lean-burn, high dilution, and variable geometry. Exhaust losses are being addressed by analysis and development of compound compression and expansion cycles achieved by valve timing, use of turbine expanders, regenerative heat recovery, and application of thermoelectric generators. Employing such cycles and devices has been shown to have the potential to increase heavy-duty engine efficiency to as high as 55% and light-duty vehicle fuel economy by 35% to 50%.

I. Introduction

Analyses of how “advanced combustion regimes” might impact the irreversibility losses have indicated a few directions to moderate reductions of this loss mechanism, but maximizing conversion of availability (or available energy) to work will require compound cycles or similar measures of exhaust energy utilization. The engine hardware changes needed to execute these advanced combustion regimes include variable fuel injection geometries, turbo- and super-charging to produce very high manifold pressures, compound compression and expansion cycles, variable compression ratio, and improved sensors and control methods. Larger reductions in combustion irreversibility will require a substantial departure from today’s processes but are being examined as a long-range strategy.

Most of the basic barriers to high engine efficiency hold true for both gasoline- and diesel-based engines. Recognizing the dominance of gasoline-type SI engines in the U.S., VTO has increased emphasis on their improvement. Gasoline-based engines, including E85 (85% ethanol, 15% gasoline) flexible-fuel, can be made 20% to 25% more efficient through direct injection, boosting/downsizing, and lean-burn. Real-world fuel savings might be even higher by focusing attention on the road-load operating points.

Meeting anticipated future emission standards will be challenging for high-efficiency diesel and lean-burn gasoline engines. To address this issue, research on innovative emission control strategies will be pursued through national laboratory and university projects designed to reduce cost and increase performance and durability of NOx reduction and PM oxidation systems. Project areas include development of low-cost base metal catalysts (to replace expensive platinum group metals), lighter and more compact multifunctional components, new control strategies to lessen impact on fuel consumption, and improved sensors and onboard diagnostics for meeting upcoming regulations. Furthermore, simulations of the catalyst technologies are being developed to enable industry to perform more cost-effective system integration during vehicle development. As advanced combustion approaches evolve and engine-out emissions become cleaner, the requirements of emission controls are expected to change as well.

The majority of lean-NOx emission controls development has been focused on diesel engines. With the potential introduction of high-efficiency lean-burn gasoline engines, these technologies will require further research and development as well as emission controls for managing HC/CO emissions. Engine-out PM emissions from lean-burn gasoline engines, although lower in mass than the diesel engine, are also a concern due to smaller particle sizes and morphology.

Enabling technologies being developed will address fuel systems, sensors, engine control systems, and other engine technologies. Fuel systems R&D focuses on injector controls and fuel spray development. Engine control systems R&D focuses on developing engine controls and sensors that are precise and flexible for enabling improved efficiency and emission reduction in advanced combustion engines. This also includes a better understanding of stochastic and deterministic in-cylinder processes that limit the speed/load range of many advanced combustion strategies. Control system technologies will facilitate adjustments to parameters such as intake air temperature, fuel injection timing, injection rate, variable valve timing, and EGR to allow advanced combustion engines to operate over a wider range of engine speed/load conditions. Engine technologies development will be undertaken to achieve the best combination that enables advanced combustion engines to meet maximum fuel economy and performance requirements. These include variable compression ratio, variable valve timing, variable boost, advanced sensors and ignition systems, and exhaust emission control devices (to control HC emissions at idle-type conditions) in an integrated system. Upcoming EPA onboard diagnostic requirements will be addressed through research on advanced sensors, improved understanding of emission control aging, and development of models that are integral to the diagnostic method. Work in developing enabling technologies for more efficient, emission-compliant engine/powertrain systems will continue to be pursued.

The Solid State Energy Conversion activity will continue on developing advanced thermoelectric generators for converting energy from engine waste heat directly into useful electrical energy for operating vehicle auxiliary loads and accessories to improve the vehicle’s fuel economy. Achieving the vehicle-based performance goals requires reduction in the cost of thermoelectric materials, scaling them up into practical devices, reduction in the manufacturing cost of vehicular thermoelectric generators at the production scale for the vehicle market, and making them durable enough for vehicle applications. The cost-shared projects initiated in FY 2011 with three competitively selected teams will continue in the design and development of cost-competitive manufacture of thermoelectric generators for selected passenger vehicle platforms.

The remainder of this report highlights progress achieved during FY 2013 under the Advanced Combustion Engine Program. The following 69 abstracts of industry, university, and national laboratory projects provide an overview of the exciting work being conducted to address critical technical challenges associated with R&D of higher efficiency, advanced ICEs for light-duty, medium-duty, and heavy-duty vehicles. We are encouraged by the technical progress realized under this dynamic Program in FY 2013, but we also remain cognizant of the significant technical hurdles that lay ahead, especially those to further improve efficiency while meeting the light-duty EPA Tier 3 emission standards and future heavy-duty engine standards for the full useful life of the vehicles.

Gurpreet Singh, Program Manager
Advanced Combustion Engine Program
Vehicle Technologies Office

Roland M. Gravel
Vehicle Technologies Office

Kenneth C. Howden
Vehicle Technologies Office

Leo Breton
Vehicle Technologies Office

I.2 Project Highlights

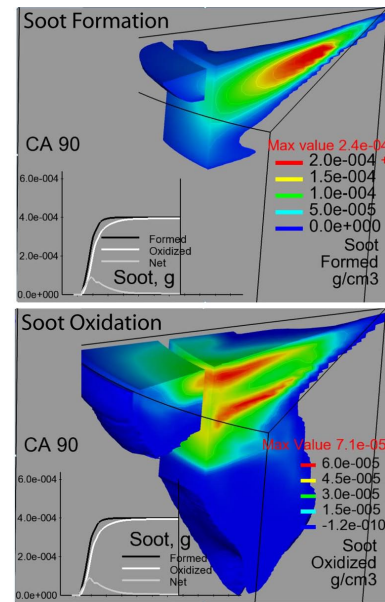
The following projects highlight progress made in the Advanced Combustion Engine Program during FY 2013.

ADVANCED COMBUSTION AND EMISSION CONTROL RESEARCH FOR HIGH-EFFICIENCY ENGINES

A. Combustion Research

The objective of these projects is to identify how to achieve more efficient combustion with reduced emissions from advanced technology engines.

- Sandia National Laboratories (SNL) is providing the physical understanding of the in-cylinder combustion processes needed to minimize the fuel consumption and the carbon footprint of automotive diesel engines while maintaining compliance with emissions standards. In FY 2013 they developed and improved diagnostic techniques that permit the quantitative evaluation of equivalence ratio distributions formed from injection of diesel-like fuels. They also explored the applicability of pilot injection strategies to low-temperature combustion (LTC) techniques; examined the impact of pilot mass, injection pressure, ambient temperature and swirl ratio on the mixture formed by the pilot fuel injection; quantified the impact of ambient temperature, oxygen concentration, and mixture formation on the ignition of the pilot fuel; and evaluated the ability of computational models to accurately capture the pilot ignition process. (Miles, SNL)
- SNL is developing fundamental understanding of how in-cylinder controls can improve efficiency and reduce pollutant emissions of advanced LTC technologies. In FY 2013 SNL developed a conceptual framework of exhaust soot-reduction dependencies for post injections that were close-coupled to the main injection to maintain fuel-efficient combustion phasing; showed interactions between the post-injection jet and residual main-injection products via multi-plane soot and combustion diagnostics, which is a first step to building a conceptual model for multiple injections; achieved good agreement between computer models and experiments, and used the model predictions to gain insight into three-dimensional (3-D) in-cylinder processes; and quantified effects of post-injection load, duration, and dwell effects on LTC efficiency and identified in-cylinder processes responsible for combustion efficiency improvements. (Musculus, SNL)
- SNL is facilitating improvement of engine spray combustion modeling, accelerating the development of cleaner, more efficient engines. In FY 2013 they expanded a comprehensive spray combustion dataset working collaboratively with more than 10 different experimental institutions from around the world. SNL led the ECN via monthly web-meetings and frequent exchanges. ECN experimental targets are now the focus of engine combustion modeling activities worldwide. They applied novel diagnostics to quantify evaporation and mixing in a multi-hole gasoline injector with the focus of understanding stochastic variability in direct-injection fueling systems, and demonstrated how the spray collapse during the end-of-injection phase affects mixing and evaporation in iso-octane and ethanol fuel sprays. (Pickett, SNL)
- SNL is providing the fundamental understanding (science-base) required to overcome the technical barriers to the development of practical Low-Temperature Gasoline Combustion (LTGC) engines, including Homogeneous Charge Compression Ignition (HCCI) and partially stratified variants of HCCI, by industry. In FY 2013 they completed the following. First, an investigation of fuel composition effects combined with early direct injection, partial fuel stratification fueling produced higher efficiencies and



Time-integrated spatial distribution of soot formation (top) and soot oxidation (bottom) predicted by computer models, (Musculus, SNL)

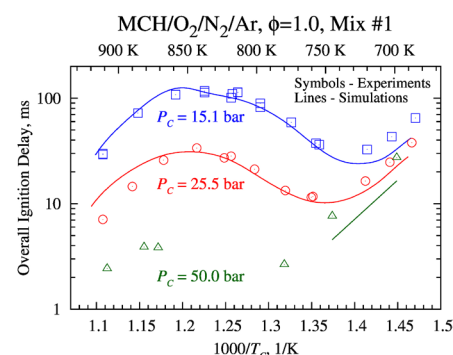
significant increases in the maximum load for a given intake-boost level. Second, the effect of raising the compression ratio from 14:1 to 16:1 was investigated and found to offer further improvements in thermal efficiency. Third, progress has been made toward an investigation of how the in-cylinder thermal stratification is affected by the piston-top temperature. Additionally, a new study has been initiated to understand the relationship between combustion noise level and ringing intensity as metrics for acceptable LTGC engine operation, and efforts are underway to upgrade their research engines for investigations of spark-assisted LTGC. (Dec, SNL)

- SNL is researching a negative valve overlap (NVO) strategy for controlling HCCI combustion. In FY 2013 they: (1) characterized species produced during NVO reactions as a function of NVO fuel-injection timing; (2) applied CHEMKIN simulation to identify the NVO reaction products responsible for chemically enhancing main HCCI combustion; and (3) performed joint experiments with ORNL that identified optimal NVO injection parameters for production of hydrogen and carbon monoxide gas in rich NVO environments. Such onboard generation of synthesis gas could benefit gasoline engine operation through enhanced dilution tolerance and knock avoidance. (Steeper, SNL)
- Argonne National Laboratory (ANL) is developing and validating robust and predictive nozzle flow and turbulence models for diesel engine applications aided by high-performance computing tools. In FY 2013 they: (1) Performed 3-D, transient, turbulent in-nozzle flow simulations. For the first time, needle off-axis (wobble) motion has been accounted for in the simulations. For multi-hole injectors the needle wobble is shown to have a profound influence on mass flow rate from each orifice. (2) Demonstrated grid-convergence on diesel spray using LES turbulence models. (3) Demonstrated that LES can capture cyclic variability and performs both qualitatively and quantitatively better than Reynolds Averaged Navier-Stokes for spray calculations. (4) Performed engine simulations on 1,024 processors in a scalable fashion. (5) Developed and validated a 106 species-based reduced reaction model for n-dodecane as surrogate for diesel fuel. (Som, ANL)
- ANL is making detailed measurements of the sprays from fuel injectors using X-ray absorption. The technique is non-intrusive, quantitative, highly time-resolved, and allows them to make detailed measurements of the spray, even in the densely-packed region very near the nozzle. In FY 2013, ANL completed measurements of the needle lift and internal geometry of the Engine Combustion Network (ECN) "Spray B" injectors. They also performed parametric studies to learn the conditions that are most and least likely to result in gas bubbles that are pulled inside of diesel injectors at the end of injection which may be a factor in injector damage as well as unburned hydrocarbon and particulate matter emissions. They continued to develop a new diagnostic for droplet sizing in the near-nozzle region of sprays: Small-Angle X-Ray Scattering. With further development and validation, this may become a unique and valuable method for studying near-nozzle spray structure, providing new data for spray model development and validation. (Powell, ANL)
- SNL is combining unique state-of-the-art simulation capability based on the large eddy simulation (LES) technique with Advanced Engine Combustion R&D activities. In FY 2013 they established the first quantitative explanation that shows a distinct gas-liquid interface does not exist for a wide range of diesel-relevant injection conditions at high pressures, demonstrated that the classical view of jet atomization (which is currently widely assumed) is not applicable at these conditions, and performed detailed analysis of high-pressure injection processes using LES and real-fluid thermodynamics and compared LES with ECN experimental target data. (Oefelein, SNL)
- ANL is collaborating with combustion researchers within DOE's Offices of Basic Energy Science and Vehicle Technologies Office programs to develop and validate predictive chemical kinetic models for a range of transportation-relevant fuels. In FY 2013: (1) A high-fidelity modeling framework has been developed to simulate chemicophysical processes within ANL's rapid compression machine, where refinements to this are ongoing. This activity enhances the validation and improvement of chemical kinetic mechanisms for transportation-relevant fuels. (2) ANL's rapid compression machine has been used to acquire autoignition data for additive-doped gasoline surrogate blends. Chemical kinetic models have been assembled for these fuels with predictions compared against experimental measurements. Improvements to the base fuel mechanisms seem to be necessary in order to adequately capture the sensitizing effects of fuel additives. (3) Comprehensive expressions have been developed for a reduced-order, control-oriented ignition model which cover low and high temperatures for fuels with a wide range

I. Introduction

of reactivity. Future work will unify these expressions across temperatures from 500 to 2,000 K. (Goldsborough, ANL)

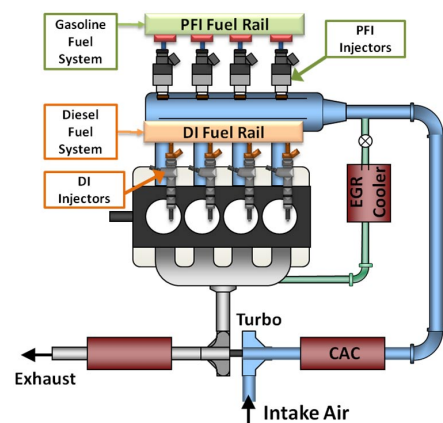
- Lawrence Livermore National Laboratory (LLNL) is developing detailed chemical kinetic models for fuel components used in surrogate fuels for compression ignition, HCCI and RCCI engines. In FY 2013 they: (1) developed improved models for n-propyl benzene, n-butyl benzene, and their mixtures and validated them for ignition and flame speeds; (2) developed a new chemical kinetic model for α -methyl naphthalene and validated it for high-temperature ignition in a shock tube and oxidation in a flow reactor; (3) developed a fuel surrogate model for gasoline-ethanol mixtures and validated it by comparison to flame speeds in a flat-flame burner and intermediate heat release in an HCCI engine; and (4) developed an improved model for methylcyclohexane and validated it for ignition at engine conditions and for species measurements in low-pressure flames. (Pitz, LLNL)
- LLNL is gaining fundamental and practical insight into HECC regimes through numerical simulations and experiments. In FY 2013 they: (1) validated new multi-zone scheme, and quantified accuracy and fidelity for zone strategies; (2) implemented advanced solvers with CONVERGE™ multi-zone, yielding orders of magnitude reduction in simulation time; (3) validated multi-dimensional simulations of iso-octane Premixed Charge Compression Ignition (PCCI) using CONVERGE™ multi-zone with detailed chemistry; (4) demonstrated computational fluid dynamics/multi-zone applied to gasoline direct-injection spark ignition and PCCI operation; and (5) partnered with Cummins/CONVERGE™ to integrate a graphical processing unit-based solver into multidimensional computational fluid dynamics, developed and tested graphical processing unit combustion chemistry with potential 8x speedup. (Whitesides, LLNL)
- LLNL is applying mathematics underpinning efficient algorithms and developing combustion software on new computing architectures. In FY 2013 they: (1) developed a sensitivity analysis tool for use by chemical kineticists that reduces the time to solution for a typical fuel from one week to less than an hour; (2) created a computer processing unit-accelerated algorithm to calculate thermochemistry functions an order of magnitude faster than the computer processing unit-based version; (3) tested and validated the adaptive preconditioner technique for new mechanism classes key to the development of “real fuel” surrogates; (4) extended the adaptive preconditioner technique to calculate the ignition delay characteristics for a 39,000 species mechanism in two minutes (compared to five months using the traditional approach); and (5) developed a reaction timescale analysis tool to aid in mechanism design. (McNenly, LLNL)
- Los Alamos National Laboratory (LANL) is developing algorithms and software for the advancement of speed, accuracy, robustness, and range of applicability of the KIVA internal engine combustion modeling—to be more predictive. In FY 2013 they: (1) developed parallel hp -adaptive predictor-corrector split using a Petrov-Galerkin finite element method for all flow regimes, from incompressible to high-speed compressible; (2) developed 3-D overset grid method for moving and immersed actuated parts such as valves for robust grid movement; (3) validated KIVA multi-component particle/spray injection algorithm into the predictor-corrector split finite element method solver; (4) validated KIVA chemistry package into the predictor-corrector split finite element method solver; (5) validated KIVA splash, break-up, collide and wall-film models into the predictor-corrector split solver; and (6) developed large eddy simulation turbulence modeling for wall-bounded flows. (Carrington, LANL)
- The University of Michigan is exploring new high-pressure lean-burn combustion strategies that can enable future gasoline engines with 20-40% improved fuel economy. In FY 2013 (1) Two engine models of spark-assisted compression ignition were developed. (2) Experiments and modeling studies on stratification have shown complex behavior of burn rate when injection timing and boost pressure are varied. (3) Optical engine studies of spark-assisted compression ignition have confirmed that phasing changes in autoignition are the result of a relatively small amount of flame heat release, which



Comparison of the methylcyclohexane model with experimental ignition data from a rapid compression machine, for a stoichiometric mixture, over a range of temperatures, and at pressures of 15, 25 and 50 bar. (Pitz, LLNL)

is determined by a tradeoff between time available and changes in flame speed. (4) Experiments in a Cooperative Fuel Research engine have shown that a microwave-assisted spark plug helps with early flame kernel development but has little effect on overall burn characteristics. (5) Computational studies of the effect of buffer gas on autoignition show significant effects on ignition delay, especially in the negative temperature coefficient region, and on heat release, with CO₂ dilution resulting in the lowest peak heat release rate. (Wooldridge, University of Michigan)

- Michigan State University is demonstrating a spark ignition HCCI dual combustion mode engine for a blend of gasoline and E85 (85% ethanol and 15% gasoline) for the best fuel economy. In FY 2013 (1) The engine simulation model was further improved with an updated physics-based charge mixing model based upon the test data. (2) Multi-injection and multi-ignition capability was added to the engine control system to enable multiple injections and ignitions during the mode transition, and the electrical variable valve timing operational range was extended to 85 degrees to increase recompression. (3) Stable HCCI combustion was achieved with around 2% coefficient of variance for the target single-cylinder metal engine without external electric heater. (4) Smooth combustion mode transition was achieved between SI and HCCI combustion within eight engine cycles. It was found that the proposed concept of using the hybrid combustion mode during the mode transition is the key enabler for fast and smooth combustion mode transition. (Zhu, Michigan State University)
- Oak Ridge National Laboratory (ORNL) is developing and applying innovative strategies that maximize the benefit of high-performance computing resources and predictive simulation to support accelerated design and development of advanced engines to meet future fuel economy and emissions goals. In FY 2013 they initiated metamodel development for highly dilute spark-ignition combustion by launching initial grid optimization and parameter sensitivity sweeps, developed a computational framework for job management and component optimization, and performed initial parameter sweeps for model validation. (Edwards, ORNL)
- ANL is optimizing the operating conditions to use low cetane fuel to achieve clean, high-efficiency engine operation and demonstrate the use of LTC as an enabling technology for high-efficiency vehicles. In FY 2013 they achieved 1.3 bar brake mean effective pressure (BMEP) to 20 bar BMEP using only 87 anti-knock index fuel; demonstrated the effectiveness of cetane enhancers (ethyl hexyl nitrate) in facilitating low-load performance; and attained a 26% fuel economy improvement using LTC in a conventional powertrain vehicle over a similar port fuel injected vehicle on the combined Urban Dynamometer Driving Schedule and Highway Fuel Economy Test cycles in a 2007 Cadillac vehicle. (Ciatti, ANL)
- ANL is quantifying the efficiency potential and combustion stability limitations of advanced GDI combustion systems including lean, boosted and EGR-dilute concepts. In FY 2013 they quantified the sensitivity of lean and EGR-dilute combustion to air/fuel ratio and combustion phasing perturbation. A novel, Reynolds Averaged Navier-Stokes approach characterized by low numerical diffusion was applied to qualitatively evaluate cycle-to-cycle variability and combustion stability in an internal combustion engine. They also implemented an advanced directed energy ignition system ignition system providing fully programmable multi-spark and sustained spark features. (Wallner, ANL)
- ORNL is gaining and utilizing knowledge of the recurring patterns that occur in cyclic variability in spark-ignition engines to predict and correct for low-energy cycles such as misfires that reduce engine efficiency at the dilution limit. In FY 2013 they experimentally quantified the effects of various engine control parameters on combustion stability (injection and cam timing, ignition timing, composition) and found that external EGR affects the dynamics of cyclic variations beyond the dilution limit imposed by combustion stability requirements. (Kaul, ORNL)
- ORNL is developing and evaluating the potential of High Efficiency Clean Combustion (HECC) strategies with production-viable hardware and aftertreatment on multi-cylinder engines. In FY 2013 they attained the 2013 technical target of



ORNL Multi-Cylinder RCCI Engine (Curran, ORNL)

I. Introduction

developing a Reactivity Controlled Compression Ignition (RCCI) engine map suitable for use in vehicle system drive cycle simulations, attained the 2013 technical target of demonstrating greater than 20% improvement in modeled fuel economy with multi-mode RCCI operation as compared to a 2009 port fuel injected (PFI) gasoline baseline, performed drive cycle estimations of fuel economy and emissions using vehicle systems modeling with experimental data with multi-mode RCCI/conventional diesel combustion operation, and evaluated the hydrocarbon and CO reduction effectiveness of multiple diesel oxidation catalysts with RCCI. (Curran, ORNL)

- ORNL is defining and analyzing specific advanced pathways to improve the energy conversion efficiency of internal combustion engines from nominally 40% to as high as 60%, with emphasis on opportunities afforded by new approaches to combustion. In FY 2013 they: (1) demonstrated that in-cylinder non-catalytic reforming is a thermodynamically inexpensive pathway to forming a high-octane reformatre stream rich in hydrogen; (2) successfully collaborated with SNL on quantifying chemical species formed during NVO associated with in-cylinder non-catalytic reforming; and (3) determined that very low concentrations of sulfur (~2 ppm) can significantly deactivate the nickel-based thermochemical recuperation reforming catalyst, and that this is the most likely cause of the reforming degradation. (Daw, ORNL)
- SNL is studying the effects of continuous operation (i.e. gas exchange) on indicated thermal efficiency and emissions of an opposed free-piston linear alternator engine utilizing HCCI combustion at high compression ratios (~20-40:1). In FY 2013: (1) passive synchronization of the pistons was successfully demonstrated through continuous motoring tests; (2) low equivalence ratio HCCI combustion with hydrogen was successfully demonstrated; (3) new, low-friction pistons were designed, fabricated and installed; and (4) extended duration (~30 sec) combustion tests have shown a path to greater than 50% indicated fuel conversion efficiency and greater than 55% work-to-electrical efficiency. (Johnson, SNL)
- ORNL is assessing the fuel economy and emissions benefits of VCR technology. In FY 2013 they tested a prototype VCR engine but encountered mechanical problems with the timing chain system. (Domingo, ORNL)
- ANL is performing engine benchmarking to accelerate the development of high-efficiency internal combustion engines for light-duty vehicle applications, while meeting the future emission standards, using numerical simulations. In FY 2013 they completed engine and vehicle testing of a 2012 Audi A4 with twin variable geometry turbochargers, direct injection and variable valve lift 2.0-liter engine for testing. They also completed engine and vehicle testing of a 2012 Mini Cooper with a 1.6-liter turbocharged direct-injected variable valve timing engine. (McConnell, ANL)
- ORNL is applying the historically successful approach of developing and applying minimally invasive advanced diagnostic tools to resolve spatial and temporal variations within operating engines and catalysts. In FY 2013 they developed an improved multiplex laser-based exhaust gas recirculation (EGR) probe, and improved analysis techniques. This multiplex setup allowed for simultaneous measurements from four EGR probes positioned at various locations in the engine system. The result was a profound increase in the efficiency of system mapping. (Partridge, ORNL)

B. Emission Control R&D

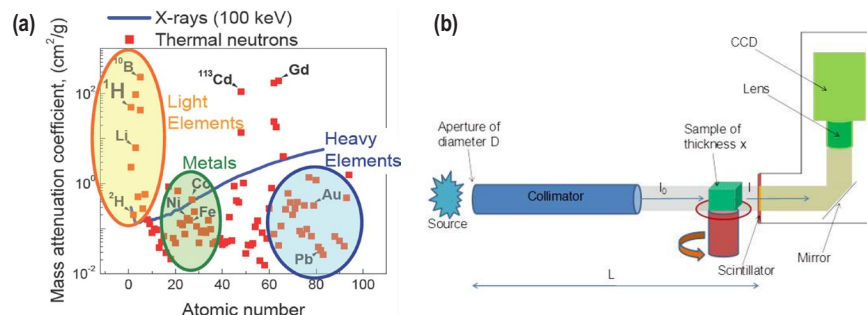
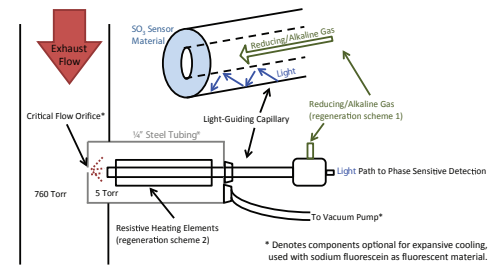
The following project highlights summarize the advancements made in emission control technologies to both reduce exhaust emissions and reduce the energy needed for emission control system operation.

- ORNL is coordinating the Cross-Cut Lean Exhaust Emission Reduction Simulation (CLEERS) activity for the DOE Advanced Engine Cross-Cutting Technology Development Team. In FY 2013 they led and facilitated CLEERS Focus teleconferences; created an initial bibliographic database for evaluation by selective CLEERS members and established an ORNL Sharepoint site for an expanded experimental database of engine exhaust and aftertreatment measurements and simulation algorithms and modeling tools; continued further refinement of LNT and SCR catalyst characterization protocols in coordination with the CLEERS Kinetics task; conducted the 2013 CLEERS Industry Priority Survey; organized the 2013 CLEERS workshop; maintained the CLEERS website; and increased utilization of models and kinetic parameters produced by CLEERS projects in full system simulations of conventional and hybrid advanced light- and heavy-duty powertrains. (Daw, ORNL)

- ORNL is collaborating with Pacific Northwest National Laboratory (PNNL) to support industry in the development of accurate simulation tools for the design of catalytic emissions control systems that enable advanced high-efficiency combustion engines to meet emissions regulations while maximizing fuel efficiency. In FY 2013 they: (1) completed detailed flow reactor characterization of the BMW GDI LNT catalyst; (2) demonstrated that NO oxidation to NO_2 does not play a role in the reaction mechanism for NO SCR by NH_3 ; (3) investigated N_2O formation during low-temperature regeneration of LNT catalysts, and identified mechanistic steps that account for observed LNT N_2O trends; (4) evaluated changes in SCR catalyst model parameters required to capture impacts of aging on catalyst functionality; and (5) developed experimental protocols and analysis techniques for direct measurement of NH_3 adsorption enthalpy as a function of coverage on zeolite SCR catalysts. (Daw, ORNL)
- PNNL is developing improved computational tools for simulating realistic full-system performance of lean-burn engines and the associated emissions control systems. In FY 2013 they: (1) identified an important reaction intermediate for NH_3 selective catalytic reduction (SCR) with small-pore zeolite-based Cu SCR catalysts; (2) mechanisms for Pt stability on spinel magnesium aluminate support materials in lean-oxides of nitrogen (NOx) traps (LNTs) were determined; (3) detailed reaction kinetics measurements of NH_3 SCR demonstrated the importance of intra-particle diffusion control for reactivity over a wide temperature range; and (4) proposed a two-site SCR global kinetics model that includes NH_3 oxidation, NO oxidation, and the standard SCR reaction, and provides a simple means of representing performance changes due to aging of the copper chabazite zeolite catalyst. (Muntean, PNNL)
- PNNL is identifying approaches to significantly improve both the high- and low-temperature performance, and the stability of the catalytic NOx reduction technologies via pursuit of a more fundamental understanding. In FY 2013: (1) Catalysts were characterized before and after incorporation of Cu by X-ray diffraction, electron paramagnetic resonance and temperature-programmed reduction. (2) Baseline reactivity measurements were performed on these catalysts in preparation for mechanistic studies of high- and low-temperature performance loss. (3) A variety of model K-titania catalysts were prepared at PNNL based on materials described in the open literature. (4) Detailed studies of the sensitivity to high temperatures (required for desulfation) were conducted of these model catalysts. (Peden, PNNL)
- PNNL is developing and demonstrating mixed metal oxide-based catalysts as a low-cost replacement for platinum in the oxidation of NO to NO_2 in lean engine exhaust, an essential first step in controlling NOx emissions. In FY 2013 they demonstrated the stability of Ce-Mn mixed oxides against high-temperature aging, determined the effect of Mn loading on the catalyst activity, demonstrated that ceria stabilizes Mn in a higher oxidation state leading to easier Mn reducibility and lower temperature for NO oxidation, and Mn addition to ceria was shown to lower the energy required for oxygen vacancy formation. (Karim, PNNL)
- PNNL is developing a fundamental understanding of the integration of SCR and diesel particulate filter (DPF) technologies for on-road heavy-duty diesel applications. In FY 2013 they developed improved understanding of soot oxidation performance with a coupled active SCR process and the pathway towards optimizing its performance for heavy-duty diesel applications; developed an understanding of SCR processes and the nature by which improved integration with coupled soot oxidation processes can be accomplished achieving optimum performance for both; and continued to develop the ability to accurately predict how changes in active species concentrations will affect system performance. (Rappe, PNNL)
- ORNL is developing emission control technologies that perform at low temperatures ($<150^\circ\text{C}$) to enable fuel-efficient engines with low exhaust temperatures to meet emission regulations. In FY 2013 they investigated an innovative Au@Cu (core@shell) catalyst for oxidation, demonstrated the synergy of mixing of Au@Cu and Pt catalysts and the potential to overcome inhibitions, and synthesized and evaluated new catalysts using a new support. (Toops, ORNL)
- ORNL is assessing and characterizing catalytic emission control technologies for lean-gasoline engines. In FY 2013 they achieved $>99\%$ NOx to NH_3 conversion over a three-way (TWC) at an equivalence ratio of 0.96; demonstrated $>98\%$ NOx reduction efficiency with a TWC+SCR approach on the lean-gasoline engine platform with a 5.6% fuel economy improvement over the stoichiometric-engine case; and identified key SCR catalyst characteristics and operating strategies required to achieve high NOx conversion while minimizing fuel penalty. (Parks, ORNL)

I. Introduction

- ORNL is researching the fundamental chemistry of automotive catalysts, identifying strategies for enabling self-diagnosing catalyst systems, and is addressing critical barriers to market penetration. In FY 2013 they characterized spatiotemporal intra-catalyst performance of a degreened commercial Cu-SAPO-34 SCR catalyst under standard and fast SCR conditions, demonstrated application of spatially resolved capillary inlet mass spectrometer (SpaciMS) intra-catalyst data for developing kinetic models, and configured Fast-SpaciMS for resolving reaction sequences related to N₂O formation mechanisms. (Partridge, ORNL)
- The University of Houston is identifying NOx reduction mechanisms operative in LNTs and in situ SCR catalysts, and is using this knowledge to design optimized LNT-SCR systems in terms of catalyst architecture and operating strategies. In FY 2013 kinetic models were developed based on measurements for the LNT and SCR chemistries, and incorporated into reactor models for design and optimization. These models have been successfully applied to determine the catalyst architectures and operating conditions that result in NOx conversion and N₂ selectivity that achieve defined threshold levels. (Harold, University of Houston)
- ORNL is using high-fidelity neutron imaging capability to advance the understanding of two components being employed in modern vehicles: the particulate filter and the in-cylinder fuel injector. In FY 2013 they: (1) implemented spray chamber with a portable fluid delivery system for high-pressure fluid delivery for diesel injectors; (2) obtained computed tomography scan of ash deposits from a continuously regenerated particulate filter and a periodically generated one; and (3) obtained 3-D computed tomography scan of a gasoline direct injection (GDI) injector with spatial resolution of 45 microns. (Toops, ORNL)



(a) Mass attenuation coefficients of a range of elements as a function of atomic number. Comparison given between neutron (squares) and X-rays (line). (b) Schematic of a neutron imaging facility at ORNL. (Toops, ORNL)

- ANL is researching gasoline particulate filter filtration/regeneration mechanisms and evaluating their performance. In FY 2013 they characterized the physical properties of GDI particulate matter emissions, such as morphology and chemistry and found numerous small nanoparticles found only from GDI engines; evaluated the effects of filter structures and emissions flow conditions on pressure drop in soot loading; and developed a numerical simulation code predicting gas dynamics and soot loading in a filter. (Lee, ANL)
- PNNL is developing a fundamental understanding of the factors affecting filtration efficiency and back-pressure, in order to promote the development of optimum filtration systems for advanced gasoline vehicles. In FY 2013 (1) Improved unit collector models have been used to explore the parameter space relevant to the design of future gasoline particulate filtration systems. (2) The ERC Exhaust Filtration

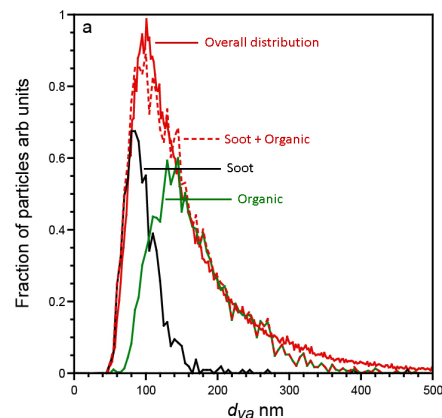
Analysis system was modified to allow filtration tests with exhaust from gasoline test engines. (3) Extensive sets of micro X-ray computed tomography data were obtained for five current filter substrates from two major manufacturers which cover a range of properties. Automated computer programs were written to extract relevant property information. (Stewart, PNNL)

- The Health Effects Institute is utilizing established emissions characterization and toxicological test methods to assess the overall safety of production-intent engine and control technology combinations that are being introduced into the market during the 2007-2010 time period. In FY 2013 they: (1) completed emissions generation and exposure characterization during chronic testing at the Lovelace Respiratory Research Institute; (2) completed the ancillary studies' analyses and received three final reports; and (3) continued analyses of health endpoints for the chronic bioassay at the Lovelace Respiratory Research Institute in Phase 3B (funded separately by the U.S. Environmental Protection Agency). (Greenbaum, Health Effects Institute)

C. High-Efficiency Engine Technologies

The objective of these projects is to research and develop technologies for more efficient clean engine/powertrain systems to improve passenger and commercial vehicle fuel economy.

- Cummins, Inc. is developing engine systems with 50% or greater brake thermal efficiency and demonstrating a tractor-trailer with 50% or greater freight efficiency improvement. In FY 2013 they demonstrated in a test cell a 51% thermal efficient engine system; this system included both exhaust and coolant/lube waste heat recovery systems contributing in a parallel fashion, and demonstrated the SuperTruck Demo 1 vehicle with 61% freight efficiency improvement, on a Texas highway drive cycle route. (Koeberlein, Cummins)
- Detroit Diesel Corporation is demonstrating a 50% total increase in vehicle freight efficiency measured in ton-miles per gallon, with at least 20% improvement through the development of a heavy-duty diesel engine capable of achieving 50% brake thermal efficiency. In FY 2013; they demonstrated 50.0% engine brake thermal efficiency in the laboratory. The waste heat recovery system design was completed, hardware and control systems developed. Testing to date has demonstrated an improvement in engine brake thermal efficiency of 2.3% via recovered exhaust and EGR energy, bringing the total engine brake thermal efficiency up to 50.0%. (Sisken, Detroit Diesel Corporation)
- Volvo is identifying concepts and technologies that have potential to achieve 55% brake thermal efficiency on a heavy-duty diesel engine. In FY 2013 they completed testing of combustion improvements, engine friction, pumping loss technologies, and a waste heat recovery system in a complete powertrain system demonstrated 48% brake thermal efficiency on a dynamometer. (Amar, Volvo)
- Delphi is developing, implementing, and demonstrating fuel consumption reduction technologies using a new low-temperature combustion process: gasoline direct-injection compression ignition. In FY 2013 they continued single-cylinder testing, initiated multi-cylinder testing, and initiated building of a demonstration vehicle with the multi-cylinder engine. (Confer, Delphi)
- Ford Motor Company is demonstrating 25% fuel economy improvement in a mid-sized sedan using a downsized, advanced gasoline turbocharged direct injection engine with no or limited degradation in vehicle level metrics. In FY 2013 they completed conversion of the high feature combustion vessel; demonstrated closed-loop control of combustion sensing (phasing and stability) on the first 3.5-L



Gasoline compression ignition particulate aerodynamic diameters under one low-load condition. (Stewart, PNNL)

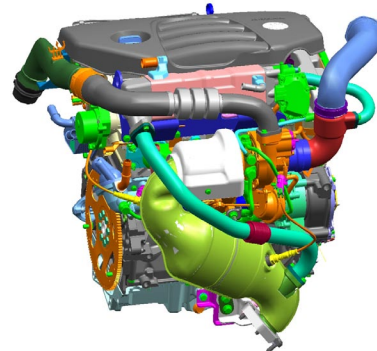


SuperTruck Demo 1 Vehicle (Koeberlein, Cummins)

I. Introduction

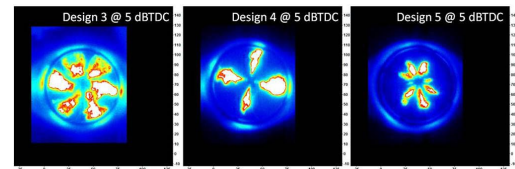
EcoBoost engine and developed algorithms and initiated testing of stochastic knock detection and control on the same engine; and completed Phase 1 testing and initiated analysis of in-cylinder temperatures and heat flux on the second 3.5-L EcoBoost engine. (Wagner, Ford Motor Company)

- General Motors (GM) is developing an advanced lean-gasoline combustion engine and aftertreatment system and will demonstrate 25% vehicle fuel economy improvement while achieving Tier 2 Bin 2 emissions. In FY 2013 they: (1) demonstrated Tier 2 Bin 2 capability with Spray Guided Engine version 5 (SG5) lean gasoline combustion system using a passive/active ammonia SCR system; and (2) developed the Lean Downsize Boost combustion system that demonstrated brake specific fuel consumption improvement of 21% compared to the 4-cylinder port fuel-injected baseline. (Smith, General Motors)
- Cummins, Inc. is demonstrating 40% fuel economy improvement over a baseline gasoline V-8 pickup truck while achieving Tier 2 Bin 2 tailpipe emissions compliance. In FY 2013 the prototype engine was acquired and installed in a vehicle. Engine testing has shown substantially higher fuel economy than the baseline mule engine values. Tailpipe emissions demonstrated on several occasions in a chassis laboratory environment, as well as tested on public roads, maintaining Tier 2 Bin 2 emission control over a variety of driving conditions while demonstrating City fuel economy more than 10% better than project goals. (Ruth, Cummins)
- Robert Bosch LLC is improving fuel economy by 25% with minimum performance penalties while achieving Super Ultra-Low Emissions Vehicle level emissions with gasoline. In FY 2013 they demonstrated up to 40% brake fuel efficiency improvement against the baseline engine at frequently visited driving cycle conditions on the ACCESS Prototype II engine, and completed vehicle simulations based on ACCESS Prototype II engine combustion optimization data, showing greater than 25% fuel economy improvement during the FTP-75 drive cycle over the baseline vehicle. (Yilmaz, Robert Bosch LLC)
- The Chrysler Group, LLC is demonstrating a 25% improvement in combined City and Highway Federal Test Procedure fuel economy in a Chrysler minivan. In FY 2013 dynamometer test modeling and simulation results show the efficiency goals are met. Development of the controls and calibrations are underway to assure the in-vehicle testing will achieve project goals. (Reese, Chrysler)
- Filter Sensing Technologies, Inc. is demonstrating and quantifying improvements in efficiency and greenhouse gas reductions through improved DPF sensing, controls, and low-pressure drop components. In FY 2013 they designed and developed alpha prototype radio frequency sensor systems, and supplied them to project partners for testing on light- and heavy-duty engine dynamometers and heavy-duty fleet vehicles. They also demonstrated potential for 50% to 75% regeneration-related fuel savings through on-road fleet testing with heavy-duty vehicles equipped with radio frequency sensors. (Sappok, Filter Sensing Technologies, Inc.)
- GM is applying the enabling technologies of high energy, extended duration ignition and novel intake charge boosting/mixing system to a current GM boosted spark ignition engine. In FY 2013 they completed the following: (1) One-dimensional engine simulation models with conventional low-pressure loop EGR and dedicated EGR have been constructed and various boost/mixing system candidates have been evaluated to determine capability of the candidate systems to supply and cool a sufficient quantity of EGR to meet the project objectives. (2) Vehicle simulation model of a current mid-size GM vehicle has been evaluated to determine the operating points for the subject engine configurations in order to generate fuel economy projections. (3) Phase 3 turbocharged 2.0-L engine with high-energy, extended-duration DCO™ ignition system, 11.0:1 compression ratio and low-pressure loop cooled EGR system testing has been completed to establish the fuel consumption and performance of this specification compared to the baseline. (4) Design work is complete to package the Phase 4 system defined as noted previously in the engine compartment of a current GM mid-size vehicle. (Keating, General Motors)



Low-Pressure Loop EGR System Packaged in GM Mid-Sized Vehicle (Keating, General Motors)

- Eaton Corporation is demonstrating fuel economy improvement through Rankine cycle waste heat recovery systems utilizing a roots expander in heavy-duty diesel applications. In FY 2013 they prototyped and air tested the single-stage roots expander demonstrating greater than 60% isentropic efficiency; built and validated organic Rankine cycle (ORC) test stand for water or ethanol usage; tested single-stage roots expander with water as working fluid on the ORC test stand; designed multistage expander and started procurement; selected heat exchanger vendor and completed specification; and completed packaging study of the entire ORC system on the engine. (Subramanian, Eaton Corporation)
- MAHLE Powertrain is demonstrating thermal efficiency of 45% on a light-duty gasoline engine platform while demonstrating potential to meet U.S. Environmental Protection Agency emissions regulations. In FY 2013 they: (1) completed optical and thermodynamic engine testing of Turbulent Jet Ignition (TJI) designs; (2) analyzed data from the optical engine to correlate jet characteristics to TJI designs; (3) demonstrated the potential of TJI to extend the lean limit into the ultra-lean region, achieving thermal efficiency parity with previous TJI studies, and demonstrated a path forward to achieve the project goal of 45% thermal efficiency; and (4) synthesized data from optical and thermodynamic engines to characterize engine performance as a function of jet characteristics. (Blaxill, MAHLE Powertrain)
- ENVERA LLC is developing a high-efficiency variable compression ratio (VCR) engine having variable valve actuation (VVA) and an advanced high-efficiency supercharger to obtain up to a 40% improvement in fuel economy. In FY 2013: (1) the VVA system was projected to attain cam lift and duration values needed for attaining engine power and efficiency targets; (2) the 4-cylinder VCR engine with advanced supercharging was projected to achieve power and torque targets; and (3) computer-aided design of the VCR engine was initiated. (Mendler, ENVERA LLC)
- Robert Bosch LLC is developing an intake air oxygen (IAO₂) sensor which directly and accurately measures the oxygen concentration in the intake manifold. In FY 2013: (1) The design concept for IAO₂ was completed. Focus of component design and research was on the subsystems sensor connector and housing as well as the protection tube. (2) Development of the protection tube led to benchmark functional performance in its design space. (3) Bench testing and endurance tests to support development work throughout the project were developed and set up and used to steer design work. (4) Testing of IAO₂ baseline sensors was completed. (5) Engine and simulation work for system evaluation and control development was conducted. (Schnabel, Robert Bosch LLC)
- LANL is developing prototype NO_x and NH₃ sensors based on mixed-potential technology. In FY 2013 they: (1) qualitatively reproduced NO_x sensitivity and selectivity of a LANL bulk sensor in a commercially manufacturable device; (2) demonstrated sensor stability for 1,000 hours in both unbiased and biased mode with no systematic degradation in sensor sensitivity; and (3) showed that the sensor tracks NO_x concentration in engine dynamometer testing performed at the National Transportation Research Center at ORNL. (Mukundan, LANL)



Optical Data @ 5 degrees before top-dead center (dTDC)
– TJI Designs 3, 4, and 5 (Blaxill, MAHLE Powertrain)

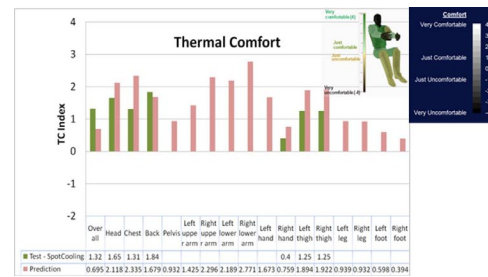
SOLID STATE ENERGY CONVERSION

Several projects are being pursued to capture waste heat from advanced combustion engines in both light- and heavy-duty vehicles using thermoelectrics (TEs). Following are highlights of the development of these technologies during FY 2013.

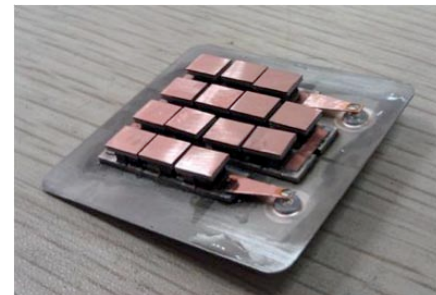
- Gentherm is designing a TE waste heat recovery system with 5% improvement in fuel economy for light-duty vehicles while providing a path towards commercialization at passenger vehicle volumes of 100,000 units per year. In FY 2013: (1) The cartridge design has been advanced and validated with physical testing. (2) Final vehicle platform/powertrain selections have been made by BMW and Ford after extensive trade-off analysis. The vehicles have been tested to measure the exhaust outputs over the US06 Cycle. (3) Design of the TE generator assemblies is advancing rapidly and the required design tools have been completed. (Barnhart, Gentherm)

I. Introduction

- GM is developing a thermal comfort model and computer aided engineering tool to predict the occupant physiological response to localized heating and cooling through human subject testing—key to balance distributed heating ventilation and air conditioning (HVAC) components and to speed execution of stratified thermal systems. In FY 2013 they delivered the completed Buick LaCrosse demonstration vehicle, achieved an estimated 30% HVAC energy saving with distributed TE components, maintained equivalent occupant thermal comfort in the demonstration vehicle, and exceeded the coefficient of performance target of 1.3 in cooling and 2.3 in heating with prototype TE devices. (Bozeman, General Motors)
- GM is developing an overall TE generator (TEG) system including all necessary vehicle controls and electrical systems fully integrated onto a light-duty vehicle to demonstrate fuel economy improvement of 5% over the US06 drive cycle. In FY 2013: (1) design specifications for the initial TEG prototype are being completed based on extensive modeling of heat flows, thermoelectric performance, and vehicle operation; (2) TE material has been fabricated and TE module fabrication is in progress; (3) final design of the heat exchangers, subassembly clamping schemes, and other TEG components is underway for the initial TEG build; and (4) bench testing, data collection, and analysis of the initial TEG will inform a redesign for the final TEG system. (Meisner, General Motors)
- GMZ Energy is demonstrating a robust, thermally cyclable TE exhaust waste heat recovery system that will provide approximately a 5% fuel efficiency improvement for a light-duty vehicle platform. In FY 2013: (1) a TE device has been subjected to 1,000 thermal cycles, between 600°C and 100°C, with <1% degradation in power output performance; (2) high-temperature TE modules, which will be integrated into the passenger vehicle and Bradley Fighting Vehicle TEGs, were successfully fabricated and characterized; (3) a new TEG design concept with a higher power output relative to the previous TEG design has been developed; and (4) achieved the 2013 technical target of finalizing a detailed mechanical design of a 1-kW TEG for integration on to a Bradley Fighting Vehicle, within specified operating parameters. (Cleary, GMZ Energy)
- Ohio State University is developing non-toxic TE materials with high figure of merit (ZT)>1 using only earth-abundant elements. In FY 2013 they found that the TE performance of the PbS system can be enhanced by means of a closely coupled phonon-blocking/electron-transmitting approach that consists of embedding endotaxially nanostructured second phases. By extension, they anticipate that this approach can be successfully applied to other material systems as well. This work shows that the ZT of p-type PbS can be increased to the record high value of ~1.3 at 923 K with CdS nanostructures. Although the same strong reduction of the lattice thermal conductivity is achieved with ZnS, CaS and SrS, the enhanced ZT of the CdS system is unique and derives from better hole mobility. This project is now complete. (Heremans, Ohio State University)
- Purdue University is developing the fundamental understanding and technology improvements needed to make viable the efficient conversion of waste heat in automotive exhaust systems to electricity. In FY 2013 they: (1) investigated carrier relaxation rates for different filling ratio of filled-skutterudite; (2) grew PbTe, Bi₂Te₃, and Ag₂Te nanowires in large quantities (>10 g/batch); (3) developed new TEG designs based on a jet impingement mechanism and developed numerical models to evaluate such designs; and (4) designed and assembled a test bench for experimental verification of system level performance with various configurations of hot- and cold-side heat exchangers and thermal interface materials and successfully characterized thermal interfaces. (Xu, Purdue University)



Thermal comfort computer-aided engineering tool validation results for one of the spot cooling test conditions. (Bozeman, General Motors)



High-temperature thermoelectric module with the hot-side casing removed. (Cleary, GMZ Energy)

- Stanford University is developing and measuring novel TE materials, including skutterudites and half-Heusler alloys. In FY 2013 they: (1) developed and characterized the performance and reliability of carbon nanotube (CNT)-based thermal interface materials bonded with reactive metal subjected to thermal cycling; (2) adapted a coarse-grained molecular simulation to predict thermal transport properties of CNT and metal nanowire arrays; (3) developed and validated in situ thermal measurement techniques for characterization and reliability testing of TEG devices using high temperature infrared thermometry; (4) established a complete electrodeposition apparatus for template-assisted fabrication of nanostructured metal thermal interface materials; (5) synthesized copper nanowire arrays with tunable properties, including lengths from 1-60 μm , diameters of 200 nm, and volume fractions from 10-50% over large areas; and (6) designed, fabricated, and calibrated microfabricated heater/thermometer devices for thermal characterization of metal nanowire arrays using the three-omega method. (Goodson, Stanford University)
- Stony Brook University is developing a scalable high-throughput, non-equilibrium synthesis process for high ZT TE materials from abundant low-cost feedstock by using thermal spray technology. In FY 2013: (1) Vacuum plasma spray (VPS) has been successfully used to synthesize magnesium silicide thick coatings and the maximum ZT achieved 30% by the traditional hot press method using the same feedstock powder. (2) VPS provides denser coating due to its high velocity and Hall Effect measurement showed carrier concentration and mobility enhanced the ZT of magnesium silicide coating for VPS compared with atmospheric plasma spray. (3) High velocity atmospheric plasma spray for filled skutterudites as quench powder has been successfully deposited on an Al substrate without obvious oxidation or evaporation. (4) TE functional layer as well as insulation and conducting layers have been thermal sprayed for TE device fabrication. (Zuo, Stony Brook University)
- Texas A&M University is synthesizing inorganic nanowires and quantum wires of both CoSb_3 and InSb , and organic conducting polymer thin films, and assembling them into inorganic-organic hybrid TE cells with sizes ranging from a few mm^2 to a few cm^2 , using conjugated linker molecules to tether the nanowires to each other or to conducting polymer thin films. In FY 2013 they fabricated bulk TE devices from mass-produced Zn_3P_2 and ZnO nanowire powders, extended the nanowire composite fabrication strategy to obtain degenerately doped zinc oxide nanowire pellets, and a phase transformation route was developed for converting single-crystalline silicon nanowires into polycrystalline/single-crystalline metal silicide nanowires. (Vaddiraju, Texas A&M University)
- The University of California, Los Angeles is developing materials and interfaces for improved thermomechanical reliability of TE vehicle exhaust waste heat harvesting devices. In FY 2013 they fabricated and optimized $\text{Cu-ZrW}_2\text{O}_8$ composites in a wide range of compositions, and characterized the $\text{Cu-Zr W}_2\text{O}_8$ composites for coefficient of thermal expansion, electrical conductivity, thermal conductivity, and microstructure. (Ju, University of California, Los Angeles)
- The University of California, Santa Cruz is developing novel TE materials based on abundant and non-toxic Zintl-phase magnesium silicide alloys. In FY 2013 they plan to: (1) optimize spark plasma sintering (SPS) of n-type Mg_2Si and effect on grain boundaries; (2) synthesize SPS of n-type Mg_2Si with embedded tungsten nanoparticles—characterization and transport modeling; and (3) identify bipolar thermal conductivity as a key factor limiting thermodynamic ZT of $\text{Mg}_2\text{Si}_{1-x}\text{Sn}_x$ at high temperatures. Proposed electron energy filtering to reduce bipolar thermal conductivity and achieve ZT>2. (Shakouri, University of California, Santa Cruz)
- Virginia Tech is fabricating and characterizing new TE materials grown with scalable techniques for production of large quantities of efficient, yet non-toxic and inexpensive elements capable of long-term operation at high temperatures over thousands of thermal cycles. In FY 2013 they: (1) manufactured several small-scale heat exchanger modules for use in experiments to validate the numerical models for heat transfer behavior characterization; (2) completed an experimental test facility to investigate heat exchanger modules previously designed and manufactured; (3) created a performance map of the heat exchanger module and the TE system over a range of operational parameters (engine speed, coolant pumping power, etc.); (4) modeled fluid flow and heat transfer behavior inside the exhaust pipe test section with internal fins (multi-louvered fins and wavy Herringbone fins) using computational fluid dynamics; (5) scaled the synthesis process for the previously developed n-type magnesium silicide materials to allow for production of over 3,000 elements/hr; (6) reduced the thermal conductivity of the ZnO materials through nanostructuring; and (7) characterized the effect of synthesis and sintering conditions

I. Introduction

on the doping mechanisms on carrier concentration and power factor in the ZnO materials. (Huxtable, Virginia Tech)

- The University of Texas at Austin is increasing the ZT of earth abundant and low-cost magnesium silicides (Mg_2Si) and higher manganese silicides ($MnSi_{1.73}$, or HMS) to the level found in state-of-the-art TE materials that contain scarce and expensive elements. In FY 2013 they: (1) obtained the TE and magnetic properties of high-purity HMS chemical vapor transport crystals; (2) developed an approach to generate high yields of HMS nanowires; (3) revealed the effect of (Al,Ge) double doping on the TE properties of HMS; (4) addressed the chemical instability problem of Mg_2Si -based compounds; and (4) designed and fabricated the first generation and the improved second generation TE devices, and measured contact resistance and power output to correlate to and validate the device model. (Shi, University of Texas at Austin)
- Ford Motor Company is developing a TE HVAC system to optimize occupant comfort and reduce fuel consumption. In FY 2013 they achieved the following: (1) zonal HVAC system successfully packaged into the test vehicle; (2) TE devices met project objectives of COP >1.3 in cooling and COP >2.3 in heating; (3) HVAC system annualized energy consumption was reduced by 12% compared to baseline vehicle; and (4) cost of TE devices tracks closely with performance and capacity requirements. This project is complete. (Maranville, Ford Motor Company)



TE Device Used in Zonal HVAC System
(Maranville, Ford Motor Company)

I.3 Honors and Special Recognitions/Patents

HONORS AND SPECIAL RECOGNITIONS

1. Paul Miles, SNL: Invited speaker “Scientific and Engineering Challenges Impacting the Design of Advanced Internal Combustion Engines,” Swedish Academy of Engineering Sciences, Stockholm, Sweden, Sept. 12, 2013.
2. Paul Miles, SNL: Invited speaker “Quantitative Measurements of Flow and Scalar Fields Supporting Predictive Simulation for Engine Design,” International Energy Agency – Energy Conservation and Emissions Reduction Task Leaders Meeting, San Francisco, CA, July 23, 2013.
3. Lyle Pickett, SNL: Election to SAE Fellow.
4. Scott Curran, ORNL: 2013 DOE Vehicle Technologies Office R&D Award for RCCI research.
5. Scott Curran, ORNL: Best Presentation Award 2012 ASME ICEF Conference – RCCI paper.
6. Scott Curran, ORNL: Speaking award for 2033 SAE World Congress – RCCI paper.
7. Joe Oefelein, SNL: ILASS Americas William Robert Marshall Award, 2012 (for best paper judged to be the most significant contribution to the ILASS 23rd Annual Conference on Liquid Atomization and Spray Systems).
8. John Dec, SNL: SAE Arch T. Colwell Award for SAE paper 2011-01-1291, SAE Int. J. Engines, 4(1): 1669-1688, 2011.
9. John Dec, SNL: Most cited article in the Proceedings of the Combustion Institute since 2008: Dec, J. E., Proc. Combust. Inst., 32: 2727-2742, 2009.
10. David Carrington, LANL: Outstanding Innovation Award – 2011 Distinguished Licensing Award. Awarded by Los Alamos National Laboratory Technology Transfer Division, August 9, 2012.
11. David Carrington, LANL: Outstanding Innovation Award – 2010 Distinguished Copyright Award. Awarded by Los Alamos National Laboratory Technology Transfer Division, August 11, 2011.
12. Sibendu Som, ANL: inducted as a “Computational Fellow” at the Computational Institute at University of Chicago.
13. Bill Partridge, ORNL: 2013 R&D100 Awarded to Da Vinci Emissions Services, ORNL and Cummins in recognition of the Da Vinci Fuel-in-Oil being one of the 100 most technologically significant new products of the year; the commercialized DAFIO was based on DOE-funded CRADA-developed Fuel-in-Oil technology.
14. Koeberlein, Cummins: 2013 SAE International Ralph Teetor Educational Award.
15. Koeberlein, Cummins: Best paper in Journal of Automobile Engineering for 2012.
16. Xu, Purdue University: K.R. Saviers, S.L. Hodson, J.R. Salvador, L.S. Kasten, T.S. Fisher, “Carbon nanotube arrays for enhanced thermal interfaces to thermoelectric modules,” 10th International Energy Conversion Engineering Conference, paper # AIAA-2012-4048, July 2012. This paper was awarded 2012 Best Aerospace Power Systems Student Paper by the AIAA Aerospace Power Systems Technical Committee.
17. Heremans, Ohio State University: Joseph P. Heremans was elected to the National Academy of Engineering
18. Kanatzidis, Northwestern University: Mercouri Kanatzidis was elected Fellow of the American Association for the Advancement of Science.

INVENTION AND PATENT DISCLOSURES

1. SNL: U.S. Patent Application Filed: Dec, J., Ji, C., Cannella, W., and Maria, A., “A Method for Extending the High-Load Limit of Internal Combustion Engines Operated in a Low-Temperature Combustion Mode,” DOE-S no. 132389.
2. ORNL: Szybist, J.P., Conklin, J.C., “Highly Efficiency 6-Stroke Engine Cycle with Water Injection,” U.S. Patent 8,291,872 B2, Issued October 23, 2012.
3. ORNL: J.E. Parks, W.P. Partridge “Optical Backscatter Probe for Sensing Particulate in a Combustion Gas Stream,” United States Patent, Patent No. US 8,451,444 B2, Date of Patent May 28, 2013.
4. ORNL: US Appl. No.: 13/912,462; J.E. Parks, W.P. Partridge, J. Yoo “EGR Distribution and Fluctuation Probe Based on CO₂ Measurements,” ORNL Ref. No.: 2759.1; Filed 6-7-2013.
5. Ford Motor Company: Submitted “Compensation of IAO2 Sensor for Purge for Correct EGR”, ID No 83336561, DOE Case No S-134,403 – 03/07/2013.

I. Introduction

6. Ford Motor Company: Submitted “Dual Coil Ignition System with Secondary Windings Connected in Series”, ID No 83228424, DOE Case No S-134,398 – 03/07/2013.
7. Chrysler Group, LLC: Invention disclosure: “Centrifugal switch Pendulum Deactivation,” for control of start/stop clatter in crank pendulum absorbers, joint with Michigan State University.
8. Chrysler Group, LLC: I. Glanfield, B. Geist, “Retainer – Pendulum”, patent application submitted for Chrysler IDR # 709297.
9. Chrysler Group, LLC: I. Glanfield, B. Geist, “Pendulum Anti Rattle Treatment”, patent application submitted for Chrysler IDR # 709298.
10. Robert Bosch LLC: E. Hellström, A. Stefanopoulou, L. Jiang, and J. Larimore, “Predictive Modeling and Reducing Cyclic Variability in Autoignition Engines”, Application US 13/621,539, Filed on September 17, 2012. Pending
11. Robert Bosch LLC: E. Hellström, A. Stefanopoulou, L. Jiang, and J. Larimore, “Dynamic Estimator for Determining Operating Conditions in an Internal Combustion Engine”, Application US 13/621,527, Filed on September 17, 2012. Pending
12. Robert Bosch LLC: S. Jade, E. Hellström, L. Jiang, and A. Stefanopoulou, “Fueling Strategy for Controlled-Autoignition Engines”, Application US 13/621,433, Filed on September 17, 2012. Pending
13. Robert Bosch LLC: S. Jade, E. Hellström, L. Jiang, and A. Stefanopoulou, “Fuel Governor for Controlled Autoignition Engines”, Application US 13/621,425, Filed on September 17, 2012. Pending
14. Robert Bosch LLC: A. Mond and L. Jiang, “Combustion Mode Switching with a Turbocharged / Supercharged Engine”, Application US 13/679,010, Filed on November 16, 2012. Pending
15. Robert Bosch LLC: L. Jiang, and N. Ravi, “Path Planning during Combustion Mode Switch”, Application US 13/681,499, Filed on December 14, 2012. Pending
16. Robert Bosch LLC: L. Jiang, J. Sterniak, and J. Schwanke, “Combustion Control with External Exhaust Gas Recirculation (EGR) Dilution”, Application US 13/951,658, Filed on July 26, 2013. Pending
17. Filter Sensing Technologies, Inc.: Bromberg, L., Sappok, A., Koert, P., and Parker, R., “System and Method for Measuring Retentate in Filters,” United States Patent No. 8,384,396, Issued February, 2013.
18. Filter Sensing Technologies, Inc.: Bromberg, L., Sappok, A., and Koert, P., “Method and System for Controlling Filter Operation,” United States Patent No. 8,384, 397, Issued February, 2013.
19. Filter Sensing Technologies, Inc.: Sappok, A., Smith III, R., Bromberg, L., “Advanced Radio Frequency Sensing Probe,” United States Patent Application No. 61,897,825, Filed 2013.
20. General Motors: United States Patent US 8,309,839: “Method of improving thermoelectric figure of merit of high efficiency thermoelectric materials” issued 13 November 2012.
21. General Motors: United States Patent US 8,443,594: “Method of controlling temperature of a thermoelectric generator in an exhaust system” issued 21 May 2013.
22. General Motors: United States Patent US 8,554,407: “Bypass valve and coolant flow controls for optimum temperatures in waste heat recovery systems” issued 8 October 2013.
23. General Motors: United States Patent US 8,575,788: “Method of operating a thermoelectric generator” issued 5 November 2013.
24. General Motors: Chinese Patent CN 102,235,212: “Exhaust bypass control for exhaust heat recovery” issued 16 October 2013; US patent pending.
25. GMZ Energy: Patent application number: 61/873,584, “Device for Exhaust Waste Heat Recovery,” V. Mittal, 2013.
26. Purdue University: U.S. and International Full Patent application filled: TiN/(Al,Sc)N Metal/Dielectric Superlattices for Metamaterial Applications in the Visible Range. Gururaj Naik, Bivas Saha, Timothy D. Sands, and Alexandra Boltasseva.
27. Texas A&M University: S. Vaddiraju, L. Brockway, M. Van Laer, Y. Kang, “Synthesis of Inorganic Nanowires and Organic Hybrids Thereof for Electronic Elements and Devices”, US Patent Application #61/800,384, 2013.

I.4 Future Project Directions

COMBUSTION RESEARCH

The focus in FY 2014 for combustion and related in-cylinder processes will continue to be on advancing the fundamental understanding of combustion processes in support of achieving efficiency and emissions goals. This will be accomplished through modeling of combustion, in-cylinder observation using optical and other imaging techniques, and parametric studies of engine operating conditions.

- SNL is providing the physical understanding of the in-cylinder combustion processes needed to minimize the fuel consumption and the carbon footprint of automotive diesel engines while maintaining compliance with emissions standards. In the coming year they plan to examine the impact of ‘stepped-lip’ piston bowl geometries on the mixture preparation process and compare with conventional bowl geometries, investigate benefits of close-coupled pilot injections on combustion noise and emissions and identify the physical processes dominating this behavior, identify and investigate multiple injection strategies suitable for limiting cold-start hydrocarbon and CO emissions, examine induction flow processes and the ability to accurately simulate asymmetric engine flows, and the impact of asymmetries on the combustion process.
- SNL is developing a fundamental understanding of how in-cylinder controls can improve efficiency and reduce pollutant emissions of advanced LTC technologies. In the coming year they plan to: (1) continue building a conceptual-model understanding of multiple-injection processes for both conventional diesel and LTC (multi-injection schedules deployed by industry; use optical geometry more similar to metal engines; compare with metal engine data where possible; identify mechanisms and critical requirements to improve emissions and efficiency); (2) determine how combustion design affects heat transfer and efficiency (measure spatial and temporal evolution of heat transfer across range of combustion modes; correlate to progression of in-cylinder combustion processes); and (3) continue to explore and upgrade fuel-injection technologies (injection rate-shaping likely very important for performance, and higher load than our current injector capability is of interest).
- SNL is facilitating improvement of engine spray combustion modeling, accelerating the development of cleaner, more efficient engines. In the coming year they plan to quantify soot, soot precursor formation, and radiation heat loss at target conditions, characterize multi-hole sprays compared to axial-hole sprays, and evaluate internal flows within transparent injectors, transitioning to near-field mixing and dispersion at the exit of the nozzle.
- SNL is providing the fundamental understanding (science-base) required to overcome the technical barriers to the development of practical Low-Temperature Gasoline Combustion (LTGC) engines, including HCCI and partially stratified variants of HCCI, by industry. In the coming year they plan to: (1) extend evaluation of engine performance with compression ratio = 16:1 over a wider range of conditions, with an emphasis on the high-load limits for both premixed and partial fuel stratification fueling; (2) conduct a comprehensive study of early direct injection, partial fuel stratification to determine the extent to which its benefits for increased thermal efficiency and load range can be applied; (3) image fuel distributions in the optical engine to guide fuel-injection strategies for early direct injection, partial fuel stratification performance studies in the metal engine; (4) install spark-plug cylinder heads, to determine effects of new intake-port geometry on LTGC performance, and initiate studies of spark-assisted compression-ignition LTGC combustion; (5) investigate the effects of piston-top temperature on amount of thermal stratification and cold-pocket distribution; and (6) expand investigations of combustion noise level and ringing intensity with an emphasis on understanding the fundamental differences in these two measurements.
- SNL is researching an NVO strategy for controlling HCCI combustion. In the coming year they plan to: (1) complete NVO sampling experiments using LBNL facilities to improve sample speciation and compare results using gasoline in place of the surrogate fuel iso-octane; and (2) initiate new research direction on innovative ignition sources required for advanced gasoline-combustion engines and identify industry needs, research capabilities, and potential partners.
- ANL is developing and validating robust and predictive nozzle flow and turbulence models for diesel engine applications aided by high-performance computing tools. In the coming year they plan to:

I. Introduction

(1) couple nozzle flow simulations with classical spray simulations to understand the influence of in-nozzle flows on spray and combustion processes; (2) implement the best practices developed for LES calculations on engine simulations with different engine geometries available in literature; (3) develop a near-nozzle Eulerian spray modeling approach which in principle is significantly different from a classical spray modeling approach that is Lagrangian in nature; (4) develop a two-component surrogate (n-dodecane and m-xylene) mechanism for diesel fuel and validate against experimental data in constant volume combustion chamber and single-cylinder engine conditions; and (5) systematically improve the fidelity of the simulations by improving the nozzle flow, spray, turbulence, and combustion models.

- ANL is making detailed measurements of the sprays from fuel injectors using X-ray absorption. The technique is non-intrusive, quantitative, highly time-resolved, and allows making detailed measurements of the spray, even in the densely-packed region very near the nozzle. In the coming year: (1) The geometry and fuel distribution from the “Spray G” GDI injectors will be measured using X-ray diagnostics, and will be made available to experimental and modeling partners in the ECN. (2) They will measure the fuel/air mixing in a GDI injection system that is being used in engine tests of advanced combustion strategies. The high precision spray measurements will be used to validate simulations of the engine’s combustion process, providing these research programs with the data that are needed for high-fidelity modeling. (3) Further studies of cavitation will be done to improve the community’s understanding of this phenomenon and its impact on fuel/air mixing and injector internal flows. (4) Further studies of bubble ingestion will be performed, with the goal of linking this phenomenon with injector dribble. Dribble is the undesirable ejection of fuel after the nominal end of the injection event; the fuel is slow-moving, poorly atomized, and likely to generate particulate matter emissions. They hope to quantify the causes of dribble, enabling injector manufacturers to minimize its impact.
- SNL is combining unique state-of-the-art simulation capability based on the LES technique with Advanced Engine Combustion R&D activities. In the coming year they plan to extend development of models and corresponding benchmark simulations to high-Reynolds-number, direct-injection processes for both diesel and gasoline direct injection engine applications over a wide range of pressures and temperatures.
- ANL is collaborating with combustion researchers within DOE’s Offices of Basic Energy Science and Vehicle Technologies Office programs to develop and validate predictive chemical kinetic models for a range of transportation-relevant fuels. In the coming year they plan to acquire additional ignition delay measurements for gasoline surrogate, and real fuels plus reactivity modifiers, and improve predictive capabilities of chemical kinetic models; incorporate novel approaches for kinetic mechanism validation/improvement, including global sensitivity analysis, as well as the use of new targets such as rate of heat release and low-temperature heat release; test and validate the performance of a new, single-piston rapid compression machine; and test and validate the reduced-order, control-oriented ignition under engine-relevant conditions.
- LLNL is developing detailed chemical kinetic models for fuel components used in surrogate fuels for compression ignition, HCCI and RCCI engines. In the coming year they plan to: (1) continue to develop detailed chemical kinetic models for larger alkyl aromatics including ones with more than alkyl side chain; (2) develop gasoline surrogate fuels for fuels for advanced combustion engines (FACE) fuels; (3) develop an additional surrogate component model to represent two-ring aromatics in diesel fuel; and (4) develop improved chemical kinetic models for the cycloalkane chemical class in diesel fuel.
- LLNL is gaining fundamental and practical insight into HECC regimes through numerical simulations and experiments. In the coming year they plan to: (1) increase accuracy and lower computational cost of the multi-zone combustion model: Jacobian or other improved remap; error-bounded zoning; (2) improve computational performance for operator-split, every-cell chemistry in computational fluid dynamics: quasi-steady-state, partial equilibrium, perturbative methods, fully coupled chemistry/advection/diffusion; (3) implement algorithms to optimize computational performance of species advection/diffusion calculations; (4) perform engine simulations with LLNL parallel computational fluid dynamics with chemistry investigating fuel effects in HCCI/PCCI engines; (5) work towards predictive diesel engine simulations by combining computational fluid dynamics, spray, soot, diesel surrogate, and the Pitz mechanism and compare with experiments at SNL; and (6) conduct chemical kinetics mechanism rate optimization through the use of sensitivity analysis, HCCI engine experiments at multiple operating points, and multidimensional HCCI simulations.

- LLNL is applying mathematics underpinning efficient algorithms and developing combustion software on new computing architectures. In the coming year they plan to improve the fluid transport calculation and other simulation bottlenecks that occur now that the chemistry solver is substantially faster; continue to create new combustion algorithms for the graphical processing unit; and explore more robust error theory for physical models in engine simulations to ensure that accuracy is maintained in a rigorous manner transparent to all users.
- LANL is developing algorithms and software for the advancement of speed, accuracy, robustness, and range of applicability of the KIVA internal engine combustion modeling—to be more predictive. In the coming year they plan to: (1) continue developing the *hp*-adaptive finite element method for multispecies flows in all flow regimes and implementing this method to perform modeling of internal combustion engines, other engines, and general combustion; (2) continue developing comprehensive comparative results to benchmark problems and to commercial software as part of the verification and validation of the algorithms; (3) continue developing 3-D robust overset grid method for immersed actuated parts such as valves, and merge overset grid method into *hp*-adaptive finite element method framework; (4) continue developing the parallel solution method for the *hp*-adaptive predictor-corrector split algorithm; (5) continue developing more appropriate turbulence models for more predictive modeling; and (6) continue to verify and validate combustion and spray models, and the local Arbitrary Lagrangian-Eulerian in three dimensions.
- The University of Michigan is exploring new high-pressure lean-burn combustion strategies that can enable future gasoline engines with 20-40% improved fuel economy. This project is now complete.
- Michigan State University is demonstrating a spark ignition HCCI dual combustion mode engine for a blend of gasoline and E85 (85% ethanol and 15% gasoline) for the best fuel economy. This project is complete except for the final report.
- ORNL is developing and applying innovative strategies that maximize the benefit of high-performance computing resources and predictive simulation to support accelerated design and development of advanced engines to meet future fuel economy and emissions goals. In the coming year they plan to complete development and validation of a metamodel of highly dilute spark-ignition combustion, couple OpenFOAM® spray model to in-cylinder flow and combustion simulations, and optimize the injector design for improved fuel economy and emissions, and transfer knowledge and methodologies to industry partners.
- ANL is optimizing the operating conditions to use low-cetane fuel to achieve clean, high-efficiency engine operation and demonstrate the use of LTC as an enabling technology for high-efficiency vehicles. In the coming year they plan to continue to extend low-load operation to idle using uncooled EGR and different injector umbrella angles for enhancing local richness in the combustion chamber; explore the opportunity to utilize a turbocharger/supercharger combination to enhance intermediate temperature heat release to further enhance low-load operation; analyze the particulate matter coming from LTC and study the formation/oxidation process to relate particulate matter to engine operating conditions; and conduct additional engine performance tests for Autonomie simulations to support LTC development as applied to vehicles.
- ANL is quantifying the efficiency potential and combustion stability limitations of advanced GDI combustion systems including lean, boosted and EGR-dilute concepts. In the coming year they plan to implement detailed ignition energy measurement to allow direct, objective comparison of advanced coil-based ignition systems, evaluate potential of laser ignition in lean, boosted and EGR-dilute operation, expand three-dimensional computational fluid dynamics simulation to include EGR-dilute combustion, and implement characteristics of advanced ignition systems in 3-D computational fluid dynamics simulation to enable cycle-to-cycle variation prediction.
- ORNL is gaining and utilizing knowledge of the recurring patterns that occur in cyclic variability in spark-ignition engines to predict and correct for low-energy cycles such as misfires that reduce engine efficiency at the dilution limit. In the coming year they plan to: (1) characterize sensitivity of control parameters to data sampling quality; (2) demonstrate potential of next-cycle control strategies for combustion stability improvements and efficiency gains; and (3) evaluate the feasibility and potential benefits of same-cycle control strategies to prevent misfires.

I. Introduction

- ORNL is developing and evaluating the potential of HECC strategies with production-viable hardware and aftertreatment on multi-cylinder engines. In the coming year they plan to: (1) evaluate transient RCCI performance including controls and stability concerns; (2) evaluate the potential of increasing combustion efficiency through combustion optimization and engine hardware design (i.e. combustion chamber geometry); (3) characterize aftertreatment performance (including effect on particulate matter) over the over light-duty operating range; and (4) achieve the 2014 milestone of demonstrating 23% increase in fuel economy over a 2009 PFI gasoline vehicle in vehicle simulation due to improved powertrain efficiency.
- ORNL is defining and analyzing specific advanced pathways to improve the energy conversion efficiency of internal combustion engines from nominally 40% to as high as 60%, with emphasis on opportunities afforded by new approaches to combustion. In the coming year they plan to: (1) complete construction of a new engine platform at ORNL designed to be sufficiently flexible to demonstrate proof-of-principle of the various reforming concepts being pursued in this project on a multi-cylinder engine; (2) apply the in-cylinder non-catalytic reforming concept to the new flexible multi-cylinder engine experiment to quantify efficiency gains from simultaneous production and consumption of reformate in the same engine; and (3) select, procure, and conduct flow reactor evaluations of a sulfur-tolerant thermochemical recuperation reforming catalyst formulation for use in future engine experiments.
- SNL is studying the effects of continuous operation (i.e. gas exchange) on indicated thermal efficiency and emissions of an opposed free-piston linear alternator engine utilizing HCCI combustion at high compression ratios (~20-40:1). In the coming year they plan to continue to perform combustion experiments and extend run times to measure indicated thermal efficiency and emissions at various compression ratios and equivalence ratios with hydrogen, and based on experimental results and modeling predictions, assess the overall engine design and performance with respect to the target fuel-to-electricity conversion efficiency of 50% at 30 kW output.
- ORNL is assessing the fuel economy and emissions benefits of VCR technology. In the coming year they plan to: (1) re-design present timing chain system to fix mechanical issues; (2) fabricate a new timing chain system; (3) add external EGR loop to the engine; and (4) evaluate durability of new timing chain system and functionality of external EGR loop.
- ANL is performing engine benchmarking to accelerate the development of high-efficiency internal combustion engines for light-duty vehicle applications, while meeting the future emission standards, using numerical simulations. In the coming year they plan to evaluate new technologies in the Nissan Micra (1.4 liter turbocharged direct-injected engine) and another vehicle to be identified; analyze the new emerging technologies and how they are used; and conduct analysis on the new and emerging technologies to determine their maximum fuel saving potential.
- ORNL is applying the historically successful approach of developing and applying minimally invasive advanced diagnostic tools to resolve spatial and temporal variations within operating engines and catalysts. In the coming year they plan to further improve the multiplex laser-based EGR probe to enable the quantification necessary to characterize internal and external EGR partitioning and fluctuations via backflow measurements, as well as methodology development to assess net cylinder charge composition, temperature, and fluctuations from such measurements.

EMISSION CONTROL R&D

In FY 2014, work will continue on LNTs and urea-SCR to reduce NOx emissions. The focus of activities will be on making these devices more efficient, more durable, and less costly. For particulate matter control, the focus will be on more efficient methods of filter regeneration to reduce impact on engine fuel consumption.

- ORNL is coordinating the CLEERS activity for the DOE Advanced Engine Cross-Cutting Technology Development Team. In the coming year plan to: (1) continue leading the CLEERS planning and database advisory committees; (2) continue leading the Focus Groups; (3) continue archival of expanded experimental and modeling data in the CLEERS Sharepoint site and hiring of ORNL post-doctoral researcher to help manage the database if continuing budget changes permit; (4) organize and conduct the 2014 CLEERS workshop in the spring of 2014; (5) continue sharing of basic data and models with DOE Vehicle Systems projects and the ACEC Team from U.S. DRIVE; (6) continue maintenance and expansion

of the CLEERS website; (7) continue providing regular update reports to the DOE Advanced Engine Cross-Cutting Technology Development Team; and (8) complete and issue final public report on the 2013 CLEERS Industry Priority Survey.

- ORNL is collaborating with PNNL to support industry in the development of accurate simulation tools for the design of catalytic emissions control systems that enable advanced high-efficiency combustion engines to meet emissions regulations while maximizing fuel efficiency. In the coming year they plan to develop a reaction mechanism for NO SCR by NH₃ over small-pore Cu zeolite SCR catalysts that is consistent with experimental observations; determine chemical processes responsible for N₂O formation during low-temperature LNT regeneration and incorporate into a model; quantify impacts of hydrothermal aging on energetics of NH₃ adsorption for a commercial Cu zeolite SCR catalyst; identify strategies for adjusting model parameters to account for aging; and develop an experimental protocol for measuring the key properties of hydrocarbon adsorbers required for model calibration.
- PNNL is developing improved computational tools for simulating realistic full-system performance of lean-burn engines and the associated emissions control systems. In the coming year they plan to continue detailed kinetic and mechanistic studies for NO reduction over the state-of-the-art small-pore zeolite-based Cu SCR catalysts; complete studies of K-based LNT catalysts with a focus on properties of spinel magnesium aluminate supports; characterize current production and advanced DPF substrates through advanced image and statistical analysis of high resolution computed tomography data; extend the SCR global kinetic model to include fast SCR and NO₂ SCR reactions and validate its performance at intermediate aging states; and perform micro-scale flow and transport simulations to assess the accessibility of catalysts in an SCR on filter and effects of catalyst location on backpressure and filtration efficiency.
- PNNL is identifying approaches to significantly improve both the high- and low-temperature performance, and the stability of the catalytic NOx reduction technologies via a pursuit of a more fundamental understanding. In the coming year they plan to focus on the mechanisms for low- and high-temperature performance loss as a function of operation conditions of new generation CHA-based NH₃ SCR catalysts, and develop a deeper understanding of the mechanisms of NOx storage and reduction activity, and performance degradation of materials that have been reported to show good NOx storage and reduction performance at temperatures considerably higher than BaO/alumina-based materials.
- PNNL is developing and demonstrating mixed metal oxide-based catalysts as a low-cost replacement for platinum in the oxidation of NO to NO₂ in lean engine exhaust, an essential first step in controlling NOx emissions. In the coming year they plan to optimize mixed metal oxide catalyst compositions and forms for NO oxidation, to enable the noble metal content of diesel oxidation and LNT catalysts to be reduced or eliminated; investigate the effect of the Ce-Mn mixed oxide synthesis method on the activity and stability; perform a detailed characterization of mixed metal oxide catalysts using state-of-the-art analytical tools; and develop reaction pathways for MnOx clusters supported on ceria and for Mn-doped ceria to determine the nature of active centers on those catalysts; and optimize the catalyst synthesis to maximize the Mn/Ce interaction and the number of active sites.
- PNNL is developing a fundamental understanding of the integration of SCR and DPF technologies for on-road heavy-duty diesel applications. In the coming year they plan to continue to interrogate passive soot oxidation feasibility in the integrated device, including continued parametric investigations interrogating the effect of NO₂:NOx ratio, SCR catalyst loading, NH₃:NOx ratio; pursue maturation of model development activities to aid in system performance prediction and as a tool for optimizing the physical SCR-DPF integration that achieves optimum soot oxidation and NOx conversion performance; and pursue investigating alternative DPF substrates for inclusion in the technology, including possibly silicon carbide, aluminum titanite, and others.
- ORNL is developing emission control technologies that perform at low temperatures (<150°C) to enable fuel-efficient engines with low exhaust temperatures to meet emission regulations. In the coming year they plan to continue investigation on Au@Cu with ceria-zirconia and other supports, include trap materials and NOx reduction catalysts, and move from powder catalysts to washcoated cores and further validation in engine exhaust.

I. Introduction

- ORNL is assessing and characterizing catalytic emission control technologies for lean-gasoline engines. In the coming year they plan to evaluate the potential benefits of utilizing NO_x storage media on three-way catalysts to extend lean operating time with the passive SCR approach, and analyze the impact of oxygen storage components of the three-way catalyst on NH₃ production during rich-lean transitions for the passive SCR approach.
- ORNL is researching the fundamental chemistry of automotive catalysts, identifying strategies for enabling self-diagnosing catalyst systems, and addressing critical barriers to market penetration. In the coming year they plan to quantify spatiotemporal performance of a commercial Cummins SCR catalyst under lab- and field-aged conditions.
- The University of Houston is identifying NO_x reduction mechanisms operative in LNTs and in situ SCR catalysts, and to use this knowledge to design optimized LNT-SCR systems in terms of catalyst architecture and operating strategies. In the coming year they plan to accomplish the following activities: (1) further development and application of LNT/SCR dual layer model for identifying optimal catalyst composition and structural properties such as washcoat thickness; (2) extension of serial and segmented model LNT/SCR to include CO and propylene in the feed as reductants; (3) application of LNT/SCR dual-layer model for identifying optimal catalyst composition and structural properties such as washcoat thickness; (4) spatio-temporal studies of LNT-SCR serial and segmented catalysts; and (5) experimental study of combined LNT-SCR double-layer and dual-brick catalysts with the goal to identify strategies of profiling the active components to achieve higher conversion over a wide temperature range.
- ORNL is using high-fidelity neutron imaging capability to advance the understanding of two components being employed in modern vehicles: the particulate filter and the in-cylinder fuel injector. In the coming year they plan to: (1) develop a system for fluid/fuel injection with GDI; (2) probe detailed fluid dynamic study within fuel injectors using time-resolved technique; (3) incorporate ash-laden and gasoline particulate samples into the particulate filter study; and (4) share findings through collaboration with the General Motors injector team that is developing a model of the injector.
- ANL is researching gasoline particulate filter filtration/regeneration mechanisms and evaluating their performance. In the coming year they plan to evaluate ash effects on soot oxidation kinetics, evaluate differences of soot and filter properties in micro- and macro-scales between aged and fresh filters (catalyst coated), and develop a multi-functional gasoline particulate filter system combined with the three-way catalyst.
- PNNL is developing a fundamental understanding of the factors affecting filtration efficiency and back-pressure, in order to promote the development of optimum filtration systems for advanced gasoline vehicles. In the coming year they plan the following activities: (1) filtration efficiency experiments using the University of Wisconsin EFA system with spark ignition direct injection exhaust at temperatures representing close-coupled filter placement; (2) apply advanced characterization methods to particulate matter that penetrates filters; (3) attempt to correlate statistics obtained from micro-structural analysis with pressure drop and filtration efficiency; (4) use first-principals micro-scale models to further improve sub-grid modeling tools, such as the commonly used unit-collector; and (5) apply advanced particulate characterization to subsequent generations of engines—leaner operation, higher fuel efficiency.
- The Health Effects Institute is utilizing established emissions characterization and toxicological test methods to assess the overall safety of production-intent engine and control technology combinations that are being introduced into the market during the 2007-2010 time period. In the coming year they plan to: (1) complete all health analyses for the Phase 3B core study at the Lovelace Respiratory Research Institute and receive final reports on inhalation chamber exposure characterization and health outcomes; (2) peer review and publish the final Phase 2 and Phase 3B reports, hold a stakeholder webinar to present the final results of Phase 3B; and (3) present results at the Society of Toxicology Meeting in Phoenix, AZ in March 2014, the CRC Real World Emissions workshop in San Diego, CA in April 2014, and the Health Effects Institute Annual Conference in Alexandria, VA in April 2014.

HIGH-EFFICIENCY ENGINE TECHNOLOGIES

The objective of these projects is to increase engine and vehicle efficiency of both light- and heavy-duty vehicles using advanced technology engines and advanced drivetrains. The following describe what is planned for completion in FY 2014.

- Cummins, Inc. is developing engine systems with 50% or greater brake thermal efficiency and demonstrating a tractor-trailer with 50% or greater freight efficiency improvement. In the coming year they plan to complete the 68% freight efficiency improvement vehicle demonstration testing, analysis and targeted testing of technologies for achievement of a 55% thermal efficient engine, and complete the build of the 68% 24-hour freight efficiency demonstration vehicle.
- Detroit Diesel Corporation is demonstrating a 50% total increase in vehicle freight efficiency measured in ton-miles per gallon, with at least 20% improvement through the development of a heavy-duty diesel engine capable of achieving 50% brake thermal efficiency. In the coming year they plan to complete the following activities: (1) refinement of various engine systems will continue in 2014, to help refine their operating characteristics in support of vehicle testing; (2) the analysis of the pathway to achieving 55% engine brake thermal efficiency will continue, including some testing of a few components needed to make this objective possible; and (3) build and test the final engine system in the SuperTruck vehicle to demonstrate the improvements in the vehicle as part of the 50% vehicle freight efficiency improvement.
- Volvo is identifying concepts and technologies that have potential to achieve 55% brake thermal efficiency on a heavy-duty diesel engine. In the coming year they plan to: (1) use the combustion tool for the 55% brake thermal efficiency concept engine work where they will enter new regimes and explore advanced injection strategies; (2) continue development of the combustion tool, with focus on kinetic mechanisms and testing of model fuels; and (3) validate on-road fuel savings of the 48% brake thermal efficiency powertrain system and refine design requirements for next generation waste heat recovery system.
- Delphi is developing, implementing, and demonstrating fuel consumption reduction technologies using a new low-temperature combustion process: gasoline direct-injection compression ignition (GDCI). In the coming year they plan to: fully map GDCI operation on performance dynamometers; debug the Phase 2 GDCI vehicle; continue development of GDCI engine control systems; calibrate the Phase 2 GDCI vehicle; test the Phase 2 GDCI vehicle; and continue single-cylinder engine tests to refine the combustion process and component designs.
- Ford Motor Company is demonstrating 25% fuel economy improvement in a mid-sized sedan using a downsized, advanced gasoline turbocharged direct injection engine with no or limited degradation in vehicle level metrics. In the coming year they will demonstrate a vehicle with greater than 25% weighted city/highway fuel economy improvement and Tier 2 Bin 2 emissions on the FTP-75 test cycle.
- General Motors is developing an advanced lean-gasoline combustion engine and aftertreatment system and will demonstrate 25% vehicle fuel economy improvement while achieving Tier 2 Bin 2 emissions. In the coming year they will demonstrate a passive SCR system capable of high efficiency NOx conversion with relatively low engine-out NOx; further investigation into the 12-volt start/stop system; and thermal management opportunities will be explored in GM's next generation of engines.
- Cummins, Inc. is demonstrating 40% fuel economy improvement over a baseline gasoline V-8 pickup truck while achieving Tier 2 Bin 2 tailpipe emissions compliance. In the coming year they plant to continue development and optimization of the first vehicle installation of the prototype engine, measure emissions, and perform a vehicle demonstration.
- Robert Bosch LLC is improving fuel economy by 25% with minimum performance penalties while achieving Super Ultra-Low Emissions Vehicle level emissions with gasoline. In the coming year they plan to finalize and integrate advanced combustion control strategies into the engine control unit, demonstrate engine and vehicle performance during transient operations including mode switches, and analyze fuel efficiency and emission results from the vehicle, identifying commercial potentials of the proposed technology solutions.
- The Chrysler Group, LLC is demonstrating a 25% improvement in combined City and Highway Federal Test Procedure fuel economy in a Chrysler minivan. In the coming year they will complete refinement and

I. Introduction

verification of the system controls and calibration of the Alpha 2 engine on a dynamometer and in-vehicle to meet all performance, emissions, fuel economy and drivability targets.

- Filter Sensing Technologies, Inc. is demonstrating and quantifying improvements in efficiency and greenhouse gas reductions through improved diesel particulate filter sensing, controls, and low-pressure drop components. In the coming year they plan to: (1) quantify radio frequency sensor measurement accuracy relative to gravimetric standard over a range of engine platforms and aftertreatment system configurations; (2) design and develop pre-production beta radio frequency sensing system meeting manufacturer requirements, and supply systems to project partners for testing and performance evaluation; (3) develop optimized aftertreatment control strategies, utilizing input from the radio frequency sensor, and demonstrate potential fuel savings and reduced system costs enabled through accurate measurement of the filter loading state and advanced low-pressure drop aftertreatment; and (4) evaluate additional efficiency gains possible through the use of advanced combustion modes and alternative fuels in conjunction with radio frequency aftertreatment sensing and control.
- GM is applying the enabling technologies of high-energy, extended-duration ignition and novel intake charge boosting/mixing system to a current GM boosted spark ignition engine. In the coming year they plan to build and test a Phase 4 GM 2.0-L turbocharged engine defined through simulation and packaging studies.
- Eaton Corporation is demonstrating fuel economy improvement through Rankine cycle waste heat recovery systems utilizing a roots expander in heavy-duty diesel applications. In the coming year they plan to build and test the multistage roots expander in an ORC system utilizing water, ethanol or a combination of water and ethanol as the working fluid; prototype and evaluate heat exchangers, working fluid pump, valves and fluid conveyance lines; design and build a heavy-duty diesel engine Rankine cycle system with integrated roots expander for a John Deere 13.5-L diesel engine; and demonstrate roots expander capability of meeting the DOE objective utilizing the developed heavy-duty diesel engine Rankine cycle system.
- MAHLE Powertrain is demonstrating thermal efficiency of 45% on a light-duty gasoline engine platform while demonstrating potential to meet U.S. Environmental Protection Agency emissions regulations. In the coming year they plan to: (1) correlate computational fluid dynamics model to experimental data to develop quasi-predictive tool to guide TJI design refinement; (2) conduct boosted single-cylinder thermodynamic engine experiments to achieve naturally aspirated engine peak load levels at ultra-lean conditions; (3) explore TJI designs at the edges of the established design space to induce and understand engine performance differences; and (4) identify optimum engine operating strategy with TJI.
- ENVERA LLC is developing a high-efficiency VCR engine having VVA and an advanced high-efficiency supercharger to obtain up to a 40% improvement in fuel economy. In the coming year work will be conducted in the following areas: VCR crankcase design and manufacture, VVA development and cylinder head installation, and advanced supercharger integration into the engine.
- Robert Bosch LLC is developing an intake air oxygen (IAO₂) sensor which directly and accurately measures the oxygen concentration in the intake manifold. In the coming year they plan completion of the following activities: (1) development of a control algorithm that uses the accurate IAO₂ sensor oxygen concentration measurement to maximize combustion efficiency, and improve fuel economy; (2) fabrication of IAO₂ sensors; (3) validation of first generation IAO₂ sensor design (component and engine durability); (4) identification of further improvement potential on base of component validation and cool EGR system analysis; and (5) set up and conduct design work to incorporate lessons learned from component validation and cool EGR system analysis.
- LANL is developing prototype NO_x and NH₃ sensors based on mixed-potential technology. In the coming year they plan to: (1) demonstrate quantitative correlation of NO response of optimized sensor to Fourier transform infrared response during engine testing; (2) demonstrate NH₃ sensitivity of 10 ppm in an ESL-manufactured sensor; and (3) demonstrate >10 times NH₃ selectivity with respect to hydrocarbons.

SOLID STATE ENERGY CONVERSION

Research will continue in FY 2014 on TEs for converting waste heat from advanced combustion engines directly to electricity. Research will focus on development of practical systems that are suitable for future production.

- Gentherm is designing a TE waste heat recovery system with 5% improvement in fuel economy for light-duty vehicles while providing a path towards commercialization at passenger vehicle volumes of 100,000 units per year. In the coming year they plan to scale up the TE engine subassembly, TEG subsystem joining technologies, and the TEG fabrication concept; complete assembly and bench testing of light-duty vehicle TEGs; complete assembly and test of heavy-duty vehicle TEG and related system components; and deliver heavy-duty vehicle TEG and cooling system to TARDEC.
- GM is developing a thermal comfort model and computer-aided engineering tool to predict the occupant physiological response to localized heating and cooling through human subject testing—key to balance distributed HVAC components and to speed execution of stratified thermal systems. In the coming year they plan to install, calibrate and evaluate the TE system, including carry-over TE components (from the LaCrosse) and new seats with TE contact heating and cooling, in the Chevrolet Volt, and deliver the completed Chevrolet Volt demonstration vehicle to DOE by March 2014.
- GM is developing an overall TEG system including all necessary vehicle controls and electrical systems fully integrated onto a light-duty vehicle to demonstrate fuel economy improvement of 5% over the US06 drive cycle. In the coming year they plan to: (1) complete design and fabrication of initial TEG subunit for bench testing; (2) analyze performance and durability of initial TEG subunit as input for redesign of the final TEG system; (3) use vehicle level modeling to prioritize enhanced vehicle electrification schemes, such as electrification of belt driven accessories, to ensure full use of the TEG electrical power delivered; (4) complete vehicle level controls and integration to fully optimize vehicle performance with installed TEG; (5) perform extensive testing and analysis of demonstration vehicle with TEG installed, and deliver both the results and the demonstration vehicle to DOE; and (6) complete study of cost and scale up plans for TEG commercialization potential.
- GMZ Energy is demonstrating a robust, thermally cyclable TE exhaust waste heat recovery system that will provide approximately a 5% fuel efficiency improvement for a light-duty vehicle platform. In the coming year they plan to complete the following activities: (1) TE modules will be subjected to extensive thermal and mechanical reliability testing; (2) the module design is also being adapted for manufacturability; (3) fabricate the TEGs for the passenger vehicle and the Bradley Fighting Vehicle; and (4) TEGs will be integrated onboard a vehicle platform and the vehicle will be tested before and after TEG installation to demonstrate the improvement in fuel efficiency.
- Purdue University is developing the fundamental understanding and technology improvements needed to make viable the efficient conversion of waste heat in automotive exhaust systems to electricity. In the coming year they plan to complete the following activities: (1) find out how the filling ratio in skutterudite affects the electronic band structure and energy carriers in skutterudites; (2) dope nanowire materials to optimize the TE performance, develop hydrazine-free telluride nanowire synthesis methods, and make a nanocrystal-coated fiber TE device; (3) develop a theoretical model to explain the origin of such high interface thermal conductance and measurement of cross-plane electrical properties of superlattices; (4) experimental assessment of impinging and longitudinal heat exchangers for analytical model verification, allowing system optimization and initial TEG performance estimates; and (5) increase the maximum operating temperature of the test rig to at least 800°C and use CNT-based interface materials to address thermomechanical stress issues.
- Stanford University is developing and measuring novel TE materials, including skutterudites and half-Heusler alloys. In the coming year they plan to: (1) adapt the thermal and mechanical characterization metrology developed for CNT arrays during FY 2011 and FY 2012 to perform full characterization on metal nanowire arrays; (2) adapt coarse-grained molecular simulation tool to predict properties in nanostructured metal thermal interface materials, including nanowire arrays, and compare to data obtained experimentally; (3) demonstrate matrix stabilization of metal nanowire arrays to lend mechanical integrity to metal nanowire arrays as freestanding thermal interface materials; (4) utilize high-temperature infrared microscopy apparatus to make measurements on novel TE materials and nanostructured thermal

I. Introduction

interface materials at temperatures comparable to combustion exhaust streams; and (5) develop systems-level model for a complete TE generator system integrated into an automobile exhaust stream.

- Stony Brook University is developing a scalable high-throughput, non-equilibrium synthesis process for high ZT TE materials from abundant low-cost feedstock by using thermal spray technology. In the coming year they plan to: (1) evaluate the TE properties of doped magnesium silicide using thermal spray; (2) anneal thermal sprayed as-quenched powder to get filled skutterudite phase; (3) try cold spray for filled skutterudite powder for better TE properties; (4) conduct a series of experiments on thermal spray conditions to optimize the electrical conduction while suppressing heat conduction; and (5) fabricate a complete TE working device and test its efficiency.
- Texas A&M University is synthesizing inorganic nanowires and quantum wires of both CoSb_3 and InSb , and organic conducting polymer thin films, and assembling them into inorganic-organic hybrid thermoelectrics cells with sizes ranging from a few mm^2 to a few cm^2 , using conjugated linker molecules to tether the nanowires to each other or to conducting polymer thin films. In the coming year they will evaluate the TE performance of a Zn_4Sb_3 nanowire pellets and Zn_4Sb_3 nanowire-copper nanoparticle composite pellets. This system is expected to provide additional evidence that compositional disorder is useful for enhancing the efficiencies of thermoelectrics.
- The University of California, Los Angeles is developing materials and interfaces for improved thermomechanical reliability of TE vehicle exhaust waste heat harvesting devices. In the coming year they plan to further investigate flexible mechanical/thermal interfaces compatible with the TE-tailored nanocomposites and related bonding methods.
- The University of California, Santa Cruz is developing novel thermoelectric materials based on abundant and non-toxic Zintl-phase magnesium silicide alloys. In the coming year they plan to finalize papers on the latest materials synthesized and summarize the key theoretical results including the calculation of the bipolar thermal conductivity.
- Virginia Tech is fabricating and characterizing new TE materials grown with scalable techniques for production of large quantities of efficient, yet non-toxic and inexpensive elements capable of long-term operation at high temperatures over thousands of thermal cycles. In the coming year they plan to: (1) perform a sensitivity study on the performance of the system to various parameters including the number of TEG modules, engine power, vehicle speed, etc. and find the optimum operating conditions for the system; (2) modify design to perform optimally in the typical operating conditions; (3) develop a prototype of the TEG; and (4) explore methods to improve the electrical conductivity in the ZnO materials.
- The University of Texas at Austin is increasing the ZT of earth-abundant and low-cost magnesium silicides (Mg_2Si) and higher manganese silicides ($\text{MnSi}_{1.73}$, or HMS) to the level found in state-of-the-art TE materials that contain scarce and expensive elements. In the coming year they plan to: (1) improve the TE properties of silicides by nanostructuring and modulation doping; (2) understand the crystal complexity on the phonon dispersion and transport in HMS; (3) test TE devices coupled with heat exchanger and validate the system level model; and (4) incorporate thermal and electrical contact resistance in the system level model.

II. COMBUSTION RESEARCH

II.1 Low-Temperature Automotive Diesel Combustion

Paul Miles

Sandia National Laboratories
PO Box 969
Livermore, CA 94551-0969

DOE Technology Development Manager:
Gurpreet Singh

Subcontractor:
University of Wisconsin Engine Research Center,
Madison, WI

Overall Objectives

- Provide the physical understanding of the in-cylinder combustion processes needed to minimize the fuel consumption and the carbon footprint of automotive diesel engines while maintaining compliance with emissions standards
- Develop efficient, accurate computational models that enable numerical optimization and design of fuel-efficient, clean engines
- Provide accurate data obtained under well-controlled and characterized conditions to validate new models and to guide optimization efforts

Fiscal Year (FY) 2013 Objectives

- Develop and improve diagnostic techniques that permit the quantitative evaluation of equivalence ratio distributions formed from injection of diesel-like fuels
- Explore the applicability of pilot injection strategies to low-temperature combustion (LTC) techniques
- Examine the impact of pilot mass, injection pressure, ambient temperature and swirl ratio on the mixture formed by the pilot fuel injection
- Quantify the impact of ambient temperature, O₂ concentration, and mixture formation on the ignition of the pilot fuel
- Evaluate the ability of computational models to accurately capture the pilot ignition process

FY 2013 Accomplishments

The accomplishments below target the barriers of 1) lack of fundamental knowledge and 2) lack of a predictive modeling capability identified in the

Vehicle Technologies Program 2011-2015 Multi-Year Program Plan:

- Characterized the photo-physics of new laser-induced fluorescence tracers suitable for use with diesel primary reference fuels and demonstrated their application in engine measurements
- Measured the evolution of in-cylinder mixture distributions for pilot injections as pilot mass, injection pressure, ambient temperature and swirl ratio were varied
- Examined the pilot ignition processes under conventional and low-temperature diesel combustion conditions as pilot mass and injection pressure were varied
- Assessed performance of current kinetic models for predicting the ignition behavior of diesel fuels and examined the ability of multi-dimensional models to capture the impact of ambient temperature on ignition

Future Directions

- Examine the impact of 'stepped-lip' piston bowl geometries on the mixture preparation process and compare with conventional bowl geometries
- Investigate the benefits of close-coupled pilot injections on combustion noise and emissions and identify the physical processes dominating this behavior
- Identify and investigate multiple injection strategies suitable for limiting cold-start hydrocarbon (HC) and CO emissions
- Examine induction flow processes, the ability to accurately simulate asymmetric engine flows, and the impact of asymmetries on the combustion process



INTRODUCTION

Direct-injection diesel engines have the highest proven brake fuel efficiency of any reciprocating internal combustion engine technology. However, conventional diesel combustion produces elevated emissions of both soot and oxides of nitrogen (NO_x). To address this shortcoming, low-temperature combustion (LTC) techniques that prevent the formation of these pollutants within the engine are being developed. These techniques

employ low engine compression ratios and high levels of dilution that promote premixing and low soot and NO_x formation. However, a high degree of premixing can lead to excessive combustion noise and elevated HC and CO emissions.

This year, the project has focused on developing an understanding of how pilot injection strategies can be adapted to LTC strategies. Pilot injections are commonly used in conventional automotive diesel combustion systems to shorten ignition delay and control combustion noise and emissions. By decreasing the amount of premixing, HC and CO emissions stemming from overly lean mixtures are reduced as is the rapid and noisy pressure rise associated with premixed combustion.

Exploiting the potential synergy between LTC strategies and pilot injections can be difficult. The reduced premixing associated with pilot injections can compromise NO_x emissions, and soot emissions nearly always deteriorate. Moreover, with the high dilution levels and low compression temperatures associated with LTC, the pilot itself may over-mix and itself become an important source of HC and CO emissions. Under extreme conditions, the pilot may not even ignite. A major focus of this work is thus to understand and establish an ability to predict the mixture formation process during the pilot ignition delay, and its subsequent impact on the pilot ignition process as well as the emissions and combustion performance of LTC combustion strategies.

APPROACH

The overall research approach involves carefully coordinated experimental, modeling, and simulation efforts. Detailed measurements of in-cylinder flows, fuel and pollutant spatial distributions, and other thermochemical properties are made in an optical engine facility based on a General Motors 1.9-liter automotive diesel engine. Close geometric and thermodynamic correspondence between the optical engine and the production engine allow the combustion and engine-out emissions behavior of a traditional, all-metal test engine to be closely matched. These measurements are closely coordinated and compared with the predictions of numerical simulations.

The experimental and numerical efforts are mutually complementary. Detailed measurements of the in-cylinder variables permit the evaluation and refinement of the models used in the computer simulations, while the simulation results can be used to obtain a more detailed understanding of the in-cylinder flow and combustion physics—a process that is difficult if only limited measurements are available. Jointly, this approach addresses both of the principal goals of this project: 1) development of the physical understanding to guide

and 2) the simulation tools to refine the design of optimal, clean, high-efficiency diesel combustion systems.

RESULTS

Figure 1 illustrates the impact of pilot injection quantity on a low-load, LTC operating condition with a near-top-dead-center injection event. In this case, without a pilot injection the combustion is very unstable and the combustion efficiency η_c is poor. While a small (1 mg) pilot improves the combustion significantly, increasing the pilot quantity provides considerable additional reductions in HC and CO emissions at both injection pressures as well as improved combustion stability

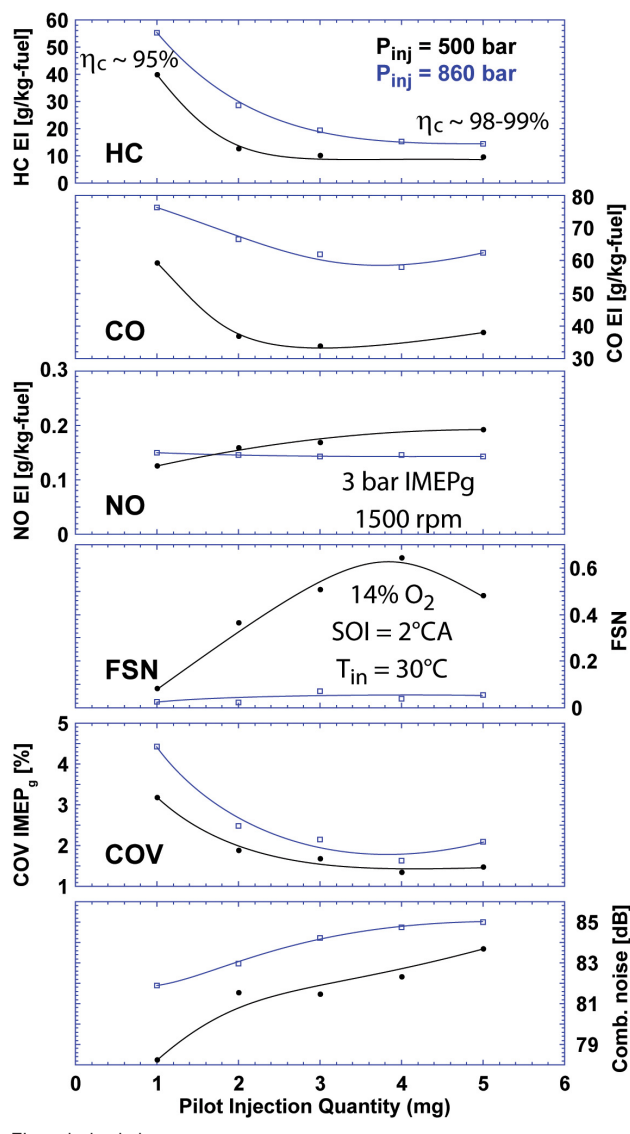


FIGURE 1. Engine emissions, stability (COV – coefficient of variation of indicated mean effective pressure), and combustion noise for two different injection pressures at a light-load, LTC operating condition.

(coefficient of variance of indicated mean effective pressure). Although NO_x changes are negligible with increased pilot mass, noise is increased modestly and soot can increase significantly at the lower injection pressure. Increased injection pressure is often cited as a remedy for increased soot emissions when pilot injections are employed; however, as seen in Figure 1 this can lead to deteriorated HC/CO emissions and poorer stability.

Under the conditions of Figure 1 we find that improvements in HC/CO and coefficient of variance occur until the pilot mass exceeds 3 mg. Examination of the heat release characteristics shown in Figure 2 shows that between 2 and 3 mg, the pilot ignition transitions to a “robust” ignition event, with a pronounced high-temperature heat release period. We find that robust ignition can be identified by requiring that ~40% of the pilot fuel lower heating value be released within 25° of crank angle of the start of pilot injection.

To investigate how the pilot ignition is impacted by charge O_2 concentration, pilot mass, and injection pressure, we examined how the minimum temperature needed for a robust pilot ignition event changed over a broad range of operating conditions. Example results are shown in Figure 3. Clearly a higher temperature is needed when the charge gas is dilute—the temperature needed can change by ~100 K as the intake charge O_2 concentration is reduced from 18% to 10%. Figure 3 also shows that richer pilot fuel-air mixtures appear to promote pilot ignition at the low-temperature threshold for robust ignition. Increased pilot mass or reduced injection pressure can both be seen to result in a lower minimum ignition temperature. Similar behavior can

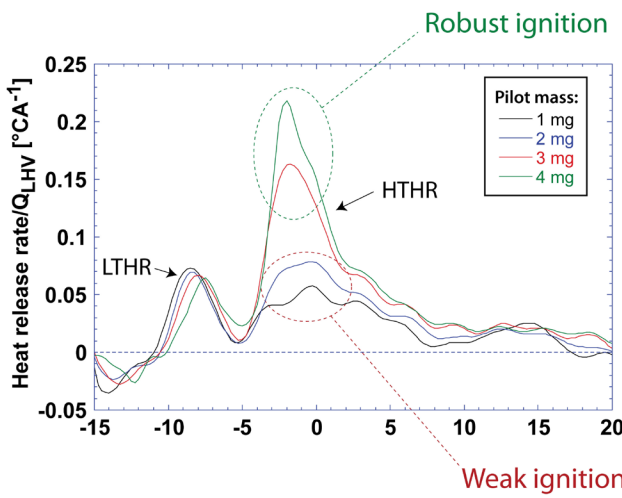


FIGURE 2. Normalized apparent heat release rate associated with the pilot injection alone, for various pilot injection quantities at an injection pressure of 860 bar. The presence of a pronounced high-temperature heat release peak corresponds to a “robust” ignition event.

be observed in the measured ignition delays; under low-temperature, dilute conditions increased pilot mass or reduced injection pressure result in a *decreased* ignition delay. In contrast, at more conventional diesel combustion conditions (higher temperatures, lower O_2 concentrations) the opposite effect is observed—increased mass or reduced injection pressure result in an *increased* ignition delay.

Simulations of the ignition of homogeneous mixtures performed using a detailed kinetic mechanism developed for the diesel primary reference fuels [1] shed light on the reason for this contradictory behavior. Figure 4 shows that at each O_2 concentration, there is an optimum equivalence ratio that promotes ignition. Under dilute or low-temperature conditions, over-mixing to excessively lean equivalence ratios will impede ignition, leading to longer ignition delays. In this case, additional pilot mass or lower injection pressure can be beneficial. Conversely, under more conventional diesel operating conditions with low dilution and generally rich mixtures at the time of ignition, the still richer mixtures associated with additional mass or lower injection pressure will impede ignition.

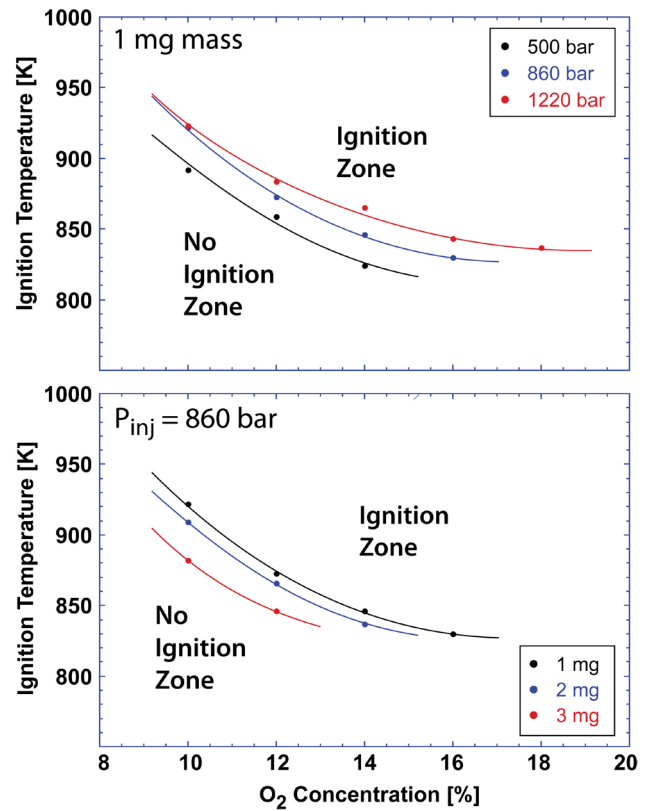


FIGURE 3. Impact of injection pressure and pilot injection mass on the minimum charge gas temperature needed to obtain a robust ignition event, for various charge gas O_2 concentrations.

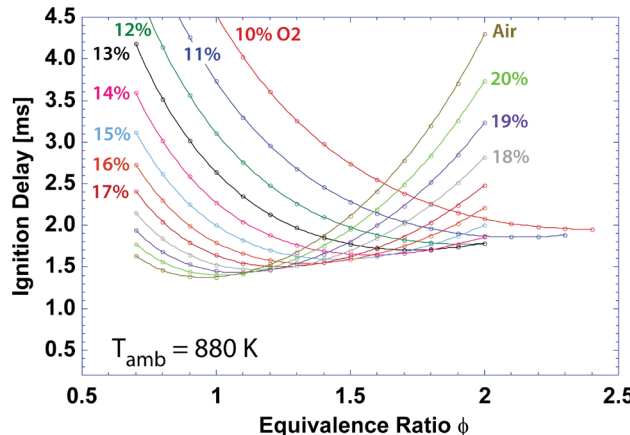


FIGURE 4. Variation of ignition delay with ϕ and O₂ at a fixed ambient temperature of 880 K.

There are at least two potential causes for this optimal equivalence ratio behavior. First, the chemical kinetics of the ignition process could be changing with ϕ , such that different chemical pathways lead to different ignition propensities. Alternatively, this behavior could also be simply related to the specific heat of the fuel-air mixture. In this latter scenario, the most favorable ϕ for ignition represents a balance between entraining enough hot mixture to rapidly initiate low-temperature reactions, but not so much as to dampen the ΔT associated with low-temperature heat release. Comparison of the mixture specific heat per unit mass of fuel, for each O₂ concentration shown in Figure 4, shows that the specific heat is nearly constant at the optimal equivalence ratio for ignition. Consequently, the latter explanation for the optimal equivalence ratio is likely the dominant effect.

The ignition delays predicted by the kinetic mechanism exceed the measured ignition delays by roughly 50%; hence, the kinetic mechanism requires further refinement. Nevertheless, because it is mainly independent of the kinetics, the existence of an optimal ϕ for ignition is expected to persist. However, the range of ϕ giving optimal ignition, currently $\phi \sim 1.0\text{--}1.6$ for modest dilution rates, may vary as the mechanism is refined.

Both the experimental results of Figure 3 and the simulation results of Figure 4 indicate that richer mixtures are responsible for the improved ignition behavior as ignition mass is increased. To directly assess this behavior, we have measured the in-cylinder ϕ distributions using a new laser-induced fluorescence technique based on the use of 1-methylnaphthalene as a tracer compound. Figure 5 shows the resulting fuel mass distributions. The distributions show that as the boundary shown in Figure 2 between non-robust (2 mg fuel) and robust ignition is crossed (3 mg fuel), a significant amount of fuel mass moves into the equivalence ratio

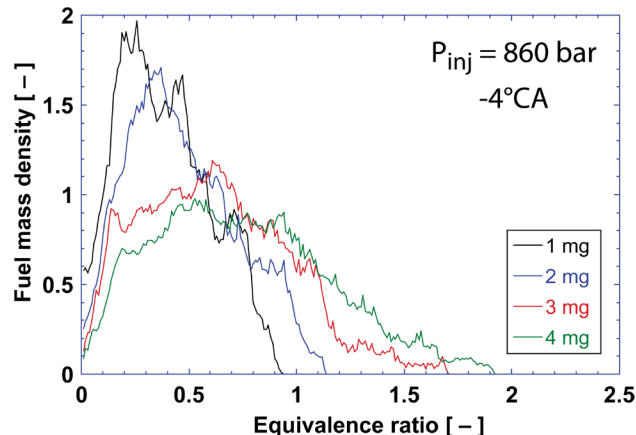


FIGURE 5. Fuel mass distributions measured for the conditions corresponding to the apparent heat release traces shown in Figure 2.

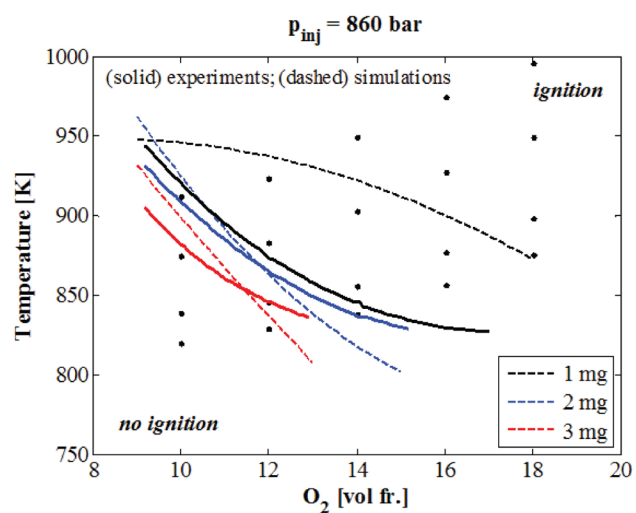


FIGURE 6. Comparison between the measured and computed minimum ignition temperatures as O₂ concentration and pilot mass are varied.

range expected to promote optimal ignition: $1.0 < \phi < 1.6$. Analogous behavior in the fuel mass distributions is observed as the boundary between non-robust and robust ignition is crossed when injection pressure is reduced.

If multi-dimensional simulations are to be employed to optimize pilot injection strategies, it will be important to capture the pilot ignition processes accurately. Currently, reduced kinetic mechanisms appropriate for multidimensional simulations do not exist for the diesel primary reference fuels. Consequently, we have instead evaluated the suitability of the lighter, gasoline primary reference fuel mechanisms to capture the kinetics of pilot ignition. Figure 6 compares the measured minimum ignition temperatures against those calculated. The simulations clearly capture the required minimum temperature well at the higher pilot masses, and the

reduction in the minimum required ignition temperature with increased pilot mass is clearly seen. However, at the smallest pilot mass, the simulation results generally predict a higher minimum ignition temperature than is seen experimentally, an artifact that is likely due in part the prediction of overly lean mixtures.

CONCLUSIONS

Under LTC operating conditions, increased pilot mass can be beneficial for reducing HC and CO emissions, as well as cycle-to-cycle variability. One key to obtaining these benefits is a robust pilot ignition event. Specific findings include:

- The minimum charge temperature needed to obtain robust ignition is strongly impacted by O₂ concentration, pilot mass, and injection pressure.
- Simulations show that the observed ignition behavior is fully consistent with a predicted optimal equivalence ratio for ignition. The optimum occurs when enough hot mixture to rapidly initiate low-temperature reactions has been entrained, but the ΔT associated with low-temperature heat release is not damped by excessive mixture entrainment.
- The measured in-cylinder fuel-air distributions are fully consistent with the measured ignition behavior and the existence of an optimal ϕ for ignition in the approximate range predicted by the simulations.
- The detailed kinetic mechanism available for diesel primary reference fuels requires refinement to accurately predict ignition delay.
- Multi-dimensional simulations indicate that pilot injections will be more difficult to ignite than is found experimentally. Accurate modeling of the pilot ignition process is a difficult problem that will require accurate prediction of both the mixture formation process and the kinetics of ignition.

REFERENCES

1. Westbrook, C.K., Pitz, W.J., et al., Detailed Chemical Kinetic Reaction Mechanisms for Primary Reference Fuels for Diesel Cetane Number and Spark-Ignition Octane Number. Proceedings of the Combustion Institute 33 (1): pp. 185-192, 2011.

FY 2013 SELECTED PUBLICATIONS/ PRESENTATIONS

1. "Diesel and Diesel Low-Temperature Combustion Systems," Andersson, Ö and Miles PC. Encyclopedia of Automotive Engineering – in Press.

2. "In-Cylinder Flow," Borée J. and Miles PC. Encyclopedia of Automotive Engineering – in Press.
3. "Fuel Concentration Imaging inside an Optically Accessible Diesel Engine using 1-Methylnaphthalene Planar Laser-Induced Fluorescence (PLIF)," Trost J, Zigan L, Leipertz A, Sahoo D, Miles PC. *International Journal of Engine Research* – in Press.
4. "Characterization of Four Potential Laser-Induced Fluorescence Tracers for Diesel Engine Applications," Trost J, Zigan L, Leipertz A, Sahoo D, Miles PC. *Applied Optics* – in Press.
5. "Pilot Injection Ignition Properties under Low-Temperature, Dilute In-Cylinder Conditions," Miles PC, Sahoo D, Busch S, Trost J, Leipertz A. Presented at the 2013 SAE/KSAE Powertrain, Fuels & Lubricants Meeting; *SAE Int. J. Engines* 6 (4): 2013.
6. "The Impact of Injection Pressure, Ambient Temperature, and Swirl Ratio on the Mixture Preparation of a Pilot Injection," Sahoo D, Miles PC, Trost J, Leipertz A. Presented at the 11th International Conference on Engines & Vehicles. *SAE Int. J. Engines*, 6 (3), 1716-1730.
7. "Analysis of the Influence of Swirl and Injected Mass on the Equivalence Ratio of Pilot Injections in a Diesel Engine During PPCI Low-Temperature Combustion Using 1-Methylnaphthalene LIF," Trost J, Leipertz A, Sahoo D, Miles PC. pp. 485-496 in XIth International Congress on Engine Combustion Processes: Current Problems and Modern Techniques, ed. A. Leipertz. ESYTEC-Verlag, Erlangen, 2013.
8. "Conceptual Models for Low-Load, Single-Injection, EGR-Diluted, Partially Premixed Low-Temperature DI Diesel Combustion," Musculus MPB, Miles PC, Pickett LM. *Prog. Energy Combust. Sci.* 39 (2): 246-283, 2013.
9. "Atmospheric Pressure Acetylene Detection by UV Photo-fragmentation and Induced C2 Emission," Miles PC, Li B, Li Z, and Aldén, M. *Applied Spectroscopy* 67 (1): 66-72, 2013.
10. "A Computational Investigation of the Effects of Swirl Ratio and Injection Pressure on Mixture Preparation and Wall Heat Transfer in a Light-Duty Diesel Engine," Perini F, Dempsey A, Reitz RD, Sahoo D, Petersen B, Miles P. Presented at the 2013 SAE World Congress, SAE Technical Paper 2013-01-1105.
11. "Effect of Cetane Improvers on Gasoline, Ethanol, and Methanol Reactivity and the Implications for RCCI Combustion," Dempsey AB, Walker NR, Reitz RD. Presented at the 2013 SAE World Congress, SAE Paper 2013-01-1678.
12. "Effect of Piston Bowl Geometry on Dual Fuel Reactivity Controlled Compression Ignition (RCCI) in a Light-Duty Engine Operated with Gasoline/Diesel and Methanol/Diesel," Dempsey AB, Walker NR, Reitz RD. Presented at the 2013 SAE World Congress, SAE Paper 2013-01-0264.
13. "Use of Low-Pressure Direct-Injection for Reactivity Controlled Compression Ignition (RCCI) Light-Duty Engine Operation," Walker NR, Dempsey AB, Andrie MJ, Reitz RD. Presented at the 2013 SAE World Congress, SAE Paper 2013-01-1605.

14. "Directions in Internal Combustion Engine Research," Reitz RD. *Combustion and Flame* 160, pp. 1-8, DOI: 10.1016/j.combustflame.2012.11.002, 2013.
15. "A Generalized Renormalization Group Turbulence Model and its Application to a Light-Duty Diesel Engine Operating in a Low Temperature Combustion Regime," Wang B-L, Lee C-W, Reitz RD, Miles PC, Han Z. *International Journal of Engine Research* 14 (3) 279-292, 2013.

SPECIAL RECOGNITIONS

1. **Invited speaker** "Scientific and Engineering Challenges Impacting the Design of Advanced Internal Combustion Engines," Miles PC. *Swedish Academy of Engineering Sciences*, Stockholm, Sweden, Sept. 12, 2013.
2. **Invited speaker** "Quantitative Measurements of Flow and Scalar Fields Supporting Predictive Simulation for Engine Design," Miles PC. *International Energy Agency – Energy Conservation and Emissions Reduction Task Leaders Meeting*, San Francisco, CA, July 23, 2013.

II.2 Heavy-Duty Low-Temperature Diesel Combustion and Heavy-Duty Combustion Modeling

Mark P.B. Musculus
Combustion Research Facility
Sandia National Laboratories
P.O. Box 969, MS9053
Livermore, CA 94551-0969

DOE Technology Development Manager:
Gurpreet Singh

Overall Objectives

This project includes diesel combustion research at Sandia National Laboratories (SNL) and combustion modeling at the University of Wisconsin. The overall objectives are:

- Develop fundamental understanding of how in-cylinder controls can improve efficiency and reduce pollutant emissions of advanced low-temperature combustion (LTC) technologies
- Quantify the effects of fuel injection, mixing, and combustion processes on thermodynamic losses and pollutant emission formation
- Improve computer modeling capabilities to accurately simulate these processes

Fiscal Year (FY) 2013 Objectives

The objectives for FY 2013 are all tied to gathering the required data and insight into in-cylinder processes to develop a conceptual model for multiple injections.

- Show the in-cylinder mechanisms that affect soot reduction by post injections at fuel-efficient combustion phasing (SNL)
- Determine the three-dimensional (3-D) interactions between close-coupled post injections and residual main-injection soot (SNL)
- Provide 3-D in-cylinder predictions to aid optical data interpretation for post-injection soot formation/oxidation (SNL)
- Evaluate efficacy and in-cylinder mechanisms of LTC combustion efficiency improvements by post injections (SNL)

FY 2013 Accomplishments

- Developed conceptual framework of exhaust soot-reduction dependencies for post injections that were close-coupled to the main injection to maintain fuel-efficient combustion phasing
- Showed interactions between the post-injection jet and residual main-injection products via multi-plane soot and combustion diagnostics, which is a first step to building a conceptual model for multiple injections
- Achieved good agreement between computer models and experiments, and used the model predictions to gain insight into 3-D in-cylinder processes
- Quantified effects of post-injection load, duration, and dwell effects on LTC combustion efficiency and identified in-cylinder processes responsible for combustion efficiency improvements

Future Directions

- Continue building a conceptual-model understanding of multiple-injection processes for both conventional diesel and LTC
 - Multi-injection schedules (pilot, post, split) deployed by industry
 - Use optical geometry more similar to metal engines (expense limit)
 - Compare with metal engine data where possible (industry partners)
 - Identify mechanisms and critical requirements (injector rate-shaping, dwell, duration, etc.) to improve emissions and efficiency
- Determine how combustion design affects heat transfer and efficiency
 - Measure spatial and temporal evolution of heat transfer across range of combustion modes; correlate to progression of in-cylinder combustion processes
- Continue to explore and upgrade fuel-injection technologies
 - Injection rate-shaping likely very important for performance, and higher load than our current injector capability is of interest



INTRODUCTION

Regulatory drivers and market demands for lower pollutant emissions, lower carbon dioxide emissions, and lower fuel consumption motivate the development of clean and fuel-efficient engine operating strategies. Most current production engines use a combination of both in-cylinder and exhaust aftertreatment strategies to achieve these goals. One in-cylinder strategy of current interest is the use of post injections of fuel that follow a conventional main fuel injection.

Previous work at SNL and in other studies in the literature have shown that close-coupled post injections, for which the dwell after the main injection is relatively short, can reduce soot emissions and/or increase combustion efficiency while maintaining or improving fuel efficiency [1]. Even so, studies in the literature are not in agreement on the mechanisms, the magnitude, or even the direction of post-injection effects on emissions. For instance, available data from studies to date show large variations in soot reduction/increase by post injections, and proposed explanations for the effects on soot also vary widely [1]. This disagreement in the literature shows that the injector and in-cylinder factors that affect post-injection performance are not well understood. The overall goal for FY 2013 is to begin to gather the required data and insight into in-cylinder processes to develop a conceptual model to explain how multiple injections affect engine performance and emissions.

APPROACH

This project uses an optically-accessible, heavy-duty, direct-injection diesel engine (Figure 1). A large window in the piston crown provides primary imaging access to the piston bowl, and other windows at the cylinder wall provide cross-optical access for laser diagnostics. For the data included here, the engine uses a Delphi DFI-1.5 light-duty injector and support system capable of precise delivery of small, closely spaced injections.

The experiments use a combination of engine-out and in-cylinder optical measurements. An AVL 415S smoke meter and a California Analytical Instruments 600 series hydrocarbon analyzer measured of the engine-out soot (smoke) and unburned hydrocarbon (UHC) emissions. Several in-cylinder techniques were utilized. Figure 1 shows a generic imaging setup, with two cameras to acquire simultaneous images from separate techniques. To probe the first-stage ignition processes, as well as to detect unburned fuel, planar laser-induced fluorescence (PLIF) of formaldehyde (H_2CO), a combustion intermediate, was employed. The second-stage ignition and concomitant completion of combustion was revealed by PLIF of the hydroxyl

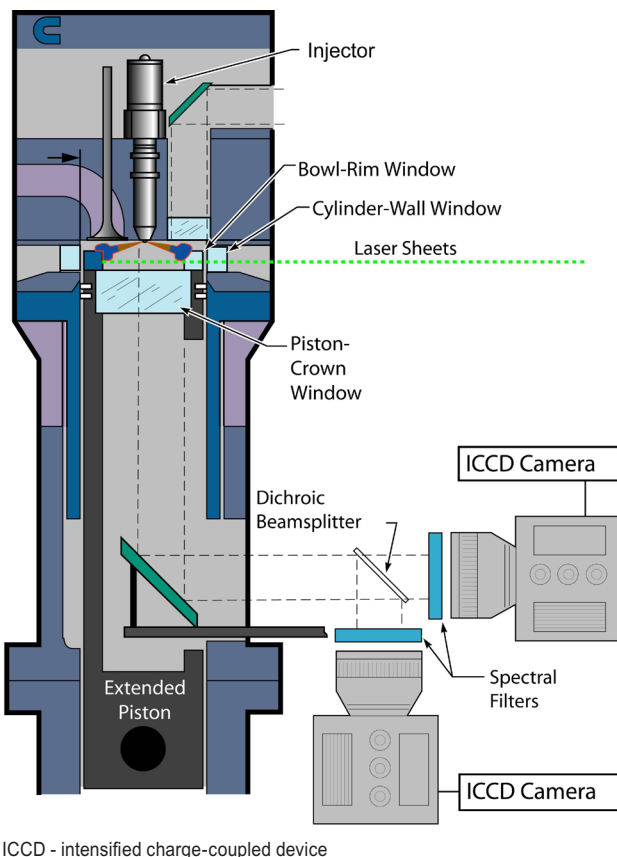


FIGURE 1. Schematic diagram of the optically accessible direct injection diesel engine and optical setup.

radical (OH), a combustion intermediate that is formed when the combustion of fuel is complete (or nearly complete) in regions of intermediate stoichiometry. In-cylinder soot was detected with both natural luminosity (soot-NL) imaging, which provides a two-dimensional (2-D) projection of the 3-D soot cloud that depends on the combustion-heated soot temperature, and planar laser-induced incandescence (PLII), which provides 2-D mapping of laser-heated soot for which the signal strength is independent of combustion-heated soot temperature. OH-PLIF and soot-PLII were also utilized simultaneously and at multiple different laser sheet elevations below the firedeck to measure the 3-D soot distribution in the ensemble.

RESULTS

The prime practical use of post injections has been to reduce engine-out soot emissions while maintaining efficiency, so this aspect is explored first, both in the exhaust and in the engine cylinder during combustion. Figure 2 shows a plot of measured engine-out soot for a range of single- and post-injection durations for engine operation at constant charge density and with

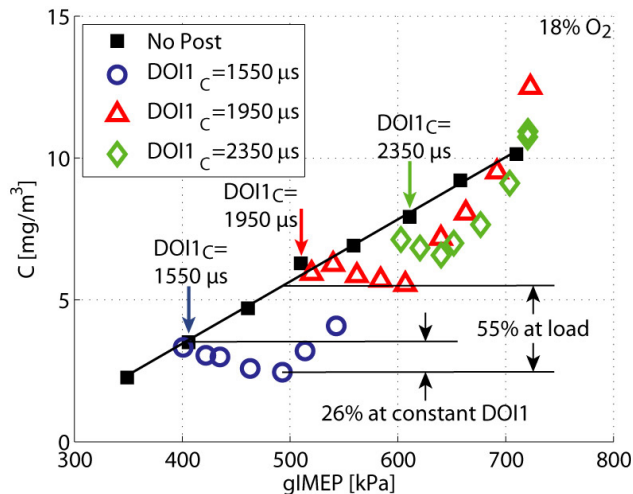


FIGURE 2. Measured engine-out soot expressed as carbon (C) concentration for a duration sweep of single injections (filled black squares) and three post-injection duration sweeps (open symbols) added to three different single-injection conditions at 18% intake oxygen fraction.

moderate exhaust gas recirculation (EGR) yielding an intake oxygen fraction of 18%. The filled black squares and solid trendline show how elemental carbon (C), which is a measure of the engine-out soot, increases with increasing engine load, quantified according to the gross indicated mean effective pressure (gIMEP). For three of the operating points, identified according to the commanded duration of main injection (DOI1_c) of 1,550, 1,950, and 2,350 microseconds, adding a post injection at first decreases the engine-out soot as the engine load increases (open symbols). As the post-injection duration increases, the engine-out soot once again increases. Similar behavior was observed across a wide range of intake oxygen fractions from 21 down to 12.6% (EGR from 0 to ~50%). Such soot reductions exceeding 60% at comparable loads were achieved with fuel-efficient close-coupled post injections using the light-duty common-rail injector specifically designed for multiple injections, which was installed in the previous FY.

The in-cylinder images from soot-NL and soot-PLII in Figure 3 provide some insight into the in-cylinder mechanisms that cause the observed engine-out emissions trends. The series of soot-NL images on the left show that the post-injection soot (outlined in red) appears to overlap with and/or pass over the soot remaining from the main injection (outlined in blue). The interactions are often more apparent from visual inspection of the dynamic soot-NL cinematographs, which are available online [2,3]. Even in dynamic cinematographs, however, the exact interaction is difficult to unravel because the soot-NL images represent a 2-D projection of a 3-D soot cloud. The uncertainties about the depth of the soot along the camera line of sight

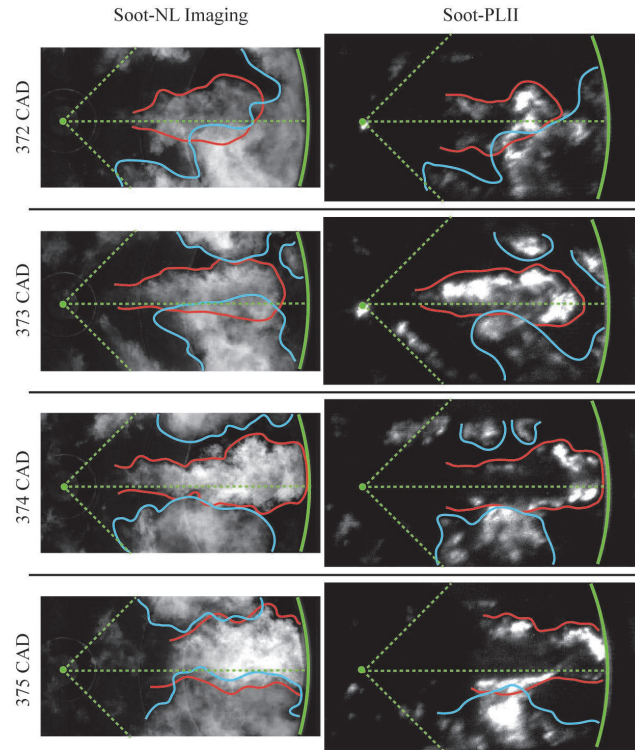


FIGURE 3. Instantaneous images of soot-NL (left) and soot-PLII (right) with the laser sheet aligned on the nominal jet axis for a post-injection condition at 18% intake oxygen fraction. The injector is on the left of the images (green dot) and the dotted green lines show nominal jet axes. The bowl wall is on the right (curved green line). To guide the eye, the approximate boundaries of the post- and main-injection soot clouds are identified by the outlines in red and blue, respectively. The left-right pairs are acquired simultaneously from the same cycle, but the pairs are from different cycles.

can be resolved, at least partially, by the simultaneous soot-PLII images on the right in Figure 3, which were acquired with the laser sheet aligned along the jet axis. The soot-PLII images frequently show that the post-injection soot overlaps with the main injection soot within the plane of the laser sheet, such as in the image at 373 crank-angle degrees (CAD) in Figure 3. The images also often show that the post jet appears to displace the main-injection soot away from the bowl wall, such as the black regions devoid of soot signal on the top- and bottom-right of the soot-PLII image at 374 CAD. Even these data, however, do not provide a complete picture of the 3-D interaction, especially including the distribution of combustion zones.

The four images in Figure 4 provide more details about key features of the 3-D soot and combustion zone distributions. The images are composites of OH-PLIF (false-colored green) along with simultaneous soot-PLII (false-colored red) acquired with the laser sheet horizontal at key elevations from firedeck as indicated

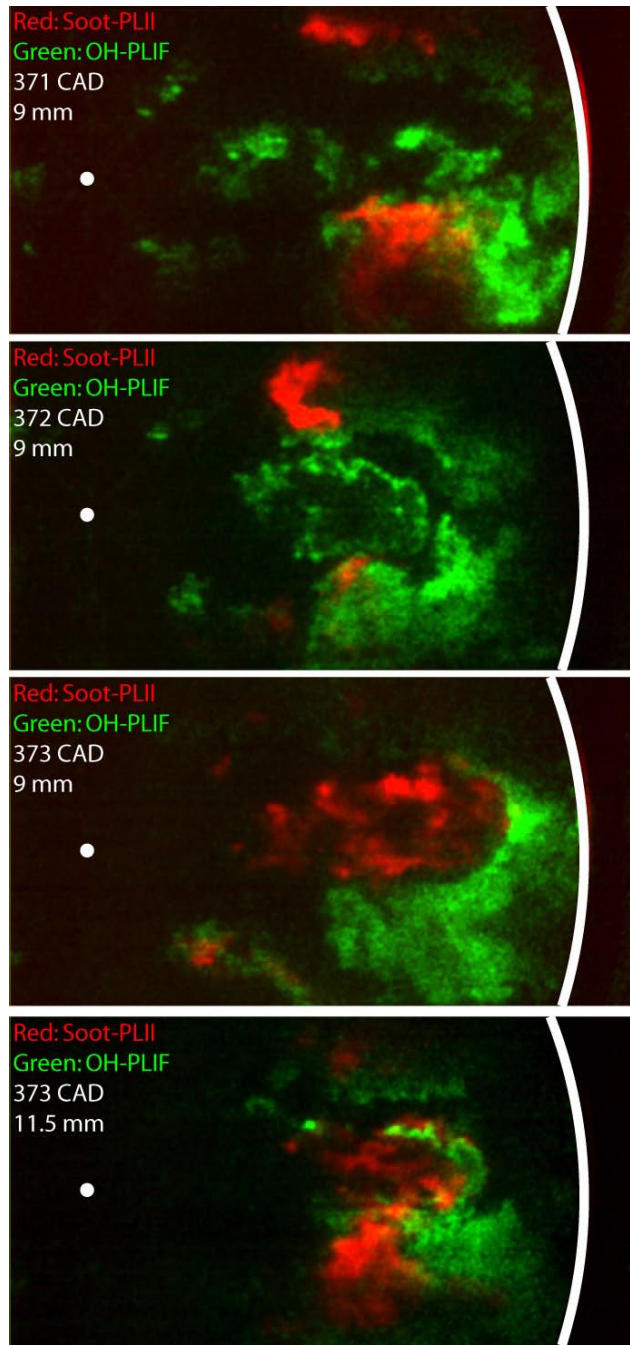


FIGURE 4. Instantaneous images of soot-PLII (red) and OH-PLIF (green) with laser sheets horizontal at elevations below the firedeck as indicated on the images. The soot-PLII and OH-PLIF are simultaneous in each image, but the images are from different cycles.

on the figures. The top image at 371 CAD shows the first appearance of combustion (green) in the post jet at the 9-mm sheet elevation. The next image shows a more defined diffusion-flame structure in the post jet, similar to Dec's conceptual model for diesel jets [4]. Another CAD later at 373 CAD shows soot (red) across the post jet cross-section, with a much broader distribution of OH-

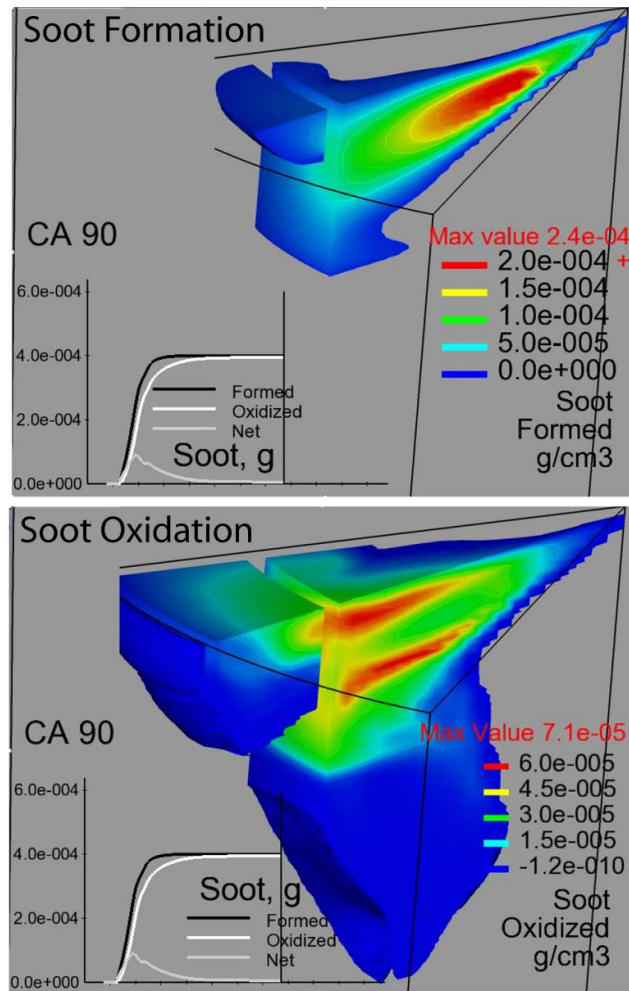


FIGURE 5. Time-integrated spatial distribution of soot formation (top) and soot oxidation (bottom) predicted by computer models.

PLIF (green) than in the 372 CAD image. The 372 and 373 CAD images are also examples of different OH-PLIF distributions that are observed on different cycles, with either a black zone free of OH between the post jet and the main-injection products (372 CAD), or a relatively broad distribution of OH-PLIF outside the post jet (373 CAD). The bottom image shows combustion at 373 CAD but in a lower plane, with a more defined diffusion flame and lack of any OH-PLIF signal near the bowl wall (right side of image), supporting the hypothesis that the post-jet injection displaces the main-injection products to some degree.

Computer-model simulations at the University of Wisconsin help to complement the experimental data by providing predictions of quantities that are difficult to measure experimentally. After confirming that the model replicates the engine-out soot trends shown in Figure 2, the predictions were analyzed in more detail to reveal the spatial distributions of soot formation and

oxidation. Figure 5 shows examples of time-integrated soot formation (top) and oxidation (bottom) predicted by the model. Although experiments can measure soot itself, separation of oxidation from formation is currently available only through computer simulations. Future analysis of computer-model predictions will provide insight into how post injections affect soot formation and oxidation processes to yield soot emissions improvements, and will also provide insight into effects of post injections on fuel efficiency. In this way, analysis of the computer-model predictions will complement experimental measurements to aid the development of a conceptual model for multiple fuel injections.

Finally, in addition to reducing soot emissions while maintaining fuel efficiency, post injections can improve combustion efficiency under conditions where over-mixed fuel does not burn to completion. Similar to Figure 2, the plot on the bottom of Figure 6 shows measured exhaust UHC dependence on injection duration for either a single injection (black filled circles) or a range of post-injection durations (open blue circles) for a high-EGR LTC condition (12.6% intake oxygen fraction). The data show that the post injection reduces UHC by 25–30% compared to a single injection at the same load, and with

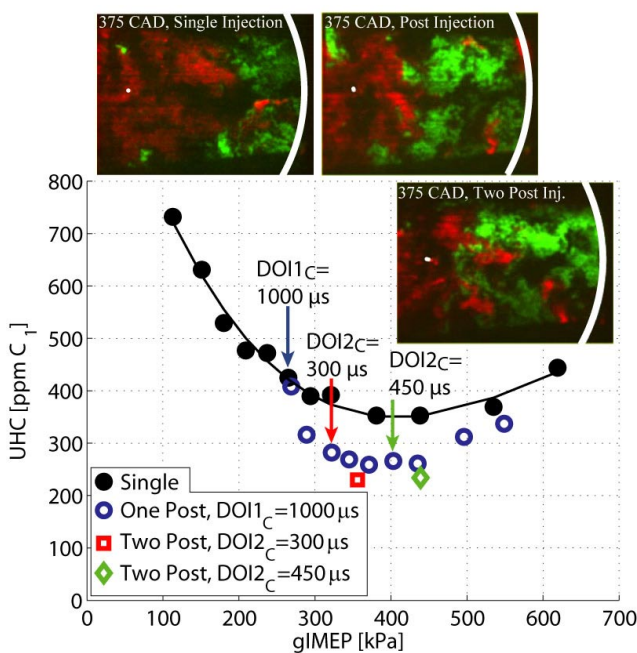


FIGURE 6. Plot: measured engine-out UHC expressed as concentration of C1 (methane) for a duration sweep of single injections (filled black circles) and a post-injection duration sweep (open blue circles) as well as two different conditions using two post injections (red and green open symbols) at a LTC condition with 12.6% intake oxygen fraction. Images: Instantaneous H_2CO -PLIF (red) and OH-PLIF (green) with laser sheets oriented along the nominal jet axis for conditions with either a single injection, one post injection, or two post injections.

very consistent performance. Such “clean” and consistent data were not achievable in previous work without the precise injection system that was installed the previous FY. Adding a second post injection (open square and diamond) can further reduce exhaust UHC, though the reductions are not as dramatic. The three images above the plot for single, post, and dual-post injections show that formaldehyde PLIF (red) is increasingly displaced by OH-PLIF (green), indicating more complete combustion in the formerly over-lean region near the injector, and hence reduced UHC emissions. Even though the post injections improve combustion efficiency by burning more of the fuel, some unburned fuel remains both in the exhaust and in the images (red), indicating that further improvements might be possible with a more optimized interaction between injections. The interaction does not appear to simply be a matter of providing more fuel after the main injection. The spatio-temporal placement and rate of mixing of the post-injected fuel appear to be important for the subsequent completeness of combustion, which suggests that the rate-of-injection could be tailored for further improvement in combustion efficiency.

CONCLUSIONS

The recent research efforts described in this report provide improved understanding of in-cylinder processes involved with post injections required by industry to build cleaner, more efficient, heavy-duty engines. Specific conclusions include:

- A new conceptual framework of exhaust soot-reduction dependencies for fuel-efficient close-coupled post injections shows how the potential for soot reduction increases with higher EGR, while the range of effective injection quantities narrows
- The post jet appears to displace main-injection soot near the bowl wall while entraining main-injection soot farther upstream, and such insight is a first step to building a conceptual model for multiple injections
- Computer models not only replicate experimental trends, but also show the spatial distribution of soot formation and oxidation with and without post injections, which provides further material for the development of a conceptual model for multiple injections
- Under LTC conditions with low combustion efficiency due to overmixing, post injections over a wide range of injection quantities extend the range of complete combustion over a wider spatial extent, thereby improving combustion efficiency

REFERENCES

1. O'Connor J and Musculus MPB. Post injections for soot reduction in diesel engines: a review of current understanding. SAE Technical Paper 2013-01-0917 SAE Int. J. of Engines 6:400-421, 2013.
2. O'Connor J and Musculus MPB. Single-injection soot-NL cinematograph. www.sandia.gov/ecn/pub-links/120329o.html, 2013.
3. O'Connor J and Musculus MPB. Post-injection soot-NL cinematograph. www.sandia.gov/ecn/pub-links/120329l.html, 2013.
4. Dec JE. A conceptual model of D.I. diesel combustion based on laser-sheet imaging. SAE Paper 970873 SAE Trans. 106(3):1319-1348, 1997.

FY 2013 PUBLICATIONS/PRESENTATIONS

1. “Conceptual models for low-load, single-injection, EGR-diluted, partially premixed low-temperature DI diesel combustion,” M.P.B. Musculus, P.C. Miles, and L.M. Pickett, Prog. Energy Combust. Sci. 39(2):246-283, 2013.
2. “Experimental facilities and measurements – fundamentals,” M.P.B. Musculus, L.M. Pickett, and S.A. Kaiser, book chapter in Encyclopedia of Automotive Engineering, accepted Oct. 2012.
3. “Effects of EGR and load on soot in a heavy-duty optical diesel engine with close-coupled post injections for high efficiency combustion phasing,” J. O’Connor and M.P.B. Musculus, submitted to Int. J. Engine Res., Dec. 2012.
4. “Effect of load on close-coupled post-injection efficacy for soot reduction in an optical, heavy-duty diesel research engine,” J. O’Connor and M.P.B. Musculus, ASME Internal Combustion Engine Fall Technical Conference, submitted March 2012.
5. “Optical investigation of the reduction of unburned hydrocarbons using close-coupled post injections at LTC conditions in a heavy-duty diesel engine,” J. O’Connor and M.P.B. Musculus, SAE Technical Paper 2013-01-0910, accepted Dec. 2012.

6. “Optical investigation of multiple injections for unburned hydrocarbon emissions reduction with low-temperature combustion in a heavy-duty diesel engine,” J. O’Connor and M.P.B. Musculus, accepted for 8th U. S. National Combustion Meeting, May 2013.
7. “Post injections for soot reduction in diesel engines: a review of current understanding,” J. O’Connor and M.P.B. Musculus, SAE Technical Paper 2013-01-0917, accepted Dec. 2012.
8. “Sandia Optical Heavy-Duty Diesel Engine and Optical Diagnostic Techniques,” presented to technical staff at Cummins and at Navistar by M.P.B. Musculus, June 2012.
9. “In-cylinder optical diagnostics of soot mitigation by close-coupled post-injections for high-efficiency heavy-duty diesel combustion,” presented to technical staff at Cummins and at Navistar by Jacqueline O’Connor, June 2012.
10. “In-cylinder optical diagnostics of soot mitigation by close-coupled post-injections for high-efficiency heavy-duty diesel combustion,” presented by Jacqueline O’Connor, AEC/HCCI Working Group Meeting, June 2012.
11. “Optical investigation of the mechanism of unburned hydrocarbons reduction using close-coupled post injections at LTC conditions in a heavy-duty diesel engine,” presented by Jacqueline O’Connor, AEC/HCCI Working Group Meeting, Feb. 2013.
12. “A conceptual model for partially premixed low-temperature combustion,” presented by M.P.B. Musculus, IEA 34th Task Leaders Meeting in Combustion Agreement, Oct. 2012.
13. “A conceptual model for low-temperature diesel combustion,” invited presentation at Chalmers University Combustion Engine Research Center Annual Review, May 2012.

II.3 Spray Combustion Cross-Cut Engine Research

Lyle M. Pickett
Sandia National Laboratories
P.O. Box 969, MS 9053
Livermore, CA 94551-9053

DOE Technology Development Manager:
Gurpreet Singh

- Evaluate internal flows within transparent injectors, transitioning to near-field mixing and dispersion at the exit of the nozzle.



INTRODUCTION

All future high-efficiency engines will have fuel directly sprayed into the engine cylinder. Engine developers agree that a major barrier to the rapid development and design of these high-efficiency, clean engines is the lack of accurate fuel spray computational fluid dynamic (CFD) models. The spray injection process largely determines the fuel-air mixture processes in the engine, which subsequently drives combustion and emissions in both direct-injection gasoline and diesel systems. More predictive spray combustion models will enable rapid design and optimization of future high-efficiency engines, providing more affordable vehicles and also saving fuel.

APPROACH

To address this barrier, we have established a multi-institution collaboration, called the ECN, to both improve spray understanding and develop predictive spray models. By providing highly leveraged, quantitative datasets (made available online [1]), CFD models may be evaluated more critically and in a manner that has not happened to date. Productive CFD evaluation requires new experimental data for the spray and the relevant boundary conditions, but it also includes a working methodology to evaluate the capabilities of current modeling practices. We have organized ECN experimental and modeling activities through frequent web conference exchanges, and made plans for an upcoming workshop. Based on standards laid out in the ECN, workshop organizers are gathering experimental and modeling results to allow a side-by-side comparison and expert review of the current state of the art for diagnostics and engine modeling for specific aspects of spray and combustion modeling.

In addition to many aspects related to diesel spray combustion, this year we have made a focused effort to characterize direct-injection gasoline sprays. Predicting spray behavior from these injection systems is difficult but important for minimization of wall wetting, preventing knock, and possibly operating in stratified-charge mode, all of which can increase efficiency. Random fluctuations in stratified combustion result in partial-burn or misfire, and eliminating these

Overall Objectives

Facilitate improvement of engine spray combustion modeling, accelerating the development of cleaner, more efficient engines.

Fiscal Year (FY) 2013 Objectives

- Lead a multi-institution, international research effort on engine spray combustion, called the Engine Combustion Network (ECN), with focus on diesel and gasoline sprays.
- Evaluated the mixing variability for direct-injection gasoline fuel injection systems at controlled conditions.
- Explore the effect of ethanol fueling on vaporization and mixing in gasoline direct injection.

FY 2013 Accomplishments

- Expanded a comprehensive spray combustion dataset working collaboratively with more than 10 different experimental institutions from around the world. Led the ECN via monthly web-meetings and frequent exchanges. ECN experimental targets are now the focus of engine combustion modeling activities worldwide.
- Applied novel diagnostics to quantify evaporation and mixing in a multi-hole gasoline injector with the focus of understanding stochastic variability in direct-injection fueling systems.
- Demonstrated how the spray collapse during the end-of-injection phase affects mixing and evaporation in iso-octane and ethanol fuel sprays.

Future Directions

- Quantify soot, soot precursor formation, and radiation heat loss at target conditions.
- Characterize multi-hole sprays compared to axial-hole sprays.

poor combustion events requires knowledge of the source. Are they caused by engine flow, ignition, or fuel delivery (i.e., the spray)? We measured the variability in fuel-air mixture linked to fuel injection hardware by experimentation in a near-quiescent pressure vessel at high-temperature conditions representative of late, stratified-charge injection. An 8-hole spark ignition direct injection spray was interrogated using high-speed schlieren and Mie-scatter imaging from multiple, simultaneous views, to acquire the vapor and liquid envelopes of the spray [2]. The mixture fraction of vaporized sections of the spray was then quantified at a plane between plumes using Rayleigh scattering. A schematic of the vessel and experimental setup for schlieren and Mie-scatter imaging is shown in Figure 1.

RESULTS

Figure 2 shows a snapshot in time indicating the vapor boundary (left, schlieren), liquid boundary from the same perspective (middle, Mie-scatter), and

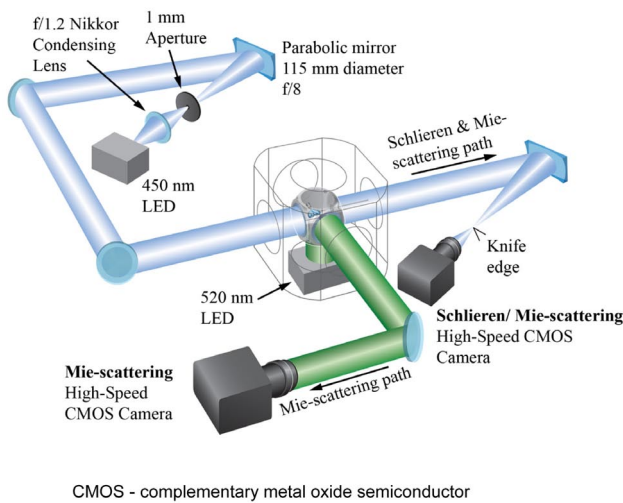


FIGURE 1. Spray chamber with combined schlieren and Mie-scattering optical setup. Schlieren and Mie-scattering imaging paths are given as blue and green, respectively. Mie-scattering was imaged along the schlieren path as well.

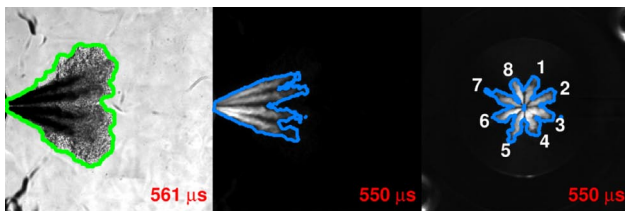


FIGURE 2. Images of schlieren (left), side-view (middle) and front-view (right) Mie-scattering. Times are referenced after start of injection. Hole numbers are indicated on the front-view Mie-scatter image at the right.

simultaneous Mie-scatter from the front view (right). The injector is orientated such that only four plumes of the 8-hole injector are visible from the side view, with the pair of plumes that fall in line, obvious from the front view (e.g., Plumes 2 and 7 fall behind one another). The vapor and liquid envelopes are distinguished by the green and blue outlines, respectively. With measurement of the plume orientation from multiple views, it is possible to reconstruct the three-dimensional orientation of each plume. Other operating conditions and description of the injector are provided at Refs. [2,3].

A composite of the liquid and vapor information together is given in Figure 3 at different times after the start of injection. The averaged (for a pair of plumes) drill angles are shown in yellow, and the averaged plume vectors are given by the red lines. At the early timing, the liquid boundary had a similar penetration to the vapor boundary as little vaporization has occurred. The plume vectors aligned with the drill angles indicates a lack of multi-hole dynamics and hole-to-hole interactions during the early part of the injection event. During the middle of injection, the bottom and top plume vectors deviate from the drill angles, moving toward the injector centerline. At the end of injection, all plumes have been noticeably attracted to the injector axis.

This plume-plume interaction, which is difficult to predict in current CFD modeling approaches, greatly affects the mixture preparation and the stochastic variability of this process. Figure 4 characterizes the variability of finding fuel vapor at the edges of a boundary from injection to injection by showing contours of probability at timings after the end of injection, when combustion is active. For instance, there is a 90% chance of producing a fuel vapor region that is the same size and penetrates the same distance as the blue region but only a 10% chance of obtaining a vapor region the size of the black region. This information is valuable for computational models that attempt to accurately reproduce the cycle-to-cycle variability seen in engines, such as large eddy simulations; the modeler can overlay their vapor boundaries on the probability contours to verify if their model agrees with experimental variability, but they must first analyze the vapor probability along the same line-of-sight as the experiment.

Shortcomings associated with line-of-sight analysis are overcome by utilizing planar mixing measurements. An example raw Rayleigh image is shown in Figure 5 at 2.2 ms after start of injection (ASI). The image plane is that depicted in Figure 4. Multiple images were acquired and converted to mixture fraction and equivalence ratio at different timings ASI, shown in Figure 6. The inner section the spray forms a “V” shape in the earliest images, which is expected considering the liquid sprays form a hollow cone. But at later times, the spray no

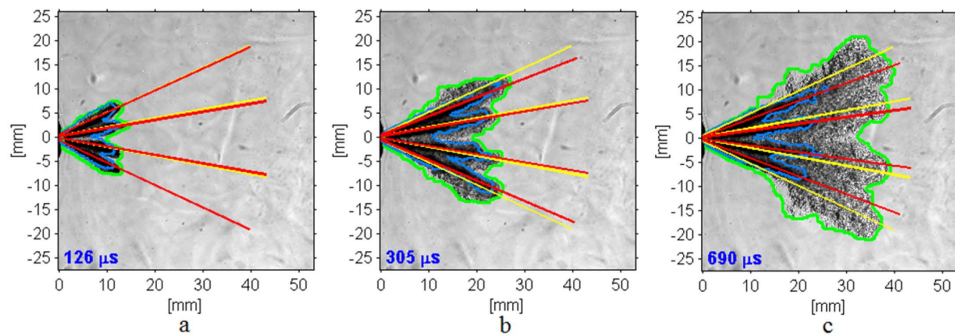


FIGURE 3. Time sequence of injection. Ambient: 900 K, 3 kg/m³, 0% O₂. Injection: iso-octane, 200 bar, 0.87 ms injection duration. Vapor and liquid envelopes are shown in green and blue, respectively. Drill angles and plume vectors are shown in yellow and red, respectively

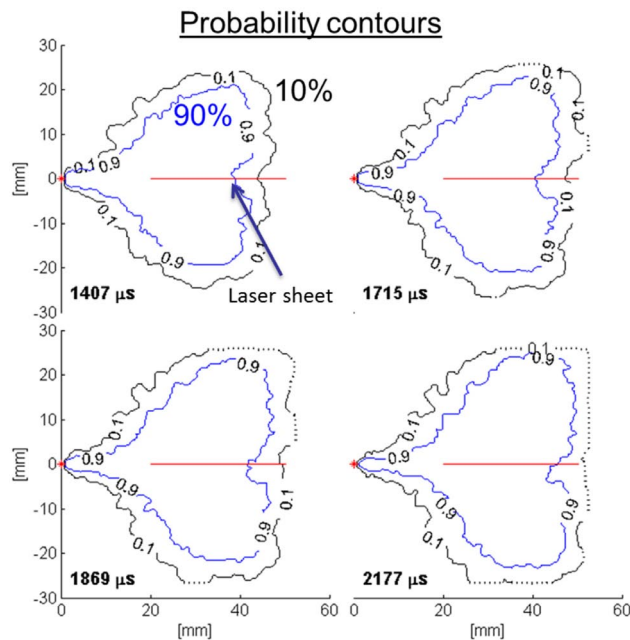


FIGURE 4. Vapor probability contours (10% and 90%) at 700 K, 6 kg/m³ conditions. Contours are derived from schlieren vapor envelopes. Dots show where the vapor crossed the field of view boundary. The red asterisk indicates the injector tip, and the red line is the laser sheet location.

longer retains this initial shape as the cone collapses as discussed above. A vapor trail appears to emerge from the center and becomes more prominent at later timings.

The equivalence ratio continues to decrease with time, and the location shifts over time. In the first two images (1,420, 1,720 μs ASI), the greatest equivalence ratio is located near the spray center with a bias toward the upper region. By the third image, the upper region clearly has a higher concentration of fuel vapor, but the fourth image shows the lower region now has a slightly greater concentration of fuel vapor. By this time, all plumes have merged and charge is carried mainly toward

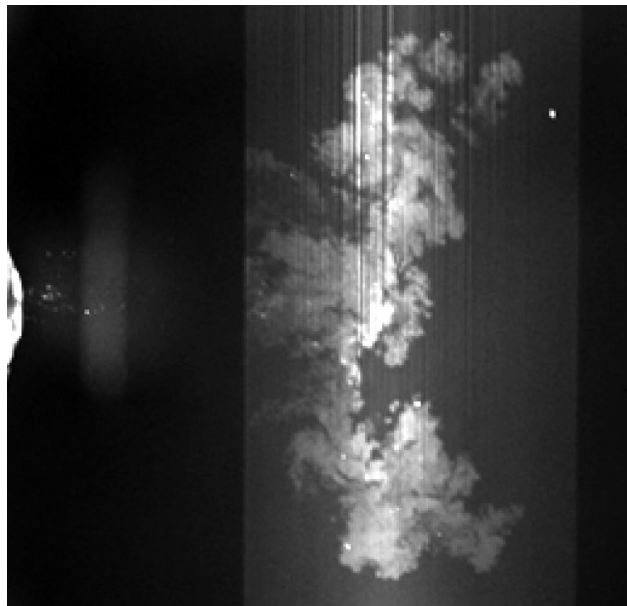


FIGURE 5. Raw planar Rayleigh scattering measurement. Molecular scattering from the ambient and the fuel jet is observable in the laser sheet area at the right.

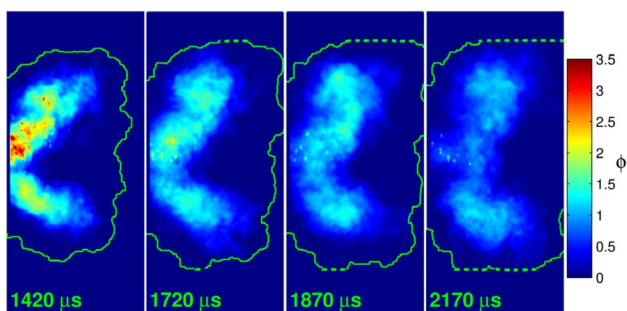


FIGURE 6. Average equivalence ratio computed from Rayleigh scatter imaging (calculated for 21% ambient oxygen). The 10% schlieren vapor probability contour is shown by the green line (with dots indicating where the vapor crossed the boundary).

the central section, filling in the middle between plumes. Understanding the plume dynamic as the injector closes is really only possible through the combination of planar measurements combined with multiple-view Mie-scatter and schlieren imaging.

CONCLUSIONS

Research this year has shown significant advances with respect to modeling and experimental coordination as a part of the ECN. In addition, a new emphasis on direct-injection gasoline sprays provides better understanding of plume interaction and quantitative mixing data that can be directly applied to model comparison and improvement. The mixture field between plumes is characterized by multi-hole and end-of-injection dynamics that attract the plumes to each other and toward the injection axis, resulting in a liquid-fuel-droplet-dense central plume in the planar measurements. Note that this type of experimentation will soon be applied to an 8-hole gasoline “Spray G” injector donated by Delphi as a target for the ECN. A dozen international laboratories have agreed to use this spray (12 identical injectors are available) as a target for future collaborative research. Research will also continue on single- and multi-hole diesel sprays. Collectively, this project provides unique information needed for the development of high-fidelity CFD models that will be used to optimize future engine designs.

REFERENCES

1. Engine Combustion Network, <http://www.sandia.gov/ECN>.
2. Blessinger, M., Meijer, M., Pickett, L.M., Manin, J., Skeen, S. Quantitative Mixing Measurements and Stochastic Variability of a Vaporizing Gasoline Direct-Injection Spray, US Combust Inst., 2013.
3. Blessinger, M., Meijer, M., Pickett, L.M., Manin, J., Skeen, S. Liquid/Vapor Penetration and Plume-Plume Interaction of Vaporizing Iso-Octane and Ethanol SIDI Sprays, ILASS, 2013.

FY 2013 PUBLICATIONS

1. Blessinger, M., Meijer, M., Pickett, L.M., Manin, J., Skeen, S. Quantitative Mixing Measurements and Stochastic Variability of a Vaporizing Gasoline Direct-Injection Spray, US Combust Inst., 2013.
2. Blessinger, M., Meijer, M., Pickett, L.M., Manin, J., Skeen, S. Liquid/Vapor Penetration and Plume-Plume Interaction of Vaporizing Iso-Octane and Ethanol SIDI Sprays, ILASS, 2013.
3. Cenker, E., Bruneaux, G., Pickett, L.M. and Schulz, C. Study of Soot Formation and Oxidation in the Engine Combustion Network (ECN), Spray A: Effects of Ambient Temperature and Oxygen Concentration. SAE Int. J. Engines 6 (1), 2013.
4. Kook, S., Zhang, R., Szeto, K., Pickett, L.M. and Aizawa, T. In-Flame Soot Sampling and Particle Analysis in a Diesel Engine. SAE Int. J. Fuels Lubr. 6 (1):80-97, 2013.
5. Kondo, K., Aizawa, T., Kook, S., and Pickett, L.M. Uncertainty in Sampling and TEM Analysis of Soot Particles in Diesel Spray Flame. SAE Technical Paper 2013-01-0908. <http://dx.doi.org/10.4271/2013-01-0908>.
6. Manin, J. Pickett, L.M., and Skeen, S.A. Two-Color Diffused Back-Illumination Imaging as a Diagnostic for Time-Resolved Soot Measurements in Reacting Sprays. SAE Int. J. Engines 6 (4), 2013.
7. Pickett, L.M., Manin, J., Payri, R., Bardi, M., and Gimeno, J. Transient Rate of Injection Effects on Spray Development. SAE Technical Paper 2013-24-0001. <http://dx.doi.org/10.4271/2013-24-0001>.

SPECIAL AWARDS AND RECOGNITION

1. Election to SAE Fellow, Lyle Pickett

II.4 HCCI and Stratified-Charge CI Engine Combustion Research

John E. Dec
Sandia National Laboratories
MS 9053, P.O. Box 969
Livermore, CA 94551-0969

DOE Technology Development Manager:
Gurpreet Singh

Overall Objectives

Provide the fundamental understanding (science-base) required to overcome the technical barriers to the development of practical Low-Temperature Gasoline Combustion (LTGC) engines, including Homogeneous Charge Compression Ignition (HCCI) and partially stratified variants of HCCI, by industry.

Fiscal Year (FY) 2013 Objectives

- Complete investigation of the effects of the ethanol content of gasoline on LTGC/HCCI thermal efficiency (TE) and load.
- Determine the potential of increasing the TE by raising the compression ratio (CR) from 14:1 to 16:1 for both premixed fueling and with partial fuel stratification (PFS).
- Complete experimental design and setup for investigations of the effect of piston-top temperatures on thermal stratification (TS) and cold-pocket distribution.
- Initiate facility upgrade for spark-assisted LTGC and higher gasoline direct injection (GDI) pressure, including design and fabrication of new cylinder heads and design of new fueling system.
- Support chemical-kinetic mechanism development at Lawrence Livermore National Laboratory (LLNL), and modeling of thermal stratification at the University of Michigan and General Motors (GM).

FY 2013 Accomplishments

- Completed evaluation of the performance effects of increasing the ethanol content of gasoline, from E0 \Rightarrow E10 \Rightarrow E20. (Base fuel, E0 \Rightarrow anti-knock index, AKI = 87, regular gasoline).
 - Evaluated the effects on stability, efficiency, high-load limit, and ability to apply PFS.

- Expanded fuels study to include investigation of: 1) E100 (pure ethanol), and 2) effects of changing the base fuel composition to a high AKI = 93 distillate fuel (certification gasoline with zero ethanol, CF-E0).
- Determined the effect of increasing the CR from 14:1 to 16:1 on the TE for both fully premixed and PFS operation.
- Optical Engine: designed and installed an aluminum piston-top with variable air-jet cooling, and evaluated vignetting/camera-position effects for boundary-layer measurements.
- With Cummins, designed and fabricated spark-plug cylinder heads, and with GM, acquired ignition systems and high-pressure GDI injectors. Designed and acquired components for high-pressure fuel-supply system.
- Conducted an initial study comparing combustion noise level (CNL) and ringing intensity (RI).
- Supported chemical-kinetic modeling at LLNL, and TS modeling at the University of Michigan and GM by providing data and analysis. Initiated collaborations with University of California, Berkeley (UC Berkeley) for computational fluid dynamics modeling of LTGC/HCCI.

Future Directions

- Extend evaluation of engine performance with CR = 16:1 over a wider range of conditions, with an emphasis on the high-load limits for both premixed and PFS fueling.
 - Analyze the potential of a Miller-cycle cam vs. increased exhaust gas recirculation (EGR) for maximizing the load range while preventing overly advanced autoignition.
- Conduct a comprehensive study of Early-direct injection (DI) PFS to determine the extent to which its benefits for increased TE and load range can be applied.
 - Determine effects of operating conditions and fuel-injection parameters.
 - Investigate the potential of multiple injections for more effective fuel stratification.
- Image fuel distributions in the optical engine to guide fuel-injection strategies for Early-DI PFS performance studies in the metal engine.
- Install spark-plug cylinder heads, and 1) determine effects of new intake-port geometry on LTGC

performance, and 2) initiate studies of spark-assisted compression-ignition LTGC combustion.

- Investigate the effects of piston-top temperature on the amount of TS and cold-pocket distribution. Also, investigate the potential of over-mixing to reduce TS.
- Expand investigations of CNL and RI with an emphasis on understanding the fundamental differences between these two metrics.
- Continue collaborations to support chemical-kinetic mechanism development at LLNL and CFD modeling of LTGC at UC Berkeley.



INTRODUCTION

Improving the efficiency of internal combustion engines is critical for meeting global needs to reduce petroleum consumption and CO₂ emissions. LTGC engines, including HCCI and partially stratified variants of HCCI, have a strong potential for contributing to these goals since they have high thermal efficiencies and ultra-low oxides of nitrogen (NO_x) and particulate emissions. Furthermore, with intake-pressure boost, LTGC can achieve loads comparable to diesel engines, as will be discussed. Perhaps most importantly, LTGC provides a means for producing high-efficiency engines that operate on light distillates, thus complementing diesel engines that use middle distillates, for more effective overall utilization of crude oil supplies and lower total CO₂ production.

Results during FY 2013 have contributed to overcoming four of DOE's technical barriers to the practical implementation of LTGC/HCCI combustion in production engines: 1) understanding fuel effects, 2) increasing the TE, 3) extending operation to higher loads, and 4) providing an improved understanding of in-cylinder processes. First, an investigation of fuel composition effects combined with Early-DI PFS fueling produced higher efficiencies and significant increases in the maximum load for a given intake-boost level. Second, the effect of raising the CR from 14:1 to 16:1 was investigated and found to offer further improvements in the TE. Third, progress has been made toward an investigation of how the in-cylinder TS is affected by the piston-top temperature. Additionally, a new study has been initiated to understand the relationship between CNL [1] and RI [2] as metrics for acceptable LTGC engine operation, and efforts are underway to upgrade our research engines for investigations of spark-assisted LTGC.

APPROACH

Studies were conducted in our dual-engine LTGC/HCCI laboratory using both the all-metal and matching optically accessible LTGC research engines (displacement = 0.98 liters). This facility allows operation over a wide range of conditions, and it can provide precise control of operating parameters such as combustion phasing, injection timing, intake temperature (T_{in}), intake pressure (P_{in}), engine speed, and mass flow rates of supplied fuel and air. The facility also allows the use of cooled EGR and is equipped with a full emissions bench (hydrocarbons, CO, CO₂, O₂, NO_x, and smoke).

The all-metal engine was used for the majority of research in FY 2013 because this work involved studies at very high loads, and precise measurements of TE and fuel effects were required. Changes in fuel composition were investigated both in terms of their fundamental effect on the propensity for autoignition, and in terms of their effects on overall performance. Differences in either the required T_{in} or the amount of cooled EGR provided a means of quantifying changes in autoignition reactivity between the fuels. The key performance parameters of peak TE and maximum load were determined by conducting knock-limited (as determined by the ringing intensity) fueling-rate sweeps over a wide range for the various fuels at several intake-boost pressures. By operating at the maximum RI without engine knock (taken to be RI = 5 MW/m² [3]) the combustion phasing was as advanced as possible, resulting in the highest TE for a given fueling rate and boost level. Since our previous work has shown that PFS produced by 100% direct-injection fueling early in the intake stroke (Early-DI PFS) has significant advantages for increasing the TE, knock-limited fueling-rate sweeps were conducted using Early-DI PFS as well as premixed fueling.

In preparation for an investigation of the effect of piston-top temperature on the development of TS, an improved optical setup was established for laser-sheet imaging measurements of TS through the cylinder-wall windows in the optical engine. Also, the piston-top window replaced with a metal piston-top instrumented with thermocouples, and an air-jet cooling system was developed to vary the temperature. For the facility upgrade, we have worked with Cummins on the design and fabrication of new cylinder heads modified to accommodate a spark plug, and with GM on obtaining higher-pressure GDI injectors.

RESULTS

The fuel's autoignition reactivity and changes in reactivity with intake boost can have a large impact on the performance of LTGC engines in terms of

stability, TE, and high-load capability. It is well known that ethanol addition can increase the octane rating of gasoline, which would be expected to decrease its autoignition reactivity at LTGC conditions. Currently, most gasoline sold in the U.S. contains 10% ethanol, and efforts are underway to increase the ethanol concentration to 15% to 20%. Also, fuels containing up to ~85% ethanol are available in some places. Accordingly, a study was conducted on the effects of ethanol blending up to 20% on LTGC performance. For this study, the base fuel was a petroleum-distillate gasoline with no ethanol (E0) and an AKI of 87, corresponding to regular-grade U.S. gasoline. Ethanol blends were produced by mixing this same gasoline with 10% and 20% ethanol (by liquid volume) to form E10 and E20, respectively. This approach eliminates variations in performance due to changes in the composition of the base fuel, while the AKI is increased by the ethanol. A certification gasoline with a higher AKI of 93 and no ethanol (CF-E0), was also investigated to understand how decreasing the fuel's autoignition reactivity without ethanol compares to ethanol addition. Finally, the performance with pure ethanol (E100) was investigated for some conditions. Table 1 gives the Research Octane Number (RON), Motor Octane Number (MON), and AKI for these fuels.

TABLE 1. Fuel Octane Numbers

| | RON | MON | AKI |
|-------|------|------|------|
| E0 | 91.0 | 82.7 | 86.9 |
| E10* | 95 | 86 | 90.5 |
| E20* | 98 | 87.5 | 92.8 |
| E100 | 109 | 90 | 99.5 |
| CF-E0 | 96.6 | 88.7 | 92.7 |

*For E10 and E20, the RON, MON and AKI are based on data in [4].

Figure 1 shows the changes in autoignition with fuel type for fully premixed LTGC (i.e. HCCI) at 1,200 rpm. As can be seen in Figure 1a, for naturally aspirated operation ($P_{in} = 1$ bar) E0, E20, and E100 have nearly identical autoignition reactivities as indicated by their very similar T_{in} and T_{bdc} values, despite large differences in their AKIs. CF-E0 requires T_{in} to be ~8°C hotter, indicating a slight lower reactivity, in line with its AKI being higher than that of E0. In contrast, Figure 1b shows that for a typical boosted condition, $P_{in} = 2.4$ bar, there is a strong consistent trend of decreasing autoignition reactivity with increasing ethanol content of the fuel, as indicated by the reduced EGR requirement (increasing percentage of intake oxygen) as ethanol content increases. This trend is in agreement with the increasing AKI of these fuels. However, it can be seen that the CF-E0 that has an AKI similar to E20 actually autoignites

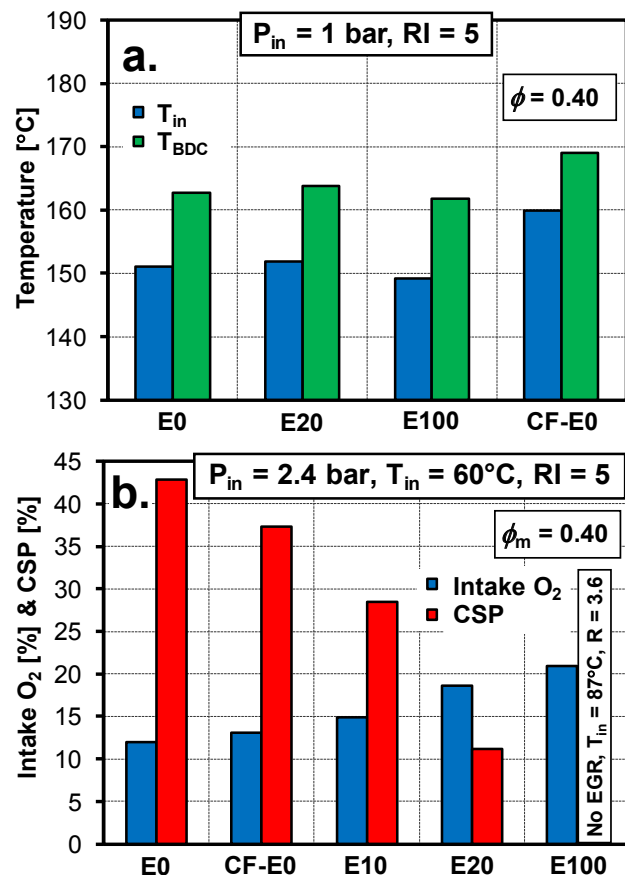


FIGURE 1. Comparison of autoignition reactivity of the fuels tested at (1a) naturally aspirated ($P_{in} = 1$ bar) and (1b) typical boosted conditions ($P_{in} = 2.4$ bar) at 1,200 rpm. In (1b), the amount of EGR is shown both by the percentage of intake oxygen and by the amount of complete stoichiometric products (CSP) introduced by the EGR (i.e. the combustion-product portion of the EGR).

more easily than E10. Thus, autoignition reactivity for boosted operation varies greatly depending on whether the AKI is increased by adding ethanol or by changing the composition of the base fuel.

Typical fueling-rate (load) sweeps for boosted operation ($P_{in} = 2.4$ bar) with premixed fueling are presented in Figure 2. As can be seen, the highest TEs occur at a moderate load for this P_{in} of about 1,000 kPa gross indicated mean effective pressure (IMEP_g). For higher loads, the TE drops because combustion phasing, as measured by the 50% burn point (CA50), must be retarded to maintain $RI \approx 5$ MW/m² (to prevent knock) as shown in Figure 2b. For lower loads, the TE drops because combustion efficiency begins to decrease rapidly as the mixture becomes overly dilute, i.e. the fuel/charge mass-ratio becomes too low, and combustion reactions do not go to completion before they are quenched by the expansion. It is interesting to note that all the fuels

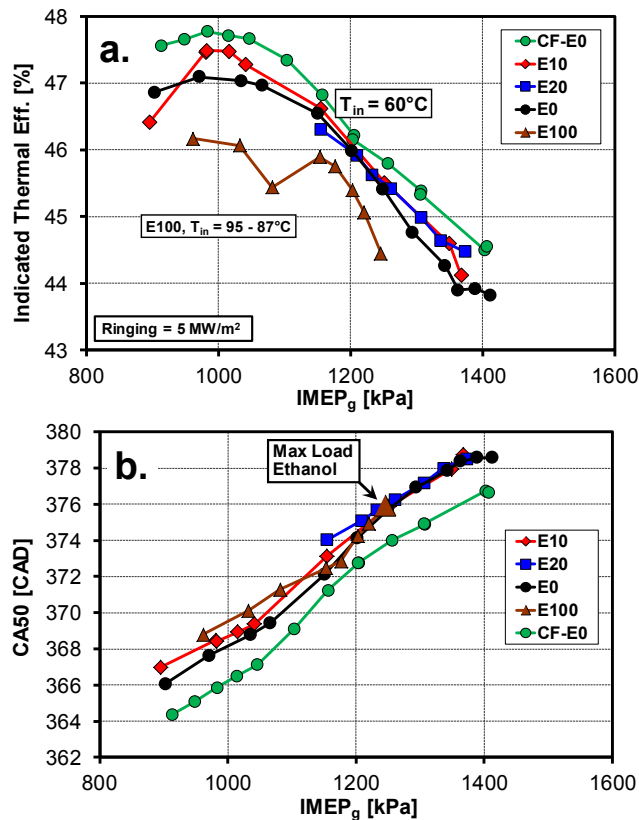


FIGURE 2. Gross indicated thermal efficiency (2a), and CA50 (2b) as a function of IMEP_g at P_{in} = 2.4 bar, RI ≈ 5 MW/m², 1,200 rpm, and T_{in} = 60°C except for E100, for which T_{in} varied from 95–87°C as load was increased.

based on E0 (E0, E10, and E20) have very similar TE (Figure 2a) and CA50 (Figure 2b) curves for all points shown. However, no E20 data are presented for loads below IMEP_g ≈ 1,150 kPa, because E20's autoignition reactivity is so low that these lower loads would have required intake heating above the T_{in} = 60°C used for the other fuels (except E100, as noted in the figure). Had additional intake heat been supplied for these lower loads, the TE would drop below that of the other fuels because heat-transfer losses would increase. This is the main reason for the lower TE with E100, which requires even more intake heating than E20 due to its lower reactivity (see Figure 1b). Thus, the TEs are similar for these fuels only as long as they have the same required T_{in}. Unlike the other fuels, CF-E0 has a higher TE at all loads even though the same T_{in} = 60°C was used. This is because less CA50 retard was required to control knock as shown in Figure 2b (most likely because CF-E0 is more sensitive to the thermal stratification). With this advantage, CF-E0 gave a peak TE of 47.8%, the highest for premixed fueling at this operating condition.

Finally, Figure 2a shows that all the fuels except E100 have about the same high-load limit at this P_{in} of ~1,400 kPa IMEP_g, in agreement with them all having

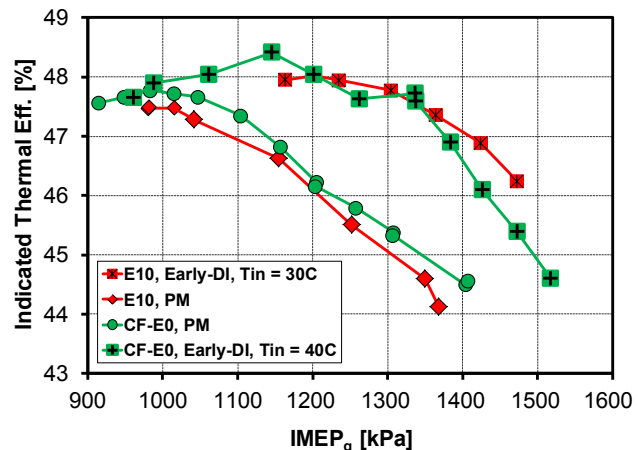


FIGURE 3. Comparison of gross indicated TE for Early-DI PFS and premixed (PM) fueling as a function of IMEP_g at P_{in} = 2.4 bar and RI ≈ 5 MW/m², 1,200 rpm. For premixed fueling, T_{in} = 60°C, and for Early-DI PFS, T_{in} = 30 or 40°C as noted in the legend.

about the same CA50 retard limit (Figure 2b). For E100, the maximum load is considerably lower because poor cycle-to-cycle stability limits CA50 retard, as shown in Figure 2b. This high instability is the result of ethanol's very weak intermediate-temperature heat release as discussed in [5,6].

As mentioned above in the Approach section and discussed in depth in [3], Early-DI PFS offers significant advantages for increased TE at intake-boosted conditions. This is because with Early-DI fueling, the charge mixture is not fully homogeneous (i.e. it is partially stratified), and for boosted operation with most distillate gasolines, regions of different equivalence ratio (ϕ) within the charge autoignite at different rates. As a result of these different ϕ regions autoigniting sequentially, the heat release rate is reduced, which allows CA50 to be more advanced while keeping RI ≈ 5 MW/m², yielding higher TEs. Additionally, with 100% DI fueling, T_{in} < 60°C can be used without concern about premixed fuel condensing in the intake system. These lower intake temperatures result in lower combustion temperatures, which reduce heat-transfer losses and increase the γ (c_p/c_v) of the combustion products allowing more work to be extracted during the expansion stroke. Therefore, Early-DI PFS with reduced T_{in} was investigated to determine its potential for increasing the TE, and for increasing the maximum load at a given boost pressure.

Figure 3 compares TEs for fueling-rate sweeps using Early-DI PFS with those for the premixed sweeps from Figure 2, for E10 and CF-E0 at P_{in} = 2.4 bar, RI ≈ 5 MW/m². For both fuels, Early-DI fueling with reduced T_{in} gives substantially higher TEs over most of the load range, and the peak TE is increased to 48.4%. Further analysis shows that CA50-advance is a major

contributor to this TE improvement, with CA50 being advanced by 4–5° CA for E10 and by 3–4° CA for CF-E0 compared to premixed fueling. Early-DI PFS was also found to work well with E0, but not for E20. The higher ethanol content of E20 was found to reduce the sensitivity of autoignition to ϕ variations, reducing the benefits from the PFS and producing some stability problems.

To investigate the potential of increasing the CR to further increase the TE, the piston geometry was changed to raise the CR from 14:1 to 16:1. With this higher CR, fueling-rate sweeps like those in Figures 2 and 3 were acquired to determine peak TE and maximum load at several intake-boost pressures and for naturally aspirated operation. Figure 4 presents an example of these results for Early-DI PFS with CF-E0 at $P_{in} = 2.4$ bar compared to data at the same conditions with CR = 14:1 (from Figure 3). As can be seen, the higher CR increases the TE by ~0.7 thermal-efficiency percent-units across the load range. Slightly greater gains in TE were found for other P_{in} , and the highest peak TE achieved increased to 49.2% with the CR = 16:1 piston.

The effects of fuel-type and fueling strategy on the high-load limits as a function of boost pressure are shown in Figure 5. Starting with premixed operation (i.e. HCCI), it can be seen that the maximum load is increased from 16.3 to 18.1 to 20.0 bar IMEP_g for E0, E10, and E20, respectively. This load increase is possible because the ethanol blending reduces the autoignition reactivity, which reduces the amount of EGR required to retard CA50 to maintain RI ≈ 5 MW/m², leaving more air available for combustion. Although this allows loads up to 20 bar IMEP_g, P_{in} must be increased up to 3.6 bar to achieve this. However, with Early-DI PFS, significantly less boost is required to obtain a given load compared to

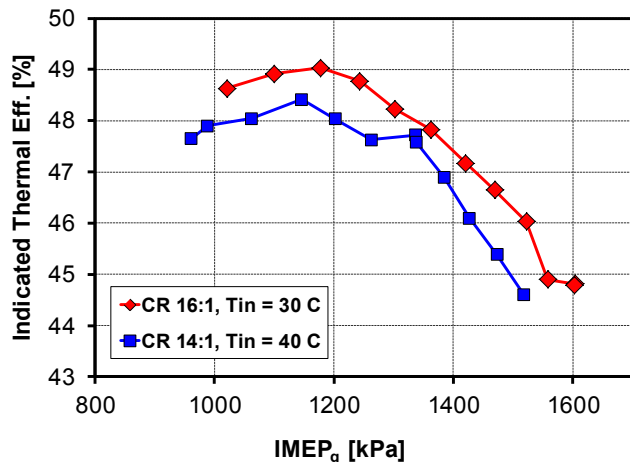


FIGURE 4. Comparison of TEs for CR = 16:1 and CR = 14:1 as a function of IMEP_g for Early-DI PFS fueling at $P_{in} = 2.4$ bar and RI ≈ 5 MW/m². $T_{in} = 30$ or 40°C as noted in the legend.

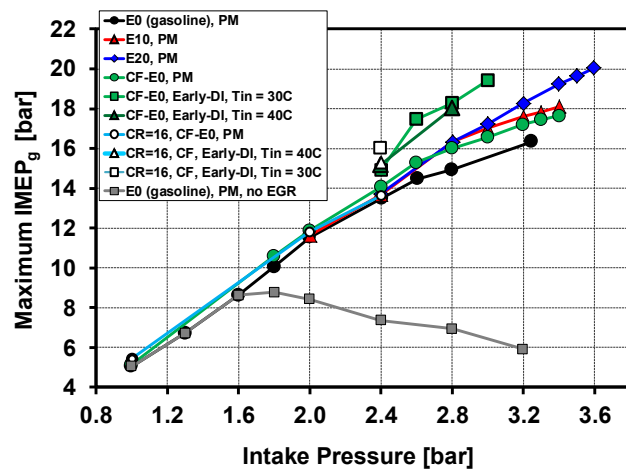


FIGURE 5. High-load limits as a function of intake pressure for premixed (PM) and Early-DI PFS fueling for several fuels. All data are for CR = 14:1, except those noted in the legend as CR = 16, for which only CF-E0 was used. All points have no knock (RI ≈ 5 MW/m²), and NOx and particulate emissions well below U.S. 2010 standards.

premixed fueling, when using a fuel whose autoignition is sufficiently sensitive to the nonuniformities in fuel distribution, such as the CF-E0 shown in Figure 5. For example, a load of 19.4 bar IMEP_g can be reached with $P_{in} = 3.0$ bar using Early-DI PFS, compared to a required $P_{in} = 3.45$ bar for premixed operation with E20. It is also evident in Figure 5 that for any given $P_{in} \geq 2.4$ bar, CF-E0 reaches a significantly higher load with Early-DI PFS than with premixed fueling.

Combustion-generated engine noise is an important issue for LTGC/HCCI as well as other forms engine combustion, and both the CNL and RI have been commonly used to quantify it. Because the relationship between these two metrics is not well understood, a study was initiated to examine these two cylinder-pressure analysis techniques, and to explain the advantages and disadvantages of each. Toward this goal, comparisons of the CNL and RI were made over a range of LTGC operating conditions. The results show that the two metrics track each other for some variations in engine operation but not for others. In general, it was found that RI better predicts the onset of engine knock (one key source of noise), while the CNL appears to better represent the overall engine-combustion noise for non-knocking operation. As indicated under “Future Directions,” this effort will continue in FY 2014 with an in-depth analysis of these two methodologies to determine how the two metrics should be applied.

CONCLUSIONS

- A comprehensive study on the effects of increasing the AKI of gasoline (i.e. reducing its autoignition

reactivity) by: 1) blending with ethanol up to 20%, or 2) by changing the composition of the base fuel showed that the two methods have quite different effects for LTGC.

- E0, E10, E20, and E100 all had nearly identical autoignition characteristics for naturally aspirated LTGC. However, for intake-boosted operation, the autoignition reactivity was progressively and substantially reduced with increasing ethanol content.
- In contrast, increasing the AKI by changing the composition of the base fuel reduced autoignition reactivity modestly at both naturally aspirated and boosted conditions.
- Overall, the AKI is not a good indicator of LTGC autoignition reactivity; however, it did indicate trends within each class of fuels (E0, E10, E20, and E100) or (E0 vs. CF-E0).
- For boosted operation with $P_{in} \geq 2.4$ bar and premixed fueling, blending with ethanol up to 20% has little effect on the TE, but CF-E0 gives a slightly higher TE because it allows CA50 to be more advanced without knock.
- Blending gasoline with up to 20% ethanol is beneficial for extending the high-load limit for premixed operation from 16.3 to 18.1 to 20.0 bar IMEP_g for E0, E10, and E20, respectively.
 - The maximum load for E100 is considerable lower, because it requires intake heating even at high boost levels and poor cycle-to-cycle stability limits CA50 retard.
- Early-DI PFS fueling provides substantial benefits for increased TE and load compared to premixed fueling when the ethanol content $\leq 10\%$, and for the high-AKI base fuel (CF-E0). However, with its higher ethanol content, E20 did not work well with PFS.
- Using Early-DI PFS, a load of 19.4 bar IMEP_g was achieved with $P_{in} = 3.0$ bar, compared to a required $P_{in} = 3.45$ bar to reach this load for premixed operation, which is a significant advantage for turbocharger design.
- Increasing the CR from 14:1 to 16:1 increased the TE at all conditions investigated.
 - A peak TE of 49.2% was achieved with CR = 16:1, compared to 48.4% for CR = 14:1.
 - The higher CR caused no reduction in maximum load for intake pressures up to 2.4 bar (using CF-E0).

- RI appears to be a better predictor of the onset of LTGC engine knock, while CNL better represents engine-combustion noise for non-knocking conditions.

REFERENCES

1. Shahlari, A., Hocking, C., Kurtz, E., and Ghandhi, J., “Comparison of Compression Ignition Engine Noise Metrics in Low-Temperature Combustion Regimes,” *SAE Int. J. Engines* 6(1):541-552, 2013, doi:10.4271/2013-01-1659.
2. Eng, J.A., “Characterization of Pressure Waves in HCCI Combustion,” SAE Technical Paper 2002-01-2859, 2002, doi:10.4271/2002-01-2859.
3. Dec, J.E., Yang, Y., and Dronniou, N., “Improving Efficiency and using E10 for Higher Loads in Boosted HCCI Engines,” *SAE Int. J. Engines* 5(3):1009-1032, 2012, doi:10.4271/2012-01-1107.
4. Anderson, J., Leone, T., Shelby, M., Wallington, T., Bizub, J., Foster, M., Linsky, M., Polovina, D., “Octane Numbers of Ethanol-Gasoline Blends: Measurements and Novel Estimation Method from Molar Composition,” SAE Technical Paper 2012-01-1274, 2012, doi:10.4271/2012-01-1274.
5. Dec, J. and Yang, Y., “Boosted HCCI for High Power without Engine Knock and with Ultra-Low NOx Emissions – using Conventional Gasoline,” *SAE Int. J. Engines* 3(1):750-767, 2010, doi:10.4271/2010-01-1086.
6. Sjöberg, M. and Dec, J.E. “Ethanol Autoignition Characteristics and HCCI Performance for Wide Ranges of Engine Speed, Load and Boost,” *SAE Int. J. Engines*, 3(1):84-106, 2010, doi:10.4271/2010-01-0338.

FY 2013 PUBLICATIONS/PRESENTATIONS

1. Yang, Y. and Dec, J.E. “Bio-Ketones: Autoignition Characteristics and Their Potential as Fuels for HCCI Engines,” DOE Advanced Engine Combustion Working Group Meeting, US Car, Southfield, MI, August 20–21, 2013.
2. Dernotte, J., Dec, J.E., and Ji, C. “Combustion noise analysis of HCCI and partially stratified HCCI-like engines,” DOE Advanced Engine Combustion Working Group Meeting, US Car, Southfield, MI, August 20–21, 2013.
3. Yang, Y. and Dec, J.E., “Bio-Ketones: Autoignition Characteristics and Their Potential as Fuels for HCCI Engines,” SAE Technical Paper 2013-01-2627, to be presented at the SAE/KSME 2013 Powertrains, Fuels and Lubricants Meeting, Seoul, South Korea, October 21–23, 2013.
4. Dec, J. E., Encyclopedia of Automotive Engineering, Section entitled “Advanced Compression-Ignition Combustion Systems for High Efficiency and Ultra-Low NOx and Soot Emissions,” Wiley and Sons, submitted August 2013, expected publication late 2013, or early 2014.
5. Dec, J. E. “Progress on Gasoline CI Combustion – Effects of Fuel Reactivity, Fueling Strategy, and CR on Efficiency

- and Load,” International Energy Agency 35th Task Leaders Meeting, San Francisco, CA, July 22–25, 2013.
- 6.** Yang, Y. and Dec, J., “Bio-Ketones: Autoignition Characteristics and Their Potential as Fuels for HCCI Engines,” Tailor-Made Fuels from Biomass – International Conference, Aachen, Germany, June 18–20, 2013.
- 7.** Ji, C., Dec, J., Dernotte, J., and Canella, W., “Increasing the HCCI Autoignition Reactivity of Gasoline Using Conventional Ignition Improvers,” 8th U.S. National Combustion Meeting, Salt Lake City, UT, May 20, 2013.
- 8.** Dec, J.E., Yang, Y., Ji, C., Dernotte, J., “The Effects of Gasoline Reactivity and Ethanol Content on Boosted HCCI Performance,” DOE Advanced Engine Combustion Working Group Meeting, Livermore, CA, February 5–7, 2013.
- 9.** Dec, J.E., “Increasing the Load Range and Efficiency of HCCI Engines using Fuel Stratification,” Combustion Energy Frontiers Research Center (CEFRC), Livermore, CA, November 14, 2012.
- 10.** Dec, J.E., Yang, Y., and Dronniou, N., “Improving Efficiency and using E10 for Higher Loads in Boosted HCCI Engines,” *SAE Int. J. Engines* 5(3): 1009-1032, 2012, doi:10.4271/2012-01-1107.

- 11.** Yang, Y., Dec. J.E., Dronniou, N. and Canella, W., “Boosted HCCI Combustion Using Low-Octane Gasoline with Fully Premixed and Partially Stratified Charges,” *SAE Int. J. Engines* 5(3): 1075-1088, 2012, doi:10.4271/2012-01-1120.
- 12.** Dronniou, N. and Dec, J.E., “Investigating the Development of Thermal Stratification from the Near-Wall Regions to the Bulk-Gas in an HCCI Engine with Planar Imaging Thermometry,” *SAE Int. J. Engines* 5(3): 1046-1074, 2012, doi:10.4271/2012-01-1111.

SPECIAL RECOGNITIONS & AWARDS/ PATENTS ISSUED

- 1.** SAE Arch T. Colwell Award for SAE paper 2011-01-1291, *SAE Int. J. Engines*, 4(1): 1669-1688, 2011.
- 2.** Most cited article in the Proceedings of the Combustion Institute since 2008: Dec, J. E., *Proc. Combust. Inst.*, 32: 2727-2742, 2009.
- 3.** U.S. Patent Application Filed: Dec, J., Ji, C., Cannella, W., and Maria, A., “A Method for Extending the High-Load Limit of Internal Combustion Engines Operated in a Low-Temperature Combustion Mode,” DOE-S no. 132389.

II.5 Automotive Low-Temperature Gasoline Combustion Engine Research

Richard Steeper
Sandia National Laboratories, MS 9053
P.O. Box 969
Livermore, CA 94551-0969

DOE Technology Development Manager:
Gurpreet Singh

Overall Objectives

- Perform fundamental engine research addressing technical barriers to the achievement of DOE efficiency and emissions goals for automotive gasoline engines.
- Develop and apply advanced diagnostics in an optically accessible Homogeneous Charge Compression Ignition (HCCI) engine to enhance our knowledge of fundamental in-cylinder processes.
- Advance the capabilities of engine simulation and analysis tools by validating with research-engine data.
- Disseminate knowledge gained from experiments through collaborative interaction with industry, academic, and national lab partners.

Fiscal Year (FY) 2013 Objectives

- Develop full-cylinder gas sampling and analysis system for the lab's research engine.
- Apply sampling system to characterize the chemistry of negative valve overlap (NVO) fueling and its effect on compression ignition. Interpret results using chemical kinetics modeling tools.
- Define and execute joint experiments with Oak Ridge National Laboratory (ORNL) to leverage common NVO research threads.

FY 2013 Accomplishments

- A full-cylinder gas sampling technique has been used to characterize species produced during NVO reactions as a function of NVO fuel-injection timing. Confirmed that acetylene is produced in sufficient quantity to chemically enhance compression ignition in the research engine. This work addresses engine manufacturer requests for physical and chemical details of strategies to control HCCI combustion phasing.

- Applied CHEMKIN simulation to identify the NVO reaction products responsible for chemically enhancing main HCCI combustion.
- Submitted proposal to Lawrence Berkeley National Lab (LBNL) to apply photoionized molecular beam mass spectroscopy for complete speciation of engine gas samples and calibration of the gas chromatograph used in the Sandia lab (see Future Directions).
- Performed joint experiments with ORNL that identified optimal NVO injection parameters for production of hydrogen and carbon monoxide gas in rich NVO environments. Such onboard generation of synthesis gas could benefit gasoline engine operation through enhanced dilution tolerance and knock avoidance.

Future Directions

- Complete NVO sampling experiments. Use LBNL facilities to improve sample speciation if proposal is accepted. Compare results using gasoline in place of the surrogate fuel iso-octane.
- Initiate new research direction on innovative ignition sources required for advanced gasoline-combustion engines. Identify industry needs, research capabilities, and potential partners. Perform scoping experiments.



INTRODUCTION

Challenges to the implementation of gasoline HCCI combustion—including phasing control, operating-range extension, and emissions control—all can benefit from advanced charge-preparation strategies. Alternative strategies such as retarded direct injection and variable valve timing can be used to modify local charge composition and temperatures, thereby controlling ignition phasing, rate of heat release, combustion efficiency, and engine-out emissions. A current focus of our research is understanding the NVO strategy for HCCI combustion. Partial fueling during the NVO period can affect main combustion both thermally (NVO reactions elevate residual gas temperature) and chemically (NVO reformation reactions produce species that are carried over to main combustion), and understanding these effects is necessary in order to take full advantage of

the strategy. Knowledge gained in this project supports DOE's goal of developing advanced energy-efficient, low-emission engine technologies.

APPROACH

Multiple diagnostics are applied in our gasoline compression-ignition engine to quantify in-cylinder processes. Direct imaging allows assessment of fuel injection; laser-induced fluorescence imaging quantifies composition and temperature distributions; chemiluminescence imaging characterizes ignition and combustion processes; laser-absorption produces time-resolved histories of select species; and dump sampling provides detailed charge compositions. Application and improvement of computational fluid dynamics/combustion models is facilitated through continuing collaborations with university and national lab partners. Regularly scheduled technical exchanges with manufacturers, national labs, and academia leverage the knowledge gained in the research project.

RESULTS

FY 2013 research has focused on directly measuring the chemical composition of the reaction products of NVO fueling. To this end, the team developed a custom sampling valve specifically suited to NVO operation. Typically, cylinder sampling relies on microvalves that are easy to deploy, but unable to deliver samples representative of entire-cylinder contents. In contrast, the dump valve developed in this project captures a large fraction of NVO products from a single cycle. The new valve, illustrated in Figure 1, is mounted in an unused spark-plug port and is triggered soon after intake valve closing (IVC), so that the collected sample is composed of NVO gases mixed with intake air. Speciation of such samples provides crucial details to understand variation in NVO composition with operating conditions, and to understand the chemical effect of NVO products on compression ignition and combustion in the engine.

Figure 2 shows the heated manifold designed to transfer extracted samples from the engine to an initially evacuated sample bottle. Each sample is captured during a single dump cycle that is triggered after establishing steady-fired NVO-HCCI operation. The volume of each of the samples captured in the bottle typically represents about 30% of engine displacement, and after performing multiple dump events, the total sample comprises a cycle-averaged composition characteristic of cylinder contents at IVC. Following sample collection, the engine is stopped, and a small volume of the sample is analyzed using a triple-column gas chromatograph configured to quantify C₁-C₈ hydrocarbons, hydrogen,

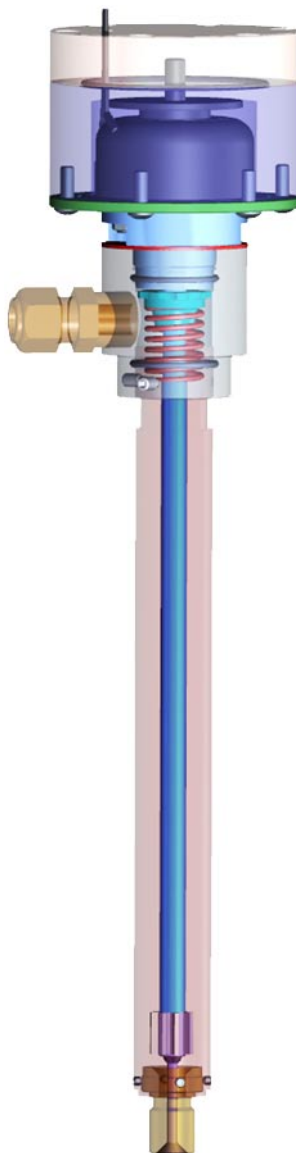


FIGURE 1. Schematic of Sandia dump valve assembly.

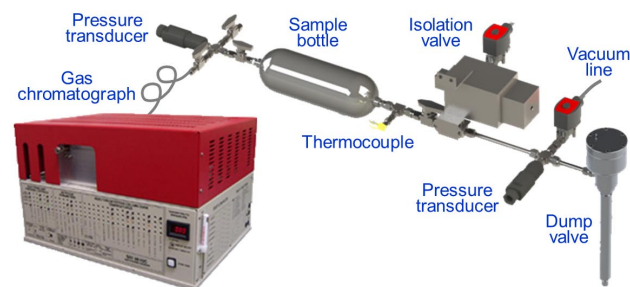


FIGURE 2. Schematic of dump valve, sample gas manifold, and gas chromatograph.

CO, CO₂, water, and oxygen. Repeated experiments and gas chromatograph analyses indicate an achieved repeatability of approximately +/-10% for the majority of measured species.

Prior experiments have provided evidence of a chemical effect of NVO fuel-injection timing on main combustion. To understand this effect, sampling experiments were performed for a sweep of fuel-injection timing ranging from 55 to 5 crank-angle degrees (CAD) before top center of NVO. Main combustion is enhanced by retarding NVO start-of-injection (SOI) timing, as witnessed in Figure 3 by an increasing apparent heat release (AHR) and an initially advancing 50% burn angle (CA50). Species profiles derived from these experiments provide important details of the chemistry responsible for this enhancement.

Several key hydrocarbon profiles are plotted in Figure 4. Not surprisingly, iso-octane, the parent fuel in these experiments, is present in the NVO product gases at relatively high concentrations compared to other detected hydrocarbons. (Note that the *main* fuel injection, which normally takes place during intake, is suppressed for the dump cycle, so that the iso-octane concentrations plotted represent unreacted NVO fuel only.) Many of the hydrocarbon products of NVO reactions show only a minor dependency on NVO SOI timing, similar to the Figure 4 trend in iso-octane data. But several small species, represented by hydrogen, methane, and acetylene/ethylene in Figure 4, show an abrupt increase in concentration associated with late-NVO injection. The observed order-of-magnitude increase in hydrogen, combined with known combustion enhancement due to hydrogen, suggests that it contributes to the observed chemical effects of NVO fueling. Based on prior seeding

experiments, acetylene is another known promoter of combustion, so the observed rise in acetylene production for late NVO SOI provides evidence that it too contributes to main combustion enhancement. Finally, it is encouraging to note that the measured NVO product concentrations validate previous experimental measurements. For example, previously recorded in-cylinder concentrations of CO using a laser-absorption diagnostic agree very well with the current CO measurements.

To gain further insight into chemical effects of specific NVO products, CHEMKIN's one-dimensional engine simulator and Lawrence Livermore National Lab's (LLNL) detailed iso-octane kinetic mechanism were used to model main combustion of the HCCI-NVO cycle. Measured concentrations of NVO products from early and late-NVO fueling were used as initial conditions for the simulations. As shown in Figure 5, a dramatic advancement in combustion phasing and an increase in peak heat release are predicted for the late NVO SOI case, in agreement with experimental trends. Furthermore, by selectively perturbing initial concentrations of key species one at a time in the simulation, acetylene was identified as the dominant factor advancing combustion phasing. A significant effect of hydrogen was also predicted (but a factor of 5 lower than acetylene), while dimethyl ether and ethylene at experimental concentrations were predicted to have an insignificant effect on main combustion.

Sandia's NVO sampling work was performed in collaboration with General Motors, LLNL, and ORNL. Sandia collaboration with ORNL notably included joint experiments to leverage the impact of each lab's project. ORNL is currently interested in exploiting reformation

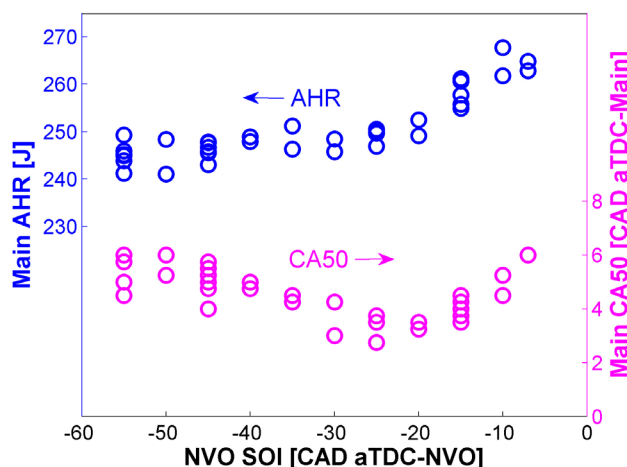


FIGURE 3. Apparent heat release and location of 50% burn point of main combustion under low-load, lean conditions for a range of NVO SOI timings.

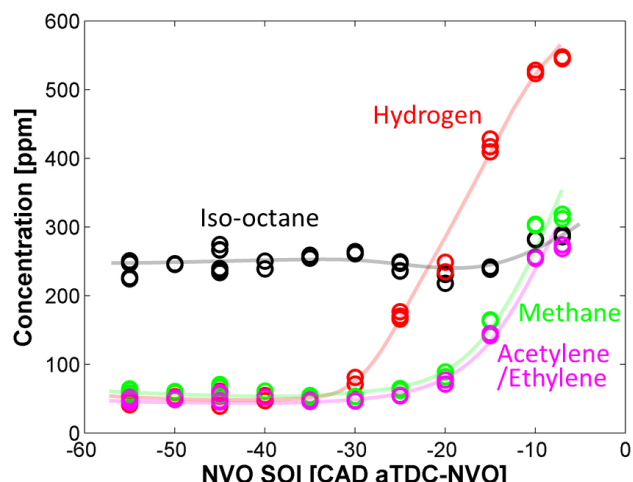


FIGURE 4. Select species concentrations determined by dump sampling and gas chromatography. Acetylene and ethylene are grouped due to inability of gas chromatograph columns to separate these C₂ species.

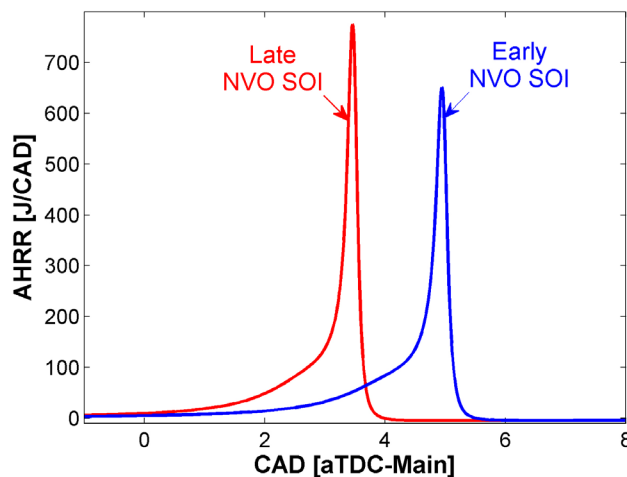


FIGURE 5. Chemical kinetics simulation of apparent heat release rate for main combustion. The two curves represent an early and a late NVO SOI case.

chemistry that occurs under rich NVO conditions, and have developed a unique 6-stroke cycle that enables sampling and analysis of NVO using technology distinct from Sandia's. Experiments at Sandia were conducted using ORNL conditions, to facilitate comparison of results. Selected species concentrations in Figure 6 illustrate the excellent agreement achieved. At the top of the figure, the principle reformation product, carbon monoxide, is plotted for the two experiments. Due to many differences in the experiments including engine geometry, load, and chemical analysis techniques, it is not surprising to see differences in absolute concentrations. Yet the near-linear trends in carbon monoxide as a function of NVO fuel-injection timing match very well. In a second example at the bottom of Figure 6, propylene exhibits a more complex, non-linear trend that is again captured well by both facilities. Results of the joint experiments enhance confidence in ORNL conclusions concerning optimization of reforming chemistry via NVO fuel-injection timing.

CONCLUSIONS

- Full-cylinder sampling in an HCCI-NVO engine enables characterization of the chemical products of NVO fueling, supporting the conclusion that late-NVO injection of iso-octane can produce acetylene and other reactive species in sufficient quantity to chemically affect main combustion.
- Chemical kinetic modeling using the current LLNL iso-octane mechanism supports the trends observed in the experiments during a sweep of NVO injection timing.

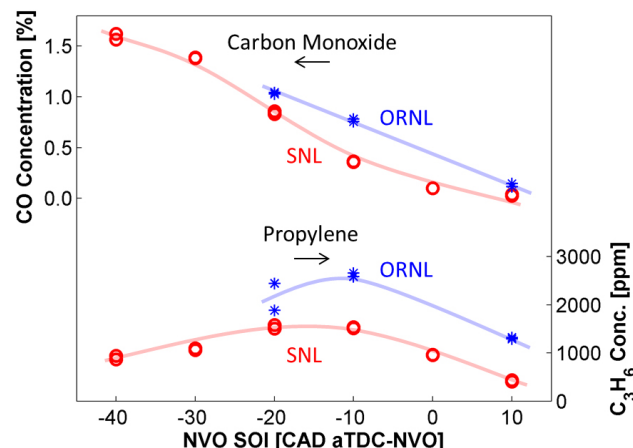


FIGURE 6. Comparison of species concentrations in NVO products measured at ORNL and Sandia under rich NVO conditions.

- Experiments performed with distinctly different equipment at ORNL and Sandia have produced very similar conclusions concerning trends in NVO reformate composition with NVO fuel-injection timing.

FY 2013 PUBLICATIONS/PRESENTATIONS

1. Steeper, R.R., "Automotive HCCI Combustion Research," DOE/OFCVT Advanced Combustion Technologies FY12 Annual Report, 2012.
2. Steeper, R.R., "Automotive HCCI Engine Research," DOE Vehicle Technologies Annual Merit Review, Arlington, VA, May 14, 2013.
3. Steeper, R.R., "Cylinder Gas Sampling during Negative Valve Overlap Operation," DOE Advanced Engine Combustion Working Group Meeting, USCAR, Detroit, August 20, 2013.
4. Steeper, R.R. and Davisson, M.L., "Analysis of Gasoline Negative-Valve-Overlap Fueling via Dump Sampling," SAE International Technical Paper 14PFL-0703, 2014.
5. Szybist, J.P., Steeper, R.R., Splitter, D., Kalaskar, V.B., Pihl, J., and Daw, C., "Negative Valve Overlap Reforming Chemistry in Low-Oxygen Environments," SAE International Technical Paper 14PFL-0435, 2014.

II.6 Spray and Combustion Modeling using High-Performance Computing Tools

Sibendu Som (Primary Contact),
Douglas E. Longman, Qingluan Xue,
Michele Battistoni
Argonne National Laboratory
9700 S. Cass Ave.
Argonne, IL 60439

DOE Technology Development Manager:
Gurpreet Singh

Overall Objectives

- Development of physics-based nozzle flow and spray models. Develop capability to perform coupled nozzle flow and spray simulations.
- Development and validation of high-fidelity turbulence models for diesel engine applications.
- Development and validation of reduced chemical-kinetic models for realistic diesel fuel surrogates.
- High-Performance Computing (HPC) tool development on codes used by the industry for internal combustion engine (ICE) applications.

Fiscal Year (FY) 2013 Objectives

- Implement in-nozzle flow models in CONVERGE code [1] followed by extensive validation against experimental data accounting for needle transients and off-axis motion.
- Demonstrate the benefits of higher-fidelity turbulence models such as large eddy simulations (LES) vs. lower-fidelity models such as Reynolds Averaged Navier-Stokes (RANS).
- Implement advanced load-balancing algorithms to ensure better speedup on high number of cores and demonstrate scalability on ~1,000 processors.
- Develop and validate a reduced chemical kinetic mechanism using n-dodecane as a surrogate for diesel fuel.

FY 2013 Accomplishments

- We have performed three-dimensional, transient, turbulent in-nozzle flow simulations. For the first time, needle off-axis (wobble) motion has been accounted for in the simulations. For multi-hole

injectors, the needle wobble is shown to have a profound influence on mass flow rate from each orifice.

- Lagrangian droplet models are widely used for engine simulations. However, many researchers have reported a strong dependency on the grid size. This large grid size dependency makes it difficult for modelers to know ahead of time what cell size to utilize. We have recently demonstrated grid-convergence on diesel sprays using LES turbulence models.
- LES was a major thrust area, and performance of LES with respect to RANS calculations was assessed in detail. It was demonstrated that LES can capture cyclic variability and performs both qualitatively and quantitatively better than RANS for spray calculations. However, the computational cost of performing LES is significantly greater than that of RANS due to the need for multiple realizations with LES.
- Typical production-type engine simulations in the industry are performed on 16-32 processors. We have performed engine simulations on 1,024 processors in a scalable fashion. These simulations were performed with a peak cell count of 50 million cells, which is the largest diesel engine simulation run to date. This simulation provided unprecedented insights into the combustion process.
- We have developed and validated a 106-species-based reduced reaction model for n-dodecane as surrogate for diesel fuel. This mechanism is being used by industry and academia extensively through the Engine Combustion Network initiated by Sandia National Laboratories [2].

Future Directions

- Perform nozzle flow simulations with production multi-hole injectors using the best-available geometry information and needle lift profiles. Couple the nozzle flow simulations with classical spray simulations to understand the influence of in-nozzle flows on spray and combustion processes.
- Implement the best practices developed for LES calculations on engine simulations with different engine geometries available in literature. This will provide a clear path for engine manufacturers to take advantage of our high-fidelity computational studies.

- Develop a near-nozzle Eulerian spray modeling approach that, in principle, is significantly different from a classical spray modeling approach, that is Lagrangian in nature [3]. Dynamically couple the nozzle flow simulations with the Eulerian approach for near-nozzle spray simulations.
- Develop a two-component surrogate (n-dodecane and m-xylene) mechanism for diesel fuel and validate against experimental data in constant-volume combustion chamber [2] and single-cylinder engine conditions.
- Systematically improve the fidelity of the simulations by improving the nozzle flow, spray, turbulence, and combustion models. The computational cost is likely to increase significantly due to the use of these robust models. Develop high-performance computing capabilities to ensure reasonable wall-clock times with these higher-fidelity models.



INTRODUCTION

ICE processes are multi-scale and highly coupled in nature and characterized by turbulence, two-phase flows, and complicated spray physics. Furthermore, the complex combustion chemistry of fuel oxidation and emission formation makes engine simulations a computationally daunting task. Given the cost for performing detailed experiments spanning a wide range of operating conditions and fuels, computational fluid dynamics (CFD) modeling aided by HPC has the potential to result in considerable cost savings. Development of physics-based CFD models for nozzle flow, spray, turbulence, and combustion are necessary for predictive simulations of the ICE. HPC can play an important role in ICE development by reducing the cost for design and optimization studies. This is largely accomplished by being able to conduct detailed simulations of complex geometries and moving boundaries with high-fidelity models describing the relevant physical and chemical interactions, and by resolving the relevant temporal and spatial scales. These simulations provide unprecedented physical insights into the complex processes taking place in these engines, thus aiding designers in making judicious choices. The major focus of our research in FY 2013 has been towards the development and validation of robust and predictive nozzle flow and turbulence models for diesel engine applications aided by HPC tools.

APPROACH

During the past year, we have focused on improving the fidelity of nozzle flow and turbulence models by using

higher temporal and spatial resolutions to ensure grid convergence [4]. Our approach to improved modeling capability is highlighted here:

1. In-nozzle flow simulations are performed by implementing a Homogeneous Relaxation Model-based two-phase flow model within a volume-of-fluid approach [5] in CONVERGE CFD code. The boundary conditions for the simulations are obtained from X-ray phase-contrast imaging at Argonne National Laboratory, which includes the needle-lift and wobble profiles [6]. The multi-hole geometry information is obtained from a previous study [7].
2. A key element in our research has been to demonstrate grid-convergence on diesel spray and engine simulations [4] within both RANS and LES frameworks. The following approach has been implemented in CONVERGE code and is critical to achieving grid convergence: adaptive mesh refinement, fully implicit momentum coupling, improved liquid-gas coupling, and improved temporal and spatial liquid mass distribution.
3. LES calculations have been performed with higher resolution compared to what is typically used in the engine modeling literature. The finest resolution simulated using LES involved minimum cell sizes of about $\sim 30 \mu\text{s}$. Three different LES models, namely Dynamic Structure, Smagorinsky, and no Sub-Grid Scale (SGS), were implemented and validated against high-fidelity experimental data [2,8].
4. In order to improve the load-balancing capability in CONVERGE, METIS [9,10] was chosen to replace the original algorithm. METIS is widely known for its efficiency in partitioning complex geometries and its capabilities to minimize the connectivity and to enforce contiguousness between partitions.

RESULTS

Some critical findings associated with the four objectives for FY 2013 are discussed here. Further details can be obtained from authors' publications in FY 2013. Figure 1 plots the mass flow rate through each orifice for a multi-hole injector [7] with needle off-axis motion along the $+x$ direction [6] and lift profile [7]. The orientation of the holes simulated is shown in the top image. It should be noted that the peak needle-off axis motion occurs during low lifts, i.e., at 0.4 ms and 1.5 ms (approximately) and at ~ 0.9 ms, which coincides with the peak needle lift of $\sim 225 \mu\text{m}$. Hence, it is not surprising that the largest hole-to-hole differences in mass flow rates are observed at low needle lift positions, i.e., ~ 0.4 ms and ~ 1.5 ms in the bottom image. At high needle-lift position of 0.9 ms, the needle lift is high, hence it does

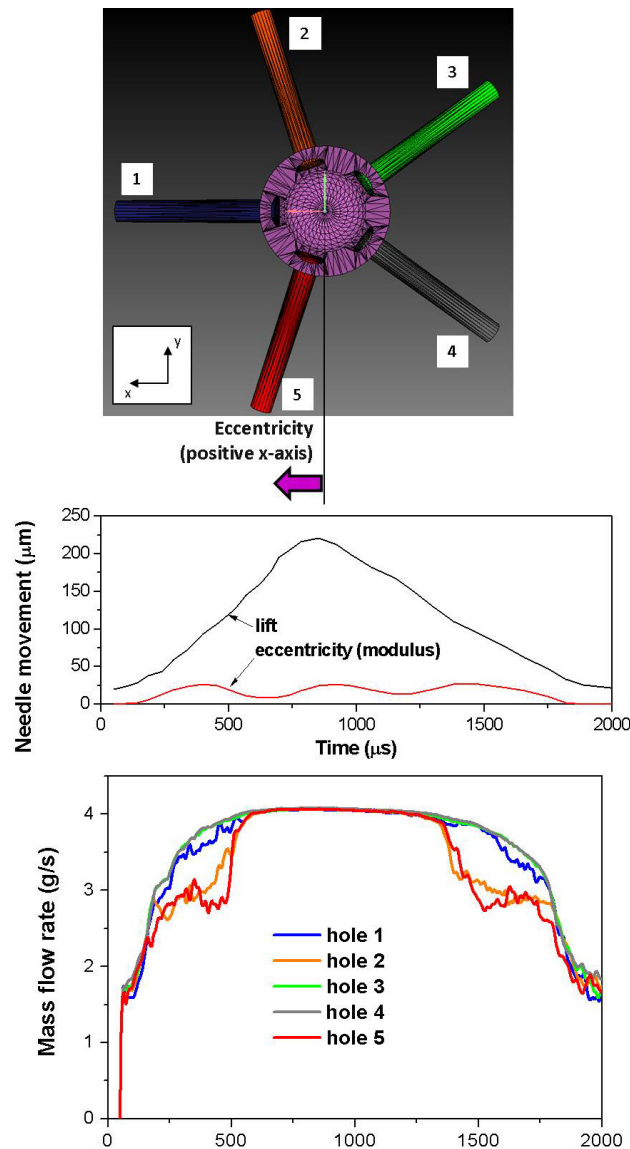


FIGURE 1. Three-dimensional transient simulation of a multi-hole injector with specified needle lift and wobble profile. The differences in mass flow rates between different orifices are clearly observed, especially during the needle transients.

not influence the flow development in the sac and orifice entry region. Between 0.55 ms and 1.35 ms, the mass flow rate predicted through each orifice is steady and on top of each other. This time period corresponds with a needle lift of $\sim 100 \mu\text{m}$ and higher. The analysis above shows that if the needle is lifted more than $100 \mu\text{m}$, the off-axis motion does not influence the flow development. It should also be noted that holes 2 and 5 are mostly affected by the needle off-axis motion and predict lower mass flow rates compared to the other orifices.

Figure 2 plots the vapor penetration profiles with RANS RNG k- ϵ (a) and LES dynamic structure

(b) models at different minimum mesh resolutions from 1 mm to 0.03125 mm. The results are from spray simulations performed using the grid-convergent approach highlighted above. It is interesting to note that both RANS and LES models can produce grid-convergent results. However, the grid-converged results with RANS do not match the experimental data, whereas the grid-converged results with LES mimic the experimental data very well. This demonstrates that LES calculations can be more predictive than RANS simulations.

Figure 3 presents the contour plots for temperature inside the combustion chamber in a non-reacting n-heptane spray experiment [2] and simulations using different RANS and LES turbulence models described earlier. It can be clearly seen that the RANS model cannot capture the flow structures, whereas all the LES models can qualitatively capture the instantaneous flow structures quite well with a minimum resolution of 0.0625 mm. Figure 2 and Figure 3 demonstrate that both qualitatively and quantitatively, LES performs better than RANS under these non-reacting spray conditions.

Figure 4 presents axial velocity profiles at different axial distances between n-dodecane non-reacting sprays [8], compared against results using the RANS RNG k- ϵ and LES dynamic structure turbulence models. Multiple injections are performed with different random number seeds to perturb the spray calculations with both the turbulence models in order to mimic the cycle-to-cycle variations observed in experiments. RANS simulations cannot capture any shot-to-shot variations since any perturbations in the flow-field are damped out. LES calculations, on the other hand, capture significant cyclic variability which is also observed in experiments [8]. It should be noted that experimental data is averaged over 20 injections. Averaged LES results over five injections are observed to capture the experimental trends quite well.

The use of higher-fidelity nozzle flow, spray, and turbulence models along with grid-convergent resolutions significantly increases the computational cost for simulations. While these simulation approaches provide a path forward for predictive ICE simulations, the computational cost could be prohibitive for engine design and optimization applications. We are also focusing towards developing high-performance computing tools to effectively load-balance the simulations so that the benefits of multi-processor simulations can be fully realized. Towards this, in FY 2012 a load-balancing approach was implemented in CONVERGE code which enabled HPC simulations up to 256 processors [9]. Figure 5 presents simulations on 128–1,024 processors for a few time-steps on the Blue-Gene machine at Argonne National Laboratory. The simulations

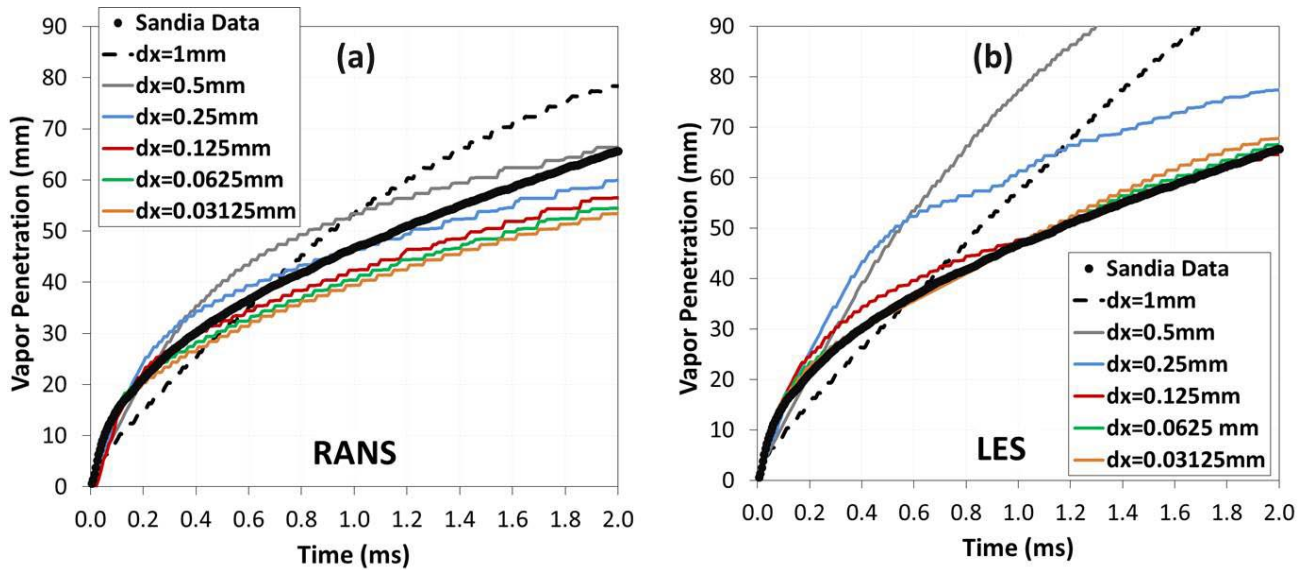


FIGURE 2. Fuel vapor penetration using RANS RNG k- ϵ and LES dynamic structure models at different minimum mesh resolutions compared against experimental data from Sandia National Laboratories [2] using n-dodecane as a surrogate for diesel fuel.

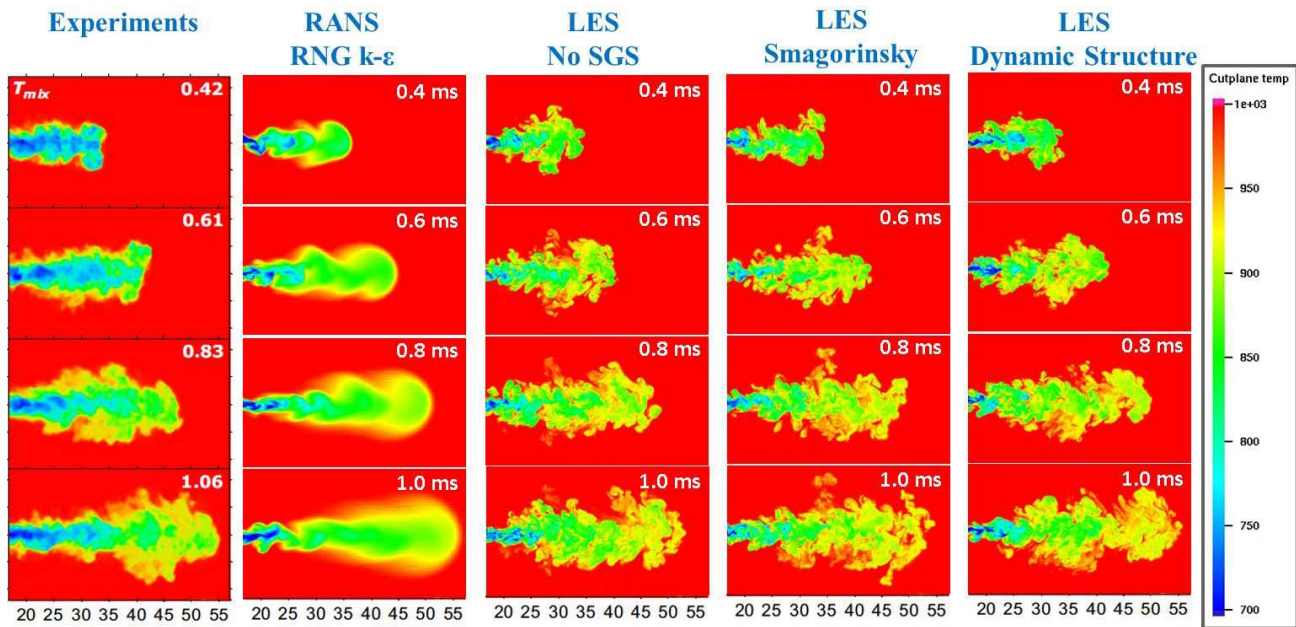


FIGURE 3. Fuel vapor temperature contours using RANS RNG k- ϵ and different LES models at a minimum mesh resolution of 0.0625 mm compared against experimental data from Sandia National Laboratories [2] using n-heptane as a surrogate for diesel fuel.

demonstrate that the code scales fairly well up to 1,024 processors, beyond which the scalability is lower than 70% of the theoretical (linear) scalability plot.

CONCLUSIONS

- In-nozzle flow simulations performed using CONVERGE software can capture the mass flow and cavitation trends very well. For the first time, the simulations accounted for needle transients, including the wobble. Differences in mass flow rates

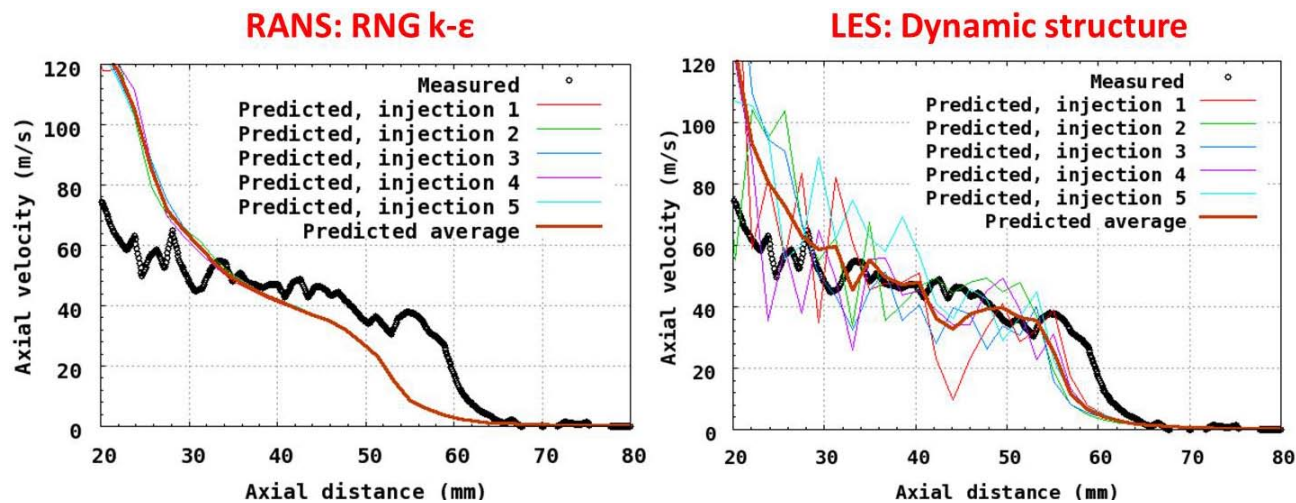


FIGURE 4. Axial velocity vs. axial distance compared between RANS RNG k- ϵ and LES dynamic structure models against experimental data from Meijer, et al. [7]. Multiple realizations show no cyclic variability with RANS, whereas significant shot-to-shot variations are captured with the LES model.

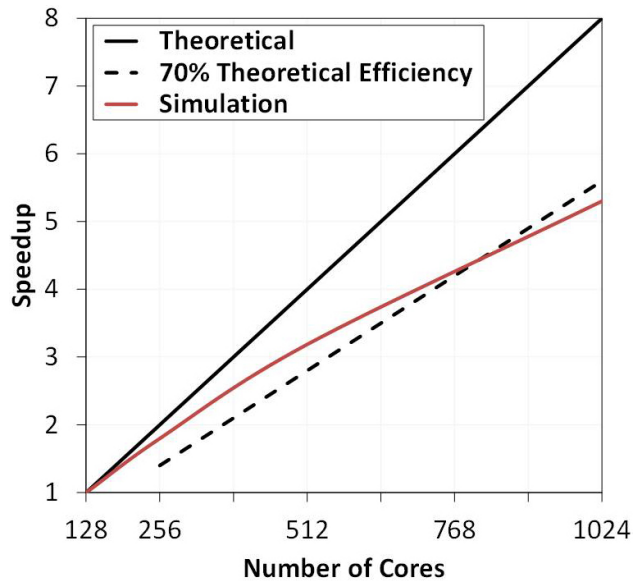


FIGURE 5. Speedup calculations for a typical internal combustion engine simulation run on 128-1,024 cores on a high-performance computing cluster at Argonne National Laboratory. Linear (ideal) speedup curve is also shown.

between different plumes were observed, especially during the needle transients.

- Grid-convergence was observed on several key nozzle flow and spray calculations using the high-fidelity turbulence models. Optimum grid resolutions have been recommended keeping in mind computational accuracy and wall-clock times.
- LES simulations can qualitatively and quantitatively capture the spray characteristics much better than

RANS calculations. LES can also capture shot-to-shot variations between different realizations that cannot be predicted by the RANS simulations. With the dramatic increase in computational resources in the past decade, this study indicates that LES is a viable alternative to RANS since it is more predictive in nature and wall-clock times can also be reasonable.

- Load-balancing in engine simulations was significantly improved by the implementation of METIS algorithm, thus enhancing computational speedup [9]. Significant speedup was demonstrated up to 1,000 processors for a typical engine simulation.

REFERENCES

1. Richards, K.J., Senecal, P.K., Pomraning, E., CONVERGE (Version 1.4.1) Manual, Convergent Science, Inc., Middleton, WI, 2012.
2. <http://www.sandia.gov/ecn/>
3. Som, S., Aggarwal, S.K., 2010, *Combustion and Flame*, Vol. 157, pp. 1179-1193.
4. Senecal P.K., Pomraning E., Richards K., Som S., *Proceedings of the ASME Internal combustion engine division fall technical conference* (2012) ICEF2012-92043.
5. Zhao H., Quan S., Dai M., Pomraning E., Senecal P.K., Xue Q., Battistoni M., Som S., *Proceedings of the ASME Internal Combustion Engine Division Fall Technical Conference*, ICEF2013-19167.
6. Kastengren, A.L., Tilocco, F.Z., Powell, C.F., Manin, J., Pickett, L.M., Payri, R., and Bazyn, T., Accepted in *Atomization and Sprays* (2013).

- 7.** Payri, R., Gil, A., Plazas, A.H., and Gimenez, B., *SAE World Congress Paper No. 2004-01-2010* (2004).
- 8.** Meijer, M., Malbec, L-M., Bruneaux, G., and Somers, L.M.T., *ICLASS 2012, Triennial International Conference on Liquid Atomization and Spray Systems*, Heidelberg, Germany, September 2–6, 2012.
- 9.** S. Som, D.E. Longman, S.M. Aithal, R. Bair, M. Garcia, S.P. Quan, K.J. Richards, P.K. Senecal, *SAE Paper No. 2013-01-1095*, 2013.
- 10.** Karypis G., “METIS – A Software Package for Partitioning Unstructured Graphs, Partitioning Meshes, and Computing Fill-Reducing Orderings of Sparse Matrices Version 5.0” (2011).

SELECTED FY 2013 PUBLICATIONS

- 1.** Q. Xue, S. Som, P.K. Senecal, E. Pomraning, “Large Eddy Simulation of Fuel Spray Under Non-Reacting IC Engine Conditions,” *Atomization and Sprays* 23(10), 925-955, 2013.
- 2.** P.K. Senecal, E. Pomraning, K.J. Richards, S. Som, “Grid-Convergent Spray Models for Internal combustion engine CFD simulations,” *Journal of Energy Resources Technology* 136 (1), 12204, 2013.
- 3.** S. Som, W. Liu, D.Y. Zhou, G.M. Magnotti, R. Sivaramakrishnan, D.E. Longman, R.T. Skodje, M.J. Davis, “Quantum tunneling affects engine performance,” *Journal of Physical Chemistry letters* 4: 2021-2025, 2013.
- 4.** E.R. Hawkes, Y. Pei, S. Kook, S. Som, “An analysis of the structure of an n-dodecane spray flame using PDF modeling,” *Proceedings of the Australian Combustion Symposium*, The University of Western Australia, November 2013.
- 5.** P.K. Senecal, E. Pomraning, Q. Xue, S. Som, S. Banerjee, B. Hu, K. Liu, J. Deur, “Large Eddy simulation of vaporizing sprays considering multi-injection averaging and grid-convergent mesh resolution,” *Proceedings of the ASME Internal Combustion Engine Division Technical Conference*, ICEF2013-19082, Dearborn, 2013.
- 6.** H. Zhao, S. Quan, M. Dai, E. Pomraning, P.K. Senecal, Q. Xue, M. Battistoni, S. Som, “Validation of a three-dimensional internal nozzle flow model including automatic mesh generation and cavitation effects,” *Proceedings of the ASME Internal Combustion Engine Division Technical Conference*, ICEF2013-19167, Dearborn, 2013.
- 7.** S. Som, Z. Wang, W. Liu, D.E. Longman, “Comparison of different chemical kinetic models for biodiesel combustion,” *Proceedings of the ASME Internal Combustion Engine Division Technical Conference*, ICEF2013-19094, Dearborn, 2013.
- 8.** M. Battistoni, S. Som, D.E. Longman, “Evaluation of different modeling approaches for nozzle cavitation prediction,” *Proceedings of the ASME Internal Combustion Engine Division Technical Conference*, ICEF2013-19093, Dearborn, 2013.
- 9.** Y. Zhu, N. Salman, K. Freeman, R. Reese, Z. Wang, R. Scarcelli, S. Som, “Numerical study of the combustion characteristics of a turbocharged DI gasoline engine with diesel micro pilot ignition and cooled EGR,” *Proceedings of the ASME Internal Combustion Engine Division Technical Conference*, ICEF2013-19170, Dearborn, 2013.
- 10.** S. Som, D.E. Longman, S.M. Aithal, R. Bair, M. Garcia, S.P. Quan, K.J. Richards, P.K. Senecal, “A numerical investigation on scalability and grid convergence of internal combustion engine simulations,” *SAE Paper No. 2013-01-1095*, Detroit, 2013.
- 11.** P.K. Senecal, E. Pomraning, K.J. Richards, S. Som, “An investigation of grid convergence for spray simulations using an LES turbulence model,” *SAE Paper No. 2013-01-1083*, Detroit, 2013.
- 12.** Z. Wang, R. Scarcelli, S. Som, S.S. McConnell, N. Salman, Y. Zhu, K. Freeman, K. Hardman, R.A. Reese, P.K. Senecal, M. Raju, S.D. Gilver, “Multi-dimensional modeling and validation of combustion in a high-efficiency dual-fuel light-duty engine,” *SAE Paper No. 2013-01-1091*, Detroit, 2013.
- 13.** Q. Xue, M. Battistoni, S. Som, D.E. Longman, H. Zhao, P.K. Senecal, E. Pomraning, “Three-dimensional Simulations of the Transient Internal Flow in a Diesel Injector: Effects of Needle Movement,” *25th Annual Conference on Liquid Atomization and Spray Systems*, Pittsburgh, 2013.
- 14.** W. Liu, S. Som, D.Y. Zhou, R. Sivaramakrishnan, D.E. Longman, R.T. Skodje, M.J. Davis, “The Role of Individual Rate Coefficients in the Performance of Compression Ignition Engine Models,” *8th US National Combustion Meeting*, Utah, 2013.

SPECIAL RECOGNITIONS & AWARDS/ PATENTS ISSUED

- 1.** Dr. Sibendu Som has been inducted as a “Computational Fellow” at the Computational Institute at University of Chicago.

II.7 Fuel Injection and Spray Research Using X-Ray Diagnostics

Christopher F. Powell (Primary Contact),
Alan Kastengren, Jin Wang
Argonne National Laboratory
9700 S Cass Ave
Argonne, IL 60439

DOE Technology Development Manager:
Gurpreet Singh

Overall Objectives

- Study the mechanisms of spray atomization by making detailed, quantitative measurements in the near-nozzle region of sprays from fuel injectors.
- Perform these measurements under conditions as close as possible to those of modern engines.
- Utilize the results of our unique measurements in order to advance the state of the art in spray modeling.
- Provide industrial partners in the spray and engine community with access to a unique and powerful spray diagnostic.

Fiscal Year (FY) 2013 Objectives

- Perform measurements of fuel density, needle life, and nozzle geometry using the hardware and conditions of the Engine Combustion Network (ECN). Share these data with computational modelers for validation and improvement of spray modeling.
- Develop diagnostics for fuel flow inside injectors, including measurements of cavitation and gas ingestion at the end of injection.
- Explore the use of X-ray diagnostics for other advanced combustion applications, such as droplet sizing, fluid dynamics of sprays, and chemical kinetics.

FY 2013 Accomplishments

- In collaboration with Sandia's ECN, we completed measurements of the needle lift and internal geometry of the ECN "Spray B" injectors. We made precision measurements of the needle lift and motion in three dimensions, and discovered significant eccentric motion in the valves of some of the injectors. The measurements are being used by computational modelers to improve spray models

that will speed the development of efficient, clean-burning engines.

- Several new pieces of equipment were completed in 2013. A fixture to mount the ECN gasoline direct injection (GDI) injectors in our existing spray chambers was completed which will enable us to study the ECN "Spray G" injectors in FY 2014. We also designed a new spray chamber that can be used to perform three-dimensional tomography of sprays at elevated pressure and temperature. This chamber will be fabricated in FY 2014. These devices significantly expand our capabilities for studying modern fuel injection hardware.
- In order to improve the fundamental knowledge of sprays, we continued work started in FY 2012 making quantitative measurements of cavitating flows. These measurements allow us to determine the exact density distribution inside a two-phase fuel flow. We made significant improvements to our experimental techniques and hardware that allowed us to carefully control the amount of air dissolved in the fuel. These measurements are being compared to cavitation simulations in collaboration with some of the world's leading cavitation modelers.
- We continued our groundbreaking studies of gas bubbles that are pulled inside of diesel injectors at the end of injection. We performed parametric studies to learn the conditions that are most and least likely to result in bubble ingestion. It is believed that these bubbles may be a factor in injector damage as well as unburned hydrocarbon and particulate matter emissions.
- We continued to develop a new diagnostic for droplet sizing in the near-nozzle region of sprays: Small-Angle X-Ray Scattering. With further development and validation, this may become a unique and valuable method for studying near-nozzle spray structure, providing new data for spray model development and validation.

Future Directions

- The ECN is beginning a program studying gasoline injection. The geometry and fuel distribution from the "Spray G" GDI injectors will be measured using X-ray diagnostics, and will be made available to our experimental and modeling partners in the ECN.
- Spray measurements will be done in conjunction with Argonne's Engine and Emissions Research group. We will measure the fuel/air mixing in a GDI

injection system that is being used in engine tests of advanced combustion strategies. The high precision spray measurements will be used to validate simulations of the engine's combustion process, providing these research programs with the data that are needed for high-fidelity modeling.

- Further studies of cavitation will be done to improve the community's understanding of this phenomenon and its impact on fuel/air mixing and injector internal flows.
- Further studies of bubble ingestion will be performed, with the goal of linking this phenomenon with injector dribble. Dribble is the undesirable ejection of fuel after the nominal end of the injection event; the fuel is slow-moving, poorly atomized, and likely to generate particulate matter emissions. We hope to quantify the causes of dribble, enabling injector manufacturers to minimize its impact.



INTRODUCTION

Fuel injection systems are one of the most important components in the design of combustion engines with high efficiency and low emissions. A detailed understanding of the fuel injection process and the mechanisms of spray atomization can lead to better engine performance. The limitations of visible light diagnostics in the near-nozzle region of the spray have led us to develop X-ray diagnostics for the study of fuel sprays. X-rays are highly penetrative, and measurements are not complicated by the effects of scattering. The technique is non-intrusive, quantitative, highly time-resolved, and allows us to make detailed measurements of the spray, even in the densely-packed region very near the nozzle.

APPROACH

This project studies the sprays from commercially available fuel injectors. Our approach is to make detailed measurements of the sprays from these injectors using X-ray absorption. This will allow us to map the fuel distribution in these sprays, extending the existing knowledge into the near-nozzle region. The X-ray measurements are performed at the Advanced Photon Source at Argonne National Laboratory. A schematic of the experimental setup is shown in Figure 1; detailed descriptions of the experimental methods are given in [1] and [2]. The technique is straightforward; it is similar to absorption methods commonly used in optical analysis. However, X-ray radiography has a significant advantage

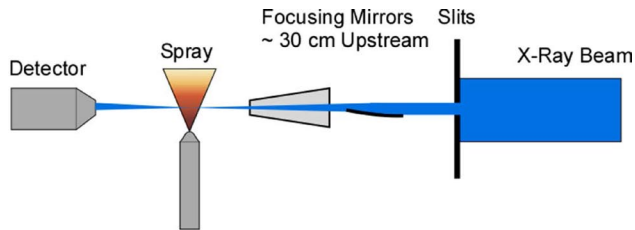


FIGURE 1. Schematic of the Experimental Setup

over optical techniques in the measurement of sprays: because the measurement is not complicated by the effects of scattering, there is a simple relation between the measured X-ray intensity and the mass of fuel in the path of the X-ray beam. This allows direct determination of the mass of fuel at any position in the spray as a function of time. It is the goal of our work to use X-ray radiography to measure sprays from commercial fuel injectors at different injection pressures, ambient pressures, and using different nozzle geometries. This will enable us to quantify how each of these variables affects the structure of the spray.

In the process of making these measurements, we will collaborate with industrial partners including engine and fuel injection system manufacturers so that they will have access to these diagnostics for improvement of their products. We will also collaborate with spray modelers to incorporate this previously unknown information about the spray formation region into new models. This will lead to an increased understanding of the mechanisms of spray atomization and will facilitate the development of fuel injection systems designed to improve efficiency and reduce pollutants.

In addition to measurements of sprays, we will explore other applications of X-ray diagnostics for combustion research. This includes X-ray imaging of the internal components of fuel injectors while they are in operation; this diagnostic allows injector manufacturers to develop and optimize injector designs. Measurements of cavitating flows provides unique data to improve the fundamental understanding of this internal fuel flow and its role in spray atomization, as well as the relationship between injector geometry, cavitation, and nozzle damage. Recent measurements have also evaluated the use of X-rays as a diagnostic for shock tubes, enabling better measurements of combustion kinetics to improve engine modeling. We will also continue to develop X-ray measurements of droplet sizing. These measurements can determine the Sauter mean diameter of the fuel parcels in the near-nozzle region, a parameter that has never before been available for validation of primary breakup models.

RESULTS

We have spent a significant part of our effort over the last few years performing experiments in collaboration with the Engine Combustion Network. This collaboration is led by Sandia National Laboratories, who has defined a specific set of operating conditions and procured a set of shared identical hardware. We have used Argonne's unique X-ray diagnostics to study both the "Spray A" and "Spray B" operating conditions, and have shared these results with the ECN community [3]. The data are now being used for validation of injector and spray models, including models that incorporate the eccentric needle motion when calculating fuel flow [4]. At the ECN2 Workshop in 2012, Argonne's data was used for validation by at least six different spray modeling groups. That activity has continued in 2013 with our group's preparations for the ECN3 Workshop; three Argonne staff members are serving as organizers for the upcoming meeting. Through this involvement in ECN, our data are being actively used to improve spray models and simplify the development of efficient, clean-burning engines.

Cavitation is an important problem in high-pressure fuel injection systems, such as those found in modern direct injection diesel engines. Cavitation—where fuel in the injector vaporizes due to a drop in pressure—can cause mechanical damage to injector components and

affect fuel/air mixing and thus pollutant formation. State-of-the-art computer models for cavitation are now being incorporated into engine modeling software to account for these factors. However, there is little information available on the accuracy of these models because cavitation is very difficult to measure experimentally. In FY 2012 we began to develop X-ray diagnostics to make precise and accurate measurements of cavitation in a transparent nozzle [5,6]. Through collaboration with modelers from both Argonne [7] and the University of Massachusetts Amherst [8], we determined that dissolved gases in the fuel were playing a significant role in our measurements and obscuring the cavitation we were trying to measure. Through a significant redesign of our fuel delivery system, we were able to eliminate dissolved gas from the fuel, and repeat the measurements of cavitation (Figure 2). University of Massachusetts Amherst is using the new data, along with the high performance computing resources at Argonne, to develop and validate high resolution computer simulations of cavitation under similar conditions to the X-ray experiments. The cavitation models developed at the University of Massachusetts Amherst are widely used in commercial engine simulations, so improvements to those models will lead to better and more accurate engine modeling software, as well as a broader understanding of this complex physical phenomenon.

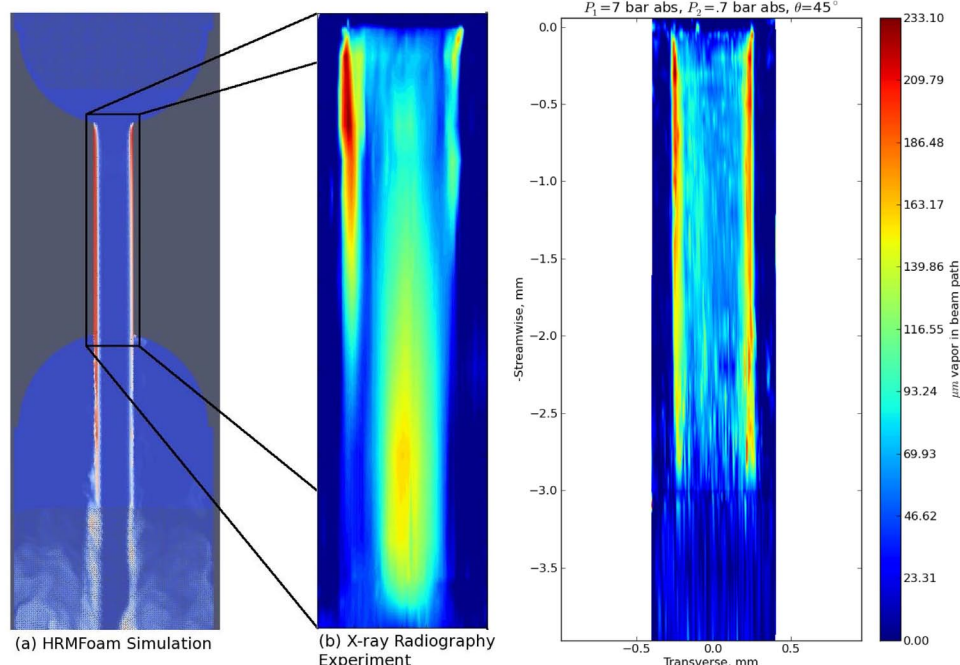


FIGURE 2. Simulations of cavitating flow (left) are compared to X-ray radiography measurements done in 2012 (middle) and 2013 (right). The newest measurements show much better symmetry, with cavitation only along the walls of the nozzle as expected. The improved measurements are being used for flow model development and validation.

High-speed imaging of injector operation was developed at Argonne in order to study the motion of steel components inside the injector, such as the valve lift. Due to improvements in our imaging technique, we recently developed the capability to image the motion of gas bubbles inside production injectors. One interesting phenomenon that was discovered is that bubbles are drawn into the injector sac through the nozzle holes at the end of injection (Figure 3). In FY 2013, additional experiments and analysis quantified that the quantity of gas in the sac after injection increases with injection pressure and decreases with ambient pressure (Figure 4). These bubbles inside the injector will likely have an impact on emissions, since the bubbles will expand when the exhaust valves open and drive any remaining fuel out of the injector into a cold combustion chamber. Further work will attempt to link the bubbles to injector dribble, and explore ways to minimize their impact on engine performance.

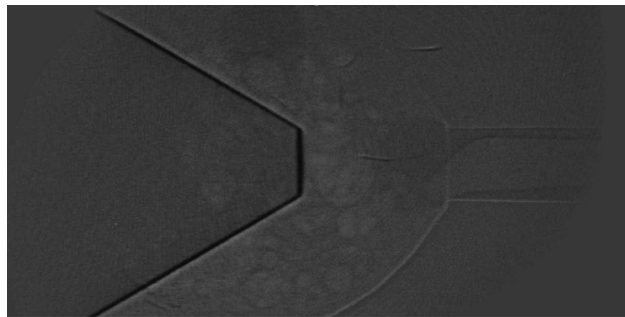


FIGURE 3. X-ray image through a steel injector nozzle showing bubbles that were drawn into the sac at the end of injection. The presence of these bubbles is likely to have an impact on emissions.

CONCLUSIONS

- The X-ray measurements can be used to help understand the mixing of fuel and air in the engine, and its impact on engine emissions and performance. Such measurements are not possible using other imaging techniques, and represent a powerful data set for validating computational models of fuel flow.
- The time-dependent mass measurements provide unique information to spray modelers, and allow them to test their models in the spray formation region, something that was impossible previously. These data are crucial for the development of accurate spray models and for the detailed understanding of spray behavior. The quantitative measurements that we have provided may help to elucidate the mechanisms of spray atomization. This could ultimately lead to the design of cleaner, more efficient engines.
- The impact of our work on the engine community is shown by the expanding list of collaborators and by the significant in-kind contributions to our work that are being made by fuel system and engine manufacturers.

REFERENCES

- “Time-Resolved Measurements of Supersonic Fuel Sprays using Synchrotron X-rays”, C. F. Powell, Y. Yue, R. Poola, and J. Wang, *J. Synchrotron Rad.* 7:356-360 (2000).
- “Spray Density Measurements Using X-Ray Radiography” A.L. Kastengren, C.F. Powell, *Journal of Automobile Engineering*, Volume 221, Number 6, 2007, pp 653-662.

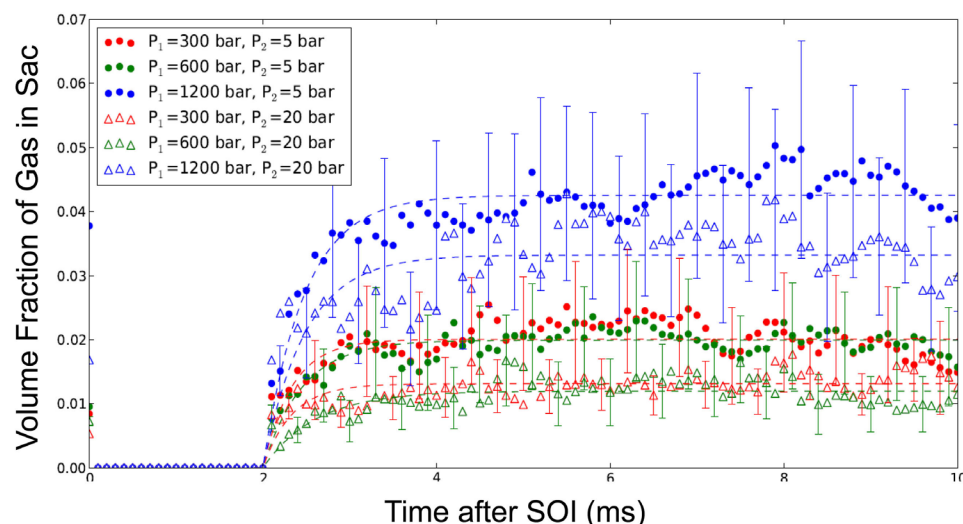


FIGURE 4. Plot showing the volume fraction of gas bubbles in the injector sac versus time after start of injection. The volume of gas quickly rises after the end of injection, then stabilizes. The gas fraction is shown for several injection and ambient pressures.

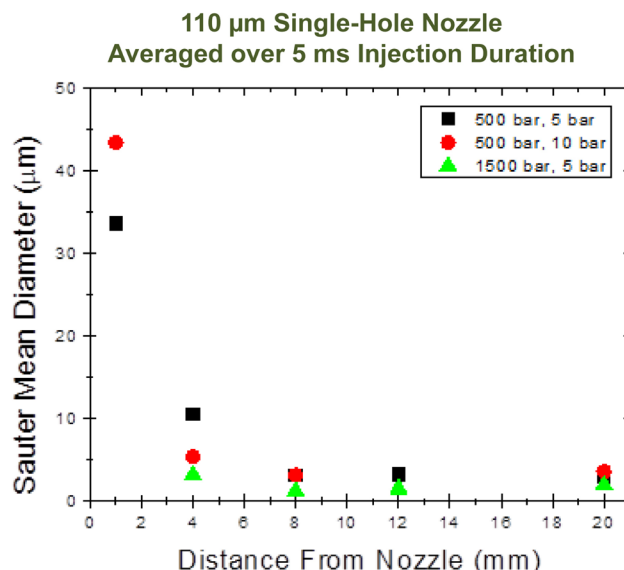


FIGURE 5. Sauter mean diameter of fuel parcels in the spray versus distance from the nozzle for two different ambient and injection pressures. These measurements were performed using X-ray small angle scattering, a new diagnostic for measuring particle size in the near-nozzle region. The results were obtained from a 110- μm single-hole nozzle.

3. “Engine Combustion Network (ECN): Measurements of Nozzle Geometry and Hydraulic Behavior”, A.L. Kastengren, F.Z. Tilocco, C.F. Powell, J. Manin, L.M. Pickett, R. Payri, T. Bazyn. Atomization & Sprays 22 (12), pp 1011-1052 (2012).
4. Q. Xue, M. Battistoni, S. Som, D.E. Longman, H. Zhao, P.K. Senecal, E. Pomraning, “Three-dimensional Simulations of the Transient Internal Flow in a Diesel Injector: Effects of Needle Movement,” 25th Annual Conference on Liquid Atomization and Spray Systems, Pittsburgh, PA, May 2013.
5. “X-Ray Radiography Measurements of Cavitating Nozzle Flow”, D.J. Duke, A.L. Kastengren, F.Z. Tilocco, A. Swantek, and C. F. Powell, Atomization & Sprays 23 (9), pp. 841-860, 2013.
6. “Synchrotron X-Ray Measurements of Cavitation”, D.J. Duke, A.L. Kastengren, F.Z. Tilocco, C.F. Powell. 25th Annual Conference on Liquid Atomization and Spray Systems, Pittsburgh, PA, May 2013.
7. M. Battistoni, S. Som, D.E. Longman, “Evaluation of different modeling approaches for nozzle cavitation prediction,” under review Journal of Engineering for Gas Turbine and Power, 2013.

8. “High Resolution Large Eddy Simulations of Cavitating Gasoline-Ethanol Blends”, D.J. Duke, D. Schmidt, K. Neroorkar, A.L. Kastengren, C.F. Powell, International Journal of Engine Research, In Press, October 2013.

9. “Measurements of Diesel Spray Droplet Size with Ultra-Small Angle X-Ray Scattering”, C.F. Powell, D.J. Duke, A.L. Kastengren, J. Ilavsky. 25th Annual Conference on Liquid Atomization and Spray Systems, Pittsburgh, PA, May 2013.

FY 2013 PUBLICATIONS

1. “X-Ray Radiography Measurements of Cavitating Nozzle Flow”, D.J. Duke, A.L. Kastengren, F.Z. Tilocco, A. Swantek, and C.F. Powell, Atomization & Sprays 23 (9), pp. 841-860, 2013.
2. “Unraveling the Geometry Dependence of In-Nozzle Cavitation in High-Pressure Injectors”, K.-S. Im, S.-K. Cheong, C.F. Powell, M.-C.D. Lai, J. Wang, Scientific Reports 3, Article number: 2067, June 2013.
3. “Measurements of Diesel Spray Droplet Size with Ultra-Small Angle X-Ray Scattering”, C.F. Powell, D.J. Duke, A.L. Kastengren, J. Ilavsky. 25th Annual Conference on Liquid Atomization and Spray Systems, Pittsburgh, PA, May 2013.
4. “Synchrotron X-Ray Measurements of Cavitation”, D.J. Duke, A.L. Kastengren, F.Z. Tilocco, C.F. Powell. 25th Annual Conference on Liquid Atomization and Spray Systems, Pittsburgh, PA, May 2013.
5. “Engine Combustion Network (ECN): Measurements of Nozzle Geometry and Hydraulic Behavior”, A.L. Kastengren, F.Z. Tilocco, C.F. Powell, J. Manin, L.M. Pickett, R. Payri, T. Bazyn. Atomization & Sprays 22 (12), pp 1011-1052 (2012).
6. “Measurements of Spatial Variations in Response of Ionization Chambers”, W.E.B. Miller, A.L. Kastengren, J Synchrotron Rad. 20 pp 160-165, October 2012.
7. “Understanding the Acoustic Oscillations Observed in the Injection Rate of a Common-Rail Direct Injection Diesel Injector”, J. Manin, A. Kastengren, R. Payri. Journal of Engineering for Gas Turbines and Power 134(12), 122801, October 2012.

II.8 Large Eddy Simulation Applied to Advanced Engine Combustion Research

Joseph C. Oefelein
Sandia National Laboratories
7011 East Avenue, Mail Stop 9051
Livermore, CA 94551-0969

DOE Technology Development Manager:
Gurpreet Singh

Overall Objectives

- Combine unique state-of-the-art simulation capability based on the large eddy simulation (LES) technique with Advanced Engine Combustion R&D activities.
- Perform companion simulations that directly complement optical engine and supporting experiments being conducted at the Combustion Research Facility and elsewhere.
- Maximize benefits of high-performance massively-parallel computing for advanced engine combustion research using DOE leadership computer platforms.

Fiscal Year (FY) 2013 Objectives

- Perform detailed LES of direct injection processes with emphasis on Engine Combustion Network (ECN; www.sandia.gov/ecn) experiments.
- Establish a new theoretical description that quantifies the effects of real fluid thermodynamics on liquid fuel injection processes at thermodynamically supercritical pressures typical of diesel engine operating conditions.
- Apply to the Spray-A (n-dodecane) cases using real-fluid thermodynamics and transport.

FY 2013 Accomplishments

- Established the first quantitative explanation that shows a distinct gas-liquid interface does not exist for a wide range of diesel-relevant injection conditions at high-pressure.
 - Knudsen-number criterion reveals that interfacial diffusion layers develop due to broadening vapor-liquid interfaces and diminished intermolecular forces.

- As pressure increases, the interface enters the continuum regime due to increasing thickness and significant decrease in mean molecular path.
- Demonstrated that the classical view of jet atomization (which is currently widely assumed) is not applicable at these conditions.
 - Distinct gas-liquid interface does not exist, conventional spray theory not valid.
 - Lack of inter-molecular forces promotes diffusion over atomization.
 - Real fluid equations of state, thermodynamics, and transport for multicomponent mixtures must be considered instead.
- Performed detailed analysis of high-pressure injection processes using LES and real-fluid thermodynamics and compared LES with ECN experimental target data.

Future Directions

- Extend development of models and corresponding benchmark simulations to high-Reynolds-number, direct-injection processes for both diesel and gasoline direct injection engine applications over a wide range of pressures and temperatures.



INTRODUCTION

Recent research has provided new conceptual insights into direct injection processes at high pressures. Imaging has long shown that under some high-pressure conditions, the presence of discrete two-phase flow processes becomes diminished. Under such conditions, liquid injection processes transition from classical sprays to dense-fluid jets, with no drops present. When this transition occurs, however, was not well understood. The theory developed here is one of the first to explain and quantify this transition, that has important implications from the standpoint of design and related development of predictive models. A key output from the theory are regime diagrams for liquid injection such as the example shown in Figure 1. Detailed analysis of the gas-liquid interfacial structure quantifies under what conditions “classical” spray dynamics transition to dense-fluid jets as a function of the pressure and temperature of the injected fuel and ambient gas. Predictions have been

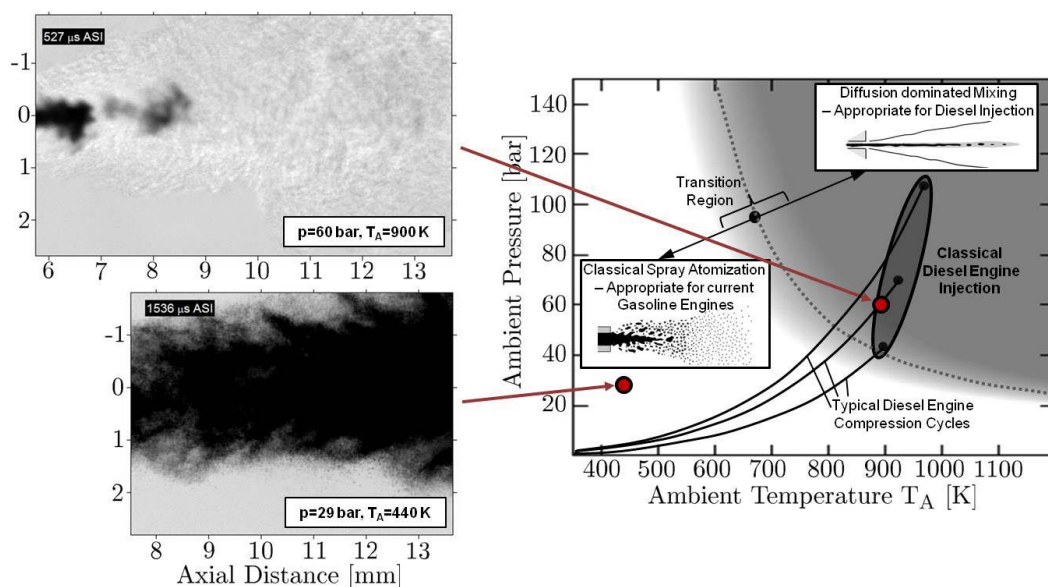


FIGURE 1. Regime diagram for n-dodecane injected at a temperature of 363 K into nitrogen suggests the presence of dense supercritical jets under diesel engine conditions without drop formation. High-speed imaging of both a dense jet and spray illustrates the significant transitional change that occurs at high supercritical pressures (images courtesy of L.M. Pickett, Sandia National Laboratories, Combustion Research Facility).

corroborated using microscopic imaging to visualize the features of dense-fluid jets (top left image in Figure 1) and classical spray atomization processes (bottom left).

Analysis of the trends with different fuels suggests that most high-performance combustion devices currently operate over ranges of pressures and temperatures in the vicinity of these transitional regimes. The pressure-temperature diagram in Figure 1 shows results for n-dodecane injected at a temperature of 363 K into gaseous nitrogen at varying ambient pressures and temperatures. The classical spray regime (highlighted in white) and diffusion-dominated mixing regime (gray) are found using an applied the Knudsen-number criterion (See Dahms and Oefelein, *Physics of Fluids*, **25** 2013). To illustrate the relevance of this diagram, ambient gas pressure-temperature traces, which span a range of conditions during different diesel engine compression cycles, are shown for three representative conditions: a) turbocharged, b) medium-load, and c) light-load operation. The corresponding initial pressures and temperatures are a) 2.5 bar, 363 K, b) 1.6 bar, 343 K, and c) 1 bar, 335 K, respectively. Fuel injection then occurs at full compression conditions, as indicated by the three respective points in the diagram. Interestingly, the cylinder pressures at full compression exceed the supercritical mixture pressure for all of the cases considered. Only under representative light-load operation does there appear to be a chance that classical spray fuel spray atomization takes place. Thus, contrary to conventional wisdom, the regime diagram suggests

that classical spray phenomena do not occur at typical diesel injection conditions. Instead, the fuel is injected as a continuous jet with diminished interfacial structure and surface tension forces leading to diffusion-dominated mixing dynamics. Such mixing layers are largely affected by non-ideal thermodynamics and transport processes and cannot support evaporation phenomena or the formation of liquid ligaments or drops.

APPROACH

To enhance the current understanding of the processes described above, the theoretical findings were combined with high-fidelity LES to gain a more detailed view into direct injection processes at high pressures. The experimental data provided by Pickett et al. were used as key targets (see www.ca.sandia.gov/ECN). The analysis is performed using a single unified code framework called RAPTOR. Unlike conventional LES codes, RAPTOR is a direct numerical simulation solver that has been optimized to meet the strict algorithmic requirements imposed by the LES formalism. The theoretical framework solves the fully coupled conservation equations of mass, momentum, total-energy, and species for a chemically reacting flow. It is designed to handle high Reynolds number, high-pressure, real gas and/or liquid conditions over a wide Mach operating range. It also accounts for detailed thermodynamics and transport processes at the molecular level, and is sophisticated in its ability to handle a

generalized sub-model framework. A noteworthy aspect of RAPTOR is it was designed specifically for LES using non-dissipative, discretely conservative, staggered, finite-volume differencing. This eliminates numerical contamination of the sub-models due to artificial dissipation and provides discrete conservation of mass, momentum, energy, and species, that is an imperative requirement for high-quality LES.

RESULTS

Using the trends highlighted in Figure 1, a series of LES calculations were performed using a real-fluid equation of state, thermodynamics, and transport for multicomponent mixtures. Emphasis was placed on the ECN Spray-A case. Non-reacting liquid n-dodecane at 363 K was injected into a quiescent gaseous mixture at 900 K and 60 bar, which are precisely the conditions represented by the medium-load compression cycle shown in Figure 1 and corresponding top image. For the present case, all of the oxygen is consumed before injection and the composition of the gaseous ambient is $Y_{O_2} = 0$, $Y_{N_2} = 0.897$, $Y_{CO_2} = 0.065$, and $Y_{H_2O} = 0.038$. The liquid fuel was injected through a 0.09 mm diameter nozzle injector. The peak injection velocity was 620 m/s, that provides the same injected mass flow rate as the experiment. A synthetic turbulent signal with a turbulent intensity of 5% was superimposed on the bulk profile. Measurements have shown that the vessel temperature is almost uniform in space, which justifies the use of adiabatic walls in the simulation. The grid spacing in the vicinity of the injector exit was approximately 4 μ s, with the grid stretched optimally in the downstream and radial directions.

Figure 2 shows the structure of the injected jet at 0.27 ms, which is the point of injection just prior to auto-ignition. Also shown are the instantaneous pressure and scalar dissipation fields along the center plane of the jet. The high-speed compressed liquid jet stays coherent for almost 20 diameters before starting to disintegrate. At approximately 20 diameters downstream, the jet exhibits self-similar behavior, which is a feature of classical gaseous turbulent jets. This trend is correlated with the presence of strong density gradients shown in Figure 3. The density of the jet is slightly above 700 kg/m^3 when exiting the injector whereas the density of the ambient gas is 23 kg/m^3 . This strong density variation results in a high-momentum flux ratio, which delays the destabilization of the jet. Once destabilization of the dense core occurs, parcels of dense fluid detach from the compressed liquid jet. These dense fragments can still be observed 70 diameters downstream of the injector exit. The presence of these fast-moving dense structures enhances local turbulence as they act as fast-moving solid objects for the surrounding gaseous

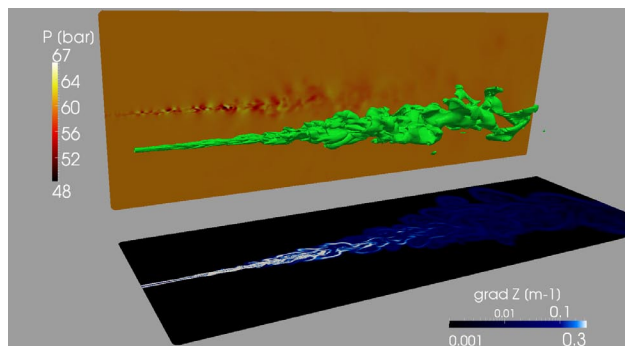


FIGURE 2. Instantaneous structure of the Spray-A case at 0.27 ms, which is the point of injection just prior to auto-ignition. The green iso-contour represents the mass fraction of n-dodecane at a value of 0.5. Also shown are the instantaneous pressure and scalar dissipation fields along the center plane of the jet.

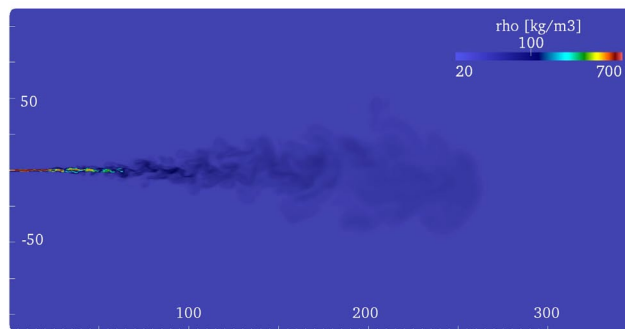


FIGURE 3. Instantaneous density field along the center plane of the jet at 0.27 ms. The spatial scale is non-dimensionalized using the jet diameter of 0.09 mm.

phase. Many vortical eddies are generated at the surface of the liquid core, and this phenomenon significantly affects the mixing of the fuel. After these structures are completely diffused, the jet behavior becomes “gas-like” and turbulent-diffusion effects become prevalent. In the region where the dense core of the jet becomes very corrugated and eventually breaks up at between 20 and 60 diameters, the presence of dense lumps evolving at high speed generates significant localized pressure variations through compression/expansion effects,. This can be seen in Figure 2. These pressure variations modify the flow and enhance mixing.

An interesting feature of the present case is illustrated in Figure 4, that shows the instantaneous Mach number field along the center plane of the jet at 0.27 ms. In this figure, one can see that the flow becomes supersonic at various locations within the mixing layer due to variations associated with the speed of sound. The compressed liquid is injected at a Mach number of 0.6 (note that the speed of sound in pure n-dodecane at 363 K and 60 bar is 1,008 m/s). In the mixing layer

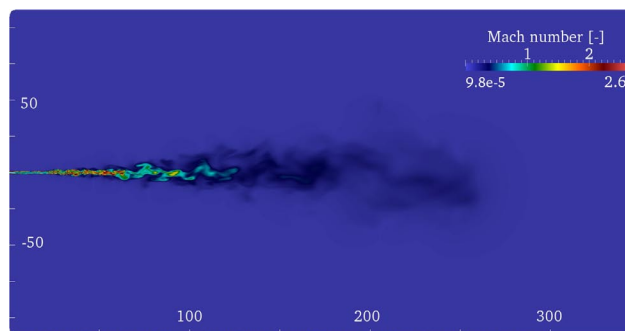


FIGURE 4. Instantaneous Mach number field along the center plane of the jet at 0.27 ms. The spatial scale is non-dimensionalized using the jet diameter of 0.09 mm.

of the jet, non-linear thermodynamic effects lead to a sharp increase in the ratio of specific heats and a significant decrease of the partial derivative of pressure with respect to density. The combined effect results in a strong decrease of the speed of sound, which reaches a minimum of 170 m/s in the mixing region of the jet in the region between 30 and 70 diameters downstream. In this area, the flow entrained by the high-speed jet has a velocity of approximately 400 m/s, which is more than two times the local sound speed. This remarkable behavior is the result of near supersonic injection of a compressed liquid at supercritical conditions. More work is required in this area to determine the exact consequences of these new observations.

CONCLUSIONS

Imaging has long shown that under some high-pressure conditions, the presence of discrete two-phase flow processes becomes diminished. Under such conditions, liquid injection processes transition from classical sprays to dense-fluid jets, with no drops present. When and how this transition occurs, however, was not well understood until recently. This research has provided a new theoretical description that quantifies the effects of real-fluid thermodynamics on liquid fuel injection processes as a function of pressure at typical diesel engine operating conditions. The implications that this has on modeling were then investigated using the LES technique coupled with real-fluid thermodynamics and transport. The established theory explains and quantifies the major differences that occur in the jet dynamics compared to that described by classical spray theory in a manner consistent with experimental observations. In particular, the classical view of spray atomization as an appropriate model at some engine operating conditions is questionable. Instead, non-ideal real-fluid behavior must be taken into account using a multicomponent formulation that applies to hydrocarbon mixtures at high-pressure supercritical conditions.

To highlight the implications and needs related to modeling, a sequence of studies was presented. LES studies were extended to the Engine Combustion Network (www.sandia.gov/ECN) Spray-A injector using n-dodecane as the fuel. The accompanying analysis revealed the structural characteristics of the inherent scalar mixing and combustion processes at conditions relevant to diesel engines. Trends demonstrate that the mixing path associated with all local states throughout the duration of injection never crosses the liquid-vapor regime (i.e., the mixture is never saturated). Instead, the fuel is injected as a compressed liquid and the interfacial mixing layer dynamics are locally supercritical. This implies that classical first order vapor-liquid phase transitions (as are typically assumed) do not occur. Instead, the injected fuel enters the combustion chamber as a compressed liquid, not a spray, and is heated at supercritical pressure. This implies 1) that applying the ideal gas assumption just prior to auto-ignition in these types of flows is not valid, and 2) the classical view of spray atomization and secondary breakup processes as an appropriate model is questionable at these particular conditions. Instead, non-ideal real-fluid behavior associated with the dense liquid jet must be taken into account.

FY 2013 PUBLICATIONS/PRESENTATIONS

1. R.N. Dahms and J.C. Oefelein. On the transition between two-phase and single-phase interface dynamics in multicomponent fluids at supercritical pressures. *Physics of Fluids*, **25**(092103):1–24, 2013.
2. J.C. Oefelein, R.N. Dahms, G. Lacaze, and A.M. Ruiz. Modeling and numerical treatment of liquid injection processes at high-pressure supercritical conditions. *Proceedings of the Fourteenth International Conference on Numerical Combustion*, April 8–10 2013.
3. R.N. Dahms, J. Manin, L.M. Pickett, and J.C. Oefelein. Understanding high-pressure gas-liquid interface phenomena in diesel engines. *Proceedings of the Combustion Institute*, **34**:1667–1675, 2013.
4. L. Lu, P.M. Najt, T.-W. Kuo, V. Sankaran, and J.C. Oefelein. A fully integrated linear eddy and chemistry agglomeration method with detailed chemical kinetics for studying the effect of stratification on HCCI combustion. *Fuel*, **105**:653–663, 2013.
5. J. Manin, M. Bardi, L.M. Pickett, R.N. Dahms, and J.C. Oefelein. Development and mixing of diesel sprays at the microscopic level from low to high temperature and pressure conditions. *Proceedings of the 7th THIESEL Conference on Thermo- and Fluid-Dynamic Processes in Direct Injection Engines*, September 11–14 2012. Valencia, Spain.
6. J.C. Oefelein, R.N. Dahms, G. Lacaze, J.L. Manin, and L.M. Pickett. Effects of pressure on the fundamental physics of fuel injection in diesel engines. *Proceedings of the 12th International Conference on Liquid Atomization and Spray Systems*, September 2–6 2012. Heidelberg, Germany.

7. J.C. Oefelein, R.N. Dahms, and G. Lacaze. Detailed modeling and simulation of high-pressure fuel injection processes in diesel engines. *SAE International Journal of Engines*, **5**(3):1–10, 2012.
8. R. Knaus, J. Oefelein, and C. Pantano. On the relationship between the statistics of the resolved and true rate of dissipation of mixture fraction. *Flow, Turbulence and Combustion*, **89**(1):37–71, 2012.
9. G. Lacaze and J.C. Oefelein. A non-premixed combustion model based on flame structure analysis at supercritical pressures. *Combustion and Flame*, **159**:2087–2103, 2012.
10. B. Hu, M.P. Musculus, and J.C. Oefelein. The influence of large-scale structures on entrainment in a decelerating transient turbulent jet revealed by large eddy simulation. *Physics of Fluids*, **24**(045106):1–17, 2012.

SPECIAL RECOGNITIONS & AWARDS/ PATENTS ISSUED

1. ILASS Americas William Robert Marshall Award, 2012 (for best paper judged to be the most significant contribution to the ILASS 23rd Annual Conference on Liquid Atomization and Spray Systems.

II.9 Collaborative Combustion Research with Basic Energy Science

S. Scott Goldsborough
Argonne National Laboratory
9700 S. Cass Avenue
Bldg 362
Argonne, IL 60439

DOE Technology Development Manager:
Gurpreet Singh

- Acquired software for a multi-zone reactor model and initiated modifications for simulations of the RCM experiments.
- Acquired new ignition delay measurements for undoped iso-octane, as well as two multi-component gasoline surrogates + 2EHN. Developed chemical kinetic models for these blends and compared predictions with experimental data.
- Created an approach to account for RON and octane sensitivities of gasoline-relevant fuels within a reduced-order, control-oriented ignition model covering low- and high-temperature conditions.

Overall Objectives

- Collaborate with combustion researchers within DOE's Offices of Basic Energy Science (BES) and Vehicle Technologies programs to develop and validate predictive chemical kinetic models for a range of transportation-relevant fuels.
- Acquire ignition delay and other necessary combustion data using Argonne National Laboratory's (ANL's) rapid compression machine (RCM) at conditions representative of today's and future internal combustion engines, including high pressure ($p = 15\text{--}80$ bar) and low to intermediate temperatures ($T = 650\text{--}1,100$ K).

Fiscal Year (FY) 2013 Objectives

- Continue upgrades to RCM components to extend experimental capabilities.
- Refine reduced-order, physics-based models necessary for novel data analysis and simulation of RCM experiments; integrate those models into multi-zone reactor framework to improve fidelity of simulations.
- Acquire ignition delay measurements for gasoline surrogate fuels + reactivity modifiers, including 2-ethyl-hexyl nitrate (2EHN); develop and validate chemical kinetic models for these blends.
- Develop a reduced-order, control-oriented ignition model covering a wide range of fuel reactivity (e.g., Research Octane Number [RON] and octane sensitivity) and charge dilution.

FY 2013 Accomplishments

- Designed new heating and fuel delivery systems to reduce experimental uncertainties.
- Improved sub-models for heat loss in the piston crevice volume, which are now more reliable and applicable across a range of RCM piston geometries.

Future Directions

- Acquire additional ignition delay measurements for gasoline/diesel surrogates and real fuels along with reactivity modifiers, and improve predictive capabilities of chemical kinetic models.
- Incorporate novel approaches for kinetic mechanism validation/improvement, including global sensitivity analysis, as well as the use of new targets such as rate of heat release and low-temperature heat release.
- Test and validate the performance of a new, single-piston RCM.
- Test and validate a new reduced-order, control-oriented ignition under engine-relevant conditions.



INTRODUCTION

Accurate, predictive combustion models are necessary in order to reliably design and control next-generation fuels and future engines which can meet mandated fuel economy and emissions standards while achieving reductions in development times and costs for new configurations [1]. The imprecision of available models prevents the adoption of detailed simulation techniques within current design processes. Existing engineering-scale models can achieve satisfactory performance at some operating points; however, the models are neither sufficiently robust to cover complete ranges of conventional engine operation, nor when novel or advanced combustion concepts are utilized. Toward this, there is a critical need to improve the understanding of the multiple physical and chemical processes that occur within combustion engines, some of which include chemical ignition, fluid-chemistry interactions, and pollutant formation/decomposition. To advance these

understandings, collaborations are necessary across multiple disciplines, for example, between combustion engineers within DOE's Vehicle Technologies Office and scientists who are supported through DOE's BES. Through these interactions, fundamental, engine-relevant data can be acquired with low experimental uncertainties, while predictive models can be developed and validated based on these datasets.

APPROACH

RCMs are highly sophisticated, experimental tools that can be employed to acquire fundamental insight into fuel ignition and pollutant formation chemistry, as well as fluid-chemistry interactions, especially at conditions that are relevant to advanced, low-temperature combustion concepts [2]. They are capable of creating and maintaining well-controlled, elevated temperature and pressure environments (e.g., $T = 600$ to $1,100$ K, $P = 5$ to 80 bar) where the chemically-active period preceding autoignition can be monitored and probed via advanced in situ and ex situ diagnostics. The ability to utilize wide ranges of fuel and oxygen concentrations within RCMs, from ultra-lean to over-rich (e.g., $\phi = 0.2$ to $2.0+$), and spanning dilute to oxy-rich regimes (e.g., $O_2 = 5\%$ to $>21\%$), offers specific advantages relative to other laboratory apparatuses such as shock tubes and flow reactors where complications can arise under such conditions. The understanding of interdependent chemicophysical phenomena that can occur at some conditions within RCMs is a topic of ongoing investigation within the combustion community, while interpretation of facility influences on datasets is also being addressed [2]. Approaches to implementing novel diagnostics that can provide more rigorous constraints for model validation compared to integrated metrics such as ignition delay times, e.g., quantification of important radical and stable intermediates such as H_2O_2 and C_2H_4 [3,4], are under development by many combustion researchers.

Argonne's existing twin-piston RCM is utilized in this project to acquire data necessary for chemical kinetic model development and validation, while improvements to the facility's hardware and data analysis protocol are continually performed to extend its capabilities and fidelity. Collaborations are undertaken with BES-funded scientists at ANL and other U.S. laboratories, as well as with researchers at national and international institutions, including complementary RCM facilities.

RESULTS

Physics-based, reduced-order models have previously been developed for RCMs [5,6] in order

to reduce uncertainties associated with modeling the chemical kinetic processes within the reaction chamber. These models take into account effects of fluid flow and heat loss which alter the thermodynamic state of the reacting mixture, and have cost and other advantages relative to conventional methodologies which employ empirical representations of the heat loss based on experiments using analogous non-reacting mixtures (e.g., O_2 replaced by N_2). Reduced-order models, as opposed to multi-dimensional computational fluid dynamics (CFD) approaches, are required in order to utilize large, detailed chemical kinetic mechanisms in the simulations. These models also have the potential to be used in data reduction algorithms in order to derive additional parameters from experimental measurements, such as the temperature rise that occurs during preliminary stages of ignition, where these can be used as new metrics for mechanism validation purposes. Efforts this year have focused on re-formulating existing correlations for fluid shear and convective heat transfer within the piston crevice volume of the RCM. Piston crevices that are machined circumferentially typically utilize geometries which are generally constrained by a particular RCM's configuration. The individual design can alter the fluid dynamics of the gas that flows into the crevice during an experiment, and thus affect the pressure/temperature history of the gas in the reaction chamber during the delay period. Existing expressions assume that the gas flow resembles motion within the annulus of a concentric pipe. More realistic, generalized expressions have therefore been developed based on detailed CFD simulations, where these are able to account for various geometries and thus can be utilized for ANL's existing RCM, as well as a new single-piston machine that is currently being fabricated, to be commissioned in FY 2014.

Additional improvement in the fidelity of RCM simulations can be accomplished by using a stratified reactor model to simulate the experiments [7]. With such an approach, the reactivity within the colder boundary layer could be taken into account, where this has been demonstrated to be influential within the negative temperature coefficient (NTC) regime. Further, rates of heat release, which are affected by boundary layer effects even for single-stage fuels, can be more realistically simulated using a stratified reactor model. To facilitate this, a multi-zone model was acquired from Lawrence Livermore National Laboratory (LLNL) in the last quarter of FY 2013, and modifications have been initiated to adapt this software to simulations of ANL's RCM, e.g., by incorporating the capability to prescribe the machine's piston trajectory. In FY 2014, physical sub-models for heat loss and crevice flows in the RCM will be integrated into the software.

Experiments have been conducted in the RCM in order to investigate the influence and effectiveness of fuel additives, specifically for gasoline-relevant fuels. Additives are useful for improving the ignition quality of low grade fuels, especially at very small quantities, e.g., 1 ppm to 1,000 ppm, and have been suggested as a means to dynamically control fuel reactivity during engine operation in order to cover a wide range of combustion modes, including conventional and low-temperature combustion modes [8]. Additives are chemical compounds that contain a weak intramolecular bond where this leads to rapid decomposition at modest temperatures, so that in the combustion chamber, they break down early in the combustion process, substantially before the fuel. The decomposition process yields active chemical species, such as alkyl radicals and nitrogen dioxide, which stimulate fuel reactivity, e.g., through the formation of OH. Though a number of studies have been conducted with fuel additives in fundamental laboratory experiments [9-16], as well as within internal combustion engines [17-25], important questions remain, including:

- How do additives interact with various fuel components (e.g., paraffins, branched alkanes, aromatics) across a range of conditions?
- What are influences of exothermicity and kinetic pathway acceleration?
- Can interactions and influences be reliably predicted, along with impacts to pollutant formation, e.g., oxides of nitrogen?
- Are there optimal additives that can be used across a range of operating modes?

Mixtures of two simple gasoline surrogates have been tested in the RCM, one a two-component blend of n-heptane/iso-octane (primary reference fuel, PRF), and a second that is a three-component blend of n-heptane/iso-octane/toluene (toluene reference fuel, TRF). The compositions of the fuels are adjusted so that the RON of each is approximately 91. The fuels are doped with 2EHN at levels of 0.1%, 1.0% and 3.0% liquid volume, and tests are conducted at a pressure of 21 bar over a temperature range from 675 K to 1,025 K. Fuel lean ($\phi < 1$), fuel rich ($\phi > 1$), and stoichiometric ($\phi = 1$) ratios are used for the PRF91 blends, while the TRF91 blend is tested at $\phi = 1$.

Chemical kinetic models are constructed which consist of a base fuel mechanism, a sub-mechanism for the fuel additive, and a sub-mechanism for the nitrogen chemistry. Two fuel mechanisms are employed for comparison, included the LLNL detailed gasoline surrogate model [26-28], and the University of Wisconsin Engine Research Center MultiChem model [29]. The sub-mechanism for 2EHN is based on ref. [30] where 2EHN decomposes in two steps. First, the interior O-N bond is cleaved to release NO₂; after this, the ethyl

hexoxy radical β-scissions into C₇H₁₆-3 and CH₂O. Two sub-mechanisms for nitrogen chemistry are utilized. The first is a skeletal compilation that includes basic pathways for the formation and consumption of NO, N₂O, and NO₂; H-atom abstractions from the surrogate fuel by NO₂; and HONO decomposition [31]. A comprehensive mechanism is also assembled that includes pathways that are described in ref. [32]. A number of fuel-specific interactions are also considered in the comprehensive mechanism, including H-atom abstractions from, and NO/NO₂ additions to, the fuel radical.

The experiment and modeling results are presented in Figures 1-3. Figure 1 illustrates the measured and computed ignition delay times for the PRF91 and TRF91 blends at the $\phi = 1$ condition. Also included here for reference are data for iso-octane/“air” mixtures (PRF100) conducted at p = 20 bar, $\phi = 1$ and 21% O₂; these are the conditions specified at the 1st International RCM Workshop [2]. The data for the PRF91 and TRF91 mixtures are seen to have measured ignition times that are significantly longer than the PRF100 mixtures, where this is due to the high level of dilution used in the additive experiments (11.4% O₂). Also visible in this figure is that while the LLNL mechanism reasonably predicts the 1st and 2nd stage ignition times for the PRF100 cases, the predictions are generally too fast for the undoped PRF91 and TRF91 mixtures. The differences in NTC behavior between the two fuels, however, that are seen in the experiments are adequately predicted by the detailed mechanism. The simulations using the University of Wisconsin Engine Research Center mechanism are even faster than the LLNL mechanism for the overall ignition

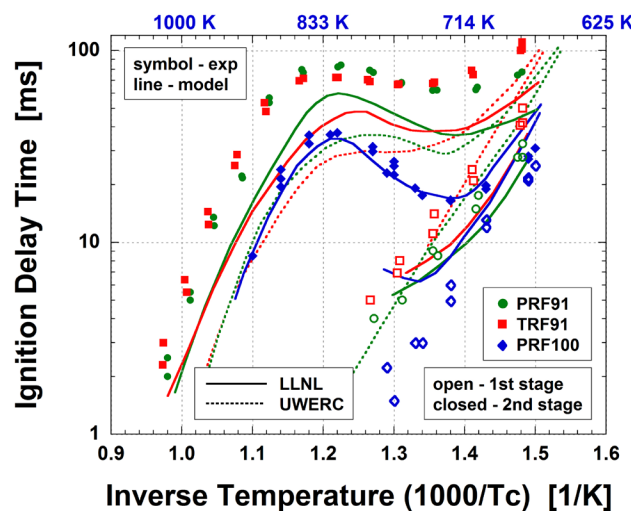


FIGURE 1. Ignition delay times as function of temperature for three undoped fuels, PRF91, TRF91 and PRF100 at 21 bar and stoichiometric conditions; PRF91 and TRF91 conducted at 11.4% oxygen, PRF100 at 21% oxygen.

times, though the computed 1st stage ignition times lie close to the experimental measurements.

Figures 2 and 3 illustrate the results for the doped experiments using PRF91 and TRF91 where the doping effectiveness is plotted as functions of temperature, with this defined as the ratio of ignition delay time for the doped to undoped mixtures, i.e., $R_{\text{eff}} = \tau_{\text{doped}} / \tau_{\text{undoped}}$. Here it can be seen that at the experimental conditions none of the chemical kinetic mechanisms adequately predict the effectiveness of the 2EHN additive. The detailed model generally over-predicts the ignition sensitization, while the reduced model generally under-predicts this sensitization. Additional work is needed to understand

the model results and improve the predictive capabilities of these mechanisms for use in internal combustion engine simulations. Nevertheless, it is clear that the experiments and simulations highlight the importance of adequately representing the base chemistry of the fuel in chemical kinetic models to achieve proper sensitization for the additive. Additional tests are planned for FY 2014 using the RCM to explore other fuel additives, and additive–fuel interactions.

A reduced-order, control-oriented ignition model is also under development within this project in order to enhance the capability to reliably predict knock and autoignition via model-based control algorithms. Conventional approaches typically utilize ignition delay correlations that are fitted to experimental or modeling results, where a knock integral is employed to indicate the time of ignition in the cycle. Existing correlations cover limited engine-relevant operating ranges and levels of fuel reactivity, e.g., RON [33]. This activity seeks to create a universal expression that can be used for a wide range of gasoline- and diesel-relevant fuels (RON = 0–120), and can account for fuel-dependent, octane sensitivities ($S = \text{RON} - \text{MON} = 0–12$), especially in the NTC regime. NTC behavior has been demonstrated to be especially important within advanced combustion regimes [33]. During FY 2013 an approach was formulated to develop expressions covering low- and high-temperature regimes ($T = 500–650$ K, 1,450–2,000 K) for 11 TRF fuel blends. In FY 2014 these expressions will be combined within the NTC region so that the complete temperature range of 500 K to 2,000 K can be covered with a unified expression.

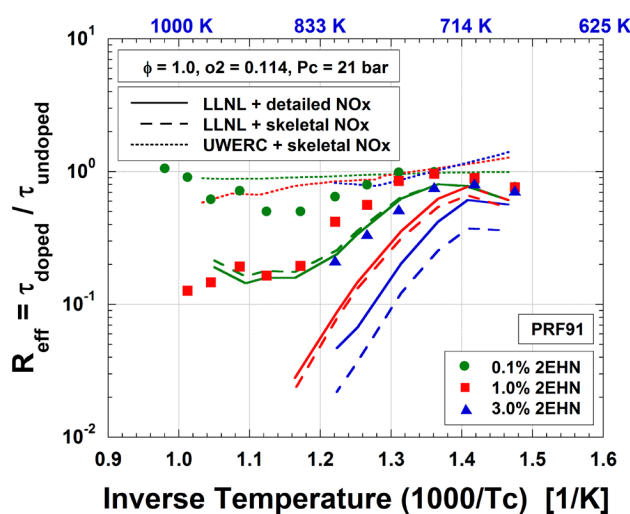


FIGURE 2. Effectiveness of 2EHN doped into a two-component gasoline surrogate, PRF91 at 21 bar and 11.4% oxygen.

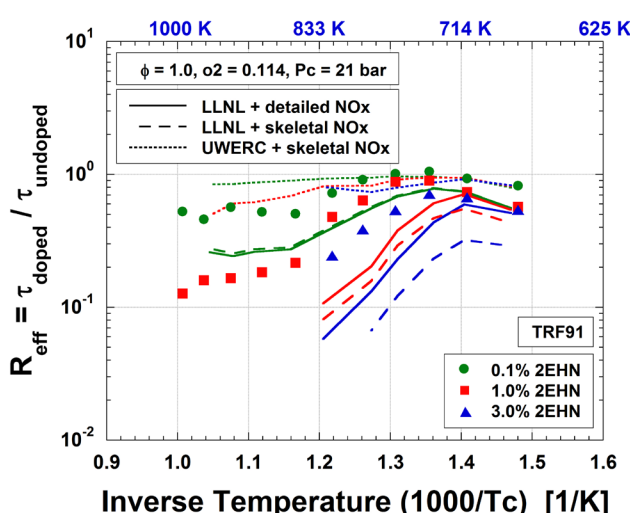


FIGURE 3. Effectiveness of 2EHN doped into a three-component gasoline surrogate, TRF91 at 21 bar and 11.4% oxygen.

CONCLUSIONS

- A high-fidelity modeling framework has been developed to simulate chemicophysical processes within ANL's RCM, where refinements to this are ongoing. This activity enhances the validation and improvement of chemical kinetic mechanisms for transportation-relevant fuels.
- ANL's RCM has been used to acquire autoignition data for additive-doped gasoline surrogate blends. Chemical kinetic models have been assembled for these fuels with predictions compared against experimental mechanisms and additive decomposition rates seem to be necessary in order to adequately capture the sensitizing effects of fuel additives.
- Comprehensive expressions have been developed for a reduced-order, control-oriented ignition model which cover low and high temperatures for fuels with a wide range of reactivity. Future work will

unify these expressions across temperatures from 500 K to 2,000 K.

REFERENCES

- 1.** Basic Research Needs for Clean and Efficient Combustion of 21st Century Transportation Fuels. (http://science.energy.gov/~/media/bes/pdf/reports/files/ctf_rpt.pdf)
- 2.** S.S. Goldsborough, D. Longman, M.S. Wooldridge, R.S. Tranter and S. Pratt, “1st International RCM Workshop Meeting Report,” August 28–29, 2012. (<http://www.transportation.anl.gov/rcmworkshop>)
- 3.** C. Bahrini, O. Herbinet, P.-A. Glaude, C. Schoemaecker, C. Fittschen and F. Battin-Leclerc, *J. Am. Chem. Soc.* (139) 11944-11947, 2012.
- 4.** I. Stranic, S.H. Pyun, D.F. Davidson, R.K. Hanson, *Combust. Flame* (159) 3242-3250, 2012.
- 5.** S.S. Goldsborough, C. Banyon, G. Mittal, *Combust. Flame* (159) 3476-3492, 2012.
- 6.** S.S. Goldsborough, G. Mittal, C. Banyon, *Proc. Comb. Inst.* (34) 685-693, 2013.
- 7.** J. Kodavasal, M.J. McNenly, A. Babajimopoulos, S.M. Aceves, D.N. Assanis, M.A. Havstad and D.L. Flowers, *Int. J. Engine Res.* (14) 416-433, 2013.
- 8.** S.L. Kokjohn, R.M. Hanson, D.A. Splitter and R.D. Reitz, *SAE Paper* 2009-01-2647, 2009.
- 9.** B. Higgins, D. Siebers and C. Mueller, Sandia Report SAND98-8243, 1998.
- 10.** G.J. Suppes, Y. Rui, A.C. Rome and Z. Chen, *Ind. Eng. Chem. Res.* 36:4397-4404, 1997.
- 11.** T. Inomata, J.F. Griffiths, A.J. Pappin, 23rd Symp. (Int.) Combust. 1759-1766, 1990.
- 12.** J.F. Griffiths, Q. Jiao, W. Kordylewski, M. Schreiber, J. Meyer, and K.F. Knoche, *Combust. Flame* 93:303-315, 1993.
- 13.** S. Tanaka, F. Ayala, J.C. Keck and J.B. Heywood, *Combust. Flame* 132:219-239, 2003.
- 14.** A. Toland, J.M. Simmie, *Combust. Flame* 132:556-564, 2003.
- 15.** M. Hartmann, K. Tian, C. Hofrath, M. Fikri, A. Schubert, R. Schiessl, R. Starke, B. Atakan, C. Schulz, U. Maas, F. Kleine Jäger and K. Kühlung, *Proc. Comb. Inst.* 32:197-204, 2009.
- 16.** Y. Stein, R.A. Yetter, F.L. Dryer and A. Aradi, *SAE Paper* 1999-01-1504, 1999.
- 17.** A.M. Ickes, S.V. Bohac and D.N. Assanis, *Energy Fuels* 23:4943-4948, 2009.
- 18.** J.A. Eng, W.R. Leppard and T.M. Sloane, *SAE Paper* 2003-01-3179, 2003.
- 19.** X. Gong, R. Johnson, D.L. Miller and N.P. Cernansky, *SAE Paper* 2005-01-3740, 2005.
- 20.** A. Gupta, D.L. Miller and N.P. Cernansky, *SAE Paper* 2007-01-2002, 2007.
- 21.** J.H. Mack, R.W. Dibble, B.A. Buchholz and D.L. Flowers, *SAE Paper* 2005-01-2135, 2005.
- 22.** D. Splitter, R. Reitz and R. Hanson, *SAE Paper* 2010-01-2167, 2010, 2010.
- 23.** R. Hanson, S. Kokjohn, D. Splitter, R. Reitz, *SAE Paper* 2011-01-0361, 2011.
- 24.** J. Kaddatz, M. Andrie, R. Reitz, S. Kokjohn, *SAE Paper* 2012-01-1110, 2012.
- 25.** A.B. Dempsey, N.R. Walker, R. Reitz, *SAE Paper* 2013-01-1678, 2013.
- 26.** M. Mehl, W.J. Pitz, C.K. Westbrook, H.J. Curran, *Proc. Comb. Inst.* 33:193-200, 2011.
- 27.** G. Kukkadapu, K. Kumar, C.-J. Sung, M. Mehl, W.J. Pitz, *Combust. Flame* 159:3066-3078, 2012.
- 28.** G. Kukkadapu, K. Kumar, C.-J. Sung, M. Mehl, W.J. Pitz, *Proc. Comb. Inst.* 34:345-352, 2013.
- 29.** Y. Ra and R.D. Reitz, *Combust. Flame* 158 (2011) 69-90.
- 30.** H. Bornemann, F. Scheidt and W. Sander, *Int. J. Chem. Kinet.* 34 (2002) 34-38.
- 31.** M. Hartmann, K. Tian, C. Hofrath, M. Fikri, A. Schubert, R. Schiessl, R. Starke, B. Atakan, C. Schulz, U. Maas, F. Kleine Jäger and K. Kühlung, *Proc. Comb. Inst.* 32:197-204, 2009.
- 32.** S.S. Goldsborough, 8th US National Combustion Meeting, Salt Lake City, UT, 2012.
- 33.** S.S. Goldsborough, T.A. Smith, M.V. Johnson, S.M. McConnell, *SAE Paper* 2012-01-1136, 2012.

FY 2013 PUBLICATIONS/PRESENTATIONS

- 1.** S.S. Goldsborough, “The influence of nitrogen chemistry on the effectiveness of alkyl nitrates as cetane enhancers: a modeling study,” 8th US National Combustion Meeting, Salt Lake City, UT, 2012.

II.10 Chemical Kinetic Models for HCCI and Diesel Combustion

William J. Pitz (Primary Contact), Marco Mehl,
Charles K. Westbrook

Lawrence Livermore National Laboratory (LLNL)
P. O. Box 808, L-288
Livermore, CA 94551

DOE Technology Development Manager:
Gurpreet Singh

- Developed an improved model for methylcyclohexane and validated it for ignition at engine conditions and for species measurements in low-pressure flames

Future Directions

- Continue to develop detailed chemical kinetic models for larger alkyl aromatics including ones with more than one alkyl side chain
- Develop gasoline surrogate fuels for fuels for advanced combustion engines (FACE) fuels
- Develop an additional surrogate component model to represent two-ring aromatics in diesel fuel
- Develop improved chemical kinetic models for the cycloalkane chemical class in diesel fuel



Overall Objectives

- Develop detailed chemical kinetic models for fuel components used in surrogate fuels for compression ignition (CI), Homogeneous Charge Compression Ignition (HCCI) and Reactivity-Controlled Compression-Ignition (RCCI) engines.
- Combine component models into surrogate fuel models to represent real transportation fuels. Use them to model low-temperature combustion strategies in HCCI, RCCI, and CI engines that lead to low emissions and high efficiency.

Fiscal Year (FY) 2013 Objectives

- Develop detailed chemical kinetic models for larger alkyl aromatics relevant to diesel fuels
- Develop more accurate surrogate kinetics models for gasoline-fueled HCCI, including ethanol
- Develop improved chemical kinetic models for larger alkyl-cyclohexanes
- Develop an improved 2-component surrogate mechanism for diesel to be used for multidimensional computational fluid dynamics (CFD) simulations

FY 2013 Accomplishments

- Developed improved models for n-propyl benzene, n-butyl benzene, and their mixtures and validated them for ignition and flame speeds
- Developed a new chemical kinetic model for α -methyl naphthalene and validated it for high-temperature ignition in a shock tube and oxidation in a flow reactor
- Developed a fuel surrogate model for gasoline-ethanol mixtures and validated it by comparison to flame speeds in a flat-flame burner and intermediate heat release in an HCCI engine

INTRODUCTION

Predictive engine simulation models are needed to make rapid progress towards DOE's goals of increasing combustion engine efficiency and reducing pollutant emissions. These engine simulation models require chemical kinetic submodels to allow the prediction of the effect of fuel composition on engine performance and emissions. Chemical kinetic submodels for conventional and next-generation transportation fuels need to be developed to fulfill these requirements.

APPROACH

Gasoline and diesel fuels consist of complex mixtures of hundreds of different components. These components can be grouped into chemical classes including n-alkanes, iso-alkanes, cycloalkanes, alkenes, oxygenates, and aromatics. Since chemical kinetic models cannot be developed for hundreds of components, specific components need to be identified to represent each of these chemical classes. Then detailed chemical kinetic models can be developed for these selected components. These component models are subsequently merged together to produce a "surrogate" fuel model for gasoline, diesel, and next-generation transportation fuels. This approach can create realistic surrogates for gasoline or diesel fuels that reproduce experimental behavior of the practical real fuels that they represent. Detailed kinetic models for surrogate fuels can then be simplified as needed for inclusion in multidimensional CFD models.

RESULTS

In FY 2013, the chemical kinetic models for n-propyl benzene and n-butyl benzene were greatly improved by including more-accurate C1-C4 base chemistry and by updating low-temperature pathways for these alkyl benzenes. These models were validated by comparing simulations to experimental data on ignition in a shock tube and a rapid compression machine (RCM) at National University of Ireland, Galway. A comparison for nbutyl benzene is shown in Figure 1 where the model well reproduces the experimental data. The models were also validated for mixtures by simulating alkyl benzenes mixed with n-heptane. Again, the comparison of simulations to experimental data from National University of Ireland, Galway was good. These well-validated alkyl benzene models are a valuable addition to the LLNL surrogate components for diesel fuel.

In addition to single-ring alkyl benzenes, diesel fuel also contains two-ring aromatics. To help simulate this chemical class, a chemical kinetic model for α -methyl naphthalene was developed by LLNL. α -Methyl naphthalene has been selected by Mueller et al. in a nine-compound diesel surrogate palette that well reproduces the ignition behavior, distillation curve, molecular structures, and density of two representative diesel fuels [1]. Simulations using the α -methyl naphthalene model were compared to high-temperature ignition measured in a shock tube and intermediate species measured in a flow reactor. A comparison of the simulations and experimental data from the flow reactor is shown in Figure 2. The agreement between the simulations and experiments is reasonable and development of this component mechanism is a significant step towards

representing the nine components in a peer-reviewed diesel surrogate palette [1].

In FY 2013, LLNL development of surrogate models for gasoline fuels has been expanded to include ethanol. We have developed new correlations to match the Research Octane Number and sensitivity of a target gasoline-ethanol fuel with a surrogate fuel mixture. Using these correlations, we have developed five-component surrogate mixtures for 15, 50, and 85% ethanol in gasoline. These mixtures used the same gasoline hydrocarbon components as used in our previous work [2]. Our gasoline-ethanol surrogate mechanism using these three surrogate formulations was able to reasonably match flame speeds for the corresponding real gasoline ethanol mixtures experimentally measured in premixed flames by Professor Egolfopoulos's group at the University of Southern California. Our new model also matched reasonably well the experimental flame speeds for neat gasoline and neat ethanol. These new gasoline ethanol formulations and corresponding chemical kinetic models were further tested in an HCCI engine for 10% and 20% ethanol gasoline mixtures (E10 and E20). The predictions of the chemical mechanism using a single-zone model compare well to HCCI engine experiments performed at Sandia National Laboratories for intermediate temperature heat release (ITHR). ITHR is an important fuel behavior whose presence allows ignition phasing to be delayed so that higher boost operation in an engine can be achieved [3].

Gasoline FACE fuels have been developed to provide researchers with controlled gasoline compositions that can be used to assess the fuel effects on engine combustion [4]. The LLNL kinetics team has formulated gasoline surrogates to match gasoline FACE A and C

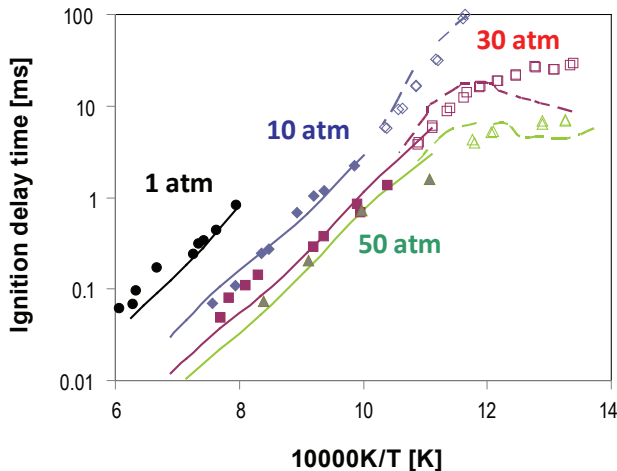


FIGURE 1. A comparison of ignition behavior from the chemical kinetic model (curves) and the experiments (symbols) for n-butyl benzene. The solid curves and closed symbols are results from the shock tube and the open symbols and the dashed curves are from the RCM.

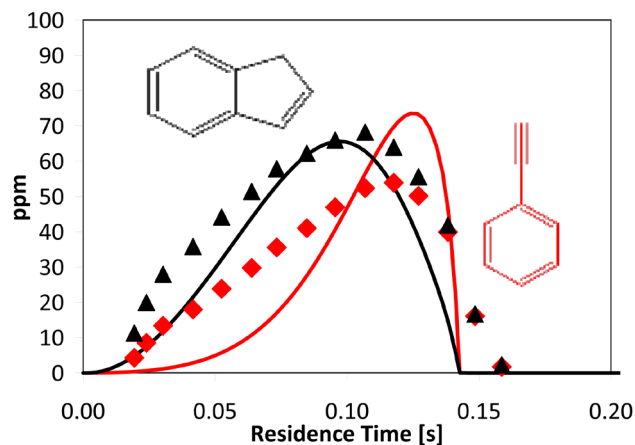


FIGURE 2. Comparison of simulations from the α -methyl naphthalene chemical kinetic model with measurements [6] of intermediate species in a flow reactor for an equivalence ratio of 0.5 at 1 atm. The intermediate species shown are indene and phenylacetylene.

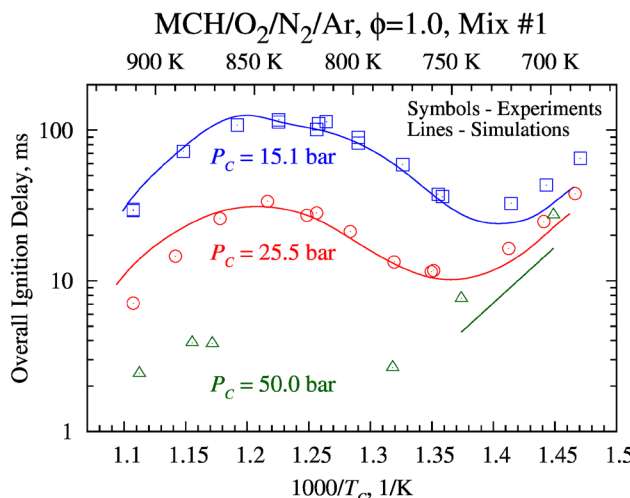


FIGURE 3. Comparison of the methylcyclohexane model with experimental ignition data from an RCM [5], for a stoichiometric mixture, over a range of temperatures, and at pressures of 15, 25 and 50 bar.

using their mixture correlations [2]. They have used the corresponding LLNL gasoline surrogate mechanism to simulate their ignition behavior measured in a shock tube at KAUST and measured in an RCM at the University of Connecticut. The LLNL mechanism and surrogate formulation is able to reasonably reproduce the experimental ignition behavior and that of a corresponding primary reference fuel 84 mixture.

The methylcyclohexane mechanism which is used to represent cycloalkanes in gasoline fuels has been significantly improved in its prediction of ignition and soot precursor species. The low-temperature chemistry of the methylcyclohexane mechanism has been improved using first-principles rate constants computed by Sandia National Laboratories. The critical abstraction rates of H atoms from the fuel have been made more accurate by using experimentally measured rate constants from Argonne National Laboratory. The fidelity of the treatment of unsaturated species has been enhanced so that soot precursor species are much better predicted. Simulations using the improved mechanism have been compared to ignition behavior in an RCM over a wide range of temperature, pressure and equivalence ratio, Figure 3 [5]. An RCM mimics conditions in an internal combustion engine. Simulations have also been compared to experimental measurements of radicals and intermediate species in a low-pressure flame using the Advanced Light Source facility at Lawrence Berkeley National Laboratory.

CONCLUSIONS

- Improved mechanisms for alkyl benzenes, and their mixtures with n-heptane have been developed and validated
- A new mechanism for α -methyl naphthalene has been developed to represent two ring aromatics in diesel fuel
- A new correlation to formulate surrogates for ethanol gasoline mixtures has been developed and used to simulate experimental flame speeds in a premixed flame and ITHR in an engine
- The methylcyclohexane mechanism has been greatly improved in its ability to simulate ignition in an RCM and soot-precursor species needed to predict soot emissions

REFERENCES

- C.J. Mueller, W.J. Cannella, T.J. Bruno, B. Bunting, H.D. Dettman, J.A. Franz, M.L. Huber, M. Natarajan, W.J. Pitz, M.A. Ratcliff and K. Wright, “Methodology for Formulating Diesel Surrogate Fuels with Accurate Compositional, Ignition-Quality, and Volatility Characteristics,” *Energy & Fuels* 26 (6) (2012) 3284–3303.
- M. Mehl, J.Y. Chen, W.J. Pitz, S.M. Sarathy and C.K. Westbrook, “An Approach for Formulating Surrogates for Gasoline with Application toward a Reduced Surrogate Mechanism for CFD Engine Modeling,” *Energy & Fuels* 25 (11) (2011) 5215–5223.
- J.E. Dec and Y. Yang, “Boosted HCCI for High Power without Engine Knock and with Ultra-Low NOx Emissions - using Conventional Gasoline,” Society of Automotive Engineers, SAE 2010-01-1086, (2010).
- FACE, “CRC Fuels for Advanced Combustion Engines Working Group (FACE),” <http://www.crao.org/publications/advancedVehiclesFuelsLubricants/FACE/index.html>, (2013).
- B.W. Weber, W.J. Pitz, M. Mehl, E.J. Silke, A.C. Davis and C.-J. Sung, “Experiments and Modeling of the Autoignition of Methylcyclohexane at High Pressure,” *Combust. Flame* Submitted (2013).
- C.R. Shaddix, K. Brezinsky and I. Glassman, “Oxidation of 1-methylnaphthalene,” *Symposium (International) on Combustion* 24 (1) (1992) 683–690.

FY 2013 PUBLICATIONS/PRESENTATIONS

- Weber, B.W., W.J. Pitz, M. Mehl, E.J. Silke, A.C. Davis and C.-J. Sung (2013). “Experiments and Modeling of the Autoignition of Methylcyclohexane at High Pressure.” *Combustion and Flame*, Submitted.
- Nakamura, H., Darcy, D., Mehl, M., Tobin, C.J., Metcalfe, W.K., Pitz, W.J., Westbrook, C.K. and Curran, H.J., “An Experimental and Modeling Study of Shock Tube and

Rapid Compression Machine Ignition of n-Butylbenzene/Air Mixtures,” Combustion and Flame (2013) <http://dx.doi.org/10.1016/j.combustflame.2013.08.002>.

3. Darcy, D., Nakamura, H., Tobin, C.J., Mehl, M., Metcalfe, W.K., Pitz, W.J., Westbrook, C.K. and Curran, H.J., “A High-Pressure Rapid Compression Machine Study of n-Propylbenzene Ignition,” Combustion and Flame (2013) <http://dx.doi.org/10.1016/j.combustflame.2013.08.001>.

4. Darcy, D., Nakamura, H., Tobin, C.J., Mehl, M., Metcalfe, W.K., Pitz, W.J., Westbrook, C.K. and Curran, H.J., “An Experimental and Modeling Study of a Surrogate Mixtures of N-Propyl- and N-Butylbenzene in N-Heptane to Simulate N-Decylbenzene Ignition,” Combustion and Flame, Submitted (2013).

5. Z. Luo, S. Som, S.M. Sarathy, M. Plomer, W.J. Pitz, D.E. Longman and T. Lu, “Development and Validation of an n-Dodecane Skeletal Mechanism for Diesel Spray-Combustion Applications,” Combustion Theory and Modelling (2013), Submitted.

6. Vuilleumier, D., Kozarac, D., Mehl, M., Saxena, S., Pitz, W.J., Dibble, R., Chen, J. and Sarathy, M., “Intermediate Temperature Heat Release in an HCCI Engine Fueled by Ethanol / N-Heptane Mixtures: An Experimental and Modeling Study,” Combustion and Flame (2013) <http://dx.doi.org/10.1016/j.combustflame.2013.10.008>.

II.11 Computationally Efficient Modeling of High Efficiency Clean Combustion Engines

Russell Whitesides (Primary Contact),
Salvador Aceves, Daniel Flowers,
Nick Killingsworth, Matt McNenly,
Geoff Oxberry, Tom Piggott, Randy Hessel
(University of Wisconsin), Robert Dibble
(University of California, Berkeley),
J.Y. Chen (University of California, Berkeley)
Lawrence Livermore National Laboratory (LLNL)
P.O. Box 808, L-792
Livermore, CA 94551

DOE Technology Development Manager:
Gurpreet Singh

Subcontractors:

- University of Wisconsin, Madison, WI
- University of California, Berkeley, CA

Overall Objectives

- Gain fundamental and practical insight into High Efficiency Clean Combustion (HECC) regimes through numerical simulations and experiments
- Develop and apply numerical tools to simulate HECC by combining multidimensional fluid mechanics with chemical kinetics
- Reduce computational expense for HECC simulations
- Democratize high fidelity engine simulation by bringing computational tools to the desktop computer for use by engine designers and researchers

Fiscal Year (FY) 2013 Objectives

- Validate and develop combustion simulation capabilities that will enable the prediction of performance and emissions in the development of new vehicle powertrain technologies
- Conduct detailed analysis of Homogenous Charge Compression Ignition (HCCI) and direct-injection engine experiments and conduct analysis of clean and efficient diesel engines that use stoichiometric and low-temperature combustion modes
- Develop fully-parallelized multi-dimensional computational fluid dynamics (CFD)-chemistry solvers for analysis of non-homogeneous engine combustion

- Distribute advanced combustion models to U.S. industrial and academic partners

FY 2013 Accomplishments

- Validated new multi-zone scheme, quantified accuracy and fidelity for zone strategies
- Implemented advanced solvers with CONVERGE™ multi-zone, yielding orders of magnitude reduction in simulation time
- Validated multi-dimensional simulations of iso-octane Premixed Charge Compression Ignition (PCCI) using CONVERGE™ multi-zone with detailed chemistry
- Demonstrated CFD/multi-zone applied to gasoline direct-injection spark ignition and PCCI operation
- Partnered with Cummins/CONVERGE™ to integrate graphical processing unit (GPU)-based solver into multidimensional CFD, developed and tested GPU combustion chemistry with potential 8x speedup
- New license agreement for advanced central processing unit (CPU)/GPU solvers with Convergent Science
- Initiated analysis of direct-injected diesel combustion for full engine geometry

Future Directions

- Increase accuracy and lower computational cost of multi-zone combustion model: Jacobian or other improved remap; error-bounded zoning
- Improve computational performance for operator-split, every-cell chemistry in CFD: quasi-steady-state, partial equilibrium, perturbative methods, fully coupled chemistry/advection/diffusion
- Implement algorithms to optimize computational performance of species advection/diffusion calculations.
- Perform engine simulations with LLNL parallel CFD with chemistry investigating fuel effects in HCCI/PCCI engines (simulations with full and reduced mechanism for RD387 [1], certification fuel, ethanol based on Dec/Sandia experiments [2])
- Work towards predictive diesel engine simulations by combining CFD, spray, soot, diesel surrogate

- [3], and Pitz mechanism (e.g. [4]) and compare with experiments at Sandia National Laboratories
- Conduct chemical kinetics mechanism rate optimization through the use of sensitivity analysis, HCCI engine experiments at multiple operating points, and multidimensional HCCI simulations
 - Continue technology transfer and licensing activities



INTRODUCTION

This project focuses on the development and application of computationally efficient and accurate simulation tools for prediction of engine combustion. Simulation of combustion aids in development of new high-efficiency and low-emissions engines by allowing detailed characterization of in-cylinder engine processes that are difficult to measure directly. Simulation also allows exploratory investigations of new concepts, such as new combustion chamber geometry, allowing valuable and limited experimental resources to be focused on the most promising strategies.

Combustion simulation is computationally demanding because it combines three-dimensional turbulent fluid flow with highly exothermic chemical reactions proceeding at rates that span several orders of magnitude. As such, simulation of an internal combustion engine cycle with chemistry and fluid flow typically requires access to large-scale computing resources. One major motivation of this research is to use physical and mathematical methods to reduce computational expense of combustion simulation with minimal loss of accuracy. These computationally efficient tools are applied to understand the fundamental physical processes occurring in engines operating with HECC strategies.

APPROACH

We use high-fidelity simulations to predict internal combustion engine operation, seeking to maximize computational performance by taking advantage of physical discretization strategies, numerical methods, and new computer architectures. Thermo-kinetic chemistry and fluid mechanics that occurs in engine combustion (diesel, spark ignition, HCCI, etc.) is challenging to simulate because of the large gradients present and the wide range of time-scales over which these processes occur, from femtoseconds to milliseconds. We developed a multi-zone solver that significantly reduces the computational burden of chemistry simulation combined with computational fluid mechanics with little loss in accuracy. The multi-zone model solves chemistry in a non-geometric thermo-chemical phase-

space, significantly reducing the number of chemistry calculations needed to calculate an engine cycle relative to the standard geometric discretization.

Multi-zone chemistry modeling allows for higher fidelity of combustion simulation through a more effective use of available computational resources. Combining multi-zone modeling with parallel CFD gives increased fidelity to the fluid mechanics part of combustion simulation along with the chemistry. However, chemistry simulation for complex fuels is still computationally expensive. This project is closely coupled to two other projects at LLNL, the Chemical Kinetics Models for Advanced Engine Combustion project led by William Pitz [5], and the Improved Solvers for Advanced Engine Combustion Simulation project led by Matthew McNenly [6]. The chemical kinetics project provides better physical models of fuel ignition, and the solvers project allows this project to effectively use these physical models to simulate engines.

RESULTS

This year's effort has been focused on continued development and application of computational tools to effectively simulate advanced high-efficiency engine combustion strategies. The multi-zone combustion model has been demonstrated to be accurate and effective for predicting HCCI and PCCI combustion using practical, engineering levels of resolution for the fluid mechanics with detailed chemical kinetic mechanisms [7-9]. The standard approach to solving chemical kinetics in computational fluid mechanics codes is to solve chemistry in every cell of the CFD grid, resulting in a requirement to solve from tens of thousands to several million chemical reactors. With detailed chemistry for realistic fuels, solving chemistry in every cell requires unreasonably long computational times, from days to weeks for a single engine cycle simulation for even modestly sized mechanisms with hundreds of species.

Figure 1 shows how physical models, computational tools, and detailed experiments are being combined in this and associated projects to study engine combustion. Mueller et al. developed a 9-component mixture of compounds that has been experimentally verified to produce combustion and emissions characteristics representative of diesel fuel [3]. The fuel chemical kinetics project has developed chemical kinetic mechanisms for many of the various components in the diesel surrogate and is currently working towards developing a comprehensive chemical kinetic mechanism for the 9-component surrogate [1,4], which will contain upwards of 10,000 chemical species. The combustion numerics project has reduced computational time for solving combustion chemical kinetics by orders of magnitude, enabling the use of these large mechanisms in

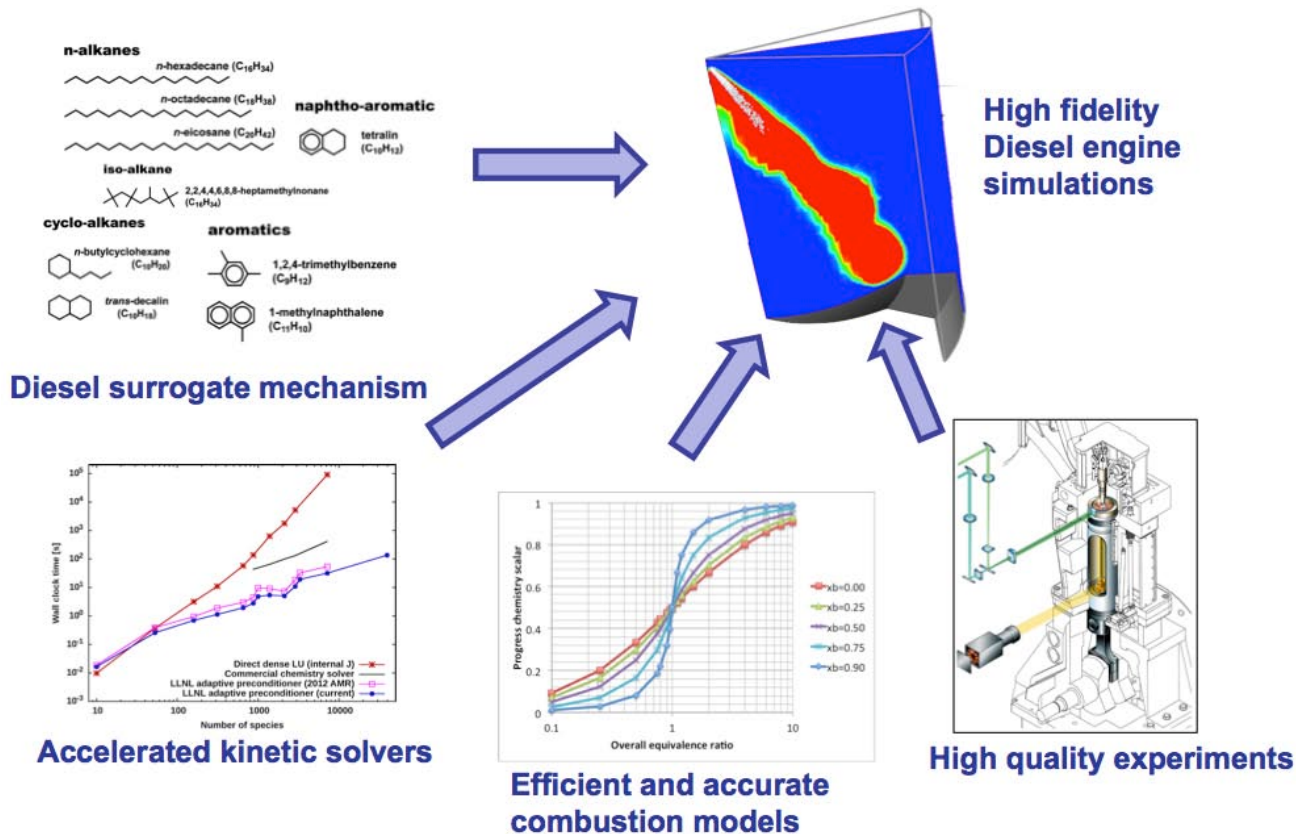


FIGURE 1. Schematic of the approach to advanced engine combustion simulation combining detailed chemical kinetics, advanced solvers, advanced combustion models, and high quality experiments.

detailed chemistry solvers [10,11]. This project develops combustion models for multi-dimensional simulations and conducts simulations of multidimensional engine operation. Simulations are conducted with close coupling to high quality engine experiments.

A reactor model has been developed to test the multi-zone combustion model zoning parameters for highly stratified combustion. The reactor model is based on an unsteady two-dimensional opposed flow laminar non-premixed flame that marches to a steady state. Figure 2 shows the temperature contours for the counterflow non-premixed laminar flame used to validate the multi-zone model. Fuel enters on the left and air enters on the right, both at specified temperatures and flow rates. Combustion products exit at the top, and the bottom is a line of symmetry. Depending on the spatial and temporal distribution in temperature and flow rate, the fuel and air will ignite to varying degrees and produce a temperature rise as a function of axial distance.

Figure 3(a) shows the temperature as a function of axial distance. The peak temperature occurs about three-quarters of the way from the fuel inlet towards the air inlet. For this initial case, hydrogen kinetics is used—as this is the simplest chemical mechanism available—with

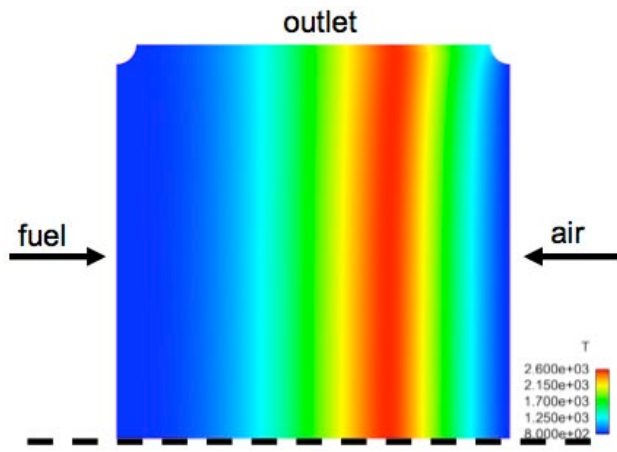


FIGURE 2. Temperature contours for two-dimensional laminar opposed laminar non-premixed reactor used for testing the multi-zone combustion model.

fuel and air temperatures at 800 K. Figure 3(a) shows calculation of temperature across the reactor for the standard approach of calculating chemistry in every cell (labeled nz) in the computational mesh as well as several different multi-zone discretizations (labeled z1, z2, z3,

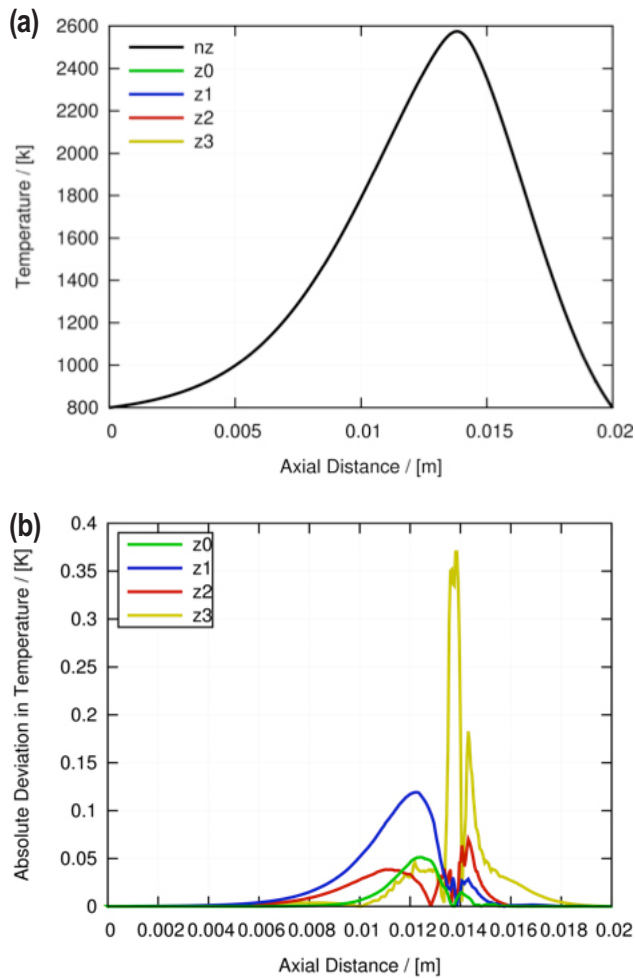


FIGURE 3. (a) Temperature versus axial distance for different zoning strategies, and (b) difference in axial temperature for different zoning strategies relative to the every cell simulation.

and z4). Table 1 shows the discretization used for the different cases. The multi-zone uses ranges of mixture fraction and temperature to aggregate cells into zones. The temperature curves in Figure 3(a) for every cell and the different zoning strategies are essentially identical. Figure 3(b) shows the difference in temperature predicted by the different zone discretizations relative to the every cell solution. The maximum absolute deviation in temperature is about 0.4 K for the coarsest discretization.

Table 1 shows the zoning used and computational time associated with the simulation results in Figures 2 and 3. The “nz” “every cell chemistry” case solves chemistry in every cell of the computational mesh, resulting in 63,680 chemical zones solved. The highest resolution “z0” multi-zone case groups cells with temperature within 1 K bands and cells with mixture fractions within increments of 0.002 (0.2%). Mixture fraction is a measure of local fuel air mixture, with all air having a mixture fraction of zero and all fuel

TABLE 1. Comparison of “every cell chemistry” to various multi-zone configurations for the opposed laminar non-premixed flame test case.

| Label | ΔT [K] | Δf | # of Zones | Chemistry Speedup | Overall Speedup |
|-------|----------------------|------------|------------|-------------------|-----------------|
| nz | Every Cell Chemistry | | 63,680 | 1 | 1 |
| z0 | 1 | 0.002 | 3,773 | 13.2 | 9.6 |
| z1 | 5 | 0.005 | 749 | 54.6 | 19.3 |
| z2 | 10 | 0.01 | 372 | 91.8 | 22.6 |
| z3 | 20 | 0.02 | 186 | 132.9 | 23.5 |

having a mixture fraction of one. The mixture fraction definition here is atomic mixture fraction excluding complete combustion products [12]. The “z0” multi-zone case reduces the number of chemical zones by 17-fold relative to the every cell simulation and reduces the chemistry computational time by 13-fold. The overall simulation time is reduced by a factor of nearly 10. As the zoning becomes coarser (larger temperature and mixture fraction bin sizes), the number of chemical kinetic zones decreases and the computational time also decreases. At the “z3” zoning discretization, the speedup of the chemistry part of the simulation is more than 130-fold relative to the every cell chemistry simulation, but the overall simulation is only slightly faster than the “z2” simulation, though both are more than 20 times faster than the every cell calculation. This is due to the multi-zone model speeding up chemistry so much that other parts of the simulation (e.g. convection, diffusion) dominate the computational cost resulting in diminishing returns from further reduction in chemistry cost. As shown in Figure 3, even the coarsest multi-zone model gives very good predictive accuracy relative to the every cell case.

The Advanced Combustion Numerics project [6] has developed chemical kinetic solvers utilizing GPUs in concert with CPUs. In collaboration with Cummins Inc., Convergent Sciences, and University of Indiana, we worked to extend this GPU solver capability to multidimensional engine combustion simulations. The key observation is that GPU-based chemistry solvers can give substantial speedup in a multi-reactor simulation, thus significant speedup may be achievable by simultaneously solving multiple reactors on the GPU. This is due to the differences in architecture between GPUs and CPUs. GPUs are most effective when a large number of calculations are done per memory access. Figure 4 shows computational speedup for using the GPU in a multi-reactor combustion chemistry simulation. Fuels of interest in engine combustion calculations typically have between 100 and 10,000 species in their kinetic mechanisms, and Figure 4 shows that by calculating parts of the kinetic solution on 256 to 1,024 simultaneous

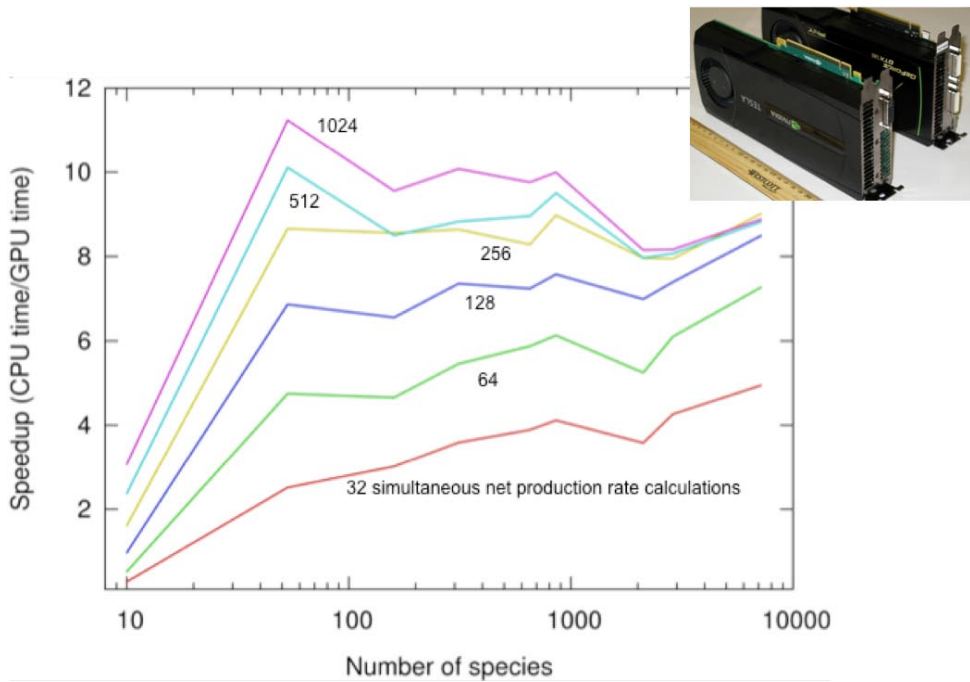


FIGURE 4. Speedup versus number of species in a chemical mechanism for calculations of combustion chemical kinetics on the GPU. Curves represent the number of reactors simultaneously solved on the GPU.

reactors on the GPU, we can achieve more than 8-fold speedup in the combustion chemistry solution time. The latest CPU and GPU based solvers have been licensed by LLNL to Convergent Science Inc. in an extension of our current license agreement for the multi-zone model. CONVERGE™ is widely used in U.S. industry for engine combustion analysis and design [13].

Ongoing work involves simulations of direct injection diesel combustion using detailed diesel fuel surrogate chemical kinetic mechanisms. The CONVERGE™ multidimensional engine CFD code is being used to simulate combustion in the optical Heavy Duty Fuels engine at Sandia National Laboratories. As shown in Figure 5(a), the engine simulation includes the full breathing features, intake runner, exhaust runner, intake and exhaust valve events, and combustion chamber. Preliminary simulations have been conducted using n-heptane as a diesel surrogate shown in Figure 5(b), with continuing effort to update geometry based on optical access modifications and update the chemistry as the detailed surrogate component mechanism are available.

CONCLUSIONS

We have made significant advances developing high performance computing tools for simulation of advanced engine combustion:

- Developing new combustion models and validation tools
- Implementing solvers combined with multidimensional engine simulations on CPU and GPU based architectures
- Collaborating with industry, academia and national labs to develop more predictive and efficient simulation tools
- Licensing tools to industry relevant software vendors to allow for rapid adoption of improved capabilities

In the next year we will continue to apply these high performance simulation tools to investigate fundamental characteristics of advanced engine combustion regimes. We will continue to distribute our latest models and solvers to support the simulation efforts of our U.S. Industry partners.

REFERENCES

1. Mehl, M., Pitz, W.J., Westbrook, C.K., Curran, H.J., "Kinetic modeling of gasoline surrogate components and mixtures under engine conditions", Proceedings of the Combustion Institute 33:193-200, 2011.
2. John E. Dec, Yi Yang, and Nicolas Dronniou, "Improving Efficiency and Using E10 for Higher Loads in Boosted HCCI Engines," SAE Int. J. Engines 5(3): 1009-1032, August 2012.

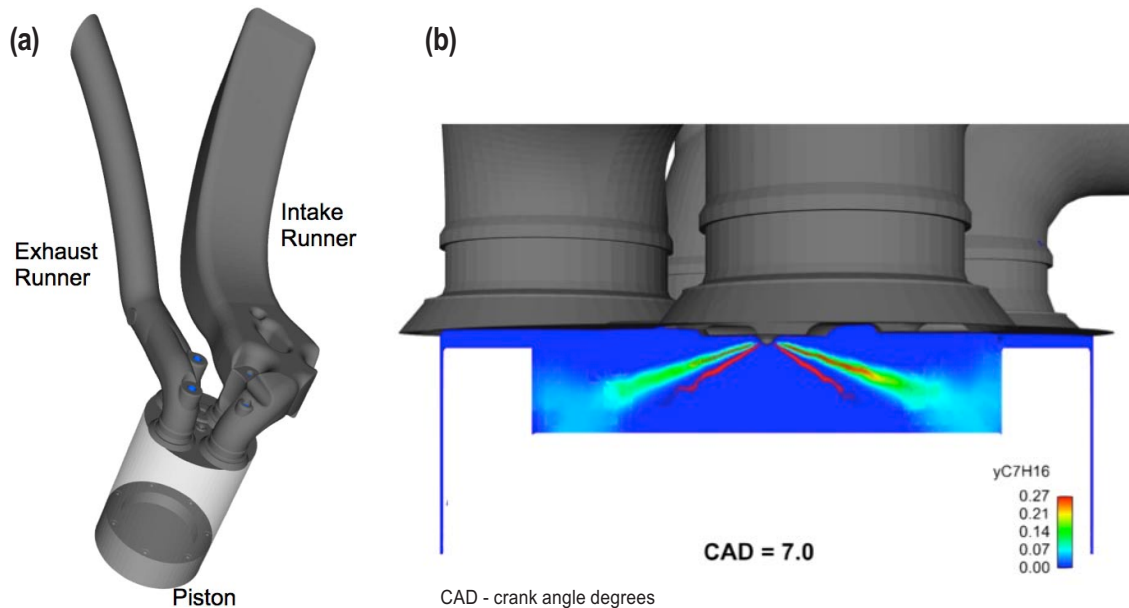


FIGURE 5. (a) Geometry of the flow domain analyzed for the Sandia Heavy Duty Fuels engine, and (b) fuel distribution at 7 degrees after top-dead center for conventional diesel operation using n-heptane as a kinetic surrogate.

3. Mueller, C.J., Cannella, W.J., Bruno, T.J., Bunting, B., Dettman, H.D., Franz, J.A., Huber, M.L., Natarajan, M., Pitz, W.J., Ratcliff, M.A. and Wright, K., Energy & Fuels 26(6):3284-3303, 2012.
4. Westbrook, C.K., W.J. Pitz, O. Herbinet, H.J. Curran, and E.J. Silke, "A Detailed Chemical Kinetic Reaction Mechanism for n-Alkane Hydrocarbons from n-Octane to n-Hexadecane," Combust. Flame 156(1): 181-199, 2009.
5. Pitz, W.J., "Chemical Kinetics Models for Advanced Engine Combustion," II.12 in Advanced Combustion Engine Research and Development 2013 Annual Progress Report, U.S. Department of Energy, 2013.
6. McEnly, M.J., Improved solvers for advanced engine combustion simulation," II.22 in Advanced Combustion Engine Research and Development 2013 Annual Progress Report, U.S. Department of Energy, 2013.
7. Babajimopoulos, A., Assanis, D.N., Flowers, D.L., Aceves, S.M. and Hessel, R.P., "A fully coupled computational fluid dynamics and multi-zone model with detailed chemical kinetics for the simulation of premixed charge compression ignition engines," International Journal Engine Research, Volume 6, Issue 5, pages 497-512, 2005.
8. Hessel, R., Babajimopoulos, A., Foster, D., Aceves, S., Davisson, M., Espinosa-Loza, F.J., Flowers, D.L., Pitz, W., Dec, J., Sjoberg, M., "Modeling Iso-octane HCCI using CFD with Multi-Zone Detailed Chemistry; Comparison to Detailed Speciation Data over a Range of Lean Equivalence Ratios, 2008-01-0047.
9. Flowers, D.L., Aceves, S.M., Babajimopoulos, A., "Effect of Charge Non-uniformity on Heat Release and Emissions in PCCI Engine Combustion," SAE Paper 2006-01-1363.

10. McEnly, M.J., Whitesides, R.A., Flowers, D.L., "Adaptive preconditioning strategies for integrating large kinetic mechanisms," The 8th US National Combustion Meeting, Park City, Utah, May 19–22, 2013.

11. Whitesides, R.A., McEnly, M.J., Flowers, D.L., "Optimizing time integration of chemical-kinetic networks for speed and accuracy," The 8th US National Combustion Meeting, Park City, Utah, May 19–22, 2013.

12. Bilger, R.W., "The Structure of Turbulent Non-Premixed Flames," Proceedings of the Combustion Institute 22(1):475-488, 1989.

13. <http://www.convergecfd.com/news-item/whitepapersasmeice2013/>

FY 2013 PUBLICATIONS/PRESENTATIONS

1. Oxberry, G.M., Keceli, M., Barton, P.I., Green, W.H., "Projection-based Model Reduction in Combustion," Combustion and Flame, in review, 2013.
2. Kodavasal, J., McEnly, M.J., Babajimopoulos, A., Aceves, S.M., Assanis, D.N., Havstad, M.A., and Flowers, D.L., "An Accelerated Multi-zone for Engine Cycle Simulation (AMECS) of HCCI combustion," International Journal of Engine Research, 14:416-433 October 2013.
3. McEnly, M.J., "Better Algorithms for Mechanism Development Tools" Advanced Engine Combustion Program Review, Southfield, Michigan, August 20–21, 2013.
4. Whitesides, R.A. "LLNL Engine Models and Simulations," Advanced Engine Combustion Program Review, Southfield, Michigan, August 20–21, 2013.

5. McNenly, M.J., Whitesides, R.A., Flowers, D.L., "Mechanism Reduction as a Preconditioning Strategy for Integrating Large Chemical Kinetic Systems," 4th International Workshop on Model Reduction in Reacting Flows (IWMRRF), San Francisco, California, June 19–21, 2013.
6. McNenly, M.J., Whitesides, R.A., Flowers, D.L., "Adaptive preconditioning strategies for integrating large kinetic mechanisms," The 8th US National Combustion Meeting, Park City, Utah, May 19–22, 2013.
7. Whitesides, R.A., McNenly, M.J., Flowers, D.L., "Optimizing time integration of chemical-kinetic networks for speed and accuracy," The 8th US National Combustion Meeting, Park City, Utah, May 19–22, 2013.
8. McNenly, M.J. "Recent Progress in Combustion Numerics," AICES Invited Talk, RWTH Aachen University, Aachen, Germany, Mar. 26, 2013
9. McNenly, M.J., "Recent progress on Combustion Numerics" Advanced Engine Combustion Program Review, Livermore, California, February 6–7, 2013.
10. Flowers, D.L., "Recent progress in Combustion Simulations," Advanced Engine Combustion Program Review, Livermore, California, February 6–7, 2013.
11. Flowers, D.L., "Simulation of High Efficiency Clean Combustion Engines and Detailed Chemical Kinetic Mechanisms Development," 2012 Directions in Engine-Efficiency and Emissions Research (DEER) Conference, Dearborn, Michigan, October 16–19, 2012.

II.12 Improved Solvers for Advanced Combustion Engine Simulation

Matthew McNenly (Primary Contact),
Salvador Aceves, Daniel Flowers,
Nick Killingsworth, Geoffrey Oxberry,
William Piggott III, Guillaume Petitpas, and
Russell Whitesides

Lawrence Livermore National Laboratory (LLNL)
7000 East Ave. (L-140)
Livermore, CA 94550

DOE Technology Development Manager:
Gurpreet Singh

Overall Objectives

- Accelerate development and deployment of high-efficiency clean-combustion engine concepts through deeper understanding of complex fluid and chemistry interactions.
- Improve physical accuracy of combustion simulations by enabling the use of large chemistry mechanisms for real transportation fuels.
- Reduce the time and resource cost for combustion simulations by designing efficient algorithms guided by applied mathematics and physics.
- Develop truly predictive combustion models and software that are fast enough to impact the engine design cycle.

Fiscal Year (FY) 2013 Objectives

- Prepare and release the LLNL combustion software (thermochemistry library and adaptive preconditioners) for wider-use by the engine simulation community.
- Identify new applications and physical models in need of acceleration to support the Advanced Combustion Engine (ACE) subprogram research.
- Implement the LLNL thermochemistry library on general-purpose graphical processing units (GPUs).
- Continue to develop, rigorously test and validate the adaptive preconditioning concept for acceleration of chemistry solvers without loss in accuracy.

FY 2013 Accomplishments

- Executed 4-year license agreement with Convergent Sciences Inc. for use of the LLNL combustion software in CONVERGE™ CFD as requested by the

memorandum of understanding's (MOU's) industrial partners.

- Developed a sensitivity analysis tool for use by chemical kineticists that reduces the time to solution for a typical fuel from one week to less than an hour.
- Created a GPU-accelerated algorithm to calculate thermochemistry functions an order of magnitude faster than the computer processing unit (CPU)-based version.
- Tested and validated the adaptive preconditioner technique for new mechanism classes key to the development of "real fuel" surrogates.
- Extended the adaptive preconditioner technique to calculate the ignition delay characteristics for a 39,000 species mechanism in two minutes (compared to five months using the traditional approach).
- Developed a reaction timescale analysis tool to aid in mechanism design.

Future Directions

- Continue efforts to distribute the project's new software to industrial and academic partners, and to the multidimensional computational fluid dynamics (CFD) software packages they use.
- Improve the fluid transport calculation and other simulation bottlenecks that occur now that the chemistry solver is substantially faster.
- Continue to create new combustion algorithms for the GPU.
- Explore more robust error theory for physical models in engine simulations to ensure that accuracy is maintained in a rigorous manner transparent to all users.



INTRODUCTION

This project aims to fill the present knowledge gap through substantial improvements in the performance and accuracy of combustion models and software. The project is focused largely on the applied mathematics underpinning efficient algorithms, and the development of combustion software on new computing architectures. It is a natural complement to the other LLNL projects in the quest to gain fundamental understanding of the new engine modes investigated under the ACE subprogram. Other LLNL projects include the multidimensional

engine modeling project led by Whitesides (see 2013 ACE R&D annual report II.7) and the high-fidelity chemistry mechanisms developed for real transportation fuels by Pitz (see 2013 ACE R&D annual report II.12). The long-term goal of this project is to develop predictive combustion software that is computationally fast enough to impact the design cycle and reduce the deployment time for new high-efficiency, low-emissions engine concepts. Toward this goal, the project developed a new thermochemistry library and chemistry solver [1-2] that achieves multiple orders of magnitude speedup over the traditional approaches found in CFD codes in use like Kiva3V [3], OpenFOAM® [4] and CONVERGE™ (v1.4 – v2.1) [5] without any loss of accuracy. Further, the new library and solver are 15 times faster than sophisticated commercial solvers. As a consequence of this project, it is now possible to model high-fidelity chemical mechanisms in multidimensional engine simulations (e.g., on the order of a thousand species).

APPROACH

The project is focused on creating combustion software capable of producing accurate solutions in a short time relative to the engineering design cycle on commodity computing architectures. The creation of fast and accurate simulation tools can speed the deployment of new engine combustion strategies. In the past, simply demonstrating that it is possible to couple detailed chemical kinetics with fluid dynamics in an engine was a feat unto itself. As a consequence, combustion software research was focused on combining existing tools and models into a single code (e.g. fluid solvers, stiff integrators, and Lagrangian spray tracking). Now that this coupled physics capability is more common, it is necessary to take a step back and study how the individual code components can be made more efficient, more accurate and better integrated.

The approach taken in this project to produce accurate and efficient combustion software has several facets. Major bottlenecks in the software are identified through detailed code profiling. New algorithms replacing the slow code sections are created from the applied mathematical exploration of the performance. These algorithms are developed with an emphasis on exploiting the nature of the physical phenomenon while maintaining mathematical consistency with the model equations. This approach leads to efficient, grid independent and reproducible solutions, which are then validated against existing experimental and computational results. Once rigorously tested, the new models and solvers can be distributed to industrial and academic partners as standalone libraries or coupled with multidimensional CFD software packages.

RESULTS

The project advanced four areas in FY 2013 to deepen the fundamental understanding of advanced combustion modes in support of the ACE subprogram goals. These advances include: (i) increasing the availability of detailed chemistry simulations for MOU engine designers, (ii) reducing the time spent by chemical kineticists waiting for simulation results and debugging reaction networks, (iii) porting key thermochemistry algorithms to the GPU for an order of magnitude speedup, and (iv) extending and verifying the performance of the adaptive preconditioner method on a broader range of mechanisms and fuel component classes.

A major achievement of the project in FY 2013 was to increase the availability of the high-performance combustion software developed in the previous year. To extend the range of users of the new software, the principal investigator of this project along with the multidimensional engine modeling project (see 2013 ACE R&D annual report II.7) met with the simulation teams at several industrial partners under the MOU. The specific goal of the meetings was to find the quickest path to wider adoption of the new software to have the greatest impact on the industrial engine design process. All the industrial partners visited (Chrysler, General Motors, Ford, Cummins and Chrysler) had independently selected CONVERGE™ CFD by Convergent Science, Inc. (CSI) to handle an appreciable amount of the multidimensional CFD modeling. It was thus natural to follow the urging of the industrial partners and build on the previous license agreement between LLNL and CSI. LNLL executed a new agreement in FY 2013 with CSI to license the thermochemistry library and adaptive preconditioner algorithms and their future GPU versions. This high-performance software delivers orders of magnitude reduction in the chemistry computation cost for a realistic fuel mechanism. It also ensures that future gains made for the GPU architecture will be available to further accelerate the design process for the advanced combustion engine community.

Another area advanced by this project in FY 2013 is the creation of new and accelerated computational tools to help design large, predictive fuel mechanisms. The high-performance software that accelerates multidimensional CFD engine simulations offers clear benefits to other time-consuming models. A particularly daunting challenge faced by the advanced engine community is the development of physically accurate, fundamental mechanisms for real transportation fuels. The creation of such mechanisms is the primary focus of another LLNL project led by Pitz (see 2013 ACE R&D annual report II.12). The promising

combustion modes investigated in this sub-program (e.g. Homogenous Charge Compression Ignition, Premixed Charge Compression Ignition, Reactivity Controlled Compression Ignition and Spark Assisted Compression Ignition) have some portion of the operation range dependent on kinetically controlled ignition. While these combustion modes have demonstrated great strides toward the efficiency and emission goals of the ACE subprogram, the most successful computational models to predict ignition behavior require the detailed fuel mechanisms developed by Pitz and colleagues [6-7]. High fidelity mechanisms for real fuel components may resolve several thousand species (e.g. 7,200 species for 2-methylalkane [8-9]). The level of complexity adds to the challenge of mechanism design by making it difficult to detect errors.

The new algorithms at the foundation of the adaptive preconditioner method can also identify erroneous kinetic rates, thermodynamic functions and reaction pathways during the simulation process. One example is using the Jacobian matrix information to detect abnormally fast reaction rates in the mechanism. Figure 1 illustrates how this new tool identified the fastest reactions by the characteristic frequency coupling two species. In the example, an early methylcyclohexane mechanism was found to have reactions more than ten orders of magnitude faster than the reactions found in the well-validated n-heptane mechanism developed by LLNL [10].

The high-performance combustion software created by this project aids chemical kineticists by accelerating the models they use for mechanism development. In FY 2013, the A-factor sensitivity calculation, identified

as one of the most time-consuming steps in the design process, was sped up significantly. In one particular instance, the waiting time using the old tool was a week. The new version reduced the wait to less than thirty minutes with no loss of accuracy. The speedup was achieved in two ways. First, the new solver is at least an order of magnitude faster than other solvers in use. Second, the new solver was parallelized to allow the users to easily manage tens of thousands of sensitivity calculations on multi-core desktops and high-performance computing architectures. These achievements along with future planned improvements (e.g. accelerated sensitivity calculations and additional chemical simulation models) will allow the mechanism developers in the advanced engine community to focus on creating new fuel component mechanisms—instead of waiting for simulations or searching for potential errors.

This project achieved another important advance in the development of GPU-based algorithms for combustion models in FY 2013. GPUs have gained a foothold in scientific computing because of their ability to deliver an order of magnitude more performance than traditional CPUs in terms of number of calculations per dollar (and per Watt). Importantly, NVIDIA has made general-purpose programming on the GPU much easier than in the past with the development of their CUDA library, which is a straightforward extension to the widely used C and C++ programming languages. While the CUDA library makes it relatively easy to convert an existing algorithm, unlocking the full performance of the GPU often requires considerable attention to code design.

The high-performance thermochemistry library developed for the CPU was ported to run eight to 10 times faster on the GPU in FY 2013. The thermochemistry library contains all the functions to calculate the thermodynamic state of a chemically reacting system as well as functions for the time evolution of the composition and heat release. Some portions of the library, such as the algorithms for computing the internal energy, enthalpy, and Gibbs free energy, are well suited to the GPU. They are easily converted to the new architecture and achieve one to two orders of magnitude of speedup. However, the calculation of the chemical reaction rates using the high-performance techniques developed for the CPU requires great care just to breakeven on the GPU.

Using a direct conversion of the code to the GPU, the calculation of the net species production rate from the reaction rates of progress is actually 50 times slower than the CPU. This performance penalty is so great as to make the GPU impractical for this application if not resolved. Fortunately, a more suitable algorithm was found by taking advantage of the fact that the simulations in the greatest need of GPU acceleration have a large number of

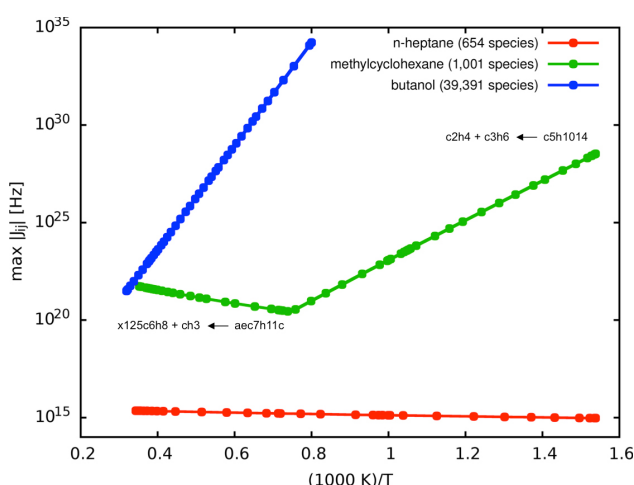


FIGURE 1. The new tool identifies the fastest reaction timescales using the Jacobian information from the adaptive preconditioner method during a simulation to provide an extra level of error-detection in mechanism development.

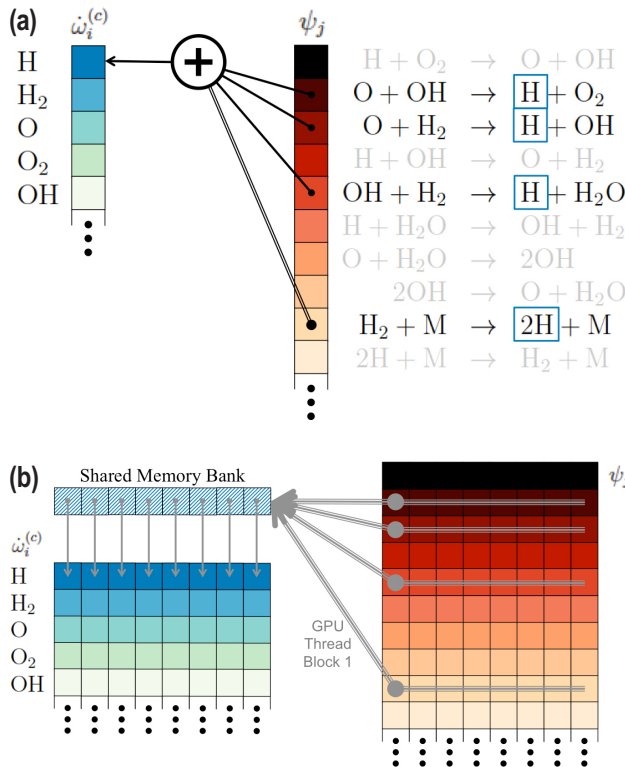


FIGURE 2. Comparison of the memory access patterns between the CPU (a) and GPU-based (b) algorithms for the net species production rate $\dot{\omega}_i$ (blue-green) computed from the reaction rates of progress ψ_j (red-brown). The CPU algorithm accesses the memory in an irregular, non-continuous pattern based on the natural mechanism ordering, which is ill suited to the GPU. The new GPU algorithm simultaneously adds multiple reaction steps (rows) for multiple compositions (columns) representing distinct fluid cells.

chemical reaction networks to evaluate together. Figure 2 illustrates the difference between the two approaches. The new GPU algorithm is more than fifteen times faster than the original CPU algorithm. Based on the new net rate algorithm, this project ultimately delivered an eight to 10-fold speedup for the calculation of time derivatives of the thermodynamic state and composition.

The final advance to mention for this project is the extension and verification of the adaptive preconditioner method to previously untested classes of molecules and mechanisms. Notable additions include: methylcyclohexane (1,000 species [11]), a 3-component biodiesel surrogate (3,300 species [12]), and an automatically generated mechanism for hydrocarbons up to C9 courtesy of Bill Green's research group, which is the largest tested to-date (39,000 species [13]). Figure 3 shows that the computation time for the ignition delay calculations with these new mechanisms follows the same linear scaling with the number of species, which stands in stark contrast to traditional methods. The average computation time to solve the ignition delay using the 39,000 species mechanism is about two minutes with

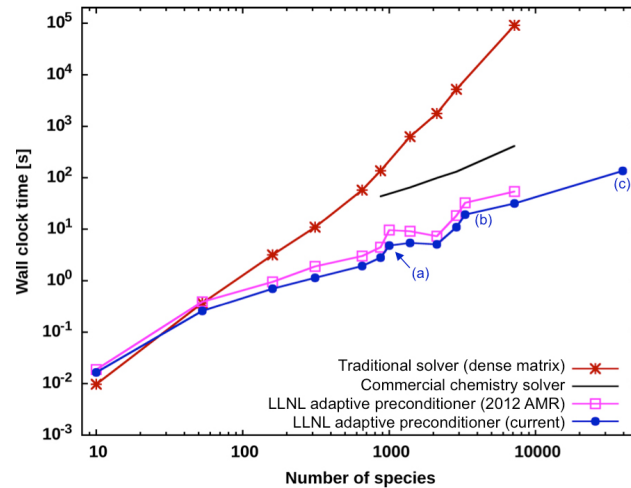


FIGURE 3. The computational cost of the adaptive preconditioner technique shows near linear scaling for new molecules and mechanism classes. Examples include: (a) methylcyclohexane (1,000 species [10]); (b) 3-component biodiesel surrogate (3,300 species [11]); and (c) and an automatically generated mechanism for hydrocarbons up to C9 (39,000 species [12]).

the new software, which is several orders of magnitude faster than the estimated 150 days using the traditional approach. This is a clear example how this project is able to improve the pace of advanced combustion engine development by delivering much higher fidelity in less time.

CONCLUSIONS

In FY 2013, this project progressed toward the goal of bringing truly predictive combustion software to the computational level needed to impact the engine design cycle for new high-efficiency clean-combustion operating modes. Key achievements included:

- Executing a 4-year license agreement with CSI for use of the LLNL combustion software in CONVERGE™ CFD, which is widely used by the MOU's industrial partners for engine simulation.
- Developed a sensitivity analysis tool for mechanism developers that reduces the time to solution for a typical fuel from one week to less than an hour.
- Created a GPU-accelerated algorithm to calculate thermochemistry functions that is an order of magnitude faster than the CPU-based version.

In FY 2014, we will continue our efforts to distribute the high performance solvers and libraries developed by this project to industrial and academic partners, and explore new algorithms to further accelerate the software used throughout the advanced combustion engine community.

REFERENCES

- 1.** McNenly, M.J., Whitesides, R.A., Flowers, D.L., "Adaptive preconditioning strategies for integrating large kinetic mechanisms," The 8th US National Combustion Meeting, Park City, Utah, May 19–22, 2013.
- 2.** Whitesides, R.A., McNenly, M.J., Flowers, D.L., "Optimizing time integration of chemical-kinetic networks for speed and accuracy," The 8th US National Combustion Meeting, Park City, Utah, May 19–22, 2013.
- 3.** Hessel, R., Babajimopoulos, A., Foster, D., Aceves, S., Davisson, M., Espinosa-Loza, F.J., Flowers, D.L., Pitz, W., Dec, J. and Sjoberg, M., "Modeling Iso-octane HCCI using CFD with Multi-Zone Detailed Chemistry; Comparison to Detailed Speciation Data over a Range of Lean Equivalence Ratios, SAE Paper 2008-01-0047.
- 4.** Website <http://www.openfoam.org/>.
- 5.** Raju, M.P. *et al.*, "Acceleration of Detailed Chemical Kinetics Using Multi-zone Modeling for CFD in Internal Combustion Engine Simulations," SAE Paper 2012-01-0135.
- 6.** Curran, H.J., Gaffuri, P., Pitz W.J. and Westbrook, C.K., "A comprehensive modeling study of iso-octane oxidation," *Combust. Flame*, 2002.
- 7.** Mehl, M., Pitz, W.J., Westbrook, C.K. and Curran, H.J., "Kinetic modeling of gasoline surrogate components and mixtures under engine conditions", *Proc. Combust. Inst.*, 2011.
- 8.** Sarathy, S.M. *et al.*, "Comprehensive chemical kinetic modeling of the oxidation of 2-methylalkanes from C7 to C20," *Combust. Flame*, 158(12):2338-2357, 2011.
- 9.** Sarathy, S.M., Yeung, C., Westbrook, C.K., Pitz, W.J., Mehl, M. and Thomson, M.J. "An experimental and kinetic modeling study of n-octane and 2-methylheptane in an opposed-flow diffusion flame," *Combust. Flame*, 158(7):1277-1287, 2011.
- 10.** Mehl, M., Pitz, W.J., Westbrook, C.K. and Curran, H.J., "Kinetic modeling of gasoline surrogate components and mixtures under engine conditions. *Proc Combust Inst* , 33:193-200, 2011.
- 11.** Pitz, W.J., Naik, C.V., Mhaolduin, T.N., Westbrook, C.K., Curran, H.J., Orme, J.P. and Simmie, J.M., "Modeling and experimental investigation of methylcyclohexane ignition in a rapid compression machine," *Proc. Combust Inst.*, 31(1):267-275, 2007.
- 12.** Herbinet, O., Pitz, W.J., Westbrook, C.K., "Detailed chemical kinetic mechanism for the oxidation of biodiesel fuels blend surrogate," *Combust. Flame*, 154(3):507-528, 2010.
- 13.** Green, W.H. *et al.*, "RMG - Reaction Mechanism Generator v4.0.1", 2013. (available online at <http://rmg.sourceforge.net/>)

FY 2013 PUBLICATIONS/PRESENTATIONS

- 1.** Oxberry, G.M., Keceli, M., Barton, P.I., Green, W.H., "Projection-based Model Reduction in Combustion." *Combustion and Flame*, in review, 2013.
- 2.** Kodavasal, J., McNenly, M.J., Babajimopoulos, A., Aceves, S.M., Assanis, D.N., Havstad, M.A., and Flowers, D.L., "An Accelerated Multi-zone for Engine Cycle Simulation (AMECS) of HCCI combustion," *International Journal of Engine Research*, 14:416-433 October 2013.
- 3.** McNenly, M.J., "Better Algorithms for Mechanism Development Tools" Advanced Engine Combustion Program Review, Southfield, Michigan, August 20–21, 2013.
- 4.** Whitesides, R.A. "LLNL Engine Models and Simulations," Advanced Engine Combustion Program Review, Southfield, Michigan, August 20–21, 2013.
- 5.** McNenly, M.J., Whitesides, R.A., Flowers, D.L., "Mechanism Reduction as a Preconditioning Strategy for Integrating Large Chemical Kinetic Systems," 4th International Workshop on Model Reduction in Reacting Flows (IWMRRF), San Francisco, California, June 19–21, 2013.
- 6.** McNenly, M.J., Whitesides, R.A., Flowers, D.L., "Adaptive preconditioning strategies for integrating large kinetic mechanisms," The 8th US National Combustion Meeting, Park City, Utah, May 19–22, 2013.
- 7.** Whitesides, R.A., McNenly, M.J., Flowers, D.L., "Optimizing time integration of chemical-kinetic networks for speed and accuracy," The 8th US National Combustion Meeting, Park City, Utah, May 19–22, 2013.
- 8.** McNenly, M.J. "Recent Progress in Combustion Numerics," AICES Invited Talk, RWTH Aachen University, Aachen, Germany, Mar. 26, 2013.
- 9.** McNenly, M.J., "Recent progress on Combustion Numerics" Advanced Engine Combustion Program Review, Livermore, California, February 6–7, 2013.
- 10.** Flowers, D.L., "Recent progress in Combustion Simulations," Advanced Engine Combustion Program Review, Livermore, California, February 6–7, 2013.
- 11.** Flowers, D.L., "Simulation of High Efficiency Clean Combustion Engines and Detailed Chemical Kinetic Mechanisms Development," 2012 Directions in Engine-Efficiency and Emissions Research (DEER) Conference, Dearborn, Michigan, October 16–19, 2012.

II.13 KIVA Development

David B. Carrington
Los Alamos National Laboratory
P.O. Box 1663
Los Alamos, NM 87545

DOE Technology Development Manager:
Gurpreet Singh

Subcontractors:

- Dr. Juan Heinrich, University of New Mexico, Albuquerque, NM
- Dr. Xiuling Wang, Purdue University Calumet, Hammond, IN
- Dr. Darrell W. Pepper, University of Nevada, Las Vegas, Las Vegas, NV

Overall Objectives

- Develop algorithms and software for the advancement of speed, accuracy, robustness, and range of applicability of the KIVA internal engine combustion modeling – to be more predictive. This is to be accomplished by employing higher-order spatially accurate methods for reactive turbulent flow, and spray injection, combined with robust and accurate actuated parts simulation and more appropriate turbulence modeling.
- To provide updated KIVA software that is easier to maintain and is easier to add models to than the current KIVA. To reduce code development costs into the future via more modern code architecture.

Fiscal Year (FY) 2013 Objectives

- Continue developing code and algorithms for the advancement of speed, accuracy, robustness, and range of applicability of the KIVA combustion modeling software to higher-order spatial accuracy with a minimal computational effort.
- Finish developing underlying discretization to an *hp*-adaptive predictor-corrector split (PCS) using a Petrov-Galerkin (P-G) finite element method (FEM) for all flow regimes.
- Implement KIVA Spray and Chemistry in the *hp*-adaptive PCS FEM solver.
- Develop three-dimensional (3-D) overset grid method for moving and immersed actuated parts such as valves for robust grid movement.

FY 2013 Accomplishments

- Developed parallel *hp*-adaptive PCS using P-G FEM for all flow regimes, from incompressible to high-speed compressible. Partially verified the *hp*-adaptive (FEM) framework and PCS solver.
- Developed 3-D overset grid method for moving and immersed actuated parts such as valves for robust grid movement.
- Validated KIVA multi-component particle/spray injection algorithm into the PCS FEM solver.
- Validating KIVA chemistry package into the PCS FEM solver.
- Validating KIVA splash, break-up, collide and wall-film models into the PCS solver.
- Developing large eddy simulation turbulence modeling for wall-bounded flows.

Future Directions

- Continue developing the *hp*-adaptive FEM for multispecies flows in all flow regimes. Continue implementing this method to perform modeling of internal combustion engines, other engines, and general combustion.
- Continue developing comprehensive comparative results to benchmark problems and to commercial software as part of the verification and validation of the algorithms.
- Continue developing 3-D robust overset grid method for immersed actuated parts such as valves. Merge overset grid method into *hp*-adaptive FEM framework.
- Continue developing the parallel solution method for the *hp*-adaptive PCS algorithm. Parallel structure to be supplied by portable implementation of Message Passing Interface with nested OpenMP paradigms.
- Continue developing more appropriate turbulence models for more predictive modeling.
- Continue to verify and validate combustion and spray models, and the local Arbitrary Lagrangian-Eulerian (ALE) in 3-D.
- Incorporate Volume of Fluid method in spray modeling for more predictive modeling capability.



INTRODUCTION

Los Alamos National Laboratory and its collaborators are facilitating engine modeling by improving accuracy of the modeling, and improving the robustness of software. We also continue to improve the physical modeling methods. We are developing and implementing new mathematical algorithms, those that represent the physics within an engine. We provide software that others may use directly or that they may alter with various models e.g., sophisticated chemical kinetics, different turbulent closure methods or other fuel injection and spray systems.

APPROACH

Development of computational fluid dynamics models and algorithms relies on basic conservation laws and various mathematical and thermodynamic concepts and statements including calculus of variations. The process encompasses a great many requirements including:

1. Expertise in turbulence and turbulent modeling for multiphase/multispecies fluid dynamics.
2. Expertise in combustion dynamics, modeling, and spray dynamics modeling.
3. Skill at developing, implementing numerical methods for multi-physics computational fluid dynamics on complex domains with moving parts.
4. Careful validation and verification of the developed code and algorithms.

RESULTS

When considering the development of algorithms and the significant effort involved producing reliable software, it is often best to create algorithms that are more accurate at a given resolution and then resolve the system more accurately only where and when it is required. We began developing a new KIVA engine/combustion code with this idea in mind [1]. This new construction is a Galerkin FEM approach that utilizes conservative momentum, species, and energy transport. Our system uses P-G and coupled pressure stabilization [2].

A projection method is combined with higher order polynomial approximation for model dependent physical variables (p -adaptive) along with grid enrichment (locally higher grid resolution— h -adaptive). Overset grids are used for actuated and immersed moving parts to provide more accurate and robust solutions in the next generation of KIVA. The scheme is particularly effective for complex domains, such as engines.

The hp -adaptive FEM is at a minimum 2nd order accurate in space and 3rd order for advection terms, but becomes higher order where required as prescribed by the adaptive procedures [2]. The hp -adaptive method employs hierarchical basis functions, constructed on the fly as determined by a stress-error measure [3].

The adaptive method, along with a conservative P-G upwinding technique, combined with the KIVA multi-component spray model accurately sprays. Shown in Figure 1 are the spray penetration curves for diesel

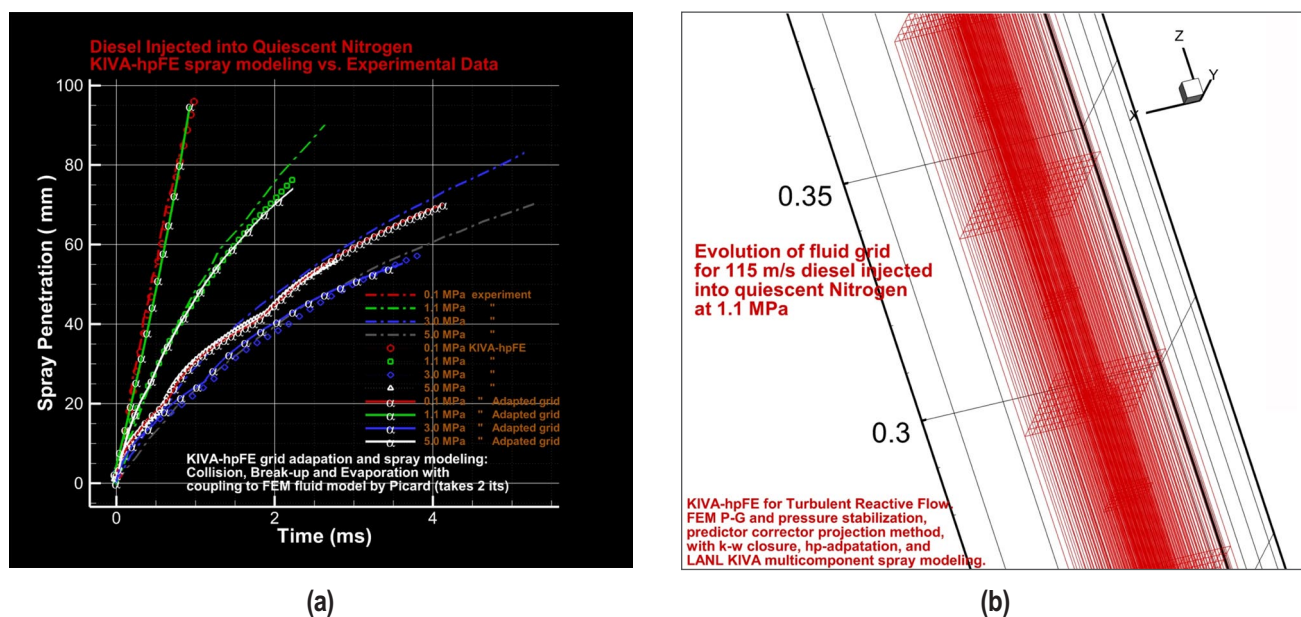


FIGURE 1. Diesel fuel injection into quiescent nitrogen at various pressures. a) Both refined and coarse grids results are compared, showing what is essentially grid independence; b) the h -adapting grid during spray evolution (spray is along the axial z -direction in the center).

injected into quiescent nitrogen. The simulations are compared to the experimental data [4] with excellent agreement shown over ambient pressures from 0.1 atmospheres to 50 atmospheres. The injected quantity and initial spray velocity is given by the experimental data.

Notice in Figure 1a, where the refined grid (shown in Figure 1b) produces nearly the same results as the courser grid, suggesting that once fluid and energy transport are resolved, so too is the spray transport—it is grid convergent. This convergence is not possible with the finite volume method as employed by the older versions of KIVA.

Using the FEM method with the spray models provides a more accurate representation of the droplets interaction with the conveying fluid and with walls than the original finite volume method of KIVA. Because the FEM method allows for a continuous representation of phase-space, grid-scale accuracy can be applied everywhere. Problems with coarse grids influencing the spray are only related to the solution accuracy—the spatial representation of the spray model is therefore convergent. The KIVA multi-component spray model, a method based the algorithm developed by Dukowicz [5] and expanded by Torres, et. al [6] for break-up, agglomeration, and surface films, has being installed in the *hp*-FEM PCS solver. We have implemented a new two-way coupling between the spray droplets and the fluid, using a successive substitution method, that is less algebraically cumbersome than the 3-step method previously used and usually only requires two iterations to converge to some very small value.

Figure 2 shows flow solved using the implemented parallel OpenMP method in the PCS adaptive FEM

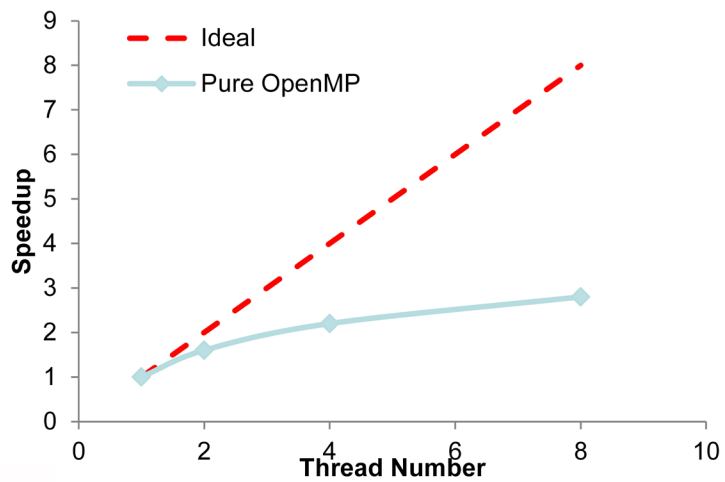
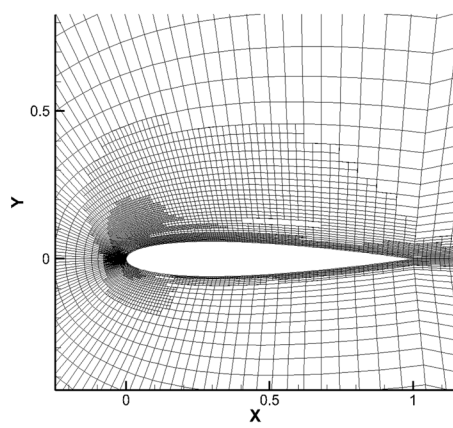


FIGURE 2. Transonic flow over a 3-D National Advisory Committee for Aeronautics 0012 airfoil at 4° angle of attack using *hp*-adaptive PCS FEM. a) adapted final grid; b) OpenMp speed-up as central processing units are increased (threading).

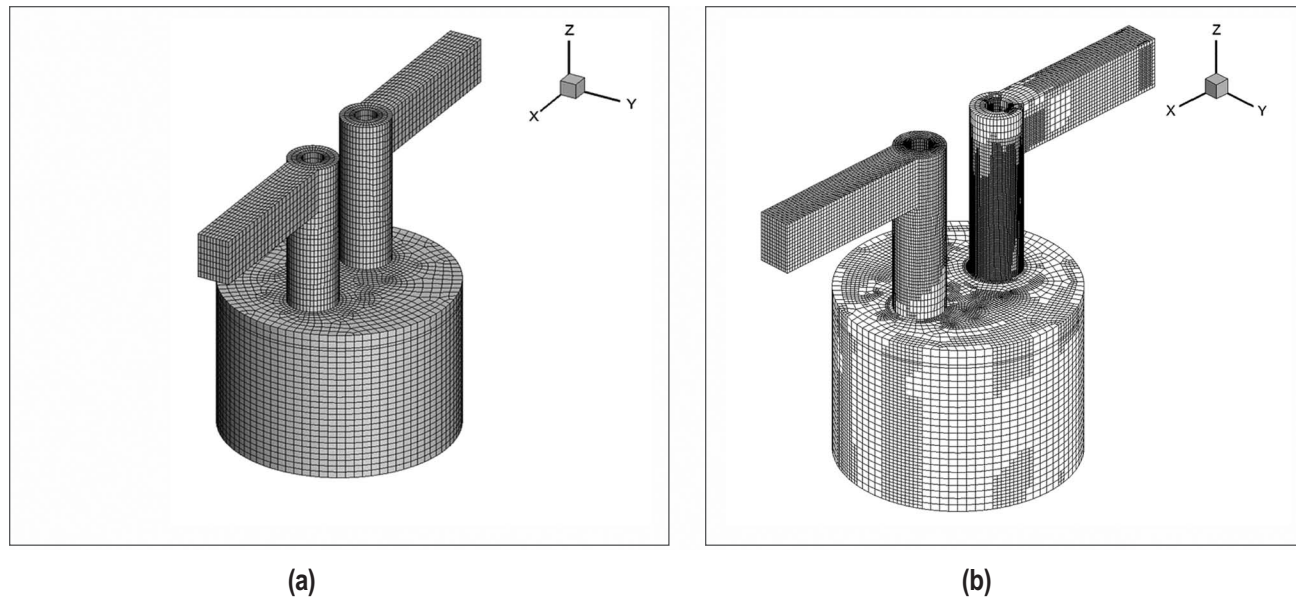


FIGURE 3. Starting grid (a) and final refined grid (b) when simulating a 2-valve engine using *hp*-adaptive PCS FEM system.

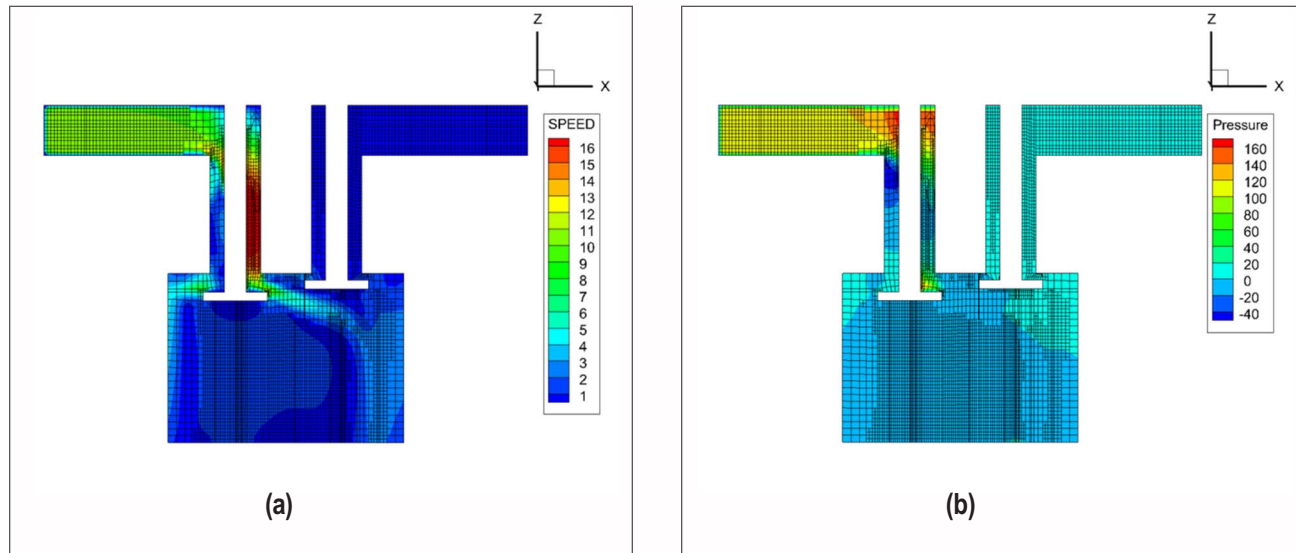


FIGURE 4. Flow in 2-valve engine simulation using *hp*-adaptive PCS FEM system. Velocity magnitude on center slice (a) and pressure on center slice (b).

the grid generation process. Hence, ports and cylinder portions of the grid are continuously represented. The overset grid method allows for computer-aided-design-to-grid in nearly a single step, providing nearly automatic grid generation.

The ALE system adjusts the grid locally as the parts move through the fluid, and maintains 2nd order spatial accuracy while never allowing the grid to tangle or producing an element that cannot be integrated accurately

[7]. Since the fluid is represented continuously, fluxing of material through the grid, as it moves is not required. This need to flux through the grid is just one portion of the error when the usual ALE method is employed with finite volumes. Here the fluid solver remains Eulerian and the moving grid portions are no longer entwined with fluid solution. The slanted piston shown in Figure 5 tests all 84 possibilities of how hexahedral elements can be sliced by moving parts. The method demonstrates 2nd order spatial accuracy and is robust.

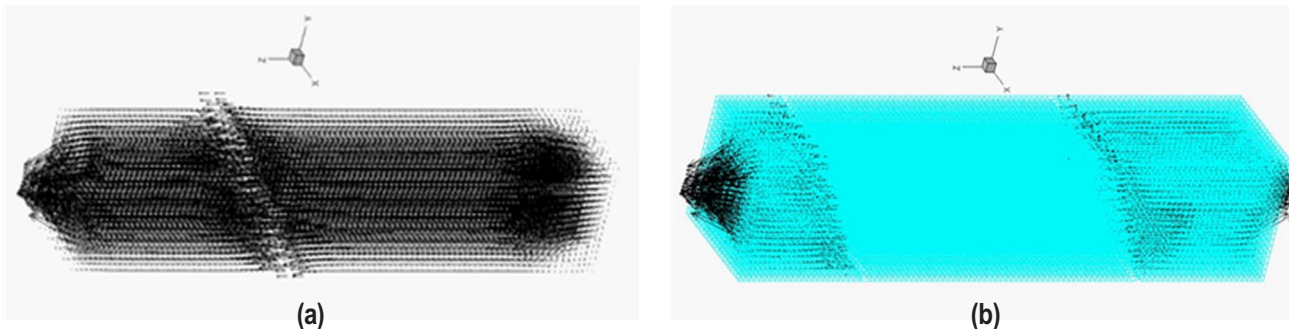


FIGURE 5. Square cylinders with moving piston showing velocity vectors and piston location in the grid. a) rectilinear motion of a slanted piston; b) rectilinear motion of two pistons moving simultaneously.

CONCLUSIONS

In FY 2013, we continue advancing the accuracy, robustness, and range of applicability internal combustion engine modeling algorithms and coding for engine simulation. We have performed the following to advance the state of the art:

- Development of an *hp*-adaptive PCS FEM for all flow regimes, with compressible flow verification and validation.
- Developed new method for immersed moving parts, extending the 2-D method to 3-D.
- Validated the KIVA spray model into the adaptive PCS FEM solver.
- Validating the KIVA reactive chemistry model into PCS FEM solver.
- Developed OpenMP parallel solution process with the *hp*-adaptive FEM.
- Developing the nested OpenMP in the Message Passing Interface parallel system.
- Developing large eddy simulation turbulence modeling for wall-bounded flows.

REFERENCES

1. CARRINGTON, D.B., Wang, X. and Pepper, D.W. (2013) A predictor-corrector split projection method for turbulent reactive flow, *Journal of Computational Thermal Sciences*, Begell House Inc., vol 5, no. 4, pp.333-352.
2. CARRINGTON, D.B., (2011) A Fractional step *hp*-adaptive finite element method for turbulent reactive flow, Los Alamos National Laboratory Report, LA-UR-11-00466.
3. Wang, X., Carrington, D.B., Pepper, D.W. (2009) An adaptive FEM model for unsteady turbulent convective flow over a backward-facing step, *Journal of Computational Thermal Sciences*, Begell House Inc..

4. Hiroyasu, H. and Kadota, T. (1977) Fuel Droplet Size Distribution in Diesel Combustion Chamber, SAE paper no. 740715.

5. Dukowicz, J.K., (1980) A particle-fluid numerical method for liquid sprays, *JCP*, Academic Press, vol. 35, no. 2, p. 229-253.

6. Torres, D.J., O'Rourke, P.J., Amsden, A.A., (2003) A discrete multicomponent fuel model, *Atomization and Sprays* vol.13, iss.2-3, p.131-172.

7. CARRINGTON, D.B., Munzo, D.A., Heinrich, J.C (2012) A local ALE for flow calculations in physical domains containing moving interfaces, to be published *Progress in Computational Fluid Dynamics, an Int. Jour.*

FY 2013 PUBLICATIONS/PRESENTATIONS

1. CARRINGTON, D.B., Wang, X. and Pepper, D.W. (2013), A predictor-corrector split projection method for turbulent reactive flow, *Journal of Computational Thermal Sciences*, Begell House Inc., vol 5, no. 4, pp.333-352.
2. CARRINGTON, D.B., Munzo, D.A., Heinrich, J.C (2012), “A local ALE for flow calculations in physical domains containing moving interfaces,” to be published *Progress in Computational Fluid Dynamics, an Int. Jour.*

SPECIAL RECOGNITIONS & AWARDS/ PATENTS ISSUED

1. Outstanding Innovation Award – 2011 Distinguished Licensing Award. Awarded by Los Alamos National Laboratory Technology Transfer Division, August 9th, 2012.
2. Outstanding Innovation Award – 2010 Distinguished Copyright Award. Awarded by Los Alamos National Laboratory Technology Transfer Division, August 11th, 2011

II.14 University Consortium on Efficient and Clean High-Pressure Lean-Burn (HPLB) Engines

Margaret Wooldridge
University of Michigan
Mechanical Engineering
2156 GGB
Ann Arbor, MI 48109-2125

DOE Technology Development Manager:
Gurpreet Singh

NETL Project Manager: Ralph Nine

Subcontractors:

- Massachusetts Institute of Technology (MIT), Cambridge, MA
- University of California, Berkeley (UCB), Berkeley, CA

Overall Objectives

- Explore new HPLB combustion strategies that can enable future gasoline engines with 20-40% improved fuel economy.
- Determine the fuel economy benefits of engines and engine cycles designed to utilize advanced combustion modes.

Fiscal Year (FY) 2013 Objectives

- Develop a simplified system model of a spark-assisted compression ignition (SACI) engine suitable for refining earlier analyses of vehicle fuel economy gains made possible by advanced, multi-mode combustion.
- Determine effects of stratification and equivalence ratio in a boosted stratified compression ignition engine. Develop models of autoignition applicable to highly stratified, turbulent combustion as it applies to gasoline Direct Injection/Homogeneous Charge Compression Ignition (DI/HCCI) engines.
- Experimentally explore flame and autoignition heat release in SACI. Determine the effects of composition and temperature on the critical combustion characteristics such as heat release rate and stability. Develop and refine computational fluid dynamics (CFD) models of SACI combustion and validate with experimental data. Explore microwave-assisted ignition as it relates to SACI.

- Determine the effects of fuel properties such as octane number on HCCI combustion. Explore the chemical kinetic effects of buffer gas on ignition and combustion characteristics of fuels relevant to HCCI and SACI combustion.

FY 2013 Accomplishments

- Completed development of a two-zone, quasi-dimensional model of spark-assisted (SA) HCCI for system level simulations of engine control strategies and vehicle fuel economy improvement, combining an existing spark ignition flame model with a new correlation for the autoignition heat release rate which takes into account combustion phasing, fraction of fuel remaining at autoignition and mixing of internal exhaust gas recirculation (EGR).
- The effects of fuel stratification in a small bore diesel engine using gasoline in Partially Premixed Compression Ignition (PPCI) mode have been determined. Three distinct combustion behaviors were observed as DI phasing was retarded from early to late. The results are explained by a complex interplay between residence time and autoignition time of the evolving fuel-air mixture.
- The flamelet-based combustion submodels including the spray vaporization effect have been implemented and validated in DI/HCCI engine conditions. The results show that for modeling ignition of late injection, stratified mixtures, the flamelet-based model gives significantly better agreement with data than current multizone approaches. This is the result of an apparent acceleration of ignition/burn rate due to small scale turbulence and mixing effects, not previously well understood.
- Fully-coupled CFD and chemical kinetics simulations were performed to model partial fuel stratification (PFS). The simulations confirmed experimental results that showed the occurrence of multi-stage combustion for PFS at $P_{in} = 2$ bar, but showed only single-stage combustion occurs with $P_{in} = 1$ bar. Analysis reveals that this effect is due to the competing effects of fuel and temperature stratification as they are affected by low temperature heat release (LTHR).
- Experiments on SACI in the fully flexible valve actuation (FFVA) engine were continued to quantify the effect of composition. Comparing dilution with EGR vs. air, the results showed significant

augmentation in the flame heat release fraction with increasing in-cylinder oxygen concentration and a corresponding decrease in peak heat release rate.

- Optical engine experiments were carried out to determine the effects of spark assist with a reference gasoline (E0) and a blend of 30% ethanol with 70% gasoline (E30). The results show that global ignition of SA HCCI is dominated by autoignition, and the heat released during flame propagation is less than ~20% of the total available. The compression heating caused by flame propagation primarily serves to accelerate autoignition of local sites which are already thermally preferred, that then accelerates global autoignition. Complementary experiments were conducted in a spark plug-equipped Rapid Compression Facility (RCF) using high-speed optical and pressure diagnostics.
- Open cycle SACI simulations using the previously developed KIVA-CFMZ model were performed for the geometry of the metal FFVA engine. Analysis of the results suggests that the decrease in peak heat release that is known to accompany higher flame heat release is due to preferential consumption of higher reactivity (hotter, less dilute) regions by the flame.
- A matrix of tests was conducted on a single-cylinder Cooperative Fuels Research (CFR) engine comparing the microwave-assisted spark ignition mode to the spark-only ignition mode with wet ethanol as a fuel. The microwave-assisted spark ignition mode allows stable engine operation in regions with higher dilution than possible with spark-only ignition. To assist future modeling efforts, a chemical kinetic mechanism has been developed for methane combustion that includes plasma reactions such as electron impact dissociation and recombination reactions.
- New experiments on HCCI burn rate with lower octane fuels were carried out in the FFVA engine with carefully controlled composition and combustion phasing. Over a range of engine speeds from 1,000-2,000 RPM, primary reference fuel 40 (PRF40) burned faster and had higher peak heat release rates than gasoline and could be retarded further at constant coefficient of variance (COV) of indicated mean effective pressure (IMEP), confirming the previous reported results. This was true even at 1,000 RPM where PRF40 exhibited two-stage combustion with LTHR. Varying negative valve overlap (NVO) had only a modest effect on burn rate.
- Computational simulations of ignition delay time and heat release rate of isoctane, n-heptane, and

n-butanol were used to characterize the effects of buffer gas composition. The buffer gases considered were argon, nitrogen, water, and carbon dioxide. Ignition delay times and heat release rates were found to be sensitive to the particular buffer gas, especially in the negative temperature coefficient (NTC) region.

Future Directions

The work of this three-year consortium has now been completed and results documented in the final technical report [1]. Much was learned about advanced combustion modes, and the associated benefits and challenges. A significant number of publications have resulted from the work, some still in preparation. Future directions leading from the results are:

- Utilize the system models developed in the project to find solutions to the control and stability issues that arise with complex engine-vehicle systems needed to enable advanced combustion.
- Focus new combustion studies on factors influencing cycle-to-cycle instabilities that have been found to be significant in SACI mode.
- Expand CFD work to enhance understanding of thermal gradients and their large effect on burn rates in advanced combustion.
- Continue work on small scale mixing, particularly as it relates to DI injection, and wall wetting where concentration gradients are high.
- Continue to investigate alternate fuels and their ignition characteristics as they affect engine-fuel optimization.



INTRODUCTION

Low-Temperature Combustion (LTC) is a desirable thermodynamic regime that can provide improved fuel efficiency in gasoline engines with low emissions, because the properties of the working fluid are best at lower temperature, and because oxides of nitrogen (NOx) emissions are reduced. Unfortunately, practical and reliable combustion under these dilute conditions has traditionally been unattainable due to spark ignition limits. HCCI is one method to achieve good combustion; the method works by increasing the charge temperature to induce autoignition and by diluting the mixture to reduce heat release rates. Because of the limited loads possible with HCCI, advanced combustion modes such as SACI, stratified or dual-fuel mixtures are being considered as a way to increase achievable engine loads.

At the same time turbocharging is another means of improving fuel economy, by capturing some wasted exhaust energy, but more importantly and in combination with engine downsizing, by permitting an increase of engine load without excessive temperatures while also reducing the relative importance of friction.

As seen in previously reported results shown in Figure 1, thermodynamic analysis indicates that advanced combustion modes at high pressures can provide significant efficiency improvement and vehicle fuel economy gains of up to 55%, exceeding the DOE Vehicle Technologies Office target of 20-40% improvement. Accordingly, the goal of the consortium is to explore how this improvement can be achieved; in particular to look at means of enabling the required advanced combustion under the highly dilute, boosted, high-pressure conditions necessary for optimal engine-vehicle fuel economy.

APPROACH

This research project, now at the end of its third year, combines experiments and modeling at three university research centers in order to acquire the knowledge and technology to explore the HPLB advanced combustion

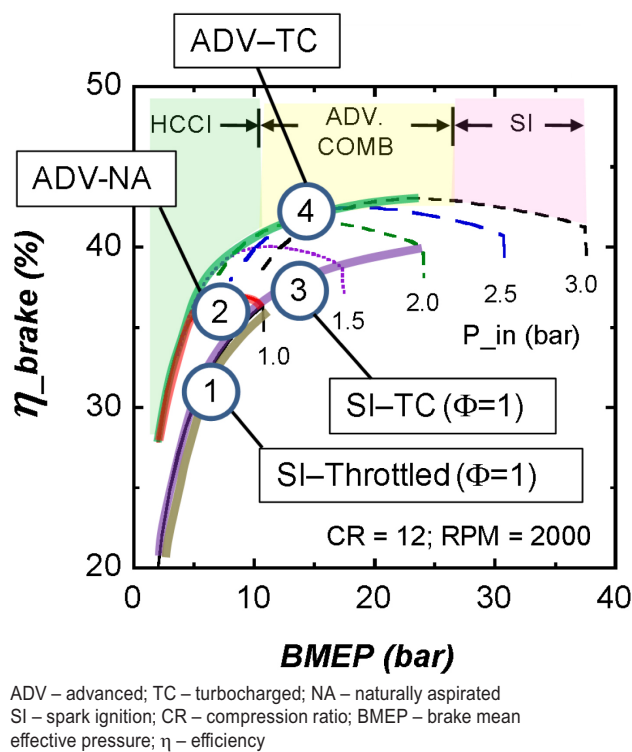


FIGURE 1. Brake efficiency projections for various combustion and boosting strategies, showing advantage of advanced combustion modes, e.g., SACI.

regime, which is key to achieving optimal fuel economy. To accomplish this, both single-cylinder and multi-cylinder engine experiments are being used to investigate direct fuel injection strategies, fuel and thermal stratification, turbo/supercharging, advanced ignition and combustion modes as well as the ignition characteristics of alternate fuels and blends with gasoline.

At the same time an array of modeling tools are being developed and refined, and brought to bear on the specific limit problems of importance. These models cover a range of detail from system models for engines and vehicles, through fully coupled CFD/kinetic models, to detailed chemical mechanisms. Our intent is to take advantage of the broad range of capabilities of the university partners and the collaborative relationships among the partners and their connections with industry and U.S. research facilities.

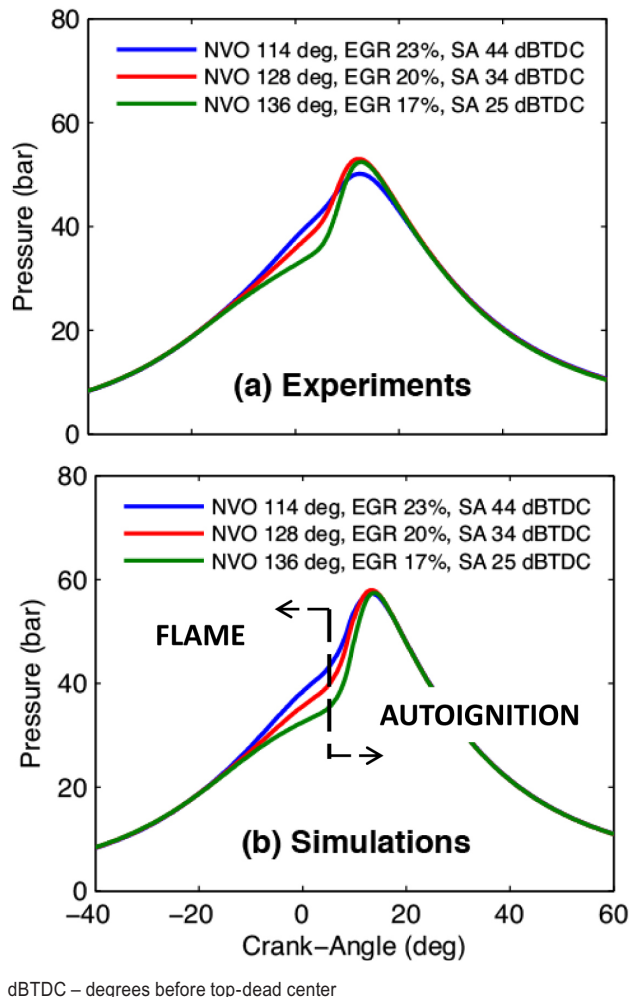
The overall technical approach is focused on light-duty automotive engine application using primarily gasoline and gasoline blends with alcohols as the fuel. The research agenda addresses the following areas:

- Thermodynamics of engines and engine cycles operating in advanced combustion modes.
- Fuel and thermal stratification and its interaction with fuel properties and heat transfer.
- Advanced multi-mode ignition and combustion.
- Novel fuel opportunities for improved efficiency.

RESULTS

Thermodynamics and System Models

GT-POWER® was used as a programming environment to develop a new phenomenological model of SACI for use in fast engine and vehicle oriented fuel economy assessments for which the drive cycle framework has been developed previously. The new model is a quasi-dimensional, multi-mode combustion formulation and employs a turbulent flame calculation that has primary input laminar flame speed correlations for highly dilute flames as reported previously. The chemical kinetics in the end gas is computed, either by an autoignition integral or by direct detailed kinetics until autoignition occurs, after which, the remaining heat is released with a rate determined according to an empirical correlation derived from experimental data. Figure 2 shows a comparison of simulation results vs. experimental data for three sets of inlet temperature and spark timings. The results clearly show the influence of the flame heat release and demonstrate that spark assist can compensate for changes in input conditions.



PPCI Engine Experiments

PPCI engine experiments were carried out in a production Renault/Mitsubishi F9Q B800 common rail diesel engine that was modified by lowering the compression ratio to 15:1 and converted to single-cylinder operation. A certification gasoline (Haltermann 437) with Research Octane Number of 97 is used for all experiments. To study charge stratification effects, the engine employs two fuel injection systems that could be used separately or simultaneously. A port fuel injector is added at the intake runner. The fuel distribution was changed by varying the ratio of DI vs. fuel injected in the intake port as well as by changing the phasing of the DI pulse.

Three distinct combustion behaviors were observed as DI phasing was retarded from early to late and stratification increased. Combustion phasing retards at

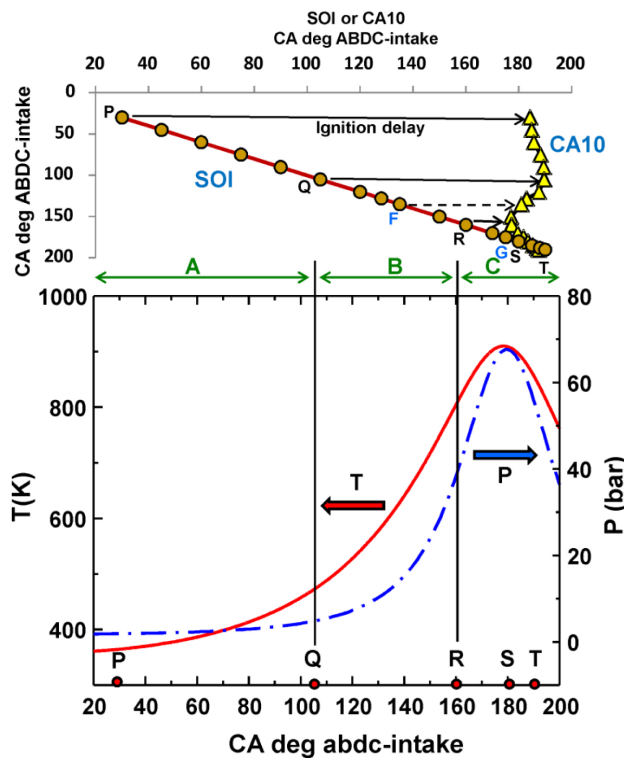


FIGURE 3. Phasing behavior of PPCI showing three regimes, A, B, and C as SOI of the DI fuel is retarded. Also shown are the compression temperature and pressure values, representative of the charge into which the DI fuel is injected. 1,200 rpm; 1.8 bar manifold absolute pressure; EGR=15%; $\Phi = 0.3$.

first in regime A, advances in regime B, then retards again in regime C. In all three regimes, rate of pressure rise is higher for earlier phasing. This is shown in Figure 3. In regime A, the ignition event behavior with injection retard appears to be controlled by a tradeoff between the time available for the ignition process (decreasing) and the rate of ignition reaction (increasing) provided by the increasing compression pressure and temperature. The net result is that ignition, and hence the crank angle for 10% burned (CA10), retards with retard of start of injection (SOI). In regime B, fuel is injected into a much hotter and denser environment and hence the ignition delay is shorter. Also the fuel is more stratified here than in regime A and fuel rich regions in the high-temperature environment have a preferentially shorter ignition delay. The net effect of the shorter ignition delay and later injection results in advancement of ignition and CA10. In regime C, the ignition delay becomes very short and the time required to physically prepare the mixture (evaporation and mixing) overpowers the gain in shortening the delay because of the hotter and denser charge and because of stratification. Thus combustion is

effectively mixing limited and the trend reverses again with combustion retarding with SOI.

Flamelet-Based Modeling

High fidelity direct numerical simulation of autoignition of a variety of reactant mixtures at HPLB engine-like conditions were conducted in order to provide fundamental insights into the ignition and combustion characteristics influenced by different levels of mixture stratifications. Full-cycle, multi-dimensional CFD simulations of ignition and combustion processes were also conducted using KIVA-3V with flamelet-based combustion submodels. Simulations were conducted for two parametric conditions, early injection (PPCI) and late injection (DI). The results were compared with those from KIVA-multizone (KIVA-MZ) calculations as well as experimental data. While the two alternative models yielded comparable fidelity for the early injection condition, for later injection, the flamelet approach showed better agreement with experimental results. The improved fidelity for the flamelet model is attributed to the ability to capture the subgrid scale fluctuations on chemical reactions that reveal an apparent acceleration of ignition/burn rate due to small-scale turbulence and mixing effects, not previously well understood.

Modeling of Partial Fuel Stratification

Fully-coupled CFD and chemical kinetics simulations were performed using a modified version of KIVA-3V that computes chemistry using CHEMKIN and with CONVERGE™ in order to provide fundamental insights into the physical processes governing PFS. A 96-species reduced mechanism for a 4-component gasoline surrogate was developed for this purpose. The simulations correctly predict the occurrence of multi-stage combustion for PFS at $P_{in} = 2$ bar as evidenced by the inflected pressure curves seen in Figure 4. In contrast only single-stage combustion occurs with $P_{in} = 1$ bar (not shown).

Analysis of the results reveals that this effect is due to the competing effects of fuel and temperature stratification. Although the richer regions are initially colder from evaporative cooling of the liquid fuel spray, the observed LTHR occurs in the richer regions of the mixture, increasing their temperature. This Φ and temperature distribution results in t_{ign} being shorter for richer regions. As such, the richer regions ignite first followed by the leaner regions and multi-stage combustion is observed. Conversely, at $P_{in} = 1$ bar, the richer regions are colder than the leaner regions ($0.3 \leq \Phi \leq 0.75$) due to evaporative cooling from the liquid fuel spray and the absence of LTHR.

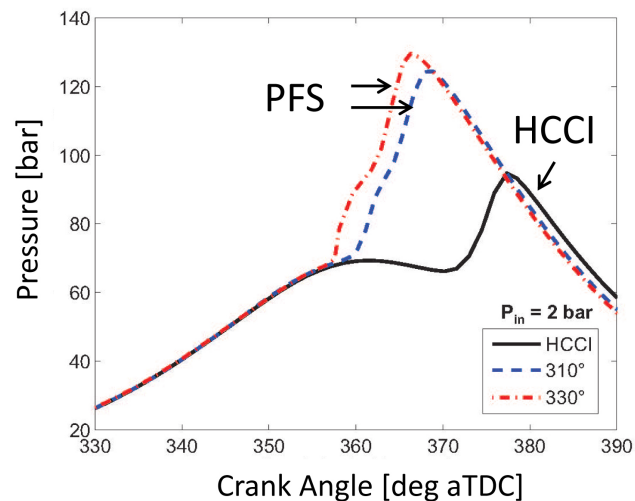


FIGURE 4. CFD simulations comparing in-cylinder pressure for HCCI (solid curve) and PFS mode (dashed) at 2 bar intake pressure. Inflected PFS pressure curves indicate two-stage burning caused by LTHR in the richer parts of the charge and the resulting alteration in the temperature-equivalence ratio distribution. Dashed labels denote the crank angle at SOI.

Metal Engine SACI Experiments

Single-cylinder metal engine experiments were used to investigate the burn rate, combustion limits, performance and emissions from SACI combustion in an FFVA NVO enabled engine. It was found that with careful manipulation of spark advance, internal EGR rates (via NVO), and external EGR rates the usable load range was doubled compared to pure HCCI combustion while maintaining high thermal efficiency. The use of SACI permitted variable burn rates at a constant phasing (CA50), thus addressing a major shortcoming of conventional HCCI combustion. Under the conditions examined, the stratification associated with NVO was found to have little effect on the rate of combustion. However diluent composition was shown to have a dramatic effect on SACI burn rates. In this case, as the mixture EGR was replaced by air (i.e., made leaner), the temperature at intake valve closing had to be decreased to maintain constant phasing. Despite the lower temperatures, the rate of flame based heat release increased. Analysis indicates that this results from higher flame speeds and burned gas temperatures during the flame-based heat release due to the higher O_2 concentrations that accompany replacing EGR with air.

Optical Engine Experiments

Experiments were carried out to determine effects of spark assist with an E0 reference gasoline and E30. A range of spark timings was considered for fuel/air equivalence ratios $0.4 \leq \Phi \leq 0.5$. High-speed imaging

together with concurrent in-cylinder pressure data was used to understand connections between spark initiated flame propagation, autoignition, and engine performance including heat release rate, IMEP and mass fraction burned. Cycle-to-cycle variations and time averaged data were evaluated. Figure 5 shows a sequence of views seen upward through the piston of a spark-assisted autoignition.

The results show that global ignition of SA HCCI is dominated by autoignition, and the heat released during flame propagation is less than ~20% of the total available. The compression heating caused by flame propagation primarily serves to accelerate autoignition of local sites which are already thermally preferred, that then accelerate global autoignition. The timing of SA is a tradeoff between (1) advancing SA and initiating flames at colder bulk temperatures (potentially quenching the flame or slowing flame progress) to give the flames more time to expand and heat the remaining unburned charge and (2) retarding SA and initiating flames at later times when bulk temperatures are higher (yielding higher flame speeds), leaving less time for the flames to heat the unburned gases. Local conditions and fuel specific flame speeds will affect the range of useful SA timing. Regardless of spark timing, the charge must already be sufficiently close to autoignition that compression heating by small fractions of the fuel/air charge can have an impact.

Rapid Compression Facility

Complementary experiments were conducted in a spark plug-equipped RCF using high-speed optical and

pressure diagnostics. Fast image processing algorithms were coupled with pressure measurements to determine key quantitative metrics of reaction fronts initiated by the spark discharge and propagated into premixed iso-octane and air. Depending on the state conditions and composition of the mixtures, the presence of flames accelerated ignition compared to conditions when no flames were initiated and sustained. The predicted adiabatic flame temperature has been identified as a good indicator of the effect of spark on the autoignition timing. A spark-initiated lean flammability limit was determined for equivalence ratios of $\Phi = 0.20$ to 0.99 , inert to oxygen dilution levels of 3.76:1 to 7.47:1, temperatures of 963 ± 10 K, and pressures of 8.0 ± 0.3 atm. Figure 6 shows pressure histories with and without spark, for a case in which the flame was viable.

CFD Modeling of SACI

Open-cycle SACI simulations using the previously developed KIVA-CFMZ model were performed with a 156,000-cell detailed mesh corresponding to the geometry of the metal FFVA engine described previously. These simulations modeled the gas exchange process and the trapping and recompression of in-cylinder residuals during NVO operation as well as direct fuel injection and charge preparation. Figure 7 shows the predicted heat release from a series of runs varying spark timing while maintaining fixed composition and CA50 by adjusting NVO and EGR. These results are in good qualitative agreement with the experimental results.

The figure shows an increase in flame heat release for the earlier spark case as well as a decrease in peak

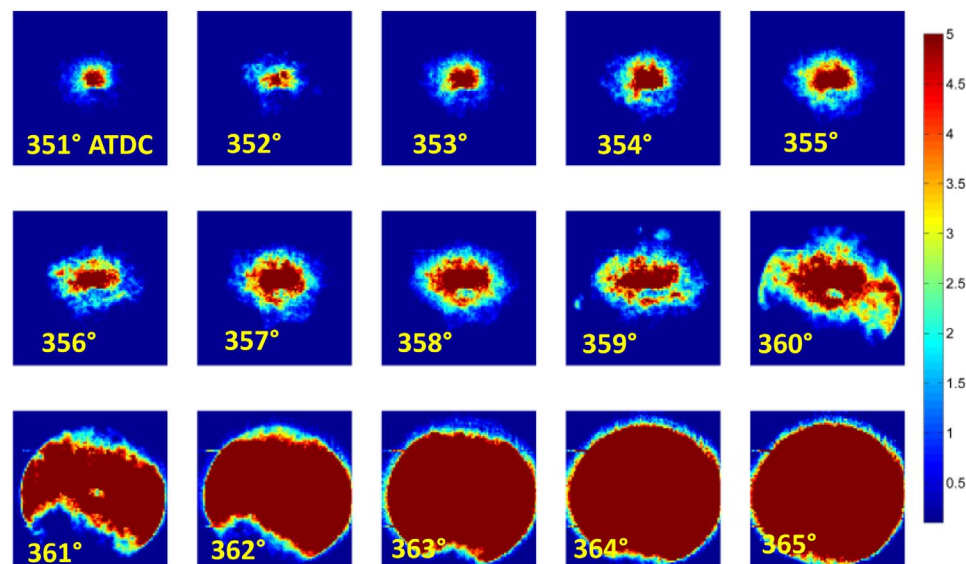


FIGURE 5. Sequence of SACI images from optical engine showing rapid transition from flame to autoignition. Average chemiluminescent intensity for E30 with SA at 40° before top-dead center and $\Phi=0.45$ at 700 RPM.

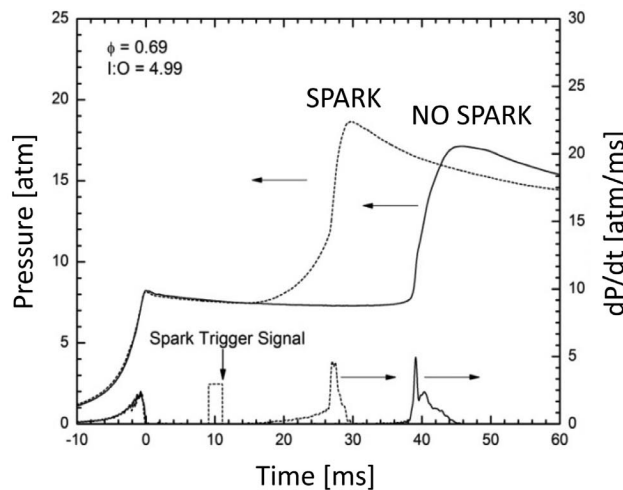


FIGURE 6. Pressure traces from the RCF showing the effect of spark on ignition delay with iso-octane: O_2 ; N_2 mixture at 7.9 atm. Testing over a wide range of conditions was used to establish limiting conditions for SACI.

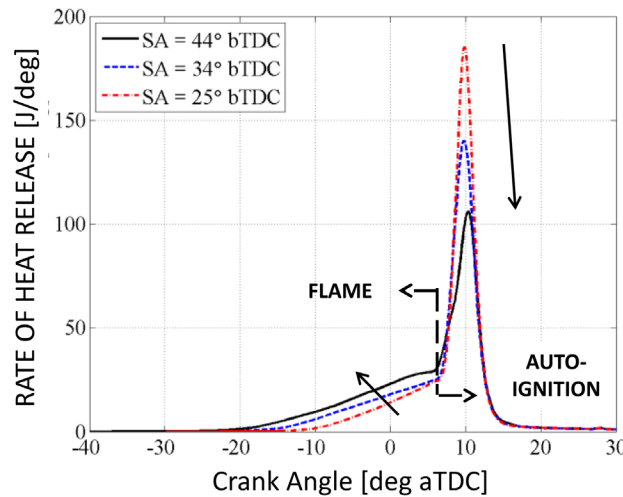


FIGURE 7. KIVA-CFMZ model predicted rate of heat release for three SACI cases. Advancing the spark timing and decreasing NVO with fixed CA50 increases the fraction of flame heat release and significantly reduces the peak rate of heat release during compression ignition.

autoignition heat release. Analysis of the results reveals that although the flame speed decreases for the advanced spark case, the additional time is sufficient to consume more of the charge before autoignition occurs. Further analysis suggests that the decrease in peak heat release is also affected by preferential consumption of higher reactivity (hotter, less dilute) regions by the flame.

Microwave-Assisted Spark Plug

A matrix of tests was conducted on a single-cylinder CFR engine comparing the microwave-assisted spark ignition mode to the spark-only ignition mode with wet

ethanol as a fuel. The microwave-assisted spark ignition mode allows stable engine operation in regions with higher dilution than possible with spark-only ignition. Microwave-assisted ignition can improve stability when operation destabilizes due to charge dilution with both air and water. The observed diminished effects of microwave-assisted spark ignition at near-stoichiometric conditions can be explained by elevated in-cylinder pressures that diminish microwave effectiveness. Combustion enhancement by microwaves appears more-strongly dependent on pressure than temperature.

The effectiveness of a microwave-assisted spark plug was also investigated in a constant volume combustion chamber for initially quiescent methane-air mixtures. High-speed schlieren imaging is used to visualize the early flame kernel development. While the initial flame kernel growth was augmented with the microwave ignition under the leanest conditions studied, overall rate of heat release did not change between at any equivalence ratio, initial pressure, microwave duration, or microwave timing delay investigated in this study, indicating that the present microwave system only affects early heat release rates and early flame kernel growth.

Further development of practical combustion applications implementing microwave-assisted spark technology will benefit from predictive kinetic models which include the plasma processes governing the observed combustion enhancement. With this in mind, a chemical kinetic mechanism has been developed for methane combustion that includes plasma reactions such as electron impact dissociation/recombination reactions, vibrational and electronic excitation reactions, and electron-neutral momentum transfer. A corresponding zero-dimensional reactor model has also been developed to include an equation for the electron energy and associated electric field input.

Fuel Effects in an NVO Engine

Previously reported comparisons of fuel octane number in HCCI combustion mode indicated that lower octane number fuel resulted in shorter burn durations and could be retarded further, enabling a higher load without exceeding the ringing limit. These experiments were carried out in an NVO-enabled (internal EGR) engine without external EGR and limited intake temperature range. As a result, definitive analysis of the results was confounded by changes in composition and internal EGR distribution that necessarily accompanied the NVO variations.

New experiments have been conducted taking full advantage of the FFVA system to more accurately control these variables. Small changes in intake valve closing time (independent of NVO) and intake pressure together with external EGR and intake temperature control were

used to maintain constant composition, fueling rate and CA50 over a range of NVO, fuel type, and engine speed. Over a range of engine speeds from 1,000-2,000 RPM, PRF40 burned faster and had higher peak heat release rates than gasoline and could be retarded further at constant COV of IMEP, confirming the previous results. This was true even at 1,000 RPM where PRF40 exhibited two-stage combustion with LTHR. Varying NVO, which more than doubled internal EGR from ~15% to ~35% produced only a modest decrease in peak heat release (<14%). Thus, compositional stratification due to incomplete mixing of internal EGR appears to have only a small effect on overall burn characteristics.

Buffer Gas Effects on Ignition

Computational simulations of ignition delay time and heat release rate of iso-octane, n-heptane, and of n-butanol were used to characterize the effects of buffer gas composition. A detailed description of the approach and results is provided in Wagnon and Wooldridge [28]. The fuels and simulation conditions were selected based on relevance to engine operating conditions and previously published ignition studies. Iso-octane and n-heptane were studied over a range of initial pressures from 9 atm to 60 atm and for two dilution levels of buffer gas, over a temperature range of 600-1,100 K. All mixtures were stoichiometric. The buffer gases considered were argon, nitrogen, water, and carbon dioxide.

In the negative temperature coefficient (NTC) region, the simulation results predicted changes of greater than a factor of 2 in ignition delay time and heat release rate as a function of buffer gas composition for n-heptane and iso-octane. Outside the NTC region, the predicted effects of changes in buffer gas composition were small (<20%). The heat release rates were also sensitive to buffer gas composition, with carbon dioxide exhibiting relatively low levels of early and late heat release relative to the other buffer gases.

The relationships between ignition delay time and heat release rate were quantified for the different diluent compositions for n-heptane. For n-heptane at the air levels of dilution and $P = 9$ atm, the results show characteristic times for heat release correlate linearly with the autoignition times, and the composition of the buffer gas has a larger effect on heat release at faster ignition delay times. The effects of buffer gas composition on heat release are amplified at higher levels of dilution and higher pressures, with over an order of magnitude difference between the characteristic time for heat release for CO_2 and N_2 at $P = 60$ atm for the same autoignition time. The results indicate that strategies that fix engine autoignition phasing will yield different combustion rates based on the buffer gas composition,

and higher engine speeds will be affected more than lower engine speeds.

CONCLUSIONS

The consortium has made considerable progress toward assembling the knowledge and tools needed to achieve the fuel economy goals of the Vehicle Technologies Office for gasoline engines.

- Two engine models of SACI were developed. The first, a system level model combining phenomenological flame model and correlations of autoignition burn rates will be used to project engine performance in the advanced combustion mode. The second, a full CFD representation has been used to provide insight into the reasons for experimentally observed benefits of higher air vs. EGR and the reduced peak heat release with SACI.
- Experiments and modeling studies on stratification (PPCI and PFS) have shown complex behavior of burn rate when injection timing and boost pressure are varied. The explanations involve tradeoffs between ignition delay and available time after injection, and the interaction of evaporative cooling, LTHR, and ignition enhancement in richer regions of the charge.
- Optical engine studies of SACI have confirmed that phasing changes in autoignition are the result of a relatively small amount of flame heat release, which is determined by a tradeoff between time available and changes in flame speed. Similar optical testing in the RCF has been used to determine the lean limit of SACI with high dilution.
- Experiments in a CFR engine have shown that a microwave-assisted spark plug helps with early flame kernel development but has little effect on overall burn characteristics. Also the effect is diminished at higher pressures.
- Controlled experiments on fuel effects in an NVO-enabled HCCI engine showed that a PRF40 fuel exhibits higher heat release than gasoline with more stability, confirming previous observations of higher maximum HCCI load for the lower octane fuel.
- Computational studies of the effect of buffer gas on autoignition have been conducted with N_2 , Ar , H_2O , and CO_2 . The results show significant effects on ignition delay, especially in the NTC region, and on heat release, with CO_2 dilution resulting in the lowest peak heat release rate.

FY 2013 PUBLICATIONS/PRESENTATIONS

1. University Consortium on Efficient and Clean High Pressure Lean Burn (HPLB) Engines, Final Technical Report, DOE project DE-EE0000203, October 2013.
2. Assanis, Dim., Wagnon, S.W., Wooldridge, M.S., "Rapid Compression Facility Studies of Iso-Octane Flame and Autoignition Interactions," in preparation for submission to Combustion and Flame, 2013.
3. Bedoya, I.D., Saxena, S., Cadavid, F.J., Dibble, R.W., Numerical Analysis of Biogas Composition Effects on Combustion Parameters and Emissions in Biogas Fueled HCCI Engines for Power Generation, ASME Journal of Engineering for Gas Turbines and Power, 135(7): 071503, 2013, doi: 10.1115/1.4023612.
4. Fatouraie, M., Wooldridge, M.S., "A High-Speed Imaging Study of the Effects of Ethanol/Gasoline Blends on Spark-Assisted HCCI," submitted to ASME Journal of Engineering for Gas Turbines and Power, in review March 2013.
5. Gupta, S., Keum, S.H., Im, H.G., 2013, "Modeling of Scalar Dissipation Rates in Flamelet Models for HCCI Engine Simulation," in preparation.
6. Gupta, S., Keum, S.H., Im, H.G., 2013, "Flamelet-Based Mixing Models for Low Temperature Combustion Engine Simulations," 9th Asia-Pacific Conference on Combustion, The Combustion Institute, May 19–22, Gyeongju, Korea.
7. Karwat, D.M.A., Wagnon, S., Wooldridge, M.S., Westbrook, C.K., "Low Temperature Chemical Kinetic and Speciation Studies of n-Heptane," accepted to Combustion and Flame, in press September 2013. Also submitted for presentation as Karwat, D.M.A., Wagnon, S., Wooldridge, M.S., Westbrook, C.K., "Chemical Kinetics of n-Heptane Ignition in a Rapid Compression Facility," National Combustion Meeting, Park City, Utah, May 2013.
8. Keum, S.H., Babajimopoulos, A., Im, H.G., Assanis, D.N., 2013, "Effect of Injection Parameters on HCCI Combustion at Low Load Conditions," in preparation.
9. Kozarac, D., Vuilleumier, D.M., Saxena, S., Dibble, R.W., Numerical Analysis of Influence of EGR on combustion of Biogas fueled HCCI engines and the Possibility to use EGR for reducing High Intake Temperature Requirements, 2013 SDEWES conference, Dubrovnik, Croatia.
10. Lavoie, G., Ortiz-Soto, E., Babajimopoulos, A., Martz, J., and Assanis, D. (2013) Thermodynamic sweet spot for high efficiency, dilute, boosted gasoline engines. *Int. J. Engine Res.*, Vol. 14, No. 3, 260-278, doi:10.1177/1468087412455372.
11. Manofsky-Olesky, L., Lavoie, G.A., Assanis, D.N., Wooldridge, M.S., Martz, J.B., "The Effects of Diluent Composition on the Rates of Spark Assisted Compression Ignition Combustion," in preparation for submission to Applied Energy, 2013.
12. Maria, A., Cheng, W., Kar, K., and Cannella, W., "Understanding Knock Metric for Controlled Auto-Ignition Engines," SAE Int. J. Engines 6(1):533-540, 2013, doi:10.4271/2013-01-1658.
13. Maria, A., Cheng, W., Kar, K., Cannella, W., (2013) "Understanding Knock Metric for Controlled Auto-Ignition Engines," SAE Paper 2013-01-1658, 2013.
14. Olesky, L.M., Martz, J.B., Lavoie, G.A., Vavra, J., Assanis, D.N., and Babajimopoulos, A. (2013) The effects of spark timing, unburned gas temperature, and negative valve overlap on the rates of stoichiometric spark assisted compression ignition combustion. *Applied Energy*, Vol. 105, No. 0, 407-417, doi:<http://dx.doi.org/10.1016/j.apenergy.2013.01.038>.
15. Ortiz-Soto, E.A., Lavoie, G.A., Martz, J.B., Babajimopoulos, A., Wooldridge, M., Assanis, D. (2014) Enhanced Heat Release Analysis for Advanced Multi-Mode Combustion Engine Experiments. Submitted to SAE World Congress 2014, 14PFL-1132.
16. Ortiz-Soto, E.A., Lavoie, G.A., Wooldridge, M., Assanis, D. (2014) A New Empirical Burn Rate Model of End-Gas Auto-Ignition for Computational Studies of SI, HCCI and SACI Engines. In preparation.
17. Ortiz-Soto, E.A., Lavoie, G.A., Wooldridge, M., Assanis, D. (2014) An Integrated Multi-Mode Combustion Model for Engine System Simulations of Advanced SACI Combustion. In preparation.
18. Ortiz-Soto, E.A., Lavoie, G.A., Wooldridge, M., Assanis, D. (2014) A New Flame Propagation Model for Engine System Simulations of Spark-Ignited Combustion. In preparation.
19. Ortiz-Soto, E.A., Lavoie, G.A., Wooldridge, M., Assanis, D. (2014) The Load Extension and Efficiency Improvement Potential of Advanced SACI Combustion Engines. In preparation.
20. Pal, P., Im, H. G., 2013, "Validation of Flamelet and Multi-zone Combustion Models for Direct-Injection HCCI Engines," 6th European Combustion Combustion Meeting, The Combustion Institute, June 25–28, Lund, Sweden.
21. Pal, P., Keum, S.H., and Im, H.G., 2013, "Applicability of Flamelet and Multi-zone Combustion Modelling Approaches to Direct Injection HCCI Engines," in preparation.
22. Pal, P., Keum, S.H., and Im, H.G., 2013, "Applicability of Flamelet and Multi-zone Combustion Modelling Approaches to Direct Injection HCCI Engines," 8th Mediterranean Combustion Symposium, The Combustion Institute, September 8–13, Cesme, Turkey.
23. Sang, W, Maria, A., Cheng, W., "The Nature of Heat Release in Gasoline PPCI Engines," paper submitted to the SAE Congress, 2014.
24. Sang, W., "Knock Mitigation on Boosted Controlled Auto-Ignition Engines with Fuel Stratification and EGR," PhD thesis, Dept. of Mech. Eng., MIT, 2014.
25. Saxena, S. and Bedoya, I.D., Fundamental Phenomena affecting Low Temperature Combustion and HCCI Engines, High Load Limits and Strategies for Extending these Limits, *Progress in Energy & Combustion Science*, 39(5):457-488, 2013, doi: 10.1016/j.pecs.2013.05.002.

- 26.** Saxena, S., Bedoya, I.D., Shah, N., and Phadke, A., Understanding Loss Mechanisms and Identifying Areas of Improvement for HCCI Engines using Detailed Exergy Analysis, ASME Journal of Engineering for Gas Turbines and Power, 135(9): 091505, 2013, doi: 10.1115/1.4024589.
- 27.** Saxena, S., Bedoya, I.D., Shah, N., Phadke, A., Understanding Optimal Engine Operating Strategies for Gasoline-Fueled HCCI Engines using Crank-Angle Resolved Exergy Analysis, Article in Press for Applied Energy, 2013.
- 28.** Wagnon, S. W., and Wooldridge, M.S., “Chemical kinetic effects of buffer gas composition during ignition” Combustion and Flame, in press, 2013.
- 29.** Wolk, B. and Chen, J.Y. (2013) Computational study of partial fuel stratification for HCCI engines using gasoline surrogate reduced mechanism. 8th US National Meeting of the Combustion Institute, Park City, Utah, USA, May 19–22, 2013, paper 070IC-0003 (submitted).
- 30.** Wolk, B. and Chen, J.Y. (2013) Computational study of partial fuel stratification for HCCI engines using gasoline surrogate reduced mechanism. Combustion Science and Technology (in revision).
- 31.** Wolk, B. and Chen, J.Y. (2013) Computational study of partial fuel stratification for HCCI engines using gasoline surrogate reduced mechanism. 8th US National Meeting of the Combustion Institute, Park City, Utah, USA, May 19–22, 2013, paper 070IC-0003.
- 32.** Wolk, B., DeFilippo, A., Chen, J.Y., Dibble, R., Nishiyama, A., and Ikeda, Y. (2013) Enhancement of flame development by microwave-assisted spark ignition in constant volume combustion chamber. Combustion and Flame, doi:<http://dx.doi.org/10.1016/j.combustflame.2013.02.004> (in-press).
- 33.** Wolk, B., DeFilippo, A., Chen, J.Y., Dibble, R., Nishiyama, A., and Ikeda, Y. (2013) Enhancement of flame development by microwave-assisted spark ignition in constant volume combustion chamber. Combustion and Flame, 160(7), pp. 1225-1234, doi:<http://dx.doi.org/10.1016/j.combustflame.2013.02.004>.

II.15 Flex-Fuel Optimized SI and HCCI Engine

Guoming (George) Zhu (Primary Contact) and Harold Schock

Michigan State University
Mechanical Engineering
Energy and Automotive Research Lab
1497 Engineering Research Court, Room E148
East Lansing, MI 48824

DOE Technology Development Manager:
Gurpreet Singh

NETL Project Manager: Nicholas Damico

Subcontractor:
Chrysler, LLC, Auburn Hills, MI

Overall Objectives

- Demonstrate a spark ignition (SI) and Homogeneous Charge Compression Ignition (HCCI) dual combustion mode engine for a blend of gasoline and E85 (85% ethanol and 15% gasoline) for the best fuel economy.
- Develop a cost effective and reliable SI and HCCI dual combustion mode engine.
- Develop a control-oriented (real-time) SI, HCCI and SI-HCCI combustion model and implement it into a hardware-in-the-loop (HIL) simulation environment.
- Develop model-based combustion mode transition control strategies for smooth mode transition between SI and HCCI combustion.
- Utilize closed-loop combustion control to minimize efficiency degradation with satisfactory engine-out exhaust emissions under any blend of gasoline and E85.

Fiscal Year (FY) 2013 Objectives

- Complete the HCCI combustion dynamometer tests and determine the HCCI operational range.
- Develop the final test plan and complete the SI and HCCI combustion mode transition performance tests.
- Complete the test data analysis and final project report.

FY 2013 Accomplishments

- The engine HIL simulation model was further improved with an updated physics-based charge

mixing model based upon the test data. The results were summarized in a journal paper for the IEEE Transaction on Vehicle Technology accepted in late 2013.

- The target multi-cylinder metal engine was converted into a single-cylinder setup, and the corresponding engine control system was reconfigured for the corresponding single-cylinder setup.
- Multi-injection and multi-ignition capability was added to the engine control system to enable multiple injections and ignitions during the mode transition, and the electrical variable valve timing (EVVT) operational range was extended to 85 degrees to increase recompression.
- Stable HCCI combustion was achieved with around 2% coefficient of variance (COV) for the target single-cylinder metal engine without external electric heater.
- Smooth combustion mode transition was achieved between SI and HCCI combustion within eight engine cycles. It was found that the proposed concept of using the hybrid combustion mode during the mode transition is the key enabler for fast and smooth combustion mode transition.
- Over the past years, three journal and three conference papers were published.

Future Directions

Complete and submit the final report of this project.



INTRODUCTION

To obtain the benefit of high efficiency of compression ignition engines and low emissions of SI engines, there has been a rekindled interest in HCCI engines in recent years. The major advantage of HCCI engines is realized by eliminating the formation of flames which results in a much lower combustion temperature [1-5]. As a consequence of low-temperature combustion, the formation of NOx emissions is greatly reduced. The lean burn nature of the HCCI engine also enables un-throttled operation to improve vehicle fuel economy. The main challenge of HCCI engines is the accurate control of the start of combustion and combustion duration. The practical application of the HCCI principle to gasoline engines is envisioned in a dual-mode combustion engine

concept. At partial load conditions, the engine would operate under an un-throttled HCCI combustion mode, and at low- or high-load conditions, the engine operation needs to transition to the conventional SI combustion mode to avoid engine misfire or knock. The objective of this project is to demonstrate an SI and HCCI dual-mode combustion engine for a blend of gasoline and E85. The operating efficiencies will be obtained through closed-loop control, which will result in minimal efficiency degradation when E85 fuel or any blend of gasoline and E85 are used.

APPROACH

This research activity adopts a model-based control approach to develop control strategies for smooth mode transition between SI and HCCI combustion with the support from our industrial partner, Chrysler, LLC. The model-based control methodology is used to develop the combustion mode transition control strategies.

First, the characteristics of both HCCI and SI-HCCI hybrid combustion processes were experimentally studied using an optical engine under HCCI combustion. Second, a control-oriented combustion model that unifies SI, HCCI, and SI-HCCI combustion was developed along with the entire engine model, and the developed model was calibrated based upon both GT-POWER simulation results and optical/metal engine experimental data. Third, the calibrated control-oriented engine model was used to study SI and HCCI combustion modes as well as the SI-HCCI hybrid (also called the spark assistant HCCI) combustion mode during combustion mode transition. Finally, the feed-forward control strategy of mode transition between SI to HCCI combustion, utilizing the hybrid combustion mode, was developed and calibrated through the HIL simulations and also validated on the target metal engine. The smooth mode transition between SI and HCCI combustion was demonstrated.

RESULTS

For HCCI combustion, mixture heterogeneity should be considered in the control-oriented model to predict accurate combustion phase and duration. In FY 2013, a two-zone HCCI combustion model was developed, where the in-cylinder charge is divided into the well-mixed and unmixed zones as the result of charge mixing (see Figure 1). Simplified fluid dynamics is used to predict the residual gas fraction before the combustion phase starts for real-time simulations, which defines the mass of the unmixed zone. Note that the unmixed zone size not only determines how well the in-cylinder charge is mixed, which affects the start of HCCI combustion, but also the resulting peak in-cylinder pressure and temperature during the combustion process. The developed control-

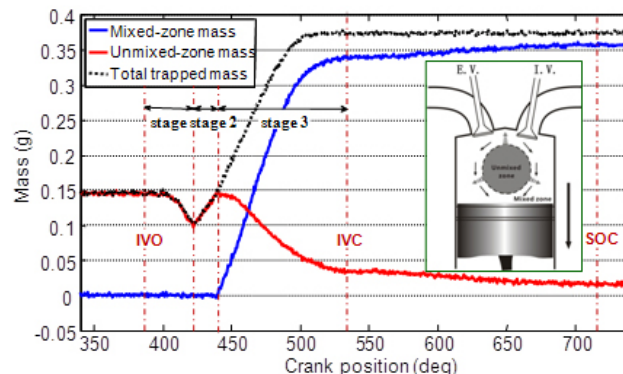


FIGURE 1. Simulated Charge Mixing Responses of the Turbulence-Based Model

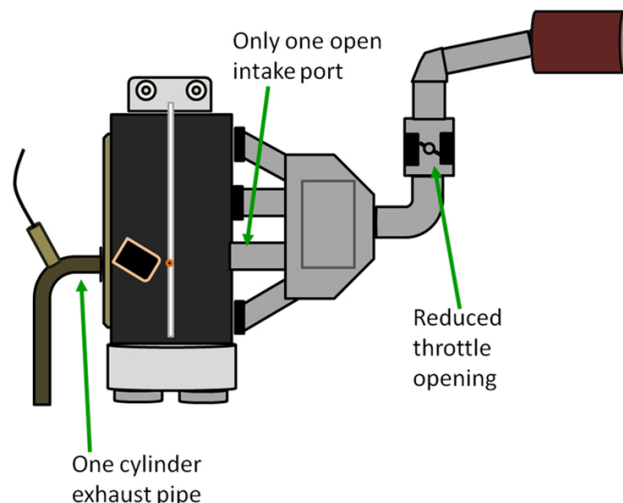


FIGURE 2. Reconfigured Single-Cylinder Metal Engine Diagram

oriented model was validated in the developed HIL simulation environment. The HIL simulation results show that the proposed charge mixing and HCCI combustion model provides better agreement with the corresponding high fidelity GT-POWER simulation results than the previously developed one-zone model [6,7].

The multi-cylinder engine was converted into the single-cylinder operation (see Figure 2) to focus on investigation of the combustion mode transition. The single-cylinder engine configuration can be found in Figure 2. The corresponding engine control system was also modified to meet the single-cylinder engine requirement. The single-cylinder engine operation was validated in engine dynamometer with modified engine cam phasing range.

Without any external electric heating device, smooth HCCI combustion was achieved for the single-cylinder metal engine, where the engine charge cooler was used to increase the charge temperature during HCCI operations.

Figure 3 shows the engine indicated mean effective pressure (IMEP) and peak cylinder pressure signals over 200 engine cycles. It can be seen that the engine IMEP fluctuation is very small with COV around 2% even though the engine peak cylinder pressure variation is relatively large.

From the mode transition study it was found that the proposed 5-cycle mode transition strategy (see Figure 4) needs to be extended to 7-9 cycles due to the increased response time of the EVVT, where the number of hybrid combustion cycles is increased to five. The slow cam phasing response is mainly due to the cam valve-train load increment from one cylinder to four cylinders.

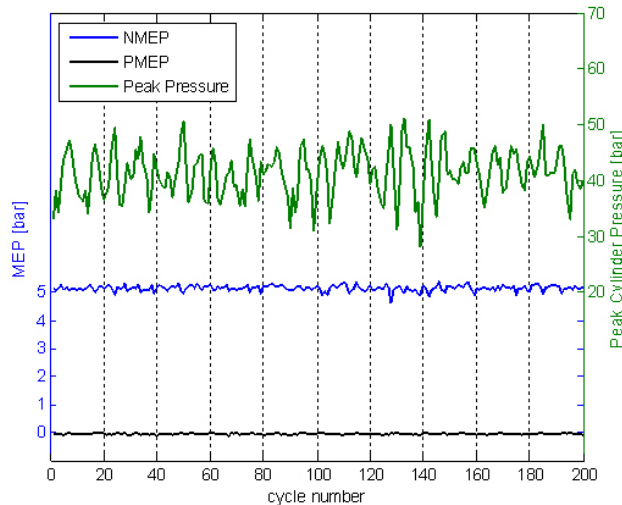


FIGURE 3. 200 Cycles of the IMEP and Peak In-Cylinder Pressure Signals

One of the key findings in FY 2013 is that it is feasible to achieve smooth combustion mode transition using the proposed hybrid combustion mode that starts with SI combustion and ends with HCCI combustion with the production-ready EVVT and two-step valve lift systems. With the help of the hybrid combustion the mode transition can be completed within eight engine cycles (see Figure 5). The mode transition number of cycles could be further reduced if the EVVT response time would be reduced. Also, the air/fuel ratio overshoot observed in Figure 5 is consistent with simulated response.

The proposed fast mode transition between SI and HCCI combustion is validated in both HIL simulations and experiments. The proposed 5-cycle mode transition was extended to 8 cycles due to slow EVVT response time. Furthermore, the experimental mass fraction burned curves (see Figure 6) of the hybrid SI-HCCI combustion during the mode transition are consistent with the simulated curves (see Figure 4) obtained based upon the developed control-oriented engine model. This also confirms that model-based combustion control is feasible for mode transition control.

CONCLUSIONS

The research conducted in FY 2013 leads to the completion of the proposed technologies and the specific accomplishments are listed in the following:

- The developed control-oriented crank-resolved engine model, implemented in the HIL simulation environment for real-time simulations, provides

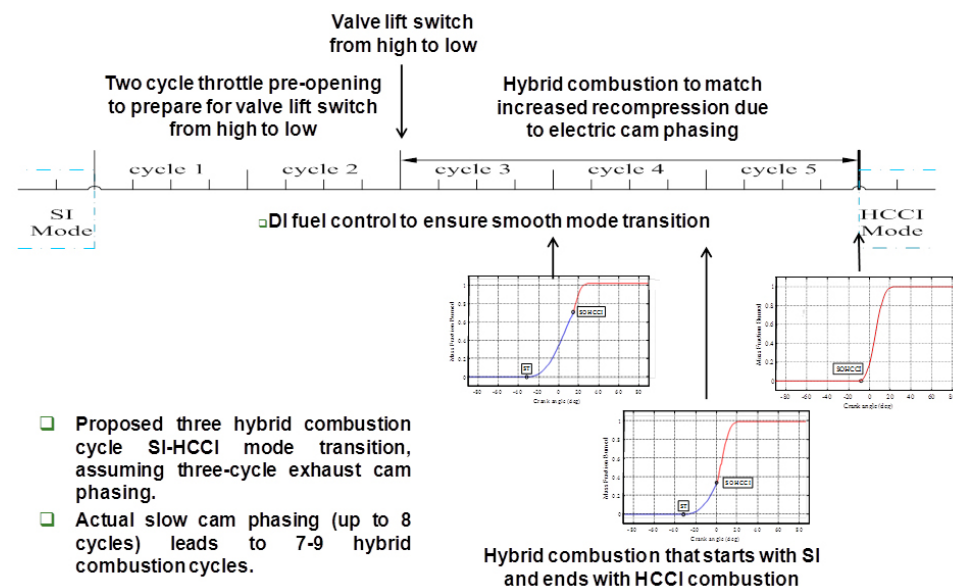


FIGURE 4. Proposed Hybrid Combustion Mode during the SI-HCCI Mode Transition

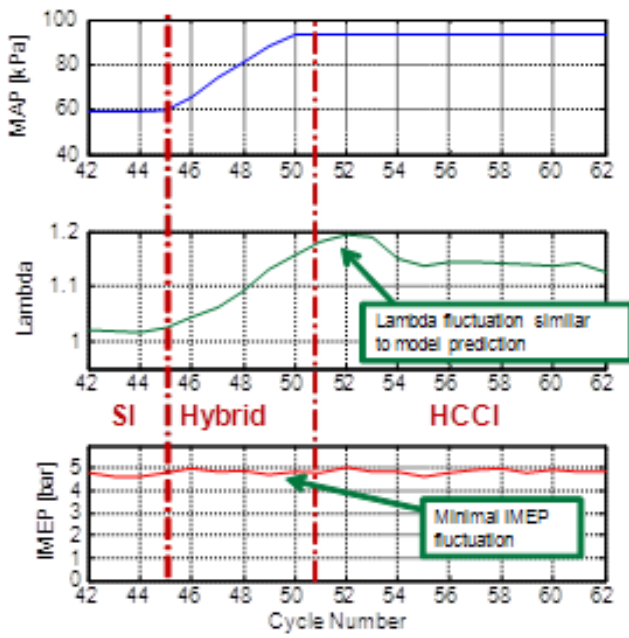


FIGURE 5. IMEP and Air/Fuel Ratio during the Combustion Mode Transition Responses

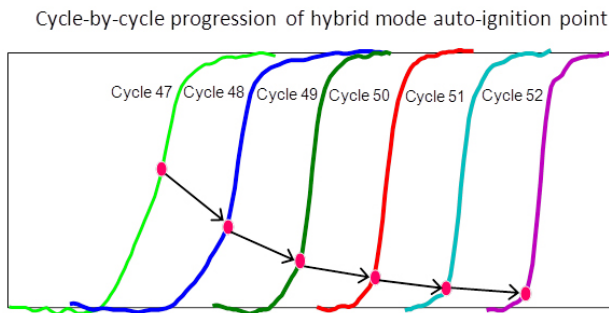


FIGURE 6. Experimental Hybrid Combustion Mass Fraction Burned Curves during the SI-HCCI Mode Transition

a key platform for developing and validating combustion mode transition control strategies.

- The simplified physics-based charge mixing model predicts the in-cylinder pressure, temperature, and the properties of the mixed and unmixed zones accurately. Note that the developed real-time model provides a solid foundation for model-based combustion control.
- Stable HCCI combustion can be achieved without external heater for charge air.
- The experimental mass fraction burned curves of the hybrid SI-HCCI combustion during the mode transition are consistent with the simulated ones obtained based upon the developed control-oriented engine model. This confirms that the model-based

combustion control is feasible for mode transition control.

- The key finding from this research project is that it is feasible to have smooth mode transition using the proposed hybrid combustion mode that starts with SI combustion and ends with HCCI combustion with the production ready EVVT and two-step valve lift systems. With the help of the hybrid combustion the mode transition can be completed within eight engine cycles.

REFERENCES

- G. Shibata, K. Oyama, T. Urushihara, and T. Nakano, “The effect of fuel properties on low and high temperature heat release and resulting performance of an HCCI engine,” *SAE Technical Paper*, SAE 2004-01-0553, 2004.
- G. Haraldsson, J. Hyvonen, P. Tunestal, and B. Johansson, “HCCI closed-loop combustion control using fast thermal management,” *SAE Technical Paper*, SAE 2004-01-0943, 2004.
- H. Persson, M. Agrell, J.-O. Olsson, and B. Johansson, “The effect of intake temperature on HCCI operation using negative valve overlap,” *SAE Technical Paper*, SAE 2004-01-0944, 2004.
- G.M. Shaver, et al, “Dynamic modeling of residual-affected homogeneous charge compression ignition engines with variable valve actuation,” *ASME Journal of Dynamic Systems, Measurement, and Control*, Vol. 127, 2005, pp. 374-381.
- G.M. Shaver, “Physics based modeling and control of residual-affected HCCI engines using variable valve actuation,” *PhD thesis*, Stanford University, 2005.
- S. Zhang, G. Zhu, and Z. Sun, “A control-oriented charge mixing and two-zone HCCI combustion model,” *IEEE Transactions on Vehicular Technology* (Accepted in September, 2013), DOI: 10.1109/TVT.2013.2285074.
- Y. Yoon, Z. Sun, S. Zhang and G. Zhu, “A control-oriented two-zone charge mixing model for HCCI engines with experimental validation using an optical engine,” *Submitted to ASME Journal of Dynamic Systems, Measurement and Control* (August, 2013).

FY 2013 PUBLICATIONS/PRESENTATIONS

- X. Yang and G. Zhu, “SI and HCCI combustion mode transition control of a multi-cylinder HCCI capable SI engine,” *IEEE Transaction on Control System Technology*, Vol. 21, Issue 5, 2013, pp. 1558-1569 (DOI: 10.1109/TCST.2012.2201719).
- S. Zhang, G. Zhu, and Z. Sun, “A control-oriented charge mixing and two-zone HCCI combustion model,” *IEEE Transactions on Vehicular Technology* (Accepted in September, 2013) DOI: 10.1109/TVT.2013.2285074.
- Z. Ren and G. Zhu, “Modeling and control of an electrical variable valve timing actuator,” *ASME Journal of Dynamic Systems, Measurement and Control* (Accepted in October, 2013)

4. S. Zhang, A. White, J. Yang, and G. Zhu, “LPV control of an electronic throttle,” *2013 ASME Dynamic System and Control Conference*, Polo Alto, CA, October, 2013.
5. Y. Yoon, Z. Sun, S. Zhang, and G. Zhu, “Development of control-oriented charge mixing model and experimental validation using graphical analysis,” *2013 American Control Conference*, Washington DC, June, 2013.
6. A. White, J. Choi, and G. Zhu, “Dynamic, output feedback, gain-scheduling control of an electric variable valve timing system,” *2013 American Control Conference*, Washington DC, June, 2013.
7. G. Zhu and H. Schock, “Flex fuel optimized SI and HCCI engine,” *DOE Vehicle Technology Program Annual Merit Review*, Arlington, VA, May, 2013.
8. G. Zhu and H. Schock, “Update on flex fuel optimized HCCI engine project,” *DOE ACE/HCCI working group meeting*, Livermore, CA, February, 2013.

II.16 Engine Efficiency Fundamentals – Accelerating Predictive Simulation of Internal Combustion Engines with High Performance Computing

K. Dean Edwards (Primary Contact),
C. Stuart Daw, Wael Elwasif,
Charles E.A. Finney, Sreekanth Pannala,
Miroslav K. Stoyanov, Robert M. Wagner,
Clayton G. Webster

Oak Ridge National Laboratory (ORNL)
National Transportation Research Center
2360 Cherahala Blvd
Knoxville, TN 37932

DOE Technology Development Manager:
Gurpreet Singh

- Developed computational framework for job management and component optimization and performed initial parameter sweeps for model validation.

Future Directions

- Complete development and validation of metamodel of highly dilute SI combustion.
- Couple OpenFOAM® spray model to in-cylinder flow and combustion simulations and optimize the injector design for improved fuel economy and emissions.
- Transfer knowledge and methodologies to our industry partners.
- Develop additional tasks with industry partners.



INTRODUCTION

This project supports rapid advancements in engine design, optimization, and control required to meet increasingly stringent fuel economy and emissions regulations through the development of advanced simulation tools and novel techniques to best utilize HPC resources such as ORNL's 20+ petaflop machine, Titan. This effort couples ORNL's leadership role in HPC with experimental and modeling expertise with engine and emissions-control technologies. Specific project tasks evolve to support the needs of industry and DOE. Two tasks were supported during FY 2013:

- Task 1:** Use of highly parallelized engine simulations to understand the stochastic and deterministic processes that drive cycle-to-cycle variability in dilute combustion systems. Collaborative effort with Ford Motor Company and Convergent Science, Inc.
- Task 2:** Use of detailed computational fluid dynamics (CFD) simulations to understand and optimize the design of direct-injection gasoline fuel injectors for improved engine efficiency. Collaborative effort with General Motors.

Fiscal Year (FY) 2013 Objectives

- Initiate development of metamodel for investigating cycle-to-cycle combustion variability in highly dilute spark-ignited (SI) engines.
- Develop and validate supervisory framework to automate and optimize fuel injector design.

FY 2013 Accomplishments

- Supported two ongoing tasks with direct industry collaboration.
- Initiated metamodel development for highly dilute SI combustion by launching initial grid optimization and parameter sensitivity sweeps.

APPROACH

The aim of this project is to develop and apply innovative approaches which use HPC resources for simulation of engine systems to address specific issues of interest to industry and DOE. The specific issues addressed and approaches applied for the two current tasks are described in the following.

Task 1: Dilute combustion provides a potential pathway to simultaneous efficiency and emissions improvements in light-duty engines. However, at sufficiently high dilution levels, flame propagation becomes unstable, and small changes in initial cylinder conditions can produce complex cycle-to-cycle combustion variability, forcing the adoption of wide safety margins and failure to achieve the full potential benefits of charge dilution. There is growing interest in the use of computational simulations to understand the physics and chemistry behind the combustion stability limit to facilitate control of the instabilities allowing operation at the ‘edge of stability’. A major challenge is that many of the associated dynamical features are very subtle and/or infrequent, requiring simulation of hundreds or thousands of sequential engine cycles in order to observe the important unstable events with any statistical significance. Complex CFD simulations with full chemical kinetic modeling can require days of computational time for a single cycle making serial simulation of thousands of cycles time-prohibitive. In this task, we address these computational challenges by replacing simulations of many successive engine cycles with multiple, concurrent, single-cycle simulations which exhibit statistically similar behavior. Results from these simulations are then used to generate lower-order metamodels which retain the key dynamic features of the complex model but computationally are simple enough to allow simulation of serial combustion events and detailed studies of the parameters that promote combustion instability.

Task 2: Multi-hole injectors utilized by SI, direct-injection engines offer the flexibility of manufacturing the nozzle holes at various orientations to engineer a variety of spray patterns. The challenge is to determine the optimal design to maximize efficiency and emissions benefits for a given application. Detailed analytical tools, such as CFD, can provide a cost-effective approach to reduce the number of potential injector concepts for a given combustion system. However, each CFD simulation requires substantial run-time and conducting a thorough investigation of the design and operating parameter space to optimize injector design remains tedious and labor-intensive. In this task, we are working with General Motors to develop and validate a high-fidelity, multi-processor simulation tool to accelerate design and optimization of fuel injector hole patterns

for direct-injection gasoline applications. Our approach involves the use of an optimization routine (such as a genetic algorithm) to coordinate parallel fuel-spray and combustion simulations with different injector geometries to hasten convergence on an optimal design.

RESULTS

Our efforts in FY 2013 have focused on development and application of the tools and methodologies required for each task in close collaboration with our industry partners.

Task 1: Efforts for this task during FY 2013 were focused on demonstration of our metamodel approach developed in FY 2012 on a detailed CFD model of an SI engine with high dilution due to external and internal exhaust gas recirculation. An open engine geometry model and experimental data provided by Ford were used to develop and calibrate a CONVERGE™ model of the engine cylinder and intake and exhaust flow paths. An extensible supervisory framework was developed to manage case setup, job creation, file handling, progress monitoring and data post-processing on Titan. Using the latest version of the adaptive sparse grid sampling algorithm developed over the past year, initial grid optimization and parameter sensitivity sweeps were launched on Titan in mid-September, totaling 401 parallel cases (using 6,416 cores on Titan). These runs are being used to provide guidance to and refine the sampling control framework which is being used by industry partners in their related HPC studies. Completion and evaluation of those runs will carry over into the beginning of FY 2014.

Task 2: Efforts for this task during FY 2013 were focused on developing and assembling the required tools and culminated in launch of the initial set of spray simulations on Titan. The foundation of this effort is an injector spray model developed by General Motors using OpenFOAM® and validated against experimental data. The spray model was ported for use on Titan and then validated against prior results obtained using General Motors’s computing resources. A scaling study was conducted and determined that 128 cores per simulation provided optimum computational efficiency on Titan’s architecture. A Python-based computational framework was developed that enables implementation of massively parallel parameter and design sweeps to take full advantage of the high performance computing architecture. This framework greatly accelerates the simulation process by replacing labor-intensive, manual generation of model iterations with automatic selection of design parameters, generation of a computer-aided design model, meshing, launching, and monitoring of the models. Using this framework, we successfully

completed the initial run of 42 parallel cases (using 5,376 cores on Titan) to validate the model against experimental data and perform an initial set of sweeps to determine parameter sensitivity.

CONCLUSIONS

Increasing industry interest in utilizing HPC resources to hasten design advancements in internal combustion engines has led to collaborative efforts with industry stakeholders in two important areas: understanding and controlling cycle-to-cycle variability in dilute combustion and optimization of fuel injector design. Early progress on these tasks is on track and showing great promise.

FY 2013 PUBLICATIONS/PRESENTATIONS

1. RM Wagner, S Pannala (2012). *High performance computing: Accelerating the development of high-efficiency engines*. 2012 Global Powertrain Congress. Troy, MI, USA; 25 October 2012.
2. CG Webster, MK Stoyanov, CEA Finney, S Pannala, CS Daw, RM Wagner, KD Edwards, JB Green Jr (2013). *High-dimensional multiphysics metamodeling for combustion engine stability*. 2013 SIAM Computational Science and Engineering Conference. Boston, MA, USA; 25 Feb-1 March 2013.
3. MK Stoyanov, CG Webster, CEA Finney, S Pannala, CS Daw, RM Wagner, KD Edwards, JB Green Jr (2013). *High dimensional multiphysics surrogate modeling for combustion engine stability*. 2013 SIAM SEAS Annual Meeting. Knoxville, TN, USA; 22-24 March 2013.
4. CG Webster, MK Stoyanov, CEA Finney, S Pannala, CS Daw, KD Edwards, JB Green Jr, RM Wagner (2013). *High dimensional multiphysics metamodeling for combustion engine stability*. 2013 SIAM Annual Meeting. San Diego, CA, USA; 08-12 July 2013.
5. RM Wagner (2013). *Accelerating the development of high-efficiency engines*. Fifth International Symposium on Clean and High-efficiency Combustion in Engines. Tianjin, China; July 2013.
6. MK Stoyanov (2013). *Hierarchy-direction selective approach for locally adaptive sparse grids*. ORNL Tech Report. ORNL/TM-2013/384.

II.17 Use of Low Cetane Fuel to Enable Low-Temperature Combustion

Stephen Ciatti
Argonne National Laboratory
9700 S. Cass Ave.
Bldg. 362
Argonne, IL 60439

DOE Technology Development Manager:
Gurpreet Singh

Subcontractors:
University of Wisconsin-Madison Engine Research
Center, Madison, WI

Overall Objectives

- Optimize the operating conditions to use low cetane fuel to achieve clean, high-efficiency engine operation.
- Demonstrate the use of low-temperature combustion (LTC) as an enabling technology for high-efficiency vehicles.

Fiscal Year (FY) 2013 Objectives

- Quantify the engine operating parameters of LTC by using cetane enhancers to study chemical (not fluid) characteristics upon LTC performance.
- Optimize the engine control parameters (injection strategy, exhaust gas recirculation [EGR], intake temperature) for 87 anti-knock index (AKI) gasoline fuel to achieve wide range (low-load/idle to full-load) performance using pump gasoline.
- Demonstrate the efficiency benefits of LTC using an Autonomie simulation to validate higher efficiency vehicles.

FY 2013 Accomplishments

- Achieved 1.3 bar brake mean effective pressure (BMEP) to 20 bar BMEP using only 87 AKI fuel.
- Demonstrated the effectiveness of cetane enhancers (ethyl hexyl nitrate, EHN) in facilitating low-load performance.
- Attained a 26% fuel economy improvement using LTC in a conventional powertrain vehicle over a similar port fuel injected (PFI) vehicle on the combined Urban Dynamometer Driving Schedule (UDDS) and Highway Fuel Economy Test (HWFET) cycles in a 2007 Cadillac vehicle.

Future Directions

- Continue to extend low-load operation to idle using uncooled EGR and different injector umbrella angles for enhancing local richness in the combustion chamber.
- Explore the opportunity to utilize a turbocharger/supercharger combination to enhance intermediate temperature heat release (results from John Dec's work at Sandia) to further enhance low-load operation.
- Analyze the particulate matter (PM) coming from LTC and studying the formation/oxidation process to relate PM to engine operating conditions.
- Conduct additional engine performance tests for Autonomie simulations to support LTC development as applied to vehicles.



INTRODUCTION

Current diesel engines already take advantage of the most important factors for efficiency—no throttling, high compression ratio, and low heat rejection. However, diesel combustion creates a significant emissions problem. Mixing or diffusion combustion creates very steep gradients in the combustion chamber because the ignition delay of diesel fuel is extremely short. PM and oxides of nitrogen (NO_x) are the result of this type of combustion, requiring expensive after-treatment solutions to meet Environmental Protection Agency emissions regulations.

The current work seeks to overcome the mixing-controlled combustion dilemma by taking advantage of the long ignition delay of gasoline to provide much more premixing of fuel and air before ignition occurs. This premixing allows for the gradients of fuel and air to be much less steep, drastically reducing the PM-NO_x tradeoff relationship of mixing controlled combustion.

APPROACH

The intent of this project is to utilize the long ignition delays of low cetane fuels to create an advanced combustion system that generates premixed (but not homogeneous!) mixtures of fuel and air in the combustion chamber. As reported in several articles, if the local equivalence ratio is below 2 (meaning at most, twice as much fuel as oxidizer) and the peak combustion temperature is below 2,000 K (using EGR to drop the

oxygen concentration below ambient 21%, thereby slowing the peak reaction rates and dropping the peak combustion temperature), a combustion regime that is very clean and yet retains reasonably high power density is achieved.

The challenge to this type of combustion system is the metering of fuel into the combustion chamber needs to be precise, both in timing and amount. If too much fuel is added too early, a “knocking” type of combustion occurs, which creates unacceptably high combustion noise or worse. If not enough fuel is added, ignition may not occur at all and raw hydrocarbon exits the exhaust. Control over the relevant operating parameters is very important—fuel properties, injection strategy, compression ratio and intake temperature all have large influence upon ignition propensity.

Different injection strategies were employed this year to extend low-load operation operating on only 87 AKI fuel and 87 AKI fuel with trace amounts of EHN (effectively creating 84 and 75 AKI fuels using 0.2% and 0.4% EHN to keep fluid properties constant). This was done to explore the chemical effects of fuel characteristics on low-load operation.

RESULTS

Injection strategy was altered in an effort to determine how much premixing is necessary to achieve the low-load goals. First, one injection was used, with

injection timing swept from -9 deg after top-dead center (ATDC) to -42 deg ATDC. Rail pressure was held constant at 500 bar and 250 bar during these sweeps. Fuel rate was adjusted at each injection timing/pressure to the minimum allowed while maintaining a 3% coefficient of variance (COV) of indicated mean effective pressure (IMEP) or better for combustion stability. No EGR was used for these tests.

As expected, there is a location of minimum fueling that demonstrates an optimal injection timing that produces the required local richness necessary for ignition (see Figure 1).

Additional points were run for the Autonomie simulations (building upon FY 2012’s work) to refine the vehicle potential for fuel economy improvement. A 2007 Cadillac vehicle was chosen as the example vehicle because it can be purchased with a PFI engine or the General Motors diesel engine upon which the LTC engine is based. With the additional points and a further refined vehicle simulation, the fuel economy improvement was found to be 26% based upon the combined drive cycles for UDDS and HWFET (see Table 1).

CONCLUSIONS

- A specific study was performed with the aim of extending the low-load limit toward idle. 1.2 bar BMEP was achieved using 87 AKI fuel, which is significantly lower than the FY 2012 accomplishment

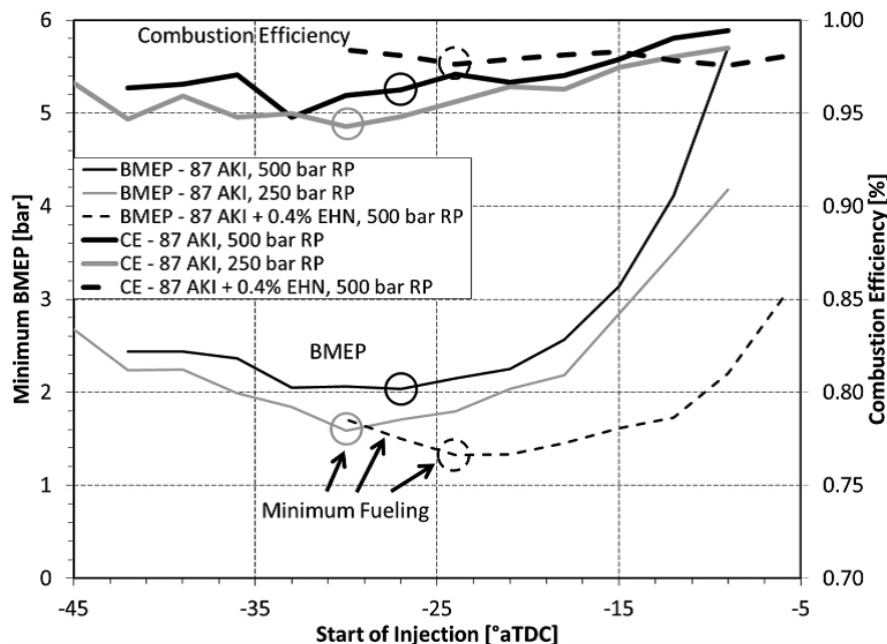


FIGURE 1. Minimum Fueling Rates for 500 bar and 250 bar Injection Pressure

TABLE 1. Cadillac Fuel Economy Comparisons – LTC vs. PFI

| Fuel Economy [mpg, unadjusted] | PFI | LTC |
|-----------------------------------|------|------|
| UDDS | 26.3 | 32 |
| HWFET | 33.2 | 45.3 |
| Combined[55/45] | 29 | 37 |
| Improvement over PFI | | 26% |

of 3.5 bar BMEP—while maintaining 3% COV of IMEP.

- Injection timing sweeps at two injection pressures (500 bar and 250 bar) were done. Single injections around -24 deg ATDC provided the minimum load possible.
- Using 250 bar rail pressure extended the low-load limit beyond the ability of 500 bar rail pressure—probably due to decreased mixing and enhanced local richness for ignition.
- The use of EHN extended the low-load range even further and allowed for delayed injection timing, due to increased ignition propensity from a chemical kinetics perspective.

FY 2013 PUBLICATIONS/PRESENTATIONS

1. Ciatti, S.A., Johnson, M.V., Das Adhikary, B., Reitz, R., Knock, A., (April 2013), SAE 2013-01-0263, “Efficiency and Emissions Performance of Multizone Stratified Compression Ignition Using Different Octane Fuels”, SAE World Congress, Detroit, MI.
2. Das Adhikary, B., Reitz, R. Ciatti, S.A., (April 2013), SAE 2013-01-0900, “Study of In-Cylinder Combustion and Multi-Cylinder Light Duty Engine Performance Using Different RON Fuels at Light Load Conditions”, SAE World Congress, Detroit, MI.
3. Presentation for President Obama’s visit to Argonne – “How can LTC strategies assist US Automakers in achieving 54.5 in 2025?” (March 2013).
4. Ciatti, S.A., (October 2012), ASME Mechanical Engineering Magazine, “The Gasoline Diesel”, ASME, NY, NY.

II.18 High Efficiency GDI Engine Research

Thomas Wallner (Primary Contact),
Riccardo Scarcelli, Nicholas Matthias
Argonne National Laboratory
9700 S. Cass Avenue
Lemont, IL 60439
DOE Technology Development Manager:
Gurpreet Singh

Overall Objectives

- Quantify efficiency potential and combustion stability limitations of advanced gasoline direct injection (GDI) combustion systems including lean, boosted and exhaust gas recirculation (EGR)-dilute concepts
- Optimize lean, boosted and EGR-dilute combustion strategies through implementation of advanced coil-based ignition systems
- Demonstrate the potential of R&D, non-coil based ignition systems
- Develop and implement three-dimensional computational fluid dynamics (3D-CFD) simulation models capable of predicting cyclic variability for conventional and advanced ignition systems

Fiscal Year (FY) 2013 Objectives

- Establish representative baseline data of a state-of-the-art GDI engine
- Characterize combustion stability implications of lean and EGR-dilute combustion
- Demonstrate ability of 3D-CFD simulation to predict combustion stability
- Initiate quantification of potential of high-energy spark plug and multi-spark operation

FY 2013 Accomplishments

- Completed set up and shake-down of modular single-cylinder GDI research engine platform that allows for comprehensive assessment of lean, boosted and EGR-dilute operation
- Quantified sensitivity of lean and EGR-dilute combustion to air/fuel ratio and combustion phasing perturbation
- A novel, Reynolds Averaged Navier-Stokes (RANS) approach characterized by low numerical diffusion

was applied to qualitatively evaluate cycle-to-cycle variability and combustion stability in an internal combustion engine

- Implemented advanced Directed Energy Ignition System (DEIS) ignition system providing fully programmable multi-spark and sustained spark features

Future Directions

- Implement detailed ignition energy measurement to allow direct, objective comparison of advanced coil-based ignition systems
- Evaluate potential of laser ignition in lean, boosted and EGR-dilute operation
- Expand 3D-CFD simulation to include EGR-dilute combustion
- Implement characteristics of advanced ignition systems in 3D-CFD simulation to enable cycle-to-cycle variation prediction



INTRODUCTION

The market share of light-duty vehicles powered by spark ignition internal combustion engines in 2010 was approximately 98%. While the Energy Information Agency reference scenario predicts an increased market share of flexible fuel, hybrid, plug-in hybrid, and diesel as well as electric vehicles, more than 90% of light-duty vehicles sold in 2040 are predicted to be (partially) powered by a spark-ignition engine [1]. That being the case, improvements in gasoline internal combustion engine efficiency have immediate effect and are a critical building block to meeting future efficiency and emissions regulations.

Downsizing, boosting as well as dilute combustion, in the form of lean or EGR-dilute operation, are known to offer efficiency improvements which are in some cases also paired with emissions benefits. However, those operating modes are also known to deteriorate combustion stability, and combustion systems are currently limited by combustion stability issues [2,3]. This project aims to identify the fundamental limitations of lean, boosted, and EGR-dilute combustion through experimental R&D combined with advanced 3D-CFD simulation and extending the lean and dilute limits by combining fundamental findings with benefits offered by advanced ignition systems.

APPROACH

This project employs a three-pronged approach to achieving its goals where the main thrust areas are to (1) expand the fundamental understanding of characteristics and limitations of lean, boosted and EGR-dilute combustion; (2) perform a technology evaluation of advanced coil-based ignition systems on a consistent state-of-the-art automotive engine platform; and (3) assess the potential of advanced, non-coil-based ignition systems (e.g., laser ignition).

The project includes experimental, as well as simulation-focused components, to better understand the current limitations of lean, boosted, and EGR-dilute combustion. 3D-CFD simulation is applied to broaden the understanding of current operating limitations. A main component of the project also focuses on expanding simulation capabilities to allow (1) representation of cyclic variability with a RANS approach and (2) realistic simulation of advanced and non-coil-based ignition systems.

RESULTS

A basic assessment of general trends of dilute operation on efficiency, emissions, and combustion characteristics is summarized in Figure 1. At the 2,000 RPM, 6 bar indicated mean effective pressure (IMEP) operating point dilution was accomplished through EGR up 8% and lean operation up to a relative air/fuel ratio λ of 1.5. All operating points were run at maximum brake torque (MBT) spark timing.

Starting from a baseline efficiency of approximately 37% at stoichiometric operation without EGR, efficiency increases to approximately 39% at 8% EGR while reducing oxides of nitrogen (NO_x) emissions from over 15 g/kWh to below 3 g/kWh. However, the combustion stability decreases from a coefficient of variance of IMEP (COV_{IMEP}) around 2 at the baseline point to 3.5 at 8% EGR. The moderate EGR addition also increases ignition delay as well as combustion duration almost by a factor of 2.

In comparison, lean operation results in a more significant increase in indicated efficiency with a peak at 41.7% at a relative air/fuel ratio λ of 1.5. Over the air/fuel ratio range an increase in NO_x emissions compared to stoichiometric operation is observed and only at the $\lambda=1.5$ point, NO_x emissions dropped slightly below the baseline. Lean operation also continuously degrades combustion stability with a COV_{IMEP} almost at 5 at $\lambda=1.5$. In terms of combustion stability operation at 8% EGR is similar to lean operation at $\lambda=1.4$. Both ignition delay and combustion duration increase moderately with lean operation.

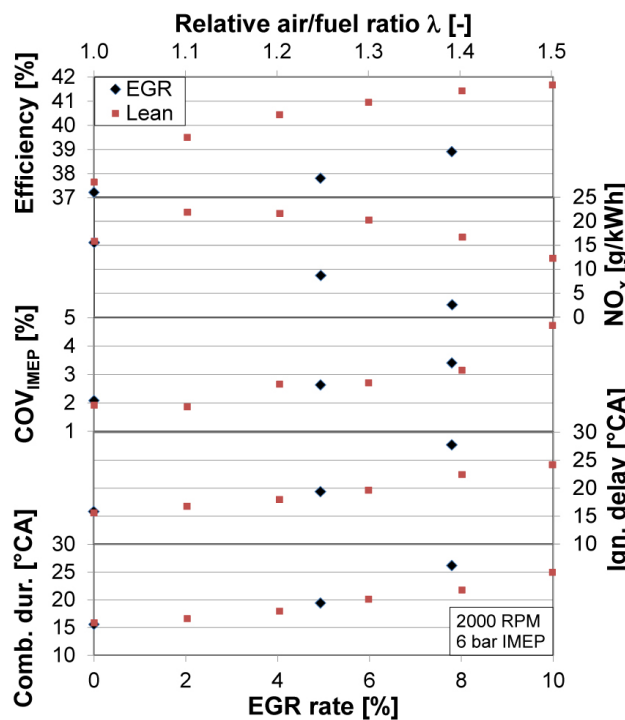


FIGURE 1. Trends of Efficiency, NO_x Emissions, Combustion Stability, Ignition Delay, and Combustion Duration with Increasing Dilution at 2,000 RPM, 6 bar IMEP

The engine exhibits natural cyclic variability during steady-state operation that increases with dilution. In an attempt to identify dominant engine control parameters affecting natural cyclic variability, a sensitivity study was carried out wherein control parameters were intentionally varied. The control parameters of particular interest are ignition timing and injection duration. The sensitivity study was carried out by first setting the steady-state operating condition including EGR rate, average relative air/fuel ratio, and optimal combustion phasing. Then a binary low-high perturbation was induced on a cycle-by-cycle basis at three levels: MBT $\pm 2^\circ$ crank angle (CA), $\pm 4^\circ$ CA, $\pm 6^\circ$ CA and injection duration $\pm 2\%$, $\pm 4\%$, $\pm 6\%$.

Results from a sensitivity study show that COV_{IMEP} is far less sensitive to ignition perturbation than to injection perturbation while the sensitivity is similar in terms of efficiency. This is true for both lean and EGR-dilute operation (Figure 2). However, one difference that stands out with EGR is the sensitivity of COV_{IMEP} to ignition perturbation. Increased sensitivity to ignition perturbation is likely the result of longer ignition delay which is critical for early flame kernel development.

The knowledge that ignition is critical to lean and EGR-dilute operation motivates the study of ignition system hardware. The most common class of modern

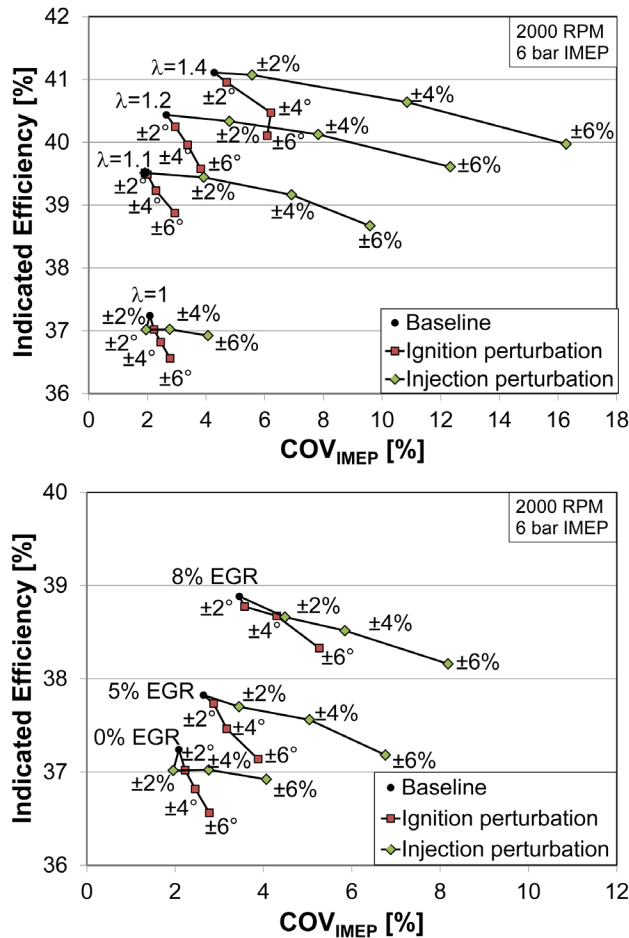


FIGURE 2. Effect of Injection and Ignition Perturbation on Combustion Stability and Efficiency in Lean (top) and EGR-Dilute (bottom) Operation

ignition systems is coil-based and there are a number of strategies that may enhance engine performance with coil-based ignition. Prominent examples are multi-spark and sustained spark. With multi-spark, each spark discharge extinguishes before more energy is added while sustained spark requires the addition of energy before the initial spark is allowed to extinguish.

One technology that allows the study of advanced coil-based ignition strategies is DEIS developed by Altronic. Preliminary results with two distinct DEIS spark profiles are shown in Figure 3. Spark profiles that are superimposed on the plot are based on the measured current through the secondary ignition coil (delivered to the spark plug). The lower energy single spark is much like a conventional coil while the higher energy sustained spark is an example of the aforementioned advanced strategies. A higher energy sustained spark ignition profile provides improved performance in terms of COV_{IMEP} predictability. The difference in predictability can be seen on the plot by how well combustion stability, COV_{IMEP} , correlates with ignition timing. There are also

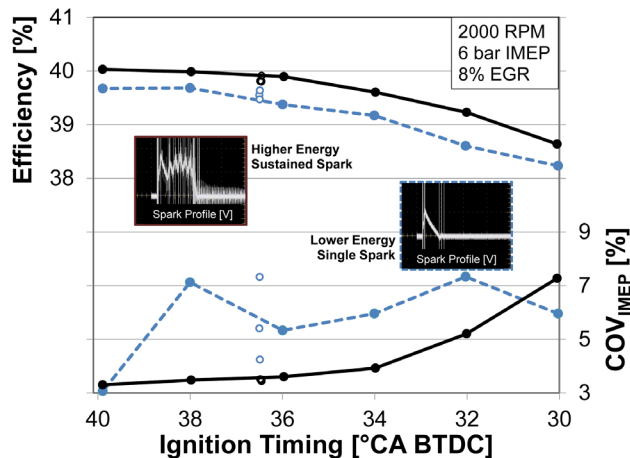


FIGURE 3. Combustion Stability and Indicated Thermal Efficiency for Two Distinct Spark Profiles Generated by the DEIS Ignition System

three iterations of the same operating point with MBT ignition timing, 36.5 °CA before top-dead center, shown as circles on the plot where three iterations are much more consistent with higher energy sustained spark. In addition to more predictable combustion stability, the higher energy sustained spark provides improved engine efficiency throughout an ignition timing sweep. The average indicated thermal efficiency difference in Figure 3 is 0.4% with a maximum of 39.5%.

This is a cursory look at the evaluation of advanced coil-based ignition which is ongoing. The DEIS is capable of controlling the output energy per discharge event as well as spark profile which will serve to isolate the confounding effects of total energy and spark profile. Multi-spark and sustained spark will also be studied in detail in dilute combustion.

Numerical simulations focused on the fundamental understanding of combustion stability, with particular regard to premixed combustion and lean operation. Figure 4 shows the results for two different intake flow configurations at 2,000 RPM, 6 bar IMEP, and $\lambda=1.5$. The case shown on the top (open swirl plate) is characterized by higher COV_{IMEP} (7%), while the case on the bottom (closed-swirl plate) has lower COV_{IMEP} (4%) due to the modified in-cylinder turbulent field. An advanced numerical approach is employed in this study and has shown significant potential in describing cycle-to-cycle variations and combustion stability. The approach is RANS-based but with low numerical diffusion in order to maintain feedback from one cycle to the next in terms of in-cylinder turbulence. Conventional RANS simulations are typically performed with coarse meshes and other settings (i.e., low discretization order) that increase numerical diffusion thus compromising the cycle-to-cycle feedback mechanism by damping

large-scale turbulence. With the advanced numerical approach, however, turbulence varies from cycle to cycle in the entire cylinder as well as in the proximity of the spark plug, thus having a strong impact on flame development and propagation. After 10 consecutive cycles, results do not show convergence of the numerical pressure traces. The latter continue to oscillate around the average experimental pressure value and are well within the maximum and minimum experimental cycles. More importantly, an operating condition that is characterized by higher measured variability (Figure 4, top) shows large oscillation of the numerical in-cylinder pressure while cases with lower experimental variability (Figure 4, bottom) are characterized by much narrower oscillation.

While many sources of cyclic variability (i.e., the non-repeatability of the injection and ignition events) were not yet analyzed and LES strategies are typically more accurate in describing cycle-to-cycle variations, the proposed RANS approach still provides good indication

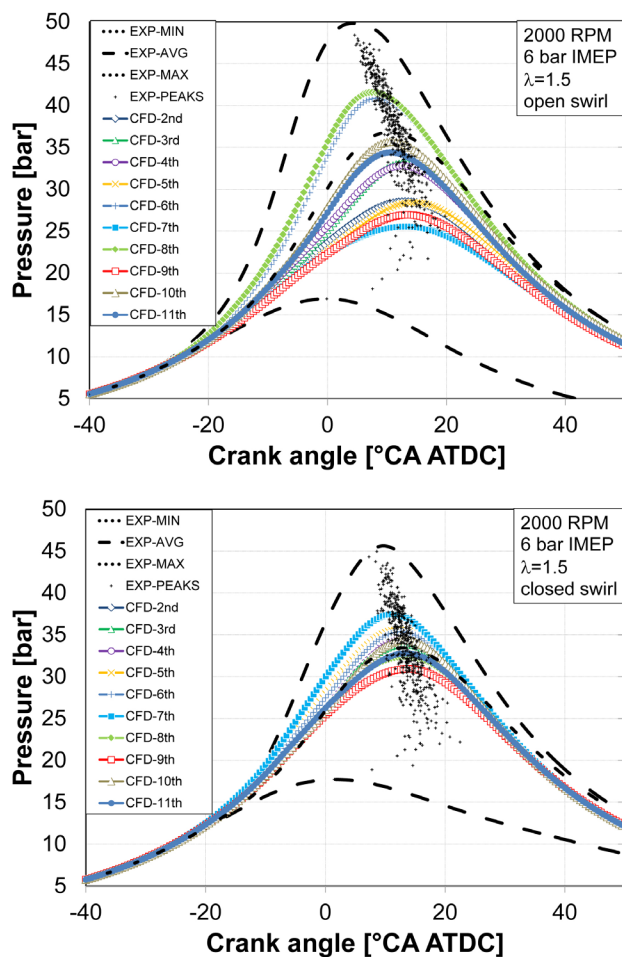


FIGURE 4. Experimental and Numerical Cyclic Variability for Two Intake Flow Configurations at 2,000 RPM, 6 bar IMEP, and $\lambda=1.5$

of combustion stability with reasonable computational times.

CONCLUSIONS

- Results from a sensitivity study show that COV_{IMEP} is far less sensitive to combustion phasing than to fueling perturbation while the sensitivity is similar in terms of efficiency. This is true for both lean and EGR dilute operation.
- With EGR, the sensitivity of COV_{IMEP} to combustion phasing is greater than in lean operation. This is likely the result of longer ignition delay which is critical for early flame kernel development.
- An alternative ignition profile consisting of higher energy and sustained spark versus a lower energy single spark ignition profile shows significant improvement in engine performance in EGR dilute operation. COV_{IMEP} is more predictable as a function of ignition timing and engine efficiency is consistently improved.
- An alternative RANS based 3D-CFD simulation approach with low numerical diffusion has proven effective at predicting cycle-to-cycle combustion variability.

REFERENCES

1. U.S. Energy Information Administration, "Annual Energy Outlook 2013 with Projections to 2040," DOE/EIA-0383(2013), 2013.
2. Kaul, B., Wagner, R. and Green, J., "Analysis of Cyclic Variability of Heat Release for High-EGR GDI Engine Operation with Observations on Implications for Effective Control," SAE Int. J. Engines 6(1):2013, doi:10.4271/2013-01-0270.
3. Hanabusa, H., Kondo, T., Hashimoto, K., Sono, H. et al., "Study on Homogeneous Lean Charge Spark Ignition Combustion," SAE Technical Paper 2013-01-2562, 2013, doi:10.4271/2013-01-2562.

FY 2013 PUBLICATIONS/PRESENTATIONS

1. Scarcelli, R., Matthias, N., and Wallner, T., "Numerical Investigation of Combustion in a Lean Burn Gasoline Engine," SAE Technical Paper 2013-24-0029, 2013, doi:10.4271/2013-24-0029.
2. Matthias, N., Scarcelli, R., and Wallner, T., "Analysis of Cyclic Variability and the Effect of Dilute Combustion in a Gasoline Direct Injection Engine," SAE Technical Paper 14PFL-0452. Scheduled for publication at the SAE 2014 World Congress.

3. Richards, K.J., Probst, D., Pomraning, E., Senecal, P.K., Scarcelli, R., “RANS Turbulence Modeling for the Prediction of Cyclic Variation in Engine Simulations”, SAE Technical Paper 14PFL-0458. Scheduled for publication at the SAE 2014 World Congress.

II.19 High Dilution Stoichiometric Gasoline Direct-Injection (GDI) Combustion Control Development

Brian C. Kaul

Fuels, Engines, and Emissions Research Center
Oak Ridge National Laboratory (ORNL)
2360 Cherahala Boulevard
Knoxville, TN 37932

DOE Technology Development Manager:
Gurpreet Singh

- Production-grade sensors and engine control units do not provide the same resolution of data acquisition as laboratory-grade equipment
- Results will determine the necessary resolution and accuracy of data to apply these control strategies in the market
- Demonstrate potential of next-cycle control strategies for combustion stability improvements and efficiency gains
- Evaluate the feasibility and potential benefits of same-cycle control strategies to prevent misfires



Overall Objectives

- Characterize dynamics of cyclic variability that limits dilution levels in spark-ignition engines
- Evaluate potential engine efficiency gains resulting from effective control of cyclic variations
- Demonstrate dilution limit extension through active control to reduce cyclic variability

Fiscal Year (FY) 2013 Objectives

- Determine effects of external exhaust gas recirculation (EGR) loop on cycle-to-cycle dynamics and differences from lean- and internal-EGR systems
- Evaluate effects of varying engine control inputs, including fuel injection timing and cam timing, on high-dilution combustion stability

FY 2013 Accomplishments

- Upgraded data acquisition system to allow for collection of longer-duration data sets (>10,000 cycles)
- Experimentally quantified effects of various engine control parameters on combustion stability (injection and cam timing, ignition timing, composition)
- Found that external EGR affects the dynamics of cyclic variations beyond the dilution limit imposed by combustion stability requirements

Future Directions

- Commission new engine control system and implement next-cycle control based on information from prior-cycle events
- Characterize sensitivity of control parameters to data sampling quality:

INTRODUCTION

Operation of spark-ignition engines with high levels of charge dilution through EGR achieves significant efficiency gains while maintaining stoichiometric operation for compatibility with three-way catalysts. At high engine loads, efficiency gains of 10-15% are achievable with current technology. Dilution levels, however, are limited by cyclic variability—including significant numbers of misfires—that increases in frequency with dilution, especially at low engine loads typical of operation on standard light-duty drive cycles. The cyclic variability encountered at the dilution limit is not random, but has been shown to be influenced by the events of prior engine cycles. This determinism offers an opportunity for dilution limit extension through active engine control, thus enabling significant efficiency gains by extending practically achievable dilution levels to the edge of combustion stability.

This project is focused on gaining and utilizing knowledge of the recurring patterns in cyclic variability to predict and correct for low-energy cycles such as misfires that reduce engine efficiency at the dilution limit. In particular, the dynamics of systems using cooled EGR loops have been elucidated for the first time, and are somewhat different from those of lean combustion systems for which similar background work has been carried out in the past. This knowledge will be utilized to develop and implement next-cycle active control strategies for extending the dilution limit.

APPROACH

A modern, turbocharged 2.0-L GDI engine, modified with a higher-than-stock compression ratio, has been installed in an engine test facility at ORNL. An external-cooled EGR loop has been installed on the engine to allow operation with external EGR. An engine controller with open access to parameters through INCA software is used to control the engine to the desired operating conditions.

Experiments have been conducted operating the engine at steady-state EGR levels beyond the practical dilution limit imposed by cyclic variability limits. The dynamics of cycle-to-cycle variations at these conditions were observed and analyzed using tools derived from chaos theory to identify recurring patterns that indicate non-random structure. Knowledge of these patterns will be used to implement control strategies based on the events of prior cycles, to stabilize combustion near the dilution limit.

RESULTS

Symbol sequence analysis of the time series of heat release data is a useful method for identifying recurring patterns in the cyclic variations. In this method, the data are binned and each bin is assigned a symbol; sequences of these symbolized data will often elucidate patterns that were obstructed by noise (i.e., stochastic variations) in the raw data. This method is described in detail by Finney, et al. [1] and by Daw, et al. [2]. A metric called modified Shannon entropy is calculated from the symbolized data to provide a quantitative measure of the level of deterministic information available. This analysis method was used to determine the optimal parameters for symbolizing this data for control applications, and Figure 1 shows that the minimum value in Shannon entropy—which corresponds to the greatest level of deterministic information—can be seen when dividing the data into 5-7 partitions and considering 3-4 cycle sequences. This result may help inform future controller architecture decisions. These results were presented at the SAE 2013 World Congress and published in the SAE International Journal of Engines (see FY 2013 Publications/Presentations).

Experiments focused on exploring the impact of valve timing and fuel injection timing on cyclic dynamics of high-EGR engine operation were also completed. The engine was operated with constant fueling and constant EGR, and the throttle was adjusted to maintain airflow/stoichiometry as the intake cam position was varied. The intake manifold pressure was affected by this, but there was no significant effect on stability or on the cyclic dynamics beyond the stable dilution limit. The engine was also operated with fixed fueling rate, constant EGR,

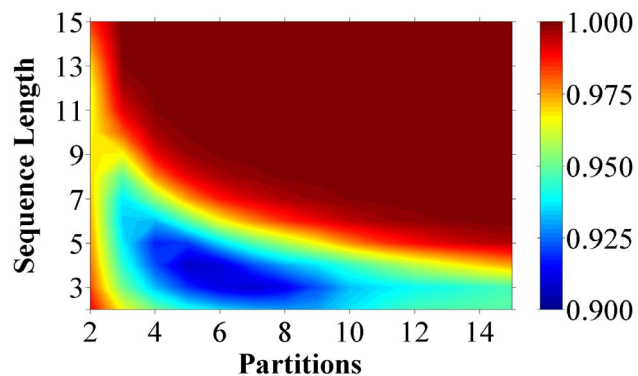
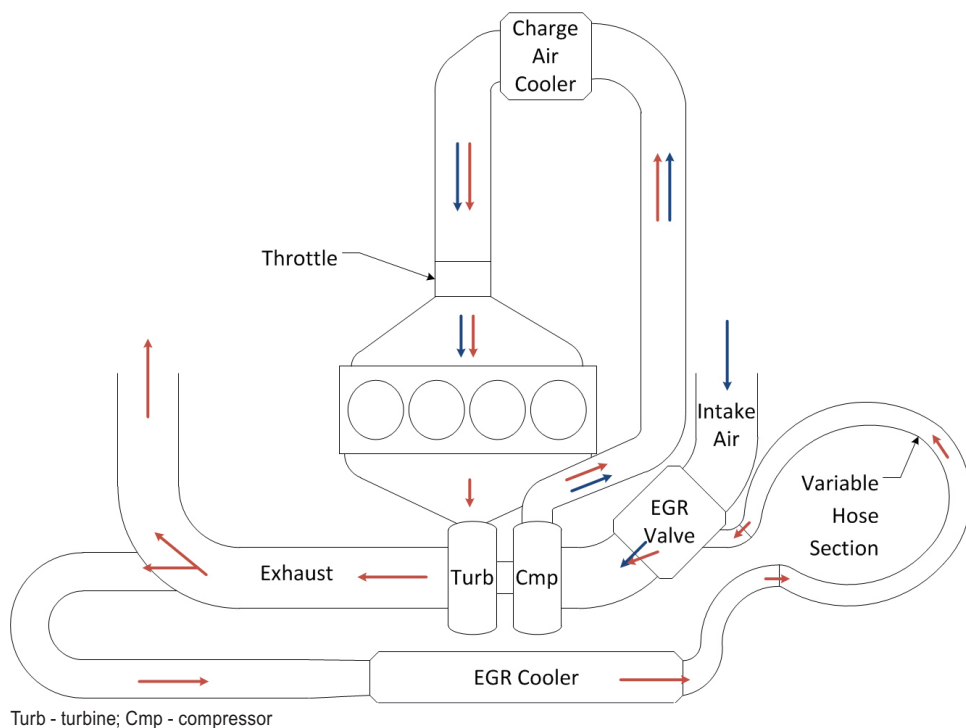


FIGURE 1. Variation of Modified Shannon Entropy with Number of Partitions and Sequence Length for 2,000 rpm, 3.8 Bar Brake Mean Effective Pressure Operation with 17% EGR

and constant cam and throttle positions while the fuel injection timing was varied. This also had no effect on engine stability at the dilution limit, nor did varying the fuel rail pressure. The effect of the external EGR masked the smaller effects of any of these parameters for the conditions tested. Unfortunately, the exhaust cam phaser on the engine was not actuating properly, so it was not possible to explore the effects of exhaust valve timing. It is possible that some impact would be detected here, as the internal trapped residual fraction would be more strongly impacted by exhaust valve timing than by intake valve timing, but later experiments showed that the dominant period of cyclic variations is primarily driven by the transit time through the external EGR loop rather than the immediate effect of the internal residual gases, and this is expected to be the case even with slight changes to the quantity of internal residuals.

Analysis focused on the importance of data quality was begun with the help of a summer student. This analysis is expected to result in several papers and yield important information regarding the quality of sensors and resolution of data acquisition required to implement control approaches based on the nonlinear dynamics analysis techniques used to detect cycle-to-cycle patterns. While examining the data, it became apparent that some dynamics are occurring for operation with external EGR that had not been previously observed in studies of cyclic variability for lean operation or other operation driven by internal trapped residual gases [3,4].

Further experiments were conducted to better understand the impact of the external EGR loop flow dynamics on cyclic variability. The length of the EGR loop was varied by replacing a section of hose indicated in Figure 2, and the transit time through the system was calculated compared to the half-period of a fast Fourier transform (FFT) of the heat release time series. A strong correlation was found between the transit time

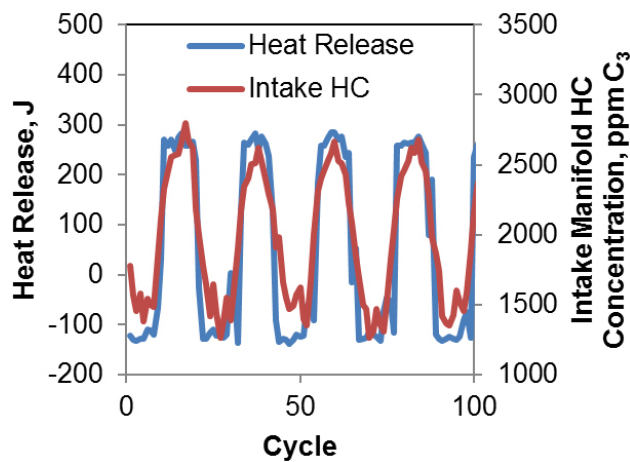
**FIGURE 2.** EGR System Diagram

of recirculated exhaust gases and a periodic high-low energy oscillation behavior observed at high EGR levels, as shown in Table 1.

TABLE 1. EGR Loop Transit Time and Half-Period of FFT of Heat Release

| EGR Loop | EGR Rate, % | Transit Time, Cycles | FFT Half-Period, Cycles |
|----------|-------------|----------------------|-------------------------|
| Short | 34 | 14.7 | 14.5 |
| Short | 39 | 13.2 | 12.8 |
| Short | 53 | 10.6 | 10.5 |
| Medium | 36 | 15.1 | 15.5 |
| Medium | 46 | 12.6 | 12.5 |
| Medium | 55 | 11 | 11.3 |
| Long | 40 | 15.2 | 6.4 |
| Long | 54 | 12.1 | 5.2 |

The correlation is excellent for the short (standard length) and medium (addition of approximately 50% to the exhaust-side EGR loop) lengths of hose. For the longest hose, which doubled the length of the exhaust-side EGR loop, the correlation breaks down as the dynamics of the system are pushed to a different fixed-point with more rapid variations. The fundamental physics causing this direct correlation between the EGR loop transit time and the cyclic variability of the engine are driven by the excess unburned fuel and air

**FIGURE 3.** Time Series of Heat Release and Intake Hydrocarbon (HC) Concentration

from cycles that do not burn fully, recirculating around and effectively reducing the dilution level for a few cycles, until the excess fuel is exhausted. The exhaust recirculated from these cycles, which burned well, contains little unburned fuel, and results in misfires or very poor combustion. A fast hydrocarbon detector was installed in the intake runner for one cylinder, and the hydrocarbon concentration was compared to the resulting heat release for each cycle. As seen in Figure 3, there is a strong correlation between the intake hydrocarbon

concentration and the resulting heat release, confirming that this is the driving mechanism behind these variations. These results have been written up in a paper and submitted to the 2014 SAE World Congress.

CONCLUSIONS

- Experiments were conducted to characterize the effects of external EGR flow loop dynamics on the cyclic variability of dilute combustion. Transit time through the EGR loop was shown to be dominant.
- Experiments were conducted to evaluate the effects of various control inputs on cyclic variability. Compared to dominant external EGR transit time effect, the effects of all other inputs were negligible.
- Modified Shannon entropy analysis of experimental data helped to determine the best parameters for symbolizing the data for control purposes.
- Analysis of the effects of data quality on control parameters was begun, and will be continued in the next year.
- Preparations were begun for upgrading engine control system to allow next-cycle control based on information gained this year.

REFERENCES

1. Finney CEA, Green JB, Daw CS. "Symbolic time-series analysis of engine combustion measurements," SAE Technical Paper 980624: 1998, doi: 10.4271/980624.
2. Daw C, Finney C, Tracy E. "A review of symbolic analysis of experimental data," Review of Scientific Instruments 74(2): 2003 February: p. 915-930, doi: 10.1063/1.1531823.
3. Wagner RM, Drallmeier JA, Daw CS. "Characterization of lean combustion instability in premixed charge spark ignition engines," International Journal of Engine Research 1(4): 2000: p. 301-320.
4. Sutton RW, Drallmeier JA. "Development of nonlinear cyclic dispersion in spark ignition engines under the influence of high levels of EGR," In Proceedings of the 2000 Technical meeting of the Central States Section of the Combustion Institute; 2000.

FY 2013 PUBLICATIONS/PRESENTATIONS

1. Kaul, B., Wagner, R. and Green, J., "Analysis of Cyclic Variability of Heat Release for High-EGR GDI Engine Operation with Observations on Implications for Effective Control," SAE Int. J. Engines 6(1):2013, doi: 10.4271/2013-01-0270.

II.20 High Efficiency Clean Combustion in Light-Duty Multi-Cylinder Diesel Engines

Scott J. Curran (Primary Contact), Zhiming Gao, Vitaly Y. Prikhodko, Adam B. Dempsey, John M. Storey, James E. Parks, and Robert M. Wagner
Oak Ridge National Laboratory (ORNL)
2360 Cherahala Blvd
Knoxville, TN 37830

DOE Technology Development Manager:
Gurpreet Singh

Subcontractor:
The University of Wisconsin, Madison, WI

The map will be developed to maximize efficiency with lowest possible emissions with production viable hardware and biofuels.

- Demonstrate improved modeled fuel economy of 20% for passenger vehicles solely from improvements in powertrain efficiency relative to a 2009 port fuel injection (PFI) gasoline baseline.
- Quantify the effectiveness of diesel oxidation catalysts on particulate matter (PM) destruction with RCCI for steady-state operation.

FY 2013 Accomplishments

- Attained the 2013 technical target of developing a RCCI engine map suitable for use in vehicle system drive cycle simulations.
- Attained the 2013 technical target of demonstrating greater than 20% improvement in modeled fuel economy with multi-mode RCCI operation as compared to a 2009 PFI gasoline baseline.
- Performed drive cycle estimations of fuel economy and emissions using vehicle systems modeling with experimental data with multi-mode RCCI/conventional diesel combustion (CDC) operation.
- Evaluated the hydrocarbon (HC) and CO reduction effectiveness of multiple diesel oxidation catalysts with RCCI.
- Collaboration with Pacific Northwest National Laboratory (PNNL) on RCCI campaign.
- Collaboration with Los Alamos National Laboratory on NO sensor.
- Partnership with MAHLE to get piston blanks for RCCI piston effect studies in the future.
- Completed RCCI noise investigation and published study.
- Completed RCCI PM study with paper submitted for 2014 SAE World Congress.
- Subcontract in place and progress made on RCCI hybrid collaboration with University of Wisconsin, Madison.
- Invited talks on HECC research.

Overall Objectives

- Develop and evaluate the potential of High Efficiency Clean Combustion (HECC) strategies with production viable hardware and aftertreatment on multi-cylinder engines.
- Expand the HECC operational range for conditions consistent with real-world drive cycles in a variety of driveline configurations (conventional, down-sized, and hybrid electric vehicle/plug-in hybrid electric vehicle).
- Improve the fundamental thermodynamic understanding of HECC in order to better identify the opportunities, barriers, and tradeoffs associated with higher efficiency combustion concepts.
- Characterize the controls challenges including transient operation and fundamental instability mechanisms which may limit the operational range of potential of HECC. This includes the development of low-order models for prediction and avoidance of abnormal combustion events.
- Understand the interdependent emissions and efficiency challenges including integration of exhaust aftertreatment for HECC and multi-mode operation.
- Support demonstration of DOE and U.S. DRIVE efficiency and emissions milestones for light-duty diesel engines.

Fiscal Year (FY) 2013 Objectives

- Develop a Reactivity-Controlled Compression Ignition (RCCI) combustion map on a multi-cylinder engine suitable for light-duty drive cycle simulations.

Future Directions

- Evaluate transient RCCI performance including controls and stability concerns.

- Evaluate the potential of increasing combustion efficiency through combustion optimization and engine hardware design (i.e., combustion chamber geometry).
- Characterize aftertreatment performance (including effect on PM) over the over light-duty operating range. Data will also be used with a vehicle model to simulate emissions performance over the light-duty drive cycle to determine aftertreatment needs for meeting Tier 2-Bin 5 and Tier 2-Bin 2 emission regulations.
- 2014 Milestone of demonstrating 23% increase in fuel economy over 2009 PFI gasoline vehicle in vehicle simulation due to improved powertrain efficiency.



INTRODUCTION

Advanced combustion concepts have shown promise in achieving high thermal efficiencies with ultra-low oxides of nitrogen (NO_x) and PM emissions. RCCI makes use of in-cylinder blending of two fuels with differing reactivity for improved control of the combustion

process. Previous research and development at ORNL has demonstrated successful implementation of RCCI on a light-duty multi-cylinder engine over a wide range of operating conditions with a focus on identifying the translational effects of going from a combustion concept to a multi-cylinder engine with production-viable hardware. Initial drive cycle modeling of RCCI/diesel multi-mode operation demonstrated at least a 15% improvement in fuel economy over a 2009 PFI baseline using vehicle systems simulations. The objective of this activity is first to develop and then use an experimental RCCI engine map in vehicle systems simulations to model fuel economy and emissions over a variety of drive cycles. Within this activity, the interdependency of fuel economy and emissions performance including the performance of exhaust aftertreatment is investigated for advanced combustion.

APPROACH

A 4-cylinder General Motors 1.9-L diesel engine installed at ORNL was modified to include a port fuel injection system using conventional gasoline injectors and pistons that were designed for RCCI operation. A schematic of the system is shown in Figure 1. A flexible microprocessor-based control system allowed for full

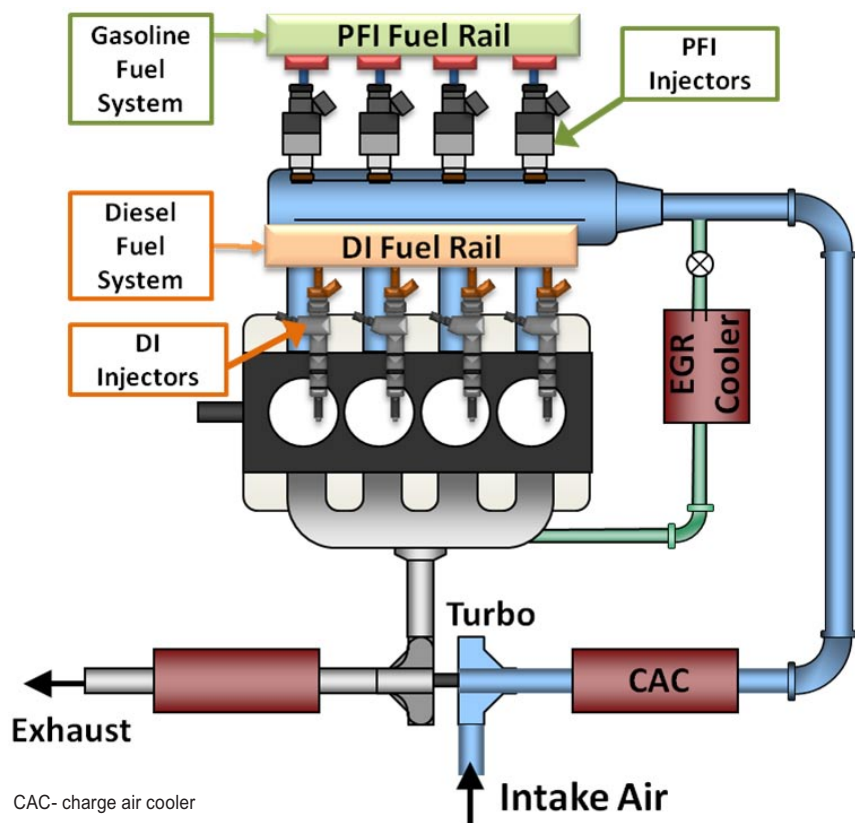


FIGURE 1. ORNL Multi-Cylinder RCCI Engine

authority of both fueling systems and other engine operating parameters. Experimental steady-state RCCI operating points on the modified RCCI engine using an in-house methodology for RCCI combustion were used to develop a speed/load map consistent with a light-duty drive cycle with sufficient detail to support vehicle simulations. The engine map was developed using a 30% ethanol blend and certification-grade diesel fuel. The potential fuel economy of RCCI operation was evaluated using vehicle systems simulations with experimental steady-state engine maps compared to representative 2009 gasoline PFI engines ranging from 1.8-L to 4.0-L as a baseline for comparison. The simulations used a multi-mode RCCI/diesel operating strategy where the engine would operate in RCCI mode whenever possible but at the highest and lowest engine operating points, the engine would switch to diesel mode as shown in Figure 2. All simulations were carried out in Autonomie using a 1,580 kg passenger vehicle (mid-size sedan, i.e., Chevrolet Malibu) over numerous U.S. federal light-duty drive cycles. RCCI fuel economy simulation results were compared to the same vehicle powered by each of the 2009 PFI gasoline engines over multiple drive cycles. Engine-out drive cycle emissions were compared to CDC and observations regarding relative gasoline and

diesel tank sizes needed for the various drive cycles are also summarized.

RESULTS

Multi-mode RCCI/CDC operation was shown through vehicle system simulations using experimental engine data to have the potential to offer greater than 20% fuel economy improvement over a 2009 gasoline PFI baseline over all hot drive cycles examined (no warm-up portion) as shown in Figure 3. The peak efficiency from the RCCI operating map was found to be within the region that is relevant to the federal light-duty drive cycles, unlike CDC whose peak efficiency is well outside the drive cycles. However, the current range of the experimental RCCI engine map does not allow full coverage of many light-duty drive cycles. RCCI fuel economy improvements were observed despite lack of complete drive cycle coverage. The results here showed that engine-out NO_x emissions are dependent on the drive cycle coverage of RCCI. Fuel usage over the drive cycles showed that nearly equal amounts of gasoline and diesel fuel would most likely be needed to be carried on board for RCCI multi-mode operation. During RCCI-only

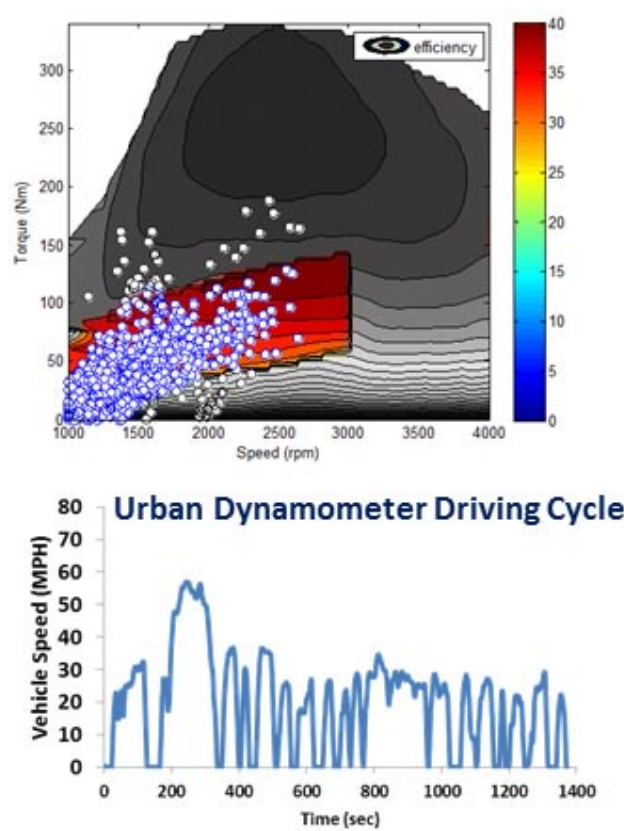
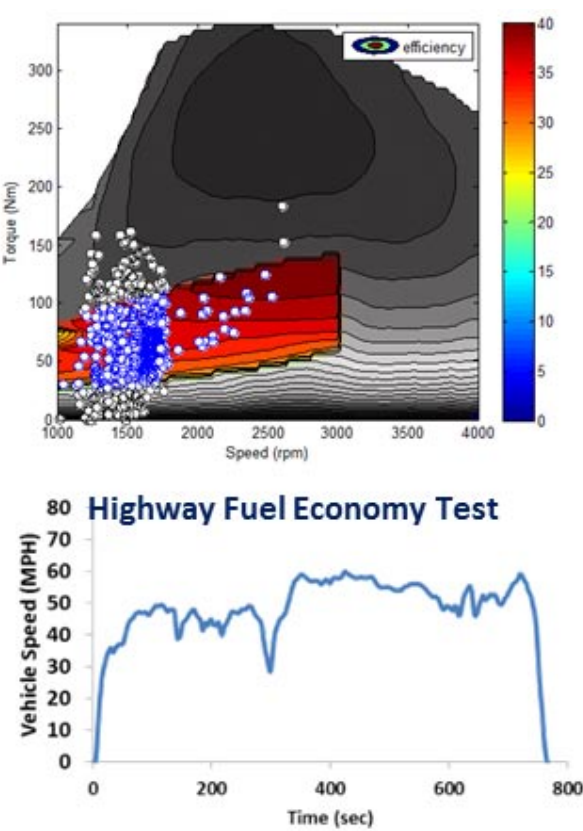


FIGURE 2. RCCI Coverage of Various Drive Cycles with Engine Speed and Load Points Overlaid



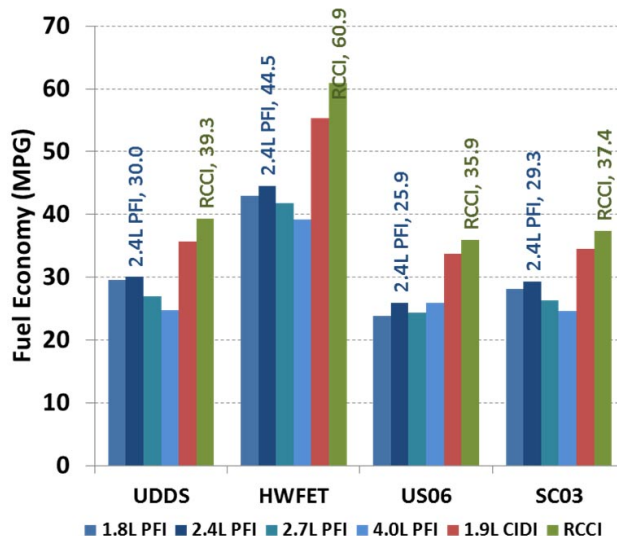


FIGURE 3. Drive Cycle Fuel Economy for PFI, CDC and Multi-Mode RCCI Operation

operation, fuel usage was found to be between 57.6% and 66.7% gasoline.

Modeled drive cycle emissions results showed between a 16% and 19% reduction in NO_x with multi-mode RCCI as compared to diesel-only operation on both city and highway driving cycles. However, HC and CO emissions increased with RCCI by a factor of 2 to 3 compared to CDC. The increased HC and CO emissions along with reduced exhaust temperatures will be a challenge for exhaust aftertreatment. The combination of high CO and HC emissions with low exhaust temperatures will be a significant challenge due to the limited effectiveness of current oxidation catalysts at low temperatures. No information on PM was collected for the mapping study for use in the vehicle systems simulations due to the difficulty in measuring RCCI PM as previously reported [1].

Previous ORNL RCCI PM research has shown that despite RCCI having a near-zero smoke number, there is still measurable PM as measured by filter or scanning mobility particle sizer after a Particle Measurement Program-style dilution system [1]. To better understand the character and composition of what is hypothesized to be condensed semi-volatile proto-soot from RCCI, a collaborative campaign was conducted with PNNL and their Single Particle Laser Ablation Time-of-Flight Mass Spectrometer (SPLAT). This technique is insightful for physically and chemically characterizing individual particles and gives a complete picture of the particle emissions from an engine. The combination of SPLAT and the advanced engine and fuel technologies at ORNL produced an unprecedented examination of exhaust emissions from RCCI under a variety of light-

duty operating conditions including the effect of a diesel oxidation catalyst on measured PM.

CONCLUSIONS

Advanced combustion techniques such as RCCI can increase engine efficiency and lower NO_x and soot emissions over the engine map. Furthermore, an RCCI/CDC multi-mode approach has been shown to allow greater than 20% fuel economy improvement over a 2009 PFI gasoline baseline in a mid-size passenger vehicle. This activity has shown the importance of taking a comprehensive engine systems approach to help meet Vehicle Technologies Program goals and milestones.

- Multi-mode RCCI operation can allow greater than 20% improvement in modeled fuel economy as compared to a 2009 PFI gasoline baseline.
- In-cylinder blending of two fuels with different fuel reactivity (octane/cetane) allows increased control over combustion compared to single fuel advanced combustion techniques.
- Increased HC/CO emissions will be a challenge and will require progress in low temperature aftertreatment.

REFERENCES

1. Prikhodko, V., Curran, S., Barone, T., Lewis, S. et al., "Emission Characteristics of a Diesel Engine Operating with In-Cylinder Gasoline and Diesel Fuel Blending," SAE Int. J. Fuels Lubr. 3(2):946-955, 2010

FY 2013 PUBLICATIONS/PRESENTATIONS

1. Curran, S.J., Szybist, J.P., and Wagner, R.M., "Combustion noise investigation with multi-cylinder RCCI", ICEF2013-19125, Proceedings of the ASME 2013 Internal Combustion Engine Division Fall Technical Conference ICEF2013 October 13–16, 2013, Dearborn, Michigan, USA.
2. Curran, S., Hanson, R., Wagner, R., and Reitz, R., "Efficiency and Emissions Mapping of RCCI in a Light-Duty Diesel Engine," SAE Technical Paper 2013-01-0289, 2013, doi:10.4271/2013-01-0289. + Presentation.
3. Curran, S., Hanson, R., Wagner, R., and Reitz, R., "Efficiency and Emissions Mapping of RCCI in a Light-Duty Diesel Engine," SAE Technical Paper 2013-01-0289, 2013, doi:10.4271/2013-01-0289.
4. S.J. Curran, R.M. Wagner, and R.M. Hanson, "Reactivity Controlled Compression Ignition (RCCI) Combustion on a Multi-Cylinder Light-Duty Diesel Engine", International Journal of Engine Research, Vol. 13, No. 3, pp. 216-225 (2012).
5. Prikhodko, V., Curran, S., Parks, J., and Wagner, R., "Effectiveness of Diesel Oxidation Catalyst in Reducing HC and CO Emissions from Reactivity Controlled Compression

Ignition,” SAE Int. J. Fuels Lubr. 6(2):2013, doi:10.4271/2013-01-0515. + Presentation

6. Hanson, R., Curran, S., Wagner, R., and Reitz, R., “Effects of Biofuel Blends on RCCI Combustion in a Light-Duty, Multi-Cylinder Diesel Engine,” SAE Int. J. Engines 6(1):488-503, 2013, doi:10.4271/2013-01-1653.

7. Daw, S., Gao, Z., Prikhodko, V., Curran, S., Wagner, R., “Modeling Emissions Controls for RCCI Engines”, CLEERS telecom, September, 2013.

8. Curran S.J., Gao, A., and Wagner, R.M., “Reactivity Controlled Compression Ignition Drive Cycle Emissions and Fuel Economy Estimations Using Vehicle Systems Simulations”, Vehicle Systems Analysis Tech Team Meeting, Aug 7, 2013, Southfield, MI.

9. Curran, S.J., Wagner, R.M., and Gao, Z., “Recent Advances in Multi-Cylinder Advanced Combustion on Light-Duty Compression Ignition Engines”, Presentation, 35th Annual International Energy Agency Task Leaders Meeting (San Francisco, CA: July 2013).

10. Curran, S.J., Storey, J.M., Dempsey, A.B., Eibl, M., Wagner, R.M., and Gao, Z., “Recent Advances in Multi-Cylinder Advanced Combustion on Light-Duty Compression Ignition Engines”, Presentation, Advanced Engine Combustion Program Review (Southfield, MI: Aug 2013).

11. Curran S.J., Gao, A., and Wagner, R.M., “Reactivity Controlled Compression Ignition Drive Cycle Emissions and Fuel Economy Estimations Using Vehicle Systems Simulations”, VSATT Meeting (Southfield, MI: Aug 2013).

12. Daw, S., Gao, Z., Prikhodko, V., Curran, S., Wagner, R., “Modeling Emissions Controls for RCCI Engines”, Engine Research Center Symposium, June, 2013 [invited].

13. Curran S.J., “High Efficiency Clean Combustion in Multi-Cylinder Engines”, 2013 VTP Merit Review, Project ID ACE016, May 15, 2013 Arlington, VA.

14. Prikhodko, V., Curran, S., Parks, J., and Wagner, R., “Diesel Oxidation Catalyst Control of PM, CO and HC from RCCI,” 2013 DOE CLEERS Workshop, April 10–12, 2013.

15. Curran, S., Hanson, R., Wagner, R., and Reitz, R., “Efficiency and Emissions Mapping of RCCI in a Light-Duty Diesel Engine,” SAE World Congress, April 17, 2013, Detroit, MI.

16. Curran S.J., Gao, A., and Wagner, R.M., “Reactivity Controlled Compression Ignition Drive Cycle Emissions and Fuel Economy Estimations Using Vehicle Systems Simulations”, SAE World Congress, April 17, 2013, Detroit, MI.

17. Curran, S.J., Gao, Z., and Wagner, R.M., “Light-Duty Reactivity Controlled Compression Ignition Drive Cycle Fuel Economy and Emissions Estimates”, Presentation at the Advanced Engine Combustion (AEC) Working Group Meeting, Livermore, CA; Feb 2013.

18. Wagner, R.M., Green, J.B., and Curran S.J., “A perspective on the future of high efficiency engines”, Current Problems and Modern Techniques (XIth Congress), (2012)

19. Curran, S.J., Wagner, R.M., and Gao, Z., “Background on RCCI and B20 RCCI Results With Both Gasoline and Ethanol Blends”, Presentation, 2012 National Biodiesel Board Biodiesel Technical Workshop, (October 30–31, 2012, Kansas City, MO. [invited]

20. Prikhodko, V.Y., Curran, S.J., Parks, J.E., and Wagner, R.M., “Effectiveness of a DOC to control CO/HC emissions from RCCI combustion”, Poster, 2012 U.S. DOE Directions in Engine-Efficiency and Emissions Research Conference, (October 15–19, 2012, Dearborn, MI).

21. Curran, S.J., Gao, Z., and Wagner, R.M., “Light-Duty Reactivity Controlled Compression Ignition Drive Cycle Fuel Economy and Emissions Estimates”, Poster, 2012 U.S. DOE Directions in Engine-Efficiency and Emissions Research Conference, (October 15–19, 2012, Dearborn, MI).

SPECIAL RECOGNITIONS & AWARDS/ PATENTS ISSUED

- 1.** 2013 DOE VTO R&D Award for PI, Scott Curran on RCCI research
- 2.** Best Presentation Award for 2012 ASME ICEF Conference – RCCI Paper
- 3.** Speaking award for 2013 SAE World congress – RCCI Paper

II.21 Stretch Efficiency – Exploiting New Combustion Regimes

C. Stuart Daw (Primary Contact),
James P. Szybist, Josh A. Pihl, Derek A. Splitter,
and Chao Xie
Oak Ridge National Laboratory (ORNL)
NTRC Site
2360 Cherahala Blvd.
Knoxville, TN 37932
DOE Technology Development Manager:
Gurpreet Singh

Overall Objectives

- Define and analyze specific advanced pathways to improve the energy conversion efficiency of internal combustion engines from nominally 40% to as high as 60%, with emphasis on opportunities afforded by new approaches to combustion.
- Implement critical measurement and proof of principle experiments for the identified pathways to stretch efficiency.

Fiscal Year (FY) 2013 Objectives

- Parametrically investigate in-cylinder non-catalytic fuel reforming and the possibility of thermochemical recuperation (TCR) using a direct injection strategy during negative valve overlap (NVO).
- Determine the effects of parent fuel composition on reformate products using the in-cylinder, non-catalytic fuel reforming process.
- Establish the cause of catalyst performance degradation from the TCR reforming catalyst used in a prior California Energy Commission-funded project by the Gas Technology Institute (GTI) and Cummins.

FY 2013 Accomplishments

- Demonstrated that in-cylinder non-catalytic reforming is a thermodynamically inexpensive pathway to forming a high-octane reformate stream rich in hydrogen.
- Successfully collaborated with Sandia National Laboratories (SNL) on quantifying chemical species formed in the NVO associated with in-cylinder non-catalytic reforming.
- Determined that very low concentrations of sulfur (~ 2 ppm) can significantly deactivate the nickel-

based TCR reforming catalyst, which is the most likely cause of the reforming degradation observed by GTI and Cummins.

Future Directions

- Complete construction of a new engine platform at ORNL designed to be sufficiently flexible to demonstrate proof-of-principle of the various reforming concepts being pursued in this project on a multi-cylinder engine.
- Apply the in-cylinder non-catalytic reforming concept to the new flexible multi-cylinder engine experiment to quantify efficiency gains from simultaneous production and consumption of reformate in the same engine.
- Select, procure, and conduct flow reactor evaluations of a sulfur-tolerant TCR reforming catalyst formulation for use in future engine experiments.



INTRODUCTION

In conventional internal combustion engines, unutilized fuel energy ends up in the form of waste heat. Waste heat cannot be utilized directly by the piston, but it can be converted into other forms that can be recycled and used to boost piston output. The goal of this project is to identify and demonstrate strategies that enable waste heat recuperation and transformation into forms that can boost the thermodynamic efficiency of single-stage engines.

Our approach to improving internal combustion engine efficiency is based on developing a better understanding of thermodynamic losses in current engines as revealed by both 1st and 2nd Law analyses and then developing ways to mitigate them. Previous studies of internal combustion engine thermodynamics conducted in collaboration with Professors Jerald Caton (Texas A&M University) and David Foster (University of Wisconsin) identified combustion irreversibility as the largest single contributor to fuel exergy loss. In addition, these studies revealed that thermal exhaust exergy is not directly usable by the piston unless it is first transformed into a more suitable state. As a result, our efforts have focused on novel concepts that transform and recuperate thermal exhaust exergy and improve dilute combustion. We are guided by combined input from industry, academia, and national labs, such as that summarized in the recently published report from the Colloquium on

Transportation Engine Efficiency held in March 2010 at the United States Council for Automotive Research [1]. In previous years we identified three promising approaches for improving engine efficiency: counterflow preheating of inlet fuel and air with exhaust heat [2], TCR [3], and chemical looping combustion [4]. Of these, TCR appears to have the greatest near-term potential, and we are pursuing TCR through fuel reforming through two pathways.

APPROACH

We are actively pursuing thermochemical recuperation through (1) a non-catalytic, in-cylinder reforming approach that thermally reforms the fuel in a hot, oxygen-deficient NVO portion of an engine cycle, and (2) a catalytic reforming of fuel in an oxygen-deficient exhaust gas recirculation (EGR) stream. Both approaches aim to use waste exhaust heat to drive endothermic reforming reactions to produce a mixed reformate and EGR stream that is rich in H₂ and CO.

In FY 2013, a novel 6-stroke engine cycle that was developed to isolate NVO reformate was used to parametrically investigate the effect of operating conditions and parent fuel composition on the extent of reforming and reformate composition. The results from this study were independently validated in a different experimental engine at SNL in collaboration with Dick Steeper. To better understand the reforming process, experimental results were also modeled using a detailed chemical kinetic mechanism in CHEMKIN.

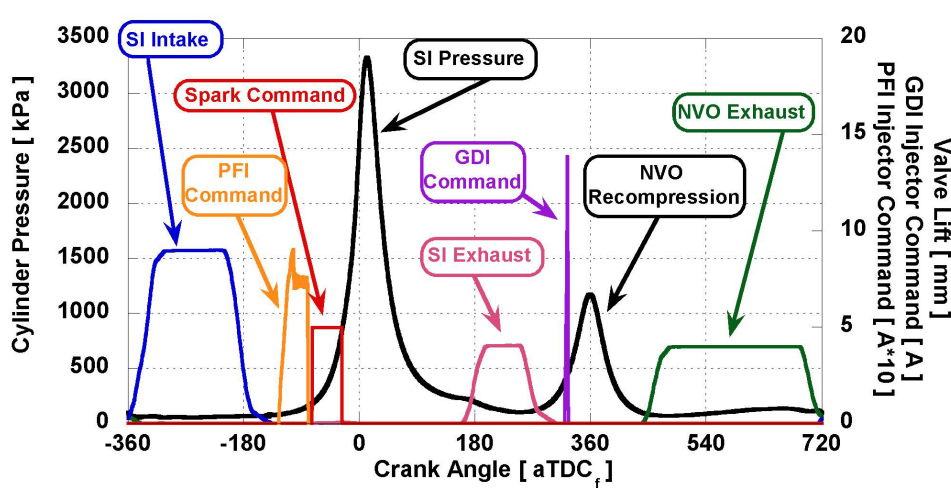
A series of flow reactor experiments were used to identify potential deactivation mechanisms for the GTI TCR catalyst. The experiments were designed to replicate the rapid performance degradation observed

during TCR experiments conducted on a Cummins natural gas engine. Three potential degradation pathways were evaluated: coking during steam reforming, catalyst oxidation during startup or shutdown, and exposure to low sulfur concentrations.

RESULTS

To investigate the reforming chemistry that occurs under in-cylinder, non-catalytic reforming conditions, a 6-stroke engine cycle was developed to isolate reformate from the remainder of the engine cycle. It should be noted that the purpose of this engine cycle is research; it is not being proposed as a production-intent engine cycle. In the engine cycle, a 4-stroke Otto cycle sets up an NVO event in which fuel is injected. In this hot, recompressed, oxygen-deficient environment, the fuel undergoes non-catalytic reforming. The engine cycle is shown in Figure 1, and complete experimental details and results can be found in publications 4 and 5 of the FY 2013 Publications list.

Experimental measurements of the results of in-cylinder reforming were made for four single-component fuels at five NVO durations and six NVO injection timings with three different residual exhaust compositions at the start of NVO. The major finding is that the fuel injection timing is the primary controlling factor for the amount of H₂ and CO formed during the reforming process. NVO duration, oxygen availability during the NVO, and NVO recompression temperature were much less important. These trends are shown in Figure 2. That fuel injection timing, which primarily affects the timescale for reforming, is the controlling variable indicates that the in-cylinder reforming process is kinetically slow, which is in agreement with reference



SI – spark ignition; GDI – gasoline direct injection; PFI – port fuel injection

FIGURE 1. The 6-stroke engine cycle that has been developed to research NVO chemistry.

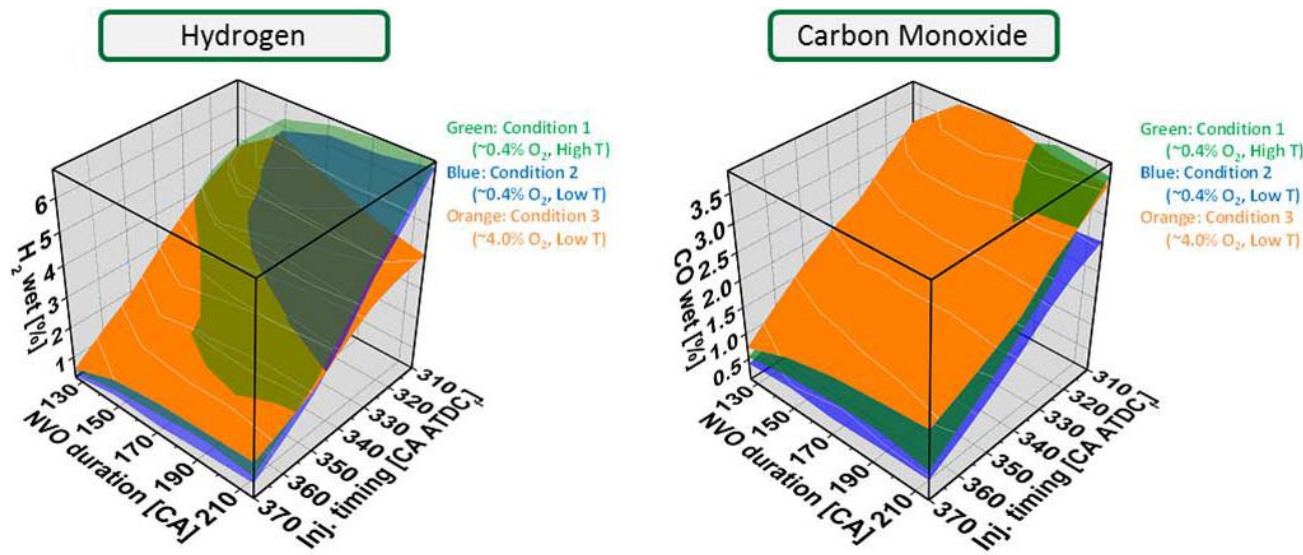
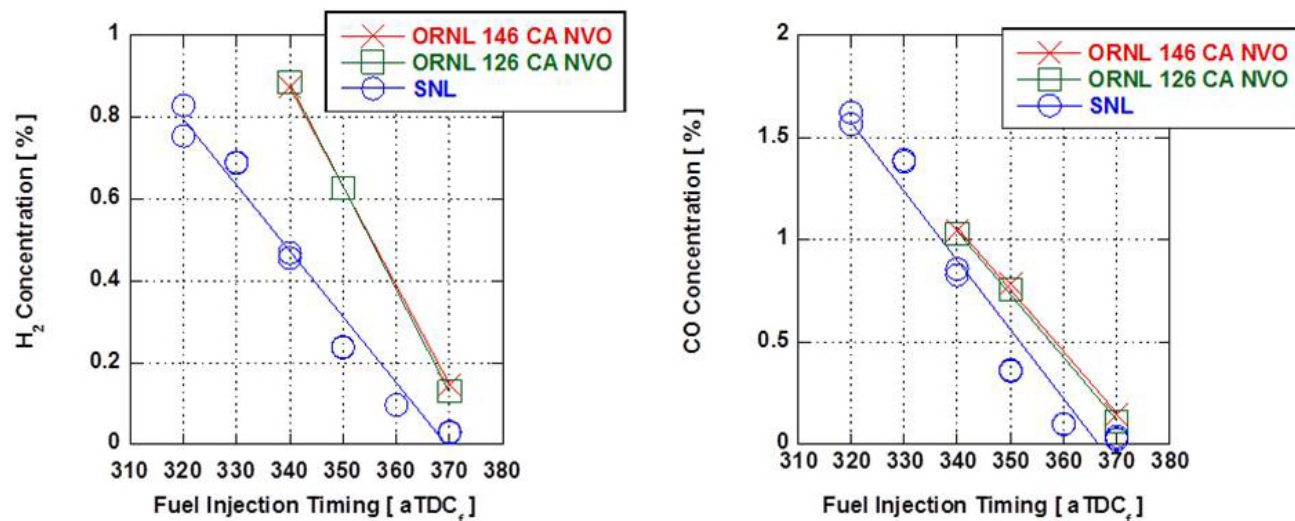


FIGURE 2. Experimental response surfaces of H_2 and CO as a function of NVO duration and fuel injection timing.



CA – crank angle; TDC – top-dead center

FIGURE 3. Comparison of ORNL and SNL experimental measurements of H_2 and CO generation as a function of fuel injection timing at comparable engine operating conditions.

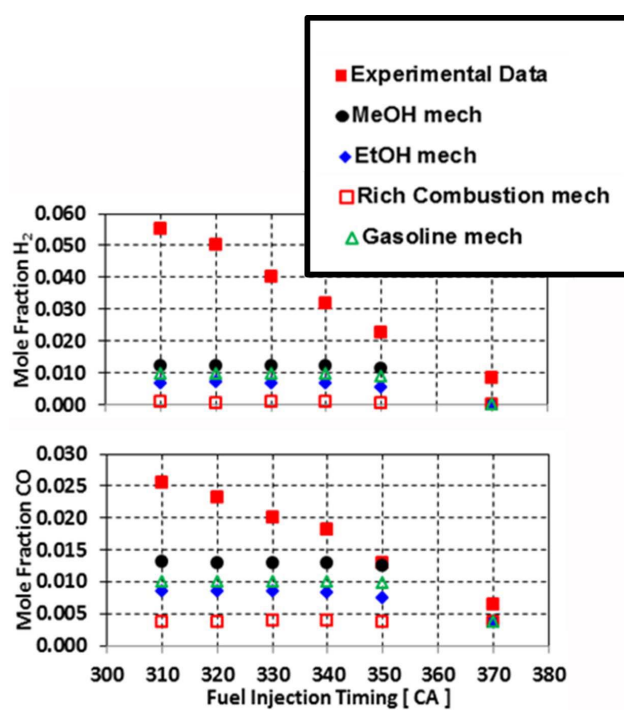
[5]. The NVO duration, a variable which showed very low sensitivity for reforming, primarily affects in-cylinder temperature and pressure conditions without changing the timescale.

In collaboration with Dick Steeper at SNL, a subset of the ORNL experimental results were replicated in order to confirm their applicability to different engine architectures and operating conditions. As shown in Figure 3, H₂ and CO production results were in excellent trend-wise agreement between the two experiments, with both sets of experiments showing a linear dependence

on the start of injection timing, again indicating that in-cylinder reforming is a kinetically slow process. This shows that despite the numerous experimental and analytical differences between the two experiments, the same reforming chemistry is observed in both systems. Further, energy balances from the two experiments show that the reforming process is thermodynamically inexpensive, meaning that while the chemical energy has changed form, it remains available for use during a subsequent combustion event. Complete results are presented in publication 5.

An attempt was made to model these same conditions using detailed reaction kinetic mechanisms and a zero-dimension engine model in CHEMKIN. Surprisingly, the simulations did not agree with the major experimental finding that the reforming process was kinetically slow and that earlier fuel injection timing led to an increase in the extent of reforming. Instead, the H₂ and CO production were predicted to be relatively constant with fuel injection timing, as shown in Figure 4. This suggests that the available kinetic mechanisms over predict key reforming reaction rates and thus do not accurately reflect the importance of reaction time. Complete details of the modeling effort are presented in publication 4.

The flow reactor experiments on the GTI TCR catalyst showed that neither coking nor catalyst oxidation result in significant loss in reforming performance. In fact, air exposure actually results in a temporary increase in H₂ production, followed by a decay back to prior performance (Figure 5). Exposure to low concentrations of sulfur (as 2 ppm SO₂) during the reforming process, however, results in rapid catalyst deactivation. This deactivation is magnified by subsequent exposure to air, as might be observed after system shutdown. While the GTI TCR catalyst was run on a natural gas engine with essentially zero fuel-borne sulfur, ppm-levels of SO₂ are expected due to lubricant oil consumption.



MeOH – methanol; EtOH – ethanol

FIGURE 4. Comparison of experimental and simulated H₂ and CO formation as a function of fuel injection timing.

Thus, the most likely cause of the GTI TCR catalyst deactivation during engine operation is sulfur exposure. Unfortunately, the sulfur loading on the engine-operated catalyst samples is lower than what can be detected through standard analytical techniques. Regardless, it is clear that a more sulfur-tolerant catalyst formulation will be required for operation in engine exhaust streams.

Based on these findings, we are developing a multi-cylinder engine experiment with a sufficiently flexible design to investigate both in-cylinder and EGR-loop reforming strategies. When investigating the in-cylinder reforming process, one cylinder will produce reformate gas, which will then be consumed in the remaining cylinders. By doing this on a multi-cylinder engine, we will be able to measure brake system efficiency. By building this experimental platform with a fully hydraulic variable valve actuation system for the reforming cylinder, we will be able to interrogate a broader range of reforming conditions than would be accessible with a cam-based system. Additionally, we will be able to operate this cylinder with conventional valve timings to investigate EGR-loop reforming for back-to-back comparisons. The modified engine cylinder head and custom valve cover for this modified engine platform is shown in Figure 6, and the engine is on track to be operational during the 2nd quarter of FY 2014.

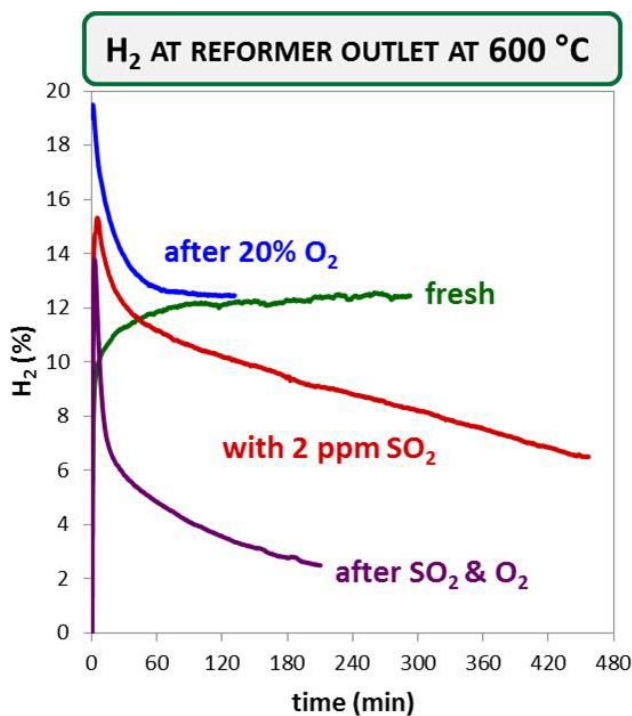


FIGURE 5. H₂ generation over the GTI catalyst for TCR as a function of time for the fresh catalyst, after exposure to O₂, in the presence of SO₂, and after exposure to SO₂ followed by O₂.



FIGURE 6. Cylinder head and custom valve cover for flexible ORNL multi-cylinder engine experiment that will be completed during FY 2014.

CONCLUSIONS

Two pathways are being pursued to boost efficiency through TCR. The first, non-catalytic, in-cylinder reforming, has been shown to be thermodynamically inexpensive, and experiments in FY 2013 have established that this process is kinetically slow. In the second pathway, catalytic EGR-loop reforming, sulfur sensitivity was identified as a major limitation on our first reforming catalyst candidate.

Moving forward, both paths will continue to be pursued in such a way as to apply them on a multi-cylinder engine to demonstrate brake thermal efficiency gains. To this end, a flexible multi-cylinder engine experiment is being developed at ORNL capable of both in-cylinder, non-catalytic reforming and EGR-loop reforming. The engine is expected to become functional during the 2nd quarter of FY 2014.

REFERENCES

1. C.S. Daw, R.L. Graves, R.M. Wagner, and J.A. Caton, "Report on the Transportation Combustion Engine Efficiency Colloquium Held at USCAR, March 3-4, 2010," ORNL/TM-2010/265, October 2010.
2. C.S. Daw, K. Chakravarthy, J.C. Conklin and R.L. Graves, "Minimizing destruction of thermodynamic availability in hydrogen combustion," International Journal of Hydrogen Energy, 31, (2006), pp 728-736.
3. V.K. Chakravarthy, C.S. Daw, J.A. Pihl, J.C. Conklin, "A Study of the Theoretical Potential of Thermochemical Exhaust Heat Recuperation in Internal Combustion Engines," Energy & Fuels, 2010, 24 (3), pp 1529-1537.

4. V.K. Chakravarthy, C.S. Daw, and J.A. Pihl, "A thermodynamic analysis of alternative approaches to chemical looping combustion," Energy & Fuels, 25 (2011), pp 656–669.

5. Song H.H., and Edwards C.F., 2009, "Understanding chemical effects in low-load-limit extension of homogeneous charge compression ignition engines via recompression reaction," International Journal of Engine Research, 10(4), pp. 231–250.

FY 2013 PUBLICATIONS/PRESENTATIONS

1. Szybist, J.P., Splitter, D.A., Kalaskar, V.B., Pihl, J.A., and Daw, C.S., "An Investigation of Non-Catalytic In-Cylinder Fuel Reforming," Invited Talk at the 2013 SAE International High Efficiency Internal Combustion Engine Symposium, (April 14th, 2013, Detroit, MI).
2. Szybist, J.P., Splitter, D.A., Kalaskar, V.B., Pihl, J.A., and Daw, C.S., "An Investigation of Non-Catalytic In-Cylinder Fuel Reforming," Invited Talk at the Southwest Research Institute HEDGE Consortium Meeting, (June 4th, 2013, Southwest Research Institute, San Antonio, TX).
3. Szybist, J.P., Daw, C.S., Pihl, J.A., Splitter, D.A., Kalaskar, V.B., Xie, C., and Gao, Z., "Stretch Efficiency for Combustion Engines: Exploiting New Combustion Regimes," Presented at the 2013 DOE Annual Merit Review, Project ID: ACE015, May 15, 2013.
4. Kalaskar, V.B., Szybist, J.P., Splitter, D.A., Pihl, J.A., Gao, Z., and Daw, C.S., "In-Cylinder Reaction Chemistry and Kinetics during Negative Valve Overlap Fuel Injection under Low-Oxygen Conditions," Proceedings of the ASME ICEF Conference, Technical Paper 2013-19230, Dearborn, MI, October, 2013.
5. Szybist, J.P., Steeper, R.R., Splitter, D.A., Kalaskar, V.B., Pihl, J.A., and Daw, C.S., "Negative Valve Overlap Reforming Chemistry in Low-Oxygen Environments," Draft manuscript 14PFL-0435, to be presented at the 2014 SAE World Congress.

SPECIAL RECOGNITIONS & AWARDS/ PATENTS ISSUED

1. Szybist, J.P., Conklin, J.C., "Highly Efficiency 6-Stroke Engine Cycle with Water Injection," U.S. Patent 8,291,872 B2, Issued October 23, 2012.

II.22 Free-Piston Electric Generator (FPEG)

Terry Johnson (Primary Contact) and
Mike Leick

Sandia National Laboratories
PO Box 969, MS 9661
Livermore, CA 94551-0969

DOE Technology Development Manager:
Gurpreet Singh

Subcontractor:
Ron Moses, Los Alamos, NM

Overall Objectives

- Study the effects of continuous operation (i.e. gas exchange) on indicated thermal efficiency and emissions of an opposed free-piston linear alternator engine utilizing homogeneous charge compression ignition (HCCI) combustion at high compression ratios (~20-40:1)
- Concept validation of passively synchronizing the opposed free pistons via the linear alternators, providing a low cost and durable design
- Proof of principle of electronic variable compression ratio control, allowing optimized combustion timing and fuel flexibility, by means of mechanical control of bounce chamber air pressure
- Provide a research tool to explore the free-piston engine operating envelope across multiple inputs: boost level, equivalence ratio, alternative fuels

Fiscal Year (FY) 2013 Objectives

- Motor the engine continuously for tens of seconds to minutes at a time to assess piston synchronization, thermal response, and compression ratio control
- Perform combustion experiments and measure indicated thermal efficiency and emissions at various compression ratios and equivalence ratios with hydrogen
- Characterize a new design for the pistons intended to reduce frictional losses and improve overall efficiency
- Based on experimental results and modeling predictions, assess the overall engine design and performance with respect to the target fuel-to-electricity conversion efficiency of 50% at 30 kW output

FY 2013 Accomplishments

- New lubrication system and valve plates installed
- Numerous motoring tests at ~10 sec duration demonstrate passive piston synchronization to within 4 mm over the 220 mm stroke
- Motoring tests show work-to-electrical efficiency of ~50%
- Initial single-shot experiments show viability of HCCI with low equivalence ratios of 0.024 to 0.1
- First combined motoring/combustion experiment with ~10 sec duration at equivalence ratio of 0.036
- New pistons installed with redesigned compression rings for reduced friction and increased efficiency
- A number of combustion experiments have been carried with 15-30 sec durations over a range of equivalence ratios from 0.1 to 0.24 and compression ratios from 30:1 to 70:1
- First tests with greater fuel energy input than air drive energy
- Indicated fuel conversion efficiency increase with fuel load demonstrated up to 50% with 0.24 equivalence ratio and compression ratio of 33:1
- Demonstrated work-to-electrical efficiency of 55% during several combustion experiments

Future Directions

- Continue to perform combustion experiments and extend run times to measure indicated thermal efficiency and emissions at various compression ratios and equivalence ratios with hydrogen
- Based on experimental results and modeling predictions, assess the overall engine design and performance with respect to the target fuel-to-electricity conversion efficiency of 50% at 30 kW output.



INTRODUCTION

As fuel efficiency of the typical American automobile becomes more important due to hydrocarbon fuel cost and availability issues, powertrain improvements will require smaller output engines combined with hybrid technologies to improve efficiency. In particular, the plug-in hybrid concept will require

an electrical generator of approximately 30 kW output. Unfortunately, current crankshaft spark-ignition internal combustion engines with optimized power outputs of 30 kW have thermal efficiencies of less than 32%.

The free-piston generator of this project has a projected fuel-to-electricity conversion efficiency of 50% at 30 kW output. The project has progressed by conducting idealized combustion experiments, designing and procuring the linear alternators required for control and power conversion, and conducting computational fluid dynamics design of the inlet/exhaust processes. The current proof-of-concept engine was designed and fabricated based on this initial work. As it has been experimentally evaluated, the engine design has been improved to enable further evaluation of motoring control and eventually combustion efficiency.

APPROACH

By investigating the parameters unique to free-piston generators (linear alternator, opposed piston coupling, uniflow port scavenging) as separate entities, each piece can be used at its optimum design point. More importantly, upon assembly of a research prototype for performance demonstration (the goal of this project), understanding of the pieces in the device will allow the proper contribution of each component to the combined performance of the assembly.

Demonstration of the research prototype has been carried out in stages. First, synchronous starting of the opposed pistons was demonstrated followed by synchronous motoring. Modeling has been used to guide design modifications and experimental procedures leading to combustion.

RESULTS

Figure 1 shows the Sandia FPEG research prototype. Bounce chamber cylinders, air injection valves, vent manifolds, and pistons were all obtained and fully assembled in FY 2011 except for the magnets. Instrumentation and data acquisition systems were also installed in FY 2011 and described in the FY 2011 report. The permanent magnet arrays for the linear alternator were assembled on backirons and integrated with the pistons in FY 2012. In addition, most of the air injection and bounce chamber vent system was redesigned and replaced in FY 2012. This effort was described in the FY 2012 report.

In late FY 2012, these various system improvements resulted in short duration motoring tests. In early FY 2013, two more modifications enabled motoring duration to rapidly increase from one second in November to 13 seconds by February. The first of these was a new

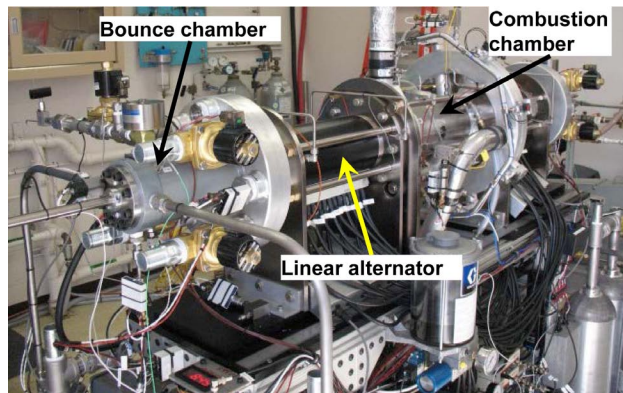


FIGURE 1. Sandia FPEG Research Prototype

lubrication distribution system. The new system enabled continuous lubrication and much finer control over oil injection to the combustion and bounce chamber cylinders which improved friction and minimized combustion of oil vapor. The second modification was the culmination of a series of bounce chamber valve plate designs which resulted in robust operation.

As shown in Figure 2, these longer duration tests demonstrated that the passive piston synchronization concept works. The graph shows piston synchronization error for five of the longest duration tests. This error is the relative difference in the piston positions with respect to the engine centerline. For many tests this error is just a few mm, compared to the 220 mm travel of each piston that occurs every half cycle at about 30 cycles per second and at a maximum velocity of up to 20,000 mm/sec. Based on simulation results, asynchronous motion is initiated by a difference in friction between the two pistons. However, as the separation grows, the electromagnetic drag on the pistons works to restore synchronous motion. Importantly, this data shows that the FPEG system can be operated without complex active controls to keep piston motion in sync. Other data has shown that good synchronization is necessary for high efficiency. For example, a synchronization error of 11 mm results in a 25% reduction in the electrical output of the linear alternators.

Figure 3 shows an energy balance for 16 of the longest duration motoring tests. The results indicate that about 50% of the input energy, which is calculated from the bounce chamber pressure-volume (P-V) integral, is converted to electrical output that is calculated from measured current and known load resistances. The remaining 50% is split among a number of loss terms, the largest of which is frictional loss. Combustion chamber P-V integrals show losses assumed to be primarily thermal, but potentially due to gas blowby as well. This term is on the order of 10%, but varies test to test.

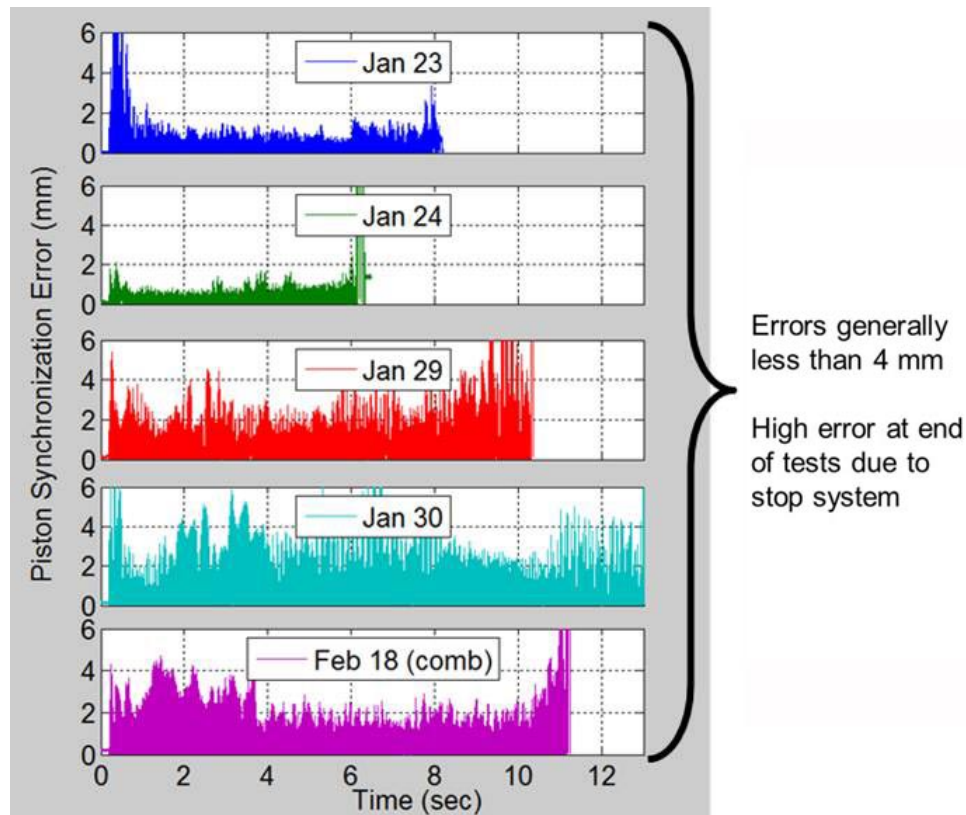


FIGURE 2. Passive Piston Synchronization Demonstrated during Motoring and Combustion Tests

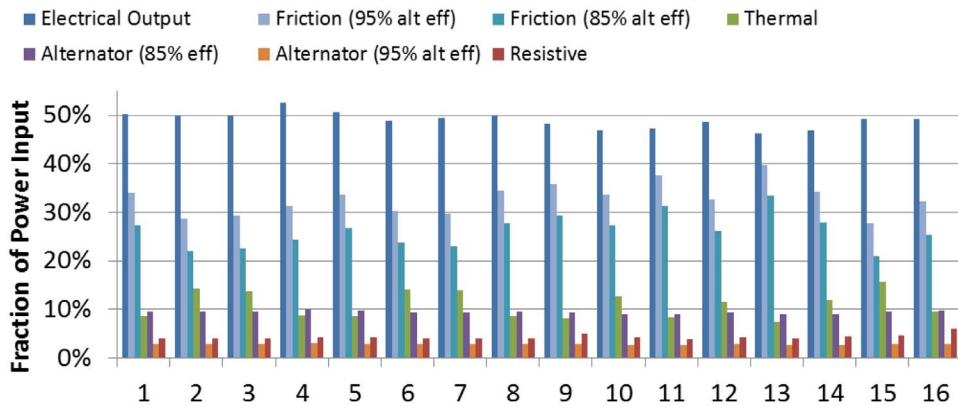


FIGURE 3. Output Energy Distribution from Motoring Tests of the FPEG

Losses to resistive heating in the linear alternator coils and lead wires are fairly small at a few percent. Eddy current losses in the alternators are not measured, but assumed by bounding the alternator efficiency between 85 and 95%. These bounds give two values for alternator losses; ~9% if efficiency is low or ~2% if efficiency is high. Since friction cannot be measured, it is taken as the remainder of the energy balance. Thus, there are two values shown for friction for each test as well. For low

alternator efficiency, friction estimates range from 22 to 32%, for high alternator efficiency, friction losses vary from 29 to 39%. Note that this analysis was performed using the original pistons.

Hydrogen combustion experiments were initiated in December, 2012 with single-shot experiments that were carried out to exercise the hydrogen injection system and to verify that compression ignition of low equivalence ratio mixtures would occur at reasonable compression

ratios. Following the successful completion of those tests, integrated combustion and motoring experiments were pursued. Early tests were carried out with a very lean fuel/air mixture (equivalence ratio of .024). Several tests were run with this mixture and the results showed inconsistent combustion that lasted for just a little over a second. The fuel load was then increased by 50% to an equivalence ratio of 0.036. The resulting test ran for significantly longer, ~10 seconds, and showed fairly consistent cycle to cycle values for combustion energy.

These initial hydrogen combustion experiments, although limited, were encouraging. However, before pursuing combustion further, the pistons were replaced with a new design. Due to the high frictional losses that were found with the original pistons, new pistons were designed and fabricated as discussed in the FY 2012 report and the decision to replace the pistons was made in March 2013. Figure 4 shows the new pistons. The primary modifications to reduce frictional losses were integrated rider rings and thinner compression rings on combustion and bounce chamber ends. Single-shot and motoring tests were run with the new pistons to assess friction. While lower friction force was estimated from this data, unfortunately the reduction was not as significant as expected based on FY 2012 tests.

Following the friction evaluation of the new pistons, combustion experiments were resumed. Over the next couple of months, a number of longer duration (14-27 sec) tests were run with increasingly higher fuel loads with equivalence ratios from 0.036 up to 0.16. In order to accommodate the higher combustion energy, the air

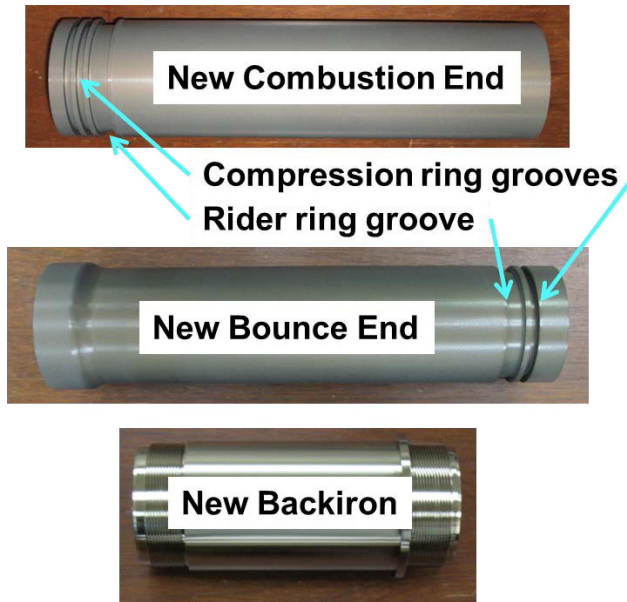


FIGURE 4. New Piston Design Incorporates Rider Rings and Thinner Compression Rings

drive energy was reduced by increasing the bounce chamber vent pressure. This was done by controlling a butterfly valve on the bounce chamber exhaust piping. With the butterfly valve fully open, the bounce chamber vent pressure reaches a steady value of about 120 kPa (17.4 psia). For the highest fuel-air mixtures tested, the vent pressure was brought up as high as 235 kPa (34.1 psia).

Figure 5 shows an example of the data from one of these longer duration combustion tests. The plot shows calculated energy values for each cycle of the ~900 cycle test (27 sec). Combustion chamber and bounce chamber energy is calculated using P-V integrals while alternator energy is calculated based on measured currents. This test was initiated with the fuel injectors set to deliver 5 mg of H₂ per cycle. This value was then increased to 6 mg/cycle and then stepped up to 9 mg/cycle in 1 mg steps. Each fuel load was maintained for about 5 sec. between steps. Initially, the bounce chamber vents to vacuum to enable start up which results in high bounce chamber energy. This value drops quickly to less than 600 J/cycle as the vent pressure increases to a steady value of about 235 kPa by cycle 100. The steps in fuel can be seen in the combustion chamber energy which increases from about 300 J/cycle to almost 600 J/cycle. Alternator energy output stays fairly constant over the duration of the test at about 470 J/cycle. In addition to the energy values, compression ratio and operating frequency are shown on the same axis by scaling them by a factor of 10. Compression ratio is initially very high at over 80:1 but drops with bounce chamber energy to between 35:1 and 38:1 for most of the test. Operating frequency is nearly constant over the test duration at about 34 Hz.

Several tests like the one shown in Figure 5 were run with slight differences in bounce chamber vent pressure and drive pressure that resulted in a range of bounce chamber input energy. Figure 6 shows two plots that examine the data sets as a whole. The top plot

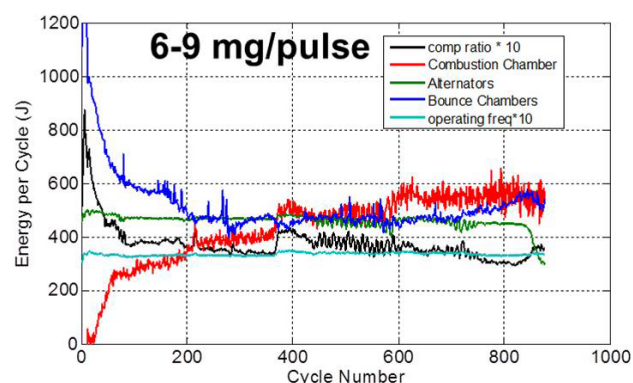


FIGURE 5. Energy Balance During Example Combustion Experiment

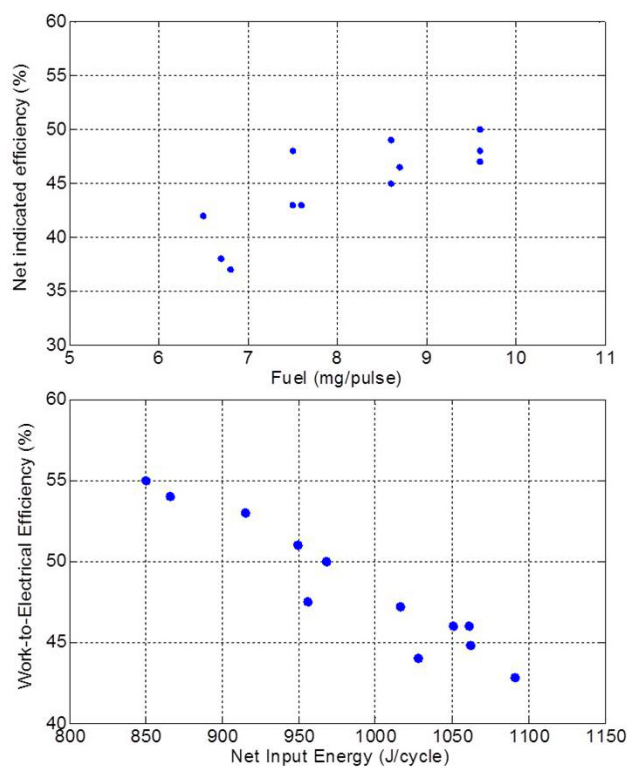


FIGURE 6. Efficiency Trends From Combustion Experiments

shows how indicated fuel conversion efficiency (ratio of net combustion chamber energy to hydrogen chemical energy) varies with fuel load. As more hydrogen is injected per cycle, the thermal and pressure losses become a smaller fraction of the combustion energy which results in a higher net indicated efficiency. The bottom plot shows how electrical output efficiency varies with the net input energy. Work-to-electrical efficiency is the ratio of the alternator energy to the sum of the bounce chamber and combustion chamber energies (net input energy). It was found that this efficiency increased with decreasing net input energy up to a maximum value of 55% and 850 J/cycle net input energy.

The next steps for the FPEG are to extend combustion run times even further, further increase fuel loading, and make emissions measurements. Up to this point, only manual control of fuel load and bounce chamber vent pressure has been used. For extended run times with higher fuel loading, automated feedback control will be required. This capability has been put in place, but has not yet been exercised. Longer run times will be necessary to make meaningful emissions measurements since the analyzers require at least 30 seconds of continuous gas flow to stabilize. However, piston temperatures may limit the duration of experiments. During the 27 sec test shown in Figure 5, piston temperature increased from 25°C to over 50°C. The permanent magnets can be damaged by temperatures exceeding 100°C, so run times may be limited to less than 90 seconds.

CONCLUSIONS

- Passive synchronization of the pistons was successfully demonstrated through continuous motoring tests
- Low equivalence ratio HCCI combustion with hydrogen was successfully demonstrated
- New, low-friction pistons were designed, fabricated and installed
- Extended duration (~30 sec) combustion tests have shown a path to greater than 50% indicated fuel conversion efficiency and greater than 55% work-to-electrical efficiency

FY 2013 PUBLICATIONS/PRESENTATIONS

1. T.A. Johnson and M.T. Leick, “Free-Piston Engine”, 2013 DOE Hydrogen and Vehicle Technologies Merit Review (Washington, DC; May 2013).

II.23 Variable Compression Ratio (VCR) Assessment to Enable Higher Efficiency in Gasoline Engines

Norberto Domingo
Oak Ridge National Laboratory (ORNL)
2360 Cherahala Boulevard
Knoxville, TN 37932

DOE Technology Development Manager:
Roland Gravel

Subcontractor:
ENVERA, Los Angeles, CA

Overall Objectives

- Under subcontract with Envera LLC, design, prototype, and deliver to ORNL one VCR engine with gasoline direct injection (GDI) engine with combined direct fuel injection and port fuel injection (PFI) capabilities. Conduct high-load dynamometer testing prior to delivery to ORNL to validate functionality of all mechanical systems.
- Set up VCR engine at ORNL and quantify the fuel economy benefit of VCR engine technology to a modern GDI engine, and the impact on emissions.
- Map VCR engine performance and emissions over multiple control variables, including compression ratio (CR), spark timing, and cam phasing.
- Utilize experimental engine maps as inputs to drive cycle simulation software to estimate the real-world fuel economy and emissions impact.

Fiscal Year (FY) 2013 Objectives

- Deliver all engine components to Automotive Specialist in Concord, NC, for engine assembly.
- Demonstrate custom VCR engine functionality at Automotive Specialist by running a series of dynamometer tests with the prototype engine.
- Conduct a post-test inspection of engine components by Automotive Specialist and reassemble engine for delivery to ORNL.
- Set up VCR engine at ORNL engine dynamometer facility.
- Generate an experimental baseline of the prototype engine performance at ORNL.

FY 2013 Accomplishments

- The ENVERA VCR engine was delivered, assembled, and first tested at Automotive Specialists in December 2012.
- After a number of mechanical problems were addressed, additional VCR engine tests were conducted in February 2013 at light loads, from idle speed to 5,000 rpm, at CRs of 9:1 and 15:1. One low-speed point was carried out at 19:1 CR. Overall run time for these tests was 30 minutes. The engine was disassembled, inspected, and reassembled. No visual wear was observed during teardown.
- The engine was shipped to ORNL and installation at the ORNL engine dynamometer test facility was completed in mid-September 2013.

Future Directions

- Re-design present timing chain system to fix mechanical issues
- Fabricate a new timing chain system
- Add external exhaust gas recirculation (EGR) loop to the engine
- Evaluate durability of new timing chain system and functionality of external EGR loop



INTRODUCTION

Basic thermodynamics dictate that the efficiency of internal combustion engines is proportional to CR. However, CRs of modern gasoline engines are relatively low from a thermodynamic standpoint, in the range of about 8.5 to 12.5, because of practical constraints at higher CR such as engine knock, increased friction work, and increased heat transfer. It is only the knock-prone conditions (low speed, high load) that constrain the engine CR. The efficiency of most part-load engine conditions can be increased by raising the CR, and it is these part-load conditions that have the most direct impact on the real-world fuel economy.

Recent trends in fuel economy improvements have illustrated that downsizing and down-speeding is a path forward to higher efficiency and lower fuel consumption. However, to meet torque and power requirements, a smaller engine needs to do more work per stroke. This

is typically accomplished by boosting the incoming charge with either a turbocharger or supercharger so that more energy is present in the cylinder per stroke to do the work. With current production engines the degree of engine boosting (which correlates to downsizing) is limited by engine knock at high boost levels. Engine knock or detonation can be prevented by lowering the CR and using premium octane fuel, but as stated earlier, lowering CR reduces engine efficiency and using premium fuel increases customer cost.

VCR technology eliminates the limitation of engine knock at high loads by reducing CR to ~8.5:1 (or whatever level is appropriate) when high boost pressures are needed and regular grade fuel is used. By reducing the CR during high load demand periods there is increased volume in the cylinder at top-dead center which allows more charge (or energy) to enter the cylinder without increasing the peak pressure. Cylinder pressure is thus kept below the level at which the engine would begin to knock. When loads on the engine are low the CR can be raised (to as much as 18:1) providing high engine efficiency. It is important to recognize that for a well designed VCR engine cylinder pressure does not need to be higher than found in current production turbocharged engines. As such, there is no need for a stronger crankcase, bearings and other load bearing parts within the VCR engine.

APPROACH

We propose to investigate the effect of VCR on engine efficiency at the maximum brake torque spark timing over the engine map with a VCR research engine designed and built by Envera LLC. This state-of-the-art engine will combine a production cylinder head utilizing direct fuel injection, cam phasers, and a custom engine block containing the VCR mechanism. Specifications for the engine are shown in Table 1.

Engine experiments will combine parametric sweeps of spark timing, CR, and cam phasing to determine the optimal efficiency at each engine speed/load operating condition. Emissions from the engine will also be measured.

The experimental data of engine performance and emissions will be used to generate composite engine maps of engine efficiency and emissions (i.e. at best efficiency, constant CR, lowest emissions, etc). The engine maps can then be used as inputs for computer simulations of vehicle drive cycles using the PSAT software to determine the real-world impact of variable CR on fuel economy and emissions.

TABLE 1. ORNL Envera GDI-VCR Engine Specifications

| | |
|----------------------------|--|
| Cylinders | Inline 4-cylinder |
| Displacement | 1.886-L |
| Bore/Stroke | 81.0/91.5 mm |
| Variable Compression Ratio | |
| Maximum: | 18:1 (18.95:1 as measured) |
| Minimum: | 8.5:1 (9.92:1 as measured) |
| Crankcase Material | A356 aluminum |
| Cooling | Electric water pump |
| Oil Pump | External (not engine driven) |
| Valvetrain | 16-valve dual overhead camshaft |
| Phase Shifters | Intake and exhaust camshafts |
| Fuel Delivery | Port fuel injection, Gasoline direct injection |
| Aspiration | Naturally aspirated |

RESULTS

The Envera VCR engine was assembled with a PFI head on December 2012 at Automotive Specialists in Concord, NC. Figure 1 shows the VCR engine setup at the Automotive Specialists dynamometer stand. The engine was started using a MoTeC engine controller and ran for a few minutes but a number of mechanical problems were encountered almost immediately into the tests, some more serious than others. Among the most serious problems were timing chain tensioning, failure of the original equipment manufacturer (OEM) exhaust cam phaser, oil supply obstruction to the cylinder head valvetrain, and EGR flow path obstruction. Failure of the exhaust cam phaser resulted in damage to the timing chain and supporting guide as shown in Figure 2. One

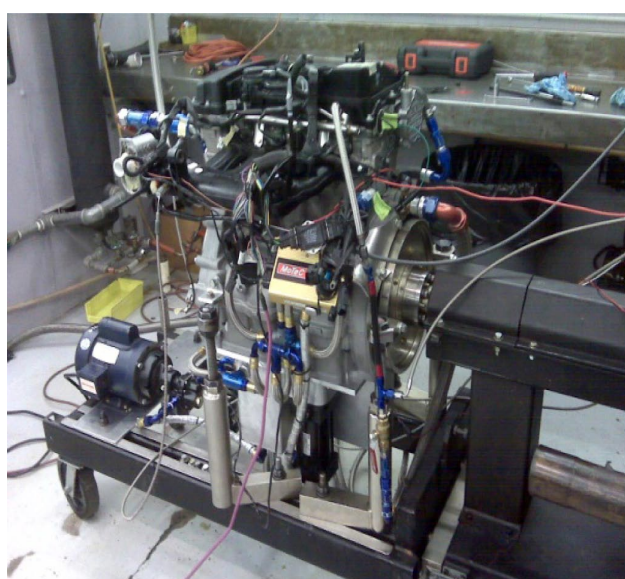


FIGURE 1. VCR Engine at Automotive Specialists Dynamometer Stand

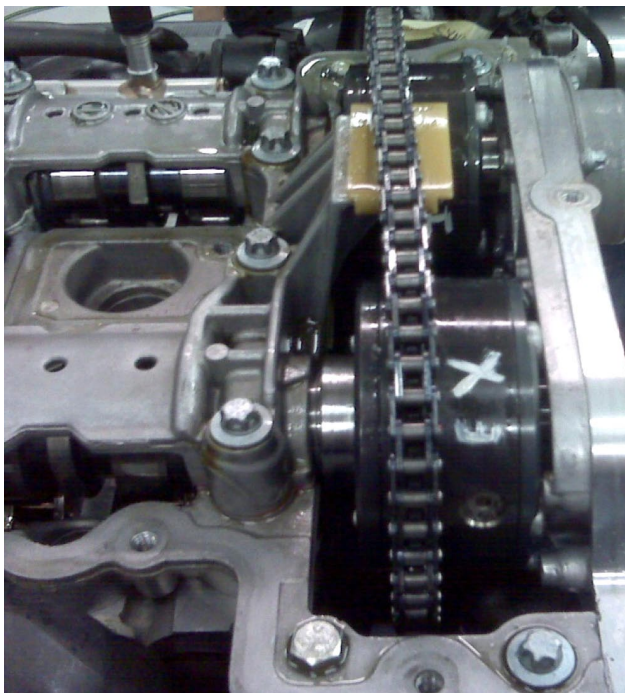


FIGURE 2. Failed Exhaust Cam Phaser Mechanism



FIGURE 3. Oil Passage Mismatch between ENVERA Engine Block and OEM Cylinder Head Gasket

probable cause for the exhaust cam phaser failure may have been due to the lack of oil supply to its internal rotor because the valvetrain was not being supplied with oil. The lack of oil to the valvetrain was attributed to a mismatch between the oil ports in the custom short block and the OEM cylinder head. Figure 3 shows that the oil passages on the ENVERA engine block were not designed correctly to match the OEM cylinder head gasket. A similar mismatch situation, as shown in Figure 4, was noted between the inside EGR passages in the OEM cylinder head and the block. Consequently, the EGR passages on the OEM head had to be plugged, thus disabling engine EGR. Some mechanical problems were corrected. Oil to the cylinder head was corrected by tapping into an oil passage in the block and running hoses to the cylinder head as shown in Figure 5. Other mechanical problems, like the timing chain system and EGR system will require re-design. The engine was re-assembled and tested again with the PFI cylinder head in February 2013 at Automotive Specialists. About an hour of testing was carried out at various operating points. Demo tests were



FIGURE 4. Internal EGR Passage Mismatch between ENVERA Block and OEM Head Gasket

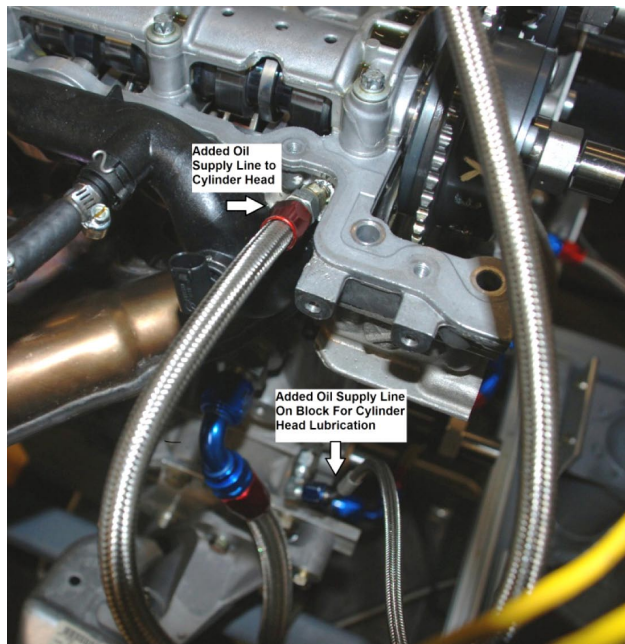


FIGURE 5. Added Oil Supply Line from Engine Block to Cylinder Head

conducted at light loads, from idle speed to 5,000 rpm. Runs were carried out at compression ratios of 9:1 and 15:1. One low-speed point was carried out at 19:1 CR. Following these tests, the engine was disassembled, inspected, and reassembled. No visual wear was observed during the teardown.

The engine was shipped to ORNL and installation in the ORNL engine dynamometer test facility was completed in mid-September 2013. Figure 6 shows the VCR engine setup at the ORNL engine dynamometer facility.

Using a MoTec engine controller, baseline tests were initiated. With minimal engine operation at ORNL (~4 hours) the timing chain failed. This failure caused significant damage to the chain guides. Figure 7 shows the timing chain system with guides as installed on the engine prior to failure. This unconventional guide mechanism is supposed to move up and maintain chain firmness as the chain rotates clockwise during operation. There is no tensioning device. Figures 8 and 9 show deep grooves and chain wear to the guides and one of the support plates that holds the guides. Groove depth on the guides was measured to be 0.080" to 0.120". Fortunately, there was no damage to the valves because the engine was running at a low CR setting at the time of failure. It is evident that the timing chain design on this engine is unreliable and needs to be modified. One obvious problem is that the system lacks a tensioning device to maintain tautness on the chain during operation. We plan to re-design the timing chain system and evaluate its

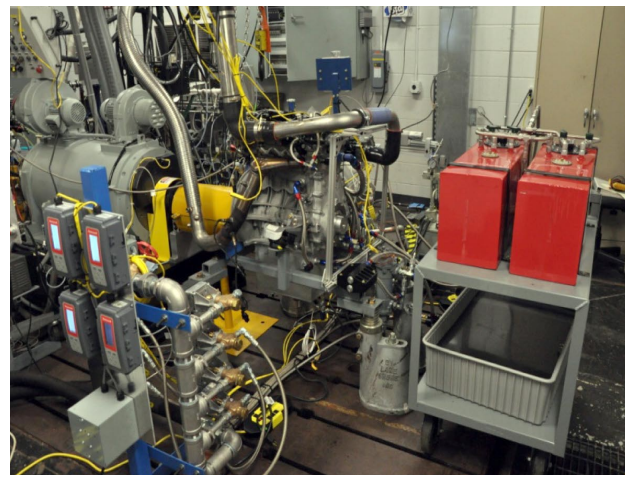


FIGURE 6. VCR Engine at ORNL Engine Test Facility



FIGURE 7. VCR Engine Timing Chain System

durability over a long operating period during FY 2014. Also an external EGR loop will need to be added due to the fact that the internal EGR ports on the OEM head had to be plugged because a mismatch exists between the ENVERA engine block and OEM cylinder head gasket. Internal EGR cannot be added to this engine without a complete redesign of the ENVERA engine block. Therefore an external EGR loop is the best option.

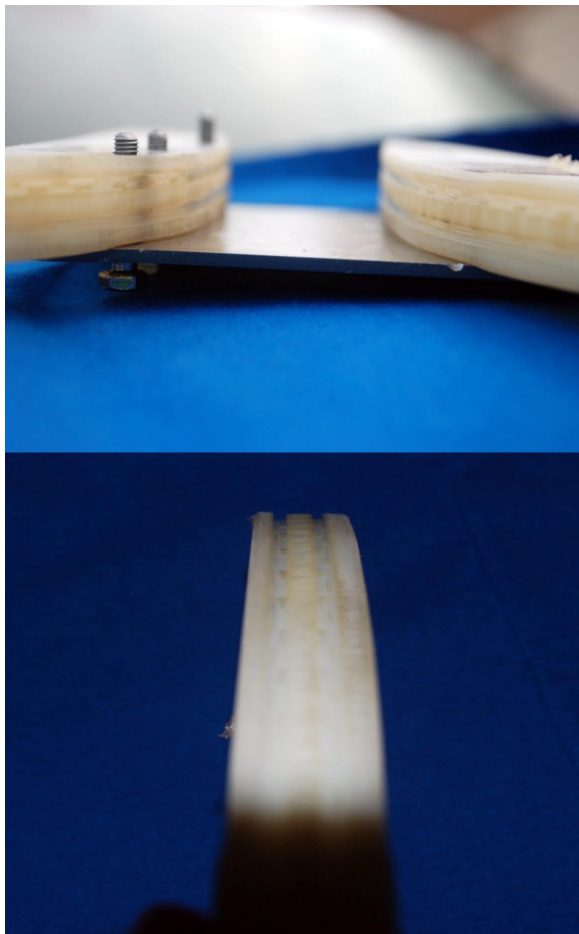


FIGURE 8. Damaged VCR Engine Timing Chain Guides



FIGURE 9. Chain Rub and Damage to Guide Support Plate

CONCLUSIONS

Under the current project, Envera delivered a prototype VCR engine compatible with both PFI and direct injection cylinder heads. The engine was assembled and its functionality was validated at Automotive Specialist. The engine was then shipped and installed at the ORNL dynamometer test facility. During shakedown tests at ORNL, the engine timing chain failed causing significant damage to the timing chain guides and supporting mechanism. ORNL is evaluating the root cause of this failure and what design modifications need to be made to the timing chain system to fix this problem and produce a reliable and durable VCR engine platform.

II.24 Engine Benchmarking CRADA Annual Report

Steve McConnell (Argonne National Laboratory), David Lancaster (General Motors), Tom Leon (Ford), John Opra (Chrysler)
Argonne National Laboratory
9700 South Cass Avenue
Argonne, IL 60439
United States Council for Automotive Research (USCAR)
1000 Town Center Drive
Suite 300
Southfield, MI 48075

DOE Technology Development Manager:
Gurpreet Singh

Subcontractor:
David Gian, FEV, Auburn Hills, MI

Overall Objectives

- Identify state-of-the-art engine and vehicle technologies currently in production, such as 2-stage lift exhaust valves, advanced turbochargers, spray-on engine liners and advanced engine controls
- Quantify the benefits of the state-of-the-art vehicle technologies currently in production
- Optimize vehicle performance using advanced vehicle level modeling such as Autonomie® and the performance maps advanced technologies evaluated in this Cooperative Research and Development Agreement (CRADA)
- Accelerate the development of high-efficiency internal combustion engines for light-duty vehicle applications, while meeting the future emission standards, using numerical simulations
- Support DOE with data and analysis of advanced vehicle technologies

Fiscal Year (FY) 2013 Objectives

- Identified and procured two vehicles with multiple advanced technologies for testing
- Supplied five data sets from the engine benchmarking database to United States Driving Research and Innovation for Vehicle efficiency and Energy sustainability (U.S. DRIVE) goal setting
- Currently testing two vehicles and evaluating the advanced technologies within each vehicle

FY 2013 Accomplishments

- Attained the 2012 Audi A4 with twin variable geometry turbochargers, direct injection and variable valve lift 2.0 liter engine for testing:
 - The vehicle level testing is complete and the vehicle has been torn down for engine level and component testing.
 - The engine level testing is complete with an emphasis on speed/load areas where the variable geometry turbocharger and variable valve lift are operated.
- Attained the 2012 Mini Cooper with a 1.6 liter turbocharged direct-injected variable valve timing engine:
 - Vehicle- and engine-level testing is complete. Final reports were supplied by the end of November 2012.
- Supplied vehicle data sets from the BMW 530i, Toyota Prius, and Toyota Auris to the vehicle systems group for the U.S. DRIVE goal setting exercise.
- Obtained two Nissan Micra (1.4 liter turbocharged direct-injected engine) vehicles. One for vehicle-level testing and one for engine-level and component testing. The relatively low cost of the vehicles allows for parallel testing and faster delivery of the data.

Future Directions

- Evaluate new technologies in the Nissan Micra (1.4 liter turbocharged direct-injected engine) and another vehicle to be identified
- Analyze the new emerging technologies and how they are used
- Conduct analysis on the new and emerging technologies to determine their maximum fuel saving potential



INTRODUCTION

The goal of this engine benchmarking CRADA is to accelerate the development of high-efficiency internal combustion engines for light-duty vehicle applications, while meeting the future emission standards, using numerical simulations. The CRADA will support this

goal by gathering engine and engine component data for use in DOE's programmatic efforts.

APPROACH

The CRADA partners continuously research current and future model engines and vehicles with new features to assist the USCAR and Laboratory members in selecting vehicles for investigation, CRADA will provide a brief one-page summary of published specifications and features for each vehicle under consideration.

Once procured, the vehicle baseline testing will then be conducted followed by instrumentation and the vehicle level investigation. The vehicle investigation may include electronic control unit (ECU) mapping to determine calibration settings. The testing will document the engine controller features, inputs and outputs with an ECU analysis report. The powertrain will then be removed from the vehicle and prepared for engine dynamometer testing. The engine, in the as-installed vehicle configuration, would be installed in an engine test cell for full load performance and a full engine map to investigate emission characteristics, fuel consumption, performance and implementation of engine control hardware. As an option, additional motored stripped-down engine tests could be conducted to analyze friction losses following the thermodynamic investigations. The final step in the engine investigation will be a detailed design analysis and documentation of all of the engine components. The entire engine will be disassembled and the parts will be documented and described in detail with regard to their function and geometry.

RESULTS

- Attained the 2012 Audi A4 with twin variable geometry turbochargers, direct injection and variable valve lift 2.0 liter engine for testing:
 - Vehicle- and engine-level testing is complete. Final reports were supplied by the end of November 2012.

- Attained the 2012 Mini Cooper with a 1.6 liter turbocharged direct-injected variable valve timing engine:
 - Vehicle- and engine-level testing is complete. Final reports were supplied by the end of November 2012.
- Supplied vehicle data sets from the BMW 530i, Toyota Prius, and Toyota Auris to the vehicle systems group for the U.S. DRIVE goal setting exercise.
- Obtained two Nissan Micra (1.4 liter turbocharged direct-injected engine) vehicles. One for vehicle-level testing and one for engine-level and component testing. The relatively low cost of the vehicles allows for parallel testing and faster delivery of the data.
- Supplied data from the 2012 Audi A4, 2012 Mini Cooper, BMW 530i, Toyota Prius, and Toyota Auris to the vehicles systems group for the Government Performance Results Act evaluation.

CONCLUSIONS

- Engine maps provided by this CRADA aided the U.S. DRIVE goals setting team in developing its goals by showing the possibilities of various technologies and their effects on engine efficiency.
- Engine maps provided by this CRADA have been used to support the Government Performance Results Act study so that DOE managers can tailor their portfolio of research technologies. The state-of-the-art engine maps help establish the baseline performance for present technologies and give a better idea of where the technology could evolve. This is done by simulating low-, medium- and high-technology cases from 2015 out to 2045.
- Engine maps provided by this CRADA have aided in the goal setting and research roadmap development for the Advanced Combustion and Emissions Control Tech Team at USCAR.

II.25 Cummins-ORNL Combustion CRADA: Characterization and Reduction of Combustion Variations

Bill Partridge¹ (Primary Contact),
Sam Geckler², Jon Yoo¹, Anthony Perfetto²,
Rodrigo Sanchez-Gonzalez¹, Jim Parks¹,
Maggie Connatser¹, Vitaly Prikhodko¹
¹Oak Ridge National Laboratory (ORNL)
2360 Cherahala Blvd.
Knoxville, TN 37932
²Cummins, Inc.

DOE Technology Development Manager:
Ken Howden

- EGR probe applied to CRADA and SuperTruck measurement campaigns in Columbus, IN
- Numerical design tools assessed based on EGR probe measurements:
 - Tuned model predicts shape, phase, frequency and amplitude of EGR measurements
- EGR probe acquisition software improved to allow monitoring range of transients from crank-angle to tens-of-minutes timescales
- EGR probe measurements distinguish between cylinder-residual backflow and external-loop EGR-air charge
- U.S. patent granted on DOE-sponsored CRADA-developed Fuel-in-Oil technology licensed to Da Vinci Emissions Services and commercialized as the DAFIO
- DAFIO received a 2013 R&D100 Award, recognizing it as one of the 100 most technologically significant new products of the year

Overall Objectives

- Improve engine efficiency through better combustion uniformity
- Develop and apply diagnostics to resolve combustion-uniformity drivers
- Understand origins of combustion non-uniformity and develop mitigation strategies
- Address critical barriers to engine efficiency and market penetration

Fiscal Year (FY) 2013 Objectives

- Develop multiplex laser-based exhaust gas recirculation (EGR) probe
- Apply improved EGR probe to Cooperative Research and Development Agreement (CRADA) and SuperTruck projects to assess specific hardware, validate and improve numerical design tools, and gain fundamental insights into performance drivers
- Measure cylinder-residual backflow and distinguish from external-loop EGR

FY 2013 Accomplishments

- Multiplex laser-based EGR probe developed and demonstrated:
 - Simultaneous measurements from four EGR probes
 - Faster, linear and more sensitive response
 - Simultaneous pressure and temperature information in addition to concentration

Future Directions

- Advance EGR probe for quantification and distinguishing of exhaust and intake temperature CO₂ and simultaneous temperature measurement
- Apply improved EGR probe to monitor cylinder-charge components and their fluctuations
- Develop methodologies to monitor net cylinder-charge composition, temperature and fluctuations
- Apply improved EGR probe with CRADA partners to development of next-generation engine efficiencies:
 - Assess hardware performance
 - Assess performance of numerical design tools
 - Assess advanced control strategies
- Improve EGR probe to achieve CRADA goals:
 - Exhaust temperature applications
 - Fast temperature and pressure measurements and corrections
- Identify and develop diagnostics for addressing efficiency barriers



INTRODUCTION

A combination of improved engine and aftertreatment technologies are required to meet increased efficiency and emissions goals. This CRADA section focuses on engine and combustion-uniformity technologies, while a parallel section (NO_x Control and Measurement Technology for Heavy-Duty Diesel Engines) focuses on emissions and catalyst technologies. Improved efficiency, durability and cost can be realized via combustion-uniformity improvements which enable reduction of engineering margins required by nonuniformities; specifically, these margins limit efficiency. Specific needs exist in terms of reducing cylinder-to-cylinder and cycle-to-cycle combustion variations. For instance, combustion variations mandate system-calibration tradeoffs which move operation away from optimum efficiency points. Combustion variations are amplified at high EGR conditions which are expected in advanced engine systems. Advanced efficiency engine systems require understanding and reducing combustion variations. Development and application of enhanced diagnostic tools is required to realize these technology improvements, and is a major focus of this CRADA.

APPROACH

The CRADA applies the historically successful approach of developing and applying minimally invasive advanced diagnostic tools to resolve spatial and temporal variations within operating engines and catalysts. Diagnostics are developed and demonstrated on bench reactors and engine systems (as appropriate) at ORNL prior to field application at Cummins.

Diagnostics are applied at ORNL and Cummins to study the nature and origins of performance variations.

For example, this may be manifested in cylinder-to-cylinder CO₂ variations due to nonuniform fueling, air and/or EGR charge, fuel spray, component tolerance stacking, or other variations. Detailed measurements are used to assess the performance of specific hardware designs and numerical design tools, and identify nonuniformity origins and mitigation strategies; e.g., hardware and control changes.

RESULTS

Development of an Advanced Multiplex Laser-Based EGR Probe

A major accomplishment for FY 2013 was development and application of an improved multiplex laser-based EGR probe, and improved analysis techniques; the laser-based diagnostic was applied to a CRADA campaign October 22–26, 2012 at the Cummins Technical Center, and the full multiplex laser-based diagnostic was applied during a separate SuperTruck campaign December 10–14, 2012 in Columbus, Indiana. The multiplex laser-based EGR probe is shown in Figure 1a, where the laser housing is apparent on the right-hand side with an orange stripe, followed by a mechanical shutter used for infrared (IR) background measurements relevant to applications in high-temperature environments; the shutter is followed by the multiplex unit in a row at the picture bottom, which splits the laser into four beams; these four beams are directed to four individual EGR probes via purged (see purge tubing at bottom) hollow waveguides (HWGs); a row of four probe-dedicated IR detectors is along the top of Figure 1a; the detectors receive the return light and purge gas from the four EGR probe via HWGs; the eight silver HWGs connecting the instrument to the EGR

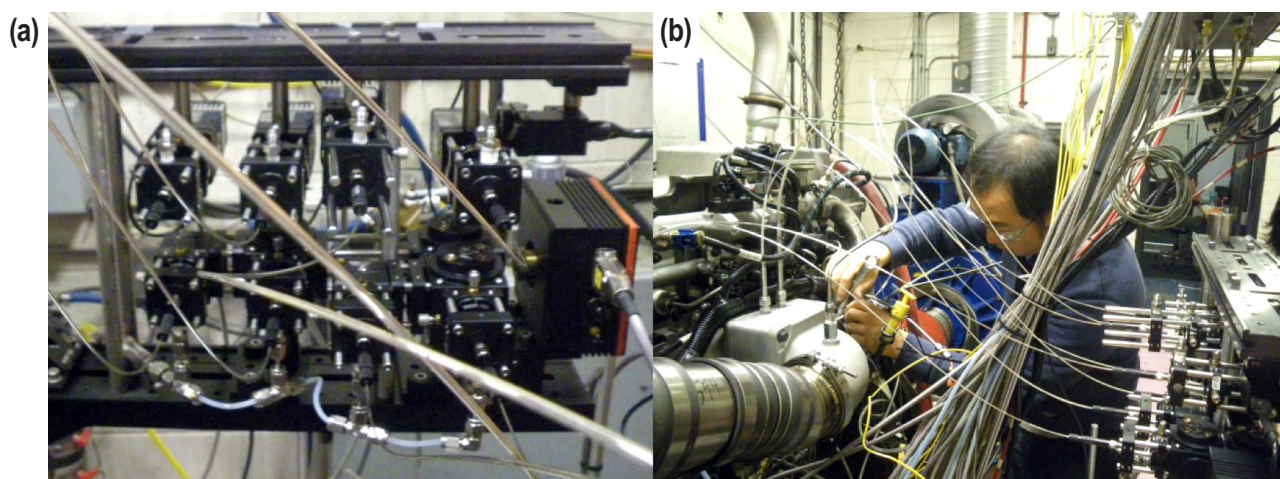


FIGURE 1. Multiplex laser-based EGR probe instrument (a, left) and EGR probe installation in the engine (b, right).

probes are apparent in the picture too. Figure 1b shows the instrument connected to the four EGR probes and their installation in the SuperTruck project engine for spatiotemporal EGR characterization. This multiplex setup allowed for simultaneous measurements from four EGR probes positioned at various locations in the engine system. The result was a profound increase in the efficiency of system mapping; indeed, the primary experimental matrix for the SuperTruck campaign was completed by mid week, which allowed for further transient EGR mapping for higher-level assessment of the hardware and design tools. Another improvement based on feedback from our CRADA campaign was faster data processing allowing results to be presented in concentration rather than arbitrary units for real-time assessment during the campaign week; the data is further processed post campaign with improved calibrations, but this analysis improvement was a significant achievement and benefit. A final notable improvement was modification of the acquisition software to allow a range of transient timescales from crank-angle to tens-of-minutes to be resolved; such broad transient ranges occur throughout engine operation such as individual valve events and intra-valve events and throttle, speed, load and EGR valve transients. This improvement was implemented in the field in response to specific project needs; the modification performed excellent and is another significant achievement and diagnostic advancement. Both the CRADA and SuperTruck EGR probe measurement campaigns were a success.

EGR Probe Application to Assess Design Tools, Hardware and Mixing Fundamentals

The improved laser-based EGR probe was applied to assess detailed spatial and temporal EGR mixing in an advanced intake architecture during a CRADA measurement campaign at Cummins Technical Center October 22–26, 2012. The results indicated that EGR uniformity can differ when assessed in the steady-state averaged and temporally resolved domains, that can in turn elucidate origins of performance variation. Moreover, spatiotemporal analysis suggests various models for fundamental performance nature which can be assessed against other measurements and modeling to understand performance drivers and identify pathways to improved performance. And, the EGR probe measurements have been key in validating certain aspects of the numerical design tools used in developing Cummins' next-generation efficiency engines systems. We have used the EGR probe results to make progress in all these areas. In general the probe continues to be robust and provide unique insights to developing high-efficiency engine systems.

Figure 2 shows a comparison of the port-to-port EGR for a specific mixer and engine condition, as measured

by the EGR probe and predicted by the baseline mixing model. Ideally, all bars would be the same height indicating uniform EGR throughout the intake manifold. Notably, the measurement and simulations predict maximum and minimum EGR at the same locations within the manifold. Although there are differences in the port-to-port EGR as predicted by the measurements and simulations, these differences are typically within 3-8%. By observing results at other mixer and engine-condition combinations, it is apparent that certain locations within the intake manifold have greater fluctuations.

Figure 3 shows measured transient EGR as measured by the EGR probe and results of the transient EGR simulation before and after tuning of the EGR Mixing Model. The baseline model results predict EGR transients of the same phase, frequency and shape as the measurements. Tuning the model based on the measurement results greatly improves the amplitude and shape of the EGR transients predicted by the EGR Mixing Model. Moreover, the specific tuning

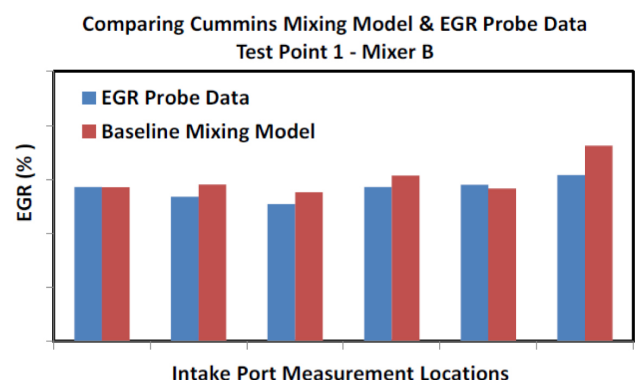


FIGURE 2. Comparison of the intake port-to-port EGR as measured by the EGR probe and predicted by the baseline mixing model for Mixer B and engine condition Test Point 1.

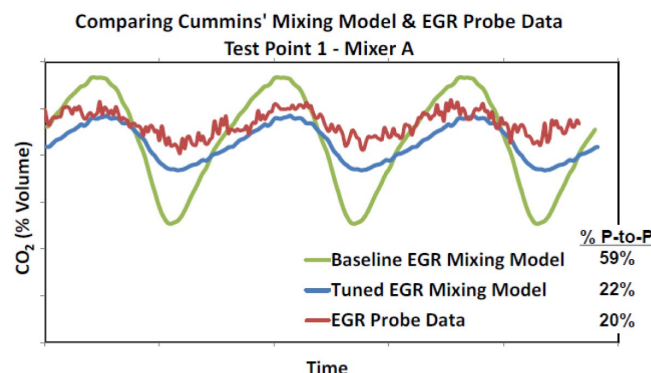


FIGURE 3. Comparing transient EGR for Mixer A and a given engine condition as measured by the EGR probe to the EGR Mixing Model results before and after tuning.

parameters and approach suggested by the measurements and the corresponding tuned-simulation results gives insights regarding the model. These results are enabling improvements to the numerical design tools for accelerating development of fuel-efficient engine systems.

Measuring Residual Exhaust Backflow with the Improved EGR Probe

Cumulative EGR is composed of external EGR flowing through the EGR loop and internal EGR composed of residual exhaust remaining in the cylinder from the previous combustion event. While external EGR can be somewhat controlled via the dampening effect of the EGR loop, cooler and mixer, the internal EGR quantity, composition and temperature can vary based on timing and the previous combustion event. Fluctuations in internal EGR or cylinder residual can cause control challenges and limit overall engine performance efficiency. One way to characterize cylinder residual is to measure its backflow into the intake runner. The EGR probe has been shown to have sufficient temporal resolution to capture the fast transient residual backflow, and experiments were performed to demonstrate this measurement. The work was performed in partnership with the Cummins-ORNL SuperTruck project, and leveraged an experimental facility and ongoing experiments for an open DOE project (Characterization of Gasoline-Range Fuel Effects on High Efficiency Combustion Regimes Using a Flexible HVA Valve Train).

The ORNL single-cylinder direct-injection (DI) spark-ignited engine was used for the residual-backflow measurements. This engine is equipped with hydraulic variable valve actuation, to allow completely independent timing and lift of the two intake and two exhaust valves;

the system imposes a ca. top-hat valve-lift profile. Experiments were performed with and without external EGR, DI and 30% ethanol-70% gasoline fuel was used throughout, and the EGR probe was inserted through an existing port fuel injector port. Figure 4 shows a schematic and picture of the engine used for the study, and the orientation of the EGR probe used for backflow measurements. The probe was located ca. 4 inches behind the intake valves, and in an end-on-angled orientation, which is not optimum for intra-probe flow and temporal resolution; a better orientation would be as indicated by the blue arrow in the center picture, but this was not an option for the initial proof-of-principle experiments. Figure 4 also shows how quick modifications were implemented on an existing EGR probe to incorporate chamfers on the probe-duct edges along the flow axis; these and other EGR probe modifications were recommended from separate computational fluid dynamics analysis performed in the Cummins-ORNL SuperTruck project, and new probes were later fabricated with the complete probe modifications.

Four types of experiments were performed to investigate residual backflow: (1) constant (exhaust-intake) overlap timing sweep, (2) variable overlap timing sweep, (3) pilot breathing timing sweep, and (4) pilot breathing width sweep. The first two experiments (1 and 2) were implemented with various valve overlap and using the low-lift valve configuration, as some valve-opening timings used were near or at top-dead center (TDC). In the second two experiments (3 and 4) pilot breathing refers to opening one intake valve in the low-lift configuration during the main exhaust event; for these experiments there was no overlap between the main exhaust and intake events that used low- and high-lift, respectively.

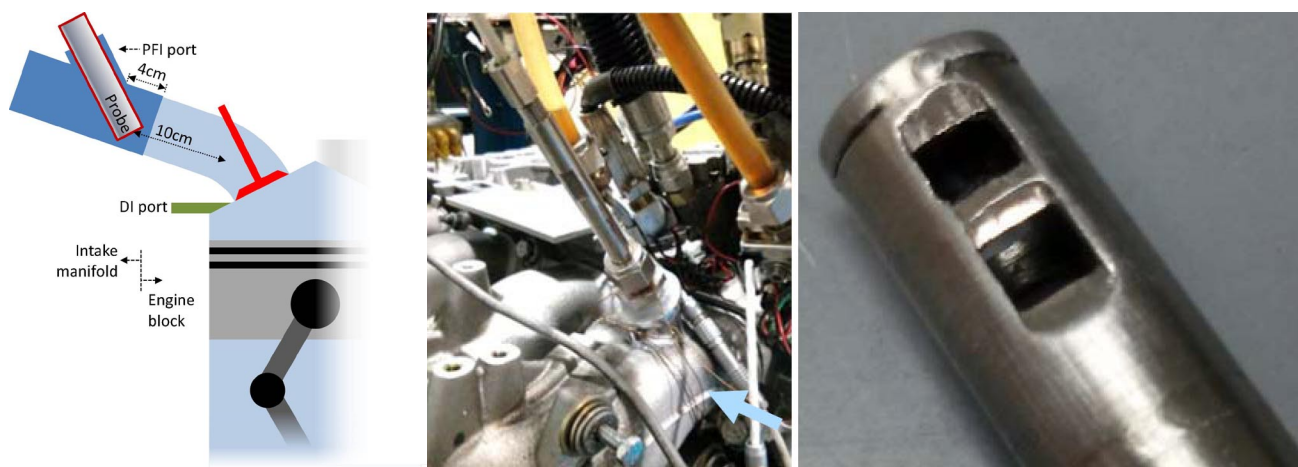


FIGURE 4. Schematic (left) of the single-cylinder engine and picture (center) of the EGR probe installed in the intake runner. The EGR probe (right) was modified to incorporate chamfers along the flow-orientation axis as recommended by computational fluid dynamics analysis.

The (1) constant overlap timing sweep was implemented with constant valve overlap, and sweeping the overlap-center timing through 40° and 20° before TDC (BTDC), TDC, and 20° and 40° after TDC (ATDC). Figure 5 shows the 16-cycle averaged EGR probe measurements at 40° BTDC with and without external EGR; note, a baseline offset has been added to the measurements. Residual backflow is apparent as the CO₂ dynamic synchronous with the valve overlap, whereas external EGR is apparent from the relatively constant baseline; i.e., the ca. 2.4 vs. 2.0 a.u. baseline in Figure 5 is due to external EGR. Indeed, the two EGR components can be distinguished. In general, the residual backflow decreased as the valve overlap timing was advanced, with little backflow being measured at the 40° ATDC timing; not measuring backflow could be simply due to it not reaching the probe location. Cycle- and crank-angle resolved measurements revealed apparently structured cycle-to-cycle fluctuations that could vary by 100%. While certain challenges exist to quantifying residual backflow from external EGR, it is apparent that with such quantification and cycle-resolved data like Figure 5, the partitioning between internal and external EGR, and their fluctuations could be measured and applied to improve combustion control and efficiency.

The (2) variable overlap timing sweep experiments were implemented by varying the degree of valve overlap approximately centered at TDC, and with constant exhaust-open and intake-close timings. Figure 6 shows a schematic and data reflecting two valve overlap timings, and crank-angle resolved residual backflow measurements at three overlap timings; residual backflow is indicated by the transient CO₂ synchronous with valve overlap as discussed in relation to Figure 5. The right portion of Figure 6 shows the variation in measured

residual backflow as a function of overlap, and indicates that the backflow reaches the EGR probe at ca. 10° overlap. The measured residual backflow increases beyond this threshold, indicating increasingly greater backflow deeper into the intake runner.

The experiments demonstrated that residual backflow can be measured with the EGR probe, and that variations with valve timing, piston speed and cycle-to-cycle fluctuations can be resolved. The measurements could be improved via synchronous high-speed pressure measurements at the EGR probe location, and by locating the probe in a more optimum configuration and location. Future work will investigate correlating the backflow fluctuations with engine and combustion fluctuations.

Further EGR probe improvements are needed to enable the quantification necessary to characterize internal and external EGR partitioning and fluctuations via backflow measurements, as well as methodology development to assess net cylinder charge composition, temperature and fluctuations from such measurements. This will be the focus of continued work in the Combustion CRADA.

CONCLUSIONS

- Improved multiplex laser-based EGR probe functions excellently in off-site engine measurement campaigns:
 - Improved speed, linearity and sensitivity
 - Faster mapping with four simultaneous probes
 - Simultaneous pressure measurements used to distinguish EGR concentration dynamics from pressure dynamics

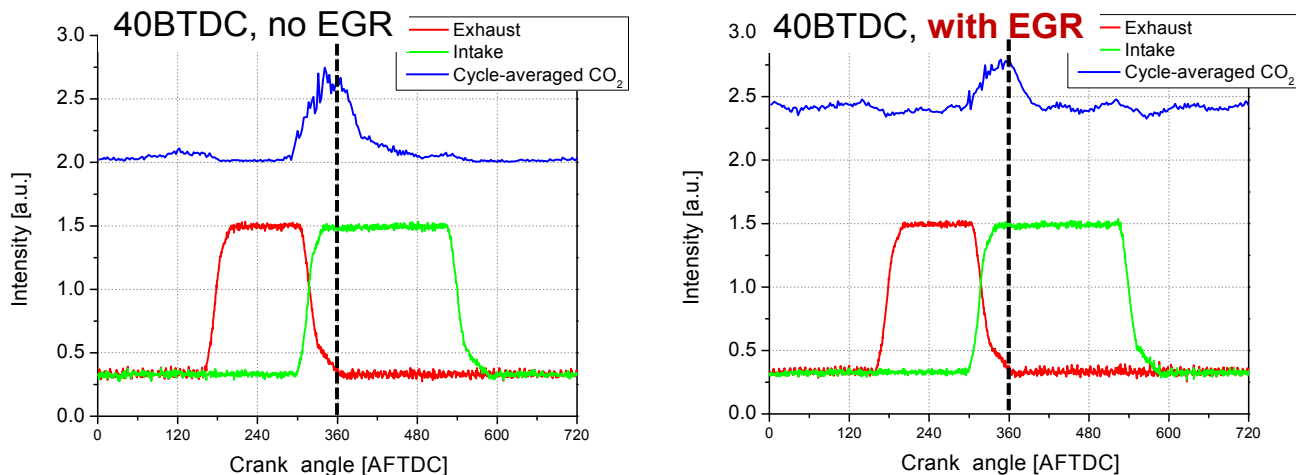


FIGURE 5. EGR probe residual backflow measurements with intake-exhaust valve overlap centered at 40° BTDC and with and without external EGR; the vertical black dashed line indicates TDC.

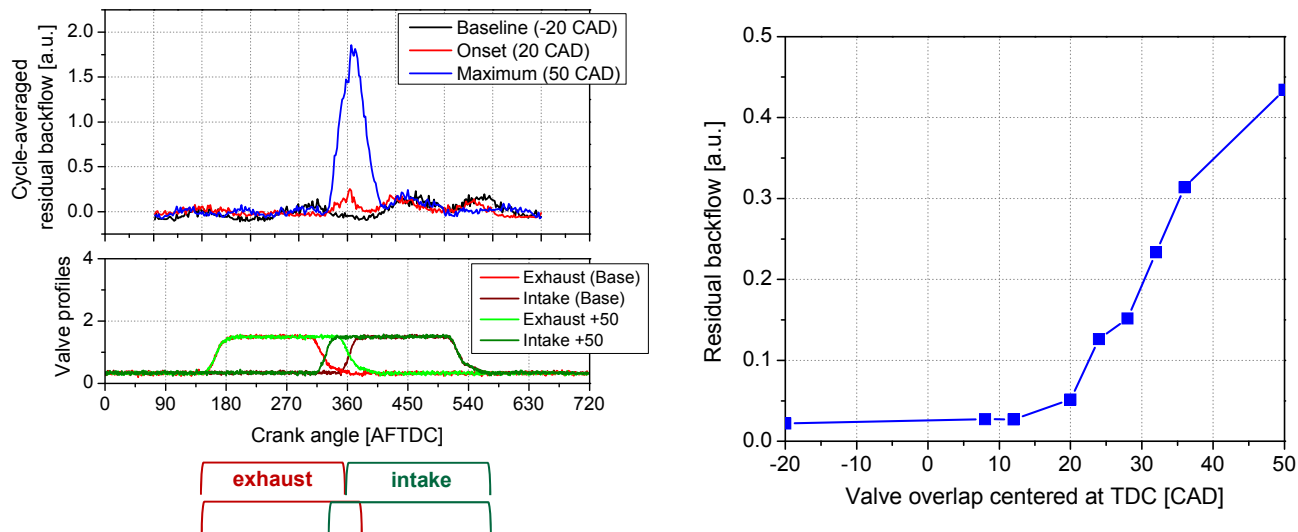


FIGURE 6. EGR probe residual backflow measurements with increasing intake-exhaust valve overlap approximately centered at TDC.

- Improved EGR probe applied in CRADA to:
 - Improve numerical design tools
 - Assess spatial and temporal mixing, hardware and mixing fundamentals
- Improved EGR probe applied to Cummins SuperTruck project
- Residual backflow and external-loop EGR measured and distinguished by EGR Probe:
 - Demonstrates components of cylinder charge can be measured
 - Provides pathway for quantify cylinder charge composition, temperature and fluctuations

FY 2013 PUBLICATIONS/PRESENTATIONS

Oral Presentations

1. R.M. Connatser, J.E. Parks, V. Prikhodko, W.P. Partridge, S. Geckler, N. Currier. "Ammonia Sensors Based on Doped-Sol-Gel-Tipped Optical Fibers for Catalyst System Diagnostics," Emission Control Technologies, 18th Directions in Engine-Efficiency and Emissions Research (DEER) Conference, Detroit, Michigan, October 17, 2012.
2. W.P. Partridge, J. Yoo, R.M. Connatser, V. Prikhodko, R.S.-Gonzalez, J. Parks, S. Geckler, A. Perfetto, A. Beck, M. Dane, R. Booth, D. Koeberlein, "Cummins/ORNL FEERC Combustion CRADA: Characterization & Reduction of Combustion Variations," 2013 DOE Vehicle Technologies Program Annual Merit Review, Arlington, Virginia, May 16, 2013.

Poster Presentations

1. J. Yoo, J.E. Parks, V. Prikhodko , W.P. Partridge, S. Geckler. "EGR Spatial Uniformity & Cylinder-Resolved Transients – measurements using an absorption spectroscopy probe," Emission Control Technologies, 18th Directions in Engine-Efficiency and Emissions Research (DEER) Conference, Detroit, Michigan, October 16, 2012.
2. R. Maggie Connatser, W.P. Partridge, Jr., J.M.E. Storey, S.A. Lewis, Sr., J.E. Parks, II. "Catalyst-Tipped Optical Fibers for Catalyst System Development: Sensing Ammonia, Oxidation State, & Sulfur Interactions," Southeastern Catalysis Society Meeting, Asheville, North Carolina, September 30, 2013.

SPECIAL RECOGNITIONS & AWARDS/ PATENTS ISSUED

Awards

1. 2013 R&D100 Awarded to Da Vinci Emissions Services, ORNL and Cummins in recognition of the Da Vinci Fuel-in-Oil being one of the 100 most technologically significant new products of the year; the commercialized DAFO was based on DOE-funded CRADA-developed Fuel-in-Oil technology.

Invited Lectures

1. Jon Yoo, Jim E. Parks, Vitaly Prikhodko, Anthony Perfetto, Sam Geckler, Rick Booth, David Koeberlein, William P. Partridge. "Single-Cylinder Information from Multi-Cylinder Engines: Measuring EGR Uniformity with Crank-Angle Resolution using a Practical & Minimally Invasive EGR Probe," US DOE Advanced Engine (ACEC & Diesel) Crosscut Team meeting; USCAR HQ, Detroit, MI and participation by Phone/Web; presentation via teleconference from Oak Ridge National Laboratory, January 10, 2013.

2. Bill Partridge, Jae-Soon Choi, Jim Parks, Maggie Connatser, Jon Yoo, Rodrigo Sanchez, Vitaly Prikhodko, Neal Currier, Sam Geckler, Mike Ruth, Rick Booth, David Koeberlein, Alex Yezerets. “Diagnostics Development & Applications for Enabling Advanced Efficiency Automotive Systems,” International Society of Automation (ISA) Oak Ridge Section, January Meeting, Knoxville, Tennessee, January 22, 2013.

3. Bill Partridge, Jae-Soon Choi, Jim Parks, Maggie Connatser, Jon Yoo, Rodrigo Sanchez, Vitaly Prikhodko, Neal Currier, Sam Geckler, Mike Ruth, Rick Booth, David Koeberlein, Alex Yezerets. “Advanced Diagnostics for Automotive Catalysts, Exhaust Gas Recirculation & Oil Dilution,” Department of Mechanical Engineering, Czech Technical University; Prague, Czech Republic, February 25, 2013.

4. Bill Partridge, Jae-Soon Choi, Jim Parks, Maggie Connatser, Jon Yoo, Rodrigo Sanchez, Vitaly Prikhodko, Neal Currier, Sam Geckler, Mike Ruth, Rick Booth, David Koeberlein, Alex Yezerets. “Advanced Diagnostics for Automotive Catalysts, Exhaust Gas Recirculation & Oil Dilution,” Korea Institute of Industrial Technology (KITECH), Automotive Components Center, Honam Technology Application Division (Dr. Inchul Choi, Senior Researcher, hosting), Gwangju (aka Kwangju), Korea, August 28, 2013.

Patents

1. J.E. Parks, W.P. Partridge “Optical Backscatter Probe for Sensing Particulate in a Combustion Gas Stream,” United States Patent, Patent No. US 8,451,444 B2, Date of Patent May 28, 2013.

Patents Filed

1. US Appl. No.: 13/912,462; J.E. Parks, W.P. Partridge, J. Yoo “EGR Distribution and Fluctuation Probe Based on CO₂ Measurements,” ORNL Ref. No.: 2759.1; Filed 6-7-2013.

III. EMISSION CONTROL R&D

III.1 Cross-Cut Lean Exhaust Emission Reduction Simulation (CLEERS): Administrative Support

Stuart Daw

Oak Ridge National Laboratory (ORNL)
National Transportation Research Center
2360 Cherahala Boulevard
Knoxville, TN 37932-6472

DOE Technology Development Manager:
Ken Howden

Other key ORNL personnel involved in this activity are Vitaly Prikhodko, Charles Finney, and Zhiming Gao.

Subcontractor:

Richard Blint, N2Kinetics Research,
Shelby Township, MI

- Coordinated with advisory team regarding database activities.
- Continued further refinement of lean-oxides of nitrogen (NOx) trap (LNT) and selective catalytic reduction (SCR) catalyst characterization protocols in coordination with the CLEERS Kinetics task.
- Conducted the 2013 CLEERS Industry Priority Survey and identified areas where DOE national lab projects need to be better aligned with industry partner needs.
- Provided regular update reports to the DOE Advanced Engine Cross-Cutting Technology Development Team.
- Organized the 2013 CLEERS workshop at University of Michigan, Dearborn on April 10–12, 2013.
- Maintained CLEERS website (www.cleers.org) including functionalities, security, and data to facilitate web meetings and serve Focus Group interactions.
- Increased utilization of models and kinetic parameters produced by CLEERS projects in full system simulations of conventional and hybrid advanced light and heavy-duty powertrains.
- Assisted the Advanced Combustion and Emissions Control (ACEC) low-temperature task force in completing the final report regarding R&D needed to address barriers in meeting increasingly stringent emissions standards as engine-out exhaust temperatures from advanced engines continue to decline.

Overall Objectives

Coordinate the CLEERS activity for the DOE Advanced Engine Cross-Cutting Technology Development Team to accomplish the following:

- Promote development of improved computational tools for simulating realistic full-system performance of lean-burn engines and associated emissions controls.
- Promote development of performance models for emissions control components such as exhaust manifolds, catalytic reactors, and sensors.
- Provide consistent framework for sharing information about emissions control technologies.
- Help identify emissions control R&D needs and priorities.

Accomplishments

- Continued leadership of the CLEERS Planning Committee and facilitation of the CLEERS Focus teleconferences with strong domestic and international participation (typically 30–50 participants).
- Created initial bibliographic database for evaluation by selective CLEERS members and established an ORNL Sharepoint site for expanded experimental database of engine exhaust and aftertreatment measurements and simulation algorithms and modeling tools.

Future Directions

- Continue leading the CLEERS planning and database advisory committees.
- Continue leading the Focus Groups.
- Continue archival of expanded experimental and modeling data in the CLEERS Sharepoint site and hiring of ORNL post-doctoral researcher to help manage the database if continuing budget changes permit.
- Organize and conduct the 2014 CLEERS workshop in the spring of 2014.
- Continue sharing of basic data and models with DOE Vehicle Systems projects and the ACEC Team from U.S. DRIVE.

- Continue maintenance and expansion of CLEERS website.
- Continue providing regular update reports to the DOE Advanced Engine Cross-Cutting Technology Development Team.
- Complete and issue final public report on the 2013 CLEERS Industry Priority Survey.



INTRODUCTION

Improved catalytic emissions controls will be essential for utilizing high-efficiency lean-burn engines without jeopardizing the attainment of much stricter U.S. Environmental Protection Agency emission standards that will begin taking effect after 2013. Simulation and modeling are recognized by the DOE Advanced Engine Cross-Cutting Technology Development Team as essential capabilities needed to address the continually evolving regulatory environment and advances in combustion engine and emissions control technology. In response to this need, the CLEERS activity was initiated several years ago to promote improved computational tools and data for simulating realistic full-system performance of lean-burn engines and the associated emissions control systems. Specific activities supported under CLEERS include:

- Public workshops on emissions control topics.
- Collaborative interactions among DOE Cross-Cutting Team members, emissions control suppliers, universities, and national labs under organized topical focus groups.
- Development of experimental data, analytical procedures, and computational tools for understanding performance and durability of catalytic materials.
- Establishment of consistent frameworks for sharing information about emissions control technologies.
- Recommendations to DOE and the DOE Cross-Cutting Team regarding the most critical emissions control R&D needs and priorities.

ORNL is involved in two separate DOE-funded tasks supporting CLEERS:

- Overall administrative support.
- Joint development of benchmark emissions control catalyst kinetics in collaboration with other national labs and university and industry partners.

APPROACH

In the administrative task, ORNL coordinates the CLEERS Planning Committee, the CLEERS Database Advisory Team, the CLEERS Focus groups, CLEERS public workshops, the biannual CLEERS industry survey, and the CLEERS website (<http://www.cleers.org>). ORNL acts as a communication hub and scheduling coordinator among these groups and as the spokesperson and documentation source for CLEERS information and reports. The latter includes preparation and presentation of status reports to the Advanced Engine Cross-Cutting Technology Development Team, responses to requests and inquiries about CLEERS from the public, and summary reports from the biannual industry surveys.

RESULTS

The updated industry priority survey was completed in 2013 using modified questionnaires based on participant feedback from previous surveys and suggestions from the CLEERS Planning Committee, individual industry partners, and members of the U.S. DRIVE ACEC Technical Team. There were two major parts in each questionnaire, one part focused on identifying the highest priority concerns of responders regarding current emissions control technology barriers and the other part focused on ranking the importance of specific CLEERS activities. Questionnaires were sent to all member organizations of the DOE Advanced Engine Cross-Cutting Technology Development Team and their close partners among the emission controls and fuel supplier communities.

Twenty-four responses were returned, including 15 from original equipment manufacturers (OEMs), five from emission control suppliers, two from government agencies outside of DOE, and two from fuel suppliers. Ten of the responses were from responders who identified their main business interests as being in the gasoline sector of the market, while seven responders identified themselves as primarily involved in the heavy-duty diesel market and the remaining seven in the medium-duty diesel market. A draft report summarizing the findings is currently under review, and a finalized version is expected to be publicly released early in FY 2014.

Briefly, the findings from the survey revealed that the highest overall technology concerns centered on the following emissions control areas:

- On-board diagnostics and multi-functionality for particulate filters.
- The mechanisms and dynamics of ammonia (NH_3) storage and release in NOx SCR.

- Low-temperature catalysts for NOx reduction and oxidation of hydrocarbons and carbon monoxide.
- Passive hydrocarbon adsorbers (also called traps) and multi-zone catalysts.
- LNT catalysts with lower levels of platinum group metals.

Although the above issues tended to be the top concerns among all the different responder groups, group-related differences were still visible in detailed statistical breakdowns of the results. For example, OEMs in the gasoline market also ranked three-way catalyst (TWC) technology as an area of high concern. However, since TWC technology is clearly not applicable to diesel exhaust, diesel OEMs did not give this area a high priority ranking. Such differences emphasize the broad diversity of the CLEERS community and the difficulty in identifying R&D targets that meet the needs of all participants simultaneously.

Rankings for the CLEERS activities were generally high over all categories, although specific helpful suggestions for improvements were also provided by several responders. The greatest benefits to the industry partners as a whole appear to be coming from:

- The annual CLEERS public workshop.
- Coordination of national lab emissions control R&D.
- The monthly technical focus telecom presentations.

In spite of the effort made to simplify and carefully word the updated questionnaires for the 2013 survey, it appeared that there was still some confusion among the responders that contributed to ambiguous trends in the analysis. This appeared to be particularly true for questions related to micro-scale kinetics modeling, non-urea generation of NH₃, modeling of hybrid electric vehicles, and the need for national labs to investigate commercially relevant catalysts. Thus it is clear that additional improvements in the questionnaire design will be warranted in any future surveys of this type.

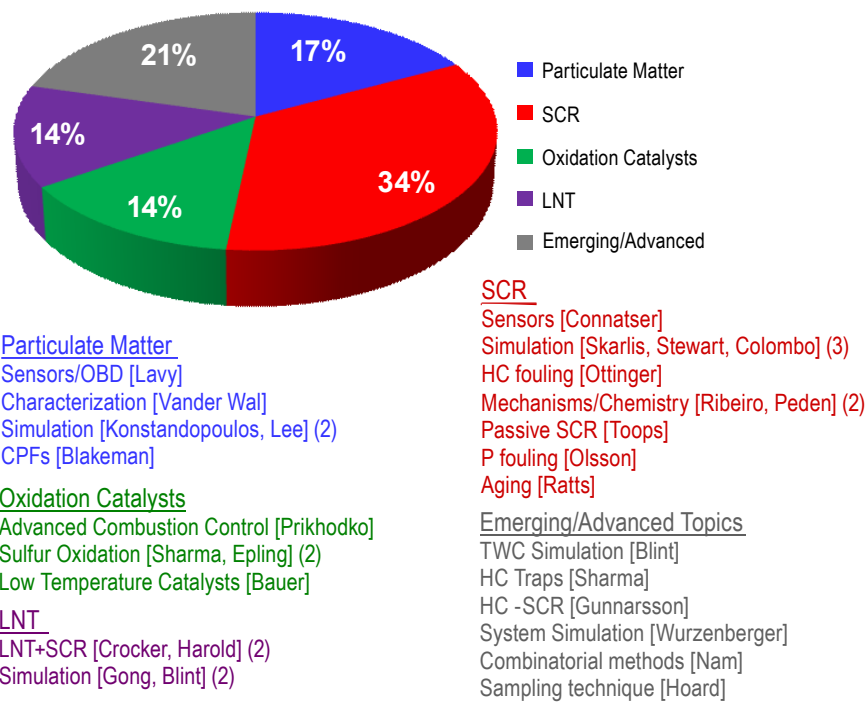
CLEERS technical teleconferences continued this year on roughly a monthly basis. The presentations covered a wide range of research results in emissions control experimentation, modeling, and simulation by members of the CLEERS Focus Group as well as outside experts including: Mike Harold (University of Houston), Joe Kubsh (Manufacturers of Emission Controls Association), George Muntean (Pacific Northwest National Lab), Chenxi Sun and Andre Boehman (University of Michigan), Mario Trujillo (University of Wisconsin), Isabella Nova (Politecnico di Milano), Feng Gao (Pacific Northwest National Lab), and Scott Curran, Stuart Daw, Vitaly Prikhodko, and Zhiming Gao (ORNL). As previously, we have continued to restrict

teleconference attendance to members of the Advanced Engine Cross-Cutting Technology Development Team and their direct collaborators, because these teleconferences sometimes include unpublished or sensitive information. In some cases, presentations include pre-publication or sensitive information and are made only via live Web link without distributing electronic copies of slides to the participants. Attendance continues to increase and is now typically between 30 and 50 participants. International participation continues to be good and is mostly from Europe.

The 2013 (16th) CLEERS Workshop was held April 10–12, 2013 at the Institute of Advanced Vehicle Studies on the Dearborn campus of the University of Michigan. These dates were selected in order to immediately precede the 2013 SAE Congress in Detroit, allowing international participants to attend both events in a single trip. As has been the tradition, the workshop was a fully public event and open to participants from any organization or institution. The workshop program included four invited speakers: Jacques Lavy (IFP Energies Nouvelle) “PM Sensor Development and Simulation for Diesel Particulate Filter On-Board Diagnostic”; Phil Blakeman (Johnson Matthey) “Catalyzed Exhaust Filters: Future Directions”; Fabio Ribeiro (Purdue University) “Investigations of Ammonia SCR on Cu-Chabazite”; and Mark Crocker (University of Kentucky) “Synergy of LNT and SCR Catalysts in Coupled LNT-SCR Systems”. Besides the invited speakers there were also 27 contributed talks and 12 posters by researchers from industry, universities, and national labs. As illustrated in Figure 1, the oral presentations and poster included a wide range of technical topics, including particulate matter, oxidation catalysts, LNTs, SCR NOx reduction, and emerging and advanced emission control methods such as passive adsorbers. Additional details can be found on the CLEERS website (www.cleers.org) under the 2013 Workshop heading [1].

The industry panel discussion topic at the CLEERS Workshop this year was “Perspectives on the emissions control challenges associated with increasingly lower exhaust temperatures from advanced combustion engines.” This topic was selected to help acquaint the wider CLEERS community with the key technical issues and industry concerns raised earlier in the ACEC Low Temperature Exhaust Workshop [2]. Panel members were: Mike Zammitt (Chrysler), Neal Currier (Cummins), Christine Lambert (Ford), Chang Kim (GM), and Phil Blakeman (Johnson Matthey). Key issues and concerns discussed by the panel members included:

- Additional computational simulation needs arising from specific challenges posed by low-temperature exhaust.



OBD – onboard diagnostics; CPF – catalytic particulate filter; HC – hydrocarbon; P – particulate

FIGURE 1. Distribution of Emission Control Topics in the 2013 CLEERS Workshop Oral Presentations

- What is currently known about the impact of sulfur on low-temperature catalyst activity and durability.
- Comparisons of exhaust reheating with fuel vs. use of electric heat addition to maintain exhaust temperature.
- How industry partners deal with the regulatory acceptance processes and potential commercial risk associated with introducing new aftertreatment materials in their products.
- Summaries of what is known/unknown regarding current oxidation and NOx reduction catalyst performance at exhaust temperatures of 150°C, (including aging effects at high temperatures and currently available passive trap materials).
- Potential onboard generation of H₂ by fuel reforming and subsequent use for low-temperature aftertreatment.

ORNL's collaborations with Sandia National Laboratories (SNL) and Pacific Northwest National Laboratory (PNNL) under CLEERS have continued to transition. After completion of joint publications on LNT modeling and Rich Larson's retirement, no new emission control modeling activities have been initiated at SNL. Discussions are still underway with SNL to identify an appropriate new SNL CLEERS collaborator and research focus. ORNL's collaboration with PNNL has continued to center on the characterization and modeling

of commercial chabazite copper-zeolite SCR catalysts, with a particular emphasis on modeling NH₃ storage and release. This change in focus is in response to both recent experimental and modeling observations at ORNL and PNNL and feedback from our industry partners regarding their concerns for urea-SCR diagnostics and controls. Additional details about the measurement and quantification of NH₃ storage are described in the 2013 CLEERS Kinetics activity annual report. One key result from this work so far has been the recognition that it will probably be necessary to include equilibrium isotherm measurements of NH₃ storage as part of the CLEERS SCR catalyst protocol.

Collaborations with university and industry partners in both the U.S. and Europe continue to be very active. Our European university partners include Petr Koci at the Institute for Chemical Technology in Prague, Louise Olsson at Chalmers University of Technology, and Isabella Nova at Politecnico di Milano. This year ORNL hosted student researchers from both Prague and Milano, who conducted laboratory experiments in the Fuels, Engines, and Emissions Research Center to develop improved kinetic mechanisms for LNT and SCR catalysts. We are also continuing close interactions with Gamma Technologies via sharing of detailed experimental reactor and engine dynamometer data. Gamma is sharing the results of their analyses with us to help improve estimates of key model parameters

and also make improvements to the CLEERS catalyst characterization protocols. Both the improved model parameter estimates and modified protocols are being shared with the CLEERS community in the expanded CLEERS database.

CONCLUSIONS

The results of the 2013 CLEERS Industry Priority Survey confirm that CLEERS is continuing to provide a unique link for technical collaboration among emissions control researchers across industry, national labs, and universities. Mechanisms are now in place to build a much expanded repository of shared, pre-proprietary data as well as reference computational algorithms and modeling components is intended to reduce duplication of effort and more effectively target fundamental research at the national labs and universities. Industry feedback to CLEERS researchers at national labs is providing a critical, fast-response mechanism to help redirect activities and maximize the commercial relevance of R&D efforts at DOE labs. CLEERS is also providing DOE with key information needed for strategic planning. The important role for CLEERS in facilitating new directions has been exemplified this year by CLEERS' support of the U.S. DRIVE ACEC Team in identifying and prioritizing new R&D directions for emissions controls of advanced, high-efficiency combustion engines with low-temperature exhaust. Participation by industry, labs, and universities in the CLEERS public workshops and technical focus meetings continues to be very high.

REFERENCES

1. 2013 (16th) CLEERS Workshop agenda and presentations at <http://www.cleers.org>.
2. "Future Automotive Aftertreatment Solutions: The 150°C Challenge Workshop Report," ACEC Low Temperature Aftertreatment Group, Michael Zammit and Craig DiMaggio(Chrysler), Chang Kim(GM), Christine Lambert(Ford), George Muntean(PNNL), Chuck Peden(PNNL), Jim Parks(ORNL), Ken Howden(DOE), draft under review.

FY 2013 PUBLICATIONS/PRESENTATIONS

1. CLEERS 2013 Workshop presentation: "Global Kinetic SCR Model with Two Ammonia Adsorption Sites," by Mark Stewart, PNNL, April 10–12, 2013.
2. SAE 2013-01-1578, "1D Model of a Copper Exchanged Small Pore Zeolite Catalyst Based on Transient SCR Protocol," M. Devarakonda, J. Lee, G. Muntean, G., J. Pihl, and S. Daw.
3. "Summary of the 2013 CLEERS Workshop," Jim Parks and Stuart Daw, Presentation to Advanced Combustion Engine and Emissions Control Tech Team, USCAR, May 9, 2013.
4. "CLEERS Updates to the DOE Advanced Engine Crosscut Team," C.S. Daw, W. Li, and R. Blint, January, 10, 2013; March 14, 2013; May 9, 2013; July 18, 2012; and September 12, 2013 (limited distribution).
5. "CLEERS Coordination & Joint Development of Benchmark Kinetics for LNT & SCR," Josh Pihl et al, 2013 DOE Hydrogen Program and Vehicle Technologies Annual Merit Review, Washington DC, May 13–17, 2013.
6. Šárka Bártová, Petr Kočí, David Mráček, Miloš Marek, Josh A. Pihl, Jae-Soon Choi, Todd J. Toops, William P. Partridge, "New Insights on N₂O Formation Pathways during Lean/Rich Cycling of a Commercial Lean NO_x Trap Catalyst", Catalysis Today, submitted.
7. Jae-Soon Choi, Josh A. Pihl, Todd J. Toops, William P. Partridge, Petr Kočí, Šárka Bártová, Miloš Marek, "Factors Controlling N₂O Formation during Lean/Rich Cycling of Lean NOx Trap Catalysts," presentation to the 9th World Congress of Chemical Engineering, Seoul, Korea, August 20, 2013.
8. David Mráček, Sarka Bartova, Peter Koci, Milos Marek, Jae-Soon Choi, Josh A. Pihl, C. Stuart Daw, and William P. Partridge, Jr., "N₂O Formation During Lean NOx Trap (LNT) Catalyst Regeneration," Presentation at the Southeastern Catalysis Society, Asheville, NC, September 29–30, 2013.
9. "2013 CLEERS Industry Priorities Survey Final Report," C.S. Daw, September 9, 2013, draft under review.

III.2 Cross-Cut Lean Exhaust Emissions Reduction Simulations (CLEERS): Joint Development of Benchmark Kinetics

Stuart Daw (Primary Contact), Josh Pihl,
Jae-Soon Choi, Bill Partridge, Mi-Young Kim,
Todd Toops
Oak Ridge National Laboratory (ORNL)
2360 Cherahala Blvd.
Knoxville, TN 37932-1563

DOE Technology Development Manager:
Ken Howden

- Identify chemical processes leading to N_2O formation during low-temperature LNT regeneration.
- Measure NOx reduction kinetics and ammonia storage on a commercial zeolite selective catalytic reduction (SCR) catalyst at exhaust temperatures between 150 and 200°C.
- Develop measurement and modeling strategies that capture the impacts of hydrothermal aging on the NH_3 storage capacity of a commercial zeolite SCR catalyst.

Overall Objectives

- Collaborate with the Pacific Northwest National Laboratory (PNNL) to support industry in the development of accurate simulation tools for the design of catalytic emissions control systems that enable advanced high-efficiency combustion engines to meet emissions regulations while maximizing fuel efficiency; specifically:
 - Identify reaction mechanisms occurring over catalytic devices under relevant operating conditions.
 - Develop modeling strategies that represent key catalyst processes in a computationally efficient manner.
 - Generate benchmark data sets for use in model calibration and validation.
 - Measure critical device parameters needed for model development.
- Disseminate mechanistic insights, modeling strategies, benchmark data sets, and representative device parameters through the CLEERS website, CLEERS focus group teleconferences, and CLEERS workshops.
- Utilize results from fundamental research to develop new approaches for advanced emissions control systems (e.g., with enhanced low-temperature function).

Fiscal Year (FY) 2013 Objectives

- Benchmark performance of the BMW gasoline direct injection (GDI) lean-oxides of nitrogen (NOx) trap (LNT) catalyst and provide data to modeling partners.

FY 2013 Accomplishments

- Completed detailed flow reactor characterization of the BMW GDI LNT catalyst. Shared data sets with modeling partners at Gamma Technologies, Inc. and ICT Prague.
- Demonstrated that NO oxidation to NO_2 does not play a role in the reaction mechanism for NO SCR by NH_3 . Developed a new NO oxidation mechanism consistent with reaction kinetics measurements and observed surface adsorbates (collaboration with Professors Tronconi and Nova at Politecnico di Milano).
- Investigated N_2O formation during low-temperature regeneration of LNT catalysts. Identified mechanistic steps that account for observed LNT N_2O trends (collaboration with Dr. Koci at ICT Prague).
- Evaluated changes in SCR catalyst model parameters required to capture impacts of aging on catalyst functionality (collaboration with PNNL).
- Developed experimental protocols and analysis techniques for direct measurement of NH_3 adsorption enthalpy as a function of coverage on zeolite SCR catalysts. Determined that a commercial copper zeolite SCR catalyst has two distinct NH_3 storage sites with adsorption enthalpies of 85 and 30 kJ/mol.

Future Directions

- Develop a reaction mechanism for NO SCR by NH_3 over small pore Cu zeolite SCR catalysts that is consistent with experimental observations (collaboration with Politecnico di Milano).
- Determine chemical processes responsible for N_2O formation during low-temperature LNT regeneration

and incorporate into a model (collaboration with ICT Prague).

- Quantify impacts of hydrothermal aging on energetics of NH₃ adsorption for a commercial Cu zeolite SCR catalyst. Identify strategies for adjusting model parameters to account for aging (collaboration with PNNL).
- Develop an experimental protocol for measuring the key properties of hydrocarbon adsorbers required for model calibration.



INTRODUCTION

Catalytic emissions control devices will play a critical role in deployment of advanced high-efficiency engine systems by enabling compliance with increasingly stringent emissions regulations. High-efficiency diesel and lean gasoline engines, for example, will require NOx reduction catalysts with very high conversion efficiencies to meet the Environmental Protection Agency Tier 3 NOx emissions standard. Low-temperature combustion strategies (such as Reactivity Controlled Compression Ignition and partially premixed combustion), on the other hand, significantly reduce engine-out NOx, but they generate a challenging combination of high hydrocarbon concentrations at low exhaust temperatures that will likely demand novel approaches to emissions control. Design of progressively more complex engine/aftertreatment systems will increasingly rely on the use of advanced simulation tools to ensure that next generation vehicles maximize efficiency while still meeting emissions standards. These simulation tools will, in turn, require accurate, robust, and computationally efficient component models for emissions control devices. Recognizing this need, the DOE Diesel Crosscut Team initiated the CLEERS activity to support the development of improved computational tools and data for simulating realistic full-system performance of lean-burn engines and associated emissions control systems.

APPROACH

ORNL is involved in two separate DOE-funded tasks supporting CLEERS: overall administrative support, and joint development of benchmark aftertreatment kinetics. Under the second activity, which is covered by this report, ORNL works closely with PNNL to support the development of accurate simulation tools for the design of catalytic emissions control systems that enable advanced high-efficiency combustion engines to meet emissions regulations while maximizing fuel efficiency. Specific activities include: identification of reaction mechanisms

that govern the performance of catalytic emission control devices under relevant operating conditions; development of modeling strategies that represent key catalyst processes in a computationally efficient manner; generation of benchmark data sets for model calibration and validation; and measurement of critical device parameters needed for model development. The resulting mechanistic insights, modeling strategies, benchmark data sets, and representative device parameters are disseminated through the CLEERS website, during monthly CLEERS focus group teleconferences, at the annual CLEERS workshop, and through publications and presentations. Research directions are guided by the DOE Advanced Engine Crosscut Team, which collectively oversees CLEERS, and by regular CLEERS industry participant priority surveys. ORNL's CLEERS research activities have focused primarily on approaches to NOx reduction in lean exhaust such as LNTs and urea SCR.

RESULTS

During FY 2013, ORNL completed benchmark evaluation of a commercial LNT formulation from a model year 2009 BMW 120i equipped with a lean GDI engine. The BMW LNT was obtained based on industry recommendations to replace the prior CLEERS "reference" LNT formulation, which had been the focus of CLEERS-related LNT research since 2005. There were two primary goals for the benchmarking process: (1) to compare the performance and properties of the new BMW LNT to the prior CLEERS reference formulation, and (2) to provide flow reactor data sets for model calibration and validation.

Figure 1 compares the NOx reduction performance and byproduct (NH₃ and N₂O) selectivity of the two LNT formulations as a function of temperature for three different reductants: H₂, CO, and C₃H₆. The newer BMW LNT has better high-temperature NOx conversion (Figure 1-a), increasing the effective operating window by 50°C. The BMW LNT also shows slightly better low-temperature NOx conversion with H₂ as the reductant. NH₃ generation persists to higher temperatures with the BMW LNT (Figure 1-b), but may be a consequence of the experimental protocol, which held the reductant composition and cycle times fixed for both LNTs, even though the BMW LNT contained less oxygen storage capacity. As a result, the BMW LNT was relatively over-regenerated, increasing NH₃ yield. The maximum N₂O yield is quite similar between the two formulations (Figure 1-c). Taking all the observations together, the overall trends in NOx conversion performance and selectivity are rather similar, implying that the findings from prior CLEERS-related research regarding surface chemistry, reaction mechanisms, and modeling strategies for the old reference LNT material are still relevant

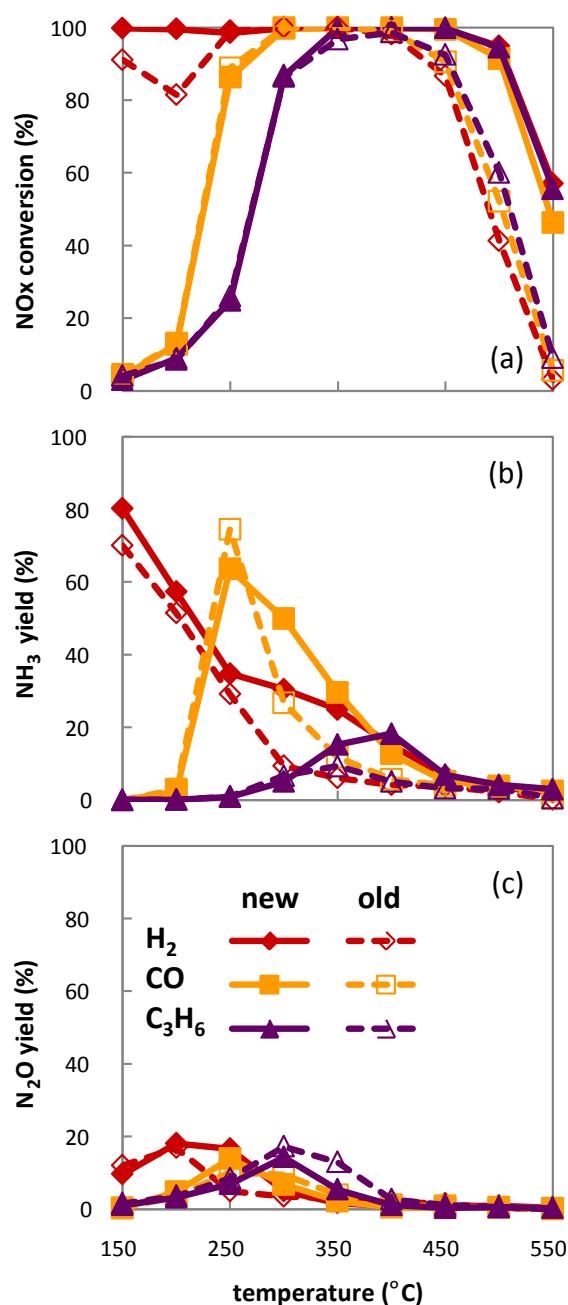


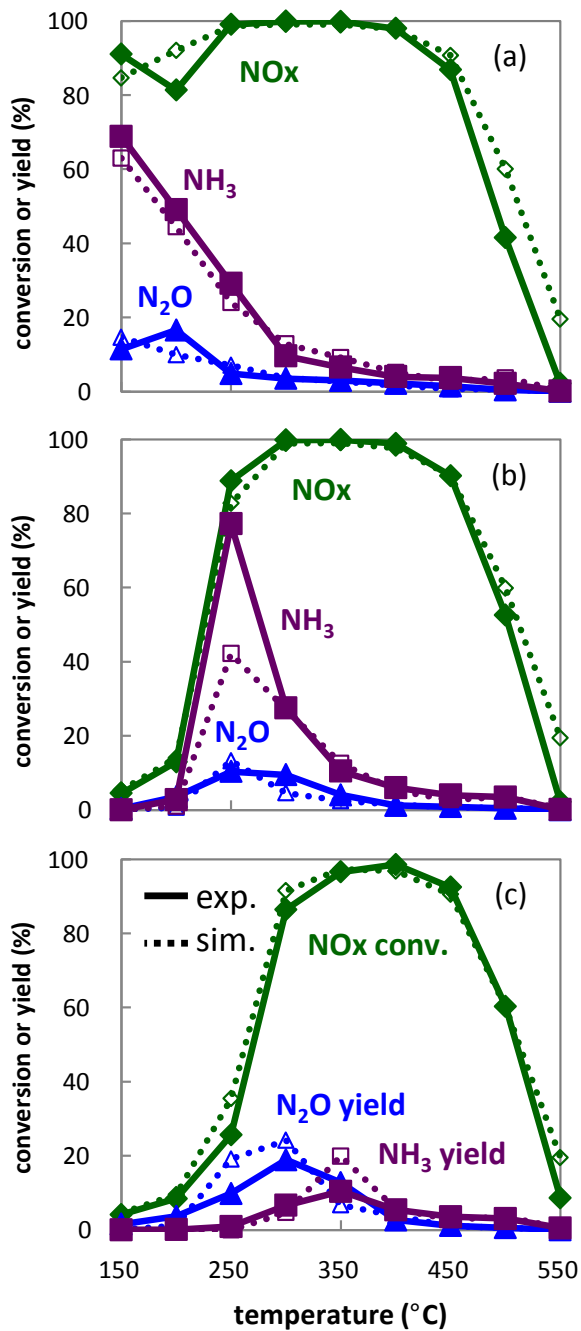
FIGURE 1. Flow reactor measurements of cycle averaged (a) NO_x conversion, (b) NH₃ yield, and (c) N₂O yield as functions of temperature and reductant composition for degreened samples of the new BMW LNT formulation (solid lines and filled symbols) and the old CLEERS reference LNT material (dashed lines and open symbols). Reactor operating conditions were: gas hourly space velocity 30,000 hr⁻¹; 60 s lean: 300 ppm NO, 10% O₂; 5 s rich: 3.4% H₂ (red diamonds) or 3.4% CO (orange squares) or 0.38% C₃H₆; both: 5% H₂O, 5% CO₂, balance N₂.

to newer catalyst formulations. The benchmark data sets have been shared with modeling collaborators at Gamma Technologies, Inc. and ICT Prague, who have recalibrated their LNT models to reflect the properties

and performance of the newer BMW LNT formulation. The data will also be posted on the CLEERS website.

Due to its potency as a greenhouse gas, N₂O will be included in upcoming emissions regulations. One of the challenges facing designers of emissions control systems is to develop component architectures and control strategies that can minimize N₂O formation while maintaining high NO_x reduction activity. This is particularly true for LNTs, that can have relatively high N₂O yields at low temperature (Figure 1-c). Therefore, it is critical that LNT simulation tools accurately capture N₂O formation. ORNL has been working closely with collaborators at ICT Prague to unravel the complex surface chemistry that drives N₂O selectivity. Detailed flow reactor investigations have revealed two distinct N₂O production processes. The primary N₂O peak occurs near the transition from lean to rich operating conditions at the beginning of the catalyst regeneration process and is largest at temperatures near the light off for a given formulation and reductant species. The secondary, somewhat smaller, N₂O peak occurs immediately after the transition from rich back to lean conditions at the end of the regeneration. ORNL and ICT Prague have proposed that the primary N₂O peak is primarily dependent on the redox state of the platinum group metal (PGM) LNT components. Fully reduced PGM surfaces are very effective at generating N₂ and NH₃ from stored NO_x species. However, if the PGM surfaces are not fully reduced, such as at very early regeneration times or at low temperatures near catalyst light off, there is a higher probability that an adsorbed N adatom will recombine with an adsorbed NO, forming N₂O. Our collaborators at ICT Prague incorporated PGM redox state into their LNT model, resulting in very good agreement between predicted and measured product selectivities over a wide temperature range for the older LNT catalyst with all three of the reductants investigated (Figure 2). Investigations into the source of the secondary N₂O peak continue.

As demonstrated above for the LNT catalyst, a thorough understanding of the rate limiting steps on the catalyst enables development of higher fidelity simulation tools. In the case of small-pore copper zeolite NO_x SCR catalysts, the controlling reaction mechanisms are still not well understood, even though these materials are already commercially applied in urea SCR systems. To overcome this knowledge gap, ORNL is collaborating with researchers at Politecnico di Milano (PoliMi) to investigate the detailed chemistry during NH₃ SCR of NO and to propose revised reaction mechanisms that account for experimental observations. It has been widely assumed that the mechanism for NO SCR by NH₃ begins with NO oxidation to NO₂; the resulting NO₂ opens up the so-called “fast SCR” pathway, which involves equal



amounts of NO and NO₂ and likely proceeds through decomposition of an ammonium nitrite intermediate. While this pathway has an appealing simplicity, the kinetics of the NO oxidation and NO SCR processes are very different.

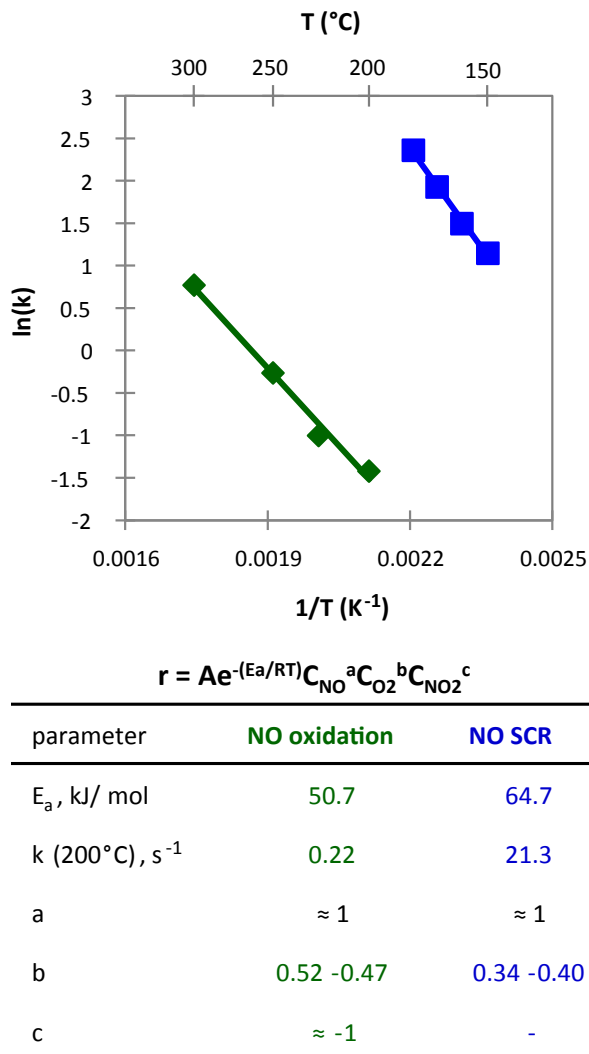


FIGURE 3. Arrhenius plot and power law rate expression parameters for NO oxidation and NO SCR over a commercial copper-exchanged small-pore zeolite.

Figure 3 illustrates an Arrhenius plot of the measured rate constants for NO oxidation and NO SCR as well as parameters for a simple power law kinetic expression that were fit to experimental data. Compared to NO SCR, NO oxidation has a significantly lower activation energy, a different dependence on oxygen concentration, and a rate that is two orders of magnitude lower. Furthermore, NO oxidation is strongly inhibited by the presence of H₂O, while NO SCR is not. These differences in kinetics are inconsistent with the assumption that NO oxidation to NO₂ is the rate determining step in the NO SCR mechanism. ORNL and PoliMi have conducted diffuse reflectance infrared Fourier-transform spectroscopy experiments to study the surface chemistry during NO oxidation, and have developed a new NO oxidation mechanism consistent

with observed surface intermediates and kinetic measurements. Development of an alternative NO SCR mechanism is ongoing. Both mechanisms will be published in the coming fiscal year.

Another key knowledge gap regarding small-pore copper zeolite SCR catalysts revolves around modeling NH₃ storage and release. Respondents to a recent survey of CLEERS industry participants indicated that this issue should be the highest priority focus of CLEERS research activities related to catalytic NOx control. Over the past fiscal year, ORNL worked closely with partners at PNNL to determine how urea SCR model parameters can be adjusted to reflect changes in catalyst properties over the vehicle lifetime, with a particular emphasis on the impact of aging on NH₃ storage. These efforts revealed that direct fitting of models accounting for storage capacity, adsorption energetics and rates, and mass transport to transient experimental measurements of NH₃ storage and release over zeolite SCR catalysts tends to generate ambiguous, non-unique estimates for the parameter values. This is because of the large number of parameters involved and the fact that, in transient experiments, there is a strong coupling among these different processes. Using parameter estimates generated this way produces predictions that are not robust to changes in operating conditions (i.e., they fail to extrapolate well).

To avoid these complications, ORNL developed a new strategy for measuring the energetics of the NH₃ adsorption process that relies on equilibrium isotherm measurements (illustrated in Figure 4-a), thereby eliminating kinetic and mass transport effects. Through straightforward thermodynamic analysis (using the Clausius-Clayperon equation), these isotherms can be used to calculate the NH₃ adsorption enthalpy as a function of NH₃ coverage (shown in Figure 4-b). In addition to providing key parameters for NH₃ storage models, a quantitative measure of NH₃ adsorption enthalpy yields insights into the NH₃ storage functionality of the catalyst, and therefore can direct the development of appropriate modeling approaches. For example, the commercial small-pore copper zeolite catalyst analyzed in Figure 4 appears to have two distinct NH₃ storage sites, with adsorption enthalpies of 85 and 30 kJ/mol. Future efforts will focus on how the NH₃ adsorption enthalpy changes with aging.

CONCLUSIONS

- Benchmark characterization of the BMW LNT catalyst has been completed. Compared to the prior CLEERS reference LNT formulation, the BMW LNT has better high-temperature NOx conversion performance, but general trends in activity and product selectivity are similar for the two catalysts.

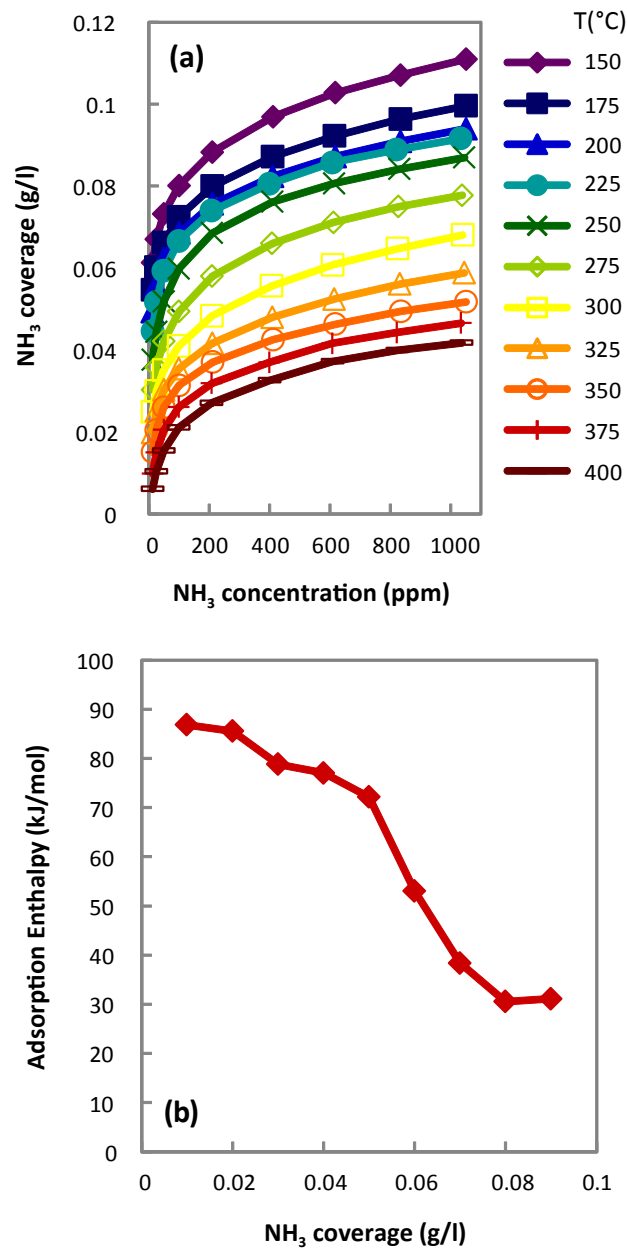


FIGURE 4. (a) Equilibrium NH₃ storage isotherms and (b) NH₃ adsorption enthalpy as a function of NH₃ coverage over a commercial copper-exchanged small-pore zeolite.

Findings from prior work on the older formulation still appear to be relevant for newer materials.

- N₂O formation during regeneration of LNTs occurs through two distinct pathways. The primary N₂O peak is due to incomplete reduction of the PGM catalyst components at low temperatures and early regeneration times. A model that accounts for PGM redox state yields excellent agreement with measured product selectivities. The chemistry that leads to the secondary N₂O peak is under investigation.

- NO SCR by NH₃ does not proceed through NO oxidation to NO₂, followed by fast SCR. A new mechanism for NO oxidation that is consistent with experimental observations has been developed. Work continues on a new NO SCR mechanism.
- Traditional experimental protocols for measuring NH₃ storage capacity generate complicated data sets that convolve thermodynamics, kinetics, and transport. Models calibrated from these data sets are not robust to extrapolation. A new strategy for measuring NH₃ storage capacities through equilibrium isotherms has been developed. Thermodynamic analysis of the resulting data sets yields direct calculations of NH₃ adsorption enthalpies. A commercial small-pore copper zeolite SCR catalyst analyzed with these methods has two distinct NH₃ storage sites with adsorption enthalpies of 85 and 30 kJ/mol.

FY 2013 PUBLICATIONS/PRESENTATIONS

1. Petr Kočí, Šárka Bártová, David Mráček, Miloš Marek, Jae-Soon Choi, Mi-Young Kim, Josh A. Pihl, William P. Partridge (2013). "Effective Model for Prediction of N₂O and NH₃ Formation During the Regeneration of NO_x Storage Catalyst," Topics in Catalysis 56, 118-124; doi: 10.1007/s11244-013-9939-y.
2. Mi-Young Kim, Jae-Soon Choi, Todd J. Toops, Eun-Suk Jeong, Sang-Wook Han, Viviane Schwartz, Jihua Chen, "Coating SiO₂ support with TiO₂ or ZrO₂ and effects on structure and CO oxidation performance of Pt catalysts", Catalysts 3 (2013) 88-103.
3. Šárka Bártová, Petr Kočí, David Mráček, Miloš Marek, Josh A. Pihl, Jae-Soon Choi, Todd J. Toops, William P. Partridge, "New Insights on N₂O Formation Pathways during Lean/Rich Cycling of a Commercial Lean NO_x Trap Catalyst", Catalysis Today, submitted.
4. Yaying Ji, Todd. J. Toops, Mark Crocker, "Isocyanate formation and reactivity on a Ba-based LNT catalyst studied by DRIFTS", Applied Catalysis B: Environmental 140-141 (2013) 265-275.
5. Xiaobo Song, Gordon Parker, John H. Johnson, Jeffrey D. Naber, Harsha Surenhalli, Josh A. Pihl, "Modeling Study of a Cu-zeolite SCR based on spatially resolved measurements and NH₃ storage distributions," Ind. Eng. Chem. Res., submitted, 2013.
6. Xiaobo Song, Gordon Parker, John H. Johnson, Jeffrey D. Naber, Josh A. Pihl, "A Modeling Study of SCR Reaction Kinetics from Reactor Experiments," SAE Technical Paper Series 2013-01-1576, 2013; doi:10.4271/2013-01-1576.
7. Maruthi Devarakonda, John Lee, George Muntean, Josh Pihl, Stuart Daw, "1D Model of a Copper Exchanged Small Pore Zeolite Catalyst Based on Transient SCR Protocol," SAE Technical Paper Series 2013-01-1578, 2013; doi:10.4271/2013-01-1578.
8. Josh Pihl, Jae-Soon Choi, Mi-Young Kim, Bill Partridge, Todd Toops, Stuart Daw, "Joint Development of Benchmark Kinetics for LNT & SCR," presentation to the Vehicle Technologies Office Annual Merit Review, Arlington, VA, May 15, 2013.
9. Mark Stewart, Cameron Hohimer, George Muntean, Ken Rappe, Maruthi Devarakonda, Josh Pihl, Stuart Daw, "Global Kinetic SCR Model with Two Ammonia Storage Sites," presentation to the 2013 DOE Crosscut Workshop on Lean Emissions Reduction Simulation, Dearborn, MI, April 12, 2013.
10. Dominik Artukovic, Dick Blint, Stuart Daw, Ryan Dudgeon, Enrico Pautasso, Josh Pihl, Syed Wahiduzzama, "Development of an LNT reaction mechanism for the BMW 120i LNT catalyst, phase 1: NO_x Adsorption and Oxygen Storage," presentation to the 2013 DOE Crosscut Workshop on Lean Emissions Reduction Simulation, Dearborn, MI, April 12, 2013.
11. Šárka Bártová, David Mráček, Petr Kočí, Miloš Marek, Jae-Soon Choi, Josh A. Pihl, William P. Partridge, Mi-Young Kim, C. Stuart Daw, "Lean NO_x trap regeneration selectivity towards N₂O - similarities and differences between H₂, CO and C₃H₆ reductants", oral presentation at the 18th Directions in Engine-Efficiency and Emissions Research (DEER) Conference, Dearborn, Michigan, October 15–19, 2012.
12. Mi-Young Kim, Jae-Soon Choi, Todd J. Toops, Viviane Schwartz, Jihua Chen, Eun-Suk Jeong, Sang-Wook Han, "Hydrothermally stable, sulfur-tolerant platinum-based oxidation catalysts via surface modification of SiO₂ with TiO₂ and ZrO₂", poster presentation at the 18th Directions in Engine-Efficiency and Emissions Research (DEER) Conference, Dearborn, Michigan, October 15–19, 2012.
13. Sarka Bartova, Petr Koci, Milos Marek, Josh A. Pihl, Jae-Soon Choi, Todd J. Toops, William P. Partridge, Jr., "New Insights on N₂O Formation Pathways during Lean/Rich Cycling of a Commercial Lean NO_x Trap Catalyst," presentation to the 23rd North American Catalysis Society Meeting, Louisville, KY, June 5, 2013.
14. Maria Pia Ruggeri, Isabella Nova, Enrico Tronconi, Josh A. Pihl, Jae-Soon Choi, Todd J. Toops, William P. Partridge, Jr., "Role of NO Oxidation to NO₂ in NH₃-SCR Reactions: Kinetics and Mechanism," poster presentation to the 23rd North American Catalysis Society Meeting, Louisville, KY, June 3, 2013.
15. Jae-Soon Choi, Josh A. Pihl, Todd J. Toops, William P. Partridge, Petr Kočí, Šárka Bártová, Miloš Marek, "Factors Controlling N₂O Formation during Lean/Rich Cycling of Lean NO_x Trap Catalysts," presentation to the 9th World Congress of Chemical Engineering, Seoul, Korea, August 20, 2013.
16. William P. Partridge, Jr., Josh A. Pihl, Mi-Young Kim, C. Stuart Daw, Xavier P. Auveray, Louise Olsson, Jae-Soon Choi, Krishna Kamasamudram, Alex Yezerski, Neal Currier, "Understanding NH₃ Coverage Distributions based on the Common Intra-Catalyst Nature of Model & Commercial SCR Catalysts," presentation to the 9th World Congress of Chemical Engineering, Seoul, South Korea, August 18, 2013.

- 17.** David Mráček, Šárka Bártová, Petr Kočí, Miloš Marek, Jae-Soo Choi, Josh A. Pihl, C. Stuart Daw, William P. Partridge, “N₂O Formation During Lean NOx Trap (LNT) Catalyst Regeneration,” presentation to the Southeastern Catalysis Society, Asheville, NC, September 30, 2013.

III.3 CLEERS Aftertreatment Modeling and Analysis

George Muntean (Primary Contact), Feng Gao,
Chuck Peden, Mark Stewart, Ken Rappe,
Janos Szanyi, Jerry Birnbaum

Institute for Integrated Catalysis
Pacific Northwest National Laboratory (PNNL)
902 Battelle Boulevard
Richland, WA 99352

DOE Technology Development Manager:
Ken Howden

Overall Objectives

- Promote the development of improved computational tools for simulating realistic full-system performance of lean-burn engines and the associated emissions control systems
- Provide the practical and scientific understanding and analytical base required to enable the development of efficient, commercially viable emissions control solutions for ultra high efficiency vehicles

Fiscal Year (FY) 2013 Objectives

- Lead and contribute to the Cross-Cut Lean Exhaust Emissions Reduction Simulations (CLEERS) activities, e.g., lead technical discussions, invite distinguished speakers, and maintain an open dialogue on modeling issues
- Continue detailed kinetic and mechanistic studies for NO reduction over the state-of-the-art small-pore zeolite-based Cu selective catalytic reduction (SCR) catalysts
- Continue fundamental studies of novel high-temperature lean-oxides of nitrogen (NOx) trap (LNT) formulations
- Characterize current production and advanced diesel particulate filter (DPF) substrates through advanced image and statistical analysis of high resolution Computed Tomography (CT) data and extend these studies to include DPFs coated with SCR catalysts for integrated DPF/SCR systems
- Develop and validate SCR aging models based on CLEERS transient protocol data

FY 2013 Accomplishments

- Identified an important reaction intermediate for NH₃ SCR with small-pore zeolite-based Cu SCR catalysts. A publication on these results was highlighted in the journal, *Science*, and in the ACS magazine, *Chemical and Engineering News*.
- Mechanisms for Pt stability on spinel magnesium aluminate support materials in LNTs were determined.
- Detailed reaction kinetics measurements of NH₃ SCR demonstrated the importance of intra-particle diffusion control for reactivity over a wide temperature range. This result suggests the possibility that small particle zeolites may offer significant advantages for overall performance.
- Proposed two-site SCR global kinetics model that includes NH₃ oxidation, NO oxidation, and the standard SCR reaction and provides a simple means of representing performance changes due to aging of the copper chabazite zeolite (Cu-CHA) catalyst.
- Obtained and analyzed four extensive sets of micro X-ray CT data for a bare high-porosity filter substrate and for the same substrate commercially coated with three different loadings of a Cu-CHA SCR catalyst for integrated filtration and NO_x abatement functionality.

Future Directions

- Continue detailed kinetic and mechanistic studies for NO reduction over the state-of-the-art small-pore zeolite-based Cu SCR catalysts. A new focus for these studies will be small-pore Fe SCR catalysts, which provide considerable advantages for high-temperature performance over Cu-based catalysts.
- Complete studies of K-based LNT catalysts in this coming year with a focus on properties of spinel magnesium aluminate supports.
- Characterize current production and advanced DPF substrates through advanced image and statistical analysis of high resolution CT data and extend these studies to include DPFs coated with SCR catalysts for integrated DPF/SCR systems.
- Attempt to extend the SCR global kinetic model to include fast SCR and NO₂ SCR reactions and validate its performance at intermediate aging states.
- Publish the SCR global kinetic modeling methodology and results in a peer-reviewed journal.

- Perform micro-scale flow and transport simulations to assess the accessibility of catalysts in an SCR on filter and effects of catalyst location on backpressure and filtration efficiency.
- Begin preliminary investigations of novel passive NO_x adsorber formulations.



INTRODUCTION

CLEERS is an R&D focus project of the Diesel Cross-Cut Team. The overall objective is to promote the development of improved computational tools for simulating realistic full-system performance of lean-burn engines and the associated emissions control systems. Three fundamental research projects are sponsored at PNNL through CLEERS: DPF, SCR, and LNT. Resources are shared between the three efforts in order to actively respond to current industrial needs.

APPROACH

SCR: Considerable progress has been made in updating SCR kinetics models to accurately describe the performance of state-of-the-art Cu-CHA catalysts. However, a need still exists for accurate yet relatively simple global kinetics models for design of aftertreatment systems. Moreover, systems designers need a simple method to account for changes in performance due to aging over the life of an SCR unit. The global SCR kinetics model for a current Cu-CHA catalyst, which had been previously developed in cooperation with Oak Ridge National Laboratory, was extended in FY 2013 to cover a range of aging states expected to be encountered over the first few years of device deployment. Investigations of SCR catalysts involve the coordinated efforts of modeling, testing and research. In FY 2013 PNNL bolstered its test capability with the development of an automated protocol reactor system (described in the following).

LNT Fundamentals Research: PNNL fundamental studies of possible new LNT formulations able to function at higher temperatures than the current generation of Ba-based materials has focused on changes in the composition of both the NO_x storage and support materials. In particular, substituting K for Ba as the NO_x storage material, and substitution of traditional alumina supports with spinel magnesium aluminate are known to provide higher temperature performance. During FY 2013, we have continued our studies of the effects of LNT catalyst supports and K-loading on the NO_x reduction performance of K- and Ba-based catalysts.

DPF/Multi-Functional Exhaust Filters: Performance of exhaust filters depends upon the detailed structure of the porous filter substrate material. This structure is altered by the addition of catalysts in multi-function filter devices. In FY 2013, automated methods were developed for analyzing the three-dimensional pore networks in exhaust filters using high-resolution X-Ray CT data and image processing techniques similar to those employed in machine vision applications.

RESULTS

SCR Kinetics Model: Reaction kinetics data was gathered at Oak Ridge National Laboratory with fresh and aged samples using the CLEERS transient SCR protocol and temperature programmed desorption (TPD) experiments. The fresh catalysts were removed from actual vehicles and then hydrothermally aged to various degrees, up to a maximum aging state intended to approximate 135,000 miles on a vehicle [1]. The proposed model uses two SCR storage sites to account for observed changes in SCR storage behavior as the catalyst ages. For convenience and simplicity, kinetic parameters for various chemical reactions (including NH₃ oxidation, NO oxidation, and standard SCR) were also associated with the two storage sites. As the catalyst ages, the proportions of the two sites are postulated to change, although the total storage capacity remains nearly constant over the aging states examined. The various kinetic parameters were fit such that a reasonable match was achieved between experiments and model predictions for storage behavior and the extents of the various reactions before and after aging. Figure 1 shows NH₃ release during TPD predicted by the model and observed in experiments for three different aging states.

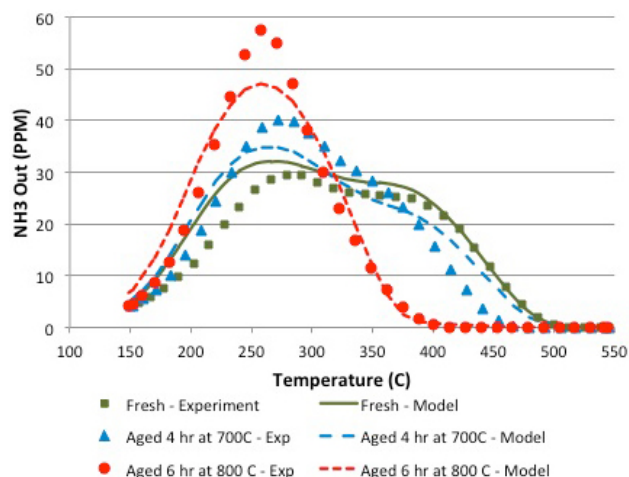


FIGURE 1. NH₃ release from Cu-CHA catalyst during TPD at various aging states.

SCR Protocol Testing: PNNL developed a laboratory-based steady-state test bench capability in support of SCR model development activities with applicability to a wide range of reactive processes. The test bench includes electronically controlled mass flow controllers for accurate exhaust simulation, integrated water vaporizer for accurate humidification, various heated zones for exhaust pre-heating and accurate catalyst thermal control, and heated Fourier transform infrared and chemiluminescent analytical capabilities for accurate and reproducible analyses of reactive exhaust species that avoids problematic condensable species. The test bench can accept catalyst core dimensions of varying diameters and lengths to make standardized comparisons to collaborator test capabilities easily.

The test bench is equipped with the capacity to autonomously execute a multi-step test sequence of varying temperature, space velocity and simulated exhaust concentration make-up. Through programming, the test bench can automatically track complex sets of user-defined reactive and adsorptive/desorptive processes for generating high-confidence data sets in support of empirical or modeling studies. The test bench has been demonstrated through successful execution of 12-step CLEERS protocol that supports SCR model development activities through characterization of NH₃ adsorption/desorption properties (capacity and rate), NO oxidation properties, and standard, fast, and NO₂-only SCR reactive processes. The test capability is expected to support catalyst development and characterization activities in support of low-temperature exhaust after-treatment.

SCR Fundamentals Research: During FY 2013, PNNL researchers continued fundamental studies of state-of-the-art small pore Cu chabazite zeolite catalysts with a focus on both the chemical and physical nature of the active Cu site and the mechanism of the SCR reaction. Extensive kinetics studies of the performance of these catalysts and spectroscopic measurements of the Cu-CHA materials under realistic reaction conditions are performed. This work has been documented in a number of publications as listed at the end of this report. Highlight here are results that suggest an especially important reaction intermediate in the NH₃ SCR reaction. The publication describing this work [2] was highlighted in both *Science* and *Chemical and Engineering News* [3,4].

Understanding the mechanisms of catalytic processes requires the identification of reaction centers and key intermediates, both of which are often achieved by the use of spectroscopic characterization tools. This can be straightforward for enzymes because they often possess catalytically active centers with precisely defined coordination environments that are only able

to accommodate intermediates relevant to the specific catalytic process. Via high magnetic field solid state magic angle spinning nuclear magnetic resonance and Fourier transform infrared spectroscopies, recent studies have identified side-on Cu⁺-NO⁺ complexes as the key intermediates in the SCR of NO over Cu-SSZ-13 zeolite catalysts (Figure 2). Analogous species have been observed and characterized in nitrite reductase enzymes, and shown to be the critical intermediates in the formation of N₂ for anaerobic ammonium oxidation reactions. The identification of this key reaction intermediate, combined with the results of prior kinetic studies, allows the proposal of a new reaction mechanism for the selective catalytic reduction of NO with NH₃ under oxygen-rich environments over Cu-SSZ-13 zeolites, a key reaction in automotive emission control [5].

LNT Fundamentals Research: MgAlO_x mixed oxides have been employed as support materials for potassium-based LNTs in high-temperature applications. Effects of support composition, K/Pt loadings, thermal aging and catalyst regeneration on NOx trapping capacity were systematically investigated, and the catalysts carefully characterized by X-ray diffraction, NOx-TPD, electron microscopy (transmission electron microscopy and high angle annular dark field scanning transmission electron microscopy), and in situ X-ray absorption fine structure (CHFP4). The results demonstrate that the MgAlO_x oxide support (Mg/Al = 0.6) exhibits significant advantages over the conventional Al₂O₃-based catalyst, in terms of high temperature NOx trapping ability and thermal stability. First, MgAlOx can better stabilize the stored nitrates in the form of KNO₃, that is crucial for NOx trapping at high temperature. Meanwhile, MgAlOx can prevent irreversible Pt sintering during thermal aging, in

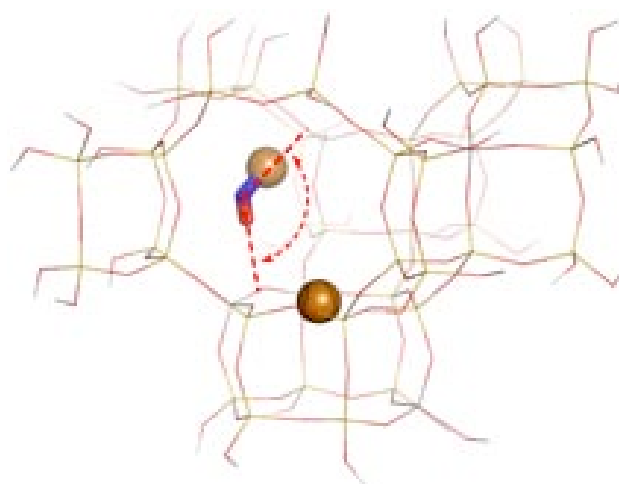


FIGURE 2. Density functional theory-optimized geometry of Cu-SSZ-13 with an additional Cu-NO present.

contrast to the Al_2O_3 -supported catalysts as demonstrated in Figure 3. After regeneration, the MgAlOx catalyst exhibits much better performance in the entire temperature range than the Al_2O_3 catalyst. Additionally, the results of Pt/K loading effects indicate that NO_x trapping is kinetically limited at low temperature, while thermodynamically limited at high temperature.

DPF/Multi-Functional Exhaust Filters: Micro-X-ray CT data were obtained for an advanced high-porosity substrate that had been commercially coated with three different loadings of a current Cu-CHA SCR catalyst to integrate DPF and SCR functionality. Automated techniques were developed to discover where the catalyst is deposited within and upon the porous walls, and which pores remain open to exhaust flow. Figure 4 shows an example cross-section image of the most heavily loaded sample where estimated catalyst locations are shown in black, the cordierite substrate is shown in gray, and

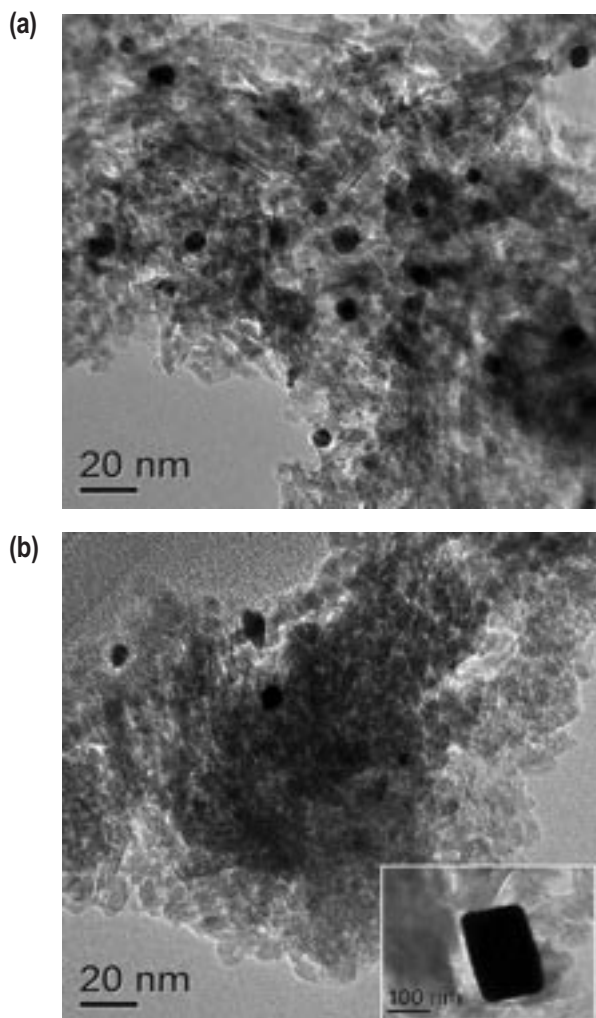


FIGURE 3. (a) TEM images for aged/reduced 10K/Pt/MG30 (b) aged/reduced 10K/Pt/ Al_2O_3 catalysts.

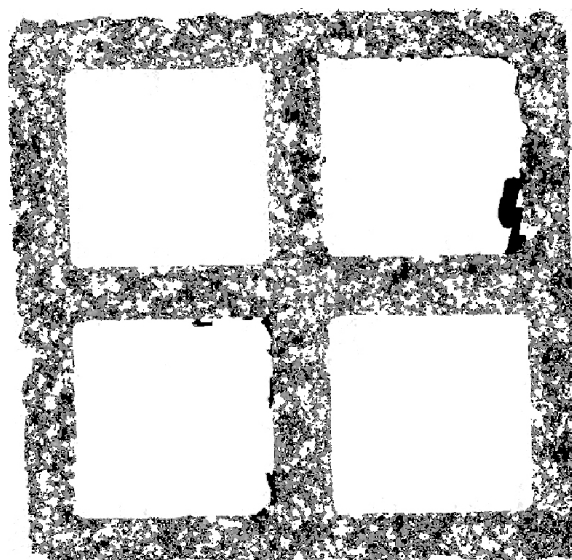


FIGURE 4. Processed micro-X-ray CT cross-section of a catalyst filter sample showing the porous substrate in gray and the catalyst in black.

open pores and channel volume are shown in white. The majority of the catalyst appears to reside inside the porous filter wall, but large lumps and flakes of catalyst can also be seen on the wall surface. In order to remain viable as a filter, the catalyst must be coated in such a way that gas flow paths remain open through the filter wall. It is possible that these flow paths bypass much of the catalyst volume. This analysis could ultimately lead to more efficient use of catalysts in integrated devices as well as improved overall performance.

Having been developed under the CLEERS project, the micro-structural analysis capability for catalyzed samples is now being employed in a new Cooperative Research and Development Agreement effort with Ford to examine additional advanced catalyst/filter combinations for new diesel and gasoline applications.

CONCLUSIONS

- A new reaction intermediate for Cu-CHA catalyzed NH₃ SCR, similar in structure to a species involved in nitrate reduction to N₂ in nitrate reductase enzymes, has been identified.
- Clear advantages of spinel magnesium aluminates as supports for LNTs over traditional alumina have been demonstrated.
- A relatively simple global SCR kinetics model with two ammonia storage sites was able to describe changes in ammonia storage behavior and the extents of various reactions in fresh and hydrothermally aged Cu-CHA catalyst samples.

- Commercial coatings of SCR catalysts in multi-functional filters appear to fill some of the internal pores while leaving some major flow pathways through the filter walls relatively open. At higher loadings, some of the catalyst remains on one surface of the filter wall.

REFERENCES

- Schmieg, S.J., S.H. Oh, C.H. Kim, D.B. Brown, J.H. Lee, C.H.F. Peden, and D.H. Kim, “Thermal durability of Cu-CHA NH₃-SCR catalysts for diesel NOx reduction”, *Catalysis Today*, 2012. 184(1): p. 252-261 DOI: 10.1016/j.cattod.2011.10.034.
- J.H. Kwak, J.H. Lee, S.D. Burton, A.S. Lipton, C.H.F. Peden, J. Szanyi, “A Common Intermediate for N₂ Formation in Enzymes and Zeolites: Side-on Cu-Nitrosyl Complexes”, *Angewandte Chemie International Edition* **52** (2013) 9985-9989.
- J.S. Yeston, “NO Switching Sides on Cu”, *Science* 341 (2013) 1153.
- M. Jacoby, “Pinpointing Intermediates”, *Chemical and Engineering News* 91 (2013) 9.
- J.Y. Luo, F. Gao, A.M. Karim, P. Xu, C.H.F. Peden, in preparation.
- F. Gao (speaker) and C.H.F. Peden, “Cu-CHA SCR Catalysts: Beyond the “Seagull-Shaped” NOx Conversion Curves,” Cummins Symposium on Cu-Based SCR Catalysts, Columbus, IN, June 2013.
- C.H.F. Peden, “Cu-CHA Catalysts for NH₃ Selective Catalytic Reduction of NOx,” 9th World Congress of Chemical Engineering, Seoul, Korea, Republic Of, August 2013.
- C.H.F. Peden, “Some Future Challenges for Catalytic Vehicle Emission Control,” given at the following locations:
 - Heesung Catalyst Corporation, Seoul, South Korea, August 2013;
 - Pohang University of Science and Technology – POSTECH, Pohang, South Korea, August 2013;
 - Ulsan National Institute of Science and Technology – UNIST, Ulsan, South Korea, August 2013.
- C.H.F. Peden, “Microporous Cu-CHA Materials for the Selective Catalytic Reduction of NOx with NH₃: Catalyst Structure/Function and Mechanistic Studies,” Fall ACS National Meeting, Indianapolis, IN, September 2013.
- J. Szanyi, “Spectroscopy Studies on Cu-SSZ-13 NH₃ SCR Catalysts: Mechanistic implications”, 5th International Symposium Advanced Micro and Mesoporous Materials, Golden Sands, Bulgaria, September 2013.
- Stewart, M.L., C. Hohimer, G. Muntean, K. Rappe, M. Devarakonda, J. Pihl, S. Daw. “Global Kinetic SCR Model with Two Ammonia Storage Sites,” DOE CLEERS Workshop, Dearborn, MI, April 2013.

FY 2013 PUBLICATIONS/PRESENTATIONS

Invited Presentations

- C.H.F. Peden, “Cu-SSZ-13 catalysts for the selective catalytic reduction of NOx with NH₃: Catalyst characterization and reaction mechanisms,” 2012 Fall AIChE Meeting, Pittsburgh, PA, October 2012.
- C.H.F. Peden (speaker) and G.G. Muntean, “Scientific and Technical Challenges for Low Temperature Aftertreatment,” Workshop on Future Automotive Aftertreatment Solutions: The 150° Challenge, Southfield, MI, November 2012.
- C.H.F. Peden, “Nano-Materials Science of Next Generation Automobile Emission Control Catalysts,” Western Washington University’s Advanced Materials Science and Engineering Center (AMSEC) “Materials After Dark” Lecture, Bellingham, WA, February 2013.
- C.H.F. Peden, “Cu-CHA catalysts for the selective catalytic reduction of NOx with NH₃: Catalyst structure/function and mechanistic studies,” Spring ACS National Meeting, New Orleans, LA, April 2013.
- G.G. Muntean, “CLEERS Aftertreatment Modeling and Analysis,” DOE Annual Merit Review, May 2013.
- C.H.F. Peden, “New Insights into the Mechanisms of Two Important Catalytic Reactions,” 2013 Annual Spring Symposium of the Michigan Catalysis Society, Dearborn, MI, May 2013.

7. F. Gao (speaker) and C.H.F. Peden, “Cu-CHA SCR Catalysts: Beyond the “Seagull-Shaped” NOx Conversion Curves,” Cummins Symposium on Cu-Based SCR Catalysts, Columbus, IN, June 2013.

8. C.H.F. Peden, “Cu-CHA Catalysts for NH₃ Selective Catalytic Reduction of NOx,” 9th World Congress of Chemical Engineering, Seoul, Korea, Republic Of, August 2013.

9. C.H.F. Peden, “Some Future Challenges for Catalytic Vehicle Emission Control,” given at the following locations:

- Heesung Catalyst Corporation, Seoul, South Korea, August 2013;
- Pohang University of Science and Technology – POSTECH, Pohang, South Korea, August 2013;
- Ulsan National Institute of Science and Technology – UNIST, Ulsan, South Korea, August 2013.

10. C.H.F. Peden, “Microporous Cu-CHA Materials for the Selective Catalytic Reduction of NOx with NH₃: Catalyst Structure/Function and Mechanistic Studies,” Fall ACS National Meeting, Indianapolis, IN, September 2013.

11. J. Szanyi, “Spectroscopy Studies on Cu-SSZ-13 NH₃ SCR Catalysts: Mechanistic implications”, 5th International Symposium Advanced Micro and Mesoporous Materials, Golden Sands, Bulgaria, September 2013.

12. Stewart, M.L., C. Hohimer, G. Muntean, K. Rappe, M. Devarakonda, J. Pihl, S. Daw. “Global Kinetic SCR Model with Two Ammonia Storage Sites,” DOE CLEERS Workshop, Dearborn, MI, April 2013.

Contributed Presentations

- F. Gao, E.D. Walter, E.M. Karp, J.H. Kwak, J. Szanyi, C.H.F. Peden, “Structure-activity relationships in NH₃-SCR over Cu/SSZ-13 as probed by reaction kinetics and EPR,” DOE CLEERS Workshop, Dearborn, MI, April 2013.
- F. Gao, E.D. Walter, E.M. Karp, J.Y. Luo, R.G. Tonkyn, J.H. Kwak, J. Szanyi, C.H.F. Peden, “Structure-activity relationships in NH₃-SCR over Cu/SSZ-13 as probed by reaction kinetics and EPR studies”, 23rd North American Catalysis Society Meeting, Louisville, KY, June 2013.
- J. Szanyi, J.H. Kwak, H. Zhu, C.H.F. Peden, S.D. Burton, A.S. Lipton, “Spectroscopy Studies on Cu-SSZ-13 NH₃ SCR Catalysts: mechanistic implications”, 23rd North American Catalysis Society Meeting, Louisville, KY, June 2013.

Publications

- G.G. Muntean, M. Devarakonda, F. Gao, J.H. Kwak, J.Y. Luo, C.H.F. Peden, M.L. Stewart, J. Szanyi, D. Tran, “CLEERS Aftertreatment Modeling and Analysis,” FY2012 Progress Report for Advanced Combustion Engine Research and Development, pp. III-3 – III-7.
- H. Zhu, J.H. Kwak, C.H.F. Peden, J. Szanyi, “In situ DRIFTS-MS studies on the oxidation of adsorbed NH₃ by NOx over a Cu-SSZ-13 zeolite,” *Catalysis Today* **205** (2013) 16-23.

- 3.** F. Gao, E.D. Walter; E. Karp, J. Luo, R.G. Tonkyn, J.H. Kwak, J. Szanyi, C.H.F. Peden, "Probing Structure-Activity Relationships in NH₃-SCR over Cu-SSZ-13: Reaction Kinetics and EPR Studies," *Journal of Catalysis* **300** (2013) 20-29.
- 4.** X. Wang, J.C. Hanson, J.H. Kwak, J. Szanyi, C.H.F. Peden, "Cation Movements during Dehydration and NO_x Desorption in a Ba-Y,FAU zeolite: an in situ Time-resolved X-ray Diffraction Study," *Journal of Physical Chemistry C* **117** (2013) 3915-3922.
- 5.** J. Szanyi J.H. Kwak, H. Zhu, C.H.F. Peden, "Characterization of Cu-SSZ-13 NH₃ SCR Catalysts: an in situ FTIR Study", *Physical Chemistry Chemical Physics* **15** (2013) 2368-2380.
- 6.** J.H. Kwak, J.H. Lee, S.D. Burton, A.S. Lipton, C.H.F. Peden, J. Szanyi, "A Common Intermediate for N₂ Formation in Enzymes and Zeolites: Side-on Cu-Nitrosyl Complexes", *Angewandte Chemie International Edition* **52** (2013) 9985-9989.
- 7.** F. Gao, J.H. Kwak, J. Szanyi, C.H.F. Peden, "Current Understanding of Cu-exchanged Chabazite Molecular Sieves for use as Commercial Diesel Engine DeNOx Catalysts", *Topics in Catalysis* (2013) in press.
- 8.** Devarakonda, M., J.H. Lee, G. Muntean, S. Daw, and J. Pihl, "1D Model of a Copper Exchanged Small Pore Zeolite Catalyst Based on Transient SCR Protocol". SAE World Congress, 2013. 2013-01-1578.

III.4 Enhanced High- and Low-Temperature Performance of NO_x Reduction Catalyst Materials

Feng Gao, George Muntean, Chuck Peden
(Primary Contact)

Institute for Integrated Catalysis
Pacific Northwest National Laboratory (PNNL)
P.O. Box 999, MS K2-12
Richland, WA 99354

DOE Program Manager: Ken Howden

CRADA Partners:

Neal Currier, Krishna Kamasamudram, Ashok Kumar,
Junhui Li, Randy Stafford, Alex Yezerski,
- Cummins Inc.
Mario Castagnola, Hai-Ying Chen, Howard Hess -
Johnson Matthey

- Continue catalyst characterization of these model high-temperature NSR catalysts with a variety of state-of-the-art methods.
- Comparative studies of the synthesis of model Cu-SAPO-34 CHA-based catalysts for ammonia SCR.
- Initiate performance and thermal durability studies of model Cu-SAPO-34 CHA-based catalysts.

FY 2013 Accomplishments

Two research thrusts continued this year:

- Mechanisms for high- and low-temperature performance stability of CHA-based catalysts (primary activity; focus of this report):
 - Based on prior literature reports, several synthesis efforts were carried out at PNNL to prepare model CHA-based catalysts.
 - Catalysts were characterized before and after incorporation of Cu by X-ray diffraction (XRD), electron paramagnetic resonance and temperature-programmed reduction.
 - Baseline reactivity measurements were performed on these catalysts in preparation for mechanistic studies of high- and low-temperature performance loss.
- Fundamental studies of high-temperature NSR catalysts prepared by PNNL:
 - A variety of model K-titania catalysts were prepared at PNNL based on materials described in the open literature.
 - Detailed studies of the sensitivity to high temperatures (required for desulfation) of these model catalysts were performed this year.

Future Directions

- The primary activities will be focused on the mechanisms for low- and high-temperature performance loss as a function of operation conditions of new generation CHA-based NH₃ SCR catalysts. For these studies, we will utilize the model catalysts prepared via methods studied in this past fiscal year (FY 2013). These fundamental studies will be carried out in conjunction with baseline performance and stability experiments on fully formulated catalysts.

Overall Objectives

Identify approaches to significantly improve both the high- and low-temperature performance, and the stability of the catalytic oxides of nitrogen (NO_x) reduction technologies via a pursuit of a more fundamental understanding of:

- the various roles for the multiple catalytic materials
- the mechanisms for these various roles
- the effects of high temperatures on the performance of these catalyst component materials in their various roles
- mechanisms for higher temperature NO_x storage performance for modified and/or alternative storage materials
- the interactions between the precious metals and the storage materials in both optimum NO_x storage performance and long term stability
- modes of thermal degradation of new generation chabazite zeolite (CHA)-based selective catalytic reduction (SCR) catalysts
- the sulfur adsorption and regeneration mechanisms for NO_x reduction catalyst materials

Fiscal Year (FY) 2013 Objectives

- Initiate studies of the thermal stability and sensitivity to sulfur of model high-temperature NO_x storage and reduction (NSR) catalysts based on K/titania materials.

- Some studies aimed at determining performance limitations, sulfur sensitivity and desulfation behavior of candidate alternative support, and NOx storage materials that provide improved high temperature performance will continue. An overall goal of the work will continue to be to develop a deeper understanding of the mechanisms of NOx storage and reduction activity, and performance degradation of materials that have been reported to show good NSR performance at temperatures considerably higher than BaO/alumina-based materials. We expect studies of K-based high temperature NSR materials to be completed this next year.



INTRODUCTION

Two primary NOx aftertreatment technologies have been recognized as the most promising approaches for meeting stringent NOx emission standards for diesel vehicles within the Environmental Protection Agency's 2007/2010 mandated limits, NSR and NH₃ SCR; both are, in fact, being commercialized for this application. Small pore copper ion exchanged zeolite catalysts with a CHA structure have recently been shown to exhibit both remarkable activity and very high hydrothermal stability in the NH₃ SCR process [1]. The NSR (also known as the lean-NOx trap, LNT, or NOx absorber) technology is based upon the concept of storing NOx as nitrates over storage components, typically barium species, during a lean-burn operation cycle, and then desorbing and subsequently reducing the stored nitrates to N₂ during fuel-rich conditions over a precious metal catalyst [2]. However, in looking forward to 2015 and beyond with expected more stringent regulations, the continued viability of the NSR technology for controlling NOx emissions from lean-burn engines such as diesels will require at least two specific, significant, and inter-related improvements. First, it is important to reduce system costs by, for example, minimizing the precious metal content while maintaining, even improving, performance and long-term stability. A second critical need for future NSR systems, as well as for NH₃ SCR, will be significantly improved high- and low-temperature performance and stability. Furthermore, these critically needed improvements will contribute significantly to minimizing the impacts to fuel economy of incorporating these aftertreatment technologies on lean-burn vehicles. To meet these objectives will require, at a minimum, an improved scientific understanding of the following things:

- the various roles for the precious and coinage metals used in these catalysts

- the mechanisms for these various roles
- the effects of high temperatures on the active metal performance in their various roles
- mechanisms for higher temperature NOx storage performance for modified and/or alternative storage materials
- the interactions between the precious metals and the storage materials in both optimum NOx storage performance and long term stability
- the sulfur adsorption and regeneration mechanisms for NOx reduction materials
- materials degradation mechanisms in CHA-based NH₃ SCR catalysts

The objective of this project is to develop a fundamental understanding of these issues. Model catalysts that are based on literature formulations are the focus of the work being carried out at PNNL. In addition, the performance and stability of more realistic catalysts, supplied by the industrial partners, are being studied in order to provide baseline data for the model catalysts that are, again, based on formulations described in the open literature.

For this short summary, we will briefly highlight results from our recent studies of the stability of candidate K-based high-temperature NSR materials, and comparative studies of methods used to synthesize Cu-SAPO-34 CHA catalysts for NH₃ SCR.

APPROACH

In microcatalytic reactor systems, catalyst performance is evaluated in two separate fixed bed reactors. In the NSR technology, the state of the system is constantly changing so that performance depends on when it is measured. Therefore in studies at PNNL, we obtain NOx removal efficiencies as “Lean conversion (30 minutes)”, that measures NOx removal efficiencies for the first 30 minutes of a lean period that follows multiple lean-rich cycles to insure consistent behavior. We have established a reaction protocol, that evaluates the performance of samples after various thermal aging and sulfation conditions. In this way, we could identify optimum desulfation treatments to rejuvenate catalyst activities.

Based on formulations and synthesis procedures described in the literature, PNNL has prepared model NSR and NH₃ SCR catalysts. Activity and performance stability measurements were performed. State-of-the-art catalyst characterization techniques were utilized to probe the changes in physicochemical properties of the PNNL-prepared model catalyst samples under

deactivating conditions, e.g., thermal aging and SO₂ treatment.

RESULTS

High-Temperature NSR Catalysts Prepared by PNNL

K-loading and thermal stability of model Pt-K/TiO₂ NSR catalysts: To date in this project, we have studied various characteristics of PtK/Al₂O₃ and PtK/MgAl₂O₄ LNT catalysts including the effect of K loading on nitrate formation/decomposition, NO_x storage activity, and durability [3-6]. Due to issues of K morphology stability, we have performed a number of studies on titania-supported K NSR catalysts over the last year. These experiments were inspired by research reports of special stability for this class of NSR catalysts [7]. Although the prior literature described using the potassium titanate, K₂Ti₂O₅, for NO_x storage, we first prepared titania-supported K catalysts via dry impregnation. In this report, we briefly present some of the initial results we obtained for these titania-supported materials. Figure 1A shows NO_x storage performance for catalysts prepared with varying K loading. As we have seen for both alumina and magnesium aluminate supported catalysts, the extent of performance (NO_x adsorption capacity) and the temperature for maximum performance show a strong dependence on K-loading. These catalysts showed quite poor stability, however, as evidenced in Figure 1B. Even after calcination at the relatively modest temperatures of 650°C and 700°C, the best catalyst, containing a loading of 10% K, shows

significant deactivation. Even in this temperature range, XRD results (not shown here) indicate the formation of K-titanates via a solid-state reaction between K and the titania support material. In this next year, we will complete our studies of titania-supported K-based NSR catalysts, including results obtained with the use of crystalline K-titanate materials.

Synthesis and Initial Evaluation of Model Cu-CHA Catalysts at PNNL

SCR catalysts with the best performance (activity, hydrothermal stability, etc.) are CHA materials, with Cu/SSZ-13 and Cu/SAPO-34 being two specific examples [1]. While the synthesis of Cu/SSZ-13 is rather straightforward, Cu/SAPO-34 preparation is significantly more complicated. For example, SAPO-34 is prone to hydrolysis in both acidic and basic solutions; therefore, care must be taken during solution ion exchange [8]. Over the past year or so, we have systematically investigated several commonly used Cu/SAPO-34 preparation methods, including solution ion exchange (IE) and solid state ion exchange (SSIE), and so-called one-pot methods [9,10]. For these studies, we are using SAPO-34 substrates generated with various structure directing agents including tetraethyl ammonium hydroxide, triethyl amine (TEA), diethyl amine, morpholine (MOR), and their mixtures. Reaction studies that include standard NH₃-SCR, and NO and NH₃ oxidation measurements, coupled with various catalyst characterizations, allow us to elucidate the key factors in obtaining highly active and selective catalysts.

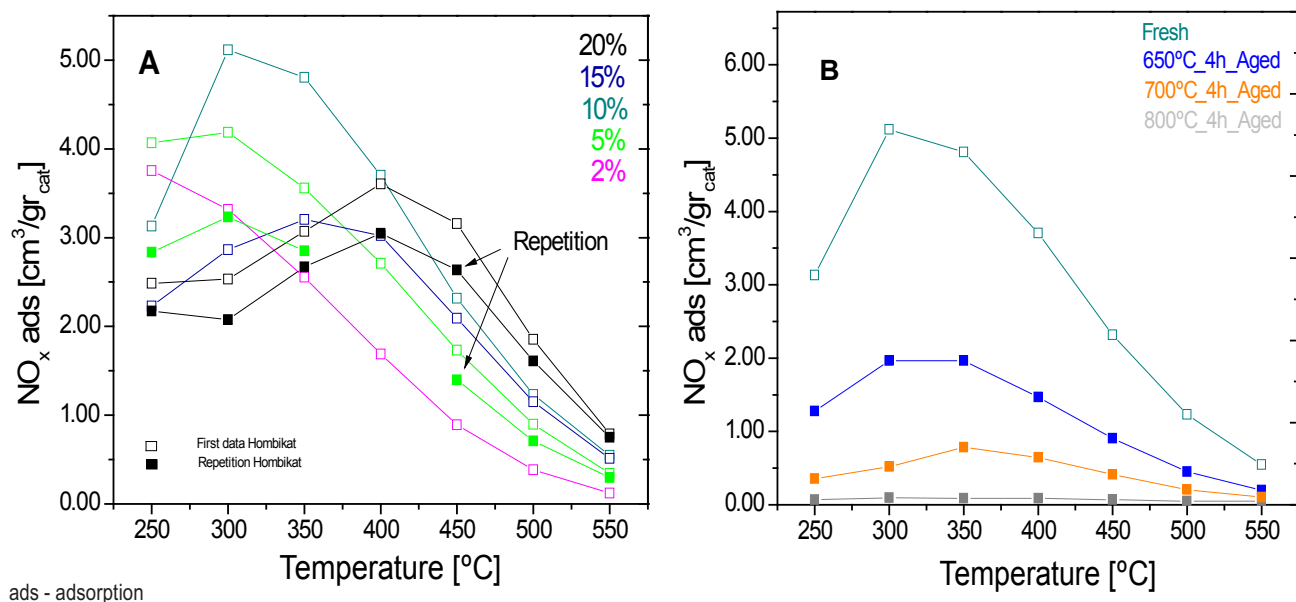


FIGURE 1. Panel A: Amounts of stored NO_x during NO_x storage tests on fresh Pt(1)K(x)/TiO₂, K = 2, 5, 10, 15, 20 w/w%. Panel B: NO_x stored amounts during NO_x storage tests on fresh and aged (at 650°C, 700°C and 800°C for 4 h) Pt(1)K(10)/TiO₂.

Solution IE: Brunauer-Emmett-Teller (BET) and micropore surface areas of the SAPO-34 samples prior to and after IE of Cu were obtained (data not shown) [9]. Interestingly, the extent of irreversible hydrolysis for different SAPO-34 samples was markedly different. The SAPO-34-TEA sample only experienced slight surface area and pore volume drop (~8%). In contrast, the SAPO-34-MOR and SAPO-34-MIX samples decomposed to a significant extent (~60% and ~80% of surface area and pore volume drop, respectively). XRD patterns for the pairs of SAPO-34 and the corresponding Cu-SAPO-34 samples are displayed in Figure 2. While the XRD pattern for SAPO-34-TEA is less-well defined indicating relatively low crystallinity, the other two SAPO-34 samples are highly crystallized. For each SAPO-34 material, the XRD patterns prior to and after ion exchange are fully consistent with the surface area/pore volume measurements. For example, the SAPO-34-TEA sample underwent the least irreversible hydrolysis during IE and, indeed, the XRD patterns are very similar prior to and after IE. On the other hand, the SAPO-34-MOR/MIX samples experienced significant surface area and pore volume loss during IE, and a substantial drop in crystallinity was observed via XRD. A broad feature is also detected between 15° and 30° for the Cu-SAPO-34-MOR/MIX samples clearly indicating the formation of an amorphous phase upon SAPO-34 hydrolysis during

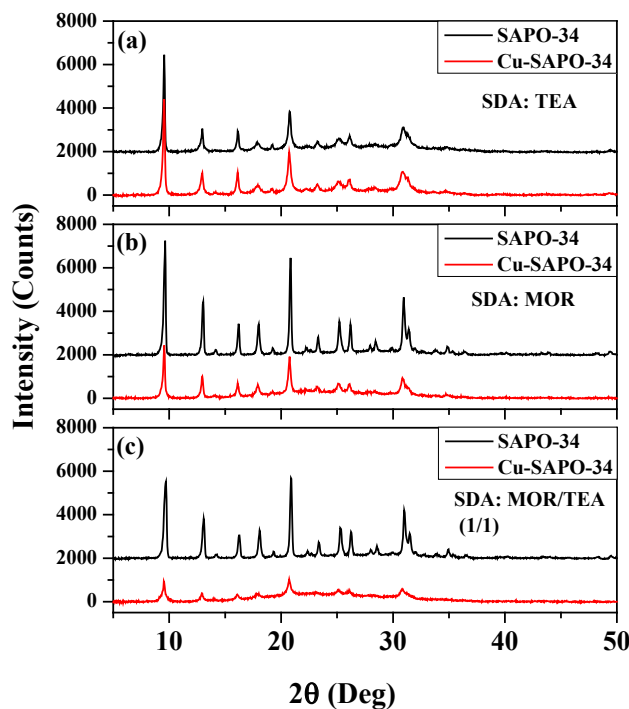


FIGURE 2. XRD patterns for SAPO-34, and Cu-SAPO-34 samples prepared by IE. SAPO-34 samples were formed using (a) TEA, (b) MOR and (c) mixed (MOR/TEA = 1/1) structure directing agents.

IE. As indicated from these results, the best material we obtained via IE, Cu-SAPO-34-TEA, was tested for standard SCR and nonselective NH₃ oxidation. While this catalyst displayed reasonably good activity and stability (data not shown) [9], the presence of some amorphous material after synthesis reduces its utility as a good model catalyst for fundamental studies. As noted above, this situation led us to explore alternative methods for the preparation of Cu-SAPO-34 materials.

SSIE: SSIE was first tested via a high-temperature reaction of mixtures of anhydrous CuCl₂ and SAPO-34 under dry N₂. Likely due to an acidic environment formed by the dissolution of the reaction product, HCl, into residual H₂O, this method led to the complete decomposition of SAPO-34. Instead, we found [10] that reasonably good catalysts could be made by mixing nanosized CuO (Sigma-Aldrich, ~50 nm) with the zeolite and then carrying out a high-temperature calcination (600-800°C for 1-16 hours). As displayed in Figure 3, the Chabazite was quite stable under these conditions and, in fact, samples aged at 700°C for 5 h and at 800°C for 1 h and 5 h actually became more crystalline. However, a weak diffraction feature appeared at 2θ = 21.3° for samples aged at 800°C (due to a tridimite [SiO₂] dense phase), indicating some SAPO-34 decomposition. All samples also gave rise to extremely weak diffraction peaks at 35.4° and 38.0° attributed to CuO, indicating incomplete reaction between SAPO-34 and CuO. Finally, the BET and micropore surface areas and micropore volumes for the samples decreased monotonically as the calcination conditions became more severe. Still, even for samples calcined at 800°C, total surface areas were dominated by micropore surface areas demonstrating the remarkable thermal stability of the SAPO structure, as

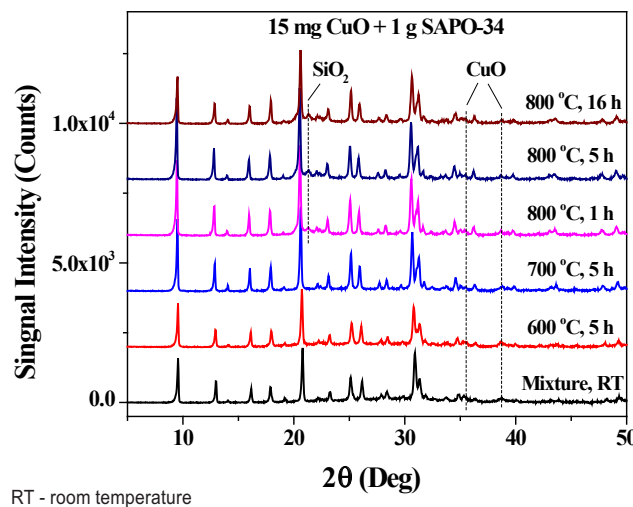


FIGURE 3. XRD patterns of the SAPO-34/CuO physical mixture and the SSIE samples. Calcination conditions are listed adjacent to the XRD patterns.

also evident by the lack of amorphous phase formation. Significantly, this method allowed us to prepare catalysts with varying Cu loading in a relatively straightforward manner. SCR activities for these samples will be shown in the following.

One-Pot Synthesis Methods: For the one-pot synthesis approach, CuSO_4 and CuO (first dissolved in phosphoric acid) were chosen as the Cu sources, and could be added directly at any stage of the zeolite synthesis gel preparation steps. After hydrothermal synthesis at 200°C for 30 h continuously, samples were separated, dried at 120°C, and calcined in air at 600°C for 5 h, or at 800°C for 16 h [10]. XRD patterns for these samples are given in Figure 4, that clearly show that highly crystallized SAPO-34 can still be synthesized in the presence of Cu. The product also showed excellent thermal stability at 800°C where only a very small portion decomposed to give rise to the tridimite phase (marked with an * in the figure). Also especially notable is the absence of CuO diffraction features in these samples. Surface areas and pore volumes of the two calcined samples at 600°C and 800°C (not shown) were quite similar to those of SAPO-34 synthesized without Cu. A possible drawback to this method may be the state of Cu after synthesis and before calcination. Our results [10] indicate that Cu is present as nano-sized CuO highly and very homogeneously dispersed in the CHA zeolite. This Cu needs to be converted to isolated Cu ions via high temperature calcination, a step similar to that used for the SSIE method. If high loadings of Cu are desired, it appears possible that the formed CuO clusters can catalyze SAPO-34 decomposition, thereby limiting the Cu loadings achievable by this method.

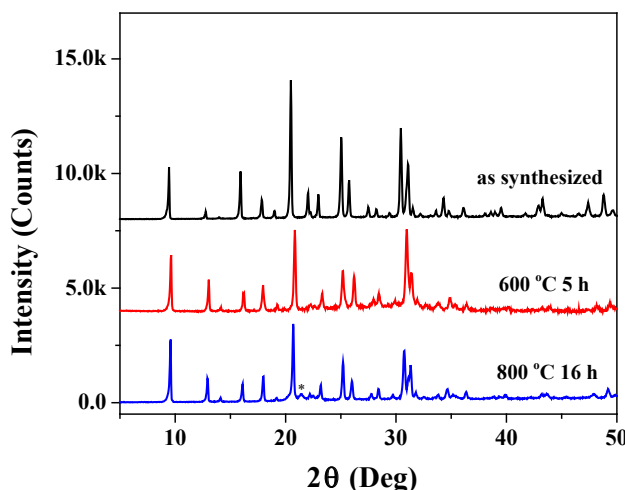


FIGURE 4. XRD patterns for the one-pot samples formed using CuO as a Cu source during gel preparation. The as-synthesized sample (dried, prior to structure directing agent removal) and the calcined samples at 600°C for 5 h, and 800°C for 16 h are displayed.

Standard SCR reactivity of SSIE-prepared catalysts: By simply varying the quantity of nano-sized CuO used for SSIE, CuSAPO34 catalysts with varying Cu loadings were successfully prepared [10]. However, as noted above, full dispersion of all of the precursor CuO was not achieved even after extended times at 800°C. From Figure 5, the use of 30.4 mg of CuO during the synthesis provided the optimum catalyst with reactivity similar to that for CuSSZ13 materials. At lower loadings, the catalysts performed poorly over the entire range of temperatures studied. For the catalyst prepared with 60 mg of CuO, reactivity degraded at temperatures above 500°C due to the early onset of non-selective NH_3 oxidation over a presumably considerable amount of residual CuO [10].

CONCLUSIONS

PNNL and its partners from Cummins Inc., and Johnson Matthey have been carrying out a project aimed at improving the higher temperature performance and stability of candidate NOx reduction technologies.

Results obtained this year demonstrate that titania-supported K-based NSR catalysts have significant issues with respect to thermal stability even though good performance is displayed for the freshly-synthesized catalysts. Recent studies and those to be completed over the next year are focused on the stability of these materials and the mechanisms for performance loss with hydrothermal treatment.

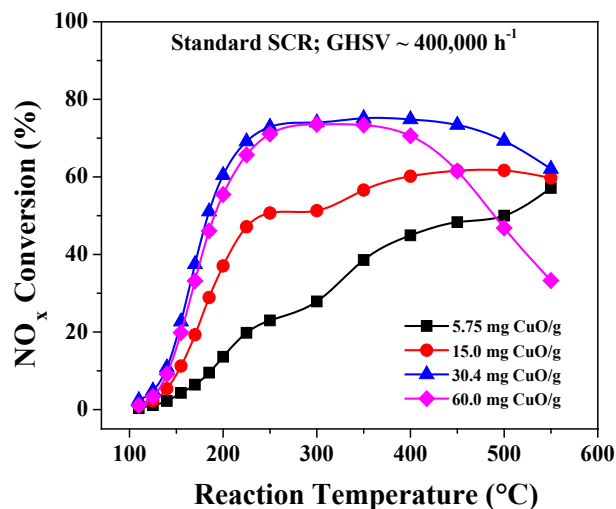


FIGURE 5. NOx NH_3 conversion as a function of temperature on Cu-SAPO-34-ACS samples formed by calcining xx mg CuO/1g SAPO-34 mixture at 800°C for 16 h. Standard SCR reactant feed contains 350 ppm NO, 350 ppm NH_3 , 14% O_2 , 2.5% H_2O balanced with N_2 . Samples are denoted as 5.75 (■), 15.0 (●), 30.4 (▲) and 60.0 (◆) mg CuO/g, respectively. Gas hourly space velocity (GHSV) = 400,000 h^{-1} .

Two alternative Cu-SAPO-34 synthesis methods to more traditional solution IE, notably SSIE and one-pot synthesis, have been used to prepare model catalysts for fundamental studies of their performance and stability. Compared with the IE method, both SSIE and one-pot procedures lead to Cu-SAPO-34 samples with significantly higher surface area/pore volumes and higher crystallinity. Performance tests of these latter catalysts show excellent NH₃-SCR performance and selectivity. The improved materials provide useful model catalysts for detailed fundamental studies of mechanisms for low- and high-temperature performance and hydrothermal stability.

REFERENCES

1. J.H. Kwak, D. Tran, S.D. Burton, J. Szanyi, J.H. Lee, C.H.F. Peden, *Journal of Catalysis* 287 (2012) 203-209.
2. W.S. Epling, L.E. Campbell, A. Yezerets, A., N.W. Currier, J.E. Parks, *Catalysis. Review.—Science and Engineering* 46 (2004) 163.
3. D.H. Kim, K. Mudiyanselage, J. Szanyi, J.H. Kwak, H. Zhu, C.H.F. Peden, *Applied Catalysis B* 142-143 (2013) 472478.
4. G.G. Muntean, M. Devarakonda, F. Gao, J.H. Kwak, J.Y. Luo, C.H.F. Peden, M.L. Stewart, J. Szanyi, D.N. Tran, K. Howden, in *Advanced Combustion Engine Research and Development: FY2012 Annual Progress Report*, III-3 – III-7.
5. J.Y. Luo, F. Gao, C.H.F. Peden, *Catalysis Today*, submitted for publication.
6. D.H. Kim, K. Mudiyanselage, J. Szanyi, H. Zhu, J.H. Kwak, C.H.F. Peden, *Catalysis Today* 184 (2012) 2-7.
7. Q. Wang, J.H. Sohn, J.S. Chung, *Applied Catalysis B* 89 (2009) 97-103.
8. A. Frache, B.I. Palella, M. Cadoni, R. Pirone, H.O. Pastore, L. Machese, *Topics in Catalysis* 22 (2003) 53-57.
9. F. Gao, E.D. Walter, N.M. Washton, J. Szanyi, C.H.F. Peden, *ACS Catalysis* 3 (2013) 2083-2093.
10. F. Gao, E.D. Walter, N.M. Washton, J. Szanyi, C.H.F. Peden, *ACS Catalysis*, submitted for publication.

FY 2013 PUBLICATIONS

1. F. Gao, E.D. Walter, N.M. Washton, J. Szanyi, C.H.F. Peden, “Synthesis and Evaluation of Cu-SAPO-34 Catalysts for Ammonia Selective Catalytic Reduction. 1. Aqueous Solution Ion Exchange”, *ACS Catalysis* 3 (2013) 2083-2093.
2. F. Gao, D.H. Kim, J.Y. Luo, G.G. Muntean, C.H.F. Peden, K. Howden, N. Currier, K. Kamasamudram, A. Kumar, J. Li, R.J. Stafford, A. Yezerets, M. Castagnola, H.-Y. Chen and H. Hess, “Enhanced High Temperature Performance of NOx Storage/Reduction (NSR) Materials”, in *Advanced Combustion Engine Research and Development: FY2012 Annual Progress Report*, III-8 – III-12.

3. D.H. Kim, K. Mudiyanselage, J. Szanyi, J.H. Kwak, H. Zhu, C.H.F. Peden, “Effect of K Loading on Nitrate Formation/Decomposition on and NOx Storage Performance of PtK₂O/ γ Al₂O₃ NOx Storage-Reduction Catalysts”, *Applied Catalysis B* 142-143 (2013) 472478.

4. F. Gao, E.D. Walter, N.M. Washton, J. Szanyi, C.H.F. Peden, “Synthesis and Evaluation of Cu-SAPO-34 Catalysts for Ammonia Selective Catalytic Reduction. 2. Solid-State Ion Exchange and One-Pot Synthesis”, *ACS Catalysis*, submitted for publication.

5. J.Y. Luo, F. Gao, D.H. Kim, C.H.F. Peden, “Effects of Potassium Loading and Thermal Aging on K/Pt/Al₂O₃ High-Temperature Lean NO_x Trap Catalysts”, *Catalysis Today*, submitted for publication.

6. D.H. Kim, K. Mudiyanselage, J. Szanyi, J.C. Hanson, C.H.F. Peden, “Effect of H₂O on the Morphological Changes of KNO₃ Formed on K₂O/ γ Al₂O₃ NOx Storage Materials: Fourier Transform Infrared (FTIR) and Time-Resolved X-ray Diffraction (TR-XRD) Studies”, *Journal of Physical Chemistry C*, submitted for publication.

FY 2013 PRESENTATIONS

1. D.H. Kim, K. Mudiyanselage, J. Szanyi, J.H. Kwak, C.H.F. Peden, “Characteristics of PtK/MgAl₂O₄ NOx Storage-Reduction Catalysts”, presentation at the AIChE Fall Meeting, Pittsburgh, PA, October 2012.
2. F. Gao, J.Y. Luo, G.G. Muntean, C.H.F. Peden, N. Currier, K. Kamasamudram, A. Kumar, J. Li, A. Yezerets, M. Castagnola, H.Y. Chen, H. Hess, “Enhanced High Temperature Performance of NOx Storage/Reduction (NSR) Materials”, invited presentation (**Chuck Peden**) at the DOE Combustion and Emission Control Review, Washington, DC, May 2013.
3. F. Gao, E.D. Walter, N.M. Washton, J.H. Kwak, J. Szanyi, C.H.F. Peden, “Synthesis and evaluation of Cu-SAPO-34 Catalysts for use in NH₃-Selective Catalytic Reduction (SCR)”, presentation at the 245th ACS National Meeting, New Orleans, LA, April 2013.
4. F. Gao, E.D. Walter, S.D. Burton, N.M. Washton, J.H. Kwak, J. Szanyi, C.H.F. Peden, “A Comparative Study Between Solution Ion Exchange (IE) and Solid State Ion Exchange (SSIE) in the Synthesis of Cu-SAPO-34 Catalysts for NH₃ SCR”, presentation at the 23rd North American Catalysis Society Meeting, Louisville, KY, June 2013.
5. J.Y. Luo, F. Gao, C.H.F. Peden, “Advantages of MgAlO_x over Al₂O₃ as a Support Material for Potassium-Based High Temperature Lean NO_x Traps”, presentation at the 23rd North American Catalysis Society Meeting, Louisville, KY, June 2013.
6. F. Gao, E.D. Walter, N.M. Washton, J. Szanyi, C.H.F. Peden, “Comparative Reactivity of Cu/SSZ-13 and Cu/SAPo-34 Catalysts After Hydrothermal Aging: No Answers”, invited presentation (**Chuck Peden**) at the Cummins Symposium on Cu-Based SCR Catalysts, Columbus, IN, June 2013.

7. F. Gao, E.D. Walter, N.M. Washton, J. Szanyi, C.H.F. Peden,
“Synthesis and Evaluation of Cu/Fe-Chabazite Catalysts for use
in Selective Catalytic Reduction (SCR)”, invited presentation
(Feng Gao) at the 246th ACS National Meeting, Indianapolis,
IN, September 2013.

III.5 Investigation of Mixed Oxide Catalysts for NO Oxidation

Ayman M. Karim (Primary Contact),
Larry R. Pederson, Ja Hun Kwak,
Donghai Mei, Diana Tran, Darrell R. Herling,
George G. Muntean, Janos Szanyi,
Charles H.F. Peden
Pacific Northwest National Laboratory (PNNL)
902 Battelle Blvd, PO Box 999
Richland, WA 99352

DOE Technology Development Manager:
Ken Howden

metal content of DOC and LNT catalysts to be reduced or eliminated.

- Investigate the effect of the Ce-Mn mixed oxide synthesis method on the activity and stability.
- Perform a detailed characterization of mixed metal oxide catalysts using state-of-the-art analytical tools and develop reaction pathways for MnO_x clusters supported on ceria and for Mn-doped ceria to determine the nature of active centers on those catalysts.
- Optimize the catalyst synthesis to maximize the Mn/Ce interaction and the number of active sites.



Overall Objectives

- Develop and demonstrate mixed metal oxide-based catalysts as a low-cost replacement for platinum in the oxidation of NO to NO₂ in lean engine exhaust, an essential first step in controlling oxides of nitrogen (NO_x) emissions.
- Improve the understanding of the nature and structure of active sites of mixed metal oxide catalysts for NO oxidation in diesel oxidation catalysts (DOCs) and lean-NO_x traps (LNTs).

Fiscal Year (FY) 2013 Objectives

- Determine the structure of catalyst prepared by incipient wetness impregnation.
- Determine the effect of aging on the catalyst activity.
- Perform density functional theory (DFT) computational studies to investigate the effect Mn on the oxygen vacancy formation in CeO₂.

FY 2013 Accomplishments

- Demonstrated the stability of Ce-Mn mixed oxides against high-temperature aging.
- Determined the effect of Mn loading on the catalyst activity.
- Demonstrated that ceria stabilizes Mn in a higher oxidation state leading to easier Mn reducibility and lower temperature for NO oxidation.
- Using DFT, Mn addition to ceria was shown to lower the energy required for oxygen vacancy formation.

Future Directions

- Optimize mixed metal oxide catalyst compositions and forms for NO oxidation, to enable the noble

INTRODUCTION

The oxidation of engine-generated NO to NO₂ is an important step in the reduction of NO_x in lean engine exhaust because NO₂ enhances the activities of both ammonia selective catalytic reduction catalysts [1] and LNTs [2]. For selective catalytic reduction catalysts, an NO: NO₂ ratio of 1:1 is most effective for NO_x reduction, whereas for LNT catalysts, NO must be oxidized to NO₂ before adsorption on the storage components. However, NO₂ typically constitutes less than 10% of NO_x in lean exhaust, so catalytic oxidation of NO is essential. Platinum has been found to be especially active for NO oxidation, and is widely used in diesel oxidation and LNT catalysts. However, because of the high cost and poor thermal durability of Pt-based catalysts, there is substantial interest in the development of alternatives. The objective of this project, in collaboration with partner General Motors (GM), is to develop mixed oxide catalysts for NO oxidation, enabling lower precious metal usage in emission control systems.

APPROACH

This Cooperative Research and Development Agreement project with GM and PNNL is aimed at replacing or reducing platinum usage in DOC and LNT catalysts, and was initiated in 2012. This project builds on success achieved recently by GM researchers, who reported excellent NO oxidation efficiency over substituted lanthanum-based mixed oxides, such as LaCoO₃ and LaMnO₃, when compared to a commercial Pt-based DOC [2].

Well-coordinated and complementary research activities are being performed at GM and PNNL. The

principal focus of GM research is on catalyst formulation, evaluation of catalytic activity under conditions relevant to lean engine exhaust, and catalyst aging. State-of-the-art analytical and computational techniques are applied at PNNL to characterize the structure of the catalysts and to determine the concentration and nature of active sites. Surface and bulk properties of catalyst materials are established as a function of catalyst composition, and correlated to trends in catalytic activity. Computational analyses of active sites and possible reaction mechanisms are probed using DFT, which provides information concerning the interaction between reactants and active sites. It is anticipated that this research will lead to the development of low-cost, durable, and active catalysts for the oxidation of NO to NO₂.

RESULTS

Mixed metal oxide catalysts containing manganese and cerium oxides were identified that show significant activity for NO oxidation. The catalysts were prepared at GM by co-precipitation methods and at PNNL by an incipient wetness method, and their structure and catalytic properties evaluated. During the first year we showed that catalysts prepared by the two methods with 30.7 wt% Mn loading showed similar activities. We further investigated the effect of Mn weight loading on the catalysts prepared by incipient wetness as well as the effect of aging on their activity. Figure 1 shows the 30.7 wt% MnO_x/CeO₂ catalyst activity before and after

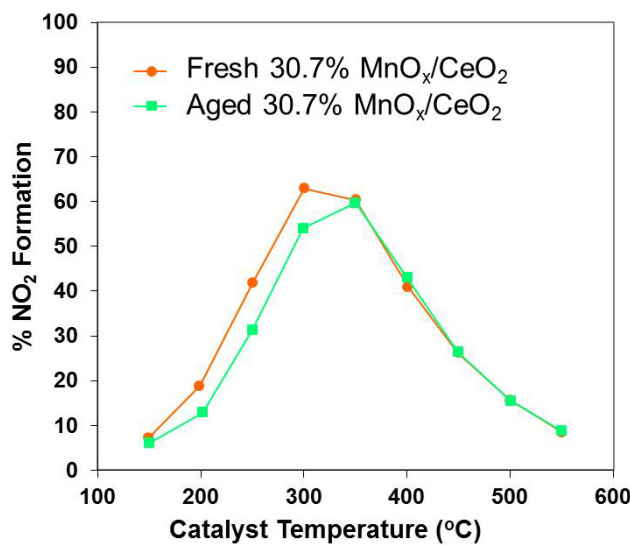


FIGURE 1. Effect of aging on the activity of 30.7% MnO_x/CeO₂ catalyst prepared by incipient wetness impregnation. Aging was performed in 10% steam in air at 700°C for one hour. Reaction conditions: 50 mg catalyst, 156 sccm total flowrate, gas composition: 200 ppm NO, 10% O₂, 10% steam, balance N₂.

aging at 700°C in 10% steam in air for one hour. The catalyst was weakly affected by aging and similar results were obtained for other Mn loading. Figure 2 shows the effect of Mn loading on the catalyst activity. The MnO_x/CeO₂ showed much higher activity than the pure CeO₂. Additionally, it can be seen that while the Mn loading was varied by an order of magnitude, the activity was not significantly affected. This is a remarkable result since it suggests that the active sites are only a small percentage of the Mn loaded on CeO₂. It is expected that the lower Mn loading results in more interaction between Mn and CeO₂. Figure 3 shows the effect of Mn weight loading on the Mn reducibility by temperature programmed reduction. The low Mn loading showed higher reducibility at low temperature (the peak at 100°C) which could be attributed to the higher fraction of Mn in close contact with the CeO₂ for the 3.4% compared with the 30.7 wt% Mn loading. This is in agreement transmission electron microscopy (not shown) where the higher loading of Mn resulted in the formation of large islands of Mn on top of the CeO₂.

In order to provide further insights on the Mn/CeO₂ interaction, we performed in situ X-ray photoelectron spectroscopy (XPS) on the MnO_x/CeO₂ catalysts. Figure 4 shows the Mn2p XPS spectra for the catalyst after oxidation in air at 500°C and after reduction in 100% H₂ at 500°C for one hour. The catalysts were transferred to the XPS analysis chamber without any exposure to air. It can be seen that after oxidation the Mn2p binding energy was the highest for the 3.4 wt% Mn/CeO₂ catalyst while the three catalysts showed similar binding energy after reduction. These results

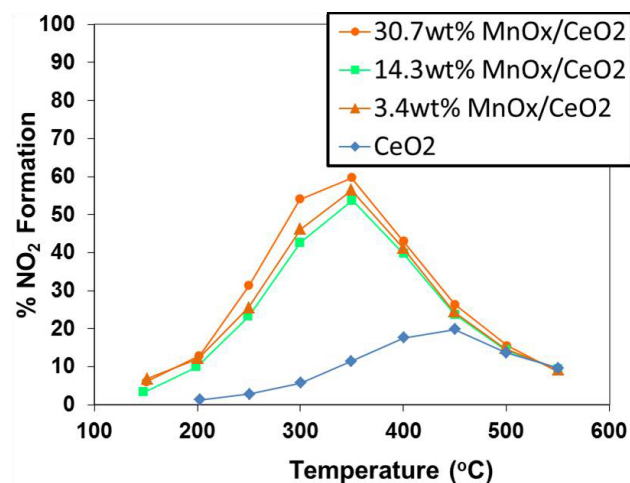


FIGURE 2. Effect of Mn loading on the activity of MnO_x/CeO₂ catalysts prepared by incipient wetness impregnation after aging. Aging was performed in 10% steam in air at 700°C for one hour. Reaction conditions: 50 mg catalyst, 156 sccm total flowrate, gas composition: 200 ppm NO, 10% O₂, 10% steam, balance N₂.

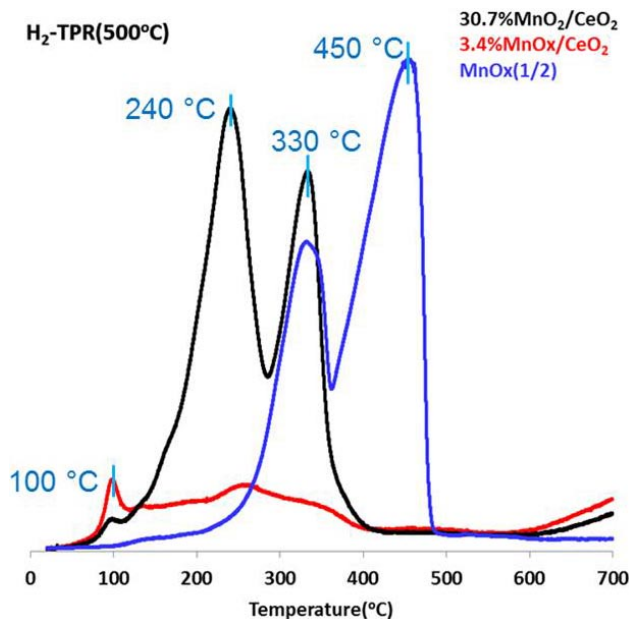


FIGURE 3. Temperature programmed reduction for 3.4 and 30.7% MnO_x/CeO₂ prepared by incipient wetness impregnation compared with pure MnO_x. All samples were calcined at 500°C for one hour prior to the temperature programmed reduction measurements.

show that the Mn in the lower loading catalysts is present at a higher oxidation state. Since we have shown that low Mn loading resulted in a larger fraction of Mn in close contact with CeO₂, we can conclude that CeO₂ helps stabilize Mn in a higher oxidation state. Moreover, since after reduction in H₂, the Mn2p binding was the same for the different Mn weight loadings, this shows that the Mn species in close contact with CeO₂, not only are stabilized

at a higher oxidation state, but are also more reducible. These results are in agreement with the activity of the catalysts shown in Figure 2 where the Mn loading didn't significantly affect the activity.

DFT calculations were performed to investigate the mechanistic details of Mn/CeO₂ interactions and how they affect the NO oxidation reaction. The doping of Mn in the CeO₂ lattice was shown to stabilize Mn in 4+ oxidation state, while MnO_x clusters on top of CeO₂ were more stable in a lower oxidation state. Additionally, the Mn in the ceria lattice was found to lower the energy of oxygen vacancy formation (either with or without the reaction with NO) from 2.3 eV for ceria, to 1.2 eV for Mn doped in the ceria lattice, to 1.7 eV for MnO_x clusters on top of ceria. These results suggest that Mn doping in the ceria lattice is more likely to be the active site and we are currently developing the full mechanistic models for NO oxidation on both systems to identify the active site and reaction pathways.

CONCLUSIONS

- Mn supported on ceria is an active and stable catalyst for NO oxidation, and it is a promising candidate to minimize the loading of precious-grade metals in catalysts for exhaust gas treatment.
- The Mn loading showed a weak effect on activity suggesting that only the Mn sites in contact with ceria are active.
- XPS results showed that Mn in contact with ceria is stabilized in a higher oxidation state and is more reducible.

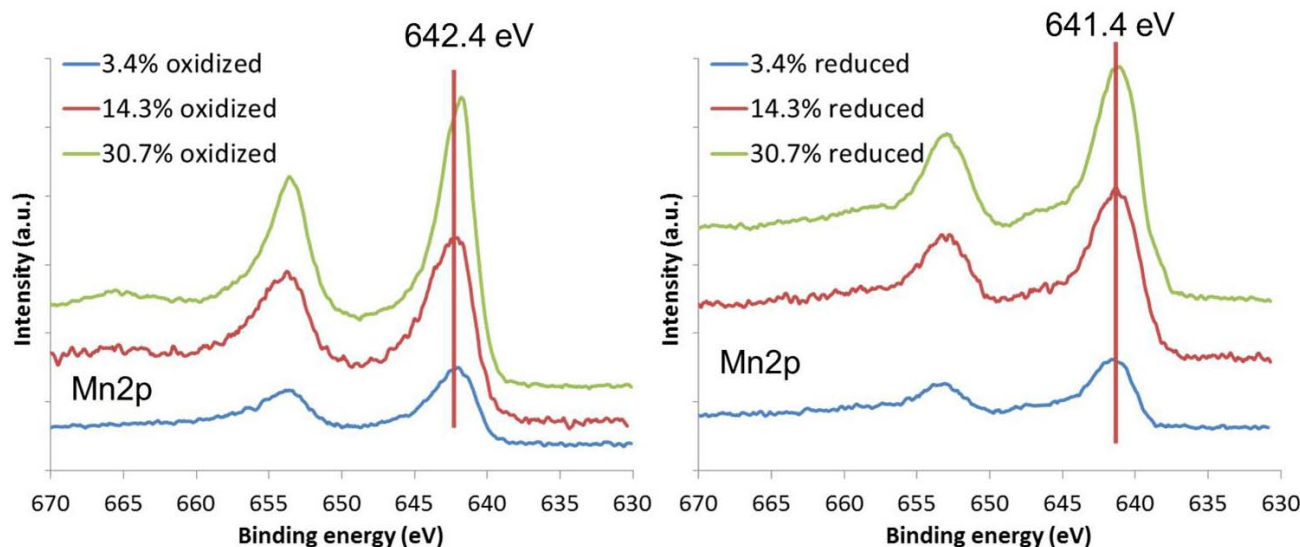


FIGURE 4. XPS spectra for the MnO_x/CeO₂ catalysts prepared by incipient wetness impregnation after oxidation (left) and after reduction (right) in air and H₂, respectively, at 500°C for one hour.

- DFT calculations show that Mn doping in ceria is more effective in lowering the energy required for oxygen vacancy formation than MnO_x clusters supported on ceria.

REFERENCES

1. M. Koebel, G. Madia, and M. Elsener, *Catalysis Today* 73, 239 (2002).
2. C.H. Kim, G.S. Qi, K. Dahlberg, and W. Li, *Science* 327, 1624 (2010).

FY 2013 PUBLICATIONS/PRESENTATIONS

1. Karim, A.M., Peterson, L., Muntean, G., Kwak, J.H., Mei, D., Peden, C. and Herling, D. "Investigation of Mixed Oxide Catalysts for NO Oxidation," 2012 DOE Vehicle Technologies Program Annual Merit Review and Peer Evaluation Meeting, May 16, 2013, Washington, D.C.
2. LR Pederson, JH Kwak, D Mei, DR Herling, GG Muntean, CHF Peden, "Investigation of Mixed Oxide Catalysts for NO Oxidation", Advanced Combustion Engine Research and Development, FY2012 Progress Report (2012) in press.

III.6 Integration of DPF and SCR Technologies for Combined Soot and NO_x After-Treatment

Kenneth G. Rappé (Primary Contact),
George G. Muntean, Mark L. Stewart,
Gary D. Maupin
Pacific Northwest National Laboratory
Post Office Box 999
Richland, WA 99354

DOE Technology Development Manager:
Ken Howden

Overall Objectives

- Develop a fundamental understanding of the integration of selective catalytic reduction (SCR) and diesel particulate filter (DPF) technologies for on-road heavy-duty diesel applications.
- Probe the DPF-SCR couple with a view towards maximum SCR conversion efficiency, optimum soot oxidation performance, and acceptable pressure drop.
- Determine performance limitations and define basic design and operating requirements for efficient integration with the engine that minimizes impact on vehicle efficiency.

Fiscal Year (FY) 2013 Objectives

- Quantify the effect of the presence and the nature of the active SCR reactive process on the soot oxidation performance exhibited in the system.
- Develop improved knowledge that could lead to advanced strategies for maximizing passive soot oxidation capacity in the integrated system in the presence of the active SCR process.
- As a facilitator, continue to develop an intimate understanding of the dynamics of the SCR process in the integrated system through modeling and simulation.

FY 2013 Accomplishments

- Developed improved understanding of soot oxidation performance with coupled active SCR process and the pathway towards optimizing its performance for heavy-duty diesel applications.
- Developed an understanding of SCR processes and the nature by which improved integration

with coupled soot oxidation processes can be accomplished achieving optimum performance for both.

- Continued to develop the ability to accurately predict how changes in active species concentrations will affect system performance.

Future Directions

- Continue to interrogate passive soot oxidation feasibility in the integrated device, including continued parametric investigations interrogating the effect of NO₂:NO_x ratio, SCR catalyst loading, NH₃:NO_x ratio.
- Pursue maturation of model development activities to aid in system performance prediction and as a tool for optimizing the physical SCR-DPF integration that achieves optimum soot oxidation and NO_x conversion performance.
- Pursue investigating alternative DPF substrates for inclusion in the technology, including possibly silicon carbide, aluminum titanite, and others. Consider quick screening studies for comparison to cordierite wash coating results.



INTRODUCTION

Exhaust after-treatment is considered an enabler for widespread adoption of more fuel efficient diesel engines. In the last decade extensive research has resulted in the development and advancement of many after-treatment technologies. However there are still many unanswered questions that relate to how these technologies can work together synergistically, especially when tightly integrated. It is anticipated that in the future there will be a need to minimize the volume and mass of after-treatment systems on ever increasingly more complex truck platforms. However, to date research focused on combining technologies into an integrated system has been relatively sparse. With the inevitable need to consider how SCR and DPF technologies will function in synergy to reduce both NO_x and PM, as well as how CO and hydrocarbons (HCs) need to be managed, an integrated investigation and approach is essential. The determination of important synergies will require study both under steady-state and through transient conditions.

APPROACH

The primary thrust is to study the synergies of integrated DPF and SCR technologies (SCRF®) systems to develop a pathway to a singular catalytic brick that combines the function of both a DPF and SCR. Corning has provided proprietary ultra-high porosity (UHP) cordierite as the current subject of study for the DPF. Corning UHP DPF samples were directionally loaded by BASF locating catalyst predominantly on the downstream portion of the filter microstructure. The samples were empirically tested for SCR of NO_x and passive soot oxidation through loading with soot to an initial concentration of 4 g/L.

For model development, a single flat wall was used with exhaust flow normal to the wall. Channel scale transport effects and axial variations were ignored. A simplified SCR reaction network was employed, and included the NH₃ oxidation reaction, the standard SCR reaction (NO only) and the fast SCR reaction (equimolar NO and NO₂). A simplified porous media model was employed with similar porosity and tortuosity as the SCRF samples used in the empirical studies. Catalyst distribution employed in the model included 90 g/L of SCR catalyst evenly distributed throughout the wall plus 60 g/L of SCR catalyst on the downstream channel wall surface. A Lattice-Boltzmann model was used to solve for the gas flow field. A soot oxidation kinetic model was employed by Messerer et al., [1]. Soot was presented as a cake layer on the upstream channel wall surface, and was assumed 50% oxidized.

RESULTS

Empirical studies were performed on SCRF samples to develop an understanding of the effect of soot

oxidation on NO_x reduction. Similarly, investigations were performed to develop an understanding of NO_x reduction on soot oxidation, with particular focus on passive oxidation. Figure 1 shows the NO_x reduction efficiency and the post-catalyst NO₂ concentration for 500 ppm NO_x with an NH₃ to NO_x ratio (ANR) of 1 with and without 4 g/L soot loading; the simulated exhaust in the left figure had NO₂/NO_x = 0.35 whereas the right had NO₂/NO_x = 0.5. Similarly, Figure 2 shows analogous performance with an NO₂/NO_x = 0.65.

The relative NO_x conversion efficiencies combined with post-catalyst NO₂ concentration have provided insight into the impact of soot oxidation on the SCR catalytic process. At low NO₂/NO_x fraction (0.35) superior SCR performance was observed in the absence of soot at <300°C, with very little NO₂ present in the effluent stream. This is attributed to the relative participation of standard (NO only) and fast (equimolar NO:NO₂) SCR reactions. In the presence of soot, a fraction of NO₂ is converted to NO through passive soot oxidation, which is reflected in the NO₂ effluent concentrations. The result is comparatively greater dependency of NO_x conversion on standard versus fast SCR reactions. At low temperatures, standard SCR reaction proceeds at comparatively slower rate versus fast SCR; the result is inferior SCR performance in the presence of soot. However, at high NO₂/NO_x fraction (0.65) superior SCR performance was observed in the presence of soot at <300°C with significant NO₂ present in the effluent stream. This is attributed to the participation of NO₂-only SCR reactions, with standard and fast SCR reactions proceeding until a relative abundance of NO₂ remains. In the presence of soot, again a fraction of the NO₂ is converted to NO which is reflected in the NO₂ effluent concentrations. The result

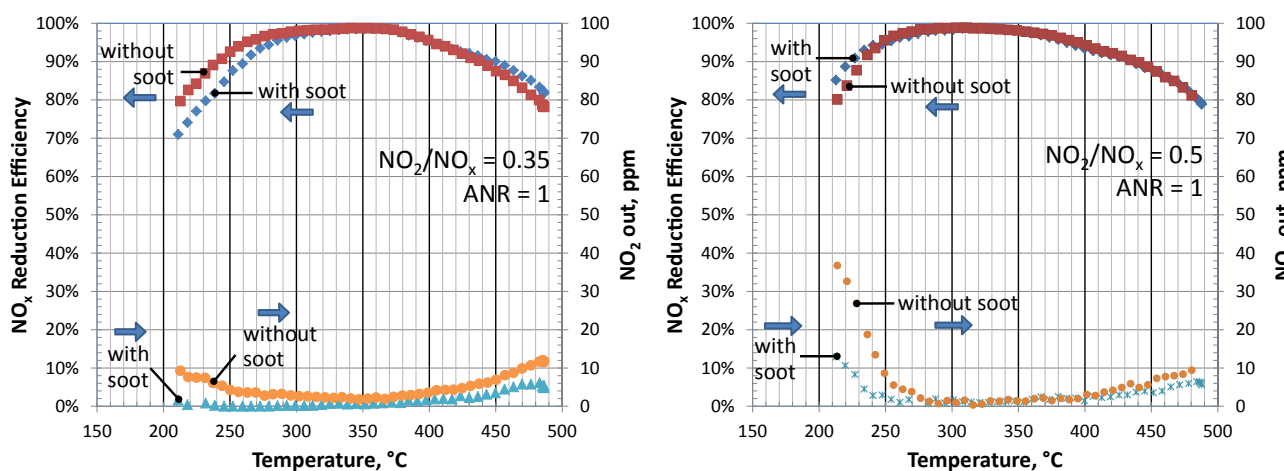


FIGURE 1. NO_x reduction performance and post-filter NO₂ concentration with simulated exhaust versus temperature for NO₂/NO_x = 0.35 (left) and 0.5 (right), 150 g/L SCR catalyst loading, with and without 4 g/L initial soot loading, 500 ppm NO_x, ANR = 1, 35,000 gas hourly space velocity (GHSV).

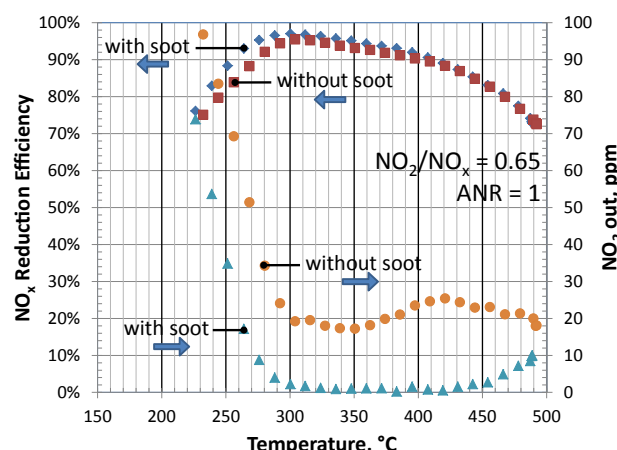


FIGURE 2. NO_x reduction performance and post-filter NO₂ concentration with simulated exhaust versus temperature for NO₂/NO_x = 0.65, 150 g/L SCR catalyst loading, with and without 4 g/L initial soot loading, 500 ppm NO_x, ANR = 1, 35,000 GHSV.

is a decreased on NO₂-only SCR reactions versus other SCR reaction pathways. At low temperatures, the NO₂-only SCR reaction proceeds at a slower rate, thus the result being superior SCR performance in the presence of soot. At equimolar NO and NO₂, SCR performance was comparable with slight superior performance in the presence of soot at <230°C. This is somewhat unexpected, and is believed to be attributed to increased ammonia storage. Thus the impact of soot oxidation on SCR performance predominantly occurs through impact on relative NO_x make-up (NO and NO₂ fractions) and the subsequent governing SCR reactions. Ammonia storage is also impacted by the presence of soot and believed to have a benefiting effect (albeit lesser) on SCR performance.

Figures 3 and 4 show temperature programmed oxidation (TPO) studies performed to characterize passive soot oxidation in the presence of NO_x reduction. The data is presented as relative (normalized) pressure drop (dP) across the SCRF sample as a function of temperature, with decrease in pressure drop being a tool to characterize oxidation of soot. The pressure drop curves combined with post-catalyst NO₂ concentration provide insight into the impact of NO_x reduction on soot oxidation, and in particular passive soot oxidation. Figure 3 shows the result of varying NO₂/NO_x ratio with constant NO_x concentration and ANR. At NO₂/NO_x = 0.5 and less, passive soot oxidation is retarded by ~50°C with coupled NO_x conversion; at higher NO₂/NO_x (0.65) the retarding effect is significantly less (~20°C). This is attributed to NO₂ balance in the system, as evident by the post-catalyst NO₂ concentration. Figure 4 shows the result of increasing NO_x concentration at NO₂/NO_x = 0.5 and 0.65. The benefiting effect of increased NO_x concentration at NO₂/NO_x = 0.65 is superior to that at NO₂/NO_x = 0.5, again attributed to NO₂ balance. The results suggest that fast SCR reactions dominate kinetics of the samples interrogated, with the rate of passive soot oxidation being a function of NO₂ balance in the system which is governed predominantly by the relative participation of fast SCR reactions.

Modeling efforts were pursued to support empirical efforts focused on optimum integration and control of coupled SCR-DPF systems. The intent is to develop an understanding of the effect of coupled SCR and DPF processes on reactive exhaust species concentrations across the filter wall. The full model locates soot and SCR catalyst as described prior; the lumped model co-locates soot and SCR catalyst in a given computational cell. Comparison of the full versus lumped model

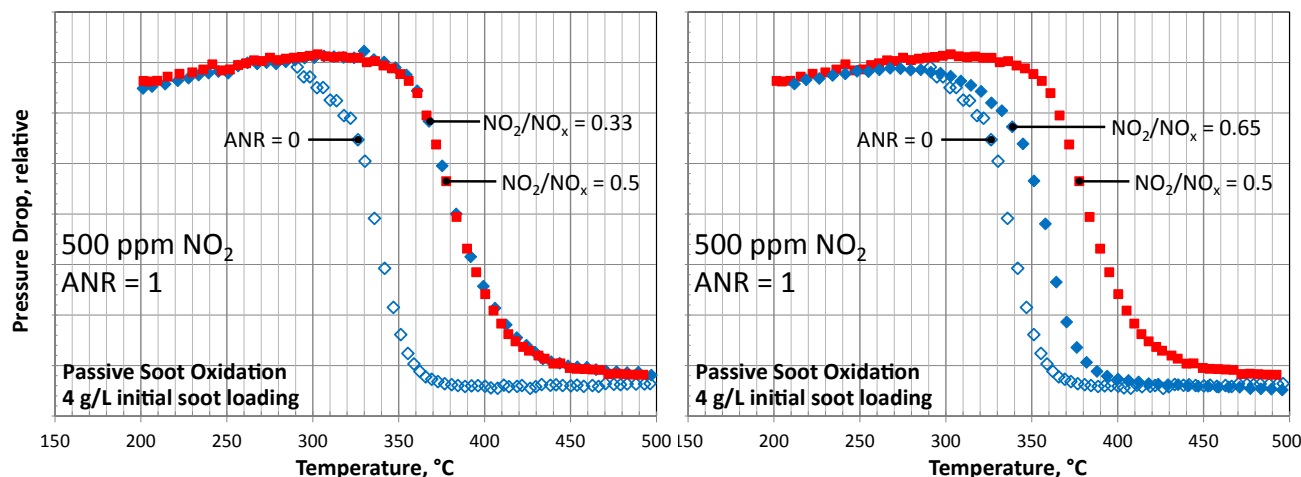


FIGURE 3. TPO studies with simulated exhaust presented as relative pressure drop versus temperature for NO₂/NO_x = 0.33 and 0.5 (left) and 0.5 and 0.65 (right), 150 g/L SCR catalyst loading, with SCR reaction (ANR=1) and without (ANR=0), 500 ppm NO_x, 4 g/L initial soot loading, 35,000 GHSV.

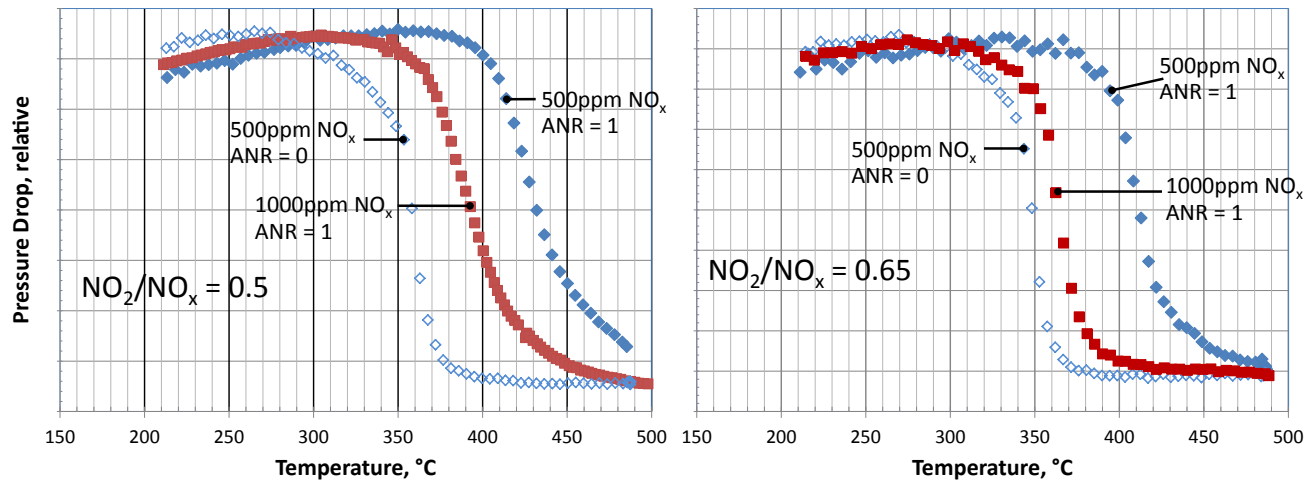


FIGURE 4. TPO studies with simulated exhaust presented as relative pressure drop versus temperature for $\text{NO}_2/\text{NO}_x = 0.5$ (left) and 0.65 (right), 150 g/L SCR catalyst loading, with SCR reaction (ANR=1) and without (ANR=0), 500 and 1,000 ppm NO_x , 4 g/L initial soot loading, 35,000 GHSV.

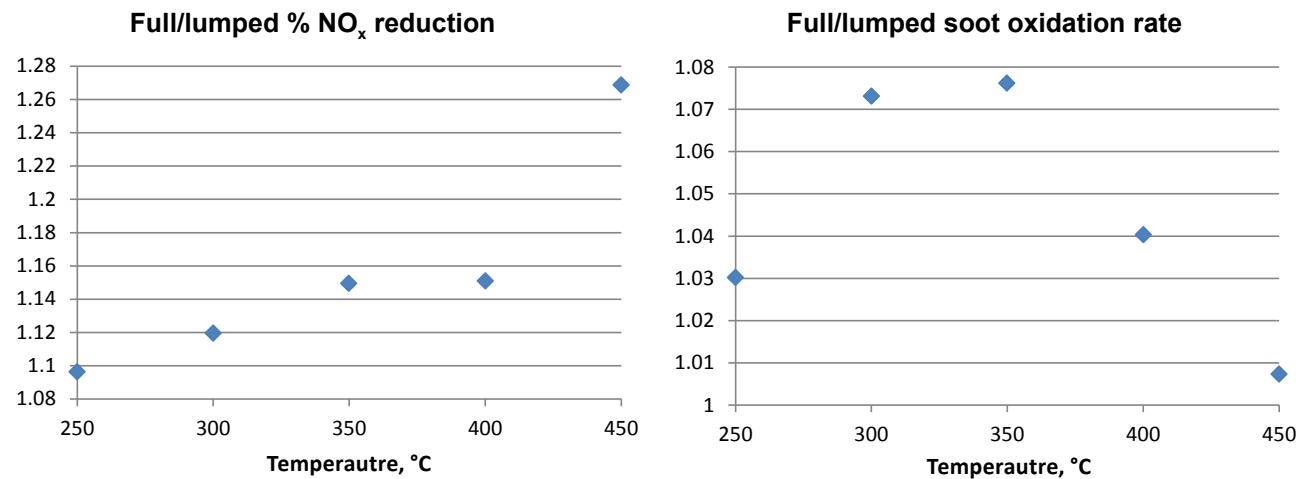


FIGURE 5. Ratio of full versus lumped SCRF model simulation as a function of temperature for NO_x conversion (left) and soot oxidation (right), 150 g/L SCR catalyst loading, 500 ppm NO_x , 4 g/L initial soot loading, $\text{NO}_2/\text{NO}_x = 0.5$, ANR = 1, 35,000 GHSV.

results provide insight into the relative magnitude of contributing reactive processes and spatial separation.

Spatially separating soot and SCR components of the SCRF system incurs reactive component concentration profiles across the filter wall. These concentration profiles are inherently a function of the location and magnitude of reaction processes in the system, convective flow, and reactive component diffusivities. Figure 5 shows the relative comparisons of the full versus lumped model for SCR performance (left) and soot oxidation performance (right) at 500 ppm NO_x , $\text{NO}_2/\text{NO}_x = 0.5$, ANR = 1 and 4 g/L soot loading. The predicted effect of spatial separation on NO_x conversion performance is significant, with 10-15% increased performance

predicted with spatial separation at 400°C and less, and 27% at 450°C. The predicted effect of spatial separation on soot oxidation performance is less significant, with a maximum of 7.6% increased performance predicted at 350°C dropping to <1% at 450°C. Combining (1) the predicted decreased effect of spatial separation on soot oxidation performance versus NO_x conversion, (2) the results from Figures 1 and 2 showing comparable measured NO_x conversion performance, and (3) the results from Figures 3 and 4 showing significantly retarded soot oxidation performance measured in the presence of SCR processes, allude to the significant dominance of SCR reaction processes. The presence and magnitude of the SCR process dominates the dynamics

of the integrated SCRF system as configured in the current study, exhibiting measureable impact on the NO_x balance in the system through strong diffusive effects that penetrate across the entire filter wall. This suggests the pathway towards optimizing the SCR-DPF couple will be through optimizing the physical arrangement of SCR integration within the porous filter wall.

CONCLUSIONS

Empirical studies and modeling efforts are helping to provide understanding of fundamental operation and pathway towards optimization of SCRF technology for heavy-duty diesel after-treatment. Empirical studies have helped to understand and quantify the primary reaction drivers in the SCRF system. Modeling efforts have helped to gain insight as to how the soot oxidation and SCR processes interact with one another, affecting active species concentration profiles across the filter wall and upstream into the inlet channel. The fast SCR process is the most significant reactive driver in the SCRF system; this leads to impacts on soot oxidation performance through diffusive effects and subsequent reaction competition, and vice versa.

FY 2013 PUBLICATIONS/PRESENTATIONS

1. K. Rappe, G. Muntean, M. Stewart, “PNNL-PACCAR CRADA: SCRF Development”, Presentation given to PACCAR at Pacific Northwest National Laboratory (Richland, WA; October 2012).
2. K. Rappe, G. Muntean, “Combination & Integration of DPF – SCR Aftertreatment”, Presentation at PACCAR Technical Center (Mount Vernon, WA; May 2013).
3. K. Rappe, “Combination & Integration of DPF – SCR Aftertreatment”, Presentation given to PNNL staff at Pacific Northwest National Laboratory (Richland, WA; January 2013).

III.7 Low-Temperature Emissions Control

Todd J. Toops (Primary Contact) and
James E. Parks

Oak Ridge National Laboratory (ORNL)
2360 Cherahala Boulevard
Knoxville, TN 37932

DOE Technology Development Manager:
Ken Howden

Overall Objectives

- Develop emission control technologies that perform at low temperatures (<150°C) to enable fuel-efficient engines with low exhaust temperatures to meet emission regulations
- Identify advancements in technologies that will enable commercialization of advanced combustion engine vehicles

Fiscal Year (FY) 2013 Objectives

- Identify novel/innovative technologies that can be implemented to address the challenges of advanced combustion strategies
- Characterize performance and surface morphology for a novel candidate catalyst

FY 2013 Accomplishments

- Investigated innovative Au@Cu (core@shell) catalyst for oxidation
 - Copper oxide surrounding Au core shows excellent low-temperature CO oxidation behavior
 - Inhibition by hydrocarbons (HCs) and oxides of nitrogen (NOx) observed
 - Durability investigated up to 800°C
- Demonstrated synergy of mixing of Au@Cu and Pt catalysts and potential to overcome inhibitions
 - Pt inhibited by CO at low temperature; improved with AuCu
 - Very high NO to NO₂ oxidation observed with mixture
- Synthesized and evaluated new catalysts using a new support
 - Improved hydrothermal durability using ceria-zirconia support

Future Directions

- Continue investigation on Au@Cu with ceria-zirconia and other supports
 - Activity in the presence of HC and NO
 - Physical mixture with Pt/Al₂O₃; Pt co-supported on ceria-zirconia
 - Additional supports while studying/characterizing metal support interactions
- Initial focus is on oxidation catalysts, but future efforts will move into trap materials and NOx reduction catalysts
 - Low-temperature NOx and HC trap materials
 - Release at moderate temperatures
 - NOx storage reduction catalysis with low-temperature release and highly active reduction chemistry
- Goal is to move from powder catalysts to washcoated cores and further validation in engine exhaust
 - Developing washcoating capability



INTRODUCTION

Removing the toxic pollutants in automotive exhaust has been an intense focus of the automotive industry over the last several decades. In particular, the emissions regulations for fuel-efficient diesel engines that were implemented in 2007 and 2010 have resulted in a new generation of emissions control technologies. These catalysts usually reach 90% conversion of pollutants between 200°C and 350°C and consequently, more than 50% of the emissions occur in the first 2-3 minutes under “cold-start” or idling conditions [1]. Thus, as emissions regulations become more stringent [2] meeting the emission regulations will require increased activity during this warm-up period. To further complicate matters, the increased Corporate Average Fuel Economy standards that will be implemented over the next decade will result in the introduction of more fuel-efficient engines [3]. This will result in lower exhaust temperatures, which further necessitates the need for increased emissions control activity at low temperatures [4]; with this in mind the Advanced Combustion and Emissions Control tech team has set a goal of achieving 90% conversion of CO/HC/NOx at 150°C. Higher Pt/Pd loadings may help to increase the catalytic efficiency,

but such methods would be too expensive for long-term success. Other options to meet the emissions standards include hydrocarbon/NOx absorbers; however, while this pathway would help mitigate cold-start emissions, the lowering of the average exhaust temperature suggests this approach alone will be insufficient and ultimately a more complete solution will be necessary. One way to accomplish this goal is to develop new catalytic materials that are active at lower temperatures.

APPROACH

To reach the goal of 90% conversion at 150°C a multi-functional approach will be pursued. Currently, there is a large effort being pursued in Basic Energy Science programs that are focused on studying catalysts with very high activity regardless of the specific application. We are initiating contact with several of these researchers and the catalysts that they are pursuing and investigating them in the harsh conditions that are present in automotive exhaust, e.g. H₂O, CO, CO_x, HC, NOx and temperatures above 800°C. Often these catalysts show exceptional activity in single-component exhaust streams, but there is significant inhibition from other exhaust species. With this in mind, we are aiming to understand the limitations of each system, but also look for synergistic opportunities when possible. This includes using traps to limit exposure of inhibiting species to active catalysts until temperatures are more amenable. Also, mixing catalytic components where the catalysts are limited by different species will be explored. Our efforts will aim to understand the processes at a fundamental level and illustrate where the shortcomings are of each catalyst we study, while striving to find compositions that will enable the very challenging goal of 90% conversion of CO/NOx/HC at 150°C. Improving this understanding of the potential limitations of catalysts will guide the reformulation of new catalysts.

RESULTS

This year, a novel catalyst was studied that has shown excellent CO oxidation behavior, silica supported AuCu. This catalyst was investigated for the application of oxidizing CO under simulated automotive exhaust conditions (CO, NO, C₃H₆). Silica was chosen due to its high surface area, good thermal stability, and high mechanical strength; additionally, recent research has indicated pathways to enhanced interactions with the metal catalysts and thus improved thermal stability and sulfur tolerance [5]. As a basis for comparison, 1.5% Pt/Al₂O₃ was also investigated. The catalyst amount and the reaction flow rate were normalized to weight to flow ratios (W/F = g·h/mol) due to the significant difference in catalyst volume for the two supports. As can be seen

in Figure 1, Pt/Al₂O₃ shows typical CO conversion behavior under lean conditions (10% O₂, 1% H₂O and Ar) with a light-off temperature (T₅₀ = 50% conversion) between 150°C–200°C, which is not greatly affected by adjustments in the weight to flow ratio. The AuCu/SiO₂ catalyst (1.5 wt% Au) under the same conditions shows very distinct differences from Pt/Al₂O₃ (1.5 wt% Pt). First, AuCu/SiO₂ is capable of oxidizing nearly 95% and 60% of the CO at a W/F = 0.25 or 0.5 g·h/mol below 100°C, respectively. Little to no activity of Pt/Al₂O₃ is observed below 150°C. A second unique feature of the AuCu/SiO₂ is a dip in the conversion curve, which begins near 70°C and begins to increase after 150°C is reached. This type of behavior is common for Au based catalysts supported on SiO₂ because it is believed that the support stores H₂O, which is capable of dissociating O₂ on the perimeter of the Au particle and the support [6].

Propylene and nitric oxide were introduced into the gas stream to represent the basic components of automotive exhaust and to study the effects they may have on CO oxidation on AuCu/SiO₂ and Pt/Al₂O₃, Figure 2. The conversion of 1% CO was performed under the same conditions from Figure 1 and all reactions were done with a W/F = 0.25 g·h/mol. The light-off temperature for CO oxidation, when AuCu/SiO₂ was used in Figure 2a, significantly increased to higher temperatures (>200°C) once 1,000 ppm of C₃H₆ or 500 ppm of NO was individually or simultaneously introduced into the reaction stream. On the other hand, Pt/Al₂O₃ was found to be much more resistant to the inhibiting effects of C₃H₆ and NO and a less dramatic increase in the light-off temperature was observed (~50°C increase in T₅₀). It is evident from the data that NO and propylene compete with CO for active sites

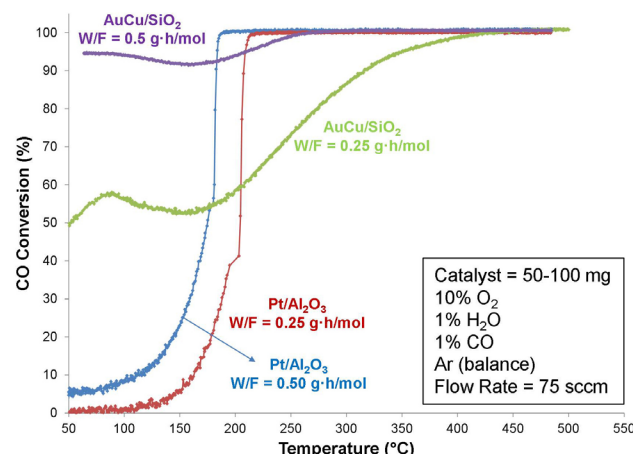


FIGURE 1. CO conversion, with different weight to flow ratios (W/F), as a function of reaction temperature for AuCu/SiO₂ and Pt/Al₂O₃. Catalysts were pretreated by calcination at 550°C for 16 h in 10% O₂, 1% H₂O and Ar (balance) at 75 sccm. Reaction conditions are in inset of the figure.

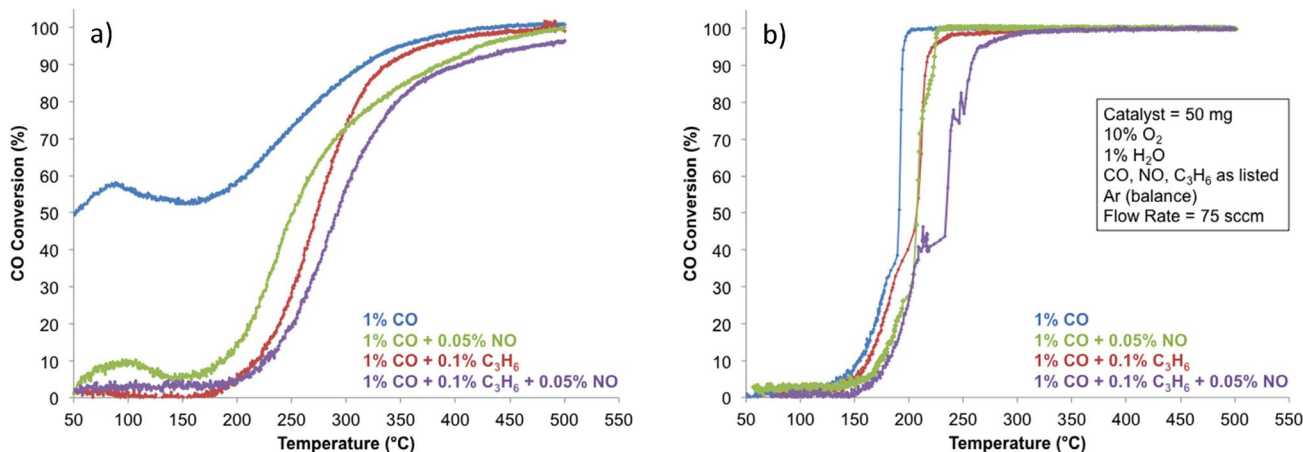


FIGURE 2. CO conversion as a function of temperature using a (a) AuCu/SiO₂ or (b) Pt/Al₂O₃ catalyst in the presence of 0.1% C₃H₆, 0.05% NO or 0.1% C₃H₆ and 0.05% NO with a W/F = 0.25 g·h/mol. Catalysts were pretreated by calcination at 550°C for 16 h in 10% O₂, 1% H₂O and Ar (balance) at 75 sccm. Reaction conditions are in inset b.

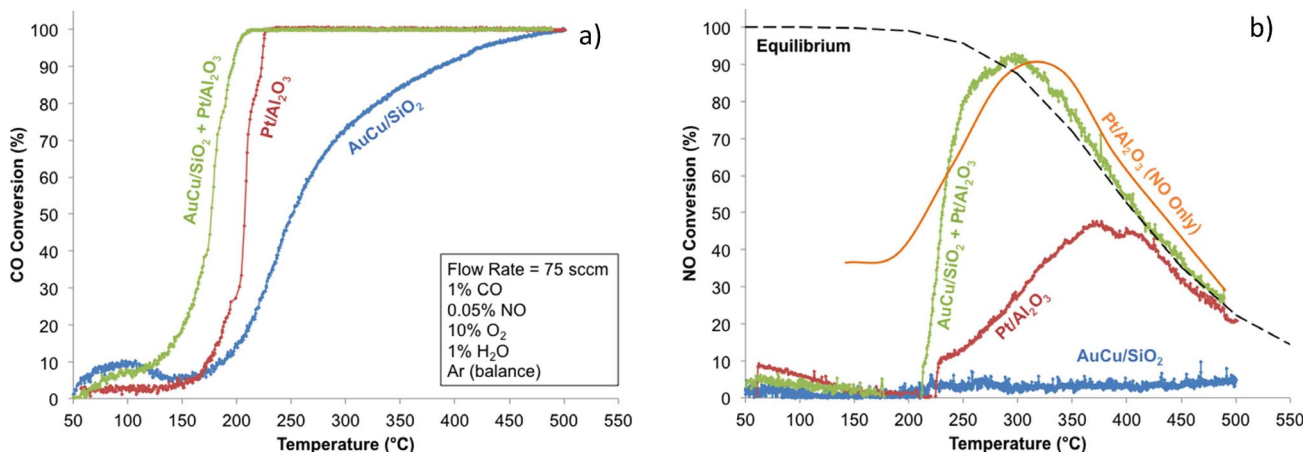


FIGURE 3. Conversion of (a) CO and (b) NO over a AuCu/SiO₂, Pt/Al₂O₃ and AuCu/SiO₂-Pt/Al₂O₃ mixture catalysts with 1% CO, 500 ppm NO, 1% H₂O, 10% O₂ and Ar with a W/F = 0.25 g·h/mol. In the case of the orange curve the reaction stream was composed of 500 ppm NO, 1% H₂O, 10% O₂ and Ar. Catalysts were pretreated by calcination at 550 °C for 16 h in 10% O₂, 1% H₂O and Ar (balance) at 75 sccm. The dashed line represents the NO/NO₂ equilibrium.

on the catalyst surface and suppress the CO oxidation reaction until temperatures near 200°C are reached. Thus under these conditions, Pt/Al₂O₃ has significantly better activity than AuCu catalysts because it is not as affected by NO and C₃H₆.

In carrying out this study we are also interested in looking for potential synergistic relationships between emerging catalysts and proven catalysts. When flowing 500 ppm of NO into the reaction stream with 1% CO and a W/F = 0.25 g·h/mol, a significant synergy between the Au-CuO_x/SiO₂-Pt/Al₂O₃ catalyst mixture is observed. Figure 3a shows that while the AuCu/SiO₂ catalyst was significantly deactivated with the presence of NO, the physical mixture of the two catalysts decrease the light-off temperature by nearly 35°C. Furthermore, the

oxidation of NO to NO₂ increases to 90% at ~300°C (in line with the NO/NO₂ equilibrium as shown in Figure 3b) while the Pt/Al₂O₃-only catalyst peaks at 40–50% conversion between 350°C–450°C. The AuCu/SiO₂ catalyst was completely inactive for the oxidation of NO into NO₂. In another study, it was found that NO had a stronger binding energy on Pt and Pd catalysts, but when AuPd alloy catalyst was used, an enhancement of CO oxidation was observed due to the weakening of NO on the catalyst surface [7]. However, in this case the Au, Cu and Pt are not alloyed and the two catalyst systems must be working in synergy. It is likely that Pt/Al₂O₃ is able to oxidize NO and reduce the inhibition on the AuCu/SiO₂ surface. At the same time, the AuCu/SiO₂ catalyst can oxidize CO that allows more active sites on the Pt/Al₂O₃

catalyst to remain open for the oxidation of NO. The orange curve in Figure 3b shows that if CO is removed from the reaction stream, NO is only present and is no longer competing with CO for active sites, the same level of NO conversion can be obtained. Interestingly, in the Pt/Al₂O₃-only case 100% CO conversion is achieved above 200°C, yet the NO to NO₂ oxidation does not reach the levels observed in the CO-free case, so this synergistic relationship goes beyond simple removal of the CO from the gas-phase.

After evaluating the effects of introducing different reactants (CO, C₃H₆ and NO) into the gas stream, the thermal stability of the AuCu/SiO₂ was investigated by ageing the catalyst in 10% O₂, 1% H₂O and Ar for 10 h. Figure 4a shows that ageing at 500°C produced the most active catalyst at low temperatures, but after 600 and 700°C the catalyst was able to reach 100% conversion at even lower temperatures than the 500°C-aged sample. As the ageing temperature increased the low temperature activity of the Au-CuO_x/SiO₂ further diminished, and after 800°C there was significant catalyst deactivation observed at the higher temperatures as well. This is consistent with a decrease in the active surface area due to particle sintering. After heating to 600°C, 700°C and 800°C for 10 h under an oxidizing atmosphere analysis of X-ray diffraction (XRD) patterns indicate the crystallite size to be 5.7 nm, 7.3 nm and 9.0 nm, respectively. Particle sizes obtained from transmission electron microscope (TEM) image analysis agree relatively well with the XRD data, Figure 4b, and show that after ageing at 600°C for 10 h a high particle density still remains (higher metal dispersion), but by 800°C there is

a lower particle density with larger particles (lower metal dispersion).

Understanding that the poor adhesion of the AuCu is limiting durability in this system, the investigation looked at different supports to aid the metal support interactions. Ceria-zirconia, which is a common commercially viable washcoat constituent, was thus employed. Figure 5a shows how the use of this washcoat significantly improves the durability, although the very high activity below 100°C is mostly lost. Under these CO-only conditions the activity approaches the target of 90% conversion at 150°C even after hydrothermal aging at 800°C. Further investigations into the activity in the presence of other exhaust constituents illustrated that both NO and HC continue to inhibit the overall activity, although this system only showed an increase in T_{90%} of 70°C compared to the ~300°C increase for the SiO₂ supported AuCu. The overall state of the research is summarized in Figure 6 for the catalysts studied during the year. While the target conversion can be reached under some conditions, the overall target in the presence of NOx and HC and after thermally aging remains elusive.

CONCLUSIONS

- In an effort to identify emissions control technologies that enable 90% conversion of NOx/CO/HC at 150°C, novel catalytic materials were fully evaluated in conditions that are relevant to automotive exhaust

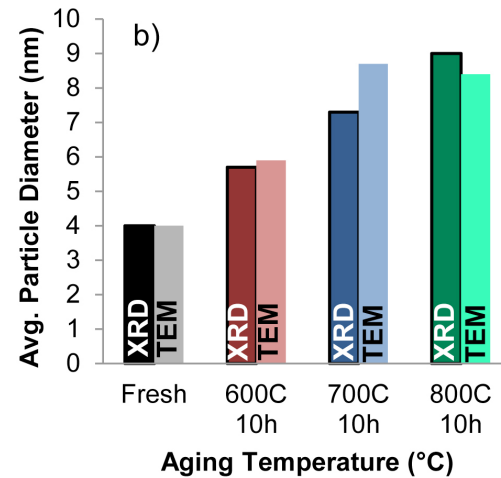
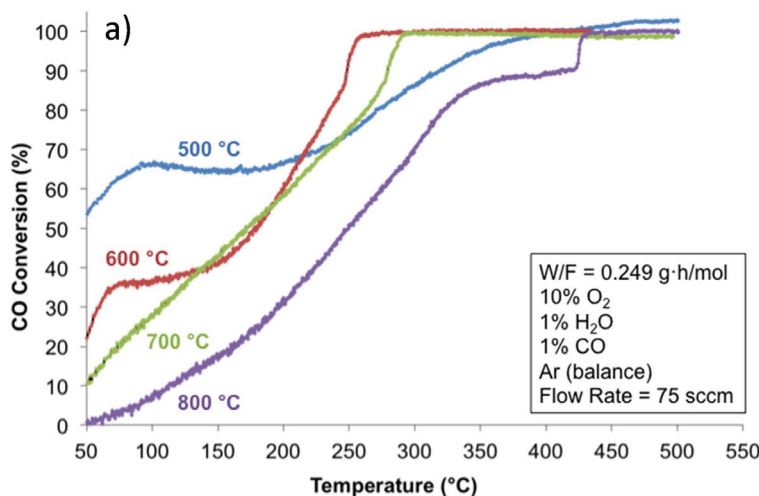


FIGURE 4. (a) CO conversion as a function of temperature after hydrothermal aging at 500, 600, 700 and 800°C for 10 h under 10% O₂, 1% H₂O and Ar. Reaction conditions: 1% CO, 1% H₂O, 10% O₂ and Ar with a W/F = 0.5 g·h/mol at a flow rate of 75 sccm. (b) The size distribution histogram of metallic particles on AuCu/SiO₂ after thermal aging.

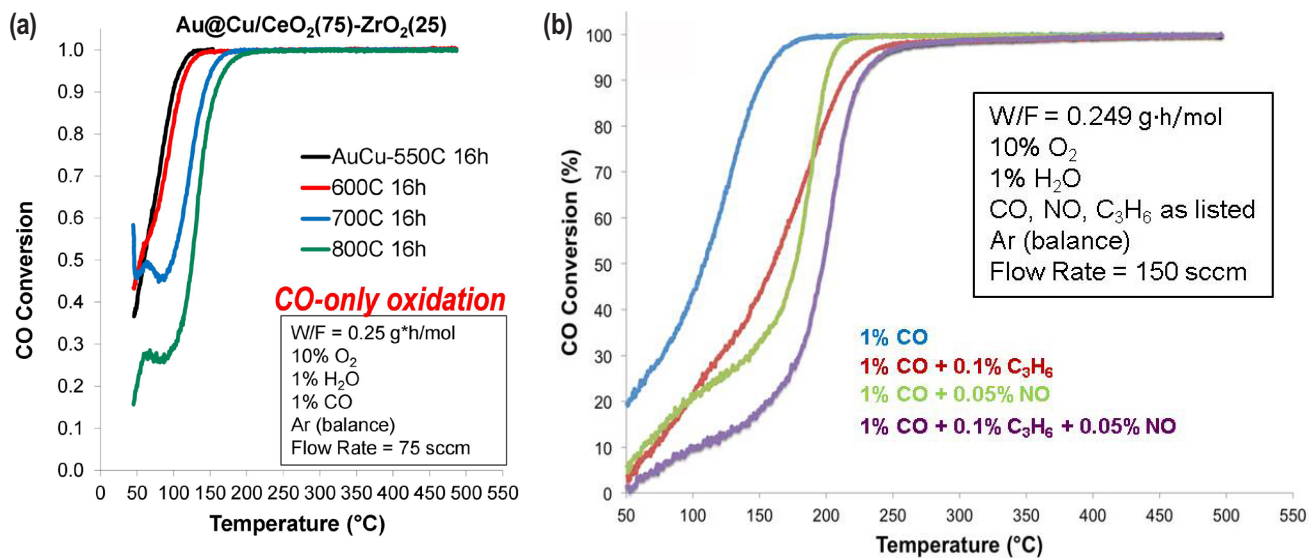


FIGURE 5. Supporting AuCu on a ceria/zirconia support showed improved durability to (a) thermal effects and (b) in the presence of NO/HCs.

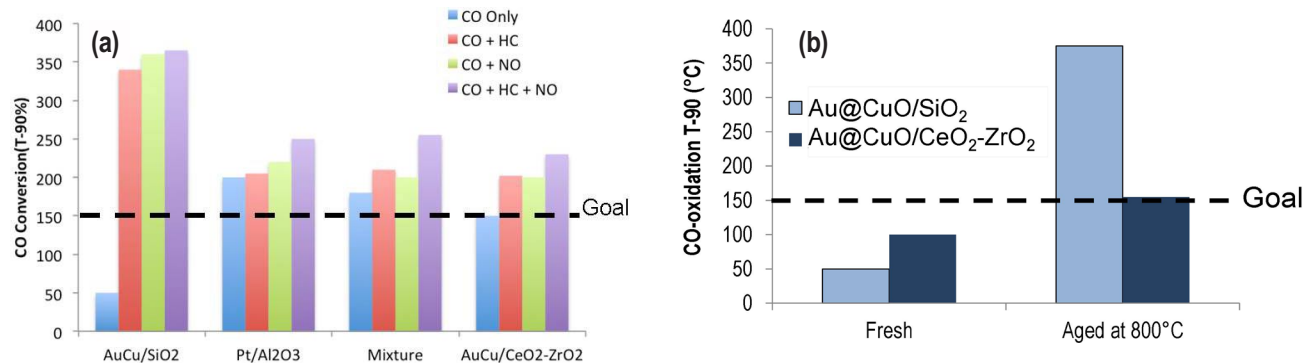


FIGURE 6. Summary of T_{90%} light-off temperatures as they are affected by (a) exhaust constituents and (b) hydrothermal aging.

- Catalysts initially developed under Basic Energy Science-funded research
- AuCu catalysts show very high CO oxidation activity at low temperatures but are limited by durability and inhibition of NO/HC.
- Thermal durability also a concern, but when supported on ceria-zirconia that activity shows only minor losses after aging to 800°C

REFERENCES

1. Kašpar, J.; Fornasiero, P.; Hickey, N.; *Catal. Today* **2003**, *77*, 419–449.
2. U.S. Environmental Protection Agency, *EPA-420-F-13-016a* **2013**, 1-4.
3. U.S. Environmental Protection Agency, Department of Transportation, National Highway Traffic Safety Administration, *Federal Register* **2012**, *77:199*, 62623-63200.

4. Prikhodko, V.; Curran, S.; Parks, J.; and Wagner, R.; *SAE Int. J. Fuels Lubr.* **2013**, *6:2*, 329-335.
5. Kim, M.-Y.; Choi, J.-S.; Toops, T.J.; Jeong, E.-S.; Han, S.-W.; Schwartz, V.; Chen, J.; *Catalysts* **2013** *3*, 88-103.
6. Daté, M.; Okumura, M.; Tsubota, S.; Haruta, M.; *Angew. Chem. Int. Ed.* **2004**, *43*, 2129–2132.
7. Hao, X.; Shan, B.; Hyun, J.; Kapur, N.; Fujdala, K.; Truex, T.; Cho, K.; *Top. Catal.* **2009**, *52*, 1946–1950.

FY 2013 PUBLICATIONS/PRESENTATIONS

1. J. Chris Bauer, Todd J. Toops, Yatsandra Oyola, James E. Parks II, “Catalytic activity and thermal stability of Au-CuO/SiO₂ catalysts for the low temperature oxidation of CO in the presence of propylene and NO,” submitted to *Catalysis Today*, October 2013.
2. Mi-Young Kim, Jae-Soon Choi, Todd J. Toops, Eun-Suk Jeong, Sang-Wook Han, Viviane Schwartz, and Jihua Chen,

“Coating Silica Support with Titania or Zirconia and Effects on Structure and CO Oxidation Performance of Platinum Catalysts”, *Catalysts* 3 (2013) 88-103; doi:10.3390/catal3010088.

3. J. Chris Bauer, Todd J. Toops, James E. Parks II, “Silica Supported Au-CuO Catalysts for Low Temperature CO Oxidation”, 23rd North American Catalysis Society Meeting (NAM), Louisville, KY, June 2–7, 2013.

4. Todd J. Toops, James E. Parks, J. Chris Bauer, “Low Temperature Emissions Control”, 2013 DOE Annual Merit Review, Crystal City, VA, May 16, 2013.

5. J. Chris Bauer, Todd J. Toops, James E. Parks II, Sheng Dai, Steve H. Overbury, “Supported Au-CuO Catalysts for Low Temperature CO Oxidation,” 2012 Directions in Engine-Efficiency and Emissions Research Conference (DEER), Dearborn, MI, October 17, 2012.

6. J. Chris Bauer, Todd J. Toops, James E. Parks II, “Supported Au-CuO Catalysts for Low Temperature CO Oxidation,” 2012 South-Eastern Catalysis Society Fall Symposium, October 1, 2012.

III.8 Emissions Control for Lean-Gasoline Engines

Jim Parks (Primary Contact), Todd Toops,
Josh Pihl, Vitaly Prikhodko
Oak Ridge National Laboratory (ORNL)
2360 Cherahala Blvd.
Knoxville, TN 37932
DOE Technology Development Manager:
Ken Howden

- Identified key SCR catalyst characteristics and operating strategies required to achieve high NO_x conversion while minimizing fuel penalty.
- Completed a study in collaboration with Pacific Northwest National Laboratory on the morphology and composition of particulate matter from lean-gasoline direct-injection engines. (Note: the particulate matter study was funded by other DOE-sponsored projects but supported by the engine platform developed for this project.)

Overall Objectives

- Assess and characterize catalytic emission control technologies for lean-gasoline engines.
- Identify strategies for reducing the costs, improving the performance, and minimizing the fuel penalty associated with emission controls for lean-gasoline engines.
- Define a technical pathway for a lean-gasoline engine to meet U.S. emission regulations (U.S. Environmental Protection Agency Tier 2 Bin 2) with minimal fuel consumption and cost.
- Demonstrate the fuel efficiency improvement of a low-emission lean-gasoline engine relative to the stoichiometric-gasoline engine case on an engine dynamometer platform.

Fiscal Year (FY) 2013 Objectives

- Commission lean-gasoline direct-injection engine platform.
- Characterize the fuel efficiency and emission performance of a three-way catalyst plus selective catalytic reduction (TWC+SCR) system on the engine dynamometer platform as a function of the ratio of lean to rich periods.

FY 2013 Accomplishments

- Completed the commission process for lean-gasoline direct-injection engine platform.
- Achieved >99% oxides of nitrogen (NO_x) to NH₃ conversion over a TWC at an equivalence ratio (λ) of 0.96.
- Demonstrated >98% NO_x reduction efficiency with a TWC+SCR approach on the lean-gasoline engine platform with a 5.6% fuel economy improvement over the stoichiometric-engine case.

Future Directions

- Evaluate the potential benefits of utilizing NO_x storage media on TWCs to extend lean operating time with the passive SCR approach.
- Analyze the impact of oxygen storage components of the TWC on NH₃ production during rich-lean transitions for the passive SCR approach.



INTRODUCTION

Currently, the U.S. passenger car market is dominated by gasoline engine powertrains that operate at stoichiometric air-to-fuel ratios (sufficient fuel is mixed in air such that all of the oxygen in the air is consumed during combustion). Stoichiometric combustion leads to exhaust conditions suitable for TWC technology to reduce NO_x, CO, and hydrocarbon (HC) emissions to extremely low levels. Operating gasoline engines at lean air-to-fuel ratios (excess air) enables more efficient engine operation and reduces fuel consumption; however, the resulting oxygen in the exhaust prevents the TWC technology from reducing NO_x emissions. It is relatively straightforward to operate an engine lean over a significant portion of the load and speed operating range; so, the largest challenge preventing fuel-saving lean combustion in gasoline applications is the control of emissions, primarily NO_x. This project addresses the challenge of reducing emissions from fuel-saving lean-gasoline engines in a cost-effective and fuel-efficient manner to enable their market introduction.

APPROACH

This project utilizes the full suite of capabilities available at ORNL's Fuels, Engines, and Emissions Research Center, including: a lean-gasoline engine on an engine dynamometer, a vehicle equipped with the

same engine on a chassis dynamometer, flow reactors for detailed catalyst evaluations under carefully controlled operating conditions, and vehicle system level modeling. The combination of catalyst studies on flow reactor and engine platforms is a key component of the project approach. Prototype catalyst formulations are first studied on flow reactors to understand catalytic function and establish operating schemes in a controlled setting; then, select catalyst combinations are studied on the engine platform to characterize performance under realistic exhaust conditions. The engine studies also enable direct measurement of fuel economy benefits from lean-gasoline engine operation as well as measurement of “fuel penalties” imposed by the emission control system to function properly.

The engine platform for the project is from a model year 2009 BMW 120i vehicle sold in Europe. The 4-cylinder, direct-injection, naturally aspirated engine operates in multiple modes including lean (excess air) and stoichiometric combustion. The BMW 120i employs both a TWC for stoichiometric operation and a lean NOx trap (LNT) catalyst for NOx reduction during lean operation. Although this engine and aftertreatment combination met the 2009 emissions regulations in Europe, as configured it does not meet the current U.S. emissions standards. Furthermore, the LNT catalyst contains high loadings of platinum group metals, which add significantly to the overall cost of the vehicle. The goal for this project is to identify emissions control technologies that could meet the U.S. Environmental Protection Agency Tier 2 Bin 2 emission levels while maximizing the fuel efficiency benefit from lean-gasoline engine operation and minimizing system cost. The project is focused primarily on NOx emission control, though HC and CO emissions targets must also be met. LNT catalysts, such as the one used on the BMW 120i, typically contain high loadings of expensive platinum group metals. Furthermore, LNTs are challenged by the high NOx concentrations and high exhaust temperatures typical of lean-gasoline applications. Cu zeolite NH₃ SCR catalysts are widely used for NOx control in the lean exhaust mixtures from diesel engines. In these systems, NH₃ is generated from a urea solution sprayed upstream of the SCR catalyst. While these catalysts have demonstrated both excellent durability and high NOx conversion activity over a wide temperature window, urea SCR may not be a viable approach for light-duty lean-gasoline engines due to high urea consumption (which scales with NOx concentration) and the cost and packaging challenges associated with the onboard urea storage and delivery system. With these challenges in mind, recent work under the project has focused on an emission control concept known as “passive SCR” [1-3]. The key to the approach is to generate NH₃ over the TWC under slightly rich conditions and then store it on a downstream SCR. When

returning to lean operation, the stored NH₃ reduces NOx that is not converted over the upstream TWC (or LNT). In this manner, the TWC controls NOx during stoichiometric and rich operation of the engine, and the SCR catalyst controls NOx during lean-engine operation.

This report highlights results from engine and flow reactor experiments conducted in FY 2013 on a passive SCR emission control system. The catalysts used in the system were either supplied or recommended by Umicore, a major catalyst supplier to the automotive industry. Frequent interaction occurred with Umicore as well as General Motors to guide project progress and relevance.

RESULTS

The engine study was conducted with a TWC and SCR catalyst installed in the engine exhaust. The TWC formulation consisted of two zones: the upstream zone was a Pd-only formulation, while the downstream zone contained Pd, Rh, and oxygen storage materials. The SCR catalyst was a small-pore Cu-zeolite catalyst and was located approximately 1 m downstream of the TWC to allow the exhaust gases to cool to more appropriate temperatures for the SCR reactions. The engine was operated at various steady-state conditions and emissions at different points in the emission control system were characterized with a Fourier transform infrared analyzer.

Initial experiments focused on the NH₃ production over the TWC; flow reactor studies of TWC formulations during FY 2012 served as a guide for the engine operating parameters. Figure 1 shows the engine-out (TWC-in) NO_x and TWC-out NH₃ as a function of λ or equivalence ratio. λ represents the ratio of the actual air-

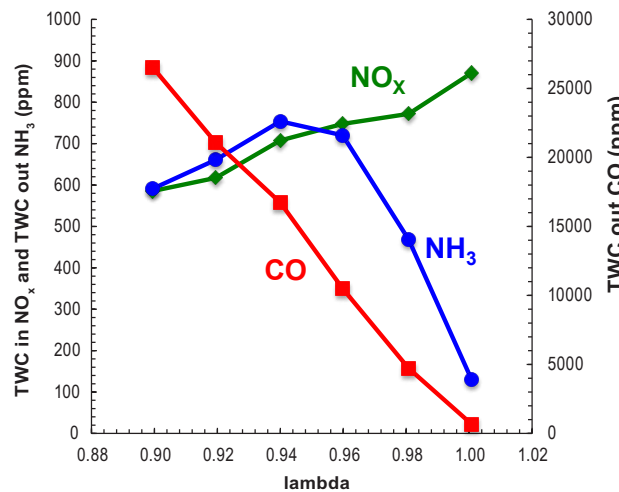


FIGURE 1. NO_x at the TWC inlet position and CO and NH₃ at the TWC outlet position as a function of equivalence ratio.

to-fuel ratio to the stoichiometric air-to-fuel ratio. Thus, for lean-engine operation, λ is greater than 1, and for rich-engine operation, λ is less than 1. As seen in Figure 1, the peak NH_3 formation occurred at $\lambda = 0.94$. Under richer conditions than $\lambda = 0.94$, NH_3 actually decreased corresponding to engine out NOx levels decreasing. Since CO increases as the engine operated more rich, the optimal operating condition for maximizing NH_3 while minimizing CO and HC emissions appears to be $\lambda = 0.96$. The engine-out NOx level affected NH_3 production over the TWC dramatically with declining NOx levels reducing NH_3 formation. As shown in Figure 2, NOx

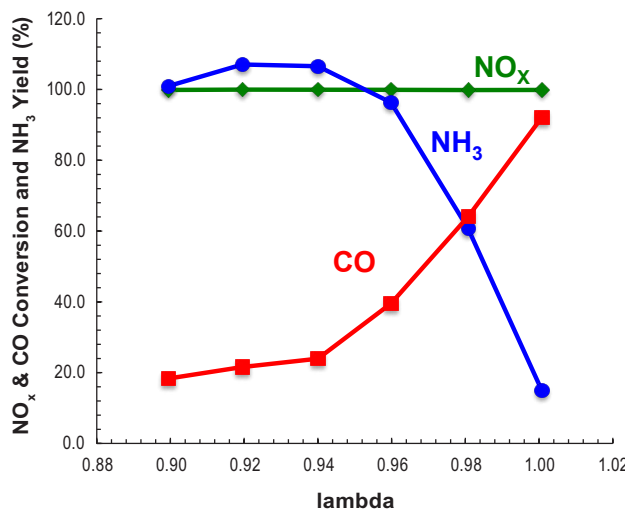


FIGURE 2. NOx and CO conversion and NH_3 yield for the same data shown in Figure 1.

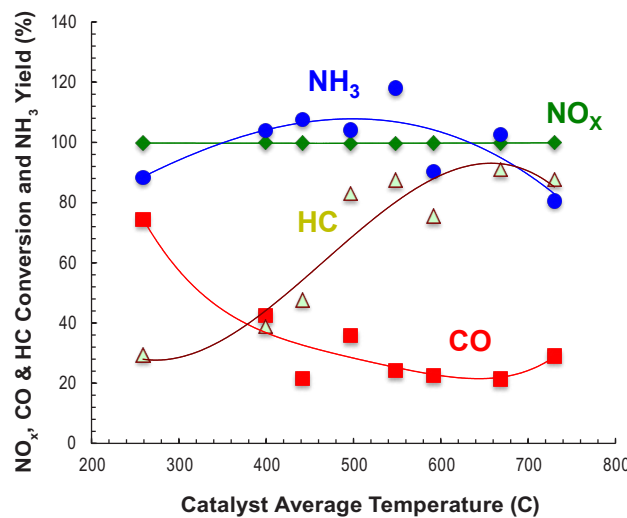


FIGURE 3. NOx, CO, and HC conversion and NH_3 yield as a function of catalyst temperature over a broad range of engine speed and load combinations.

conversion was very high with NOx being converted to NH_3 very effectively for $\lambda < 0.96$.

NH_3 production as well as NOx, CO, and HC emissions are shown in Figure 3 and give a broader picture of NH_3 formation over a wide range of engine speeds and loads for $\lambda = 0.96$. For lower catalyst temperatures, more HCs pass through the TWC unconverted. NH_3 formation is high over the entire temperature range, but CO is not converted effectively over the temperature range examined.

The combination of the TWC and SCR catalyst working together to achieve NOx reduction is demonstrated by Figure 4. Figure 4(a) shows data from FY 2012 flow reactor experiments, while 4(b) shows data from engine experiments. For both experiments, the TWC+SCR system was cycled between lean and rich simulated exhaust conditions to obtain the results; the periods of the lean vs. rich operation modes were

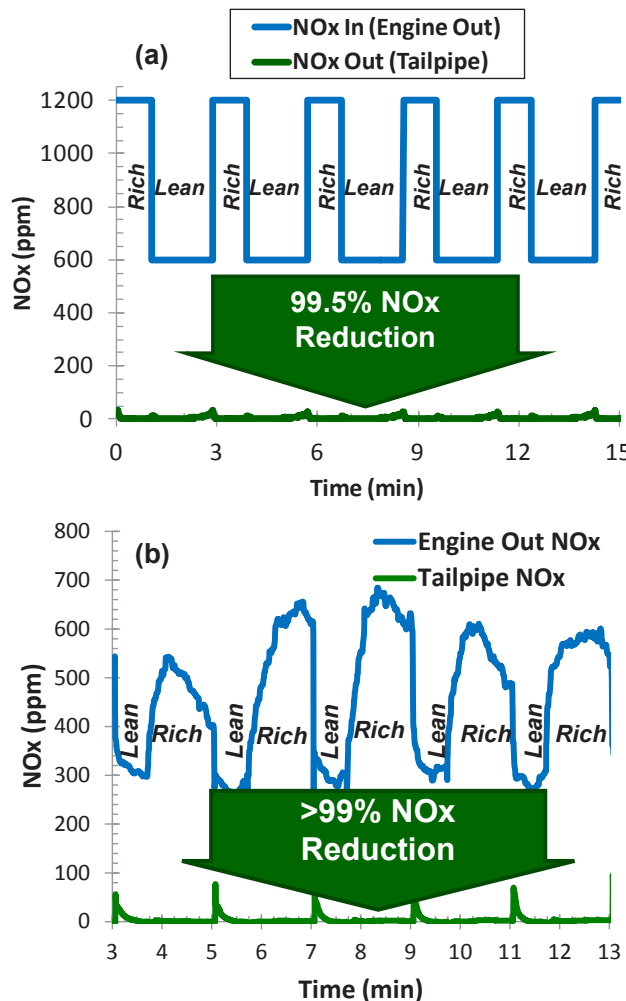


FIGURE 4. Experimental results from bench reactor (a) and engine (b) studies showing the combined performance of a TWC+SCR system. Tailpipe emission levels are also shown in Table 1.

chosen to allow highest NO_x conversion. Although actual exhaust species concentrations and catalyst temperatures differed some between the flow reactor and engine data sets, the same trends were observed in both. Specifically, enough NH₃ can be generated over the TWC to enable NO_x conversions of 99% or better over the SCR catalyst. The fuel economy benefit of the lean-rich cycle operation of the engine was 5.4% better than an engine-only operating in stoichiometric combustion modes.

The similarity in trends between the engine and flow reactor experiments is highlighted in Table 1, that shows the average and maximum species concentrations at the SCR catalyst outlet for both systems. Outlet concentrations of NO_x, NH₃, N₂O, and HC_s were quite low, but CO emissions were significant. The similarity in trends between the engine and flow reactor experiments validates the strategy of using flow reactor results to guide engine experiments.

TABLE 1. SCR Outlet Emissions for Passive SCR Operation on the Engine and Flow Reactor

| | Engine Tailpipe | | Reactor Outlet | |
|------------------|-----------------|------------|----------------|------------|
| | Avg. (ppm) | Max. (ppm) | Avg. (ppm) | Max. (ppm) |
| NO _x | 5 | 126 | 4 | 31 |
| NH ₃ | 2 | 5 | 3 | 4 |
| N ₂ O | 1 | 10 | 2 | 32 |
| CO | 1,782 | 4,658 | 1,200 | 3,900 |
| HC | <1 | 16 | 0 | 0 |

During FY 2013, flow reactor experiments focused on evaluating the impacts of operating strategies and SCR catalyst formulation on overall passive SCR system performance, and on identifying the key underlying processes that limit system performance. Investigations with a small-pore Cu zeolite generated several conclusions that will guide future engine work: (1) less than half of the SCR catalyst capacity for NH₃ storage can be utilized during passive SCR cycling to prevent excessive NH₃ slip; (2) the operating window for a small pore Cu-zeolite SCR catalyst during passive SCR cycles is between 200 and 350°C; and (3) high SCR temperatures result in oxidization of the stored NH₃ to NO_x when switching from rich to lean conditions, leading to excessive NO_x slip. Changing to an Fe zeolite formulation with lower NH₃ oxidation activity might provide a pathway around the high temperature limitations. Unfortunately, as Figure 5 illustrates, Fe zeolites also tend to have lower NH₃ storage capacity, limiting the lean operating time to just a few seconds. Thus, for the formulations studied here, the Cu zeolite was superior to the Fe zeolite at all temperatures.

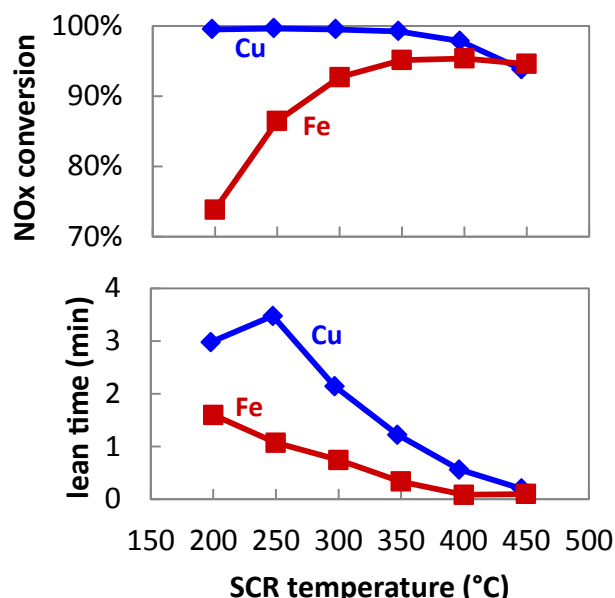


FIGURE 5. Comparison of Cu- and Fe-based performance on the bench flow reactor. In addition to higher NO_x conversions obtained with the Cu SCR, longer lean periods were obtained thereby resulting in less fuel penalty.

CONCLUSIONS

- The optimal equivalence ratio for NH₃ production with minimal CO and HC slip past the TWC is $\lambda=0.96$.
- By utilizing the TWC+SCR or passive SCR approach, high (>99%) NO_x reduction efficiencies can be achieved while still maintaining a net fuel efficiency benefit (of +5.4%) for the lean-gasoline engine. Overall, at the tailpipe position, only CO emissions were significant.
- A small pore Cu zeolite was superior to an Fe zeolite for passive SCR NO_x conversion at all SCR catalyst temperatures evaluated on the flow reactor.

REFERENCES

- Li, W., Perry, K., Narayanaswamy, K., Kim, C. et al., "Passive Ammonia SCR System for Lean-burn SIDI Engines," *SAE Int. J. Fuels Lubr.* 3(1):99-106, 2010, doi:10.4271/2010-01-0366.
- Kim, C., Perry, K., Viola, M., Li, W. et al., "Three-Way Catalyst Design for Ureless Passive Ammonia SCR: Lean-Burn SIDI Aftertreatment System," *SAE Technical Paper* 2011-01-0306, 2011, doi:10.4271/2011-01-0306.
- Guralp, O., Qi, G., Li, W., and Najt, P., "Experimental Study of NO_x Reduction by Passive Ammonia-SCR for Stoichiometric SIDI Engines," *SAE Technical Paper* 2011-01-0307, 2011, doi:10.4271/2011-01-0307.

FY 2013 PUBLICATIONS/PRESENTATIONS

- 1.** Christopher D. DiGiulio, Josh A. Pihl, James E. Parks II, Michael D. Amiridis, Todd J. Toops, “Passive-Ammonia Selective Catalytic Reduction (SCR): Understanding NH₃ formation over close-coupled Three Way Catalysts (TWC),” submitted to *Catalysis Today*, September 2013.
- 2.** Christopher D. DiGiulio, Josh A. Pihl, Jae-Soon Choi, James E. Parks II, Michael J. Lance, Michael D. Amiridis and Todd J. Toops, “NH₃ formation over a Lean NOx Trap (LNT) system: effects of lean/rich cycle timing and temperature”, *Applied Catalysis B: Environmental* 147 (2014) 698-710.
- 3.** J.A. Pihl, J.A. Lewis, J.E. Parks, T.J. Toops, “Lean NOx Trap Chemistry under Lean-Gasoline Exhaust Conditions: Impact of High Temperature and High NOx Operation”, *Topics in Catalysis* 56:1-8 (2013) 89; DOI 10.1007/s11244-013-9934-3.
- 4.** Josh A. Pihl, Todd J. Toops, Christopher D. DiGiulio, Michael D. Amiridis, James E. Parks II, “Passive SCR for lean gasoline engine emissions control”, 23rd North American Catalysis Society Meeting (NAM), Louisville, KY, June 2-7, 2013.
- 5.** Christopher D. DiGiulio, Josh A. Pihl, Jae-Soon Choi, Michael J. Lance, James E. Parks II, Michael D. Amiridis, Toops J. Toops, “Understanding NH₃ formation over Lean NOx Trap (LNT) catalysts: Effects of lean/rich cycle timing and temperature”, 23rd North American Catalysis Society Meeting (NAM), Louisville, KY, June 2-7, 2013.
- 6.** Jim Parks, Todd Toops, Josh Pihl, Shean Huff, Vitaly Prikhodko, “Emissions Control for Lean Gasoline Engines”, 2013 DOE Annual Merit Review, Crystal City, VA, May 16, 2013.
- 7.** C.D. DiGiulio, M.D. Amiridis, J.A. Pihl, J.E. Parks, T.J. Toops, “An investigation of in situ NH₃ generation for use in a downstream NH₃-SCR catalyst”, American Institute of Chemical Engineers 2012 Annual Meeting, Pittsburgh, PA, October 29, 2012.
- 8.** T.J. Toops, J.A. Pihl, J.E. Parks, C.D. DiGiulio, M.D. Amiridis, “NH₃ generation over commercial Three-Way Catalysts and Lean-NOx Traps”, 2012 Directions in Engine-Efficiency and Emissions Research Conference (DEER), Dearborn, MI, October 18, 2012.

III.9 Cummins-ORNL SmartCatalyst CRADA: NOx Control and Measurement Technology for Heavy-Duty Diesel Engines

Bill Partridge¹ (Primary Contact), Neal Currier², Maggie Connatser¹, Josh Pihl¹, Jae-Soon Choi¹, Xavier Auvray³, Soran Shwan³, Louise Olsson³, Krishna Kamasamudram², Alex Yezerets²

¹Oak Ridge National Laboratory (ORNL)
2360 Cherahala Blvd.
Knoxville, TN 37932

²Cummins, Inc.
³Chalmers University of Technology

DOE Technology Development Manager:
Ken Howden

Overall Objectives

- Understand the fundamental chemistry of automotive catalysts
- Identify strategies for enabling self-diagnosing catalyst systems
- Address critical barriers to market penetration

Fiscal Year (FY) 2013 Objectives

- Characterize distributed performance of degreened commercial Cu-SAPO-34 SCR catalyst under standard and fast selective catalytic reduction (SCR) conditions
- Compare spatially resolved capillary inlet mass spectrometry (SpaciMS) to spatially resolved capillary inlet Fourier transform infrared (SpaciIR) intra-SCR distributed measurements
- Develop Fast-SpaciMS
- Apply Fast-SpaciMS to investigate N₂O formation mechanisms
- Identify basic and practical performance characteristics consistent with enabling self-diagnosing catalyst systems

FY 2013 Accomplishments

- Characterized spatiotemporal intra-catalyst performance of degreened commercial Cu-SAPO-34 SCR catalyst under standard and fast SCR conditions.

- In collaboration with Professor Louise Olsson at Chalmers University of Technology, demonstrated application of SpaciMS intra-catalyst data for developing kinetic models:
 - Applications to SCR (PhD student Xavier Auvray) and lean-NOx trap (LNT) (M.Sc. student Soran Shwan) catalysts.
 - Kinetic parameters determined from SpaciMS data: differential conditions necessary to determine kinetic parameters often do not exist at operating temperatures and space velocities, and different operating values must be used to achieve differential conversion. By resolving the conversion distribution throughout the catalyst, SpaciMS allows the kinetic parameters to be determined under the actual operating conditions.
 - Kinetic parameters incorporated into full distributed models for both the LNT and SCR catalyst applications; transient analysis included in the SCR model.
 - Experimental data acquired at ORNL, and kinetic analysis and modeling led by Professor Olsson at Chalmers.
- Configured Fast-SpaciMS for resolving reaction sequences related to N₂O formation mechanisms.
- Cooperative Research and Development Agreement (CRADA) fiber-sensor research provided foundation for successful ORNL project to develop an in situ SO₃ sensor.
- In collaboration with Professors Enrico Tronconi and Isabella Nova of the Politecnico di Milano (PoliMi), started an effort to investigate fundamental reactions relevant to SCR performance. As part of this collaboration, PoliMi PhD student Maria Pia Ruggeri is spending 6 months at ORNL as a Visiting Student Researcher focused on this effort.
 - Joint presentations related to the importance of NO oxidation on the standard SCR mechanism, and a manuscript prepared.
- Worked in collaboration with the Cross-Cut Lean Exhaust Emissions Reduction Simulations program and the Institute of Chemical Technology, Prague to identify N₂O formation pathways in LNT catalysts; hosted visiting scientist Dr. Petr Kočí, and Institute of Chemical Technology, Prague PhD student David Mráček.

- Joint presentations and an archival presentation resulted from this work.

Future Directions

Quantify spatiotemporal performance of commercial Cummins SCR catalyst under lab- and field-aged conditions.



INTRODUCTION

A combination of improved technologies for engine and aftertreatment control of NO_x and particulate emissions are required to efficiently meet increasingly stringent emission regulations. This CRADA section focuses on catalyst technologies, while a parallel section (Characterization and Reduction of Combustion Variations) focuses on combustion and engine technologies. Improved catalyst system efficiency, durability, and cost can be achieved through advanced control methodologies based on continuous catalyst-state monitoring; the overarching goal of this CRADA is to enable self-diagnosing of smart-catalyst systems. Self-diagnosing catalyst technologies are enabled by basic and practical insights into the transient distributed nature of catalyst performance, improved catalyst models, insights suggesting control methodologies, and instrumentation to demonstrate and drive advanced control technologies. These catalysis advances require development and application of enhanced diagnostic tools to realize these technology improvements. While the CRADA has a strong diagnostic focus, it is involved, often through synergistic partnerships, in the other enabling research activities discussed previously.

APPROACH

The CRADA applies the historically successful approach of developing and applying minimally invasive advanced diagnostic tools to resolve spatial and temporal variations within operating engines and catalysts. Diagnostics are developed and demonstrated on bench reactors and engine systems (as appropriate) at ORNL prior to field application at Cummins. In some cases discrete-sensor technology is a stepping stone and may be further developed and integrated in system components; e.g., to create self-diagnosing smart-catalyst systems.

Diagnostics are applied at ORNL and Cummins to study the detailed nature and origins of catalyst performance variations; this may be spatial and temporal variations unique to each catalyst function (e.g., SCR, NH_3 storage and parasitic oxidation, NO_x storage and reduction, oxygen storage capacity, water-gas shift)

during operation and how these vary with ageing (e.g., thermal, hydrocarbon, sulfur). This detailed information is applied to understand how catalysts function and degrade, develop device and system models, and develop advanced control strategies.

RESULTS

SpaciMS and SpaciIR were used to characterize the distributed performance throughout a degreened commercial Cu-SAPO-34 SCR catalyst under standard and fast SCR conditions at 200, 300 and 400°C. In general, the reaction distribution shifted to the catalyst front with increasing temperature and for fast vs. standard SCR. Parasitic NH_3 oxidation was apparent only at the highest temperature under standard SCR conditions; specifically and on the contrary, this was not observed under fast SCR conditions at 400°C. The distributions from the two intra-catalyst analytical techniques were generally similar, and will be compared in more quantitative detail. These results will be compared to similar measurements of lab- and field-aged catalyst samples to assess the impact of ageing on distributed performance, and gain insights into ageing mechanisms and strategies for catalyst-state assessment and/or control.

A Fast-SpaciMS was configured and applied to the work with the Institute of Chemical Technology, Prague to investigate N_2O formation mechanisms during LNT regeneration. The Fast-SpaciMS uses differential sampling via a 200 μm outside x 100 μm inside diameter capillary and a ca. 25 μm orifice inlet to the MS. The result is ca. 280 $\mu\text{L}/\text{min}$ capillary sample flow rate, and ca. 200-300 ms T_{10-90} response time; this is about 4 times faster than with standard direct-sampling SpaciMS which uses ca. 28x lower capillary sampling flow. The capillary flow can be further increased to reduce the measurement response time, within the constraints of the specified minimally invasive nature.

Research related to development of an optical fiber-based sensor for NH_3 and catalyst oxidation state was performed; the sensor uses Cu-exchanged zeolite SCR catalyst as the transducer, which is incorporated in a sol-gel coating on an optical fiber, and optical spectroscopies are used to probe the state of the transducing material. The probe has promise for both applied and more basic applications related to urea dosing and catalyst control, and elucidating detailed reaction parameters related to SCR catalyst performance. This approach builds on previous CRADA work focused on temperature, O_2 , CO_2 and CO measurement with similar fiber-based diagnostics. The probe has been used to measure NH_3 transients; FY 2014 work will focus on cross sensitivities, uniformity of probe-to-probe sensor response, and

extending the measurement to quantify local oxidation state. This CRADA work also provided the background and foundation for an ORNL-funded effort to develop a diagnostic for in situ SO_3 measurements. Table 1 compares state-of-the-art methods for sulfur-compound detection, and reveals a distinct need for in situ measurement strategies, that avoid the complications of transfer lines and extractive methods. This high-risk, high-reward project uses the spectroscopic properties of copper-exchanged SCR catalyst material to study sulfur trioxide interactions with the catalyst material; Figure 1 shows the planned probe. The overarching goal of the

proposed research is two-fold, the first being developing access to improve understanding of sulfur chemistry in a catalyst material environment, and second to improve diagnostics for driving down costs of resources and time required to create new materials for high efficiency, cleaner energy production.

CONCLUSIONS

- Distributed performance of a degreened commercial Cu-SAPO-34 SCR catalyst under standard and fast SCR conditions and at a range of temperatures.

TABLE 1. Comparison of Methods Currently used to Detect Sulfur Compounds in Exhaust

| Method | Sampling Approach | Species Detected | Detection Mode | Limit of Detection | Limitations |
|--|-------------------------------------|----------------------------|--|---|---|
| Environmental Protection Agency Method 8 | Solvent selective gas entrainment | H_2SO_4 | Wet titration with colorimetric complex | 0.5 ppm in condensate | Hours of sampling time 100s of liters sample volume No spatial resolution |
| Quantum Cascade Laser Absorption | Line-of-sight open gas path | SO_3, SO_2 | Infrared absorbance | 1 ppmv | Low pressures (300 Torr) Ultra-delicate instruments Path length dependent |
| $\text{SO}_2^{\text{in}} - \text{SO}_2^{\text{out}}$ across catalyst | Transfer lines to infrared gas cell | SO_2 | Difference of dual Fourier transform infrared measurements | 10 ppm | Assumption-dependent Minimal spatial resolution within catalyst |
| Fiber Tip Luminescence | Optical probe in gas stream | SO_3, SO_2 | Catalyst luminescence quenching | ~0-100 ppm range to be evaluated | Relative Advantages Millisecond response time 100s of sec recovery time Minimally invasive for intra-catalyst spatial resolution |

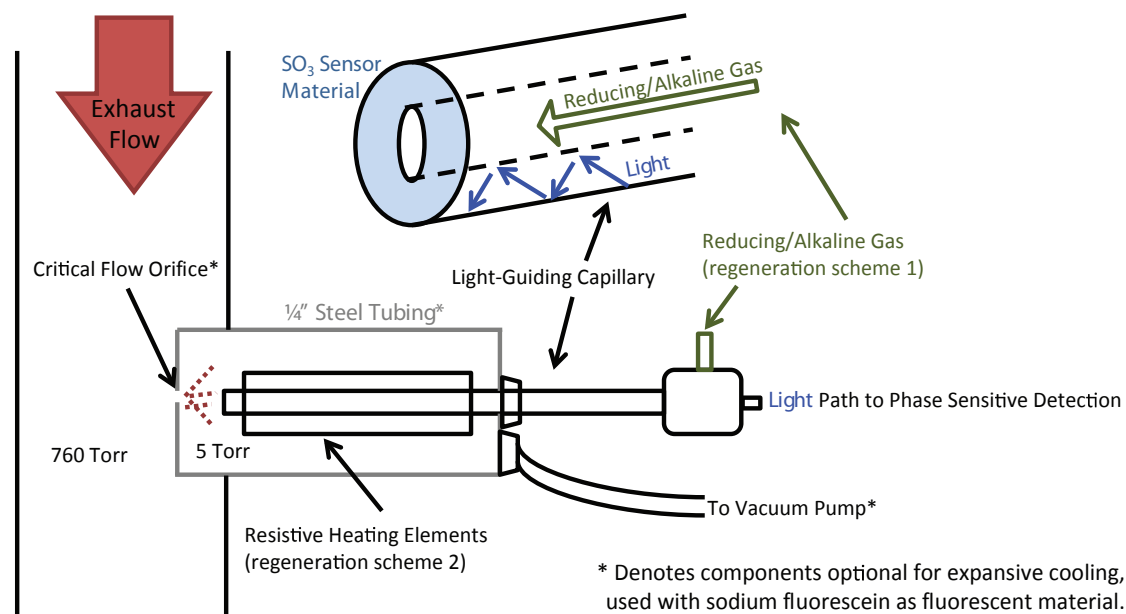


FIGURE 1. The probe concept can exploit expansive cooling from atmospheric to near-vacuum pressure, and a light-guiding capillary allows the sol gel containing a material, copper zeolite, sensitive to SO_3 and to be interrogated with laser induced luminescence and regenerated with an alkaline gas.

- In collaboration with Chalmers, intra-catalyst distributed performance measurements used to determine kinetic parameters for both SCR and LNT catalysts under actual operating conditions; and used to develop distributed-performance models.
- Fast-SpaciMS developed and demonstrated for fast-response intra-catalyst measurements.
- NH₃ sensor demonstrated.
- CRADA sensor experience used to leverage new SO₃ diagnostic project.
- Multiple collaborations benefit DOE and CRADA objectives:
 - SCR fundamentals including impact of NO oxidation on standard SCR.
 - N₂O mechanistic pathways during catalyst operation.
 - Determining kinetic parameters of catalyst-reactions under normal operating conditions.

FY 2013 PUBLICATIONS/PRESENTATIONS

Archival Publications

1. Petr Kočí, Šárka Bártová, David Mráček, Miloš Marek, Jae-Soon Choi, Mi-Young Kim, Josh A. Pihl, William P. Partridge (2013). “Effective Model for Prediction of N₂O and NH₃ Formation During the Regeneration of NO_x Storage Catalyst,” Topics in Catalysis 56, 118-124; doi: 10.1007/s11244-013-9939-y.

Oral Presentations

- 1.** R. Maggie Connatser, William P. Partridge, Jr., and James E. Parks, II, “State Assessment of SCR Catalyst: Copper Zeolite/Sol-Gel-Tipped Optical Fiber Probes,” Southeastern Catalyst Society 11th Annual Symposium, Asheville, North Carolina, October 1, 2012.
- 2.** Šárka Bártová, David Mráček, Petr Kočí, Miloš Marek, Jae-Soon Choi, Josh A. Pihl, William P. Partridge, Mi-Young Kim, C. Stuart Daw. “Lean NOx trap regeneration selectivity towards N₂O – similarities and differences between H₂, CO and C₃H₆ reductants,” Emission Control Technologies, 18th Directions in Engine-Efficiency and Emissions Research (DEER) Conference, Detroit, Michigan, October 19, 2012.
- 3.** R. Maggie Connatser, William P. Partridge, Jr., Josh A. Pihl, and James E. Parks, II, “Ammonia & Oxidation State Sensing Based on Catalyst-Tipped Optical Fibers,” 2013 DOE Crosscut Workshop on Lean Emissions Reduction Simulation, University of Michigan, Dearborn, Michigan, April 11th, 2013.
- 4.** W.P. Partridge, J.A. Pihl, J.-S. Choi, L. Olsson, F. Coelho, X. Auvray, N. Currier, A. Yezers, K. Kammasudram, “Cummins/ORNL FEERC Emissions CRADA: NO_x Control & Measurement Technology for Heavy Duty Diesel Engines,”

2013 DOE Vehicle Technologies Program Annual Merit Review, Arlington, Virginia, May 16, 2013.

- 5.** Šárka Bártová, Petr Kočí, Miloš Marek, Josh A. Pihl, Jae-Soon Choi, Todd J. Toops, William P. Partridge. “New Insights on N₂O Formation Pathways during Lean/Rich Cycling of a Commercial Lean NO_x Trap Catalyst,” 23rd North American Catalysis Society Meeting, Louisville, Kentucky, June 5, 2013.
- 6.** David Mráček, Šárka Bártová, Petr Kočí, Miloš Marek, Jae-Soon Choi, Josh A. Pihl, Stuart Daw, William P. Partridge. “N₂O Formation During Lean NO_x Trap (LNT) Catalyst Regeneration,” Southeastern Catalysis Society Meeting, Asheville, North Carolina, September 30, 2013.

Poster Presentations

- 1.** Maria Pia Ruggeri, Isabella Nova, Enrico Tronconi, Josh A. Pihl, Jae-Soon Choi, Todd J. Toops, William P. Partridge, “Role of NO oxidation to NO₂ in NH₃-SCR reactions: kinetics and mechanism,” 23rd North American Catalysis Society Meeting, Louisville, Kentucky, June 3, 2013 (Poster).
- 2.** R. Maggie Connatser, W.P. Partridge, Jr., J.M.E. Storey, S.A. Lewis, Sr., J.E. Parks, II. “Catalyst-Tipped Optical Fibers for Catalyst System Development: Sensing Ammonia, Oxidation State, & Sulfur Interactions,” Southeastern Catalysis Society Meeting, Asheville, North Carolina, September 30, 2013.

SPECIAL RECOGNITIONS & AWARDS/ PATENTS ISSUED

Invited Lectures

- 1.** Maria Pia Ruggeri, I. Nova, E. Tronconi, J.A. Pihl, J.S. Choi, T.J. Toops, W.P. Partridge. “Role of NO Oxidation to NO₂ in SCR Reactions,” presentation to the Catalyst Technology Group, Corporate Research and Technology, Cummins Inc.; presentation at the Cummins Technical Center, Columbus, Indiana, February 8, 2013.
- 2.** Bill Partridge, Jae-Soon Choi, Jim Parks, Maggie Connatser, Jon Yoo, Rodrigo Sanchez, Vitaly Prikhodko, Neal Currier, Sam Geckler, Mike Ruth, Rick Booth, David Koeberlein, Alex Yezers. “Advanced Diagnostics for Automotive Catalysts, Exhaust Gas Recirculation & Oil Dilution,” Monolith Research Group, Department of Chemical Engineering, Institute of Chemical Technology, Prague; Prague, Czech Republic, February 27, 2013.
- 3.** William Partridge, Josh Pihl, Mi-Young Kim, Stuart Daw, Xavier Auvray, Louise Olsson, Jae-Soon Choi, Krishna Kammasudram, Aleksey Yezers, Neal Currier. “Understanding NH₃ Coverage Distributions based on the Common Intra-Catalyst Nature of Model & Commercial SCR Catalysts,” 3 invited presentations at:
 - 9th World Congress of Chemical Engineering, Seoul, Korea, August 20, 2013.
 - Pohang University of Science and Technology (POSTECH), Chemical Engineering Department

(Professor In-Sik Nam, hosting), Pohang, Korea, August 26, 2013.

- Chonnam National University (CNU), Department of Applied Chemical Engineering (Professor Gon Seo, hosting), Gwangju (aka Kwangju), Korea, August 27, 2013.

III.10 Development of Optimal Catalyst Designs and Operating Strategies for Lean NO_x Reduction in Coupled LNT-SCR Systems

Michael P. Harold (Primary Contact, University of Houston), Mark Crocker (University of Kentucky, UK)
University of Houston (UH)
Dept. of Chemical & Biomolecular Engineering
S325 Engineering Building 1
Houston, TX 77204

DOE Technology Development Manager:
Ken Howden

Overall Objectives

The overarching goal of this project is to identify the oxides of nitrogen (NO_x) reduction mechanisms operative in lean-NO_x traps (LNTs) and in situ selective catalytic reduction (SCR) catalysts, and to use this knowledge to design optimized LNT-SCR systems in terms of catalyst architecture and operating strategies. The project is organized in three phases.

Phase 1

- Elucidate the mechanism of the non-NH₃ pathway for NO_x reduction by means of bench-scale reactor, in situ diffuse reflectance infrared Fourier-transform spectroscopy (DRIFTS) reactor, and temporal analysis of products (TAP) reactor studies
- Map LNT selectivity to NH₃ as a function of catalyst composition (ceria content and type) and relevant process parameters (NO_x loading, purge duration, purge lambda and space velocity)
- Develop a microkinetic LNT model that takes into account the catalyst composition (storage component such as ceria and barium loading as well as precious metal such as Pt loading/dispersion) and H₂, CO, and C₃H₆ reductants
- Develop low-dimensional models for the LNT and the coupled LNT-SCR unit for different catalyst architectures incorporating microkinetics

Phase 2

- Determine optimum ceria type and content in model LNT catalysts to achieve best net NO_x conversion in serial LNT-SCR catalysts
- Determine the level of precious-grade metal (PGM) reduction possible in the serial LNT-SCR catalyst

system while providing equivalent performance to the corresponding LNT-only system

- Establish the optimal operating strategy of serial and double layer catalyst systems with respect to NO_x conversion level and fuel penalty
- Develop microkinetic SCR model that includes non-NH₃ mechanism
- Carry out experimental optimization study of segmented LNT-SCR catalyst configurations
- Perform simulations of the LNT and coupled LNT-SCR unit using the low-dimensional models to examine the performance features and to identify optimal periodic operation and how it depends on the axial and transverse distribution of the catalytic components

Phase 3

- Study the surface chemistry and dynamics associated with NH₃ storage and consumption during LNT-SCR lean-rich cycling
- Quantify the NO_x storage-reduction behavior of aged LNT-SCR systems so as to pin-point the effects of aging on the different catalyst functions
- Complete microkinetic model for the LNT-SCR system
- Carry out modeling study of the LNT-SCR systems for real-time simulation and optimization
- Experimentally verify model predictions of different segmented LNT-SCR reactor configurations
- Use low-dimensional models to identify the optimal catalyst architectures and operating strategies of the overall LNT-SCR unit

Fiscal Year (FY) 2013 Accomplishments

During the fourth year of the project most of the Phase 1, 2 and 3 objectives were completed. Since project inception, about 33 peer-reviewed publications have appeared or are in print, with four additional papers currently under review. One of the publications includes a comprehensive chapter focused on SCR on Fe-exchanged zeolite catalysts. Additionally, nearly 40 presentations have been delivered at conferences. The latter includes at least four invited “keynote” lectures. The grant has supported the doctoral thesis research of at least seven doctoral students and one post doc at UH and UK. Three more students completed their degrees in 2013 (UH).

students Prasanna Dasari, Bijesh Shakya, who will join Johnson Matthey and UK student Vence Easterling, who joined UH as a post-doctoral research associate). To this end, the project has also been productive in terms of training new researchers, several of whom have taken positions in the emissions area. Highlights of activities over the year are as follows:

NO_x Storage and Reduction: Regeneration Mechanisms, Kinetics, and Ammonia Generation

- Systematic study of NO_x storage and reduction with CO as reductant in the absence and presence of H₂O
- Comparative study of NO_x uptake, storage and reduction with H₂ and CO as reductants in the absence and presence of CO₂

Selective Catalytic Reduction: Kinetics, Mechanisms, and Catalyst Comparisons

- Modeling and experiments of the steady-state and transient oxidation of propylene in the absence and presence of NO/NO₂/NH₃ on Cu/chabazite monolith catalyst

Coupled LNT/SCR

- Further development and application of LNT/SCR dual layer model for identifying optimal catalyst composition and structural properties such as washcoat thickness
- Extension of serial and segmented model LNT/SCR to include CO and propylene in the feed as reductants
- Application of LNT/SCR dual-layer model for identifying optimal catalyst composition and structural properties such as washcoat thickness
- Spatio-temporal studies of LNT-SCR serial and segmented catalysts
- Experimental study of combined LNT-SCR double-layer and dual-brick catalysts with the goal to identify strategies of profiling the active components to achieve higher conversion over a wide temperature range



INTRODUCTION

The LNT is a promising NO_x reduction technology for light-duty diesel and gasoline lean-burn applications but has the challenge of meeting the needs of heavy-duty vehicles. On the other hand, SCR using aqueous urea has emerged as the technology of choice for heavy-duty vehicles but has too high of a cost for light-duty

vehicles. For these reasons, the combination of LNT and SCR has utility potential for moderate-size vehicles with possible use in an even wider range of applications. The overarching goal of this project is to advance our understanding of the LNT/SCR technology and to identify the best reactor designs and operating strategies for reducing NO_x with NH₃ generated from engine-out NO_x.

APPROACH

The project activities encompass catalyst synthesis and characterization, kinetics and reactor modeling, vehicle exhaust testing, and systems integration. In Phase 1 of the project, the studies focus on two main goals: first, elucidating the mechanism of the non-NH₃ pathway for NO_x conversion in LNT-SCR systems and second, developing mechanistic-based kinetic models that describe the dependence of LNT selectivity to NH₃ and of NO_x reduction with NH₃ as a function of relevant process parameters and catalyst composition. In Phase 2, efforts are directed towards improving the individual LNT and SCR catalyst functions in terms of NH₃ generation and NO_x to N₂ conversion, respectively, and in elucidating the synergies between the LNT and SCR functions during periodic operation of the LNT/SCR. This is accomplished through targeted kinetics, catalyst synthesis, bench-scale reactor, TAP and DRIFTS measurements and complementary modeling studies, all with the goal of establishing the optimal catalyst architectures (Figure 1) and operating strategies of LNT-SCR catalyst systems that maximize NO_x conversion to N₂. Experiments and modeling are applied to assess the potential for PGM reduction in the LNT-SCR catalysts such as the use of dual-layer SCR and LNT/SCR catalysts. In Phase 3 of the project, LNT/SCR reactor

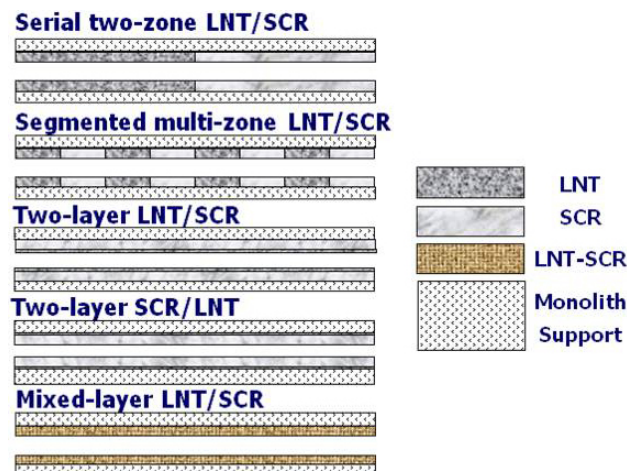


FIGURE 1. Several catalyst formulations and architectures evaluated in the project.

models based on refined LNT and SCR models are used to evaluate different catalyst architectures spanning segmented zone and dual-layer catalysts. Complementary bench-scale reactor studies are conducted, for model verification and testing of promising designs predicted by the model.

RESULTS

Selected results are reported to illustrate activities that have been completed or are in progress.

NO_x Storage and Reduction: Regeneration Mechanisms, Kinetics, and Ammonia Generation

Comparative Study of NO_x Uptake, Storage and Reduction with H₂ and CO as Reductants in the Absence and Presence of CO₂

The low to moderate temperature (<300°C) behavior of a Pt/Ba LNT catalyst is of interest especially during vehicle startup. Recent studies by our group have reported a nonmonotonic dependence of cycle average NO_x conversion versus temperature during the cyclic reduction of NO_x on Pt/Rh/Ba/Al₂O₃ in the presence of excess CO₂ [1-3]. At a catalyst temperature of about 200°C the NO_x conversion exhibits a noted minimum whereas this feature is not observed in the absence of CO₂. To determine the origin of this behavior, the formation and stability of barium carbonate and nitrite/nitrate species on a model Pt-Rh/Ba/Al₂O₃ LNT catalyst was studied using gas phase Fourier transform infrared spectroscopy. The catalyst was exposed to various mixtures including CO₂+O₂, NO+O₂, and NO+O₂+CO₂ in the temperature range of 150 to 350°C. The temporal effluent gas composition revealed that surface carbonates exist over the entire temperature range, but are relatively less stable at temperatures exceeding 230°C. During exposure to NO+O₂+CO₂ nitrite/nitrate formation competes with carbonate formation. The competition is manifested as a nonmonotonic uptake of nitrites/nitrates as the temperature is increased over the stated range. A phenomenological picture of the uptake is proposed to account for the measurements. At low temperatures (<200°C) NO_x stores on Ba sites in the proximity of the Pt, apparently relying on the spillover of adsorbed O and NO species. At higher temperatures the increased rate of NO oxidation reaction forms NO₂, which stores on the Ba sites further from the PGM sites through a disproportionation mechanism. The local minimum in NO_x conversion at ~200°C is a result of the drop in NO_x storage capacity of the catalyst due to the competition offered by CO₂ for storage sites, while at higher temperatures (>230°C) the storage capacity is partly restored due to the decrease in the carbonate stability.

SCR on Metal-Exchanged Zeolite Catalysts for LNT/SCR

NO Inhibition Effects During Oxidation of Propylene on Cu-chabazite Catalyst

Bench-flow reactor and in situ DRIFTS experiments were carried out to elucidate the features of propylene+NO+O₂ reaction system on Cu-SSZ13 (chabazite) monolithic catalyst. Experiments were conducted under both steady-state and transient conditions for application-relevant feed conditions. Steady-state conversion data of the C₃H₆ light-off in the presence of excess O₂ (5%) shows inhibition by a much smaller amount of NO (500 ppm). Corresponding data in the presence of NO₂ reveals a transition in the C₃H₆ light-off curve; for temperatures below 350°C the C₃H₆ conversion is higher in the presence of NO₂ as compared to O₂ whereas above 350°C the C₃H₆ conversion in the absence of NO₂ is higher. The reduction of NO₂ to NO and N₂ is enhanced by the addition of C₃H₆, which facilitates the reduction of Cu sites favorable for the NO₂ reduction. Spatially-resolved concentration profiles show that NO₂ is completely reduced in the front part of monolith at temperatures above 350°C. On the other hand, NO that is formed from the NO₂ reduction increases along the length in the temperature range of 200°C-350°C and exhibits a maximum value above 350°C. Similarly, C₃H₆ oxidation is inhibited by NO at the light-off temperature of the C₃H₆ oxidation reaction (~350°C) while there is no effect of NO on C₃H₆ oxidation reaction below the light-off temperature. The results clearly suggest that inhibition is not due to a competitive adsorption process but due to the generation of partially oxidized hydrocarbon species that react with NO to form O- and N-containing surface intermediates which serve to block the active catalytic sites. In-situ DRIFTS measurements confirm the formation and existence of -NCO like species over catalyst surface on exposure to NO after a 45 min of exposure to C₃H₆ and O₂ (Figure 2). A phenomenological reaction mechanism is proposed that involves the formation of inhibiting intermediates through the reaction of NO with oxygenates, which then react further to form N₂.

A predictive microkinetic based model of the propylene + NO + O₂ system is being developed that will eventually be combined with NH₃ to provide the first such model of the Cu-catalyzed SCR reaction system.

Isotopic Studies of Standard SCR With Propylene + NH₃ Mixtures

Systematic isotopic studies of feeds containing mixtures of NH₃ and C₃H₆ revealed complex interactions. For example, a feed containing labeled NO and propylene revealed the production of an adsorbed NH₃ or related

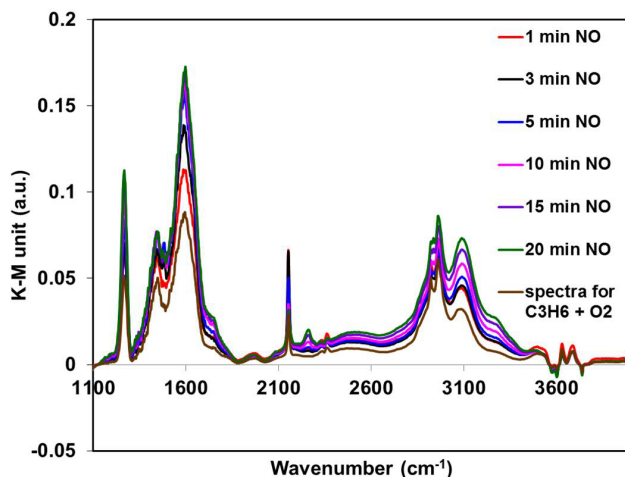


FIGURE 2. Emergence of new peak upon exposure to 500 ppm NO after 45 minutes of exposure to 500 ppm C_3H_6 at 380°C (500 ppm C_3H_6 , 500 ppm NO, 1% O_2 , balanced by He).

intermediate during lean-rich cycling on a Cu-chabazite monolithic catalyst. Isotopic labeling also showed that propylene may inhibit the utilization of NH_3 during SCR. These and other effects have a dramatic effect on the performance of the commercial SCR catalyst. Any co-reductant mixture may require such effects to be accounted for in a mechanistic model.

SCR in Dual-Layer and Dual-Brick Fe+Cu Catalysts

An optimization study of the dual component Fe+Cu SCR catalyst system was conducted to determine the composition for both dual layer and dual brick architectures. The comprehensive study determined a slight advantage for the dual-brick catalyst (Figure 3).

LNT/SCR Studies – Understanding Synergies of NH_3 Generation and NOx Reduction

Experimental Studies of the Dual-Layer LNT/SCR Monolithic Catalyst Using CO and H_2 as Dual-Reductant Mixture

We evaluated different layering and zoning configurations using mixtures of CO and H_2 and mixtures without and with propylene. In experiments with H_2 and CO, monolithic catalysts consisting of a layer of SCR catalyst deposited on top of an LNT catalyst were optimized to provide high NOx conversion at both low and high temperatures with minimal PGM loading using H_2/CO reductant mixtures. The optimized dual-layer catalyst circumvents the need for urea feed and has the potential to reduce the expensive PGM loading by up to 38% from that of LNT-only catalyst under laboratory test. We investigated the impact of catalyst design variables, such as SCR and LNT zoning, the ceria level in LNT, as well as SCR zeolite type (ZSM-5, SSZ-13) layer

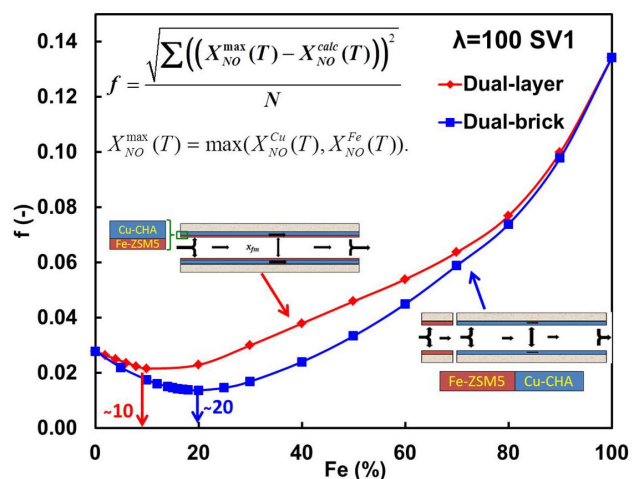


FIGURE 3. Compositional optimization of the dual-layer and brick Fe-Cu SCR catalysts.

thickness. As depicted in Figure 4, zoning of either or both the SCR and LNT in the dual-layer catalysts enables an increase of the low-temperature NOx conversion, and minimizes the high temperature (300–400°C) conversion loss caused by the SCR diffusion resistance and undesired LNT NH_3 oxidation. High ceria loading of the LNT enhanced NH_3 generation, NOx adsorption and mitigated CO poisoning at low temperatures (150–250°C). Commercial Cu-SSZ-13 exhibited a higher NH_3 storage capacity and better low-temperature SCR activity than the in-house synthesized Cu-ZSM-5, and improved the low-temperature NOx conversion of the dual-layer catalysts. The diffusion resistance in the top active Cu-zeolite layer inhibited the overall NOx reduction as shown by replacing it with an inert Na-ZSM-5 layer with a high Si/Al ratio. Washcoat diffusion limitations adversely affect the high temperature performance more than the NH_3 oxidation to NOx. The experiments revealed that for a top SCR layer loading of 1.0 g/in³ diffusion limitations started at 150°C using a pure H_2 feed and at 250°C using a CO/ H_2 feed.

Experimental Studies of the Dual-Layer LNT/SCR Monolithic Catalyst Using Propylene in the Absence and Presence of CO and H_2

In experiments with propylene, we demonstrate the application of LNT and SCR zoning in dual-layer catalysts to improve NOx reduction efficiency and show the potential to reduce the expensive PGM loading by up to 40% from that of LNT-only catalyst without degrading its deNOx performance under simulated diesel exhaust conditions. We investigated the NOx reduction pathway in the SCR layer of the dual-layer catalyst using simulated rich exhaust of $\text{C}_3\text{H}_6/\text{CO}/\text{H}_2$ as reductants. The non- NH_3 reduction pathway by N-containing organic

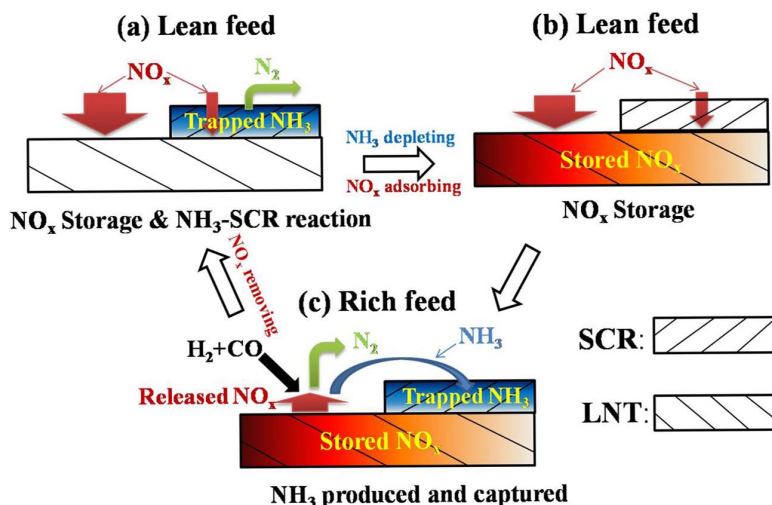


FIGURE 4. Schematic of the working principle of the dual component layered catalyst.

intermediates via the synergy of LNT and SCR catalysts can play a major role in the incremental NO_x conversion over SCR layer at low temperatures (<=225°C). The roles of NH₃ and C₃H₆ as reductants for NO_x conversion over the SCR catalyst increase with temperature (>225°C). The impact of SCR and LNT zoning as well as SCR layer thickness, were studied. Zoning of either or both the SCR and LNT in the dual-layer catalysts improved the low-temperature NO_x conversion, and minimized the high-temperature (300–400°C) conversion loss caused by the SCR layer diffusion resistance and undesired NH₃ oxidation. The performance decline due to the Cu-zeolite layer diffusion resistance was shown by replacing it with an inert Na-zeolite layer with a high Si/Al ratio.

Spatiotemporal Distribution of Reacting Species in Coupled LNT-SCR Reactor System

The spatiotemporal distribution of reactions along coupled LNT-SCR catalyst systems were measured at Oak Ridge National Laboratory to better understand interplays between LNT and SCR components under fast lean/rich cycling conditions. Specifically, we compared two different catalyst configurations: 1.5" LNT + 1.5" SCR ("sequential") vs. 0.75" LNT + 0.75" SCR + 0.75" LNT + 0.75" SCR ("sandwiched"). Both configurations were composed of the same LNT and SCR monolith cores. The experimental conditions used are summarized in the following:

Catalysts: LNT: LNT-3 (medium Ce loading); SCR: Cu-chabazite

Reactor Conditions: Total flow rate: 13,719 sccm; lean (60 s): 500 ppm NO, 8% O₂, 5% H₂O, 5% CO₂, N₂ balance; rich (5 s): 2.5% H₂ (with or without 278 ppm C₃H₆), 5% H₂O, 5% CO₂, N₂ balance; temperature: 200, 300, 400°C

The results confirm the positive impact of adding an SCR catalyst to an LNT with respect to NO_x conversion. The 10% increase in reductant as C₃H₆ at 400°C did not result in a significant increase in NO_x conversion likely due to excess amount of H₂ available (data not shown). Very similar outlet conversion levels were achieved for both LNT-SCR and LNT-SCR-LNT-SCR configurations under the conditions used in this study. As it is well known in the literature, the additional NO_x conversion levels were achieved through reactions over the SCR catalyst between NO_x and NH₃ slipped from the LNT catalyst. It is interesting to note that while NO_x conversion over the LNT sections was significantly higher at 400°C than 300°C, the overall outlet conversion was the highest at 300°C. This is likely due to greater generation from the LNT and higher subsequent storage on the SCR of NH₃ at 300°C.

A major difference between the sequential and sandwiched configurations of LNT-SCR catalysts observed in this study was N₂O yields at 200°C: considerably lower N₂O slip at the outlet for the sandwiched configuration. The N₂O profiles show that most of N₂O was generated over the LNT catalyst. Furthermore, a greater N₂O was generated over the second LNT section (0.5 L) than over the first LNT section (0.25 L) of the sequential LNT-SCR catalyst. These results seem to support the idea that NO_x reduction by NH₃ is a major contributor to the N₂O formation over LNTs as proposed in a recent LNT paper [4]. The present study also suggests that N₂O formation can be mitigated by inserting an SCR catalyst between two LNT sections. N₂O can be reduced over Cu-chabazite SCR catalysts [5], but such a pathway was not observed under the conditions used in the present study.

Simulation Studies of Dual-Layer LNT/SCR Catalysts

A simulation study of dual-layer NO_x storage/reduction (NSR) and SCR monolithic catalyst is carried out using a one-dimensional plus one-dimensional model of catalytic monolith with individually calibrated global kinetic models. The model is used to elucidate the complex spatiotemporal processes occurring within the washcoat and along the reactor length. Specifically, the simulations are used to address the following: (i) general features of dual-layer NSR+SCR configuration, (ii) effects of temperature, (iii) effects of washcoat loading of individual component, and (iv) impact of catalyst architecture. In the dual-layer configuration, NH₃ generated in the underlying NSR layer is stored in the

outer SCR layer during the rich phase which then reacts with the NO_x during the subsequent lean phase.

The dual-layer LNT/SCR simulations show that multiple combinations of catalyst loading can attain a given NO_x conversion and N₂ selectivity, and there exists a loading of SCR washcoat for a given NSR catalyst for which the NO_x conversion is maximum. Figure 5 shows simulated results in the form of a NO_x conversion contour map in the plane of SCR and LNT loading. At higher SCR loading, the NH₃ generated in the NSR is not sufficient to fully utilize the SCR catalyst. As a result, only a fraction of the SCR layer closer to the NSR layer is utilized while the rest acts as an inert layer, creating an undesired diffusional barrier lowering the NO_x conversion. Simulations of the dual-brick monolith are performed to analyze the architectural effects on performance of the combined system. Under identical conditions, the simulations show that dual-layer configuration outperforms the dual-brick in terms of NO_x conversion and NH₃ slip, largely because the NH₃ generated in the LNT layer is better utilized in the SCR layer. Finally, at higher temperatures the SCR functionality is greatly reduced because of the higher rate of NH₃ consumption in the NSR layer lowering the NH₃ yield. As a consequence, comparable performances are obtained for both the configurations.

SUMMARY

This project combines experiments spanning bench-scale kinetics and catalyst performance studies analytical methods including spatially-resolved mass spectrometry

to advance the understanding of LNT, SCR, and LNT/SCR systems. Kinetic models are being developed based on measurements for the LNT and SCR chemistries, to be incorporated into reactor models for design and optimization. These models have been successfully applied to determine the catalyst architectures and operating conditions that result in NO_x conversion and N₂ selectivity that achieve defined threshold levels.

REFERENCES

1. Ren and Harold, ACS Catalysis, 2011.
2. Liu et al., Appl. Catal. B, 2013.
3. Liu et al., Top. Catal., 2013.
4. Choi et al., Catalysis Today 184 (2012) 20-26.
5. Wang et al., Catalysis Letters 142 (2012) 1167-1174.

FY 2013 PUBLICATIONS/PRESENTATIONS

Publications

1. Liu, Y., M.P. Harold, and D. Luss, "Lean NO_x Reduction with H₂ and CO in Dual-layer LNT-SCR Monolithic Catalysts: Impact of Ceria Loading," *Top. Catal.*, **56**, 104–108 (2013).
2. Y. Ji, T.J Toops, M. Crocker, "Isocyanate formation and reactivity on a Ba-based LNT catalyst studied by DRIFTS", *Appl. Catal. B*, **140-141** (2013) 265.
3. C. Shi, Z. Zhang, M. Crocker, L. Xu, C. Wang, C. Au, A. Zhu, "Non-thermal plasma-assisted NO_x storage and Reduction on a LaMn_{0.9}Fe_{0.1}O₃ perovskite catalyst", *Catal. Today*, **211** (2013) 96.

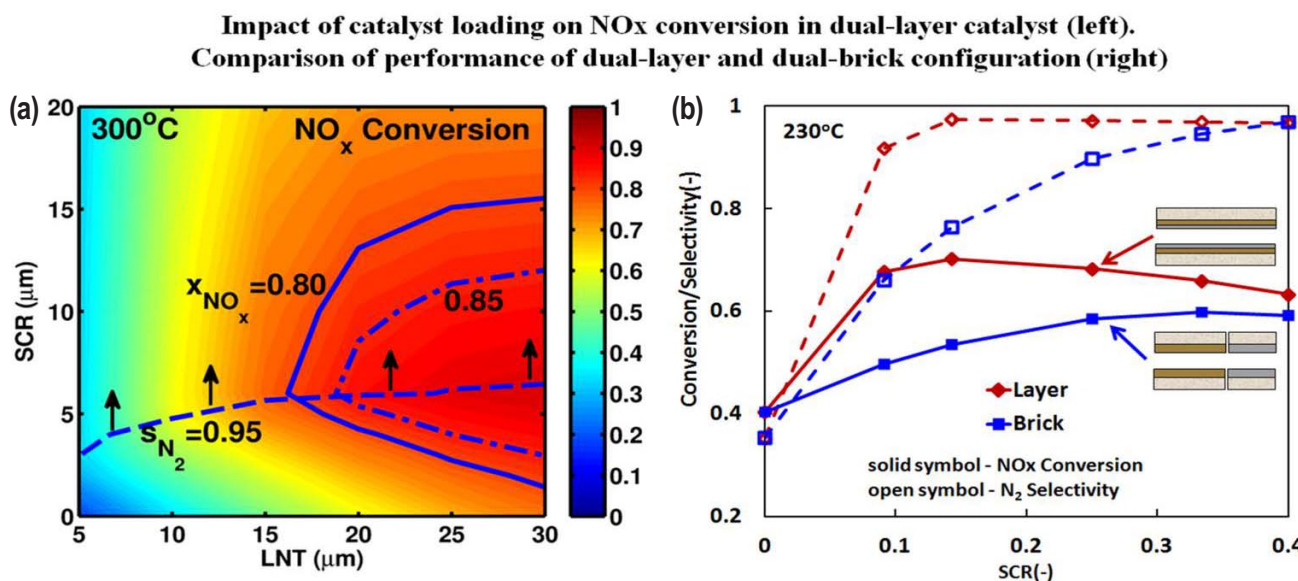


FIGURE 5. (a) Model predicted map of SCR and LNT loading showing the NO_x conversion at 300°C; (b) Dependence of NO_x conversion and product selectivity as function of SCR loading for dual-layer and dual-brick catalyst.

- 4.** Dasari, P., R. Muncrief, and M.P. Harold, “Cyclic Lean Reduction of NO by CO in Excess H₂O on Pt-Rh/Ba/Al₂O₃: Elucidating Mechanistic Features and Catalyst Performance,” *Topics in Catalysis*, in press (2013).
- 5.** Raj, R. M.P. Harold and V. Balakotaiah, “Experimental studies on NO inhibition on C₃H₆ oxidation on Cu-chabazite monolithic catalyst, elucidating the mechanistic pathway of NO_x selective reduction by C₃H₆,” *Ind. Eng. Chem. Res.*, accepted for publication (April, 2013).
- 6.** Shakya, B., M.P. Harold, and V. Balakotaiah, “Effect of cycle time on NH₃ generation on Low Pt Dispersion Pt/BaO/Al₂O₃: Experiments and Crystallite-Scale Modeling,” *Chem. Eng. Journal*, accepted for publication (June, 2013).
- 7.** J. Wang, Y. Ji, G. Jacobs, S. Jones, D.J. Kim, M. Crocker, “Effect of Aging on NOx Reduction in Coupled LNT-SCR Systems”, *Appl. Catal. B.*, in press.
- 8.** Shakya, B., M.P. Harold, and V. Balakotaiah, “Modeling and Analysis of Dual-layer NOx Storage and Reduction and Selective Catalytic Reduction Monolithic Catalyst,” *Chem. Eng. Journal*, to appear (2013).
- 9.** Y. Zheng, Y. Liu, M.P. Harold, and D. Luss, “LNT-SCR Dual-layer Catalysts Optimized for Lean NOx Reduction by H₂ and CO,” *Appl. Catalysis B. Environmental*, to appear (2013).
- 10.** M.-Y. Kim, J.-S. Choi, M. Crocker, “Roles of C₃H₆ in NH₃ Generation and NOx Reduction over a Cu-chabazite SCR Catalyst under Lean/Rich Cycling Conditions”, submitted to *Catal. Today*.
- 11.** D.J. Kim, J. Wang, M. Crocker, “Adsorption and desorption of propene on a commercial Cu-CHA SCR catalyst”, submitted to *Catal. Today*.
- 12.** Y. Zheng, M.P. Harold, and D. Luss, “Optimization of LNT-SCR Dual-layer Catalysts for Lean NOx Reduction by H₂ and CO,” *SAE Journal*, under review (2013).

Presentations

- 1.** “Lean NOx Reduction with H₂ and CO Over Dual-Layer LNT-SCR Monolithic Catalysts,” NASCRE 3, Houston, 3/13 (with Y. Zheng, presenter, and D. Luss).
- 2.** “Cyclic Lean Reduction of NO by CO in Excess H₂O on Pt-Rh/Ba/Al₂O₃: Elucidating Mechanistic Features and Catalyst Performance,” NASCRE 3, Houston, 3/13 (with P. Dasari, poster presenter).

- 3.** “Modeling and Simulation of Layered Lean NO_x Trap and Selective Catalytic Reduction Monolithic Catalysts,” NASCRE 3, Houston, 3/13 (with B. Shakya, presenter).
- 4.** “Mechanistic Studies of Selective Catalytic Reduction of NO_x with C₃H₆ on Cu based Zeolite Monolith Catalyst,” NASCRE 3, Houston, 3/13 (with R. Raj, presenter, and V. Balakotaiah).
- 5.** Y. Ji, T.J Toops, M. Crocker, “Isocyanate Formation and Reactivity on a Ba-based LNT Catalyst Studied by DRIFTS and Mass Spectrometry”, oral presentation O-W-Com-13, 23rd North American Catalysis Society meeting, Louisville, KY, June 2-7, 2013.
- 6.** J. Wang, Y. Ji, M. Crocker, “Effect of Aging on NOx Reduction in Coupled LNT-SCR Systems”, poster presentation P-W-BRC-34, 23rd North American Catalysis Society meeting, Louisville, KY, June 2-7, 2013.
- 7.** M.-Y. Kim, J.-S. Choi, M. Crocker, “Roles of C₃H₆ in NH₃ Generation and NOx Reduction over a Cu-chabazite SCR Catalyst under Lean/Rich Cycling Conditions”, poster presentation P-Tu-BRC-112, 23rd North American Catalysis Society meeting, Louisville, KY, June 2-7, 2013.
- 8.** D. Kim and M. Crocker, “Adsorption and Desorption of Propene on a Cu-Chabazite Catalyst”, poster presentation P-M-BRC-70, 23rd North American Catalysis Society meeting, Louisville, KY, June 2-7, 2013.
- 9.** “Modeling and Simulation of Layered Lean NO_x Trap and Selective Catalytic Reduction Monolithic Catalysts,” NAM, Louisville, KY 6/13 (with B. Shakya, presenter, and V. Balakotaiah).
- 10.** “Spatiotemporal Studies of NH₃ Formation Over Pt-Rh/BaO/Al₂O₃ LNT Monolith in the Presence of Excess CO₂ and H₂O,” Louisville, KY 6/13 (poster; with P. Dasari, presenter).
- 11.** “Modeling and Simulation of Transient Behavior of Multi-functional Lean NOx Catalysts,” Haldor Topsoe Catalysis Symposium, Denmark, 8/13 (invited keynote talk).
- 12.** “Modeling and Analysis of Lean NOx Traps and LNT/SCR Dual Function Catalysts”, MODEGAT III, Bad Harrenalb, Germany, 9/13 (invited keynote talk).

III.11 Neutron Imaging of Advanced Transportation Technologies

Todd J. Toops (Primary Contact),
Charles E.A. Finney, Eric J. Nafziger,
Hassina Bilheux
Oak Ridge National Laboratory (ORNL)
2360 Cherahala Boulevard
Knoxville, TN 37932

DOE Technology Development Manager:
Gurpreet Singh

Subcontractor:
Jens Gregor, University of Tennessee, Knoxville, TN

Overall Objectives

- Develop techniques and understanding that allows the use of the high-fidelity neutron imaging capability at the High Flux Isotope Reactor (HFIR) and Spallation Neutron Source on advanced transportation technologies
 - Once fully developed, this advanced capability will allow the imaging of a range of processes that occur in advanced vehicle systems
- Employ technique to aid improved design and control of complex advanced combustion systems and help to guide model validation and input
- Report findings to research community and work with industrial partners to ensure research is focused on the most critical topics

Fiscal Year (FY) 2013 Objectives

- Determine temporal and spatial resolution of neutron imaging with respect to internal fluid flow and spray pattern from fuel injectors
- Demonstrate neutron imaging capability on gasoline direct injection (GDI) devices, including obtaining three-dimensional (3-D) computed tomography (CT) scans of injectors
- Demonstrate neutron imaging capability on ash samples within particulate filters

FY 2013 Accomplishments

- Implemented spray chamber with portable fluid delivery system for high-pressure fluid delivery for diesel injectors at the HFIR
 - Investigated impact of rail pressure on fluid density profiles in the injector

- Illustrated neutron imaging can differentiate fluid density differences caused by rail pressures
- Obtained CT scan of ash deposits from a continuously regenerated particulate filter (PF) and a periodically generated one
 - Observe both dense and “fluffy” ash deposits
 - Future efforts to quantify density using standards
- Obtained 3-D CT scan of a GDI injector with spatial resolution of 50 microns
- Awarded ORNL-funded project that will allow the development of a dynamic imaging capability for internal fluid density and cavitation measurements of fuel injectors

Future Directions

- Develop system for fluid/fuel injection with GDI
 - Lower rail pressure than current system, so different pumping system required
- Probe detailed fluid dynamic study within fuel injectors using time-resolved technique
 - Requires stroboscopic approach with electronic detector trigger and fuel injector coordination
 - Aiming for 20 μ s resolution with 1 ms injection
 - Comprised of ~1 million images of each 20 μ s partition of the injection
 - Focus on cavitation studies and internal fluid dynamics
 - Identifying conditions that lead to cavitation
 - With improved spatial resolution, correlate internal injector dynamics to near nozzle spray patterns
 - Adapt chamber to eliminate fluid build-up on injector and walls
- Incorporate ash-laden and gasoline particulate samples into PF study
 - Working with partners to obtain parts as possible
 - Quantify density using standards
- Share findings through collaboration with the General Motors injector team that is developing a model of the injector



INTRODUCTION

Unlike X-rays, neutrons are very sensitive to light elements such as hydrogen atoms and can penetrate through thick layers of metals (Figure 1a) [1]. These two properties suggest neutrons are well suited to probe engine parts such as diesel particulate filters, exhaust gas recirculator coolers, fuel injectors, oil in engines, oil residues in filters, etc. Neutron imaging is based on the interactions of a sample with a neutron beam. The interactions are dependent on sample thickness/density and elemental make-up and result in absorption and scattering of neutrons within the sample. A two-dimensional position-sensitive detector placed behind the sample can measure the transmitted neutron flux, as illustrated in Figure 1b [2]. When combined with a well-controlled rotational stage it is possible to perform

CT scans and thus generate 3-D images of real-world devices. Samples can be analyzed at one cross-section or a complete reconstruction can provide a cross-section of the entire sample at a resolution of the detector; the detector resolution is currently at ~50 microns.

APPROACH

This project is focused on using this unique neutron imaging capability to advance the understanding of two components being employed in modern vehicles: the PF and the in-cylinder fuel injector. Recent efforts are aimed at investigating intra-nozzle fuel injector fluid properties and cavitation events during dynamic spraying. These efforts are designed at improving understanding of how external conditions influence internal dynamics,

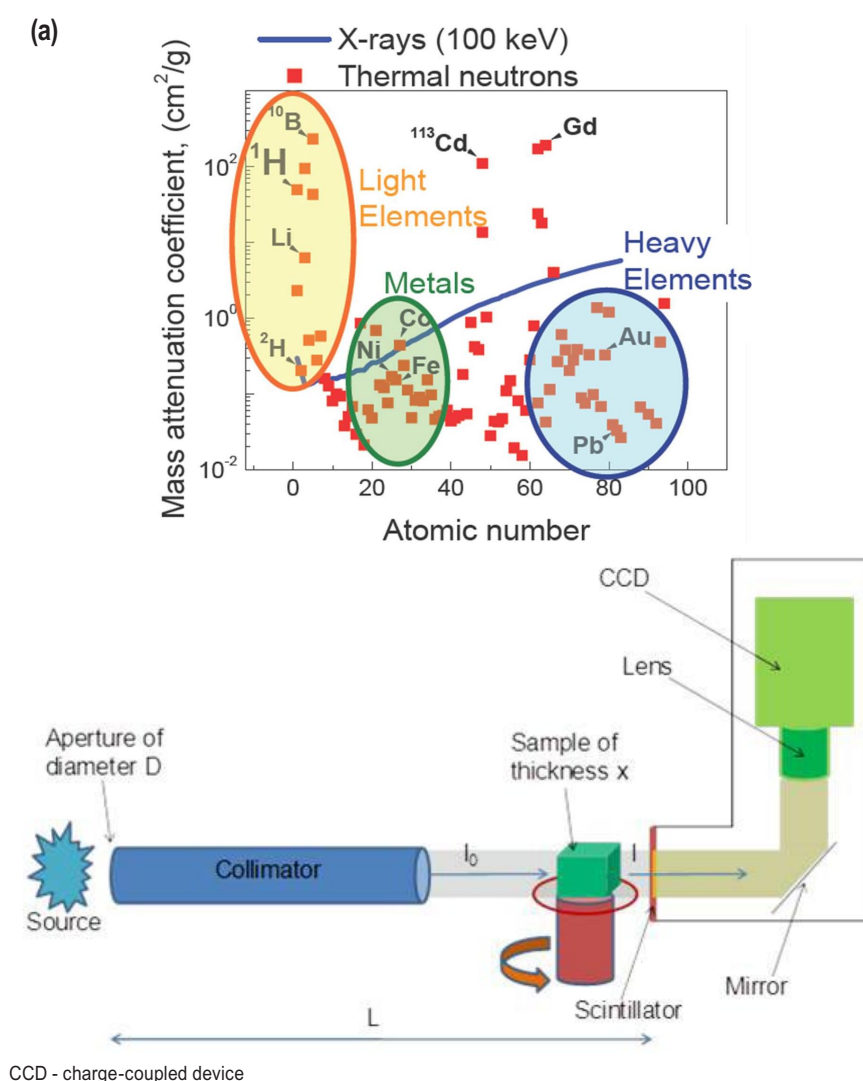


FIGURE 1. (a) Mass attenuation coefficients of a range of elements as a function of atomic number. Comparison given between neutron (squares) and X-rays (line) [1]. (b) Schematic of a neutron imaging facility at ORNL [2].

especially as it relates to advanced combustion regimes and injector durability. PFs are a key component of the emissions control system for modern diesel engines, and possibly gasoline engines in the future, yet there remain significant questions about the basic behavior of the filters. In particular, understanding how ash, or non-regenerable metal oxide-based particulate, fills the PF and interacts with the wall. The results of these measurements will provide important data to the aftertreatment modeling community on the soot and ash profiles, which change over the course of the vehicle's lifetime. In carrying out these studies, we work closely with industrial partners to obtain relevant systems and devices. The proximity of our research facility to the neutron beam allows for iterative studies when appropriate.

RESULTS

This year, efforts on the fuel injector studies were focused on two technologies: high-pressure diesel injectors and GDI-based injectors. Last year's results showed the potential of the neutron imaging technique to visualize the fluid within the diesel injector, as illustrated in Figure 2. The internal fluid has a high amount of contrast compared to the translucent injector, and it is possible to identify voids or air pockets within the fluid reservoir. Efforts this year were focused on moving into

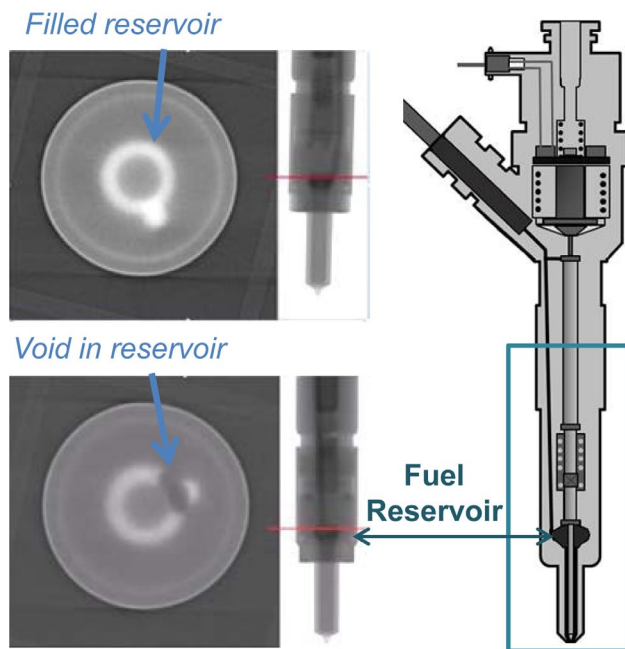


FIGURE 2. Cutaway diagram of a commercial diesel fuel injector and the corresponding image obtained with neutron radiography. Areas of highest contrast are associated with hydrocarbons inside metal fuel injector. (left) Virtual cross-section of two fuel injectors, one with the reservoir filled (top) and another with a void (bottom).

the dynamic injection studies with a focus on visualizing fluid properties within the injector and if possible, the spray. Spray images were not possible with the current set-up, but we were able to observe and analyze the fluid during injections, as illustrated in Figure 3. Under the current conditions at the HFIR, a 30-second exposure is necessary to image the internal fluid with sufficient contrast. Thus, these images are based on a composite of multiple injections and are focused on looking for areas of low overall density. A comparison between two rail pressures, 400 and 800 bar, is shown here. A feature we were able to show here is that increasing the rail pressure increases the fluid density in a manner that is detectable by the neutron technique.

In moving from the static images from last year to the dynamic imaging this year, it became clear that modifications were necessary to both the injection system and the speed of the image collection functionality. Thus a proposal was submitted to establish this capability through internal funding. This proposal has been accepted and will progress over the next two years.

In moving to the dynamic images, we will also be focusing on the GDI-based injectors that are seeing an increased market penetration as several manufacturers are now offering vehicles with this technology. The improved fuel economy from employing this technique is a main driver for this technology, but the injectors are currently a focus of significant R&D and it is being shown that modifications to the injector design can have a significant impact on both emissions formed and fuel economy gains. This year we initiated studies on static GDI-based injectors with a CT scan that is shown in Figure 4. These injectors are significantly smaller than the diesel-based systems and the spray holes/orifices are significantly larger than their diesel analogs.

While a significant effort has been placed on the injectors this year, we are continuing to use the proven techniques that we have deployed for use with PFs. The resources do not allow for time to be used for filling and regenerating PFs at ORNL, but we have increased our collaborations with research teams that are in the midst of PF investigations. There are several research groups trying to understand how ash builds up in PFs and how it depends on regeneration conditions. NGK sent us a PF that was used in an accelerated ash loading study that is described in detail elsewhere [3]; sample images of the CT scan are shown in Figure 5, and it can be seen that there is a significant maldistribution of the ash in the sample. Several channels are blocked completely, while some have minimal ash build-up. Furthermore, the ash plugs have very different natures. The ash that completely fills the channel is significantly less dense (lower contrast), while there is also ash that has coarsened, become dense (brighter contrast) and has also

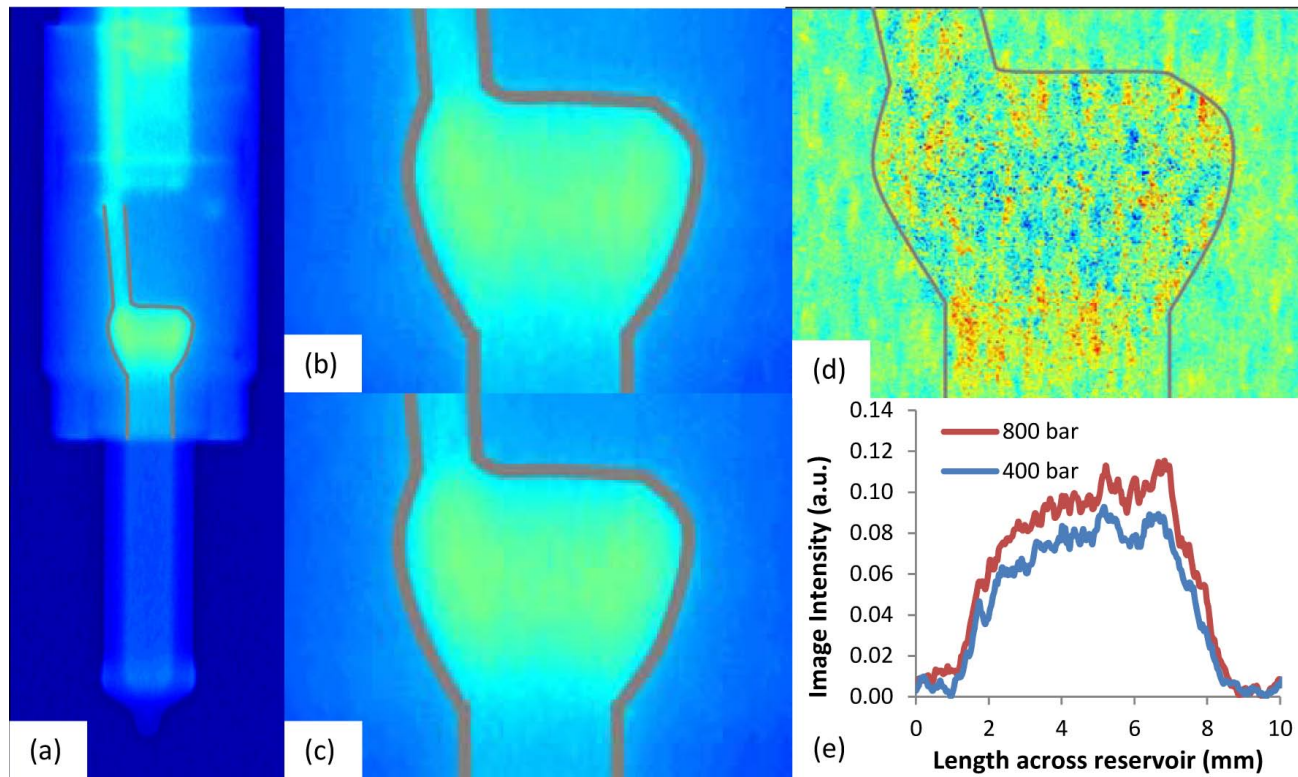


FIGURE 3. Neutron images highlighting the location and density of fuel inside of (a) diesel injectors at (b) 400 bar and (c) 800 bar. (d) Subtracted intensities illustrating a uniform density differences. (e) Graphical representation of the intensities in (b) and (c).

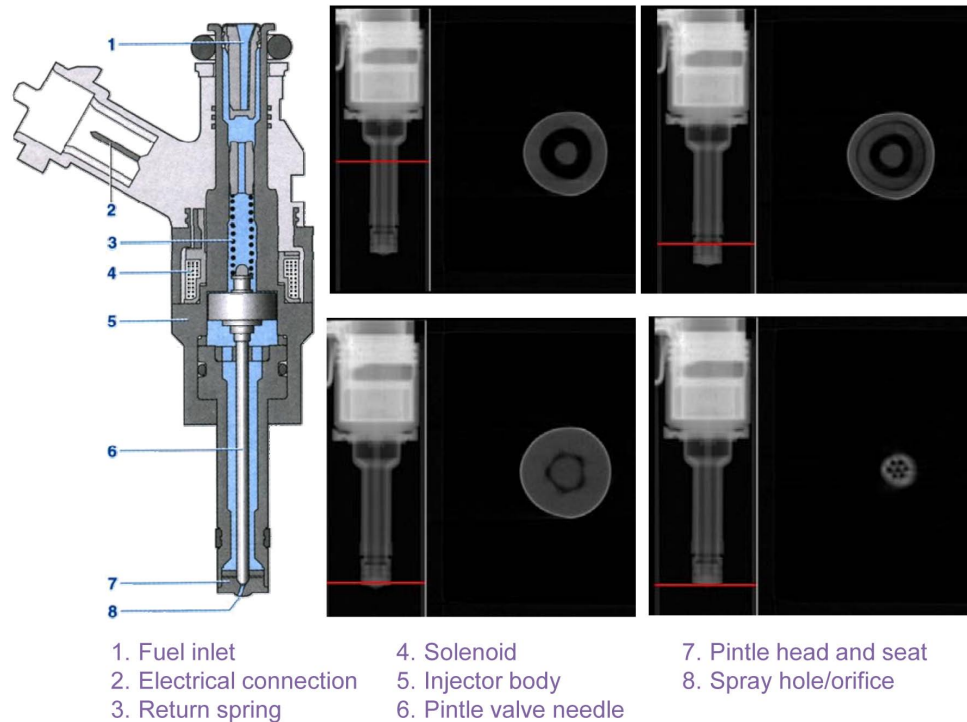


FIGURE 4. Comparison of cutaway view of a GDI-based injector, with one based on a CT scan build from neutron images.

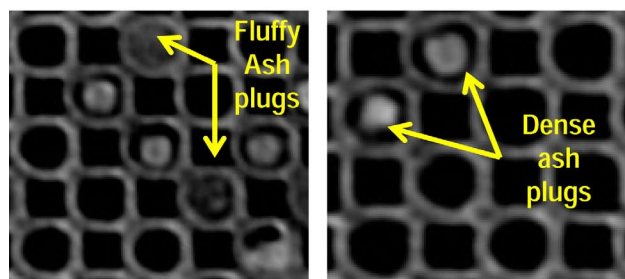
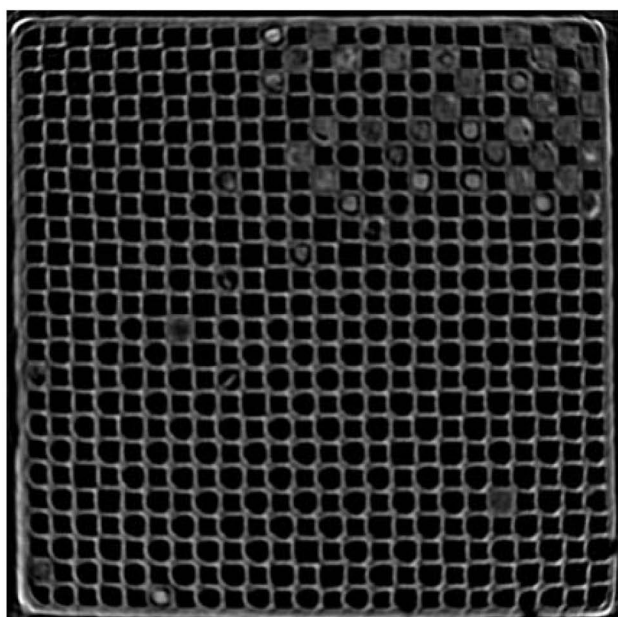


FIGURE 5. One section of a full-size SiC diesel PF containing ash plugs with varying densities, “fluffy” and “dense”.

pulled away from the wall. Further collaborations have commenced with a team at the Massachusetts Institute of Technology (MIT) that has several ash-filled PFs that have been filled to different levels and regenerated using different techniques (Figure 6). Massachusetts Institute of Technology has also supplied ash material that can be used for the standards for density determination. This collaborative effort is just beginning, but will be the basis of significant effort next year.

CONCLUSIONS

- Demonstrated the ability to detect fluid density differences within the injector under dynamic injection, but further tool modification is necessary to achieve the detailed fluid dynamic behavior that is necessary for detector work
 - Project awarded by ORNL internal funding committee to establish this capability
- Initiated GDI-based injector studies that will be the basis of much of the injector efforts going forward
- Demonstrated strong interaction of the neutrons with ash deposits in PFs which are allowing the identification of the ash density and distribution within the PF
 - Collaboration with NGK and the Massachusetts Institute of Technology have allowed this effort to proceed

REFERENCES

1. N. Kardjilov, “Absorption and phase contrast neutron imaging”, Imaging and Neutrons 2006, Oak Ridge, TN, October 23-25, 2006. http://neutrons.ornl.gov/workshops/ian2006/MO1/IAN2006oct_Kardjilov_02.pdf
2. J. Nanda, H.Z. Bilheux, S. Voisin, G. Veith, R. Archibald, L. Walker, S. Allu, N.J. Dudney, S. Pannala, Journal of Physical Chemistry C 116 (2012) 8401.
3. S. Fujii, T. Asako, “Development of Artificial Ash Accelerated Accumulation Test Method,” SAE Technical Paper Series 2010-01-2171 (2010) 1.

FY 2013 PUBLICATIONS/PRESENTATIONS

1. Todd J. Toops, Hassina Z. Bilheux, Sophie Voisin, Jens Gregor, Lakeisha Walker, Andrea Strzelec, Charles E.A. Finney, and Josh A. Pihl, “Neutron Tomography of Particulate Filters: a non-destructive investigation tool for applied and industrial research”, Nuclear Instruments and Methods in Physics Research Section A 729 (2013) 581-588.

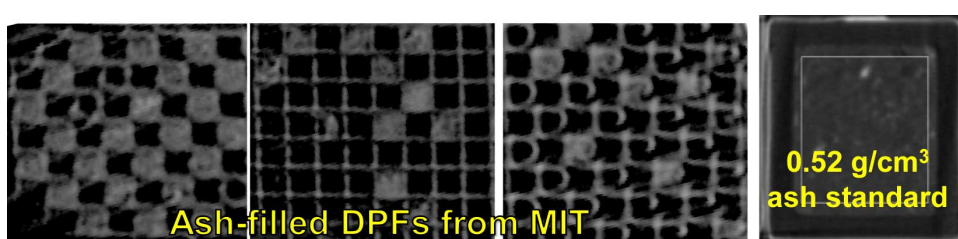


FIGURE 6. Collaborative efforts included investigating the potential of positioning full-size diesel PFs in the neutron beam for non-destructive analysis, preparing and evaluating ash standards, and CT-scans of a series of ash-filled diesel PFs. The full analysis of the standard and the ash-filled diesel PFs, will allow for quantitative evaluation ash density.

- 2.** Todd J. Toops, Charles E.A. Finney, Eric J. Nafziger, Josh A. Pihl, “Neutron Imaging of Advanced Transportation Technologies”, DOE 2012 Annual Progress Report.
- 3.** Todd J. Toops, Charles E.A. Finney, Josh A. Pihl “Neutron Imaging of DPFs and a Path Towards Quantification of Ash Distributions,” Massachusetts Institute of Technology Consortium to Optimize Lubricant and Diesel Engines for Robust Aftertreatment Systems, Fall Review Meeting, Cambridge, MA, October 10, 2013.
- 4.** Todd J. Toops, Charles E.A. Finney, Eric J. Nafziger, Josh A. Pihl, “Neutron Imaging of Advanced Transportation Technologies”, 2013 DOE Annual Merit Review, Crystal City, VA, May 15, 2013.
- 5.** Todd J. Toops, Charles E.A. Finney, Josh A. Pihl, Hassina Z. Bilheux, Sophie Voisin, Jens Gregor, “Non-destructive Neutron Imaging to Analyze Particulate Filters”, 2013 Cross-cut Lean Exhaust Emissions Reduction Simulations (CLEERS) Workshop, Dearborn, MI, April 10-12, 2013.
- 6.** Todd J. Toops, Charles E.A. Finney, Josh A. Pihl, Hassina Z. Bilheux, Sophie Voisin, Jens Gregor, “Non-destructive Neutron Imaging to Analyze Particulate Filters”, 2012 Directions in Engine-Efficiency and Emissions Research Conference (DEER), Dearborn, MI, October 17, 2012.

III.12 Particulate Emissions Control by Advanced Filtration Systems for GDI Engines

Kyeong Lee

Argonne National Laboratory
9700 S. Cass Ave.
Argonne, IL 60564

DOE Technology Development Manager:
Ken Howden

- Develop a multi-functional GPF system combined with the three-way catalyst (TWC)



INTRODUCTION

GDI engines offer such benefits as increased power output and low fuel consumption, and so the market share of passenger vehicles with these engines is markedly increasing in comparison with the market share of vehicles powered by port fuel injection engines. However, additional attention has been focused on PM emissions that are significantly higher than those from port fuel injection engines. While PM emission mass standards have continuously been updated to lower levels, regulations for nanoparticle emission standards will be in effect in a few years. To control the PM emissions, including nanoparticles, GPFs have been developed and tested by manufacturers. However, detailed mechanisms of GPF filtration and regeneration processes, which were discussed to be quite different from those of diesel particulate filters (DPFs), are still unknown. In addition, the ultimate direction of GDI engine aftertreatment systems, the multi-functional catalyzed GPF, needs to be developed.

APPROACH

First, the Argonne research team conducted soot sampling from a GDI engine at various engine conditions using a thermophoretic sampling device and analyzed its detailed physicochemical properties, including morphology, nanostructures, fractal geometry, and chemistry. The research team fabricated a GPF test bench that implemented a visualization capability of filtration and regeneration and also a capability of evaluating back-pressure effects on engine combustion. In preliminary studies, the performance of the targeted engine was evaluated for the case of virtual installation of a GPF before the TWC and the oxygen concentrations available for GPF regeneration was evaluated for the case of lean-burn operations. Numerical modeling for soot filtration and pressure drop in a filter has been performed as well.

Overall Objectives

- Find gasoline particulate filter (GPF) filtration/regeneration mechanisms and evaluate the performance
- Develop technologies to reduce GPF back pressure
- Develop multi-functional GPFs

Fiscal Year (FY) 2013 Objectives

- Define particulate matter (PM) emissions characteristics of a gasoline direct injection (GDI) engine
- Characterize filtration and regeneration processes
- Propose technical background to develop cost-efficient multi-functional GPFs

FY 2013 Accomplishments

- Installed a stock GDI engine on an engine dyno and fabricated a GPF test bench
- Characterized the physical properties of GDI PM emissions, such as morphology and chemistry and found numerous small nanoparticles found only from GDI engines
- Evaluated the effects of filter structures and emissions flow conditions on pressure drop in soot loading
- Developed a numerical simulation code predicting gas dynamics and soot loading in a filter

Future Directions

- Evaluate ash effects on soot oxidation kinetics
- Evaluate differences of soot and filter properties in micro- and macro-scales between aged and fresh filters (catalyst coated)

RESULTS

Soot Morphology and Chemistry

(For details see publication 1)

Engine Specifications and Operating Conditions: Spark-ignited single-cylinder research engine with a direct fuel injection system; displacement of 549 cc; bore x stroke = 85.96 mm x 94.6 mm; compression ratio 11.97.

The engine was operated at 2,100 rpm and 650 kPa indicated mean effective pressure with variations of injection timing (end of injection [EOI]: 220, 250, 280, and 310° before top-dead center [bTDC]) for two different equivalence ratios ($\phi=0.98, 1.13$). To keep the constant indicated mean effective pressure, the flow rates of air/fuel were controlled and the fuel rail pressure was maintained constant at 11 MPa. Tested fuels include gasoline and 20% ethanol in gasoline (E20).

Figure 1(a) shows the total number of particles per sample emission volume at different fuel injection times, measured by a scanning mobility particle sizer at dilution ratios of 25–50. Overall, the number of particles increased as the equivalence ratio increased from 0.98 to 1.13, regardless of fuel type and injection timing. For all four conditions, the largest particle number appeared at the EOI angle of 310° bTDC, while the smallest particle number appeared at either 250° or 280°, except in the E20/ $\phi=0.98$ case. The enhanced particle formation due to potential fuel impingement may have resulted in the increased number of particles at that early fuel injection time. The second largest number of particles was measured at 220° bTDC, where the relatively shorter time available for fuel-air premixing led to a poor mixing condition. Overall, no consistent fuel-dependent trend is found for the total number of particles, mainly because of two reasons: (1) this engine was not optimized

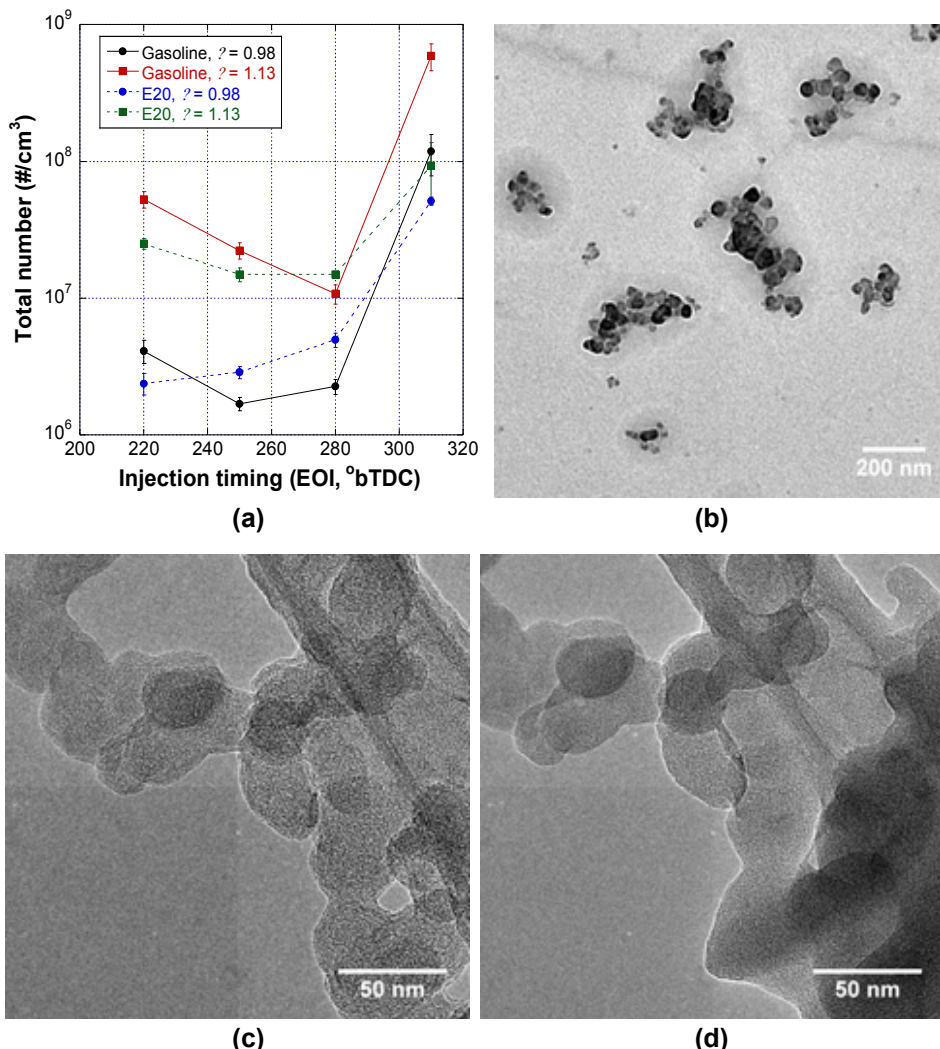


FIGURE 1. (a) Particle number distributions, (b) Observation of nanoparticles ≤ 20 nm, (c) and (d) Observation of high concentration of volatile organics from the GDI engine.

for the operation of E20 fuel and (2) the different chemical properties of ethanol in the blend should affect combustion mechanisms differently.

Figure 1(b) shows the transmission electron microscope (TEM) micrographs taken for the particulates from gasoline combustion at $\dot{\theta}=0.98$ and EOI 310° bTDC. The observed particle morphology is quite similar to that of diesel particulates in general, but an interesting observation is that the size of primary particles is quite different depending on aggregate size: the primary particles on large aggregates are overall larger than those on small aggregates. These small aggregate particles may be nascent particles that have not fully undergone graphitization processes, because their nanostructures were observed to be quite amorphous. The presence of these small nascent particles is unique and only from GDI engines; soot particles from conventional diesels are relatively uniform in size and graphitic. We believe that soot inception was enhanced at this highly advanced injection timing, where the concentration of unburned hydrocarbon from fuel impingement is anticipated to be high.

Figure 1(c) shows the TEM images for E20-derived soot particles at $\dot{\theta} = 1.13$ and 280° bTDC. Figure 1(d), a TEM image taken after the TEM electron beam energy increased at a high magnification, showed several individual primary particles to be altered from graphitic to amorphous, particularly those on the lower right-hand corner. These particles looked fused to each other and expanded. This change in morphology may come from instantaneous pyrolysis of the excess volatile organics dissolved in the particulates, as a result of the energized electron bombardment on particles. Therefore, it is quite apparent that particles from ethanol blends contain a high concentration of unburned volatile organics.

Effects of Filter Structures and Emissions Flow Conditions on Pressure Drop in Soot Loading

Clean-filter pressure drop of two different filters was measured with various flow rates at a temperature range of room temperature to 500°C . Figure 2 shows the results. The magnitude of filter A was almost twice larger than that of DPF B in the entire space velocity range, which tells that the lower permeability of filter A is caused by its low porosity and small pore size.

Characteristics of pressure drop build-up during filtration were evaluated for the two different filters at two different flow rates. The normalized ΔP_{soot} was plotted as a function of soot loading mass in Figure 3. From the graph, the amount of soot loading was evaluated in mass for depth filtration and soot cake formation. The slope of the linear fitting line evaluated for the each filtration region tells the level of pressure drop build-up per unit soot mass, defined as “pressure

drop potential” (PDP). The PDPs were evaluated for depth filtration and soot cake formation, as listed in Table 1.

During the depth filtration, the pressure drop characteristics showed quite a difference between the filters (porosity: filter A < filter B). Filter B can load 3–4 times higher amounts of soot in depth filtration

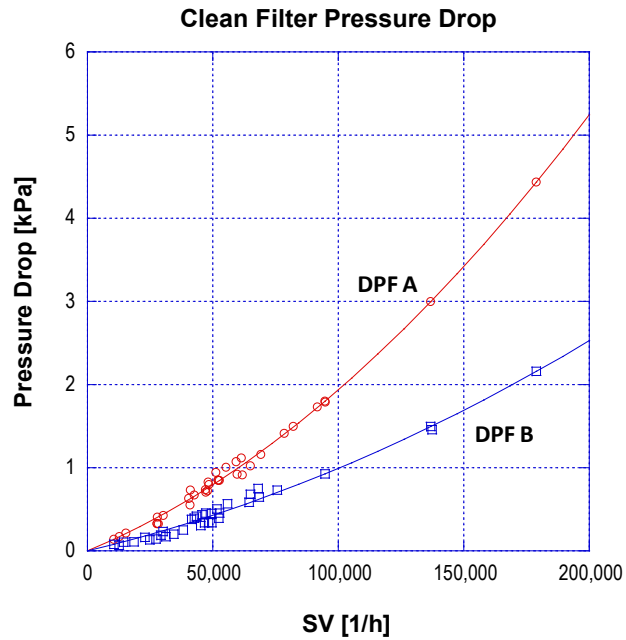


FIGURE 2. Clean filter pressure drops of two different filters.

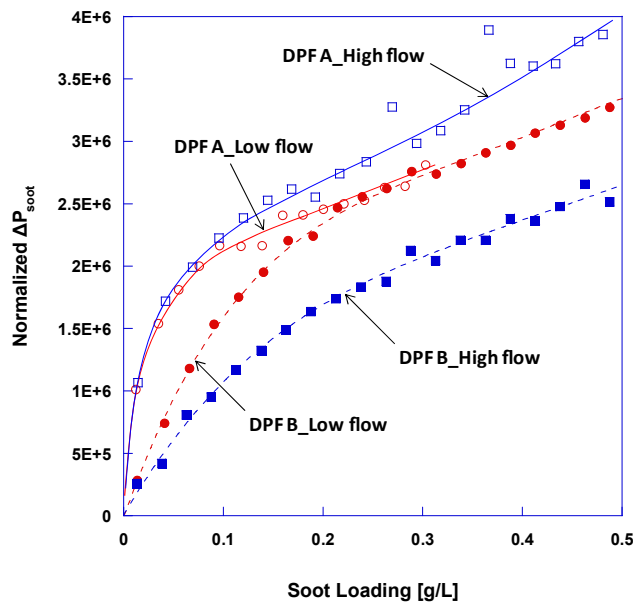


FIGURE 3. Pressure drop build-up during filtration for two different filters at two different flow rates.

TABLE 1. Comparison of Soot Deposition Characteristics of Four Filtration Conditions

| | DPF A Lowflow | DPF A Highflow | DPF B Lowflow | DPF B Highflow |
|---|------------------|-------------------|------------------|-------------------|
| Total soot loading [g/L] | 0.313 | 0.631 | 0.540 | 0.598 |
| Soot loading during depth filtration [g/L] | 0.034 | 0.033 | 0.118 | 0.163 |
| Soot loading during soot cake formation [g/L] | 0.279 | 0.598 | 0.422 | 0.435 |
| Norm. dP_{soot} at the end of depth filtration [-] | 1,991,997 | 1,801,369 | 2,169,048 | 1,770,085 |
| ΔP potential by depth filtration [Norm. ΔP_{soot} /(g/L)] | 43,796,817 | 42,837,006 | 18,372,021 | 10,518,552 |
| ΔP potential by soot cake [Norm. ΔP_{soot} /(g/L)] | 2,755,172 | 4,772,154 | 3,079,911 | 2,595,161 |

than does filter A at the same back-pressure condition. Meanwhile, the flow rate did not much affect the pressure drop of filter A in depth filtration, but did that of filter B. This behavior can be explained with the Peclet number of pore, Pe_{pore} (see Table 2). Flow conditions of soot in filter A are convection dominated ($Pe_{pore} > 1$) for both low and high flow rates, and so it shows similar soot loading mass and PDP. However, the soot flow conditions of filter B are diffusion dominated ($Pe_{pore} < 1$) for the low flow rate, resulting in such a different PDP.

During soot cake formation after the transition region, the pressure drop in filter A increased at a relatively higher rate with the high flow condition,

TABLE 2. Peclet Numbers and Other Properties Related to Soot Loading for Different Flow Conditions

| | DPF A Lowflow | DPF A Highflow | DPF B Lowflow | DPF B Highflow |
|--|------------------|-------------------|------------------|-------------------|
| Pe_{wall} | 0.236 | 0.672 | 0.271 | 0.679 |
| Pe_{pore} | 1.131 | 3.219 | 0.576 | 1.442 |
| Total soot loading [g/L] | 0.313 | 0.631 | 0.540 | 0.598 |
| Soot loading during depth filtration [g/L] | 0.034 | 0.033 | 0.118 | 0.163 |
| Gradient of ΔP profile in depth filtration [Norm. ΔP_{soot} /(g/L)] | 43,796,817 | 42,837,006 | 18,372,021 | 10,518,552 |
| Gradient of ΔP profile in soot cake formation [Norm. ΔP_{soot} /(g/L)] | 2,755,172 | 4,772,154 | 3,079,911 | 2,595,161 |

compared to three others. This result is not well correlated with the Pe_{wall} values, which indicate that the average particle flow conditions lie in all diffusion-dominated ($Pe_{wall} < 1$) and so soot particles will be more diffusive in low flow conditions. Consequently, higher-porosity filters offer better pressure drop in filtration, and the filter geometry needs to be selected with care in consideration of the flow rate range, in such a way to set Pe_{pore} slightly greater than unity.

Oxidizer Concentrations Available For GPF Regeneration at Lean-Burn Conditions

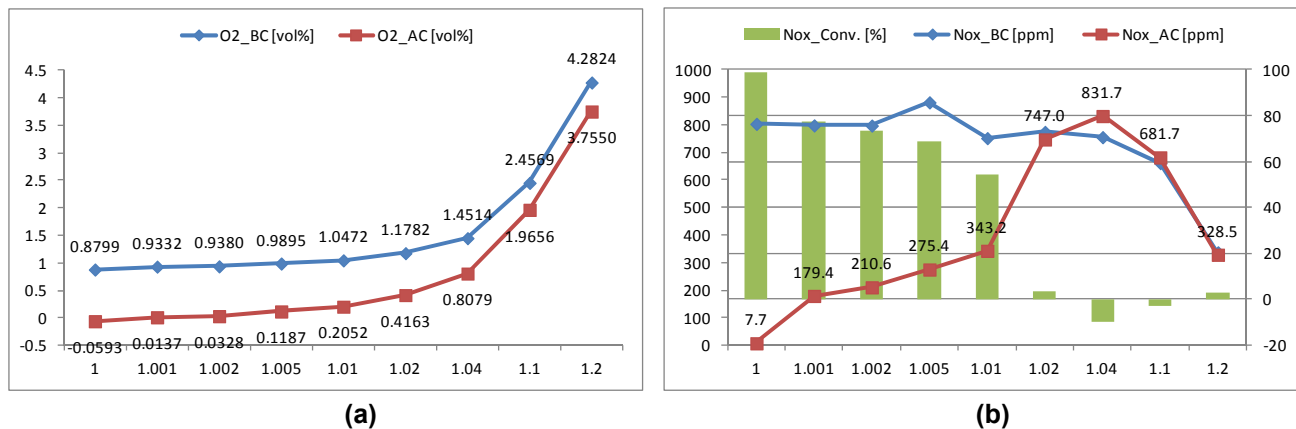
Lean-burn engine operating conditions were tested to increase the oxygen concentration available for regeneration in a post-GPF. As seen in Figure 4(a), the oxygen concentration after the TWC increased only up to 0.12 vol% as the equivalence ratio increased to 1.005 from the stoichiometric condition. At the same equivalence ratio of 1.005, however, the oxides of nitrogen (NOx) conversion efficiency by the TWC was significantly dropped to about 70% from 99%. Therefore, it turned out that lean-burn operation conditions do not offer sufficient oxidizer for GPF regeneration, while it rather worsens the NO_x conversion efficiency of TWC.

Numerical Modeling of Soot Loading in Filter Channels

Hypotheses

- The fluid is a three-dimensional (3-D) ideal gas with fully developed laminar flow.
- The particles are 3-D, constant density, and spherical in shape.
- Convective heat loss is the only heat transfer across the system boundary.
- The geometry and material properties of the filter correspond to those of 200 cell per square inch, cordierite, and uncoated filter.
- Potential energy, gravity, chemical reaction, compression effect, and ash deposition are neglected.

In this multiphase flow problem, the continuous phase (fluid) was represented by an Eulerian description; that is, the gas characteristics were calculated at fixed points within the flow. For particle-laden flows, however, the dispersed phase (particles) may be relatively sparse in the flow field, so this phase does not have to be solved in every local point of domain. Thus, use of a Lagrangian description where the motion of particles is dominated by their interaction with the fluid may be more pertinent. In the modeling, a steady-flow solver is used for the clean filter simulations where the inlet pressure is converged at a given flow rate as the code iterates, while the outlet pressure is set as a fixed boundary condition. For soot



BC – before catalyst; AC – after catalyst

FIGURE 4. Effects of lean-burn operation on oxidizer concentration and NOx conversion.

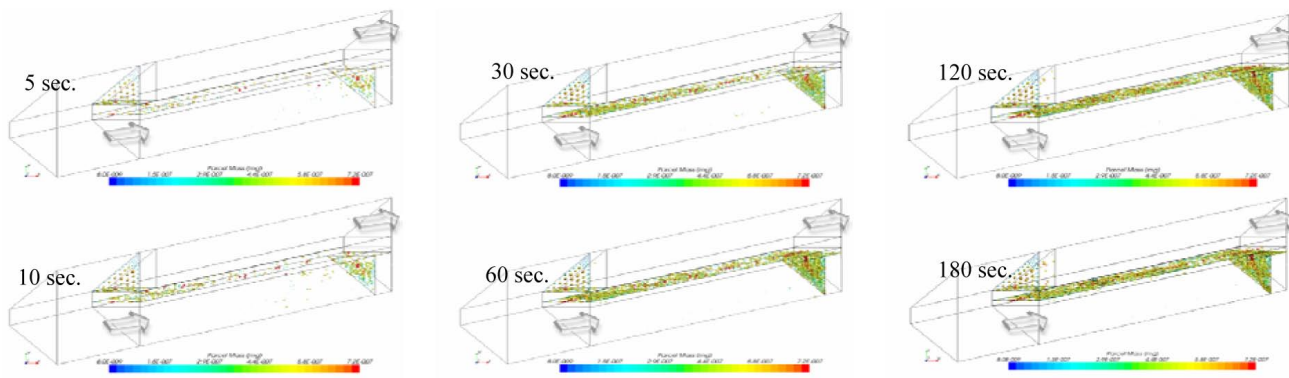


FIGURE 5. The predicted 3-D distributions of particulates during filtration at different filtration times.

loading simulations, the Lagrangian multiphase model was chosen, along with an implicit unsteady solver, to describe the transient schemes of both the continuous and dispersed phases. The predicted 3-D distributions of particulates during filtration were displayed at different filtration times in Figure 5.

CONCLUSIONS

PM emissions from a single-cylinder GDI research engine were analyzed in terms of morphology and nanostructures. The investigation found a unique result: the number of nanoparticles smaller than 23 nm significantly increased for the GDI engine, which is mainly caused by the fuel impingement due to the early fuel injection. The PM emissions from E20 turned out to contain a significant amount of unburned hydrocarbons or soluble organics. Pressure-drop characteristics of particulate filters were examined for different filter

material properties at different flow conditions. Their soot formation mechanisms were able to be interpreted by Peclet number. As a preliminary examination, a stock GDI engine was tested to examine the level of oxygen available for GPF regeneration. As a result, lean-burn conditions turned out to produce oxidizer at the levels insufficient for soot-cake regeneration, while the NOx conversion efficiency by the TWC worsened due to increased NOx emissions. Numerical modeling successfully demonstrated the temporal and spatial distributions of gas dynamics and soot loading behaviors in a filter substrate.

FY 2013 PUBLICATIONS/PRESENTATIONS

1. Lee, K., Seong, H., Sakai, S., Hageman, M., and Rothamer, D.: "Detailed Morphological Properties of Nanoparticles from Gasoline Direct Injection Engine...," SAE 2013-24-0185.

III.13 Fuel-Neutral Studies of PM Transportation Emissions

Mark Stewart (Primary Contact), Alla Zelenyuk
Pacific Northwest National Laboratory (PNNL)
902 Battelle Boulevard
Richland, WA 99352

DOE Technology Development Manager:
Ken Howden

Subcontractor:
University of Wisconsin Engine Research Center (ERC),
Madison, WI

- The ERC Exhaust Filtration Analysis (EFA) system was modified to allow filtration tests with exhaust from gasoline test engines.
- Extensive sets of micro X-ray CT data were obtained for five current filter substrates from two major manufacturers which cover a range of properties. Automated computer programs were written to extract relevant property information.

Future Directions

- Filtration efficiency experiments using the University of Wisconsin EFA system with SIDI exhaust at temperatures representing close-coupled filter placement
- Apply advanced characterization methods to particulate matter (PM) which penetrates filters
- Attempt to correlate statistics obtained from micro-structural analysis with pressure drop and filtration efficiency
- Use first-principals micro-scale models to further improve sub-grid modeling tools, such as the commonly used unit-collector
- Apply advanced particulate characterization to subsequent generations of engines—leaner operation, higher fuel efficiency



INTRODUCTION

Technologies such as SIDI and GCI offer the possibility of dramatically increasing the fuel efficiency of engines that run on gasoline and associated fuel blends. Development of this technology will blur the lines that have traditionally existed between gasoline and diesel engines. Although some similarities have been observed between diesel soot and particulates generated by lean-burn engines designed to use other fuels, significant differences could require adaptation of existing aftertreatment technologies. Gasoline particles are generally smaller than diesel particles, and PM production can vary widely between engine operating conditions.

Regulation of engine particulate emissions in Europe is moving from mass-based to number-based standards. This will place more emphasis on the reliable removal of smaller particles, which make up the vast majority of the particulates generated on a number basis. American manufacturers must already design systems to meet

FY 2013 Accomplishments

- Analysis of data from the second round of cooperative experiments at the ERC was finished and reported in several presentations and journal articles.
- Improved unit collector models have been used to explore the parameter space relevant to the design of future gasoline particulate filtration systems.

number regulations for the European market, and must also be prepared for the introduction of more stringent particulate limits in the U.S. market. Experience thus far indicates that current and future SIDI engines will likely require filtration to meet number limits. It is also likely that filtration will be required if current mass limits are tightened significantly. Furthermore, many filtration systems currently used with diesel engines may not provide adequate filtration efficiency or may result in unacceptable levels of back-pressure. Most current-generation diesel particulate filters (DPFs) rely on a soot cake to achieve high capture efficiencies. High exhaust temperatures and relatively low rates of PM production may limit soot cake formation in gasoline exhaust filtration applications.

APPROACH

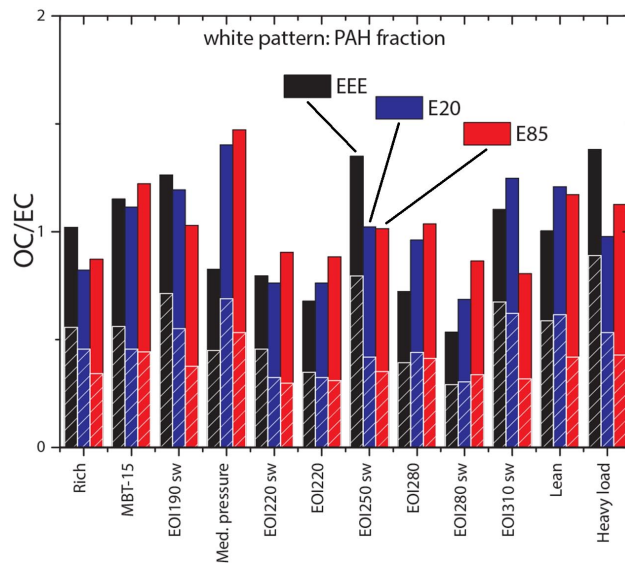
General Motors Research has provided components and guidance to develop advanced gasoline research engines at University of Wisconsin's ERC. These research engines have been configured to run with a variety of fuels over a wide range of operating conditions. Two campaigns of joint experiments conducted by PNNL and ERC have generated an extensive set of data on particulate size, shape, and composition, using standard gasoline and ethanol blends. The current focus of this project is to develop fundamental understanding of the factors affecting filtration efficiency and back-pressure, in order to promote the development of optimum filtration systems for advanced gasoline vehicles. Filtration experiments will be carried out using a variety of candidate filter substrates having a wide range of properties and different micro-structures. Experiments will include simple lab-generated particles and particulates generated with the gasoline test engines. Filter substrate microstructures will be analyzed using standard and advanced techniques, in an effort to identify length scales and morphological characteristics that correlate with filter performance. First principles micro-scale simulations will be used to refine device-scale modeling tools for better predictions of filtration efficiency.

RESULTS

Analysis of data collected in the second campaign of cooperative experiments carried out at the ERC was completed in FY 2013 and described in several presentations and publications. Experiments were conducted with GCI and SIDI engines using multiple ethanol fuel blends at dozens of relevant operating conditions, including variation in parameters such as end of injection timing, equivalence ratio, load, and temperature.

Using multiple instruments together, individual particles were selected by mass, and/or mobility diameter, and characterized by SPLAT II, an ultra-sensitive, high-precision single particle mass spectrometer developed at PNNL. Mass composition spectra for all individual particles, including those selected by mass or size, were also obtained with SPLAT II. Data collected from these multiple-instrument experiments yielded particle size, mass, aerodynamic diameter, composition, fractal dimension, primary spherule size and density, occupied volume, number of spherules per soot aggregate, and the relationships between all of these properties and engine operating conditions. One of the more interesting findings was that under certain conditions, both SIDI and GCI engines produced PM made up of distinct particle subpopulations.

Two different modes of soot particulates were observed in SIDI exhaust, appearing in different proportions depending on operating parameters such as equivalence ratio and end of injection timing. Both were found to be fractal soot particles with nearly identical compositions. While fractal dimensions were indistinguishable, the average diameters of the primary spherules making up the soot agglomerates in the two modes were found to be significantly different: 18 nm in one case, and 26 nm in the other. All of the fractal soot particles were observed to have high organic content, between 40% and 60% by mass. Figure 1 shows ratios of organic carbon to elemental carbon observed in fractal soot particles with three different fuels under various



OC - organic carbon; EC - elemental carbon; EEE - 100% gasoline; E20 - 20% ethanol, 80% gasoline; E85 - 85% ethanol, 15% gasoline; MBT - minimum for best torque; EOI - end of injection

FIGURE 1. Ratio of organic to elemental carbon in fractal SIDI particulates with three fuel blends under various conditions.

operating conditions (listed on the x axis). Particle count varied dramatically between operating conditions and fuel types. Far fewer soot particles were produced with 85% ethanol, 15% gasoline fuel blend (E85), which resulted in a larger fraction of a separate class of large, non-fractal particles. These particles are associated with lubricating oil and engine wear and tear.

In GCI exhaust, both fractal soot particles and compact organic particles were observed under low-load conditions, as shown in Figure 2. The figure shows that using composition-resolved vacuum aerodynamic diameter (d_{va}) distributions obtained with SPLAT II, the observed overall distribution of d_{va} can be separated into distributions of the two particle types. The compact organic particles disappear under higher load conditions. The fractal soot particles that remain have similar fractal dimension, but are made up of smaller primary spherules than those observed under low-load conditions.

The differing properties of the GCI particulate sub-populations can be seen in Figure 3. Effective density (ρ_{eff}) is a function of vacuum aerodynamic (d_{va}) and mobility (d_m) diameters [1]. On a log-log plot of ρ_{eff} vs d_m for a given sub-population of particles, the slope of the fit line is a function of the fractal dimension. The organic particles are shown to have a fractal dimension (D_{fa}) near 3, which is consistent with a near-spherical shape. The average effective density of these particles is $0.98 \pm 0.02 \text{ g cm}^{-3}$, which is consistent with particle compositions. Furthermore, the slight deviation of D_{fa} from 3 is due to a small increase in particle density with particle diameter, which is consistent with a

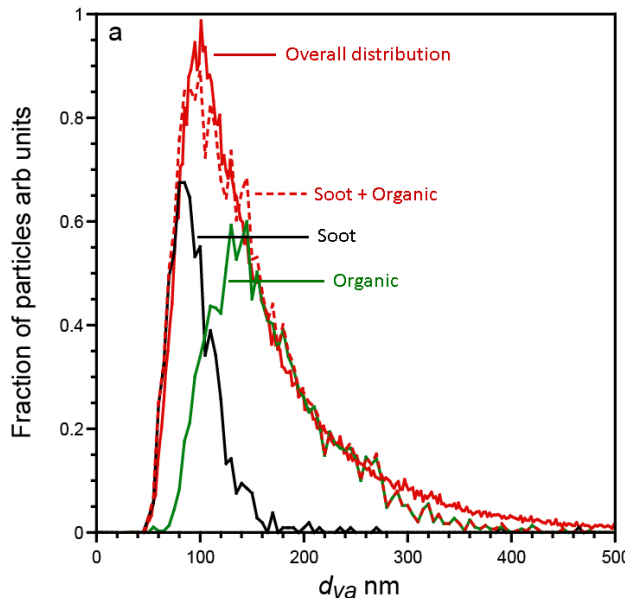


FIGURE 2. GCI particulate aerodynamic diameters under one low-load condition.

small increase in the fraction of polycyclic aromatic hydrocarbons with particle size. The soot particles found under high-load and low-load conditions both have a fractal dimension near 2, which is consistent with fractal agglomerates.

Some success has been previously reported in improving the ability of the standard unit collector model [2] to predict filtration efficiency over the particle size ranges observed in gasoline exhaust using micro-scale simulations [3]. These improved unit collector models can then be used to conduct parametric studies to help system designers manage the various tradeoffs between factors such as particulate removal efficiency, pressure drop, and system volume. Figure 4 shows an example of how filtration efficiency as a function of particle size could be expected to vary with porosity in a common cordierite filter. Back-pressure increases dramatically at low porosities, so that the optimum porosity might be the highest possible, while still meeting requirements for removal efficiency.

The standard unit collector model is based on relationships developed for loose granular beds, not for porous ceramic materials such as cordierite. Although the model has been widely used for these filter substrates, one difficulty is the selection of a value for the “collector diameter”, which would be the average grain size in a packed bed, but is often tuned to match experimental data for DPFs. System engineers have expressed the need to better understand the structure and relevant length scales of actual exhaust particulate filter substrates.

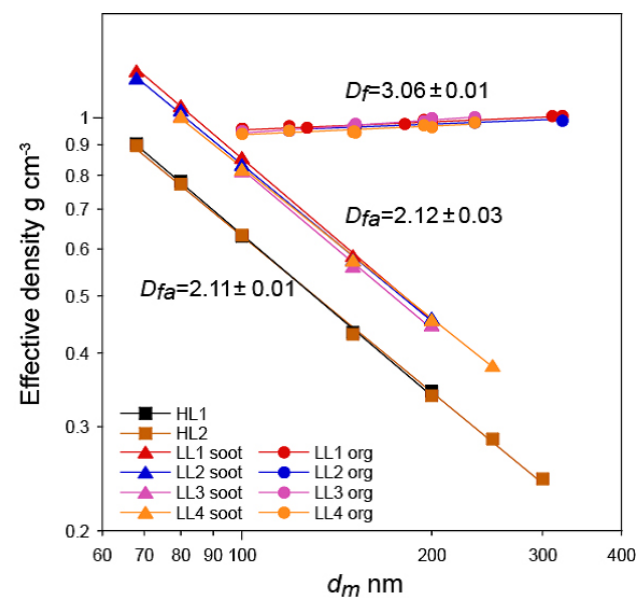


FIGURE 3. Plot of the calculated effective density as a function of mobility diameter for GCI particulates generated under low-load and high-load conditions.

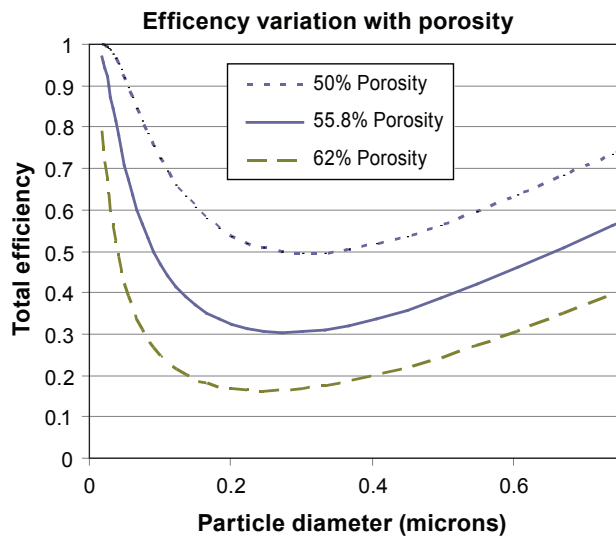


FIGURE 4. Expected variation of filtration efficiency with porosity in a typical cordierite filter.

This knowledge could lead to better application of existing materials and promote exploration of new filter technologies.

To this end, five new sets of micro X-ray CT data were collected for samples of commercially available DPF substrates. Each set contains thousands of grayscale images with a resolution of approximately 1.6 micron. These images can be combined to provide detailed three-dimensional information on the pore structure. Automated computer programs were developed to scan through the images and extract relevant parameters. Information was gathered on actual filter wall thickness and its variation within a sample, variation of porosity within the wall, and statistical metrics such as the autocorrelation function and chord length distribution [4].

Figure 5 shows an interesting feature which was common, to a greater or lesser degree, among all of the cordierite filters examined thus far. The figure shows how porosity varies throughout the wall thickness, as a function of the distance from the wall center plane. Porosity near the filter wall surface is significantly lower than in the interior of the wall. This variation in local porosity could affect overall pressure drop and filtration efficiency, as well as the transition from depth filtration to cake filtration at lower temperatures.

Figure 6 shows autocorrelation plots for the void phase in the same cordierite filter material at one wall surface and in the wall interior. The x intercept of the tangent line at low correlation lengths has been used as one relevant length scale for specification of the collector diameter in unit collector models of ceramic DPF materials [5]. It can be seen that this value also varies significantly between the filter wall surface and interior.

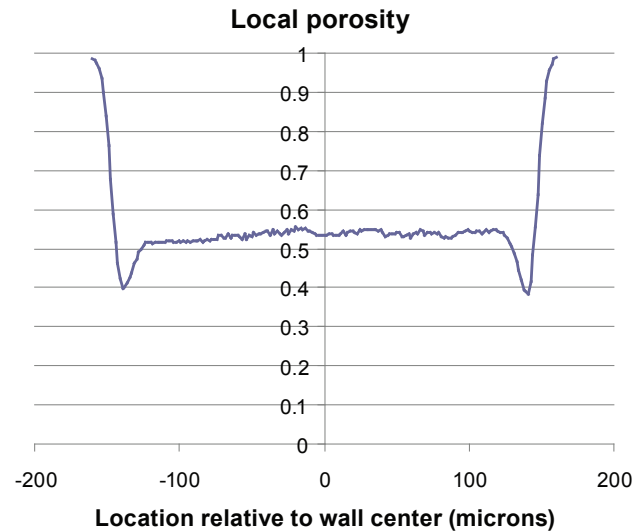


FIGURE 5. Variation of local porosity across the thickness of a single cordierite filter wall.

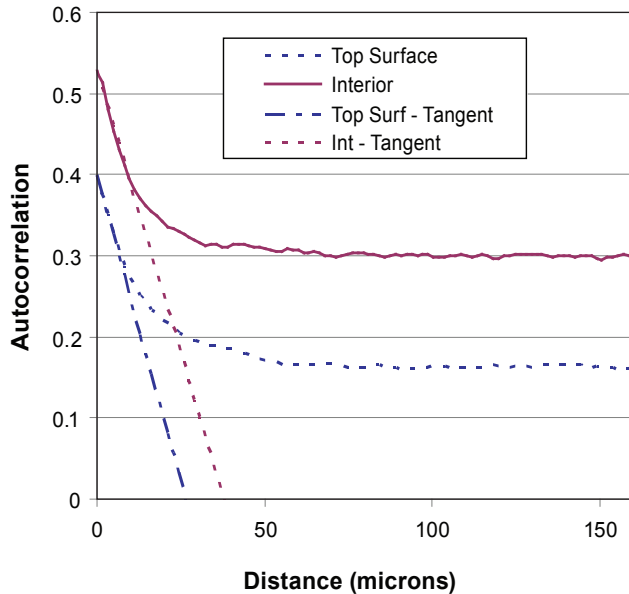


FIGURE 6. Autocorrelation plots for the void phase at the top surface and in the interior of a cordierite filter wall.

The Diesel Exhaust Filtration Analysis system [6] was upgraded and made more flexible in FY 2013 to become the new EFA system at the University of Wisconsin, Madison. Filter samples are now held in a furnace, so that sample temperature can be controlled independently from that of the inlet exhaust. The system has been made more portable, to allow experiments with actual exhaust from multiple engines. The performance of multiple candidate filter materials is currently being evaluated using exhaust from advanced gasoline engines. Further enhancements to the system will include an

upgrade of the sample holder to allow high temperature experiments, simulating close-coupled filter placement.

CONCLUSIONS

- High organic content, which was tightly bound with inorganic carbon, was observed in SIDI particulates for all fuels and operating conditions.
- Particulate populations in both SIDI and GCI exhaust were found to comprise distinct sub-populations under some conditions:
 - Two modes in SIDI soot particles were found to have similar fractal dimension but much different average primary spherule diameters.
 - Large, non-fractal particles were also observed in SIDI exhaust, that became a significant fraction of the relatively small number of particulates produced with E85.
 - GCI exhaust was found to contain large numbers of compact organic particles under low-load conditions, in addition to fractal soot particles.
 - Particulates in GCI exhaust under high-load conditions were dominated by fractal soot particles with smaller primary spherule diameters than those observed under low-load conditions.
- Parametric studies were conducted that demonstrate how a reliable device-scale filtration model could be useful in managing tradeoffs between factors such as filter system volume, pressure drop, and filtration efficiency.
- Local porosity and relevant pore length scales were found to vary significantly between the surface and interior of cordierite filter walls.

REFERENCES

1. Zelenyuk A, P Reitz, M Stewart, D Imre, P Loeper, C Adams, M Andrie, D Rothamer, D Foster, K Narayanaswamy, P Najt, A Solomon. “Detailed Characterization of Particulates Emitted by Pre-commercial Single-cylinder Gasoline Direct Injection Compression Ignition Engine”. COMBUSTION AND FLAME 2014.
2. Konstandopoulos, A and JH Johnson, “Wall-Flow Diesel Particulate Filters - Their Pressure Drop and Collection Efficiency”. SAE, 1989. 890405.
3. Long, W and M Hilpert, “A Correlation for the Collector Efficiency of Brownian Particles in Clean-Bed Filtration in Sphere Packings by a Lattice-Boltzmann Method”. ENVIRONMENTAL SCIENCE & TECHNOLOGY, 2009. 43(12). p. 4419-4424.
4. Roberts, A and S Torquato, “Chord-distribution functions of three-dimensional random media: Approximate first-passage

times of Gaussian processes”. PHYSICAL REVIEW E, 1999. 59(5): p. 4953-4963.

5. Fukushima, S, K Ohno, N Vlachos, and AG Konstandopoulos, “New Approach for Pore Structure and Filtration Efficiency Characterization”. SAE, 2007. 2007-01-1918.
6. Wirojsakunchai, E, C Kolodziej, R Yapaalo, and D Foster, “Development of the Diesel Exhaust Filtration Analysis system (DEFA)”. 2008. 2008-01-0486.

FY 2013 PUBLICATIONS/PRESENTATIONS

1. Zelenyuk A, P Reitz, ML Stewart, M Hageman, A Maier, S Sakai, D Foster, D Rothamer, M Andrie, R Krieger, K Narayanaswamy, P Najt, A Solomon, “Characterization of Pre-commercial Gasoline Engine Particulates Through Advanced Aerosol Methods,” Directions in Engine-Efficiency and Emissions Research Conference, Detroit, MI, October 2012.
2. Zelenyuk A, D Imre, J Beranek, and P Reitz. 2012. “Detailed Characterization of Shape-Selected Fractal Soot Particles.” The 31st Annual American Association for Aerosol Research (AAAR) Conference, Minneapolis, MN, October 8–12.
3. Gaddam, CK and RL Vander Wal, “Physical and chemical characterization of SIDI engine particulates”. COMBUSTION AND FLAME, 2013. 160(11): p. 2517-2528 DOI: <http://dx.doi.org/10.1016/j.combustflame.2013.05.025>.
4. ML Stewart. “Fuel-Neutral Engine Particulate Filtration Studies”, General Motors Technical Center, Warren, MI, April 10, 2013.
5. ML Stewart, “Fuel-Neutral Studies of Particulate Matter Transport Emissions”, 2013 DOE Hydrogen and Vehicle Technologies Merit Review, Washington, DC, May 2013.
6. Zelenyuk A, P Reitz, D Imre, M Stewart, P Loeper, C Adams, M Hageman, A Maier, S Sakai, D Foster, D Rothamer, M Andrie, R Krieger, K Narayanaswamy, P Najt, A Solomon. “Detailed Characterization of Particulates Emitted by Pre-commercial High-Efficiency Gasoline Engines”. The 32nd Annual American Association for Aerosol Research (AAAR) Conference, Portland, OR, Sept 30 – Oct 4, 2013.
7. Zelenyuk A, P Reitz, M Stewart, D Imre, P Loeper, C Adams, M Andrie, D Rothamer, D Foster, K Narayanaswamy, P Najt, A Solomon. “Detailed Characterization of Particulates Emitted by Pre-commercial Single-cylinder Gasoline Direct Injection Compression Ignition Engine”. COMBUSTION AND FLAME 2014, *minor revision*.

ACKNOWLEDGEMENTS

General Motors Corporation: Kushal Narayanaswamy, Paul Najt, Arun Solomon, Michael Viola, Wei Li; University of Wisconsin Madison: David Foster, David Rothamer, Matthew Coyne, Michael Andrie, Mitchell Hageman, Roger Krieger, Axel Maier, Stephen Sakai; PNNL: Josef Beranek, Paul Reitz, Cameron Hohimer

A portion of the research was performed using EMSL, a national scientific user facility sponsored by the Department of Energy's Office of Biological and Environmental Research and located at Pacific Northwest National Laboratory.

III.14 The Advanced Collaborative Emissions Study (ACES)

Dan Greenbaum (Primary Contact),
Rashid Shaikh, Maria Costantini,
Annemoon van Erp
Health Effects Institute (HEI)
101 Federal Street, Suite 500
Boston, MA 02110

DOE Technology Development Manager:
Gurpreet Singh

NETL Project Manager: Carl Maronde

Subcontractors:

- Coordinating Research Council (CRC),
Alpharetta, GA
- Lovelace Respiratory Research Institute (LRRI),
Albuquerque, NM

Overall Objectives

- Phase 1: Extensive emissions characterization at Southwest Research Institute® (SwRI®) of four production-intent heavy-duty diesel engine and control systems designed to meet 2007 standards for particulate matter (PM) and nitrogen oxides (NOx). One engine/aftertreatment system will be selected for health testing.
- Phase 2: Extensive emissions characterization of a group of production-intent engine and control systems meeting the 2010 standards (including more advanced NOx controls to meet the more stringent 2010 NOx standards).
- Phase 3: One selected 2007-compliant engine will be installed and tested in a specially-designed emissions generation and animal exposure facility at the Lovelace Respiratory Research Institute (LRRI) (Phase 3A) and used in chronic and shorter-term health effects studies to form the basis of the ACES safety assessment (Phases 3B and 3C). This will include periodic emissions characterization during both a core 24-month chronic bioassay of cancer endpoints in rats and biological screening assays in both rats and mice (Phase 3B) as well as emissions characterization during a set of shorter animal exposures and biological screening using accepted toxicological tests after the end of the chronic bioassay (Phase 3C). (NOTE: Only the emissions characterization and biological screening activities during Phase 3 are components of the DOE ACES contract.)

Fiscal Year (FY) 2013 Objectives

- Phase 2: Complete emissions characterization at SwRI® of production-intent engine and control systems meeting the 2010 standards. Review Phase 2 draft report.
- Phase 3: Complete the long-term exposures in rats. Review Phase 3B reports.

FY 2013 Accomplishments

Key Accomplishments

- Completed Phase 2 emissions characterization of three 2010-compliant engines and reviewed a draft final report from SwRI®.
- Completed Phase 3 inhalation study of animals exposed to exhaust from one 2007-compliant engine including comprehensive characterization of emissions and exposures near the end of the study; completed pathology evaluation and pathology peer review at the core laboratory (LRRI); reviewed reports from three ancillary studies to evaluate genotoxic and vascular effects.

General Oversight

- Printed and distributed copies of HEI Research Report 166 (October 2012).
- Provided briefings on ACES results to the Engine Manufacturers Association and as part of an Environmental Protection Agency (EPA) webinar on black carbon (November 2012).
- Provided a project update to the ACES Advisory and Oversight Committees (January 2013).
- Held a meeting to discuss the Phase 2 results at SwRI® with investigators and CRC Technical Panel in San Antonio (March 2013).
- Held a joint ACES Advisory and Oversight Committees meeting to review results at the HEI Annual Conference in San Francisco (April 2013).
- Presented ACES results at several meetings as listed under FY 2013 Publications/Presentations.

Phase 2

- Completed testing of the third 2010-compliant engine at SwRI® (December 2012); Completed chemical analyses of emissions from the three 2010-compliant engine at SwRI® (March 2013).

- Held a conference call with the CRC Technical Panel to discuss Phase 2 results from Oak Ridge National Laboratory regarding specific urea-related compounds (May 2013).
- Received a draft final report for Phase 2 (June 2013) and reviewed the report (July 2013).

Phase 3B

- Completed emissions generation and exposure characterization during the chronic testing at LRRI (November 2012); completed the exposures of female rats at LRRI and conducted a site visit to witness the final sacrifice of the remaining rats (December 2012).
- Completed the ancillary studies' analyses and received three final reports, by Drs. Bemis and Conklin (February 2013) and Hallberg (March 2013); held a review panel meeting to discuss the three draft Phase 3B reports (April 2013).
- Received revised reports for the ancillary studies by Drs. Bemis and Hallberg (July 2013) and Conklin (August 2013); held review panel conference calls to discuss them (September 2013).
- Continued analyses of health endpoints for the chronic bioassay at LRRI in Phase 3B (funded separately by U.S. EPA).

Future Directions

- Complete all health analyses for the Phase 3B core study at LRRI and receive final reports on inhalation chamber exposure characterization and health outcomes (November 2013).
- Peer review and publish the final Phase 2 and Phase 3B reports during 2013 (Phase 2) and 2014 (Phase 3B); hold a stakeholder webinar to present the final results of Phase 3B (Spring 2014).
- Present ACES results at the Society of Toxicology Meeting in Phoenix, AZ in March 2014, the CRC Real World Emissions workshop in San Diego, CA in April 2014, and the HEI Annual Conference in Alexandria, VA in April 2014.



INTRODUCTION

The ACES is a cooperative, multi-party effort to characterize the emissions and assess the safety of advanced heavy-duty diesel engine and aftertreatment systems and fuels designed to meet the 2007 and 2010 emissions standards for PM and NOx. The ACES project is being carried out by HEI and the CRC.

It is utilizing established emissions characterization and toxicological test methods to assess the overall safety of production-intent engine and control technology combinations that are being introduced into the market during the 2007-2010 time period. This is in direct response to calls in the U.S. EPA Health Assessment Document for Diesel Engine Exhaust [1] for assessment and reconsideration of diesel emissions and health risk with the advent of new cleaner technologies.

The characterization of emissions from representative, production-intent advanced compression ignition engine systems includes comprehensive analyses of the gaseous and particulate material, especially those species that have been identified as having potential health significance. The core toxicological study includes detailed emissions characterization at its inception, and periodically throughout a two-year chronic inhalation bioassay similar to the standard National Toxicology Program bioassay utilizing two rodent species. Other specific shorter-term biological screening studies also are being undertaken, informed by the emissions characterization information, to evaluate these engine systems with respect to carefully selected respiratory, and other effects for which there are accepted toxicologic tests. It is anticipated that these emissions characterization and studies will assess the safety of these advanced compression ignition engine systems, will identify and assess any unforeseen changes in the emissions as a result of the technology changes, and will contribute to the development of a data base to inform future assessments of these advanced engine and control systems.

APPROACH

Experimental work under ACES is being conducted in three phases, as outlined in the Objectives. Detailed emissions characterization (Phases 1 and 2) is performed by an existing engine laboratory (SwRI®) that meets the U.S. EPA specifications for 2007 and 2010 engine testing. In Phase 1, emissions from four 2007-compliant engine/control systems were characterized. One engine was selected for health testing in Phase 3. In Phase 2, emissions from three 2010-compliant engine/control systems are being characterized. In Phase 3, the selected 2007-compliant engine/control system was installed in a specially designed emission generation facility connected to a health testing facility at LRRI to conduct a chronic inhalation bioassay and shorter term biological screening in rats and mice. During the 30-month bioassay, emissions are being characterized at regular intervals throughout the testing.

The emissions characterization work is overseen by the CRC and CRC's ACES Panel. The health effects

assessment is overseen by HEI and its ACES Oversight Committee (a subset of the HEI Research Committee augmented by independent experts from several disciplines), with advice from an Advisory Committee of ACES stakeholder and other experts. The overall effort is guided by an ACES Steering Committee consisting of representatives of DOE, engine manufacturers, EPA, the petroleum industry, the California Air Resources Board, emission control manufacturers, and the Natural Resources Defense Council. Set up of the emission generation facility at LRRI (for Phase 3) and establishment of periodic emissions characterization throughout Phase 3 has been done with input from the team of investigators who conducted Phase 1 and the CRC ACES Panel.

RESULTS

The results obtained during this reporting period pertain to the Phase 2 emissions characterization at SwRI® and Phase 3B animal exposures at LRRI. Results of the three engines tested at SwRI® indicated that the intended emissions reductions were met, and in most cases exceeded. To comply with the 2010 NO_x limit, a urea-based selective catalytic reduction catalyst was placed downstream of a diesel oxidation catalyst and a catalyzed diesel particle filter used for PM emissions control. Due to technical improvements, no active regeneration of the diesel particle filter was needed during ACES Phase 2 testing, compared to the several regeneration occurrences with the 2007 technology engines tested in ACES Phase 1. Figure 1 shows that during the 16-hour cycle the average emissions of key pollutants of the three 2010-compliant engines are considerably lower than emissions from

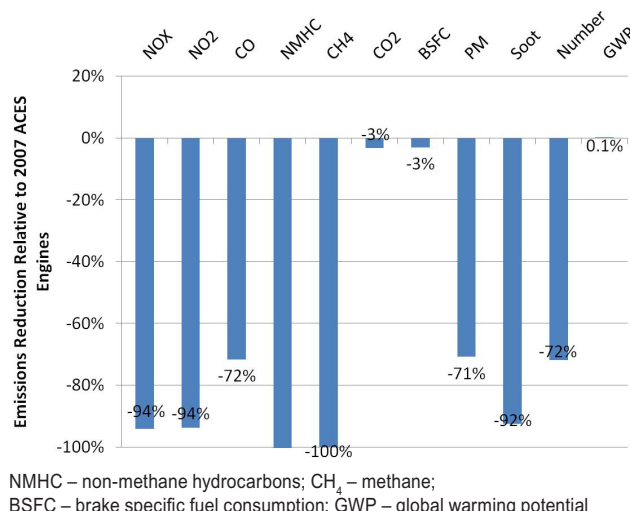


FIGURE 1. 2010 technology engines emissions reduction relative to 2007 technology engines for the 16-hr cycle.

the 2007-compliant engines tested in Phase 1, with the exception of CO₂, brake specific fuel consumption, and global warming potential. Figure 2 shows that although N₂O emissions were higher for the 2010 technology engines compared to the 2007 technology engines, they were still below the EPA 2014 N₂O emissions limit of 0.1 g/hp-hr. Reduction in particle number with the 2010 engines (data not shown) would be mainly due to the lack of sulfuric acid particle nucleation.

Figure 3 illustrates differences in composition of the PM emitted by 2010 technology engines compared to 2007 technology engines. For 2010 technology engines, the very low level of PM was dominated by organic carbon (OC; 66%), followed by elemental carbon (EC; 16%) and nitrate (14%), in contrast with 2007 technology engines, where PM was dominated by sulfate (53%), followed by OC (30%) and EC (13%). Emissions of elements were substantially lower with the 2010 vs. 2007 technology engines. The non-metallic elements were dominated by sulfur (fuel and oil derived) and metallic elements were dominated by calcium and zinc (lube oil derived) followed by iron and aluminum (engine wear) (data not shown).

Animal exposures at LRRI were completed in December 2012. Female rats were exposed for 30 months; male rats were exposed for 28 months due to reduced survival (unrelated to the exposures). Daily analysis of exposure atmospheres indicated that the 2007-compliant engine system operated reliably throughout the study and has consistently provided the targeted exposure concentrations (at 4.2, 0.8, and 0.1 ppm of NO₂) (data not shown). There were no exposure-related differences in mortality or clinically-evident morbidity in rats after 30 months of exposure. Histologic findings at 24 months showed a small increase in the extent of the tissue

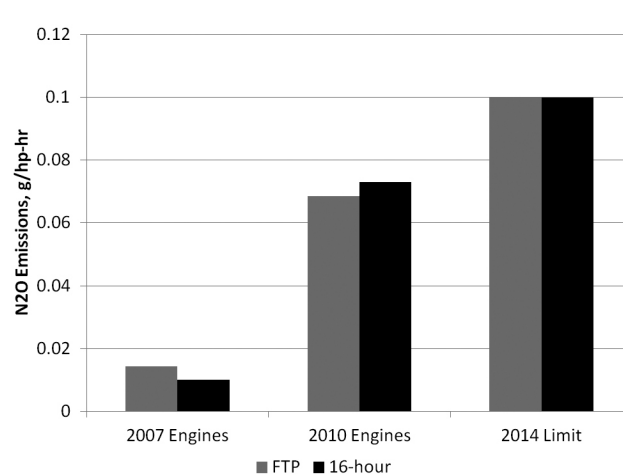


FIGURE 2. N₂O emissions comparison for 2010 and 2007 technology engines relative to the 2014 limit.

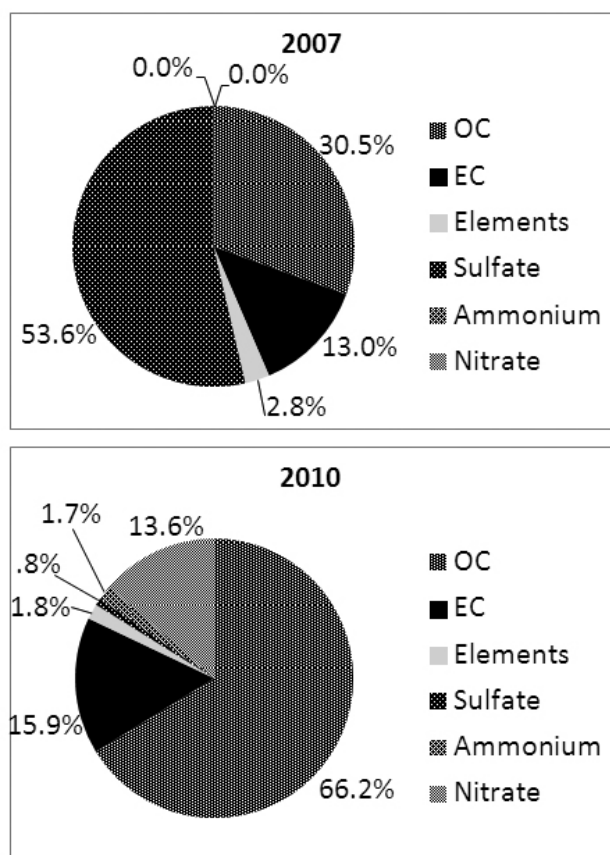


FIGURE 3. Summary of the percent composition of PM for 2010 and 2007 technology engines.

changes in the respiratory tract, but the severity of the changes remained mostly minimal and effects were observed only at the highest exposure level (Table 1).

TABLE 1. Incidence of Selected Lung Findings in Wistar Han Rats after 24 Months of Diesel Engine Exposure

| Male and Female Lung Data Combined | Control | Low | Mid | High |
|-------------------------------------|---------|------|------|-------|
| Epithelium Hyperplasia (Periacinar) | 0/20 | 0/20 | 0/20 | 20/20 |
| Interstitial Fibrosis | 0/20 | 0/20 | 0/20 | 20/20 |
| Bronchiolization | 0/20 | 0/20 | 0/20 | 2/20 |

Although a final report for the animal inhalation study has not yet been received, it is clear from the results presented and reviewed so far that 1) the great majority of health tests showed no effect of exposure; 2) several plausibly coherent responses may indicate early, exposure-related, subclinical impacts on lung inflammation, structure, and function of rats that are consistent with exposure to NO₂, an exposure which will decrease substantially with 2010-compliant engines; 3) statistically significant effects were observed primarily at

the highest exposure level (the lowest level has produced no observable effects to date); and 4) effects have not appreciably progressed from 12 to 24 or 30 months of exposure.

CONCLUSIONS

Emissions testing of 2010-compliant engines indicates that the standards are met, although some differences exist among engines from different manufacturers. Exposure of rats up to 30 months indicates that animals do not show exposure related mortality or morbidity. Preliminary results indicate some mild exposure-related changes in the lungs after 24 months of exposure that are consistent with effects seen after exposure to NO₂ alone (an exposure which, based on the Phase 2 results of 2010 engines, is expected to decrease substantially in all new engines going forward). These effects were seen only at the highest concentration of diesel exhaust (at 4.2 ppm NO₂). Results of the full assessment of potential tumor formation at 30 months will be included in the final report which is expected at HEI in November 2013. All this work has been conducted with input from the ACES stakeholders.

REFERENCES

- U.S. Environmental Protection Agency. 2002. Health Assessment Document for Diesel Engine Exhaust. EPA/600/8-90/057F. U.S. Environmental Protection Agency, National Center for Environmental Assessment, Office of Research Development, Washington D.C.

FY 2013 PUBLICATIONS/PRESENTATIONS

- Platform presentations at the DEER meeting, Dearborn, MI in October 2012:
 - "Advanced Collaborative Emissions Study (ACES)" (Tennant)
 - "ACES: Evaluation of Tissue Response to Inhaled 2007-Compliant Diesel Exhaust" (Shaikh)
- Platform presentation at the CRC Mobile Source Air Toxics Workshop in Sacramento CA, February 2013: "ACES Phase 2: Study Update" (Tim French, Truck and Engine Manufacturers Association)
- Platform and poster presentations at the Society of Toxicology annual meeting in San Antonio, TX, March 2013:
 - "IARC assessment of diesel and gasoline exhaust: overview of toxicologic evidence" (McDonald – plenary)
 - "Biomarker-based evaluation of diesel exhaust emissions from 2007-compliant engines in rats and mice exposed for defined time periods" (Hallberg – poster)

4. Platform presentation at the Diesel, Transportation, Occupational Exposures, and Health meeting in New York City, NY, April 2013: “A global perspective on improving diesel technology and fuel” (Greenbaum)
 5. Platform presentation at the CRC Real World Emissions Workshop in San Diego, CA, April 2013: “Phase 2 of the Advanced Collaborative Emissions Study (ACES): Highlights of Project Finding” (Khalek)
 6. Platform and poster presentations at the HEI Annual Conference in San Francisco, CA, April 2013:
 - a. “Results from ACES Phase 2: Emissions Characterization of 2010-Compliant Engines” (Khalek – plenary)
 - b. “Results from ACES Phase 3B: Health Effects of Chronic Exposure to Emissions from a 2007-Compliant Engine in Rats” (McDonald – plenary)
 - c. “ACES: Micronucleated Reticulocytes As an Indicator of Genotoxicity Following Exposure to Diesel Exhaust” (Bemis – poster)
 - d. “ACES: Effects of Chronic Diesel Engine Emissions on Systemic Inflammation in Rats” (Conklin – poster)
 - e. “ACES: Genotoxicity of Diesel Exhaust from 2007-Compliant Diesel Engines: A Continuation of the Study” (Hallberg – poster)
 - f. “ACES Phase 3: 52- and 104-Week Results from Rats Exposed to 2007-Compliant Diesel Emissions” (McDonald – poster)
 - g. “ACES: Update on Phase 2 of the Advanced Collaborative Emissions Study” (Tennant – poster)
7. Platform presentation at the DOE Vehicle Technologies Program Annual Merit Review in Arlington, VA, May 2013: “Advanced Collaborative Emissions Study (ACES)” (Greenbaum)
 8. Platform presentation at the Emissions 2013 Conference and Exposition in Ypsilanti MI, June, 2013: “Characterization and Health-Effects Testing of Emissions from Modern Diesel Engines” (Shaikh)

IV. HIGH EFFICIENCY ENGINE TECHNOLOGIES

IV.1 Technology and System Level Demonstration of Highly Efficient and Clean, Diesel Powered Class 8 Trucks

David Koeberlein

Cummins Inc.

PO Box 3005

Columbus, IN 47201-3005

DOE Technology Development Manager:
Roland Gravel

NETL Project Manager: Ralph Nine

Overall Objectives

Objective 1:

- Engine system demonstration of 50% or greater brake thermal efficiency in a test cell at an operating condition indicative of a vehicle traveling on a level road at 65 mph.

Objective 2:

- a Tractor-trailer vehicle demonstration of 50% or greater freight efficiency improvement (freight-ton-miles per gallon) over a defined drive cycle utilizing the engine developed in Objective 1.
- b Tractor-trailer vehicle demonstration of 68% or greater freight efficiency improvement (freight-ton-miles per gallon) over a defined 24-hour duty cycle (above drive cycle + extended idle) representative of real world, line haul applications.

Objective 3:

- Technology scoping and demonstration of a 55% brake thermal efficiency engine system. Engine tests, component technologies, and model/analysis will be developed to a sufficient level to validate 55% brake thermal efficiency.

Fiscal Year (FY) 2013 Objectives

- Complete an emission certifiable calibration of the demonstrated 50% thermal efficient engine system.
- Complete testing of the 50% freight efficiency drive cycle demonstration vehicle on a drive cycle.
- Complete the build of a 68% freight efficiency demonstration vehicle for 24-hour cycle testing.
- Complete analysis and targeted testing for a 55% thermal efficient engine system.
- Complete waste heat recovery (WHR) vehicle cooling system development tests.

FY 2013 Accomplishments

- Demonstrated in a test cell a 51% thermal efficient engine system; this system included both exhaust and coolant/lube WHR systems contributing in a parallel fashion.
- Demonstrated the SuperTruck Demo 1 vehicle with 61% freight efficiency, on a Texas highway drive cycle route.
- Completed initial development testing of the higher cylinder pressure capability, low pump parasitic engine.
- Completed design and build of the demonstrator #2 vehicle.
- Completed advanced truck model aerodynamic aid design analysis, and updated initial hardware fabrication updated on the demonstrator #2 vehicle.
- Completed initial combustion analysis with corresponding targeted testing of envisioned 55% thermal efficiency technologies and also compiled to integrated brake efficiency impacts.
- Completed vehicle tests and developmental efficiency testing of the advanced heavy-duty transmission.
- Completed a single vehicle hotel load test of the solid oxide fuel cell (SOFC) auxiliary power unit (APU) on the demonstrator #1 vehicle with comparison to baseline vehicle idling.

Future Directions

- Complete the build of the 68% 24-hour freight efficiency demonstration vehicle.
- Complete the 68% freight efficiency vehicle demonstration testing.
- Analysis and targeted testing of technologies for achievement of a 55% thermal efficient engine.



INTRODUCTION

Cummins Inc. is engaged in developing and demonstrating advanced diesel engine technologies to significantly improve engine thermal efficiency while meeting Environmental Protection Agency 2010 emission

regulations. Peterbilt Motors is engaged in the design and manufacturing of heavy-duty Class 8 trucks.

Together, Cummins and Peterbilt provide a comprehensive approach to achievement of a 68% or greater increase in vehicle freight efficiency over a 24-hour operating cycle. The integrated vehicle demonstration includes a highly efficient and clean diesel engine with 50% or greater brake thermal efficiency including advanced WHR, aerodynamic Peterbilt tractor-trailer combination, reduced rolling resistance tire technology, advanced transmission, and a lithium ion battery APU for idle management. In order to maximize fuel efficiency, each aspect associated with the energy consumption of a Class 8 tractor/trailer vehicle will be addressed through the development and integration of advanced technologies.

In addition, Cummins will scope and demonstrate evolutionary and innovative technologies for a 55% brake thermal efficiency engine system.

APPROACH

Cummins and Peterbilt's approach to project objectives emphasizes an analysis-led design process in nearly all aspects of the research. Emphasis is placed on modeling and simulation results to lead to attractive feasible solutions. Vehicle simulation modeling is used to evaluate freight efficiency improvement technologies. Technologies are evaluated individually along with combination effects resulting in our path to target measure of project status and for setting project direction.

Data, experience, and information gained throughout the research exercise will be applied wherever possible to the final commercial products. We continue to follow this cost-effective, analysis-led approach both in research agreements with the Department of Energy as well as in its commercial product development. We believe this common approach to research effectively shares risks and results.

RESULTS

Demonstrated an engine thermal efficiency of 51% in the test cell, using a combined exhaust and coolant WHR system. These results, on a Cummins 15-liter ISX engine were in combination with a diesel particulate filter/selective catalytic reduction aftertreatment system, that showed 2010 oxides of nitrogen emission regulation compliant results of 0.08 g/hp-hr on a supplemental engine test modal roll-up. Further engine friction reduction from 2012 was evident on this engine/WHR demonstration with motoring results of 30% reduced friction compared to a current production ISX15 engine. The engine exhibited an improvement in gross indicated

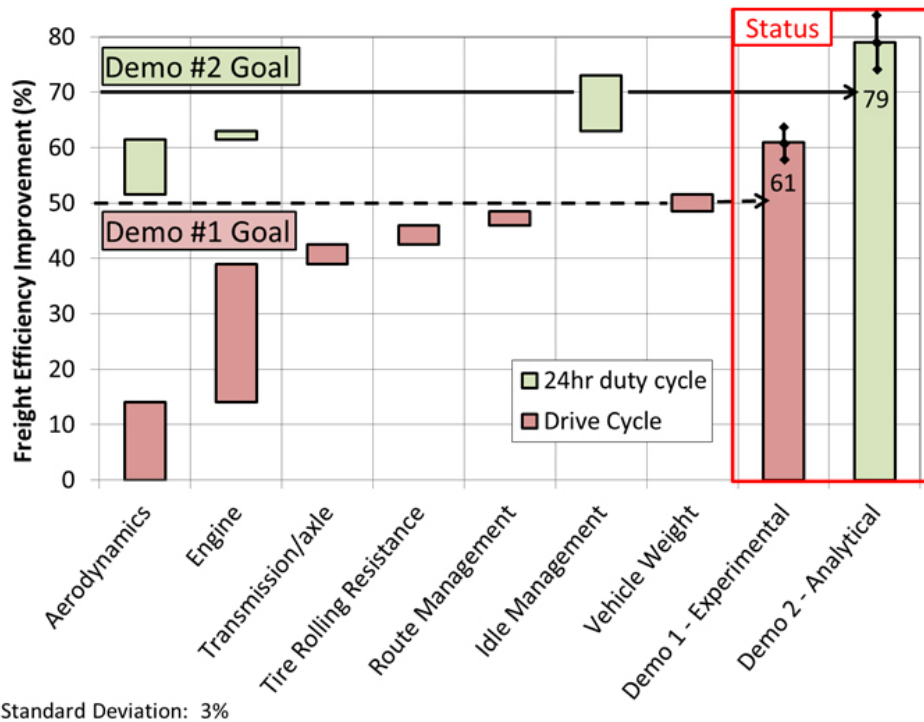
efficiency compared to the baseline engine, and a modest improvement in open-cycle efficiency. The exhaust loop of the WHR system contributed 2.8% while the coolant and lube circuit added another 0.8% to the 51% achievement. The engine-only gross indicated efficiency increased to 51.6%; approximately a 1.1% increase from result in 2012. This completed Objective 1.

The Demo 1 SuperTruck (see Figure 1), a Peterbilt Model 587 built in 2012 with advanced engine and vehicle technologies, showed freight efficiency improvements of 61% over the baseline 2009 Model 386 with a standard trailer. The Demo 1 vehicle proved lighter by approximately 1,400 pounds, despite the added weight of the engine oxides of nitrogen aftertreatment, WHR and aerodynamic aid systems. The Demo 1 vehicle achieved a 54% increase in fuel economy, averaging 9.9 mpg during testing last fall on U.S. Route 287 between Fort Worth and Vernon, Texas. The testing was conducted over 11 runs meeting SAE International test standards along a 312-mile route. The tractor-trailer had a combined gross weight of 65,000 lbs. This completed Objective 2a.

Multiple WHR-equipped vehicles are operating in test conditions. The vehicles have each completed cooling tests in a Modine climactic tunnel to understand WHR system performance on-vehicle in varying ambient and various applied heat loads. The cooling module design for the second demonstration vehicle was modified to balance coolant loop differential pressure, charge air cooler differential pressure and overall air side system restriction. The radiator was changed to a single crossflow design. The charge air cooler height was increased one tube row and the internal tube fin revised for lower restriction. External air side fin density changes were made to both radiator and charge air cooler. These fin density changes lowered the cooling module air flow. Results of these changes were a net positive. They sought to balanced engine efficiency with WHR system efficiency, where the changes to engine-side restriction showed fuel consumption improvements of 0.8%, whereas the reduction of WHR condenser performance due to reduced air flow was estimated at 0.2%.



FIGURE 1. SuperTruck Demo 1 Vehicle

**FIGURE 2.** Freight Efficiency Roadmap Targets

Following the Demo 1 drive cycle evaluations, the fuel cell APU unit was re-installed for a trial 24-hour cycle test. A hotel load was applied with a programmable load bank on both an idling baseline vehicle and the SOFC-equipped Demo 1. The hotel load profile was developed from measured accessory loads and vetted with USXpress fleet operations. The SOFC design requirements sought to minimize thermal cycle, such that warm-up, idle while driving, and shutdown fuel usage needed to be included in the overall APU operational fuel consumption. Combining the Demo 1 drive cycle results, baseline truck idling engine fueling, as well as, SOFC hotel load fuel consumption results, the estimated Demo 1 24-hour freight efficiency would increase to 64%.

The build of the integrated Demo 2, a Peterbilt Model 579 truck has been substantially completed. Testing of this truck is planned to start in the fourth quarter of 2013. This truck improves upon the Demo 1 vehicle with a higher efficiency WHR-equipped engine, improved tractor and trailer aerodynamics, an adjusted transmission shift calibration for targeted gearing combinations and a lithium-ion APU battery system. The battery APU was engineered into the truck after a Delphi decision to not pursue SOFC transportation market introduction. The electrical system and power distribution system were revised to accommodate the battery APU. The base truck was built with a combination of production assembly line and laboratory upgrade, and then re-insertion to the production assembly

line to complete its build. The truck was delivered to Cummins, in Columbus, IN for calibration and development of engine, WHR, and route management systems. In mid-July, Demo 2 returned to Denton for up fit of the truck and trailer aero package, tires, and wheels and along with additions for fuel economy test equipment.

The advanced transmission was initially built in November 2011 and since then has undergone numerous development tests. In the fourth quarter of 2012, the transmission was developed to a suitable reliability state that enabled planning for a Demo 1 transmission update. The transmission had been subjected to shift tests, full-load dyno, lube and cooling tests, shift calibration and software development and installed in a mule truck completing mileage accumulation tests. The transmission was re-installed into Demo 1, and completed drive cycle testing along with customer drive evaluations. USXpress drivers completed a 930-mile run from Irving, TX to Laredo, TX, with positive driver comments on the gear shift performance of the transmission.

Vehicle powertrain system analysis is a tool to evaluate freight efficiency improvements. The path to the target roadmap study involved an analysis of various powertrain component changes, including both hardware and control algorithms, with their resulting freight efficiency impacts. Figure 2 shows the original path to target roadmap for both the drive cycle 50% improvement

and 68% improvement on the 24-hour cycle. The chart also documents the Demo 1 experimental results of 61% on the Objective 1 drive cycle and the expected status of 79% on the 24-hour cycle test with a battery APU. We have determined uncertainty in these values of +/- 5%.

CONCLUSIONS

The SuperTruck Engine and Vehicle System Level Demonstration of Highly Efficient and Clean, Diesel Powered Class 8 Truck project has successfully completed the third year of the four-year project. The following conclusions have come from the third year:

- Demonstrated a 51% thermal efficiency engine system with combined exhaust and coolant WHR system.
- The Demo 1 truck achieved 61% freight efficiency improvement and 54% fuel economy increase on the Texas drive route.
- A Demo 2 vehicle has been built and is undergoing planned engineering updates and is scheduled for 2013 fourth quarter drive cycle and hotel load testing.
- WHR functioned well on the Demo 1 vehicle. The cooling module of Demo 2 was revised to enable higher engine efficiency, despite a modest WHR performance degradation.
- Vehicle powertrain system analysis shows the path to achievement of project freight efficiency goals.

FY 2013 PUBLICATIONS/PRESENTATIONS

Journal Paper Submissions

1. Lyle Kocher*, Mark Magee, Dan Van Alstine, Gregory M. Shaver, A Nonlinear Model-Based Controller for Premixed Charge Compression Ignition Combustion Timing in Diesel Engines, to appear at the American Control Conference, 2013.
2. Carrie M. Hall*, Dan Van Alstine, and Gregory M. Shaver, Flatness-Based Control of Mode Transitions between Conventional and Premixed Charge Compression Ignition on a Modern Diesel Engine with Variable Valve Actuation, to appear at the 2013 Dynamics Systems and Control Conference, 2-2013.

Public Presentations

1. Greg Shaver, *Automotive Research at Purdue*, Purdue, VIT (Vellore India), January 20th, 2013.
2. Greg Shaver, *Model-Based Engine Algorithm Development for Control and Virtual Sensing*, Michigan Tech University, April 4th, 2013.

3. Greg Shaver, *Poster: Model-Based Engine Algorithm Development for Control and Virtual Sensing*, NAE Symposium, April 26th, 2013.
4. Greg Shaver, *Model-Based Engine Algorithm Development for Control and Virtual Sensing*, Purdue, University of Wisconsin Engine Research Center Symposium, June 5th, 2013.
5. Bill Partridge, *Diagnostics Development & Applications for Enabling Advanced Efficiency Automotive Systems*, International Society of Automation (ISA) Oak Ridge Section, January Meeting, Knoxville, Tennessee, January 22, 2013.
6. Bill Partridge, *Advanced Diagnostics for Automotive Catalysts, Exhaust Gas Recirculation & Oil Dilution*, Department of Mechanical Engineering, Czech Technical University; Prague, Czech Republic, February 25, 2013.
7. Bill Partridge, *Advanced Diagnostics for Automotive Catalysts, Exhaust Gas Recirculation & Oil Dilution*, Monolith Research Group, Department of Chemical Engineering, Institute of Chemical Technology, Prague; Prague, Czech Republic, February 27, 2013.
8. Bill Partridge, *Cummins/ORNL FEERC Combustion CRADA: Characterization & Reduction of Combustion Variations*, 2013 DOE Vehicle Technologies Program Annual Merit Review, Arlington, Virginia, May 16, 2013.
9. Bill Partridge, *Advanced Diagnostics for Automotive Catalysts, Exhaust Gas Recirculation & Oil Dilution*, ORNL, Korea Institute of Industrial Technology (KITECH), Automotive Components Center, Honam Technology Application Division (Dr. Inchul Choi, Senior Researcher, hosting), Gwangju (aka Kwangju), Korea, August 28, 2013.
10. Bill Partridge, *Diagnostic Developments & Applications for Enabling Advanced-Efficiency Automotive Systems*, Knoxville-Oak Ridge Chapter of the American Institute of Chemical Engineers (AIChE), Knoxville, Tennessee, October 10, 2013.
11. David Koeberlein, *Cummins SuperTruck Program - Technology and System Level Demonstration of Highly Efficient and Clean, Diesel Powered Class 8 Trucks*, Cummins, 2013 DOE Vehicle Technologies Program Annual Merit Review, Arlington, Virginia, May 16, 2013.
12. Ken Damon, *DoE SuperTruck Program - Technology and System Level Demonstration of Highly Efficient and Clean, Diesel Powered Class 8 Trucks*, 2013 DOE Vehicle Technologies Program Annual Merit Review, Arlington, Virginia, May 16, 2013.
13. Bill Partridge, *Cummins/ORNL FEERC Combustion CRADA: Characterization & Reduction of Combustion Variations*, 2013 DOE Vehicle Technologies Program Annual Merit Review, Arlington, Virginia, May 16, 2013.
14. Ken Damon, *Peterbilt SuperTruck Update*, Denton Energy Summit hosted by 26th District of Texas Congressman Dr. Michael C. Burgess, Denton, Texas, July 2013.
15. Ken Damon, *Challenges of Demonstrating High Fuel Economy in Heavy Duty Trucks*, Arlington Technology Association, University of Texas/Arlington, Aug 2013.

SPECIAL RECOGNITIONS & AWARDS/ PATENTS ISSUED

1. 2013 Ralph Teeter Educational Award
2. Best paper in Journal of Automobile Engineering for 2012

IV.2 SuperTruck – Improving Transportation Efficiency through Integrated Vehicle, Engine, and Powertrain Research; Fiscal Year 2013 Engine Activities

Kevin Sisken

Detroit Diesel Corporation
HPC A-08
13400 Outer Drive West
Detroit, MI 48239-4001

DOE Technology Development Manager:
Roland Gravel

NETL Project Manager: Carl Maronde

Overall Objectives

- Demonstration of a 50% total increase in vehicle freight efficiency measured in ton-miles per gallon, with at least 20% improvement through the development of a heavy-duty diesel engine.
- Development of a heavy-duty diesel engine capable of achieving 50% brake thermal efficiency on a dynamometer under a load representative of a level road at 65 mph.
- Identify key pathways through modeling and analysis to achieving 55% brake thermal efficiency on a heavy-duty diesel engine.

Fiscal Year (FY) 2013 Objectives

- Utilizing the results of the comprehensive analytical effort performed in 2011 and the component level development and testing performed in 2012; the 2013 objective was to experimentally demonstrate an engine reaching the project goal of 50% engine brake thermal efficiency.
- Another objective in 2013 was to demonstrate the waste heat recovery system on a prototype vehicle. This was done in preparation for the 2014 requirement of building and testing a vehicle capable of demonstrating the SuperTruck goal of a 50% increase in freight efficiency.

FY 2013 Accomplishments

- Demonstrated 50.0% engine brake thermal efficiency in the laboratory on the SuperTruck demonstration engine, meeting the 2013 project targets.

- Development has continued on the core engine (meaning without waste heat recovery), with the best results to date being an engine brake thermal efficiency of 47.7%.
- The waste heat recovery system design was completed, hardware and control systems developed, and extensive testing was done in FY 2013. Testing to date has demonstrated an improvement in engine brake thermal efficiency of 2.3% via recovered exhaust and exhaust gas recirculation (EGR) energy, bringing the total engine brake thermal efficiency up to 50.0% (47.7% engine + 2.3% waste heat recovery).
- Analysis of the pathway to 55% engine brake thermal efficiency has been initiated and this effort continues.

Future Directions

- While the 50% brake thermal efficiency project goal has been achieved, there are a couple more refinements still to be tested, and this will be done to further increase engine brake thermal efficiency.
- Refinement of various engine systems will continue in 2014, to help refine their operating characteristics in support of vehicle testing.
- The analysis of the pathway to achieving 55% engine brake thermal efficiency will continue, including some testing of a few components needed to make this objective possible.
- Build and test the final engine system in the SuperTruck vehicle to demonstrate the improvements in the vehicle as part of the 50% vehicle freight efficiency improvement.



INTRODUCTION

SuperTruck is a five-year research and development project with a focus on improving diesel engine and vehicle efficiencies. The objective is to develop and demonstrate a Class-8, long-haul tractor-trailer that achieves a 50% vehicle freight efficiency improvement (measured in ton-miles per gallon) over a best-in-class 2009 baseline vehicle. The engine shall contribute 20% of the 50% improvement, specifically targeting a brake

thermal efficiency of 50%, as tested on a dynamometer under conditions representative of the SuperTruck vehicle at 65 mph. In FY 2013, the engine specific goal of 50% brake thermal efficiency was achieved in dynamometer testing, and much of the focus now turns to running this high efficiency engine in the SuperTruck vehicle.

APPROACH

The approach used in FY 2013 primarily centered on engine testing of the systems required to achieve high engine thermal efficiency. Specific engine systems being refined and tested for high engine efficiency include the combustion system, air system, fuel system, engine controls, engine parasitics, aftertreatment, and waste heat recovery. In addition, the engine was significantly downsized from the baseline engine in order to improve the engine's efficiency at conditions representative of road-load operation.

RESULTS

To date, the SuperTruck project is on track to reach the 50% freight efficiency target, helped by the fact that the engine has achieved the targeted 50% brake thermal efficiency. The building blocks to reaching this milestone are shown graphically in Figure 1. The current technical package, which enables the high brake thermal efficiency at cruise RPM, includes the following elements:

- Engine downsizing
- Higher engine-out oxides of nitrogen (NO_x) compared to baseline
- Higher engine compression ratio
- Higher peak cylinder pressures
- New piston bowl with re-matched injector
- Re-matched turbocharger
- Low viscosity oil
- Aftertreatment with high efficiency and lower pressure drop
- Variable speed coolant pump

In previous years, many of these building blocks were evaluated analytically and individually in engine testing, and in this past year, all of these items have been brought together to improve the efficiency of this demonstration engine.

Research is being conducted in the area of parasitics reduction at the Sloan Automotive Laboratory of the Massachusetts Institute of Technology as part of the SuperTruck sub-contract. One of the sub-goals of this effort on parasitic reduction is fuel economy improvement of Class-8 truck engines through

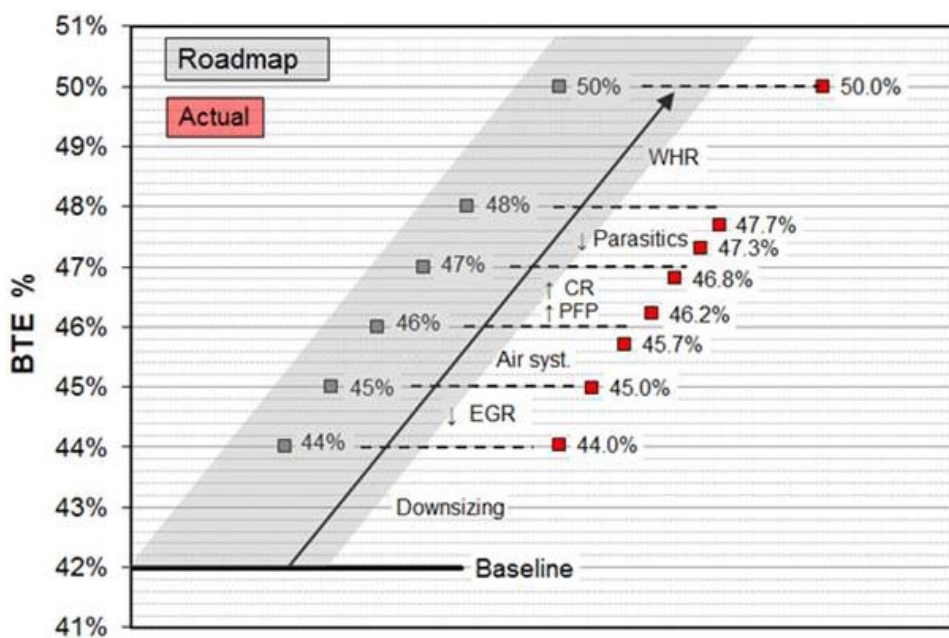
lubrication system improvements. Reduction of in-cylinder friction losses, which amount to 40-50% of the total engine mechanical losses, is an area of primary focus. Technologies related to piston kit friction reduction, oil circuit and flow optimization, and low viscosity oil are being explored, with testing taking place on the most promising of these ideas.

A novel method of engine controller is being utilized in this project, and these controls have been optimized for engine fuel efficiency improvement measures via dynamometer test cycles representative of over-the-road SuperTruck operation. The SuperTruck engine control logic is based on extensive mapping of engine operation, followed by training of neural network engine performance models. The resulting logic enables the control of engine actuators based on engine-out NO_x set-points adapted to the driving conditions. The controls have been calibrated for the high-efficiency engine and much of the work is now focused on preparing this system for testing and evaluation on the demonstration vehicle.

Progress has been made in the development of a high-efficiency, low back pressure aftertreatment system for the SuperTruck engine. One of the engine strategies is higher engine-out NO_x for increased engine efficiency matched to a high-efficiency aftertreatment system. A number of aftertreatment designs were procured and tested, and the final system was selected in previous year. Most recently, the selected aftertreatment system was tested to evaluate what the NO_x limits would be across various test cycles, to fully understand the benefits and tradeoffs with this aftertreatment hardware.

The SuperTruck waste heat recovery system will employ a Rankine cycle to harness the heat energy in the engine's exhaust and EGR cooler. Currently, the Rankine heat engine is set up to generate high pressure ethanol vapor utilizing both exhaust and EGR heat, that then energizes an expansion machine to turn a generator to produce electrical power. Significant testing and refinements of both the hardware and control system were undertaken in the last year, and a brake thermal efficiency improvement of 2.3% was realized. The Rankine system was also installed on a test vehicle in the last year, allowing for evaluation of its general performance as well as interaction with the vehicle and cooling system.

Oak Ridge National Laboratory is a partner in the SuperTruck waste heat recovery system development, and their efforts are focused on design and development of an efficient generator prototype for use with the waste heat recovery system. The expander driven generator converts mechanical input energy to electrical energy and returns this recuperated energy back to the vehicle's high voltage battery and/or hybrid drive components. The



WHR – waste heat recovery; CR – compression ratio; PFP – peak firing pressure; BTE - brake thermal efficiency

FIGURE 1. Engine Brake Thermal Efficiency Improvements

system has been designed, built, and extensively tested over the last year, including the development and testing of a second generation to further improve and refine on the first generation set of hardware. Based on this testing, development and construction of a third generation system is nearly complete and will be tested in the next fiscal year.

CONCLUSIONS

The engine project goal of demonstrating 50% brake thermal efficiency has been achieved and work continues to implement this high efficiency engine and subsystems into a vehicle. In addition, analysis and testing continues on the roadmap to a 55% brake thermal efficient engine.

FY 2013 PUBLICATIONS/PRESENTATIONS

1. Sisken, Kevin: "SuperTruck Program: Engine Project Review; Recovery Act –Class 8 Truck Freight Efficiency Improvement Project", Project ID: ACE058, DoE Annual Merit Review, May 16, 2013.

IV.3 SuperTruck Initiative for Maximum Utilized Loading in the United States

Pascal Amar (Primary Contact),
Samuel McLaughlin, Arne Andersson,
John Gibble
Volvo
13302 Pennsylvania Avenue
Hagerstown, MD 21742

DOE Technology Development Manager:
Roland Gravel

NETL Project Manager: Ralph Nine

Subcontractor:
Pennsylvania State University, State College, PA

- Optical access demonstrated on the ignition test apparatus to be used for computational fluid dynamics (CFD) validation.
- Surrogate fuel tested in 1-cylinder engine for CFD validation.
- Verified assumptions behind GT-POWER models for 55% BTE.
- Evaluated a concept capable of 55% BTE.
- Testing of combustion improvements, engine friction, pumping loss technologies and waste heat recovery (WHR) system in a complete powertrain system demonstrated 48% BTE on a dynamometer.

Overall Objectives

- Identify concepts and technologies that have potential to achieve 55% brake thermal efficiency (BTE) on a heavy-duty diesel engine. A thorough analysis of the limiting factors and potential areas for improving the engine's efficiency using analytical simulations will be performed including research into alternative thermodynamic cycles, advanced component design, fuel formulation and new engine designs, as well as development of more advanced combustion modeling tools.
- Demonstrate a heavy-duty diesel engine capable of achieving 50% BTE at the end of the SuperTruck project.

Fiscal Year (FY) 2013 Objectives

- Develop and use simulation tools and models for partially premixed combustion (PPC) and other new concepts.
- Evaluate a concept capable of 55% BTE.
- Demonstrate 47% BTE on engine dynamometer.

FY 2013 Accomplishments

- Demonstrated ability to predict rate of heat release (RoHR) and emissions within 5%.
- Demonstrated that with the transported probability density function (PDF) in place, a simple 2-equation soot model (Lindstedt et al.) is sufficient to predict soot well.

Future Directions

- The transported PDF combustion CFD tool is ready to be used for the 55% BTE concept engine work where we enter new regimes and explore advanced injection strategies.
- Continue development of the combustion CFD tool to be able to simulate PPC, with focus on kinetic mechanisms and testing of model fuels.
- Validate on-road fuel savings of the 48% BTE powertrain system and refine design requirements for next generation WHR system.



INTRODUCTION

New combustion concepts like PPC and Reactivity Controlled Compression Ignition (RCCI) have demonstrated very high indicated efficiencies together with a potential for low engine-out emissions, however the combustion is significantly more difficult to simulate than normal diesel diffusion combustion. The transported PDF combustion model has been developed to address this challenge and supports the 55% BTE concept engine work where we enter new regimes and explore advanced injection strategies.

The simulation tool development is backed up by extensive testing. A cetane ignition device equipped with optical access is used for testing of fuels and validation of spray and chemical kinetics sub-models.

The concept simulation work targeting 55% BTE has been successful. The model in GT-POWER reaches the target, but the 55% BTE concept pushes the rather

simple GT-POWER sub-models into extrapolation. We are validating the sub-models for the new regimes, one by one. So far the extrapolations have proved to be reasonably correct.

APPROACH

The Penn State effort includes CFD modeling and laboratory experiments aimed at meeting the 55% BTE target. Two simulation efforts are proceeding in parallel. One set of simulation targets high-pressure, constant-volume turbulent spray combustion in two configurations: a set of experiments available through the Engine Combustion Network and a set of experiments that is being performed at Penn State using a Cetane ID 510 device. The constant-volume simulations are focused on model development and validation for different fuels. The second set of simulations targets a Volvo heavy-duty diesel engine. The engine simulations are focused on exploring advanced high-efficiency combustion strategies, including PPC and RCCI. The modeling framework is a PDF method, with skeletal-sized chemical mechanisms (up to ~100 species) and soot models. The models are being implemented via user coding in a commercial CFD code (STAR-CD). It is anticipated that this modeling approach will be able to capture the multiple regimes of compression-ignition combustion that are of interest for this project, including conventional diesel combustion, low-temperature combustion, partially premixed combustion, and dual-fuel combustion (Figure 1).

The ignition test apparatus has been modified to introduce optical probes into the combustion chamber for high-speed fuel-spray imaging and chemiluminescence detection.

Our search for improved concepts started with an analysis of where the losses in presently used cycles occur. We identified improvement potential in a number of areas. The areas that are addressed are illustrated in Figure 2.

RESULTS

Combustion CFD

Examples of comparisons of RoHR, flame structure and soot emissions obtained with the PDF model compared to a model that neglects the influence of turbulent fluctuations on the mean chemical reaction rates (a well-stirred reactor—WSR) are shown in Figures 3-5. In general, the PDF model gives a more diffuse mean flame zone with lower peak temperatures compared to the WSR model. The RoHR is lower with consideration of turbulent fluctuations, and the results

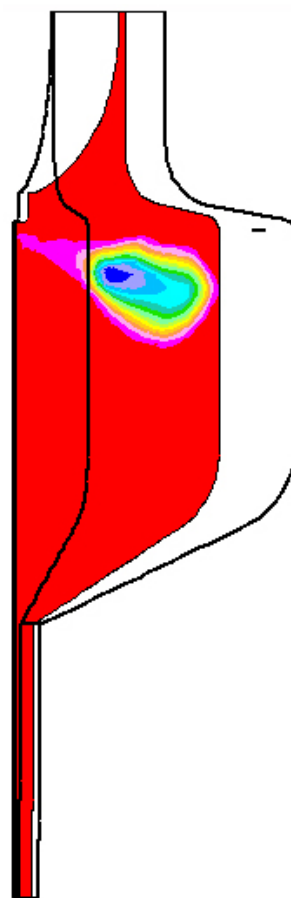


FIGURE 1. Temperature contour from transported PDF simulation of the ignition test in the Cetane ID 510. This is part of the model validation work. We perform high-speed optical imaging in the same apparatus.

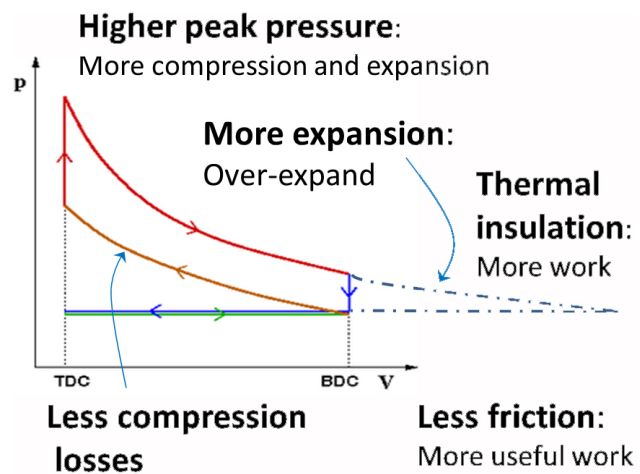


FIGURE 2. Opportunities for Higher Efficiency Cycles

with the PDF model are closer to experiment. The simple 2-equation soot model (Lindstedt et al.) is sufficient to predict soot well thanks to the PDF model. The PDF

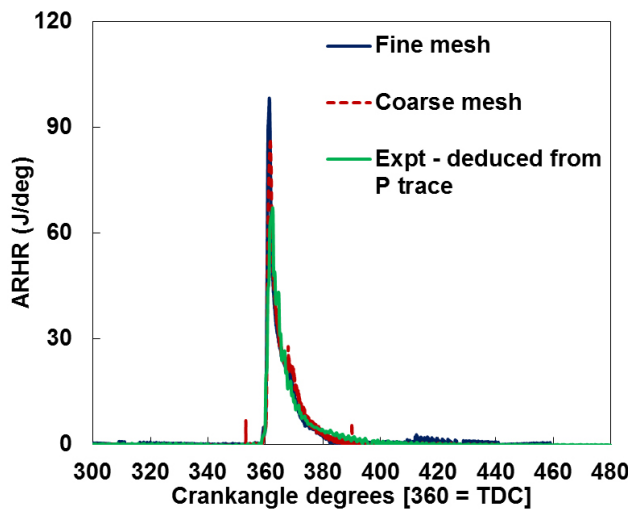


FIGURE 3. Heat-release profiles for a baseline diesel case at part load. Mesh sensitivity of the CFD heat-release prediction is also shown in the heat-release profiles.

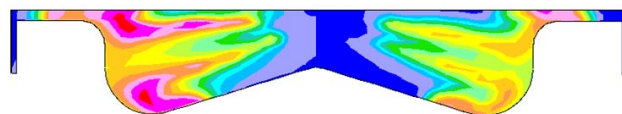


FIGURE 4. Computed mean temperature profiles @ 5° after top-dead center from a WSR model (left) and from a PDF model (right). Note the significantly lower maximum temperature with the PDF model.

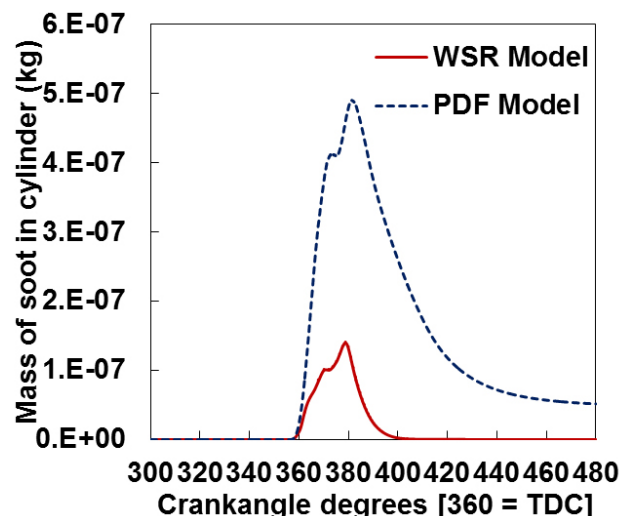


FIGURE 5. Computed (WSR versus PDF models) in-cylinder soot mass as a function of crank angle for a full-load, high exhaust gas recirculation operating condition.

model is computationally intensive, and efforts are ongoing to improve parallelization and to implement other strategies to reduce the simulation time.

Combustion CFD Validation

Regarding the constant volume combustion chamber experiments, an ignition quality test apparatus (PAC LLC, “Cetane ID 510” derived cetane number analyzer) was setup. Fuel characteristic tests were carried out for PRF fuels and high derived cetane number/low aromatics fuels.

Optical instrumentation was added to the instrumentation for visualization of spray (digital photography using a borescope, see Figure 6) and detection of the onset of chemiluminescence in the chamber (photomultiplier tube with supporting optics).

New Engine Concepts

The investigation of new engine concepts have resulted in GT-POWER models delivering 55% BTE, however the GT-POWER sub-models are not validated for the regimes simulated. Validation of sub-models by using dedicated advanced tools is on-going. So far we have not encountered any major errors in the sub-models for the investigated regimes.

WHR System

The in-house engine dynamometer testing with the Rankine WHR system was completed. The system was able to meet or exceed previous improvements in steady-state optimization despite the addition of a more efficient combustion chamber and turbocompounding, which both reduced the heat available to the system. The system was able to harvest energy in a wide range of simulated customer duty cycles, exceeding expectations related to controllability.

The WHR system was installed in a chassis for evaluation and successfully navigated multiple on-road tests with varying route profiles and vehicle loads. The vehicle performed as expected, and the WHR system generated power during normal operation.

CONCLUSIONS

PPC combustion is very demanding on simulation tools. A practical PPC engine involves combustion modes from Premixed Charge Compression Ignition to diffusion combustion. The advanced transported PDF model will be a valuable tool for combustion simulations of new regimes and advanced combustion strategies for the 55% BTE concepts.

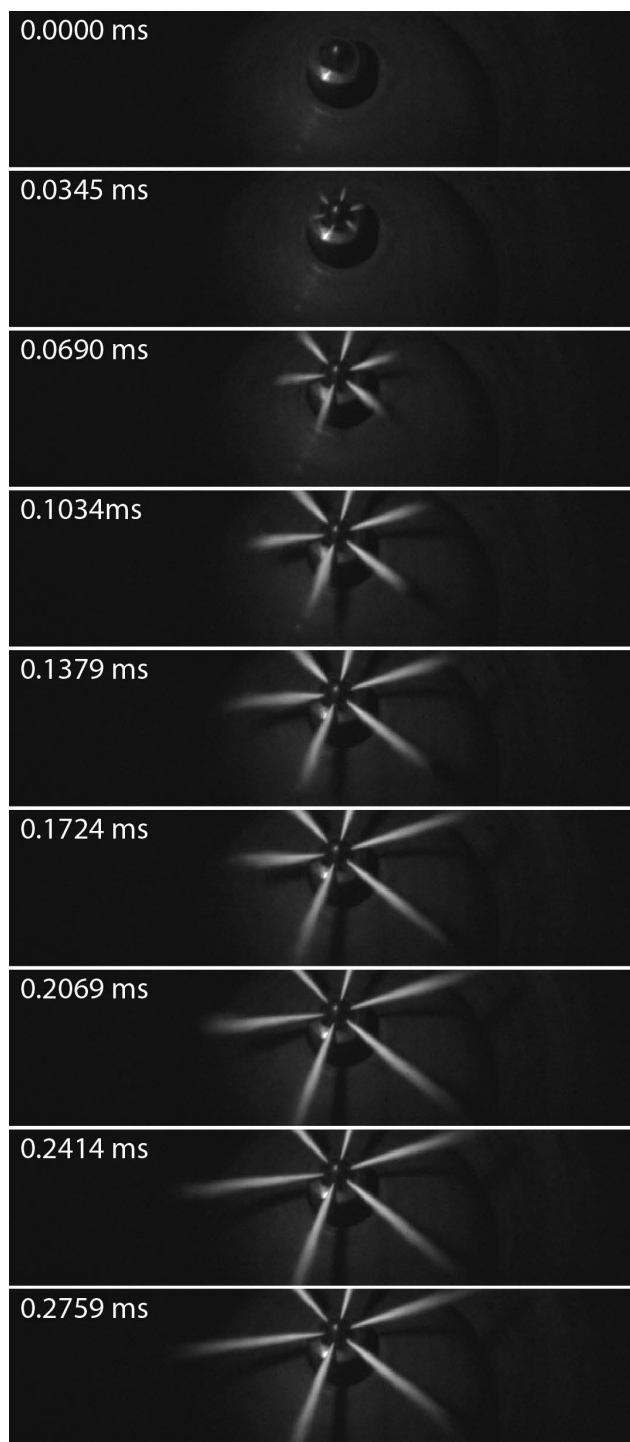


FIGURE 6. Spray injection of n-heptane in the combustion chamber of a PAC Cetane ID 510. Images captured at 29,000 frames per second with a Phantom v7.1 monochrome camera.

FY 2013 PUBLICATIONS/PRESENTATIONS

1. S. Bhattacharjee, D.C. Haworth, Combust. Flame (2013), Simulations of transient n-heptane and n-dodecane spray flames under engine-relevant conditions using a transported PDF method, <http://dx.doi.org/10.1016/j.combustflame.2013.05.003>.
2. V. Raj Mohan, D.C. Haworth, J. Li, PDF-based simulations of in-cylinder combustion in a compression-ignition engine, 8th U.S. National Combustion Meeting, Park City, UT (19–22 May 2013).
3. V. Raj Mohan, D.C. Haworth, J. Li, Transported PDF calculations of combustion in compression-ignition engines, International Multidimensional Engine Modeling User's Group Meeting at the SAE Congress, Detroit, MI (15 April 2013).
4. V. Raj Mohan, S. Bhattacharjee, D.C. Haworth, Transported probability density function modeling for high-efficiency compression ignition engines, 14th International Conference on Numerical Combustion, San Antonio, TX (8–10 April 2013).
5. D.C. Haworth, Modeling interactions among turbulence, gas-phase chemistry, soot and radiation in nonpremixed combustion, Chalmers University, Gothenburg, Sweden (8 May 2013).
6. M. Lundgren, 'Gasoline PPC: A parametric study of late cycle mixing conditions using a predictive two-zone SRM modeling tool', SAE Seoul 2013.
7. A. Andersson, F. Mauss et al, 'Combustion model for engine concept simulation', STAR Global Conference 2013.

IV.4 Gasoline Ultra-Efficient Vehicle with Advanced Low-Temperature Combustion

Keith Confer (Primary Contact), Harry Husted,
Mark Sellnau
Delphi
3000 University Drive
Auburn Hills, MI 48326

DOE Technology Development Manager:
Ken Howden

NETL Project Manager: Ralph Nine

Subcontractors:

- John Juriga, HATCI, Superior Township, MI
- Dr. Rolf Reitz, WERC LLC, Madison, WI
- Dr. Ming-Chia Lai, Wayne State University, Detroit, MI

- Project specific control system successfully used for: first warm start, first cold start, first controlled idle, mild tip-in/tip-out transient and closed-loop fuel control.
- GDCI multi-cylinder engine firing and test on performance dynamometer.
- Multi-cylinder development engine comparison study to single-cylinder concept engine.
- Initial engine mapping of GDCI combustion for planned regions of operation.
- Phase 2 demonstration vehicle build including; GDCI multi-cylinder engine, project specific transaxle, development controllers, full wiring harness, engine and charge air cooling systems.
- Single-cylinder engine development and refinement of injectors and GDCI combustion.
- Continued injector development using computational fluid dynamics/FIRE and spray chamber.
- Motoring friction evaluation of development engine.

Overall Objectives

- Develop, implement, and demonstrate fuel consumption reduction technologies using a new low-temperature combustion process: gasoline direct-injection compression ignition (GDCI).
- Refine and demonstrate several near-term fuel consumption reduction technologies including advanced valvetrain and parasitic loss reduction.
- Design and build engine hardware required.
- Develop engine control strategies.
- Demonstrate benefits of new hardware and refined engine operation.

Fiscal Year (FY) 2013 Objectives

- Continue GDCI simulation and single-cylinder combustion system development work.
- Map and refine GDCI operation using multi cylinder engines.
- Continue development of GDCI controls.
- Build Phase 2 development vehicle with GDCI multi-cylinder engine.

FY 2013 Accomplishments

- Firing and test of the start cart GDCI multi-cylinder engine.

Future Directions

- Fully map GDCI operation on performance dynamometers.
- Debug Phase 2 GDCI vehicle.
- Continue development of GDCI engine control systems.
- Calibrate Phase 2 GDCI vehicle.
- Test Phase 2 GDCI vehicle.
- Continue single-cylinder engine tests to refine the combustion process and component designs.



INTRODUCTION

This project will develop, implement and demonstrate fuel consumption reduction technologies that are focused on the improvement of thermal efficiency from in-cylinder combustion complemented by a reduction of friction and parasitic losses.

The investigation includes extensive simulation efforts combined with bench, engine and vehicle testing in a comprehensive four-year project conducted in two

phases. The conclusion of each phase is marked by an on-vehicle technology demonstration.

The single largest gain in fuel economy will come from development and demonstration of a breakthrough low-temperature combustion scheme called GDCI to be developed in Phase 2 of the project. Initial steady-state dynamometer testing of this new combustion scheme showed that thermal efficiencies can be greater for GDCI combustion than for diesel combustion. During the project, substantial development work will be done in the areas of combustion control, base engine design, fuel system design and valvetrain design to fully validate and reduce to practice a combustion scheme implementing GDCI in a gasoline engine which is suitable for mass production. Phase 2 development work spans the full four years of this project.

Phase 1 concentrated on nearer term technologies to reduce friction and parasitic losses. The on-vehicle implementation of these technologies was performed using a systems engineering approach to optimize the collective value of the technologies. The duration of Phase I was two years and was completed in June, 2012.

APPROACH

Phase 1 technologies were divided into two demonstration vehicles. These two vehicles were equipped with different Phase 1 technologies and hardware. Broadly, Vehicle 1 focused on technologies to reduce engine friction and accessory loads. Vehicle 2 focused on pumping losses and engine idling reduction. Both demonstration vehicles met the same tailpipe emissions standards as the original production vehicle from which they were derived.

For Phase 2, a wide range of analytical and experimental tools were assembled and used by small expert teams. Detailed FIRE and KIVA simulations were used in combination with spray chamber tests of physical injectors. Single-cylinder engine tests using the Design of Experiments method were combined with response surface modeling and custom combustion analysis macros to quickly process large amounts of test data. GT-POWER was used to evaluate and develop an efficient boosting system via simulation. While the multi-cylinder engine design work addressed all aspects of the engine, extra design effort was placed on valvetrain, fuel injection, thermal management and boost systems as they are key enablers for the new combustion process. Multi-cylinder GDCI engines were built for the performance dynamometer, engine start-cart, and development vehicle.

RESULTS

Phase 1

Phase 1 of this project was successfully completed in FY 2012. Two demonstration vehicles were constructed, refined and tested during that phase. One vehicle realized a combined unadjusted fuel economy improvement of 13.1% compared to the port fuel-injected (PFI) baseline vehicle. The second vehicle achieved a combined unadjusted fuel economy improvement of 13.4% compared to the PFI baseline vehicle. Minimal overlap between technologies implemented on the two vehicles suggested that the combination of compatible technologies from the two vehicles would likely offer further improvement on a single vehicle.

Phase 2

Multi-Cylinder Engine Comparison Study to Single-Cylinder Engine

Preliminary multi-cylinder engine (MCE) tests were conducted at 2,000 rpm-11 bar indicated mean effective pressure (IMEP) under conditions very similar to those used for single-cylinder engine (SCE) tests. Both the MCE and SCE were tested using the same injector design and the same gasoline with 10% ethanol. The red bars in Figure 1 show results for non-optimized MCE-1, while the blue bars show corresponding results from the SCE. The SCE results are considered optimized and are based on extensive Design of Experiments testing. Indicated specific fuel consumption (ISFC) was 175 and 172 g/kWh for the MCE and SCE, respectively. Combustion noise for the MCE was 88 dB, which is slightly lower than both the target and SCE results. Combustion duration was longer (10-90 duration) and combustion phasing was slightly later for the MCE. Oxides of nitrogen (NOx) and smoke emissions were well below targets for both engines. While CO emissions were comparable, hydrocarbon emissions for the MCE were high for this initial build.

Multi-Cylinder Engine GDCI Operation Over Complete Speed Load Range

Preliminary steady-state tests were run on the performance dynamometer for select operating conditions across the speed/load range. Initial results indicate a very efficient combustion process with good combustion stability over the complete speed/load range.

Multi-Cylinder Engine Mapping of GDCI

Initial mapping tests were performed in two sessions. The first test session was for low loads (2-4.5 bar brake mean effective pressure, BMEP) and low speeds (800-1,500 rpm) for which exhaust rebreathing is used. Results for these tests are shown in Figure 2. The second test session was for medium-to-higher loads (8-17 bar

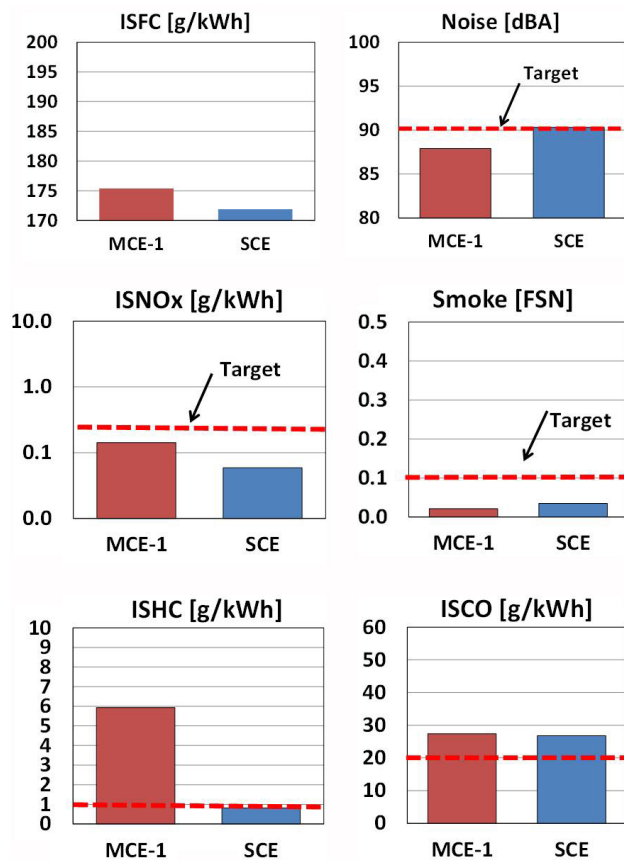


FIGURE 1. GDCI Combustion Results at 2,000 RPM-11 Bar IMEP for Multi-Cylinder Development Engine (red) And Single-Cylinder Concept Engine (blue)

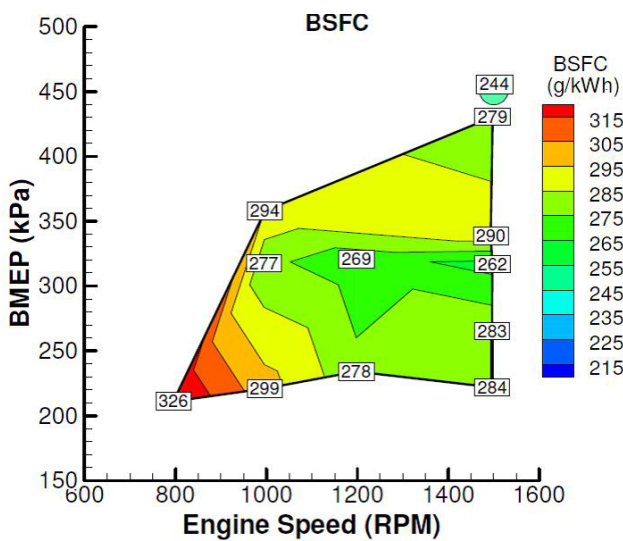


FIGURE 2. GDCI BSFC for Low Load

BMEP) in the medium speed range (1,500-2,500 rpm). Results for these tests are shown in Figure 3. Results are

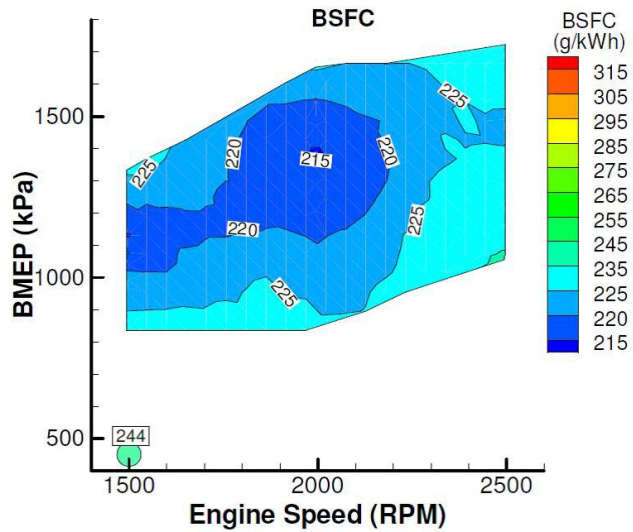


FIGURE 3. GDCI BSFC for Medium Load

considered preliminary and not yet optimized. Injection strategies vary as a function of operating condition. During low-load engine mapping, GDCI engine smoke was practically absent, combustion noise was well below targets, and combustion variability was less than 3%. The exhaust rebreathing strategy was effective to maintain exhaust temperatures above 250°C at the lowest loads. For medium-to-high loads, NOx emissions had a favourable decreasing trend with increasing load. For all tests, peak cylinder pressure was less than 160 bar and EGR was less than 45%.

Engine Controls

Controls work continues on the project including closed-loop fuel control, boost pressure control, combustion phasing control, burned gas fraction estimation and coolant system control. Control highlights for the GDCI engine on the start cart include first warm start, first room temperature start, first controlled idle, demonstration of off-idle and mid-RPM operation, and mild tip-in/tip-out capability.

Phase 2 Demonstration Vehicle Build

Construction of the GDCI demonstration vehicle was completed during this reporting period. The engine in the vehicle is identical to the MCEs used for both the performance dynamometer testing and the start cart controls development (see Figure 4). The control system implemented on the vehicle is also the same as the control system used on the start cart. The vehicle has a project specific cooling system that consists of two charge air coolers, an EGR cooler and control sensing and valve hardware. Additionally, the vehicle contains a project-specific wire harness, transmission, induction and exhaust systems, and all required instrumentation and



FIGURE 4. GDCI Demonstration Vehicle Nearing Completion at Delphi CTCM in Auburn Hills, Michigan



FIGURE 5. GDCI Demonstration Vehicle at Delphi CTCM during the August Project Review with the Department of Energy

safeties (see Figure 5). The vehicle control system is now being debugged.

CONCLUSIONS

Phase 2

- Multi-cylinder GDCI development engine results compare reasonably well to the single-cylinder concept engine that was used earlier in this project to develop the GDCI combustion process.
- Efficient GDCI combustion can be controlled over the full speed/load range including idle. Mixed mode combustion therefore is not required.

- For low speeds and light loads, rebreathing of hot exhaust gases effectively increases charge temperature and aids auto-ignition, increases exhaust temperatures for catalyst operation, and collapses the pumping loop.
- During multi-cylinder steady-state mapping, the GDCI engine NO_x, smoke, and coefficient of variance IMEP targets were fully met. BSFC at all conditions was very good with minimum BSFC of 214 g/kWh observed at 2,000 rpm-13.5 bar BMEP and ISFC was below 180 g/kWh over a wide operating range. Compared to production engines, GDCI BSFC is significantly better than gasoline engines and within 1% to 5% of light-duty diesel engines. At low-to-medium loads, GDCI BSFC was usually better than diesel engines.

2013 PUBLICATIONS/PRESENTATIONS

1. “Part-Load Operation of Gasoline Direct-Injection Compression Ignition (GDCI) Engine”, M. Sellnau et al., SAE 2013-01-0272, SAE World Congress, April 2013.
2. “Evaluation and Demonstration of a Systems Approach to Fuel Economy Improvement Technologies”, K. Confer et al., SAE 2013-01-0280, SAE World Congress, April 2013.
3. “Boost System Development for Gasoline Direct-injection Compression Ignition”, Kevin Hoyer et al, SAE 2013-01-0928, SAE World Congress, April 2013.
4. UFEV Project Merit Review Presentation, K. Confer, Merit Review, Washington, DC, May 2013.

IV.5 Advanced Gasoline Turbocharged Direct Injection Engine Development

Terry Wagner
Ford Motor Company
2101 Village Road
Dearborn, MI 48121

DOE Technology Development Manager:
Ken Howden

NETL Project Manager: Ralph Nine

Subcontractor:
Michigan Technological University (MTU),
Houghton, MI

Overall Objectives

Ford Motor Company

- Demonstrate 25% fuel economy improvement in a mid-sized sedan using a downsized, advanced gasoline turbocharged direct injection (GTDI) engine with no or limited degradation in vehicle level metrics.
- Demonstrate vehicle is capable of meeting Tier 2 Bin 2 emissions on the Federal Test Procedure (FTP)-75 cycle.

MTU

- Support Ford Motor Company in the research and development of advanced ignition concepts and systems to expand the dilute/lean engine operating limits.

Fiscal Year (FY) 2013 Objectives

- Dynamometer engine development indicates capability to meet intermediate metrics supporting vehicle fuel economy and emissions objectives.
- Demonstration vehicle and components available to start build and instrument (deferred from 12/31/2012 to 08/01/2013).
- Vehicle build, instrumentation, and development work started.
- Aftertreatment system development indicates capability to meet intermediate metrics supporting emissions objectives.

FY 2013 Accomplishments

Single-Cylinder Build and Test

- Completed combustion system verification testing to ensure combustion system meets target metrics, including fuel consumption, stability, oxides of nitrogen, CO, and particulate matter emissions; testing included part-load injection timing sweeps, cooled exhaust gas recirculation (EGR) sweeps, cold start, and idle combustion stability.
- Testing to date indicates combustion system satisfies target metrics.
- Completed an assessment of an outward opening (A-nozzle) injector, including part load, cold start, and idle. Testing showed that the outward opening injector performed similarly to the prime assumption, multi-hole injectors.
- Investigated the effects of split injection strategies on the EGR tolerance of the engine. A micro-stratification injection strategy was found to improve EGR tolerance by 3% at a low-load operating condition.
- Investigated the effects of split injection strategies on the knock tolerance of the engine.

Engine Design/Procure/Build

- Completed procurement of components and build for Engines #5–12. Engine #5 planned for performance development testing; Engine #6 for thermal management studies; Engine #7 for mechanical development studies; Engine #8 for spare; and Engines #9–12 for vehicle build.

Engine Development on Dynamometer

- Completed Engine #1 dynamometer install and engine commissioning. Substantially completed combustion system/mechanical verification testing, including partial and full factorials for optimum attributes, part-load fuel consumption and emissions, full-load performance, and advanced engine systems control (e.g. advanced boost system, electric twin independent variable camshaft timing). Testing to date indicates combustion system satisfies target metrics.
- Completed Engine #2 instrumentation, dynamometer prep, dynamometer install, and engine commissioning. Substantially completed transient

emissions verification testing, including steady-state cold fluids development and transient cold start development. Testing to date indicates combustion system satisfies target metrics.

- Completed Engine #3 instrumentation, dynamometer prep, dynamometer install, and engine commissioning. Substantially progressed engine mapping, including configuring AutoTest control for autonomous engine mapping.
- Completed Engine #4 instrumentation, dynamometer prep, dynamometer install, and engine commissioning. Completed total engine and successive component removal friction testing. Engine rebuilt to original condition for subsequent noise, vibration, and harshness (NVH) testing; completed NVH testing. Engine rebuilt to original condition for subsequent mechanical development studies.
- Continued dynamometer facility and engine instrumentation planning in support of 2013–2014 development plans.

Vehicle Installation Design and Procurement

- Completed computer-aided design (CAD) design and required computer-aided engineering (CAE) analyses of new advanced integrated powertrain systems, specifically torque converter pendulum damper and active powertrain mounts.
- Completed CAD design of supporting powertrain systems, including acoustic covers, fuel charging, and other powertrain/vehicle interfacing systems.
- Completed procurement of advanced integrated and supporting powertrain systems.

Vehicle Build

- Completed procurement of four 2013 model year CD391 Fusion vehicles for the Vehicle Calibration phase of project.
- Completed non-powertrain systems instrumentation tasks on all four vehicles in order to accelerate subsequent powertrain/vehicle integration tasks.
- Initiated powertrain/vehicle integration tasks for Vehicle #1, including removal of existing powertrain, prep for new powertrain, and prep for new advanced integrated and supporting powertrain systems. Vehicles #2–4 on-site at vehicle build facility ready to initiate the same.

Vehicle Cooling Design and Optimization:

- Completed procurement of vehicle cooling system components, including pumps, heat exchangers, fittings, lines, etc.

Vehicle Calibration

- Completed early controls and calibration development tasks on surrogate vehicle with surrogate GTDI engine to accelerate target vehicle tasks.

Aftertreatment Development

- Completed summary documentation of three-way catalyst + lean-NOx trap/selective catalytic reduction (SCR) and three-way catalyst + passive SCR systems.
- Completed procurement of exhaust system components for vehicle build, including hot and cold ends, active fresh, active aged, and inert bricks.

Combustion Research

- Progressed all facets of research and development described by the primary tasks: i) Advanced Ignition and Flame Kernel Development, ii) Advanced Ignition – Impact on Combustion, iii) GDI Air/Fuel Mixing via Planar Laser-Induced Fluorescence for Fuel Injection Optimization, iv) Combustion Sensing and Control, v) Advanced Knock Detection and Control, and vi) In-Cylinder Temperatures and Heat Transfer.
- Summarized and presented results from Task i) Advanced Ignition and Flame Kernel Development as SAE International (SAE) World Congress paper 2013-01-1627 “The Impact of Spark Discharge Pattern on flame Initiation in a Turbulent Lean and Dilute Mixture in a Pressurized Combustion Vessel”. Accepted to SAE Transactions Journal.
- Summarized and presented results from Task ii) Advanced Ignition – Impact on Combustion as SAE World Congress paper 2013-01-1630 “Impact of Ignition Energy Phasing and Spark Gap on Combustion in a Homogenous Direct Injection Gasoline SI Engine near the EGR Limit.”
- Completed conversion of the high feature combustion vessel from supporting Task i) to supporting Task iii) GDI Air/Fuel Mixing via Planar Laser-Induced Fluorescence for Fuel Injection Optimization.
- Demonstrated closed-loop control of combustion sensing (phasing and stability) on the first 3.5-L EcoBoost engine. Developed algorithms and initiated testing of stochastic knock detection and control on the same engine.
- Completed Phase 1 testing and initiated analysis of in-cylinder temperatures and heat flux on the second 3.5-L EcoBoost engine (wireless telemetry system). Initiated Phase 2 testing.

Future Direction

Vehicle demonstrates greater than 25% weighted city/highway fuel economy improvement and Tier 2 Bin 2 emissions on the FTP-75 test cycle.



INTRODUCTION

Ford Motor Company has invested significantly in GTDI engine technology as a cost-effective, high-volume, fuel economy solution, marketed globally as EcoBoost technology. This project is directed toward advancing the EcoBoost technology, as well as related additional technologies, in order to achieve the project objectives:

- Demonstrate 25% fuel economy improvement in a mid-sized sedan using a downsized, advanced GTDI engine with no or limited degradation in vehicle level metrics.
- Demonstrate vehicle is capable of meeting Tier 2 Bin 2 emissions on the FTP-75 cycle.

APPROACH

Engineer a comprehensive suite of gasoline engine systems technologies to achieve the project objectives, utilizing:

- Aggressive engine downsizing in a mid-sized sedan from a large V-6 to a small I-4
- Mid- and long-term EcoBoost advanced technologies such as:
 - Dilute combustion with cooled exhaust gas recycling and advanced ignition
 - Lean combustion with direct fuel injection and advanced ignition
 - Boosting systems with active and compounding components
 - Cooling and aftertreatment systems
- Advanced friction-reduction technologies, engine control strategies, and NVH countermeasures
- Progressively demonstrate the project objectives via concept analysis/modeling, single-cylinder engine, multi-cylinder engine, and vehicle-level demonstration on chassis rolls

RESULTS

The team progressed the project through the Single-Cylinder Build and Test, Engine Design/Procure/BUILD,

Engine Development on Dynamometer, and Vehicle tasks with material accomplishments. In addition to completing procurement of components and build for Engines #1–4, the team completed the same for the balance of the series, Engines #5–12. Engine #5 is planned for performance development testing, Engine #6 for thermal management studies, Engine #7 for mechanical development studies, Engine #8 for spare, and Engines #9–12 for vehicle build. Figure 1 shows a representative completed engine build.

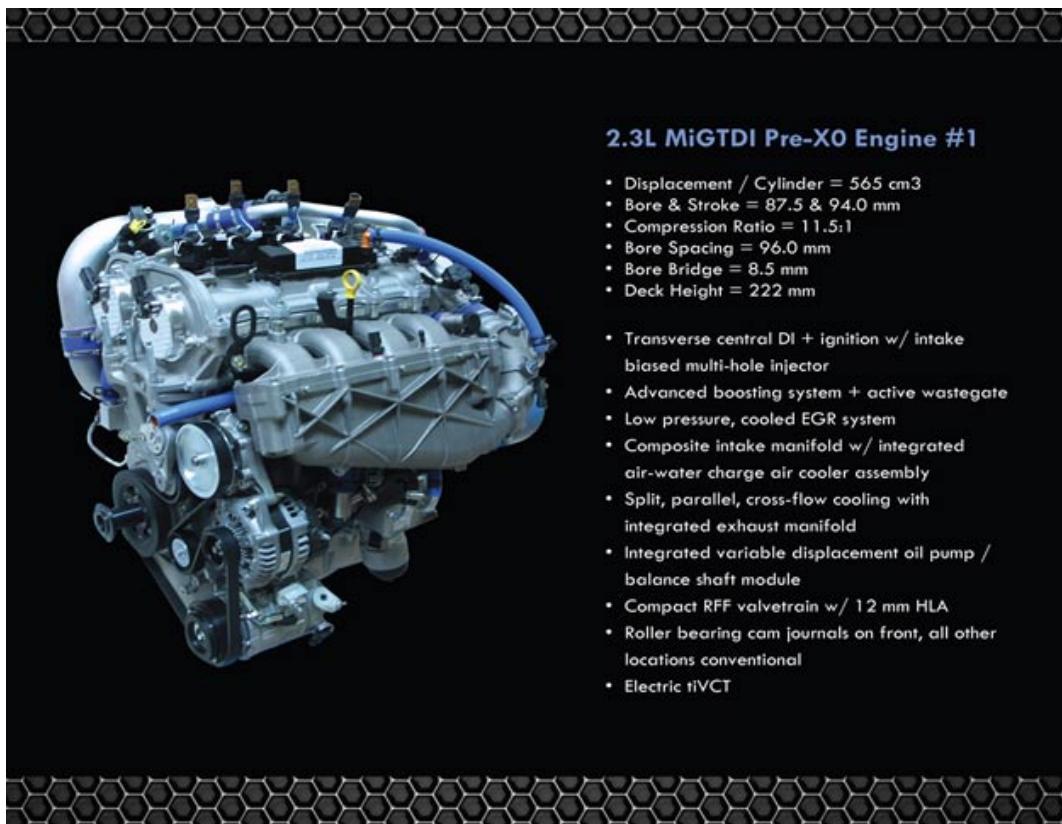
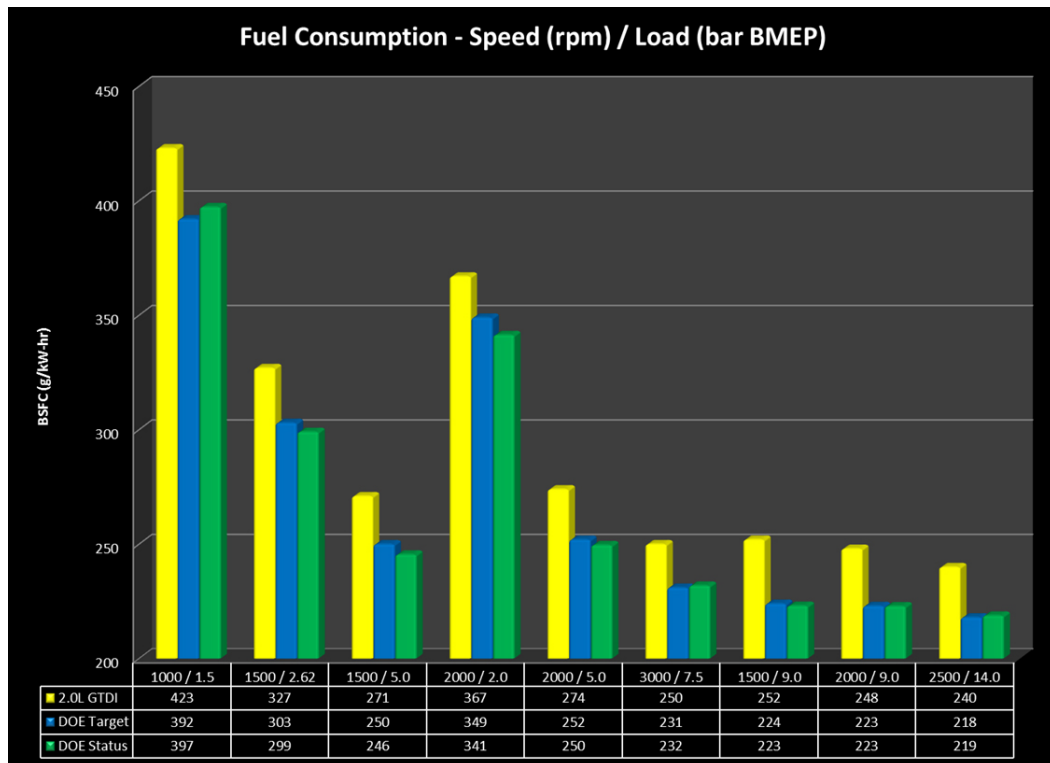
The team progressed Engines #1–4 to a high level of dynamometer development productivity, and substantially completed combustion system/mechanical verification testing, transient emissions verification testing, engine mapping, friction testing, and NVH testing. Testing to date indicates that the combustion system satisfies the target metrics, which are critical to satisfy the project objectives. For example, Figure 2 compares engine fuel consumption at critical speed/load points, all with 15% EGR; as shown, the engine overall meets the fuel consumption targets toward the project objective, and is substantially better than a comparator 2.0-L GTDI engine. Figure 3 compares engine stability at the same points, all with 15% EGR; the engine meets the stability targets, indicating good EGR tolerance. Lastly, Figure 4 compares engine CO emissions at the same points, all with 15% EGR; the engine meets the CO emissions targets, indicating good air/fuel mixing.

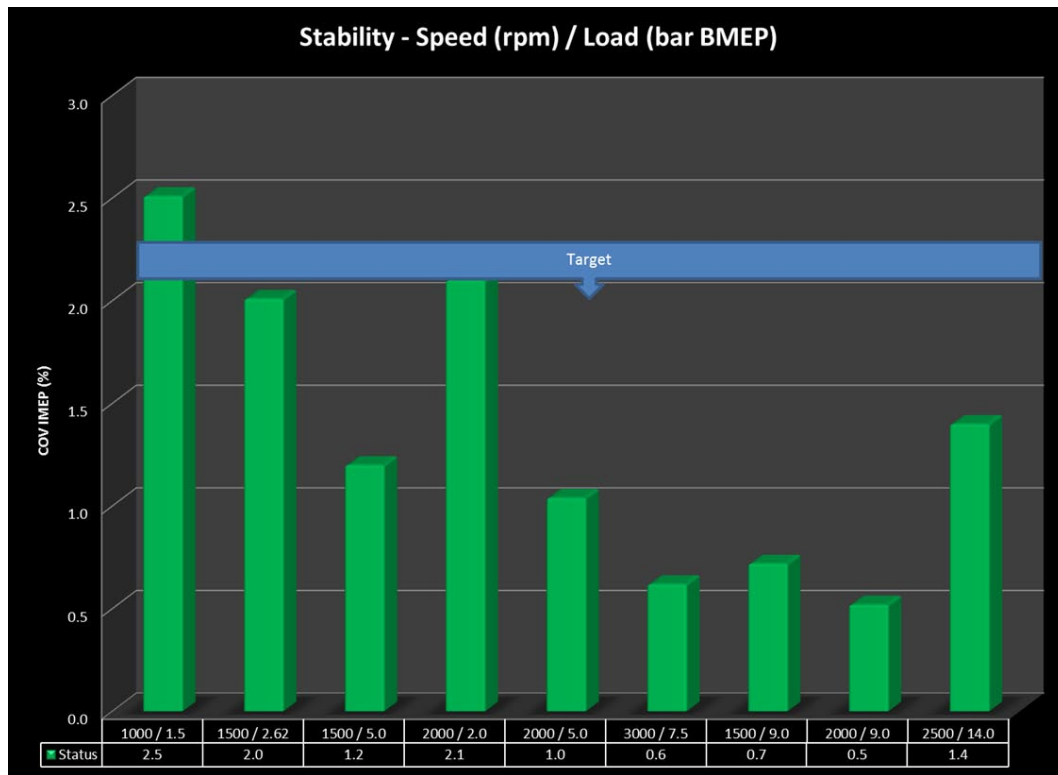
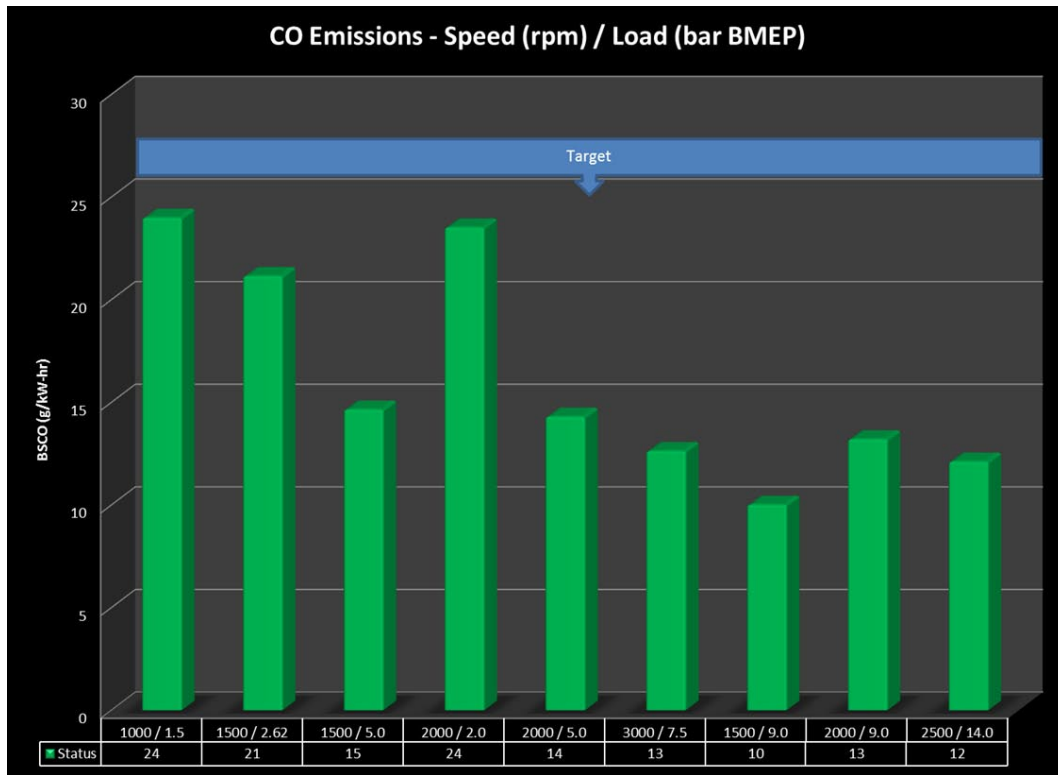
In addition to dynamometer development, the team substantially completed the vehicle design and procurement tasks, and initiated the vehicle build tasks. The team completed CAD design, CAE analyses, and procurement of advanced integrated and supporting powertrain systems, completed procurement of and instrumentation tasks on four 2013 model year CD391 Fusion vehicles, and initiated powertrain/vehicle integration tasks for Vehicle #1. Figure 5 shows the CAD representation of the powertrain as installed, and Figure 6 the actual powertrain during preliminary install in Vehicle #1.

The MTU sub-team progressed all facets of the research and development on advanced ignition concepts. Notably, the sub-team published two SAE papers from their primary tasks, and contributed significant findings on the effects spark discharge patterns on flame initiation and dilute combustion in advanced GTDI engines, directly impacting fundamental understanding of the project engine combustion system.

CONCLUSIONS

- The project will demonstrate a 25% fuel economy improvement in a mid-sized sedan using a downsized, advanced GTDI engine with no or

**FIGURE 1.** Multi-Cylinder Engine Build**FIGURE 2.** Engine Fuel Consumption

**FIGURE 3.** Engine Stability**FIGURE 4.** Engine CO Emissions

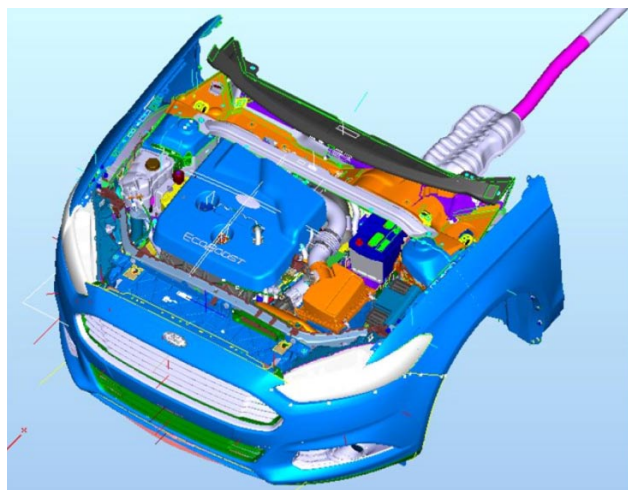


FIGURE 5. CAD Powertrain as Installed in Vehicle



FIGURE 6. Actual Powertrain as Installed in Vehicle

limited degradation in vehicle level metrics, while meeting Tier 2 Bin 2 emissions on the FTP-75 cycle.

- Ford Motor Company has engineered a comprehensive suite of gasoline engine systems technologies to achieve the project objectives and progressed the project through the Single-Cylinder Build and Test, Engine Design/Procure/Build, Engine Development on Dynamometer, and Vehicle tasks with material accomplishments.
- Ford Motor Company is in collaboration with MTU on a critical facet of the project, specifically advanced ignition concepts.

FY 2013 PUBLICATIONS/PRESENTATIONS

1. Completed presentation at 2013 U.S. Department of Energy (DOE) Hydrogen and Fuel Cells Program and Vehicle Technologies Program Annual Merit Review and Peer Evaluation Meeting (AMR), held May 13-17, 2013, Crystal City Marriott, Arlington, Virginia.
2. Completed project status presentation for Ralph Nine and Ken Howden at Ford Motor Company on August 26, 2013; reviewed status of all primary tasks and received concurrence on transitioning from Tier 2 Bin 2 to Tier 3 SULEV30 emissions. Completed a multi-cylinder lab tour, a multi-cylinder build tour, and vehicle build tour.

SPECIAL RECOGNITIONS AND AWARDS/ PATENTS ISSUED

1. Submitted “Compensation of IAO2 Sensor for Purge for Correct EGR”, ID No 83336561, DOE Case No S-134,403 – 03/07/2013.
2. Submitted “Dual Coil Ignition System with Secondary Windings Connected in Series”, ID No 83228424, DOE Case No S-134,398 – 03/07/2013.

IV.6 Lean Gasoline System Development for Fuel Efficient Small Cars

Stuart R. Smith
Powertrain Division
General Motors, LLC (GM)
895 Joslyn Avenue
Pontiac, MI 48340-2920
Phone: (248) 431-9818
Email: stuart.smith@gm.com

DOE Technology Development Manager:
Ken Howden

NETL Project Manager: Ralph Nine

Overall Objectives

- Develop an advanced lean-gasoline combustion engine and aftertreatment system
- Demonstrate 25% vehicle fuel economy improvement while achieving Tier 2 Bin 2 (T2B2) emissions
- Comprehend system level integration for an optimal combination of advanced vehicle technologies to provide the highest fuel economy for potential production implementation

Fiscal Year (FY) 2013 Objectives

- Demonstrate T2B2 emission capability on naturally aspirated SG5 Lean Gasoline Combustion system
- Develop a Lean Downsize Boost (LDB) combustion system capable of meeting FE targets
- Develop controls to enable vehicle demonstration of LDB

FY 2013 Accomplishments

- Demonstrated Tier 2 Bin 2 capability with Spray Guided Engine Version 5 (SG5) lean gasoline combustion system using a passive/active ammonia selective catalytic reduction (SCR) system.
- Developed LDB combustion system that demonstrated brake specific fuel consumption (BSFC) improvement of 21% compared to the 4-cylinder port fuel-injected (PFI) baseline.
- Controls and calibration developed to support vehicle demonstrations of both the naturally aspirated SG5 and LDB engines.

- Successfully demonstrated both SG5 and LDB engines on August 28th at the Milford Proving Grounds.

Future Directions

- Passive SCR was demonstrated capable of high efficiency NOx conversion with relatively low engine-out NOx. Further investigation into optimal washcoat technologies for NH₃ release are ongoing with various washcoat suppliers.
- A 12-volt start/stop system is in production in the 2014 Malibu. Further investigation into reducing start variation is underway, focused on repeatable engine stop position control.
- Thermal management opportunities are being explored in GM's next generation of engines. These would include expanded operation beyond "zero-flow" concepts.
- Future lean-combustion systems will require sophisticated air charging systems similar to small diesels. The combination of air and exhaust gas recirculation (EGR) requirements for small downsize boosted engines will require multi-stage boosting. There also is potential for future ignition systems to improve the engine-out NOx significantly and allow aftertreatment thrifting.



INTRODUCTION

This project accelerates development and synergistic integration of four cost-competitive technologies to improve the fuel economy of a light-duty vehicle by 25% while meeting T2B2 emissions standards. These technologies are targeted to be broadly implemented across the U.S. light-duty vehicle product line between 2015 and 2025 and are compatible with future and renewable biofuels. The technologies in this project are lean gasoline combustion, innovative passive SCR lean aftertreatment, 12-volt stop/start, and active thermal management. The project scope additionally includes risk mitigation of downsize boosting and active urea dosing.

APPROACH

The approach for 2013 focused on generating data to demonstrate performance to the project targets. This work focused on development of the LDB combustion system and integrating it into a vehicle.

The LDB combustion development in 2013 was focused on multi-cylinder engines on dynamometers. Investigations into EGR rates, ignition systems and injection strategies were performed to optimize BSFC performance. Once the hardware systems were defined, the control system was modified to include these operations within GM's internal control system. Upon completion of the controls, a DOE methodology was used to generate calibrations.

Vehicle integration work focused on packaging the new LDB powertrain, 12-volt start/stop, and thermal management systems into the vehicle. In addition to the engine and transmission, this included significant work on the cooling system due to the addition of the cool EGR and charge-air cooling systems. After the powertrain and thermal systems were installed, the vehicle electrical system was modified to support 12-volt start/stop. The mechanical work to accomplish this took 12 weeks.

RESULTS

LDB Engine

Investigations into high-energy ignition systems showed the potential for improved dilution tolerance. This increased EGR allowed the engine-out NOx to be reduced, but did not significantly improve the BSFC. The passive/active ammonia SCR aftertreatment system developed in 2012 had already demonstrated T2B2 capability at high engine-out NOx levels. The steering committee recommended dropping the high-energy ignition system from further development, as the focus for LDB was to improve BSFC, which the high-energy ignition system only marginally improved. This decision was driven in part by project timing and scope.

With the completion of the ignition study, the LDB combustion system was defined. BSFC data was generated to support vehicle fuel economy modeling. The modeling results demonstrated a 21% fuel economy advantage over the 2.4-L PFI baseline, Table 1. The BSFC results, combined with the 12-volt start/stop and thermal management gains demonstrated a final package that meets the project deliverables with a 26% improvement compared to the baseline, Table 2.

In order for a vehicle level demonstration, significant calibration work still had to occur. This

TABLE 2. LDB with Integrated Technologies vs. PFI Baseline

Phase 3 (LDB) Fuel Economy Improvement:

| Technology | City Schedule % FE Improvement | Demonstration Method |
|-----------------------|--------------------------------|----------------------------------|
| LDB combustion system | 26 | Engine dynamometer |
| 12V SS | 6 | Carryover from SG5 demonstration |
| Thermal Mgmt | 3 | Carryover from SG5 demonstration |
| LDB City FE | 35 | |

| Technology | Highway Schedule % FE Improvement | Demonstration Method |
|-----------------------|-----------------------------------|----------------------|
| LDB combustion system | 12 | Engine dynamometer |
| 12V SS | 0 | No idles |
| Thermal Mgmt | 0 | Hot test |
| LDB Highway %FE | 12 | |

12V SS – 12-volt start/stop

TABLE 1. LDB vs PFI Baseline

| | Speed (RPM) | Load (n-m) | BSFC Improvement | |
|---------|-------------|------------|------------------|------------|
| | | | PFI to Lean NA | PFI to LDB |
| Urban | Idle | 700 | 19 | 0% |
| | Zone 2 | 1335 | 27 | 17% |
| | Zone 3 | 1565 | 28 | 19% |
| | Zone 4 | 1805 | 29 | 18% |
| | Zone 5 | 1530 | 95 | -1% |
| | Zone 6 | 1821 | 80 | 3% |
| | Zone 7 | 2250 | 101 | 0% |
| Highway | Zone 8 | 1410 | 51 | 18% |
| | Zone 9 | 1669 | 60 | 9% |
| | Zone 10 | 1461 | 114 | 0% |
| | Zone 11 | 1692 | 100 | 0% |

| | Projected FE Improvement | |
|----------|--------------------------|-----|
| City | 12% | 26% |
| Highway | 8% | 12% |
| Combined | 10% | 21% |

NA – naturally aspirated; FE – fuel economy

was accomplished through a design of experiments methodology. A validation exercise on fuel specific NOx (Figure 1) and BSFC (Figure 2) was performed to confirm the DOE results.

The final three months were focused on the vehicle integration work. The mechanical work required significant redesign of the vehicle induction, cooling and electrical systems. The final four to six weeks included

integrating the 12-volt start/stop system into the LDB calibration.

The final vehicle demonstration occurred at Milford Proving Grounds on August 28, 2013.

CONCLUSIONS

- LDB combustion system demonstrated 21% fuel economy improvement over the PFI baseline

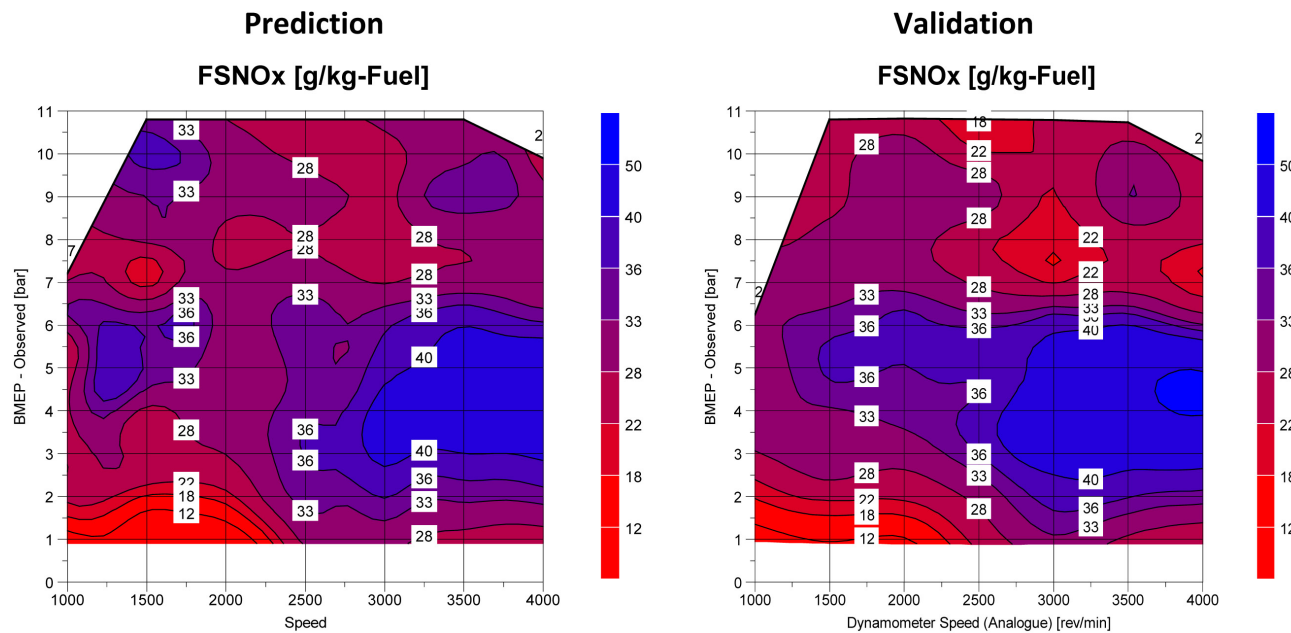


FIGURE 1. Fuel Specific NOx Predicted vs. Actual

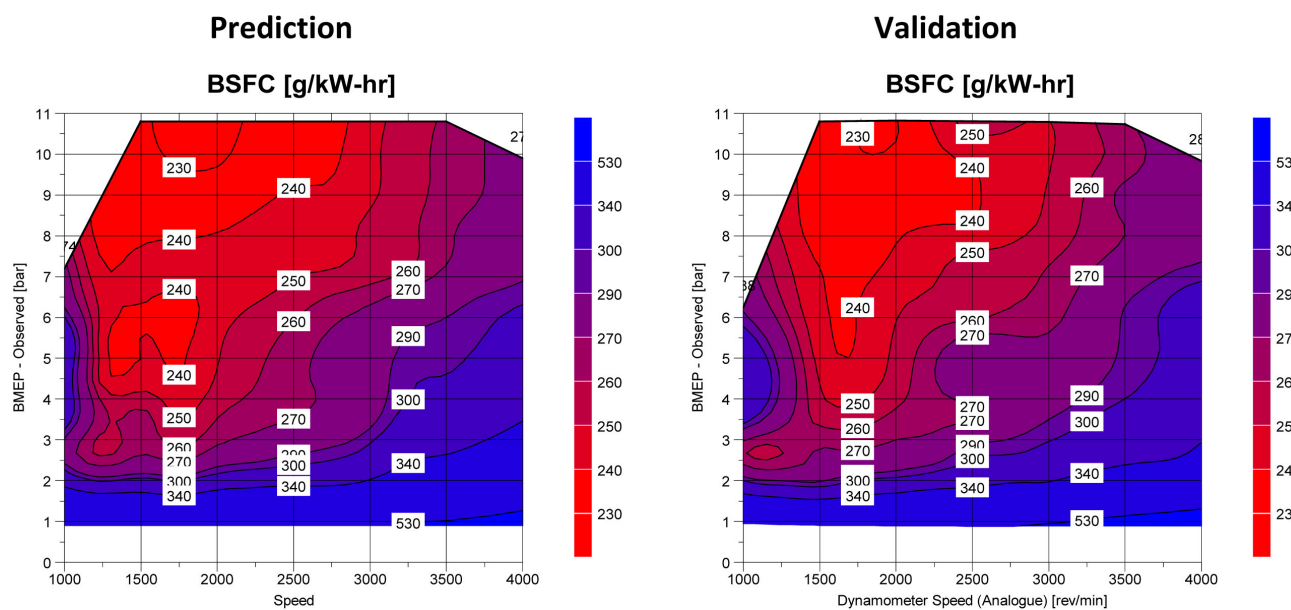


FIGURE 2. BSFC Predicted vs. Actual

- LDB combined with 12-volt start/stop and thermal management delivered 25% fuel economy improvement over the PFI baseline

FY 2013 PUBLICATIONS/PRESENTATIONS

1. Smith, Stuart “Lean Gasoline System Development for Fuel Efficient Small Car”, 2013 U.S. DOE Vehicle Technologies Program Annual Merit Review and Peer Evaluation
2. Meeting, Arlington, VA, May 16, 2013.

IV.7 Cummins Next Generation Tier 2 Bin 2 Diesel

Michael J. Ruth

Cummins Inc.

PO Box 3005

Columbus, IN 47201-3005

DOE Technology Development Manager:
Roland Gravel

NETL Project Manager: Carl Maronde

Subcontractor:

Johnson-Matthey Inc., Wayne, PA

Future Directions

- Continued development and optimization of the first vehicle installation of the ATLAS engine in T2B5 trim level (2013 demonstration did not include glow plugs, exhaust gas recirculation [EGR] cooler bypass, or optimized transmission shift control).
- T2B2 ATLAS engine-out emission demonstration in a test cell environment.
- T2B2 aftertreatment (diesel Cold Start Concept [dCSCTM] catalyst) demonstration in a test cell environment.
- T2B2 ATLAS-powered vehicle demonstration.



Overall Objectives

- Demonstrate 40% fuel economy improvement over baseline gasoline V-8 pickup truck
- Demonstrate Tier 2 Bin 2 (T2B2) tailpipe emissions compliance

Fiscal Year (FY) 2013 Objectives

- First fire of all-new, light-weight aluminum engine assembly (ATLAS engine)
- Demonstration of power and torque from ATLAS engine
- ATLAS engine installation into vehicle
- Demonstration of Tier 2 Bin 5 (T2B5) engine-out emissions from ATLAS engine in test cell
- Demonstration of T2B5 tailpipe emissions on mule vehicle

FY 2013 Accomplishments

- Completed procurement and demonstration of ATLAS engine power and torque.
- ATLAS engine assembly represented nearly 100 lb weight reduction compared to the baseline.
- ATLAS engine installed in vehicle.
- T2B5 ATLAS demonstration in test cell environment at substantially higher fuel economy than baseline mule engine values.
- T2B5 tailpipe emissions demonstrated on several occasions in chassis laboratory environment, as well as tested on public roads, maintaining T2B5 emission control over a variety of driving conditions while demonstrating City fuel economy more than 10% better than project goals.

INTRODUCTION

The overall objective of this project, Cummins Next Generation Tier 2 Bin 2 Diesel, is to design, develop, and demonstrate a state-of-the-art light-duty (1/2 ton pickup truck) diesel engine that meets U.S. Environmental Protection Agency light-duty T2B2 emission standards and increases fuel efficiency by at least 40% compared with a state-of-the-art port fuel-injected gasoline engine.

The U.S. new, personal-use vehicle fleet has changed slightly over the past two years, with car purchases increasing. By and large, pickup trucks and sport utility vehicles (SUVs) still account for nearly half of sales in this segment. An improvement in fuel economy by 40% in the light truck and SUV segment would reduce the U.S. oil consumption by 1.5M bbl/day and reduce greenhouse gas emissions by 0.5 MMT/day.

APPROACH

The project has four phases. The first phase included the baseline establishment for the target vehicle (2010 Nissan Titan) as well as the fuel consumption and emission rate of the Cummins 2.8-L ISF Euro III engine. Model development in Phase One directed technology testing and development to create a technical profile for a new engine design. The second phase of work determined viable technologies to carry forward. The third phase is a demonstration of viable technologies in preparation for the integration of the chosen technologies.

Phase Three entailed the development work required to bring the new engine to achieve T2B5 emissions with the majority of all systems working properly. The work in this phase is segmented between engine and

aftertreatment and is not necessarily developed on the same platform. The demonstration is, however, a pooling of that development into one concise demonstration. The fourth and final phase will be the optimization of all subsystems using a T2B5 demo platform, including vehicle systems such as charging and vacuum system as well as fueling and transmission shift logic. The fourth phase will be to demonstrate the ultimate goal of T2B2 emissions with at least 40% fuel economy improvement over the baseline gasoline powertrain.

RESULTS

Procurement

The ATLAS engine has been procured and built. The engine did come in slightly heavier than the design model had predicted. The total weight of the ATLAS engine was nearly 100 lb less than the production (mule) engine used in early development. Design models had pegged the weight reduction to be 120 lb. The team is working to find the differences between the model and actual parts.

The first castings procured were found to have poor control of the cast iron liner position, leading to thin sections of the liner once the assembly was finish machined. The thin sections were found to crack in testing. The cracks were not catastrophic as they only manifested themselves as high blow-by under high-load conditions. The situation was corrected by design modifications to the casting molds as well as improved material strength and dimensional changes to the liner. Subsequent testing has shown the fix to be adequate.

The synchronous timing belt arrangement also has caused failures in testing. The automatic belt tensioner has proven to have more travel than anticipated, which seems to fatigue the spring. This failure results in complete belt failure, and eventually valves and pistons come together, crashing the over head. This is a catastrophic failure, resulting in the loss of three engines. An interim fix of using a “fixed” (meaning not automatic) tensioner allows for safe operation but requires intermediate service intervals to ensure tension is maintained on the belt. The belt system supplier is working on a long-term fix.

Controls, Performance, and Emissions

The team has worked with both the mule engine and the new ATLAS engine over the past year. The mule engine development was aimed at control system development, including the system that is currently being used to run the ATLAS engine. Additionally, the controls team has now included the functional glow system and EGR cooler bypass valve.

Cold operation oxides of nitrogen (NOx) and hydrocarbons (HCs) have been reduced by more than 50%. The ATLAS engine has demonstrated cold Federal Test Procedure (FTP) NOx emissions of 0.5 grams over the first 200 seconds of operation, compared to 1.1 grams of NOx on the mule engine. The HC emissions have been reduced to a similar extent.

The ATLAS engine has demonstrated FTP-75 NOx emissions at the T2B5 engine-out target while achieving fuel economy over 22.5 mpg in the same test. This represents more than 1 mpg greater than the project goal.

Catalyst Systems

Several new dCSC™ technologies were developed and tested on the bench reactor, and the performance was compared to the reference formulation. Significant improvements in performance were observed in one of the new dCSC™ catalyst technologies. The NOx trapping efficiency, CO oxidation, and HC oxidation were compared on the bench reactor under simulated cold-start conditions. The catalysts were hydrothermally aged before evaluations. The results showed that the new technology has almost 100% NOx storage during cold-start conditions, and the NOx release profile during the temperature ramp-up portion of the test is similar to that of the reference dCSC™ catalyst. The CO and HC oxidation performance of the new technology is comparable to that of the reference dCSC™ catalyst.

Engine testing of the reference dCSC™ formulation is ongoing. The performance was evaluated under FTP-75 cycles before and after hydrothermally aging the catalysts. The results indicate that the cumulative NOx storage for the degreened part is equal to that of the aged part; hence, no degradation in NOx performance is observed due to hydrothermal aging of the dCSC™ catalyst.

Accelerated ash loading was performed by Cummins using a SCRF® catalyst, and the part was submitted for post-mortem analysis at Johnson Matthey. Reactor testing under various steady-state conditions of an ash-loaded core sample was performed to determine the effect of ash on the SCRF® catalyst performance. Further analysis determined the composition of ash and the location of ash deposits in the filter.

SCRF® catalyst development continues with testing of different formulations to improve backpressure while maintaining performance over the various regulatory cycles. One of the SCRF® formulations that was optimized for backpressure and showed low cold-flow backpressure at Johnson Matthey (bench) was tested on engine at Cummins and compared to a baseline system consisting of a diesel oxidation catalyst (DOC), platinum-grade metal catalyzed filter, and two selective

catalytic reduction (SCR) catalysts (ammonia slip catalyst removed). The SCRF® catalyst system consisted of a DOC, SCRF® catalyst, and only one SCR catalyst. Preliminary results indicated that the SCRF® catalyst system resulted in similar or slightly lower backpressure compared to the baseline system with a platinum-grade metal catalyzed filter over the FTP-75 cycle with negligible soot load on the filter.

Vehicle Results

The vehicle team has demonstrated T2B5 emissions using a limited number of the final components available—cooled EGR, SCR on filter, and direct ammonia delivery. There were no glow plugs, uncooled EGR, or dCSC™. This created a challenge to meeting emissions regulations with the cold start included. The team did meet the T2B5 requirements for full useful life mileage. This was done with margin to the fuel economy target. The majority of the emissions, as one would expect, were released at the cold start, where the engine-out emissions for this configuration were well over one gram per mile in Bag One.

Additionally, the team worked on transmission optimization to aid drivability without negatively affecting engine-out emissions. The optimization process is ongoing, but as an interim improvement, the calibration was adjusted to increase the engine speed over the drive cycle by 300 rpm on average. Tests showed no deterioration in fuel economy or engine-out emissions, but an improvement in aftertreatment temperature stabilization.

CONCLUSIONS

The Cummins next generation T2B2 light-duty diesel engine project has successfully completed the third year of the four-year project. The following conclusions have come from the second year of development:

- The new ATLAS engine has been procured and demonstrated outstanding progress toward the ultimate project goals:
 - Nearly 100 lb weight reduction from mule
 - Achieving power and torque targets
 - Demonstrating engine-out emissions and fuel economy simultaneously

- The aftertreatment development is on a path to success. The dCSC™ development appears to be on track to deliver the required storage and release characteristics for this application. The SCR method of NOx control also has been demonstrating very high effectiveness over the drive cycles.
- The direct ammonia delivery system will be critical toward achieving the goal of T2B2 tailpipe emissions. Data have shown that even without any NOx storage device, a close-coupled SCRF® plus SCR system is capable of reducing NOx over 93%, including the cold phase.
- The optimization work on transmission control has shown definite improvement with very few changes. This work has improved drivability while improving conditions for aftertreatment without negatively impacting fuel economy.

FY 2013 PUBLICATIONS/PRESENTATIONS

1. SAE Paper – April 2013; “Thermodynamic Systems for Tier 2 Bin 2 Diesel Engines,” Suresh, Langenderfer, Arnett, Ruth.
2. SAE Presentation – November 2013- Fuels Lubes and Aftertreatment; “A Systems Approach to Meet Future Fuel Economy and Emissions Regulations,” Ruth.

IV.8 Advanced Combustion Controls—Enabling Systems and Solutions (ACCESS)

Hakan Yilmaz (Primary Contact), Li Jiang,
Jeff Sterniak, Oliver Miersch-Wiemers

Robert Bosch LLC
38000 Hills Tech Drive
Farmington Hills, MI 48331

DOE Technology Development Manager:
Ken Howden

NETL Project Manager: Ralph Nine

Subcontractors:

- AVL Powertrain, Plymouth, MI
- Emitec, Auburn Hills, MI
- University of Michigan, Ann Arbor, MI
- Stanford University, Palo Alto, CA

improvement during the Federal Test Procedure (FTP)-75 drive cycle over the baseline vehicle

- Demonstrated 12 sec 300°C light-off time using the prototype three-way-catalyst with metallic substrate, critical to meeting SULEV non-methane organic carbon (NMOG) requirements
- Demonstrated Homogeneous Charge Compression Ignition (HCCI) transient and mode switch performance on the ACCESS Prototype II engine
- Completed integration of the ACCESS Prototype II engine along with start-stop functionality and base vehicle calibration for spark ignition (SI) mode into demonstration vehicle

Future Directions

- Finalize and integrate advanced combustion control strategies into engine control unit
- Demonstrate engine and vehicle performance during transient operations including mode switches
- Analyze fuel efficiency and emission results from vehicle, identifying commercial potentials of the proposed technology solutions



Overall Objectives

- Improve fuel economy by 25% with minimum performance penalties
- Achieve Super Ultra-Low Emissions Vehicle (SULEV) level emissions with gasoline
- Demonstrate multi-mode combustion engine management system

Fiscal Year (FY) 2013 Objectives

- Complete combustion concept development, quantifying the fuel efficiency improvement potentials and control challenges with advanced combustion
- Finalize the technology packages to be integrated into the demonstration vehicle
- Demonstrate vehicle performance with the ACCESS Prototype II engine integrated under spark ignition mode

FY 2013 Accomplishments

- Demonstrated up to 40% brake fuel efficiency improvement against the baseline engine at frequently visited driving cycle conditions on the ACCESS Prototype II engine
- Completed vehicle simulations based on ACCESS Prototype II engine combustion optimization data, showing greater than 25% fuel economy

INTRODUCTION

Due to availability and security of energy resources, environmental concerns, and cost factors, the automotive industry is facing the challenge of improving fuel economy and reducing the emissions without sacrificing performance. Although there are promising developments in electrification of vehicle powertrains with hybrid systems, battery electric vehicles and fuel cell electric vehicles, internal combustion engines are expected to be the mainstream power source of future high-efficiency vehicles for the next decade. The feasible future advanced engine and powertrain configuration must address the topics such as emission and fuel economy requirements for worldwide applications, transition to biofuels, and synergies with future powertrain trends.

The ACCESS project has the primary objective of developing highly capable and flexible advanced control concepts with enabling system, sub-system and component level solutions for the management of multi-mode combustion events in order to achieve 25% fuel economy improvement in a gasoline-fueled light-duty

vehicle without compromising its performance while meeting future emission standards as outlined in DOE solicitation targets.

APPROACH

The ACCESS project, through a three-phase approach, addresses the development, testing, and demonstration of the proposed advanced technologies and the associated emission and fuel economy improvement at an engine dynamometer and on a full-scale vehicle. The project investigates synergistic mainstream advanced combustion and system concepts such as:

- SI combustion with high compression ratio assisted with cooled external exhaust gas recirculation (EGR)
- HCCI assisted with boosting, external EGR, spark, valve, and fueling strategies for operation range extension
- Port-assisted direct injection (PDI) implemented with a dual-injection system for combined benefits of port fuel injection and direct injection
- Multi-hole direct injection with individual nozzle geometry design for improved mixture preparation and combustion efficiency
- Improved thermal management system for enhanced engine warm-up behaviors
- Start-stop system to eliminate fuel consumption at idling conditions

As a result, a substantial improvement in fuel efficiency by exploiting the advantages of multi-mode combustion on a turbocharged, downsized engine with high compression ratio is proposed. The research engine platform, equipped with the flexible capabilities of dual-stage turbocharging, external EGR system, electric dual-cam phasing, dual-cam profile switching, enables the investigation and development of combustion strategies to expand the HCCI operational range. In order

to cope with the complexity in combustion as well as air management, cylinder pressure sensors and Bosch's prototype intake manifold oxygen sensor supported with Bosch's latest generation engine control unit MED17 are introduced which enables development of control strategies for multi-mode combustion.

RESULTS

Multi-Mode Combustion Concept Development

Equipped with a higher than conventional compression ratio, variable valve timing and lift, multiple boosting devices, and port and direct fuel injection systems, the ACCESS prototype engine provides a powerful platform for evaluating the various methods available for exploiting the high thermal efficiencies of HCCI at higher loads. Steady-state and transient test results revealed that a combination spark assist and external EGR supplementing the internal EGR fractions afforded by negative valve overlap operation provided the best compromise of efficiency, range, and transient performance in the frequently visited areas of the engine operation map by enabling the intermediate range of dilution that exists between HCCI and conventional SI operation. Furthermore, the inclusion of external EGR in spark-assisted compression ignition (SACI) works synergistically with the benefits of cooled EGR in the upper part-load region in SI operation on high compression ratio engines, facilitating smoother mode switches and greater efficiency. This evolution of the ACCESS combustion concept from a boosted HCCI focus to include SACI and SI with cooled EGR at part loads is illustrated in Figure 1.

Engine-Level Fuel Economy and Emissions Performance

As part of the investigation, detailed maps of the efficiency and emissions performance of the combustion modes were collected. Figure 2 demonstrates the

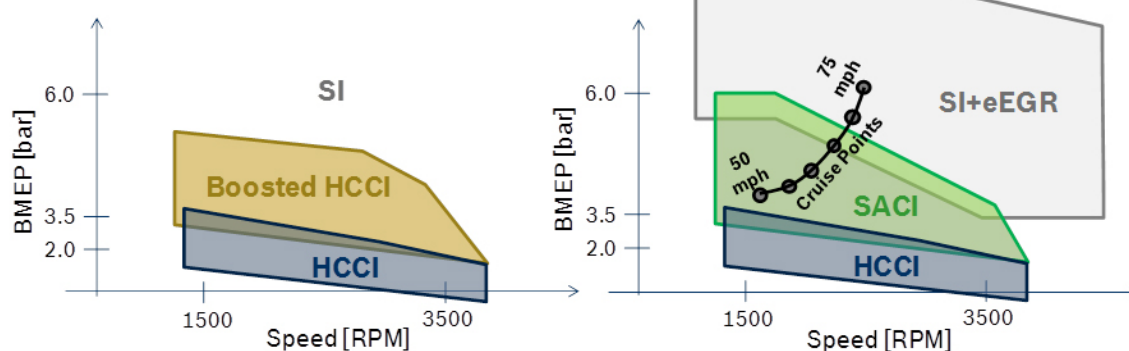


FIGURE 1. Combustion Modes and Associated Operation Ranges

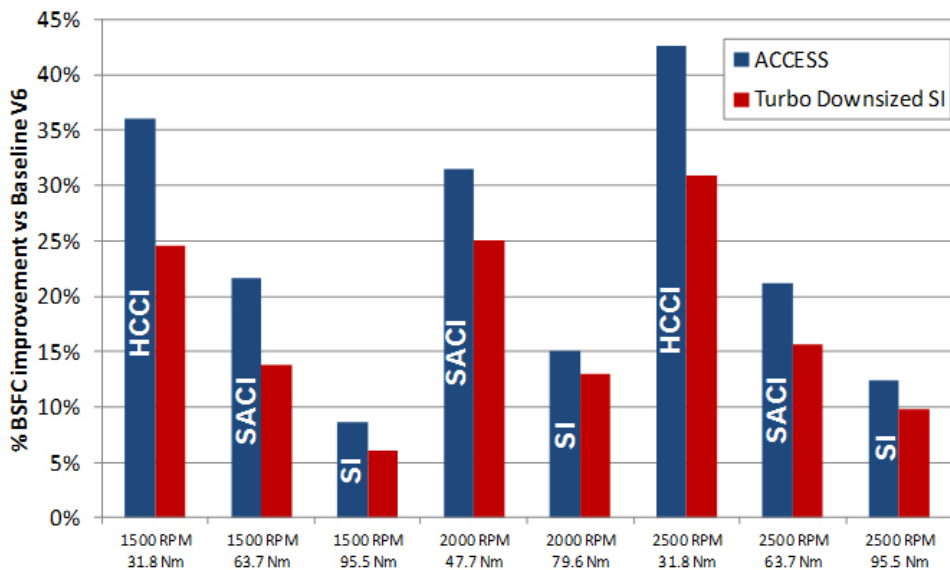


FIGURE 2. Fuel Efficiency Improvement Observed on the ACCESS Prototype II Engine at Frequently Visited Driving Cycle Operation Points

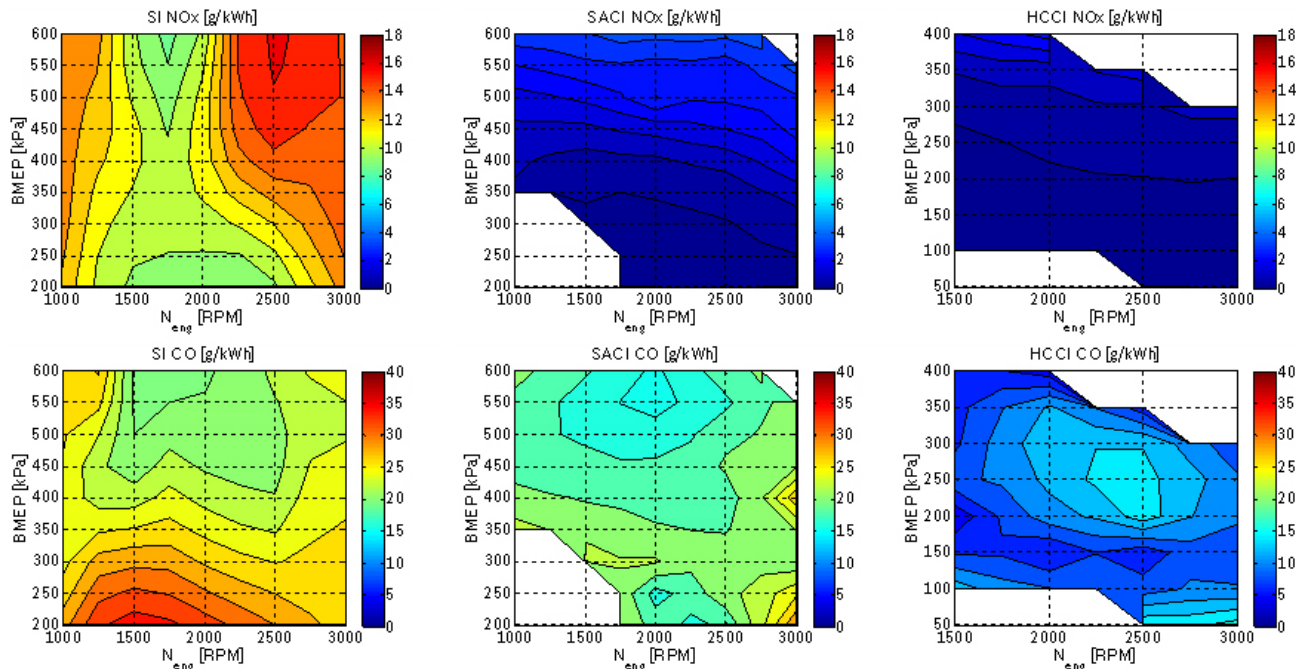


FIGURE 3. NOx and CO Engine-Out Emission Performance under Combustion Modes of SI, HCCI, and SACI Observed on the ACCESS Prototype I Engine

significant efficiency gains of the ACCESS Prototype II engine over the baseline engine with clear demonstration of the benefits of advanced combustion. The engine-out emission benefits of low-temperature combustion are also shown in Figure 3. The reduction in CO emissions shown in the first row of plots is evident,

traversing from SI to SACI to HCCI, left to right with a nearly complete reduction in oxides of nitrogen (NOx) emissions demonstrated on the second row. Although the NOx emissions in SACI operation would still likely exceed the stringent standards required for SULEV capability, the operation of SACI at stoichiometry, as

TABLE 1. Vehicle-Level Fuel Economy Simulations based on the ACCESS Prototype II Engine Combustion Optimization Data

| Engine / Combustion Modes | FE-FTP75 [mpg] | Δ FE-FTP75 [%] | FE-HWFET [mpg] | Δ FE-HWFET [%] |
|--|----------------|-----------------------|----------------|-----------------------|
| Sim: Baseline 3.6L V6 Engine / SI | 18.73 | - | 31.37 | - |
| Sim: ACCESS Prototype I Engine / SI | 23.95 | +28% | 38.05 | +21% |
| Sim: ACCESS Prototype I Engine / SI & NA HCCI (lean) | 24.77 | +32% | 38.51 | +23% |
| Sim: ACCESS Prototype I Engine / SI & NVO SACI (stoichiometric) | 24.23 | +29% | 38.45 | +23% |
| Sim: ACCESS Prototype I Engine / SI & NA HCCI (lean) & NVO SACI (stoichiometric) | 24.95 | +33% | 38.77 | +24% |
| Sim: ACCESS Prototype I Engine / SI & NVO SACI (stoichiometric) + Start-Stop | 24.83 | +32.5% | 38.48 | +23% |

shown here, enables performance of the three-way catalyst. Drive cycle simulations, updated with this steady-state Prototype II engine data, were then used to confirm the efficacy of this concept in meeting the project's fuel economy targets. Table 1 presents a variety of scenarios that could be considered with the current set of technologies developed as part of the ACCESS project and the resulting fuel economy performance, illustrating the strong potential of meeting the 25% fuel economy improvement target.

Transient Multi-Mode Combustion Emissions Performance

A variety of stoichiometric-only cases were simulated to address concerns over the transient performance of the after-treatment system in handling engine out emissions in an environment that frequently switches between lean and stoichiometric operation. As shown in Figure 4 with data from the Prototype II engine, the poor NOx conversion efficiency after sufficient lean HCCI operation to saturate the oxygen storage capacity (OSC) of the three-way catalyst and necessarily fuel-rich operation required to deplete the stored oxygen are expected to increase emissions and fuel consumption in transient operation. Augmentation of the system with a passive SCR substrate is currently underway to maximize the potential of inclusion of the lean HCCI operating area for engine-level dyno testing.

Engine Management System

Due to the lack of a direct combustion initiator, model-based control is essential for dynamic operation of HCCI combustion over driving cycle conditions. Developed based on a physics-based control-oriented model, a mid-ranging controller coordinating exhaust valve closing (EVC) and start of injection is employed in this work. The controller was validated at various

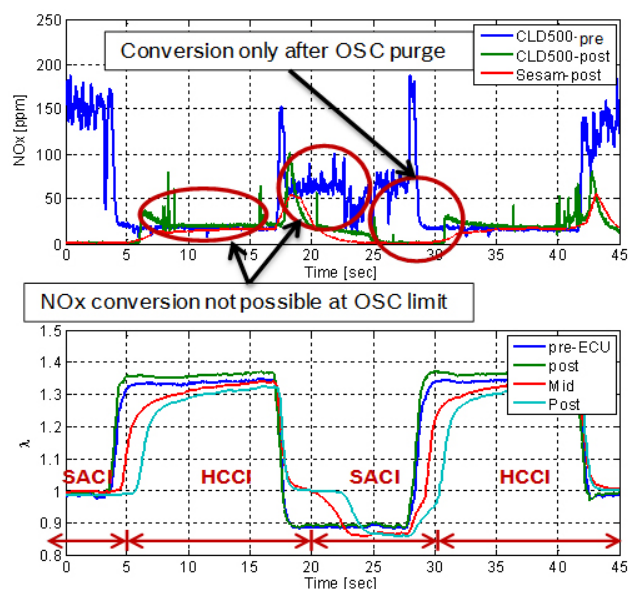


FIGURE 4. Aftertreatment Performance during HCCI-SACI Mode Switches on the ACCESS Prototype II Hardware

conditions on the single-cylinder research engine and the multi-cylinder mule engine. The proposed controller is implemented on the Prototype II engine during which it attempted to track a series of step changes in engine load, indicated by net mean effective pressure (NMEP), while maintaining a constant combustion phasing, indicated by crank angle at 50% mass fraction burn (CA50), on all cylinders. It can be observed during the experiments that the controller is able to deliver the torque steps as commanded while maintaining the desired combustion phasing through cylinder-individual injection timing and fuel mass adjustment on the cycle-to-cycle basis. With the reference cylinder set as cylinder 1 in this experiment, the controller adjusts EVC at a relatively slower pace to regulate start of injection to the set-point.

One of the major challenges with implementing HCCI on a vehicle is the requirement to switch between conventional SI mode and HCCI mode smoothly with minimal deviations in torque. Mode transitions are necessary since HCCI only covers a part of the operating range of the engine, and therefore when higher loads are required, the engine will need to transition into SI mode. A combustion mode switch strategy, during which the cam profile switching is decoupled from the combustion mode transition, was developed and first validated on the single-cylinder research engine. Such a strategy was evaluated on the Prototype II engine in an open-loop manner at selected operation conditions. Figure 5 shows the SI-HCCI mode switch performance in maintaining combustion phasing and torque output at the operation condition of 2,000 RPM, 3.8-bar NMEP on all cylinders by regulating EVC.

CONCLUSIONS

- Combustion optimization on the 2.0-L I-4 direct-injection turbocharged ACCESS Prototype II engine is completed. The proposed combustion concepts demonstrate up to 40% brake fuel efficiency improvement against the baseline 3.6-L V-6 direct-injection naturally-aspirated engine at frequently visited driving cycle conditions.
- Vehicle simulations based on the ACCESS Prototype II engine combustion optimization data, along with basic start-stop functionalities and thermal management measures, confirmed greater than 25% fuel economy improvement over the baseline 2009 Cadillac CTS vehicle over the FTP-75 driving cycle.
- A prototype three-way catalyst with metallic substrate was built and tested with the ACCESS

Prototype II engine, demonstrating 12 sec 300°C light-off time. The quick catalyst light-off performance is critical to meeting SULEV NMOC requirements.

- Control strategy development for HCCI is completed. The proposed control strategy has demonstrated desired transient performance on multiple engine platforms including the ACCESS Prototype II engine.
- Combustion and control strategies to transition between SI and HCCI modes and between SI and SACI have been developed. The proposed strategies have demonstrated desired performance at selected operating conditions on a single-cylinder research engine and the ACCESS Prototype II engine.
- The integration of the ACCESS Prototype II engine into the demonstration vehicle is completed. Start-stop functionality and base vehicle calibration for SI mode is also completed. The demonstration vehicle is ready for emission performance evaluation.

FY 2013 PUBLICATIONS/PRESENTATIONS

- J. Wheeler, D. Polovina, V. Frasinol, O. Miersch-Wiemers, A. Mond, J. Sterniak, and H. Yilmaz, "Design of a 4-Cylinder GTDI Engine with Part-Load HCCI Capability", 2013 SAE World Congress, Detroit, MI, April 16–18, 2013.
- D. Polovina, D. McKenna, J. Wheeler, J. Sterniak, O. Miersch-Wiemers, A. Mond, H. Yilmaz, "Steady-State Combustion Development of a Downsized Multi-Cylinder Engine with Range Extended HCCI/SACI Capability", 2013 SAE World Congress, Detroit, MI, April 16–18, 2013.
- J. Su, W. Lin, J. Sterniak, M. Xu, S. Bohac, "Particulate Matter Emission Comparison of Spark Ignition Direct Injection (SIDI) and Port Fuel Injection (PFI) Operation of a Boosted

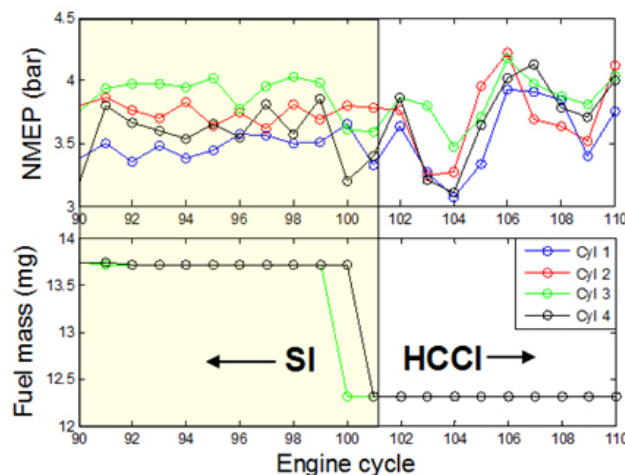
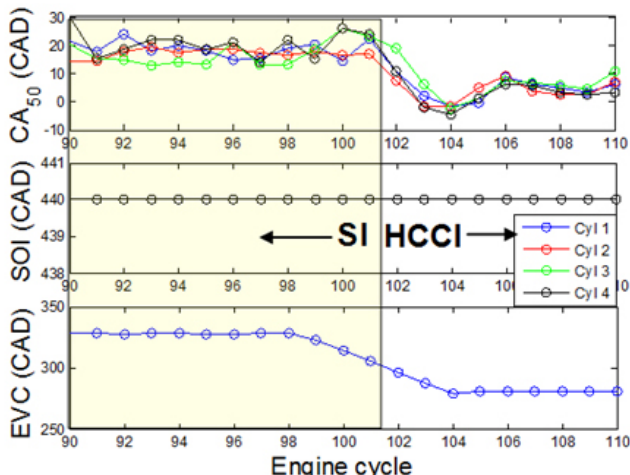


FIGURE 5. SI-HCCI Open-Loop Mode Switch—NMEP and Fuel Mass



Gasoline Engine”, ASME 2013 Internal Combustion Engine Division Fall Technical Conference, Dearborn, Michigan, October 13–16, 2013.

- 4.** W. Lin, J. Sterniak, and S. Bohac, “NOx Emissions Characterization During Transient Spark Assisted Compression Ignition (SACI) Engine Operation”, ASME 2013 Internal Combustion Engine Division Fall Technical Conference, Dearborn, Michigan, October 13–16, 2013.
- 5.** A. Vaughan, and S. Bohac, “A Dynamical System Approach to Predicting HCCI Burn Phasing During Transients and at Operating Points with High Cyclic Variability”, ASME 2013 Internal Combustion Engine Division Fall Technical Conference, Dearborn, Michigan, October 13–16, 2013.
- 6.** P. Shingne, M. Gerow, V. Triantopoulos, S. Bohac, J. Martz, “A Comparison of Valving Strategies Appropriate for Multi-Mode Combustion within a Downsized Boosted Automotive Engine Part A: High Load Operation within the SI Combustion Regime”, ASME 2013 Internal Combustion Engine Division Fall Technical Conference, Dearborn, Michigan, October 13–16, 2013.
- 7.** M. Gerow, P. Shingne, V. Triantopoulos, S. Bohac, and J. Martz, “A Comparison of Valving Strategies Appropriate for Multi-Mode Combustion within a Downsized Boosted Automotive Engine Part B: Low to Moderate Load Operation within the SACI Combustion Regime”, ASME 2013 Internal Combustion Engine Division Fall Technical Conference, Dearborn, Michigan, October 13–16, 2013.
- 8.** N. Ravi, M. Jagsch, J. Oudart, N. Chaturvedi, D. Cook, and A. Kojic, “Closed Loop Control of SI-HCCI Mode Switch using Fuel Injection Timing”, 2013 ASME Dynamic Systems and Control Conference, Palo Alto, CA, October 21–23, 2013.
- 9.** J. Larimore, E. Hellström, S. Jade, L. Jiang, and A. Stefanopoulou, “Controlling Combustion Phasing Variability with Fuel Injection Timing in a Multicylinder HCCI Engine”, 2013 American Control Conference, Washington D.C., June 17–19, 2013.
- 10.** S. Jade, J. Larimore, E. Hellström, L. Jiang, A. Stefanopoulou, “Enabling Large Load Transition on Multicylinder Recompression HCCI Engine using Fuel Governors”, 2013 American Control Conference, Washington D.C., June 17–19, 2013.
- 11.** S. Nuesch, E. Hellström, L. Jiang, A. Stefanopoulou, “Influence of Transitions between SI and HCCI Combustion on Driving Cycle Fuel Consumption”, 2013 European Control Conference, Zurich, Switzerland, July 17–19, 2013.
- 12.** J. Larimore, S. Jade, E. Hellström, J. Vanier, L. Jiang, and A. Stefanopoulou, “Online Adaptive Residual Mass estimation in a Multicylinder Recompression HCCI Engine”, 2013 ASME Dynamic Systems and Control Conference, Palo Alto, CA, October 21–23, 2013.
- 13.** E. Hellström, Anna Stefanopoulou, and Li Jiang, “A Linear Least-Squares Algorithm for Double-Wiebe Functions Applied to Spark-Assisted Compression Ignition”, In Proceedings of ASME 2013 Internal Combustion Engine Division Fall Technical Conference, Dearborn, Michigan, October 13–16, 2013.

14. E. Hellström, A. Stefanopoulou, and L. Jiang, “Cyclic variability and dynamical instabilities in autoignition engines with high residuals”, IEEE Transaction on Control System Technology, 21(5): 1527-1536, 2013.

15. V. Janakiraman, X. Nguyen, and E. Assanis, “Nonlinear Identification of a Gasoline HCCI Engine Using Neural Networks Coupled with Principal Component Analysis”, Applied Soft Computing Journal, 13(5): 2375-2389, 2013

16. V. Janakiraman, X. Nguyen, and E. Assanis, “A Lyapunov Based Stable Online Learning Algorithm for Nonlinear Dynamical Systems using Extremum Learning Machines”, 2013 International Joint Conference on Neural Networks.

17. J. Kodavasal, M. McNenly, A. Babajimopoulos, S. Aceves, D. Assanis, M. Havstad, D. Flowers, “An Accelerated Multi-Zone Model for Engine Cycke Simulation (AMECS) of HCCI Combustion”, International Journal of Engine Research, doi: 10.1177/1468087413482480, 2013.

SPECIAL RECOGNITIONS & AWARDS/ PATENTS ISSUED

- 1.** E. Hellström, A. Stefanopoulou, L. Jiang, and J. Larimore, “Predictive Modeling and Reducing Cyclic Variability in Autoignition Engines”, Application US 13/621,539, Filed on September 17, 2012. *Pending*
- 2.** E. Hellström, A. Stefanopoulou, L. Jiang, and J. Larimore, “Dynamic Estimator for Determining Operating Conditions in an Internal Combustion Engine”, Application US 13/621,527, Filed on September 17, 2012. *Pending*
- 3.** S. Jade, E. Hellström, L. Jiang, and A. Stefanopoulou, “Fueling Strategy for Controlled-Autoignition Engines”, Application US 13/621,433, Filed on September 17, 2012. *Pending*
- 4.** S. Jade, E. Hellström, L. Jiang, and A. Stefanopoulou, “Fuel Governor for Controlled Autoignition Engines”, Application US 13/621,425, Filed on September 17, 2012. *Pending*
- 5.** A. Mond and L. Jiang, “Combustion Mode Switching with a Turbocharged / Supercharged Engine”, Application US 13/679,010, Filed on November 16, 2012. *Pending*
- 6.** L. Jiang, and N. Ravi, “Path Planning during Combustion Mode Switch”, Application US 13/681,499, Filed on December 14, 2012. *Pending*
- 7.** L. Jiang, J. Sterniak, and J. Schwanke, “Combustion Control with External Exhaust Gas Recirculation (EGR) Dilution”, Application US 13/951,658, Filed on July 26, 2013. *Pending*

IV.9 Recovery Act – A MultiAir/MultiFuel Approach to Enhancing Engine System Efficiency

Ron Reese

Chrysler Group, LLC

800 Chrysler Drive

Auburn Hills, MI 48326

DOE Technology Development Manager:

Ken Howden

NETL Project Manager: Ralph Nine

Subcontractors:

- The Ohio State University (OSU), Columbus, OH
- Bosch, Farmington, MI
- Delphi, Troy, MI
- Argonne National Laboratory (ANL), Argonne, IL

Overall Objectives

- Demonstrate 25% improvement in combined City and Highway Federal Test Procedure (FTP) fuel economy in a Chrysler minivan
- Accelerate the development of highly efficient engine and powertrain systems for light-duty vehicles, while meeting future emissions standards
- Create and retain jobs in support of the American Recovery and Reinvestment Act of 2009

Fiscal Year (FY) 2013 Objectives

- Complete Alpha 2 engine procurement and builds and perform dynamometer tests to demonstrate durability and ability to meet performance, emissions and 25% fuel economy improvement goals
- Develop system controls functionality and calibration for Alpha 2 engine
- Complete the build of two vehicles and begin in-vehicle calibration work
- Complete thermal management system assessment in a surrogate vehicle and conduct drive cycle fuel economy testing in vehicle
- Update design of pendulum crankshaft and evaluate crankshaft in surrogate vehicle and incorporate in Alpha 2 engines
- Calibrate/validate Vehicle Energy Simulator model with OSU and integrate/calibrate the Vehicle Energy Model

- Continue diesel micro pilot (DMP) engine testing and simulation work at ANL to further investigate the potential efficiency improvements

FY 2013 Accomplishments

- All five Alpha 2 engines were built. Over 1,200 hours of dynamometer testing has been completed and the Alpha 2 engines have demonstrated they meet efficiency and performance targets.
- Controls and base calibration have been delivered for verification in the Alpha 2 engines.
- The first vehicle was built and verification is underway. Second vehicle build has started.
- Delphi has developed and verified algorithms to predict combustion feedback information (crank angle for 50% heat release, knock, and coefficient of variation of indicated mean effective pressure) based on the ion-sensed signals from the ignition coils.
- Thermal systems were installed in dynamometers and test vehicles. Thermal system models for both the high- and low-temperature radiators were completed.
- A third iteration of the pendulum crankshaft was created and tested. A new seven-pendulum crankshaft was installed in the surrogate engine for verification.
- DMP engine development testing done at ANL shows impressive brake specific fuel consumption results at high loads (40% brake thermal efficiency) under a slightly wider range of operation. Simulation models have been developed to determine optimized conditions for diesel mass fraction and timing, exhaust gas recirculation (EGR) rate and cam timing.

Future Directions

- Complete refinement and verification of the system controls and calibration of Alpha 2 engine on dynamometer and in vehicle to meet all performance, emissions, fuel economy and drivability targets
- Complete thermal management system control and calibration to improve fuel economy
- Optimize shift schedule and lock-up in vehicle to fully utilize the capability of the pendulum crankshaft

- Continue DMP combustion learning through continued engine testing and simulation efforts at ANL
- Perform FTP testing on rolls to demonstrate fuel economy improvement and emission levels
- Demonstrate in-vehicle drivability and performance to compare with baseline vehicle



INTRODUCTION

The purpose of this project is to demonstrate 25% improvement in fuel economy while maintaining comparable vehicle performance compared to the baseline engine (a state-of-the-art 4.0-L V-6) while meeting Tier 2, Bin 2 tailpipe emissions. This project will down-size and down-speed the engine through combustion improvements via a combination of engine technologies with concurrent development of other system enhancements.

Main technologies explored as part of this development project include in-cylinder combustion improvements, waste heat recovery via thermal management strategies, friction reduction, ancillary load management and emissions controls.

APPROACH

Complete two engine design/development iterations. Each iteration encompassed two development phases—one for design/simulation efforts, the second for procurement, engine build and test. The combination of Phases 1 and 2 resulted in the Alpha 1 engine. Phases 3 and 4 incorporated the learning from early phases to produce the Alpha 2 engine. This engine will be used in the Phase 5 Fuel Economy Demonstration.

RESULTS

Mechanical development tests were performed to prove the capability of the Alpha 1 and Alpha 2 engines. The compression ratio was increased to 12.0:1 and improvements were made to the power cell and lower end to reduce friction and improve efficiency in the Alpha 2 engine. The exhaust and turbo system were also improved to reduce temperature loss across the turbos and reduce the packaging space. Improvements in fuel efficiency have been quantified at several speeds and loads (Figure 1).

The powertrain dynamometer is operational and capable of running starts and conducting transient operations. Development and verification efforts focused

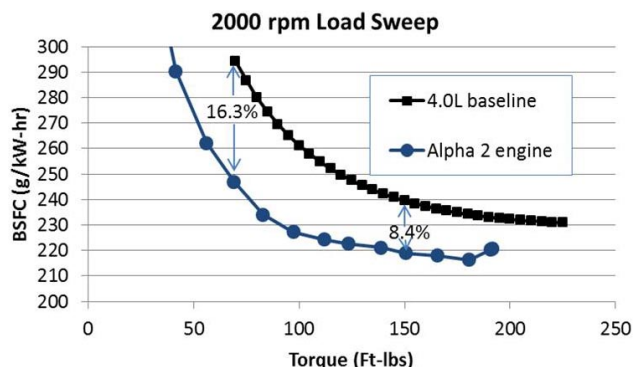


FIGURE 1. 2,000 RPM Load Sweep

on cold-start testing and successful execution of the first hill of the FTP cycle. In this environment, the Alpha 2 engine and transmission are capable of shifting through all gears and collecting emissions and temperature data.

Simulated cold-start tests were run in the engine dynamometer test cell to develop the fueling and secondary air strategy. Initial testing indicated that catalyst temperatures were lower than anticipated. Variations in injection timing, multiple injection fractions, secondary air rates and fuel enrichment were run to determine the best trade-off of emissions and catalyst temperature. Additional actions are being explored to optimize this trade-off including the addition of a turbo bypass to more directly route the exhaust to the catalyst during cold starts which further accelerates the catalyst light-off by 3 seconds (see Figures 2 and 3).

Control software for the Alpha 2 engine was delivered. Models for the high- and low-temperature radiators, and auxiliary loads charging controls were completed.

The control system was implemented to handle simultaneous control of ethanol and gasoline injection using separate injectors. This allows flexibility to modify ethanol percent content in real time for the next firing cylinder. That, coupled with the capability to measure the flame propagation, led to the development of control algorithms that predict the ethanol fuel mass necessary to optimize combustion phasing. Optimal engine operation was achieved by varying EGR and/or ramping the ethanol fraction from 20 to 90%.

Additional work on the one-dimensional/three-dimensional engine simulation was completed by Chrysler and ANL on the triple plug and DMP-equipped engine models. Genetic algorithm simulations using CONVERGE™ were run to find optimal parameter conditions for DMP resulting in a 7% indicated specific fuel consumption reduction from the baseline condition (Figure 4). Injector spray modeling work focused on

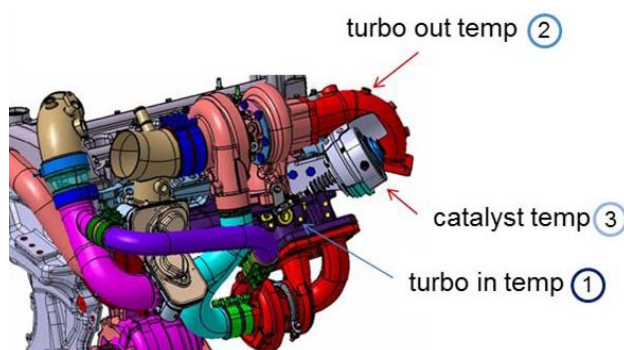


FIGURE 2. Cold-Start Catalyst Temperature Engine-Only Surrogate Test Setup



FIGURE 5. Alpha 2 Multi-Air Multi-Fuel Engine in Vehicle

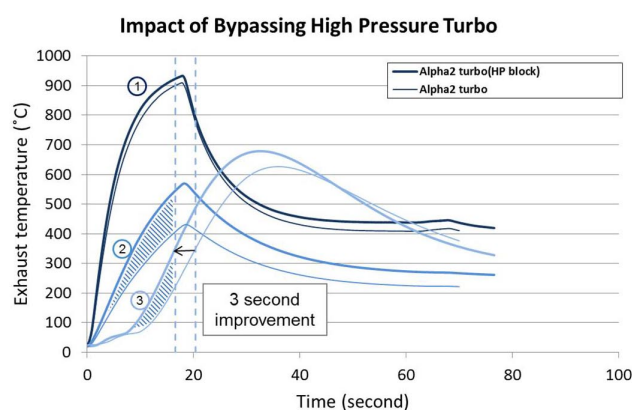


FIGURE 3. Impact of Bypassing High-Pressure Turbo

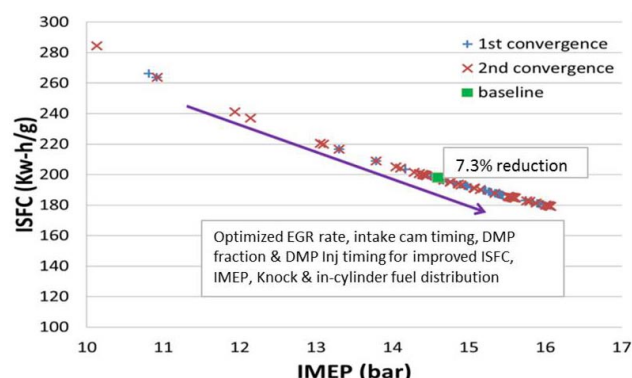


FIGURE 4. Genetic Algorithm Simulation Results—Fuel Consumption

improving the model to better correlate with the imaging data from ANL's Advanced Photon Source.

Delphi continued development of combustion feedback parameters with ion-sensed signals. Algorithm development and artificial neural network training resulted in good prediction of combustion phasing, knock detection and combustion stability predictions. Delphi's

cylinder pressure-based combustion feedback system is installed in the first vehicle for use with production-grade cylinder pressure sensors for comparison to the ion-sense results.

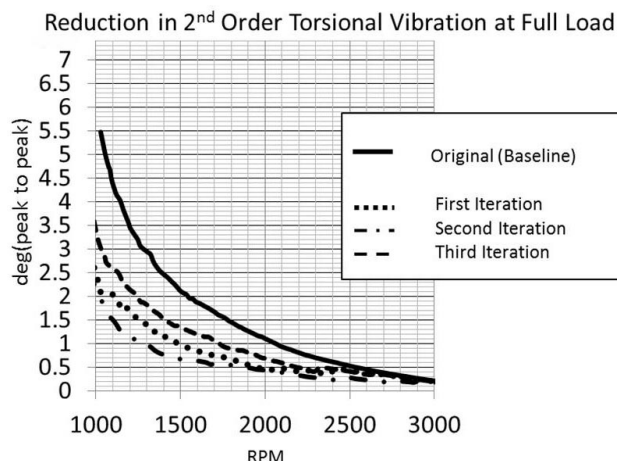
Thermal management components were installed in the powertrain dynamometer in advance of the vehicle so components would mimic the real location of such components in the vehicle. This allowed capturing gravity and transient effects of different fluids on thermal component performance and ensured realistic fluid volumes in the hose and tube routings. Thermal components were then installed in the test vehicle.

The first vehicle build was completed and communication between vehicle and powertrain was verified (Figure 5). Engine calibration and software was loaded in the fourth quarter and engine first fire was also achieved. The second vehicle build was started.

The design and verification of the pendulum crankshaft has identified necessary trade-offs between vibration correction and noise-free low-speed engine operation. High-speed video revealed the idle noise was attributable to pendulums reaching motion stops, causing noise. The tuning of the pendulums was adjusted to reduce idle noise performance but reduced correction percentages. The first iteration curve reflects 2013 corrected second order full-load torsional vibration (Figure 6). The crankshaft has been evaluated as "commercial" in terms of its noise performance at idle.

CONCLUSIONS

- Alpha 1 and Alpha 2 dynamometer test modeling and simulation results show the efficiency goals are met. Development of the controls and calibrations

**FIGURE 6.** Reduction in 2nd Order Torsional Vibration at Full Load

are underway to assure the in-vehicle testing will achieve project goals.

- Testing at ANL on the DMP system has shown improved usage range over last year, but is still too restrictive for in-vehicle use with an automatic control system and transient operation conditions. Engine efficiency at high load is improved with a diesel fuel ignition system, but only marginally better than the gasoline engine at loads up to 14 bar brake mean effective pressure. Addition of ethanol allows improved knock relief at loads above this to allow the performance goals to be reached while still running stoichiometric fueling and high dilution without the sensitivities that DMP exhibits.

FY 2013 PUBLICATIONS/PRESENTATIONS

1. 2013 DOE Vehicle Technologies Program Annual Merit Review (AMR), May 2013.
2. Advanced Engine Combustion (AEC) MOU Meeting (Sandia National Laboratory) – “Multi-Dimensional Modeling and Validation of Combustion in a High-Efficiency Dual-Fuel Light-Duty Engine”.
3. ASME Paper Number: ICEF2013-19170. Paper Title: Numerical Study of the Combustion Characteristics of a Diesel Micro Pilot Ignited DI Gasoline Engine with Turbocharging and Cooled EGR.
4. SAE Paper Presented - 2013 SAE World Congress in Detroit on April 17, 2013 by Dr. Gerard Malaczynski. Paper Number: 2013-01-0354. Paper Title: Ion-Sense-Based Real-Time Combustion Sensing for Closed Loop Engine Control.

SPECIAL RECOGNITIONS & AWARDS/ PATENTS ISSUED

1. “Centrifugal switch Pendulum Deactivation,” for control of start/stop clatter in crank pendulum absorbers, joint w/ MSU. (Disclosure number assigned: 709290)
2. I. Glanfield, B. Geist, “Retainer – Pendulum”, patent application submitted for Chrysler IDR # 709297.
3. I. Glanfield, B. Geist, “Pendulum Anti Rattle Treatment”, patent application submitted for Chrysler IDR # 709298.

IV.10 Development of Radio Frequency Diesel Particulate Filter Sensor and Controls for Advanced Low-Pressure Drop Systems to Reduce Engine Fuel Consumption

Alexander Sappok (Primary Contact),
Leslie Bromberg, Peter Koert
Filter Sensing Technologies, Inc.
P.O. Box 425197
Cambridge, MA 02141

DOE Technology Development Manager:
Roland Gravel

NETL Project Manager: Ralph Nine

Subcontractors:

- Corning, Inc., Corning, NY
- FEV Inc., Auburn Hills, MI
- Oak Ridge National Laboratory, Knoxville, TN
- Maguffin Microwaves, LLC, Andover, MA

Overall Objectives

- Demonstrate and quantify improvements in efficiency and greenhouse gas reductions through improved diesel particulate filter (DPF) sensing, controls, and low-pressure drop components.
- Design, develop, and validate radio frequency (RF) sensor performance for accurate real-time measurements of DPF loading with low-pressure drop substrates.
- Achieve breakthrough efficiencies via use of advanced combustion modes, alternative fuels, and advanced aftertreatment enabled by improved sensing and controls.
- Develop production sensor designs and commercialization plans on the scale required to significantly impact reduction in greenhouse gas emissions and fuel consumption.

Fiscal Year (FY) 2013 Objectives

- Design and develop RF sensor prototype systems (hardware and software) to measure the loading state of DPFs, and optimize engine and DPF operation.
- Quantify RF sensor performance relative to gravimetric standard for DPF soot and ash mass loading in light- and heavy-duty applications.
- Identify potential sources of error on the RF measurements, quantify effect of external variables

on measurement accuracy, and develop correction methods if needed.

- Begin 24-month on-road fleet tests to quantify potential fuel savings and evaluate RF system performance and reliability in the field.

FY 2013 Accomplishments

- Designed and developed alpha prototype RF sensor systems, supplied to project partners, for testing on light- and heavy-duty engine dynamometers and heavy-duty fleet vehicles.
- Demonstrated potential for 50% to 75% regeneration-related fuel savings through on-road fleet testing with heavy-duty vehicles equipped with RF sensors. Conducted follow-on testing to confirm results in controlled laboratory setting.
- Confirmed sensor accuracy to measure DPF soot levels up to 8 g/L.
- Identified and quantified effects of external variables on sensor accuracy including temperature, exhaust flow, water vapor, hydrocarbon dosing, and soot/ash buildup on the sensor. Quantified part-to-part variability less than 0.35% with the DPFs in this study.
- Developed and applied RF cavity models to guide sensor design and characterize spatial resolution of the RF measurement technique. Validated model results via experiments. Reported results in technical publication presented at American Society of Mechanical Engineers (ASME) Internal Combustion Engines Conference in Dearborn, MI.
- Attained sensor response time of less than 2 seconds over a 1 GHz bandwidth for accurate transient measurements.
- Developed and tested novel antenna designs, that resulted in a patent application. New antennas have an overall size and form-factor similar to conventional temperature sensors. On-road durability testing currently ongoing, with no issues to date.
- Demonstrated ability to measure DPF ash levels up to 42 g/L with accelerated ash loading and RF sensor thermal cycling equivalent to 240,000 miles of on-road use.

Future Directions

- Quantify RF sensor measurement accuracy relative to gravimetric standard over a range of engine platforms and aftertreatment system configurations through testing with project partners including Corning, Oak Ridge National Laboratory, FEV, and the City of New York Department of Sanitation.
- Design and develop pre-production beta RF sensing system meeting manufacturer requirements, and supply systems to project partners for testing and performance evaluation.
- Develop optimized aftertreatment control strategies, utilizing input from the RF sensor, and demonstrate potential fuel savings and reduced system costs enabled through accurate measurement of the filter loading state and advanced low-pressure drop aftertreatment.
- Evaluate additional efficiency gains possible through the use of advanced combustion modes and alternative fuels in conjunction with RF aftertreatment sensing and control.



INTRODUCTION

Diesel engines present one of the most promising, readily available technologies to achieve efficiency improvements in light-duty applications and are the power plant of choice for most heavy-duty vehicles. However, the need to use advanced aftertreatment systems, and DPFs in particular, to meet current emissions regulations is a significant hurdle. The Vehicle Technologies Program Multi-Year Program Plan has identified challenges associated with the use of diesel particulate filters, namely: (1) additional cost and energy usage, (2) lack of “ready to implement” sensors and controls required for sophisticated feedback systems, and (3) demanding durability requirements for both light and heavy-duty applications [1].

This project directly addressed these challenges by demonstrating a robust RF sensor and control system, for use with next-generation, low-pressure-drop aftertreatment devices, to reduce engine fuel consumption while still meeting emissions requirements. Several RF sensor prototypes were developed and tested during the first year of this project. The results show the ability to measure DPF soot and ash levels up to 8 g/L and 42 g/L, respectively. Accelerated aging studies were conducted to simulate over 240,000 miles of on-road ash aging and thermal cycling of the DPF and RF sensor. On-road fleet testing with several heavy-duty vehicles has shown the potential to reduce the fuel required for DPF

regenerations by 50% to 75%, based on measurements with the RF sensor relative to the stock control system. Compared to current pressure- and model-based control systems, direct measurement of the filter loading state will enable a step change in engine and aftertreatment system control, improved durability, and reduce system cost and complexity, while delivering tangible performance benefits.

APPROACH

The approach taken in this project is to identify, address, and overcome key technical challenges to successful RF sensor implementation early on, by leveraging knowledge gained from past research and development efforts conducted by Filter Sensing Technologies and in collaboration with national laboratories, industry, and academia [2,3]. This approach, implemented in four project phases, will develop several RF sensor prototypes, and conduct an extensive series of evaluations to quantify measurement accuracy and potential sources of error, relative to a gravimetric standard. Evaluation of the RF sensor will be carried out on a range of light- and heavy-duty applications through engine testing at Corning, Oak Ridge National Laboratory, and FEV, as well as over 48 months of cumulative on-road testing with the New York City Department of Sanitation.

Following this phased approach, sensor prototypes were developed in the first project phase, guided by RF system simulations and bench tests. Successful testing in this first phase has led to designs for the pre-production RF sensor, and resulted in a patent application covering a novel, production-intent sensor design. These pre-production sensors will be completed in the next FY, and used to develop an optimized engine and aftertreatment system control strategy based on input from the RF sensor, together with FEV. Finally, performance data with the optimized control system will be used to quantify efficiency gains and estimate aftertreatment system costs reduction and extended component life enabled by RF sensing and feedback control.

RESULTS

Development of the RF sensor followed a model-based design process, utilizing the RF cavity simulations developed at Filter Sensing Technologies. Figure 1 presents an example of the model results, showing the electric field distributions for the first two resonant modes in Figure 1(a) and Figure 1(b), respectively. Bench tests were conducted to validate the simulations by varying the soot distribution in the axial and radial directions in the DPF. Also shown in Figure 1(a) and (b) is the measured axial variation in the RF transmission parameter (S21)

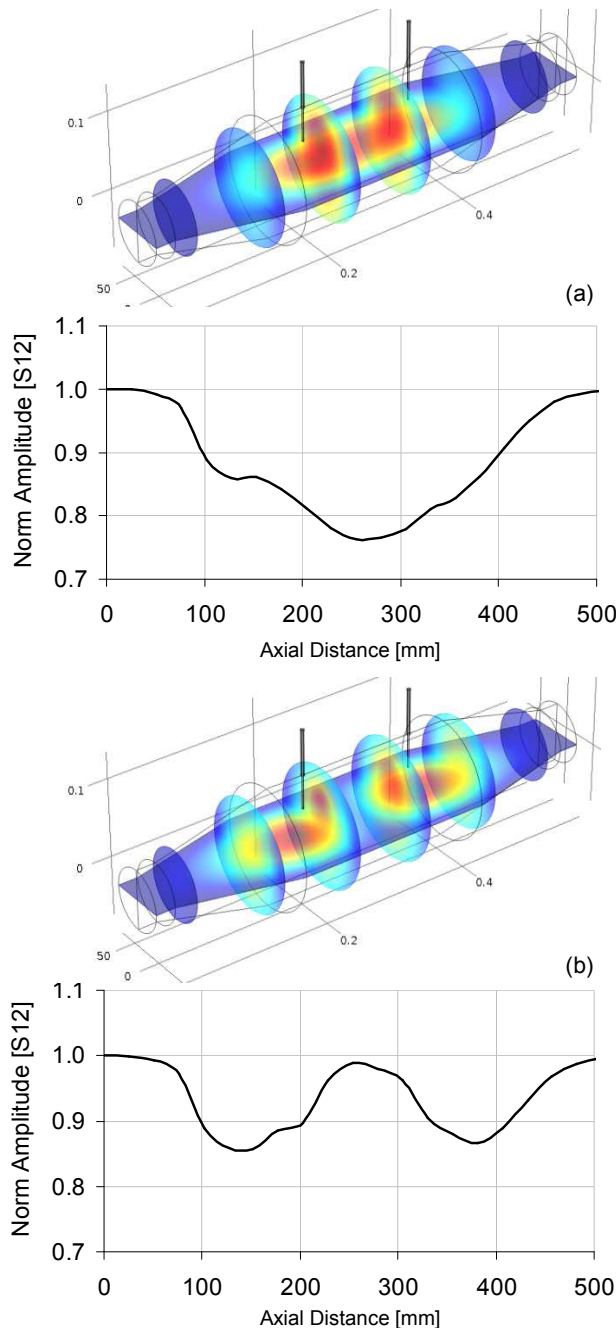


FIGURE 1. Comparison of simulation results with experiments showing predicted and experimentally-verified electric field distributions for first (a) and second (b) resonant modes. Electric field distribution corresponds to spatial resolution of the measurement.

corresponding to the first two resonant modes simulated in the model. In all, the models and experiments covered five resonant modes over a 1 GHz bandwidth, to characterize the spatial resolution of the RF measurements. The detailed results and their application to sensor design were presented in an ASME technical publication at the 2013 Fall Internal Combustion Engines Technical Conferences in Dearborn, MI.

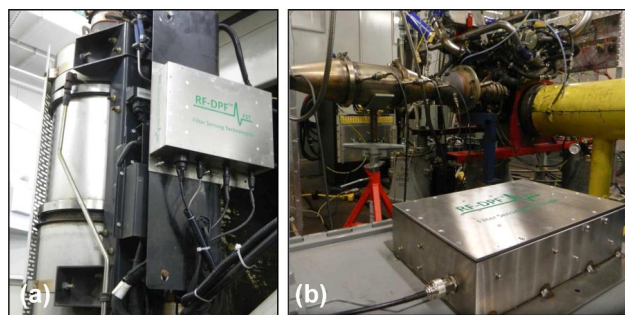


FIGURE 2. RF sensors prototype and control unit installed next to DPF on the exhaust stack of a heavy-duty truck for fleet testing (a) and installed on a light-duty General Motors engine at Oak Ridge National Laboratory (b).

In addition to guiding sensor design, the RF cavity models were also applied to parametric studies to quantify the sensitivity of the RF signal to geometric variations in the filter housing. Complementary engine and bench tests were also conducted to quantify the effects of variations in end-cone design, antenna alignment, and filter materials (cordierite and aluminum titanate), as well as filter coatings on the RF signal. Results from tests with an initial batch of heavy-duty cordierite filters supplied by Corning showed part-to-part variability less than 0.35% for the RF sensor installed on this particular sample of nominally the same filters.

Results of the parametric studies, bench tests, and simulations were used to down-select the final prototype system designs. A vector measurement system was selected for the final design, as it enabled additional degrees of freedom for the RF measurements. Figure 2(a) shows the prototype system installed adjacent to the exhaust stack on a heavy-duty vehicle equipped with a 2009 Mack MP-7 diesel engine and actively regenerated DPF. Figure 2(b) shows another prototype unit installed at Oak Ridge Nation Laboratory on a light-duty 1.9-L General Motors diesel engine. All prototype systems contained integral data acquisition and control systems, in addition to the RF electronics (which comprise only a small portion of the overall form factor). Self diagnostic functions were also developed for the sensor to detect faults with either the internal sensor electronics or external antennas, each time the system is powered on.

The prototype systems shown in Figure 2 were subjected to an extensive series of tests at Filter Sensing Technologies and with several project partners. Figure 3 presents a comparison of the soot load measured using the RF sensor with the gravimetric measurements from 0 g/L to 8 g/L. Although 8 g/L is generally above the typical measurement range for most cordierite applications, the initial tests quantified sensor performance over the full range and identified means of

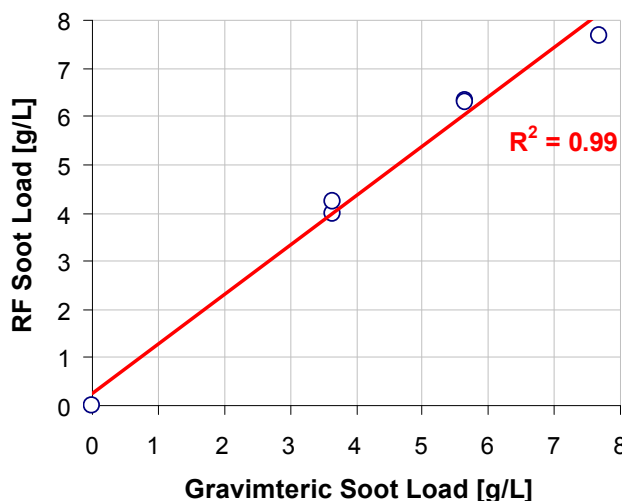


FIGURE 3. Comparison of RF and gravimetric measurements of DPF soot load up to 8 g/L.

extending the range even further, should measurement of high soot levels be required.

Figure 4 shows similar results, comparing the RF-measured ash in the DPF with gravimetric measurements, up to a maximum ash load of 42 g/L. Aside from RF sensing, the authors are unaware of commercial on-vehicle sensing technologies capable of accurately measuring both soot and ash in the DPF. The maximum ash load achieved in this study is estimated to be equivalent to approximately 240,000 miles of on-road ash accumulation. Use of a burner-based system for the accelerated ash loading also subjected the RF sensing elements to repeated high temperature regenerations (in excess of 650°C) with no detrimental effects on the antennas.

Considerable efforts were also devoted to exploring possible sources of error on the RF signal, and developing improved system designs or correction algorithms for significant error sources, as needed. The experiments and simulations covered the impacts of: water vapor, exhaust flow rate, temperature, hydrocarbon dosing and slip through the diesel oxidation catalyst, as well as soot and ash build-up on the antenna probes. Of all the variables investigated, the temperature dependence of the soot dielectric properties was found to be the most significant factor, and temperature compensation methods have been developed and implemented. Relative to the other error sources, the signal attenuation due to soot accumulation in the DPF was approximately an order of magnitude greater (normalized on a per unit mass basis). Figure 5 presents the variation in DPF pressure drop with varying exhaust flow rate, and shows no impact of flow rate variations on the RF signal.

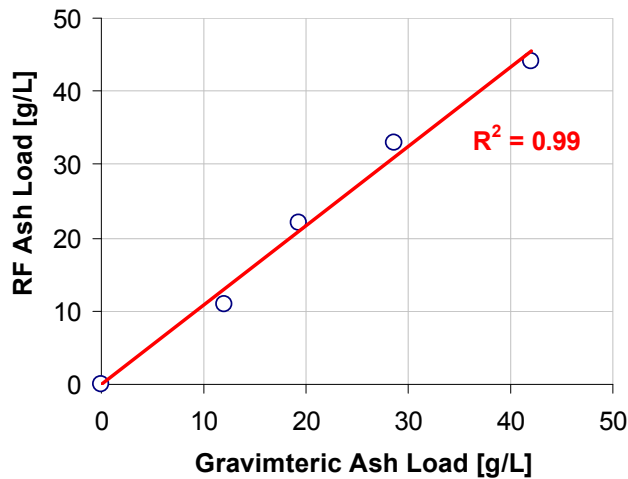


FIGURE 4. Comparison of RF and gravimetric measurements of DPF ash load up to 42 g/L. Ash level of 42 g/L corresponds to approximately 240,000 miles of on-road operation.

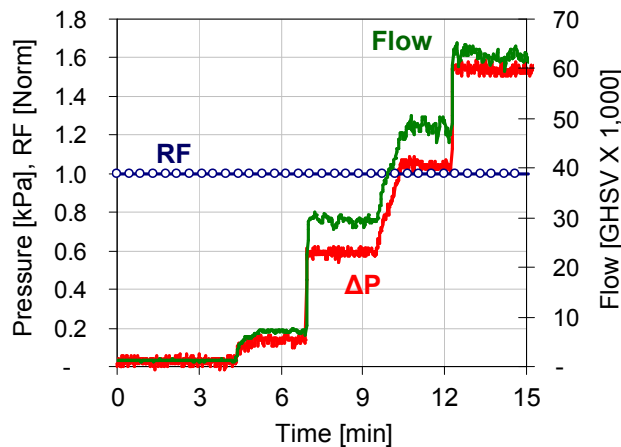


FIGURE 5. Effect of increasing exhaust flow rate through the DPF on pressure drop and RF signal response, showing the RF signal to be unaffected by variations in exhaust flow.

On-road fleet testing with two prototype systems, shown in Figure 2, was also initiated towards the end of this project phase. To date, each system has accumulated slightly over two months of on-road operation, with over 48 months of cumulative on-road testing planned by the end of this project. The systems were fitted on heavy-duty vehicles with 2009 Mack MP-7 engines, which employ an exhaust burner for DPF regeneration. The results in Figure 6 show two high-temperature regeneration events with filter inlet temperatures in excess of 700°C, measured near the periphery of the filter. Although the stock control system triggered two regeneration events in short succession, labeled (A) and (B) in Figure 6, with the first lasting 16 minutes and the second lasting 19 minutes,

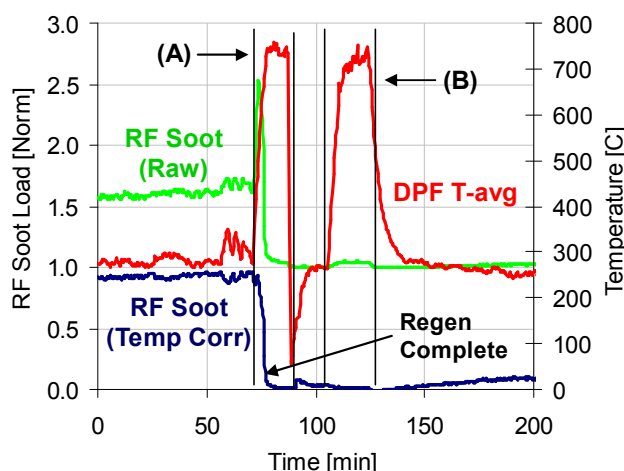


FIGURE 6. Vehicle data from a heavy-duty truck showing rapid soot oxidation during high temperature regenerations and potential for regeneration fuel savings of 50% to 75% through accurate measurement of DPF soot levels using RF sensing.

the RF sensor shows complete soot oxidation within the first 6 minutes of the first regeneration at these high temperatures. These results, typical of the regenerations observed in the fleet tests to date, have been duplicated in the lab, with similar high-temperature regenerations to confirm complete soot oxidation via gravimetric measurements and validate the RF measurements. Previous studies at Oak Ridge National Laboratory with an electrically regenerated filter have shown similar rapid oxidation at such high temperatures [4]. Thus, the data to date indicates potential regeneration fuel savings of 50% to 75% possible via accurate sensing enabled by the RF sensor.

Ongoing work will further quantify fuel savings potential over extended on-road operation with the current and next-generation pre-production sensor systems. Work with Daimler Trucks North America and FEV has served to define sensor requirements for the next iteration of the prototype, which will exhibit a form factor similar to a typical oxides of nitrogen sensor, and contain a production-intent antenna system (currently undergoing fleet testing) and the subject of a recent patent application. Proof-of-concept testing has demonstrated sensor response times less than 1.8 seconds and confirmed response times less than 1 second to be possible in the pre-production systems at no additional expense, thereby enabling accurate transient measurements. Future work will focus on controls development and extensive testing of the next-generation sensors, to quantify system performance, efficiency, and potential cost savings.

CONCLUSIONS

Completion of the first phase of this project has resulted in significant progress toward achieving the overall project objectives. Specific accomplishments are the following:

- Developed and demonstrated initial prototype RF sensors and initiated designs for pre-production systems, resulting in one new patent application covering novel RF antennas.
- Demonstrated RF sensor performance over a soot measurement range from 0-8 g/L and ash levels from 0-42 g/L, and showed good agreement with the gravimetric standard.
- Identified potential for 50% to 75% regeneration-related fuel savings through on-road fleet testing with heavy-duty vehicles equipped with RF sensors relative to stock pressure- and model-based controls, verified through follow-on laboratory testing.
- Quantified sensitivity of RF measurements to external error sources and part-to-part variability. Developed and applied temperature correction methods.

REFERENCES

- U.S. Department of Energy, “Freedom Car and Vehicle Technologies Multi-Year Program Plan: 2006-2011,” September 2006.
- Bromberg, L., Sappok, A., Parker, R., and Wong, V., “Advanced DPF Loading Monitoring with Microwaves,” CLEERS Workshop, Dearborn, MI, May 2006.
- Sappok, A., Bromberg, L., Parks, J., and Prikhodko, V., “Loading and Regeneration Analysis of a Diesel Particulate Filter with a Radio Frequency-Based Sensor,” SAE Technical Paper 2010-01-2126, 2010, doi:10.4271/2010-01-2126.
- Parks, J., Connatser, M., Prikhodko, V., Partridge, B., Lance, M., Gonze, G., and Paratore, M., “Substrate Studies of an Electrically-Assisted Diesel Particulate Filter,” DEER Conference Presentation, 2012.

PUBLICATIONS/PRESENTATIONS

- Sappok, A., Bromberg, L., “Development of Radio Frequency Diesel Particulate Filter Sensor and Controls for Advanced Low-Pressure Drop Systems to Reduce Engine Fuel Consumption (06B),” 2013 DOE Merit Review, Washington, D.C., May 2103.
- Sappok, A., Bromberg, L., “Development of Radio Frequency Sensing for In-Situ Diesel Particulate Filter State Monitoring and Aftertreatment System Control,” ASME Technical Paper ICEF2013-19199, 2013.

SPECIAL RECOGNITIONS & AWARDS/ PATENTS ISSUED

1. Bromberg, L., Sappok, A., Koert, P., and Parker, R., "System and Method for Measuring Retentate in Filters," United States Patent No. 8,384,396, Issued February, 2013.
2. Bromberg, L., Sappok, A., and Koert, P., "Method and System for Controlling Filter Operation," United States Patent No. 8,384,397, Issued February, 2013.
3. Sappok, A., Smith III, R., Bromberg, L., "Advanced Radio Frequency Sensing Probe," United States Patent Application No. 61,897,825, Filed 2013.

IV.11 The Application of High Energy Ignition and Boosting/Mixing Technology to Increase Fuel Economy in Spark Ignition Gasoline Engines by Increasing EGR Dilution Capability

Edward J. Keating

General Motors Co. (GM)

GM Powertrain – Pontiac Engineering Center

895 Joslyn Ave

Pontiac, MI 48340

DOE Technology Development Manager:

Roland Gravel

NETL Project Manager: Ralph Nine

Subcontractor:

Southwest Research Institute®, San Antonio, TX

- Test the Phase 3 turbocharged engine described above to establish fuel efficiency and full-load performance compared to the baseline engine.
- Design and acquire components to update a current GM 2.0-L turbocharged engine (Phase 4) to add the following features while packaging in a current GM mid-sized vehicle:
 1. Addition of a redesigned cylinder head featuring a two spark plug per cylinder combustion system
 2. Addition of redesigned pistons to achieve a 12.0:1 compression ratio
 3. Addition of a cooled, dedicated EGR system
 4. Addition of a dedicated EGR bypass system
 5. Addition of an intake port swirl plate system
 6. Addition of a variable geometry turbocharger assembly
 7. Addition of a port fuel injection system

Overall Objectives

- Apply the enabling technologies of high energy, extended duration ignition and novel intake charge boosting/mixing system to a current GM boosted spark ignition engine.
- Demonstrate that this GM boosted spark ignition gasoline engine operating with extensive, “high quality” exhaust gas recirculation (EGR) dilution achieves a 12% fuel economy benefit relative to a conventional NA gasoline engine at equivalent or better performance.
- Demonstrate that the GM boosted spark ignition gasoline engine solution is capable of U.S. introduction packaged in a mid-sized GM vehicle in the near- to medium-term and has the capability of meeting current and anticipated future emission standards while maintaining or exceeding competitiveness with alternate technologies.

Fiscal Year (FY) 2013 Objectives

- Design and install updates to a current GM 2.0-L turbocharged engine to add the following Phase 3 features while packaging in a current GM mid-sized vehicle:
 1. Addition of a high-energy, extended-duration DCO™ ignition system
 2. Addition of redesigned pistons to achieve a compression ratio increase to 11.0:1
 3. Addition of a conventional low-pressure-loop (LPL) cooled EGR system

Accomplishments to Date

- One-dimensional engine simulation models with conventional LPL EGR and dedicated EGR (D-EGR™) have been constructed and various boost/mixing system candidates have been evaluated to determine capability of the candidate systems to supply and cool a sufficient quantity of EGR to meet the project objectives.
- A vehicle simulation model of a current mid-size GM vehicle has been evaluated to determine the operating points for the subject engine configurations in order to generate fuel economy projections.
- The baseline 2.4-L normally aspirated engine testing has been completed to establish the fuel consumption and performance baseline.
- The Phase 3 turbocharged 2.0-L engine testing with high-energy, extended-duration DCO™ ignition system, 11.0:1 compression ratio and LPL cooled EGR system has been completed to establish the fuel consumption and performance of this specification compared to the baseline.
- Design work is complete to package the Phase 4 system defined as noted previously in the engine compartment of a current GM mid-size vehicle.

- Part acquisition is completed and engine build initiated to assemble the Phase 4 test engine configured as noted previously.

Future Directions

- Build and test a Phase 4 GM 2.0-L turbocharged engine defined through simulation and packaging studies. The base engine will be updated as follows:
 - Addition of a redesigned cylinder head featuring a two spark plug per cylinder combustion system
 - Addition of redesigned pistons to achieve a 12.0:1 compression ratio
 - Addition of a cooled, dedicated EGR system
 - Addition of a dedicated EGR bypass system
 - Addition of an intake port swirl plate system
 - Addition of a variable geometry turbocharger assembly
 - Addition of a port fuel injection system
- Evaluate results of Phase 3 and Phase 4 testing to determine performance to objectives.
- Define and build a Phase 5 GM 2.0-L turbocharged engine based on test results from Phase 3, Phase 4, and simulation.
- Test the Phase 5 engine configuration to establish final performance to objectives.



INTRODUCTION

In order to support the federal government's objective of achieving breakthrough thermal efficiencies while meeting U.S. Environmental Protection Agency emission standards, this project focuses on the enabling technologies of high-energy, extended-duration ignition and a combination boosting and mixing system. These technologies have been shown to enable engine operation with very high EGR dilution levels leading to significant thermal efficiency improvements across the engine operating range. The mechanisms for thermal efficiency improvement include lower thermal losses, improved ideal cycle efficiency, improved combustion phasing, improved combustion efficiency, and reduced pumping losses. The enabling technologies involved are production viable in the near- to medium-term.

The enabling technologies identified offer the potential additional benefit of using increased quantity and quality of cooled EGR for knock suppression at high load. This benefit should permit the specification of a

higher compression ratio leading directly to improved thermal efficiency.

APPROACH

Phase 2: Simulation

A one-dimensional engine performance simulation has been developed to evaluate the potential possibilities to generate various quantities and quality of EGR. An output of the engine simulation was the definition of various options for recirculating EGR that will best support the enhanced EGR dilution tolerance provided by an innovative ignition system. An additional output was the result of an investigation regarding the capabilities of the potential novel boost systems to efficiently generate charge boosting and enhance mixing with EGR.

A vehicle simulation was conducted following the engine simulation to define the engine dynamometer test points that are being used to predict vehicle fuel efficiency as installed in a current mid-size GM vehicle.

Phase 3: Initial High-Energy, Extended-Duration Ignition System Development

Components were designed and procured to update a suitable GM turbocharged engine with the novel high-energy, extended-duration ignition system and the EGR system as determined by simulation in Phase 2. Design work confirmed that the systems added to the engine were capable of installation in the engine compartment of a current mid-size GM vehicle. The engine was installed on the dynamometer and developed to operate at the highest thermal efficiency possible based upon the EGR dilution tolerance established with the novel high-energy ignition system.

Phase 4: Initial Boost System/Mixer and further Innovative Ignition Development

Components were designed and procured to update a GM turbocharged engine with the novel intake charge boosting/mixing system and the appropriate dedicated EGR system as determined by simulation in Phase 2. Design work confirmed that the systems added to the engine are capable of installation in the engine compartment of a current mid-size GM vehicle. The engine will be installed on the dynamometer and developed to operate at the highest thermal efficiency possible based upon the EGR dilution tolerance established with the addition of the novel intake charge boosting/mixing system, novel ignition system and dedicated EGR.

Phase 5: Engine System Development

Component designs will be updated and procured to update a GM engine with a final enabling technology solution based on the results of the first four phases. A final vehicle simulation will be conducted using the engine dynamometer data to establish performance relative to project objectives.

RESULTS TO DATE

Vehicle Simulation

A vehicle simulation of a current mid-size GM vehicle was conducted using the current U.S. Federal City/Highway/US06 test cycles. The engine speed and load operating points were compiled over these vehicle test cycles and the fuel energy used was determined. Based on this work, 11 engine speed and load operating points were established that represent approximately 95% of the fuel energy used by the mid-size GM vehicle during these test cycles. These engine speed and load points form the basis for engine testing to establish fuel consumption performance of the current baseline engine and the technologies under study.

Construct One-Dimensional GT-POWER Model of the Baseline Engine

This task was conducted to establish initial correlation between simulation results and engine dynamometer test results. The engine simulation model of the baseline engine was acquired from within GM. This engine simulation model was run at the speed and load test points determined from the vehicle simulation work to establish predicted baseline fuel consumption performance for the mid-sized GM vehicle.

Install and Test the Baseline Engine

The baseline 2.4-L Ecotec engine was installed in a test cell and the baseline test matrix was fully executed. The engine was instrumented for temperatures, pressures, and flow rates to establish a comprehensive baseline of the engine. The fully instrumented engine was installed in a test cell with control of inlet air temperature/pressure/humidity, exhaust back pressure, and engine speed/load. An emission sampling system was installed for post-catalyst and engine-out emissions measurements. Emissions measurements were conducted with a Horiba Mexa 7100DEGR exhaust emissions analysis system. Cylinder pressure analysis was conducted with an internally controlled software program.

The engine test matrix was determined by vehicle simulation (see previous) to best represent engine fuel consumption over the Federal City/Highway/US06 drive

cycles. This matrix includes 11 modes. Each mode was weighted based on vehicle fuel consumption simulations and the required engine speed and load necessary to match with the vehicle transmission and drive line constraints. Best brake specific fuel consumption (BSFC) points were determined at each of the 11 modes. Best BSFC was determined by performing sweeps of intake and exhaust cam phasers at each speed/load condition. The spark timing was adjusted to minimum for best torque (MBT), or knock-limited spark advance (KLSA). MBT spark advance was used when possible and determined by locating the 50% mass fraction burned location of the engine between 6-8 crank angle degrees after top-dead center. The full-load curve from 1,250 rpm to 6,000 rpm was acquired to verify performance. Full-load data at the test site was found to be 1.3% higher than the published SAE International full-load curve on average. This provided high confidence in engine operation and test cell acquisition.

Assessment of the engine model and engine test show strong agreement in terms of BSFC for the 11 mode points. The measured modal average BSFC was within 2% of the simulated estimations, expressing strong fidelity between simulation and experiment.

Construct One-Dimensional GT-POWER Model of the Phase 3 Engine

The model of the GM turbocharged engine that is the basis for this phase was acquired from within GM. The LPL EGR system (Figure 1) was defined and added

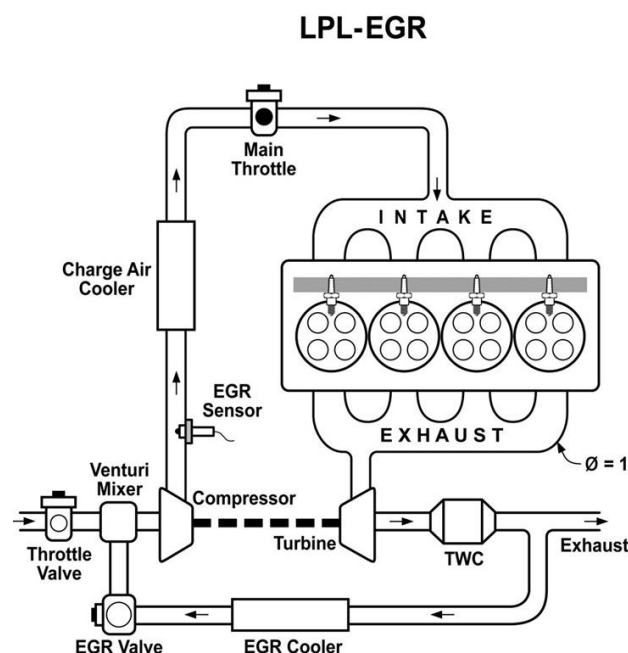


FIGURE 1. LPL EGR System Applied to Turbocharged Engine

to the engine simulation model. Engine compression ratio was increased to 11.0:1 and combustion properties of the high-energy, extended-duration ignition system were applied. The engine simulation model was run at the speed and load test points determined from the vehicle simulation work to evaluate and confirm the capability of the LPL EGR system components to provide the desired EGR flow and cooling performance required to properly evaluate the concept on the test bench and in the vehicle.

Design and Update GM 2.0-L Turbocharged Engine to Phase 3 Specification with LPL EGR System, 11.0:1 Compression Ratio, and High-Energy, Extended-Duration Ignition System that meets Performance Requirements and Packages in a Mid-Size GM Vehicle

The packaging development of the Phase 3 engine in the vehicle was completed (Figure 2). Per the project objectives, the engine system to be evaluated meets the packaging requirements of a current GM mid-size vehicle. The various components required to update the engine were manufactured and the engine was assembled for testing.

Install and Test the Phase 3 GM 2.0-L Turbocharged Engine

The engine assembled to Phase 3 specification was installed in the test cell (Figure 3). Various engine, EGR, and ignition performance testing was completed for the turbocharged GM 2.0-L 4-cylinder engine specified with 11.0:1 compression ratio, high-energy, extended-duration DCO™ ignition system and the baseline (LPL) cooled EGR system. The best BSFC points were determined

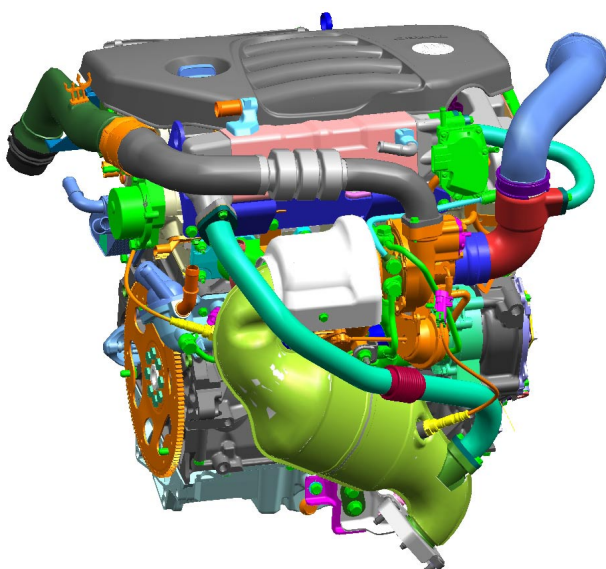


FIGURE 2. LPL EGR System Packaged in GM Mid-Sized Vehicle

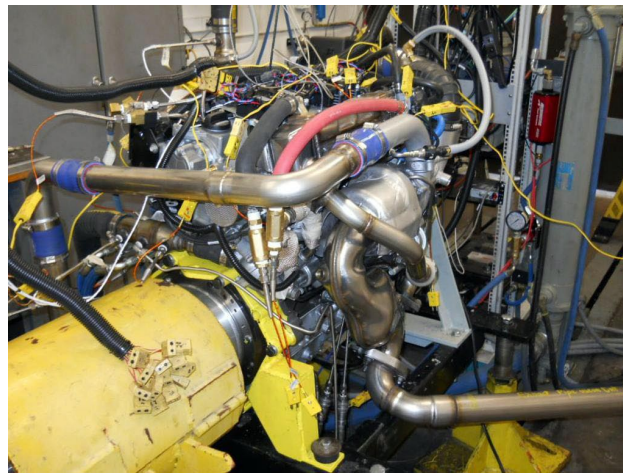


FIGURE 3. LPL EGR Turbocharged Engine Test Cell Installation

TABLE 1. Fuel Consumption of Phase 3 2.0-L Turbocharged Engine compared to Baseline

| | | | 2.4L NA | 2.0L Turbo with 11:1 CR, LPL cooled EGR and DCO ignition |
|------|--------|-----------|---------------|--|
| RPM | Torque | Weighting | Weighted BSFC | Weighted BSFC |
| 1465 | 33.0 | 0.103 | BASE | -3.4% |
| 1665 | 64.5 | 0.184 | BASE | -3.7% |
| 1500 | 87.5 | 0.212 | BASE | -3.6% |
| 1480 | 110.5 | 0.119 | BASE | -3.5% |
| 1500 | 137.5 | 0.058 | BASE | -3.6% |
| 1800 | 162.5 | 0.058 | BASE | -3.0% |
| 1800 | 187.5 | 0.046 | BASE | -0.7% |
| 2100 | 75.0 | 0.067 | BASE | -3.5% |
| 1962 | 124.6 | 0.056 | BASE | -2.1% |
| 2100 | 137.5 | 0.043 | BASE | -1.1% |
| 2600 | 196.0 | 0.054 | BASE | -1.8% |
| | | | | -3.2% |

at each of the 11 modes. Best BSFC was determined by performing sweeps of intake and exhaust cam phasers in conjunction with cooled external EGR at each speed/load condition. The spark timing was adjusted to MBT, or KLSA. The fuel consumption of the Phase 3 2.0-L turbocharged engine specified as noted above is shown (Table 1) compared to the 2.4-L naturally aspirated (NA) baseline engine at the selected 11 mode points.

An assessment was completed of simulation and engine test results achieved with the 2.4-L NA baseline engine compared to the 2.0-L turbocharged engine with 11.0:1 compression ratio, LPL cooled EGR and DCO ignition. The results show strong agreement between simulation and engine test results in terms of BSFC differences over the 11 mode points. The measured modal average BSFC improvement for the Phase 3 2.0-L turbocharged engine with 11.0:1 compression ratio, LPL

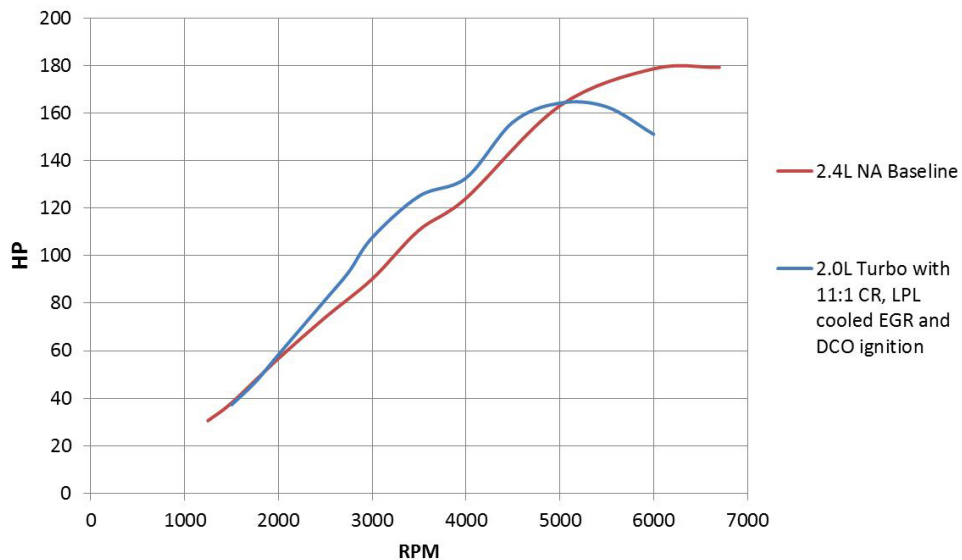


FIGURE 4. Horsepower of Phase 3 2.0-L Turbocharged Engine compared to Baseline

cooled EGR and DCO ignition compared to the 2.4-L NA baseline was predicted through simulation to be 2.4% while the engine testing resulted in a 3.2% improvement. This result illustrates strong fidelity between simulation and engine testing with the simulation results slightly more conservative regarding the predicted improvement.

Engine full-load performance testing has been completed as planned for the Phase 3 turbocharged GM 2.0-L 4-cylinder engine. Best power was determined by performing sweeps of intake and exhaust cam phasers in conjunction with 20%+ cooled external EGR at each rpm point. A stoichiometric air/fuel ratio was maintained as the turbocharger turbine inlet temperatures remained within the allowable range without excess fuel dilution due to the addition of cooled EGR. The spark timing was adjusted to MBT, or KLSA.

The horsepower output of the Phase 3 2.0-L turbocharged engine specified as noted above is shown (Figure 4) compared to the 2.4-L NA baseline engine.

Construct One-Dimensional GT-POWER Model of the Phase 4 Engine

The model of the GM turbocharged engine that is the basis for this phase was acquired from within GM. The D-EGR™ system (Figure 5) was defined and added to the engine simulation model. Engine compression ratio was increased to 12.0:1 and combustion properties of the two spark plug per cylinder ignition specification, swirl generated via the port swirl plate system and effects of the PFI fuel system were applied. In addition, the performance properties of the variable geometry turbocharger were specified. The engine simulation

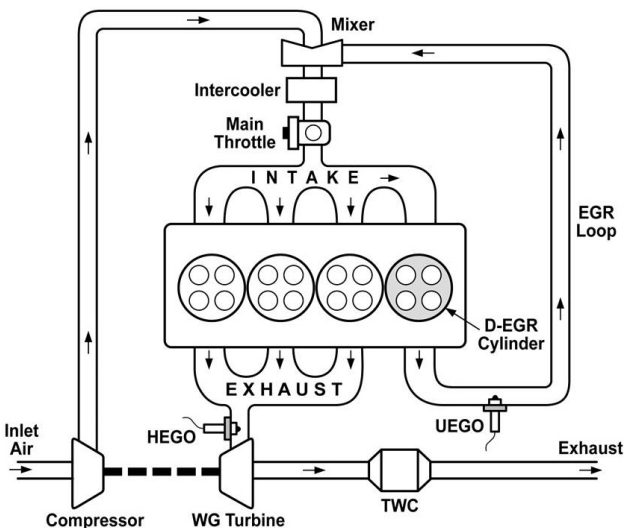


FIGURE 5. D-EGR System Applied to Turbocharged Engine

model was run at the speed and load test points determined from the vehicle simulation work to evaluate and confirm the capability of the D-EGR™ system components to provide the desired EGR flow and cooling performance required to properly evaluate the concept on the test bench and in vehicle.

Design and Update GM 2.0-L Turbocharged Engine to Phase 4 with Technology Content that meets Performance Requirements and Packages in a Mid-Size GM Vehicle

The packaging development of the Phase 4 2.0-L turbocharged engine in the vehicle has been completed.

Per the project objectives, the engine configuration to be evaluated meets the packaging requirements of a current GM mid-size vehicle.

The additions and/or updates to the engine design are as follows:

- Redesigned cylinder head featuring a two spark plug per cylinder combustion system
- Redesigned pistons to achieve a 12.0:1 compression ratio
- Cooled, dedicated EGR system
- Dedicated EGR bypass system
- Intake port swirl plate system
- Variable geometry turbocharger assembly
- Port fuel injection system

The various parts required to update the engine have been manufactured and the engine is in the process of being assembled for testing.

CONCLUSIONS

The project activities conducted to date have supported the basic assumptions used for the performance improvement projections. The activities have been completed within the constraints of the project timeline. Execution of the remaining, ongoing design activities and subsequent engine test bench evaluations will establish the performance benefits of the enabling technologies identified.

- The initial one-dimensional GT-POWER simulation and subsequent test bench results from the 2.4-L baseline engine achieved excellent correlation to the predicted performance results.

- A Phase 3 2.0-L turbocharged engine configured as follows, that packages in a current GM mid-size vehicle has been specified, designed and assembled:
 - Redesigned pistons to achieve a 11.0:1 compression ratio
 - Cooled, LPL EGR system
 - High-energy, extended-duration DCOTM ignition system
- Engine, EGR, and DCOTM performance testing has been completed for the Phase 3 turbocharged 2.0-L 4-cylinder engine. The measured modal average BSFC improvement for the Phase 3 2.0-L turbocharged engine compared to the 2.4-L NA baseline was 3.2%.
- The measured modal average BSFC improvement for the Phase 3 2.0-L turbocharged engine compared to the 2.4-L NA baseline was predicted through simulation to be 2.4% while the engine testing resulted in a 3.2% improvement. This result illustrates strong fidelity between simulation and engine testing with the simulation results slightly more conservative regarding the predicted improvement.
- A Phase 4 2.0-L turbocharged engine that is projected to meet the project performance requirements has been specified, designed, manufactured and is in the process of being assembled for testing.

FY 2013 PUBLICATIONS/PRESENTATIONS

1. 2013 U.S. DOE Vehicle Technologies Program Annual Merit Review and Peer Evaluation Meeting.

IV.12 Heavy-Duty Diesel Engines Waste Heat Recovery Using Roots Expander Organic Rankine Cycle System

Swami Subramanian (Primary Contact),
William N. Eybergen

Eaton Corporation
Corporate Research & Technology
Advance Mechanical Systems
26201 Northwestern Hwy
Southfield, MI 48076

DOE Technology Development Manager:
Gurpreet Singh

NETL Project Manager: Ralph Nine

Subcontractors:

- AVL Powertrain Engineering, Inc., Plymouth, MI
- John Deere, Waterloo, IA
- Electricore, Inc., Valencia, CA

Overall Objectives

- Demonstrate fuel economy improvement through Rankine cycle waste heat recovery (WHR) systems utilizing a roots expander in heavy-duty diesel applications of:
 - 5% (baseline objective) if only energy from the exhaust gas recirculation (EGR) loop is recovered.
 - 8% (target objective) if exhaust energy from downstream of the turbine is also used for recovery.
- Demonstrate green house gas (GHG) improvement with WHR systems in heavy-duty diesel applications of:
 - 5% (baseline objective) if only energy from the EGR loop is recovered.
 - 8% (target objective) if exhaust energy from downstream of the turbine is also used for recovery.
- Demonstrate that other pollutants, such as oxides of nitrogen (NOx), hydrocarbons, CO and particulate will not be increased as part of the overall engine/WHR/exhaust after treatment optimization.
- Demonstrate a plan for cost reduction by incorporation of a Roots-type expander.

Fiscal Year (FY) 2013 Objectives

- Prototype and evaluate the single-stage roots expander performance using air bench testing.
- Validate the performance of single-stage roots expander design in a water-based organic Rankine cycle (ORC) system.
- Design and optimize a multistage robust roots expander for a heavy-duty diesel engine ORC system.
- Model, design, and optimize heat exchangers to maximize system performance.
- Package the optimized WHR heat exchangers and roots expander on a John Deere 13.5-L diesel engine.

FY 2013 Accomplishments

- Prototyped and air tested the single-stage roots expander demonstrating greater than 60% isentropic efficiency.
- Built and validated the ORC test stand for water or ethanol usage.
- Tested the single-stage roots expander with water as working fluid on the ORC test stand.
- Designed a multistage expander and started procurement.
- Selected a heat exchanger vendor and completed specification.
- Completed a packaging study of the entire ORC system on the engine.

Future Directions

- Build and test the multistage roots expander in an ORC system utilizing water, ethanol, or a combination of water and ethanol as the working fluid.
- Prototype and evaluate heat exchangers, working fluid pump, valves, and fluid conveyance lines.
- Design and build a heavy-duty diesel engine Rankine cycle system with integrated roots expander for a John Deere 13.5-L diesel engine.
- Demonstrate the roots expander capability for meeting the DOE objective utilizing the developed heavy-duty diesel engine Rankine cycle system.



INTRODUCTION

Nearly 30% of fuel energy is not utilized and wasted in engine exhaust. ORC WHR systems offer a promising approach on waste energy recovery and improving the efficiency of heavy-duty diesel engines. One of the major technological barriers in the ORC WHR system is the turbine expander. A turbine expander is grossly mismatched for use with diesel engine exhaust heat recuperation. Eaton Corporation's comprehensive project will develop and demonstrate advanced component technology to reduce the cost of implementing ORC WHR systems on heavy-duty diesel engines. Accelerated adaptation and implementation of new fuel efficiency technology into service is critical for reduction of fuel used in the commercial vehicle segment.

Eaton's solution is to adapt an Eaton-designed Roots compressor (currently in use for supercharger boosting applications) as an expander of the ORC WHR system. Roots-based expanders will have multiple advantages over turbine expanders, including minor down speeding to match engine speed, capability to handle multiphase flow, high volumetric efficiency and a broad efficiency island. This configuration will enable faster commercialization of ORC WHR technology capable of improving engine fuel efficiency and total power output (performance). The expander technology to be demonstrated during this project will be validated during engine dynamometer testing using a John Deere 13.5-L heavy-duty diesel engine.

APPROACH

The present work has been structured to baseline the 13.5-L heavy-duty diesel engine, characterize and quantify the potential waste energy sources for construction of thermodynamic analysis models. The impacts of various WHR heat exchanger layouts on system performance will be assessed, leading to specifications of WHR components. The expander development will utilize computational fluid dynamics (CFD) analysis, bench testing, calibration, and validation to maximize efficiency and durability. The developed expander with ORC system will be tested on an engine operated over the same speed and load conditions of the baseline engine. These results will be compared to the baseline engine data at the same NO_x emission levels to provide a back-to-back demonstration of the expander technology and impact on fuel efficiency and engine system performance.

RESULTS

Expander, heat exchangers, working fluid, and working fluid pump are major components of an ORC system. Expander design and development is being carried out by Eaton Corporation. Initial specification, design and development of heat exchangers, initial specification of working fluid pump, and packaging study are being done by a collaborative team effort.

Expander Development

Roots expander development has been done systematically based on working fluid volumetric flow and pressure ratio of the ORC system. Expander size and isentropic efficiency are the major two factors involved in the design and development of the ORC system. Expander size is defined from AVL analytical input and isentropic efficiency that is driven by rotor configuration and inlet/outlet porting. Appropriate sealing, bearings, oil cavity cooling, material, and rotor coating choices were developed and implemented into the single-stage expander design. Significant design effort was focused around the selection of static and dynamic seals based on rotational speeds, pressure, and temperature. The single-stage expander depicted in Figure 1 has been evaluated through air bench testing and on the ORC test stand (Figure 2) with water as the working fluid.

Based on analytical investigations and architecture layout as outlined in Figure 3, utilization of the multistage roots expander was selected to achieve optimal performance at a wide range of operation in heavy-duty diesel engines. Figure 4 shows that most of operating points with the three-stage roots expander achieve greater than 5% brake specific fuel consumption (BSFC) improvement. This is a result of higher exhaust energy recovery rate (greater than 35% exhaust energy recovery). Different configurations of multistage roots expanders were compared and investigated. The selected

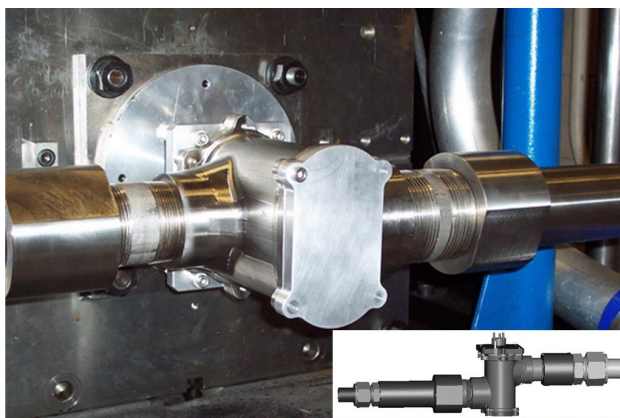


FIGURE 1. Single-Stage Roots Expander

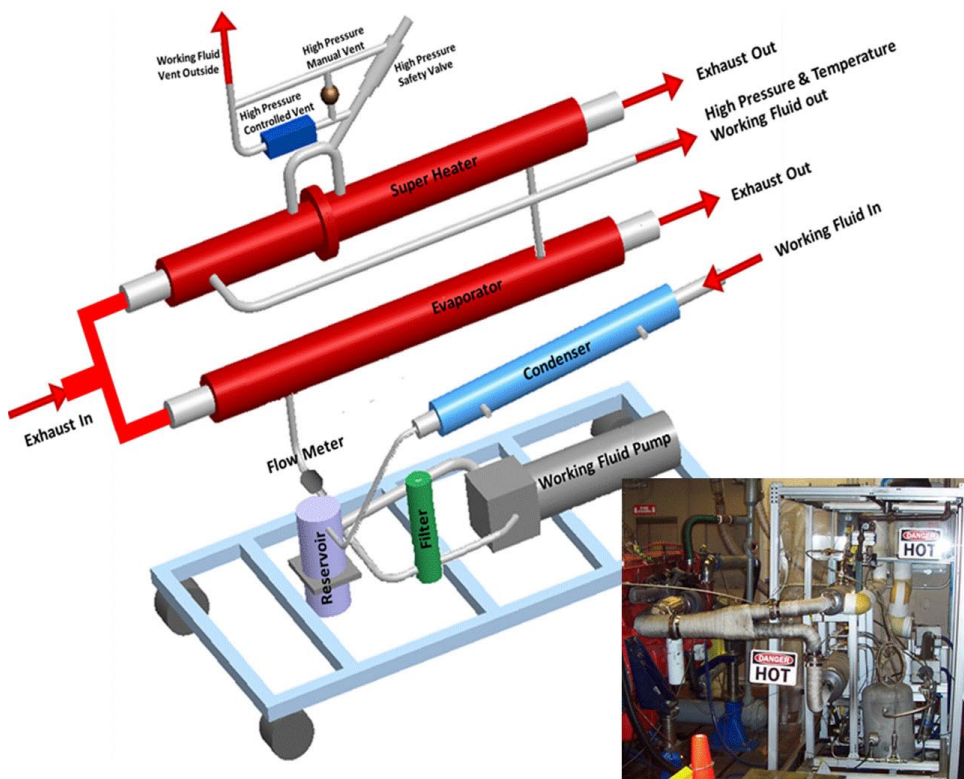


FIGURE 2. Expander Test Setup

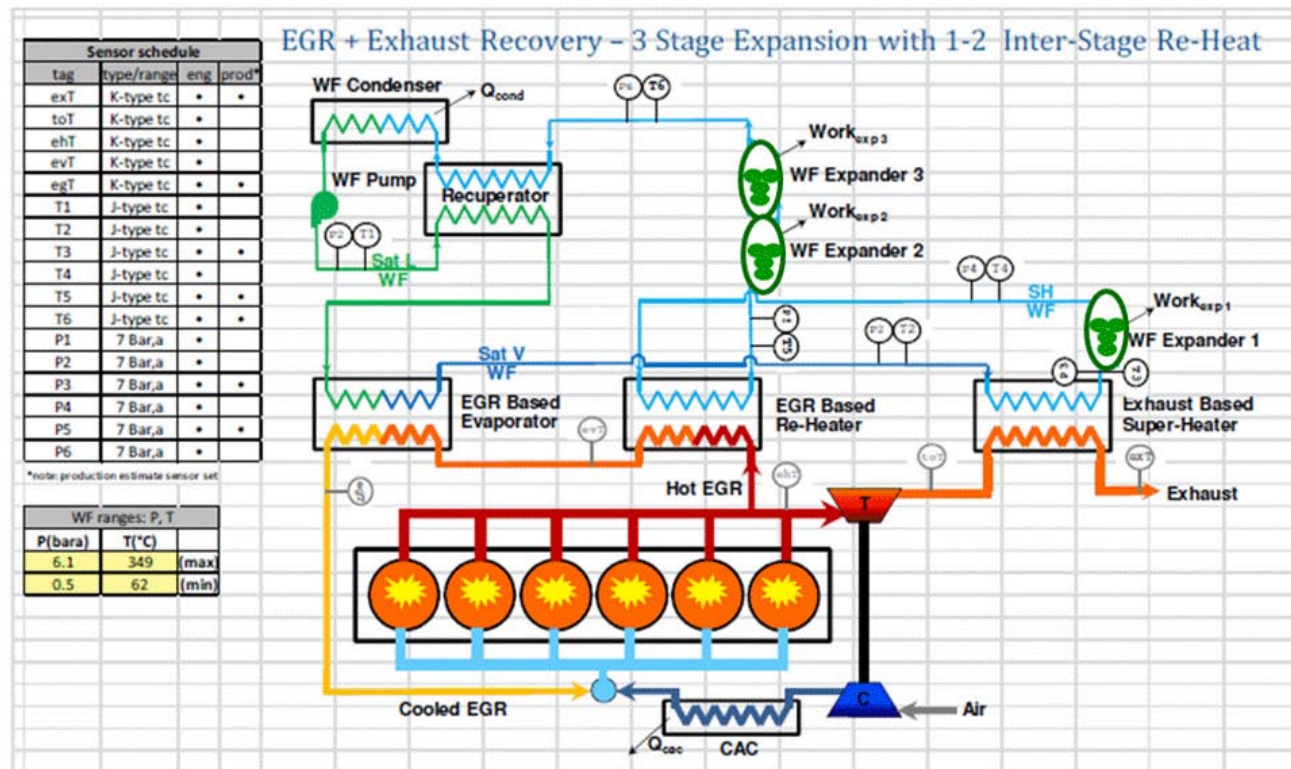


FIGURE 3. Architecture 4 - Rankine Cycle with Three-Stage Roots Expander

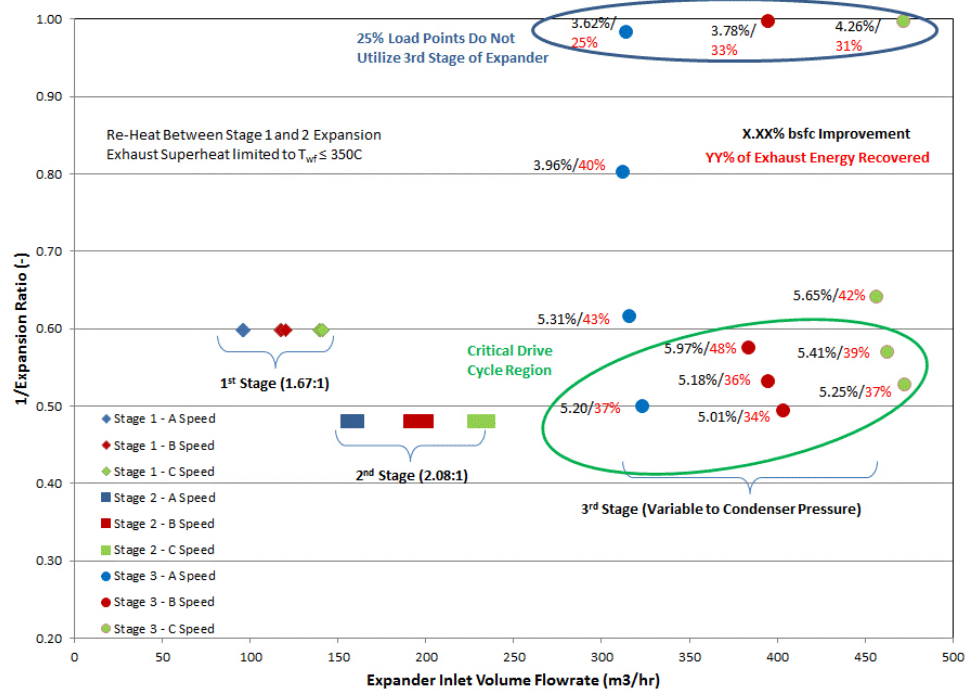


FIGURE 4. Architecture 4 – Three-Stage Expander System BSFC Improvement

design to pursue was made based on performance, flexibility to change internal drive ratios, durability and cost considerations. The inlet and outlet port configurations were optimized using CFD analysis to minimize flow losses and leaks. Figure 5 shows the compact multistage roots expander ORC system.

WHR Heat Exchangers

The WHR system being demonstrated utilizes energy recovered from both the EGR path and the post-turbine exhaust gas stream. The EGR-based energy recovery path serves to also cool the recirculated exhaust gas. The roots expander ORC WHR heat exchanger system consists of superheater, evaporator, recuperator, and condenser.

A heat exchanger vendor has been selected for WHR heat exchanger development. The vendor, Eaton, John Deere's, and AVL's expertise are involved in the heat exchanger architecture as well as system specification. These heat exchangers have been analyzed for optimal system performance in parallel and series architecture.

- Series Architecture - Working fluid passes through EGR source first (evaporator) followed by post-turbine exhaust (superheater).
- Parallel Architecture - Working fluid divides between EGR source and post-turbine exhaust. Both will evaporate and superheat the working fluid (Figure 6).

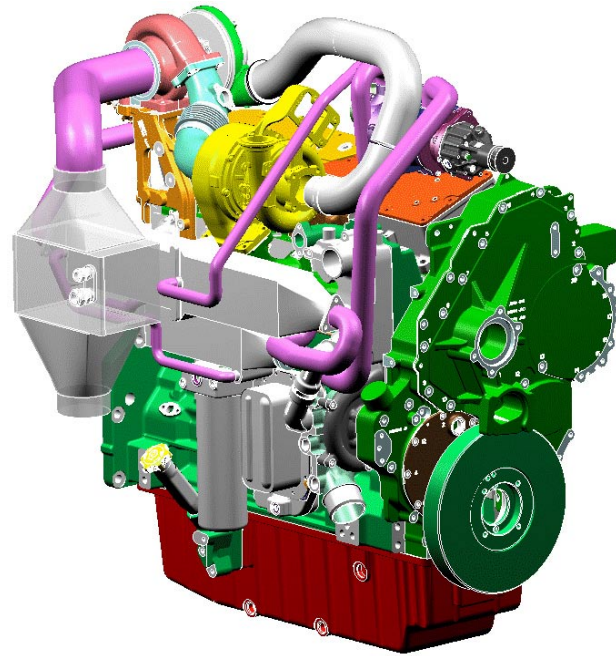
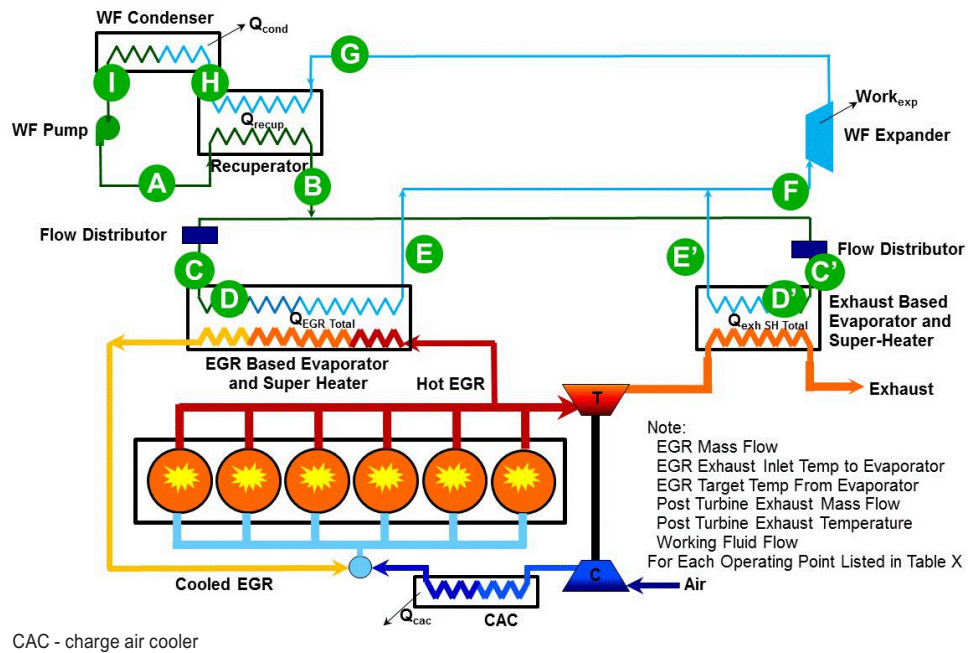


FIGURE 5. Roots Expander WHR System Packaging in John Deere Engine

Working Fluid and Heat Exchanger Architecture Evaluation

The prime path working fluid to be utilized is ethanol, but a mixture of ethanol and water will also be

**FIGURE 6.** Waste Heat Recovery System - Parallel Architecture

evaluated. The ethanol to be used will be de-natured with approximately 5% gasoline. If component durability or safety goals cannot be achieved, a mixture of water and ethanol will be used as the ORC working fluid. Heat exchangers are designed to handle the mixtures. The evaporator and superheater are designed to keep the ethanol working fluid below 275°C on exiting to prevent working fluid damage.

Working Fluid Pump Requirements

Based on the re-optimized operating conditions, the working fluid pump specifications are:

- Working fluid flow: 0 to 12 kg/min ethanol (16 L/min)
- Working pressure: 0.1 to 8 bar

CONCLUSIONS

Based on the studies documented in this report, the following summary is made:

- Simulation results for the multistage roots expander system show a BSFC improvement of approximately 6% as outlined in Figures 3 and 4.

- Air stand testing with the single-stage roots expander demonstrated greater than 60% isentropic efficiency and testing on ORC test stand with water is in progress.
- Development of a three-stage roots expander is in progress (90% completed).
- Refinements to the AVL thermodynamic model of the WHR system have been completed.
- The parallel system architecture was selected for implementation based on inherent flexibility in control and adaptability to condenser heat rejection capacity.

FY 2013 PUBLICATIONS/PRESENTATIONS

1. US DOE 2013 DOE Vehicle Technologies Program Review.

IV.13 Next Generation Ultra-Lean Burn Powertrain

Hugh Blaxill (Primary Contact), Michael Bunce, Kristie Boskey, Prasanna Chinnathambi, Eric Smith, Luke Cruff
MAHLE Powertrain (MPT)
23030 MAHLE Dr.
Farmington Hills, MI 48377

DOE Technology Development Manager:
Roland Gravel

NETL Project Manager: Ralph Nine

Subcontractor:
Delphi Corporation, Rochester, NY

- Completed thermodynamic engine testing of TJI designs.
- Analyzed data from the optical engine to correlate jet characteristics to TJI designs.
- Demonstrated the potential of TJI to extend the lean limit into the ultra-lean region, achieving thermal efficiency parity with previous TJI studies, and demonstrated a path forward to achieve project goal of 45% thermal efficiency.
- Synthesized data from optical and thermodynamic engines to characterize engine performance as a function of jet characteristics.

Future Directions

- Demonstrate thermal efficiency of 45% on a light-duty gasoline engine platform while demonstrating potential to meet U.S. Environmental Protection Agency emissions regulations.
- Demonstrate using ultra-lean-burn technology, a 30% predicted vehicle drive cycle fuel economy improvement over an equivalent conventional port-fuel-injected gasoline engine with variable cam phasing.
- Demonstrate potential to maintain typical levels of passenger vehicle performance.
- Demonstrate a cost-effective system, capable of being installed in production engines with minimum modification and showing a clear route to production.
- Develop MPT's Turbulent Jet Ignition (TJI) concept, in conjunction with turbocharging, as the enabling technology to accomplish these objectives.



INTRODUCTION

Regulation and industry trends have sought to produce engines with higher efficiency, lower fuel consumption, and lower exhaust emissions than their predecessors. Lean-burn operation provides thermal efficiency benefits but may result in higher nitrogen oxides (NO_x) emissions, requiring expensive emissions aftertreatment. Ultra-lean burn has been shown to improve thermal efficiency and simultaneously reduce NO_x formation by significantly reducing in-cylinder temperatures. However, there are challenges associated with ignition of the charge and combustion stability. In order to improve light-duty spark ignition (SI) engine efficiency and vehicle fuel economy, the industry is moving towards downsizing (smaller displacement, boosted direct injection engines), but these engines typically display poor thermal efficiency. MPT intends to use two key enabling technologies for its ultra-lean burn combustion concept: TJI and turbocharging.

Fiscal Year (FY) 2013 Objectives

- Complete single-cylinder optical engine build and installation, and acquire high-speed imaging data.
- Complete single-cylinder thermodynamic engine build and installation, and acquire data to evaluate the effects of TJI design on engine performance.
- Synthesize data from optical and thermodynamic engines to determine the relationship between jet characteristics and engine performance.

FY 2013 Accomplishments

- Completed optical engine testing of TJI designs.

APPROACH

TJI is a pre-chamber-initiated distributed ignition system that enables reliable ignition of ultra-lean main chamber air-fuel mixtures. TJI differs from other pre-chamber-based systems in that it incorporates auxiliary fueling directly in the pre-chamber and the design of the nozzle interface between pre-chamber and main chamber promotes flame quenching, thereby seeding the main chamber with active radical species. This project seeks to apply this concept to a light-duty SI engine platform in an effort to achieve 45% peak thermal efficiency, 30% drive cycle fuel economy improvement, and low NO_x emissions levels.

To meet these objectives, optical engine testing is employed to qualitatively explore effects of the turbulent radical jets on main chamber ignition and combustion. Thermodynamic engine testing is employed to determine combustion and engine performance differences as functions of different nozzle designs. Finally, optical and metal engine data are compared to quantitatively determine the physical characteristics of the jets and their comparative effect on combustion and engine performance.

RESULTS

Data demonstrate that TJI effectively extends the lean limit of the base engine. Unfueled (no auxiliary fueling) TJI results in a lean limit of approximately $\lambda=1.4$; fueled TJI can extend this limit past $\lambda=2.0$. A major contributor to stable combustion at significantly higher λ 's is the reduction in crank angle (CA) 0-10 burn duration. This duration remains much flatter over the lambda sweep with fueled TJI than with unfueled TJI. This indicates that fueled TJI provides an increased ignition potential, allowing it to continue to ignite the main charge relatively easily despite the decreasing ignitability of the main charge as it is enleaned.

Combustion temperatures are reduced as the main chamber is enleaned, which reduces NO_x emissions. This reduction is significant, with values on the order of 20 ppm at the lean limit, as displayed in Figure 1.

Due to the gamma effect, enleanment has been shown to increase net thermal efficiency (NTE) [1]. An additional gain in NTE results from the ability to increase compression ratio without enduring a knock penalty. The lower temperature combustion accompanying lean combustion coupled with the distributed ignition qualities of TJI enable this increase in compression ratio. Base engine peak NTE has been established as approximately 36.5% at stoichiometric. Previous internal TJI research [2-5] has demonstrated peak NTE reaching approximately 42% with TJI. As is observed in Figure 2,

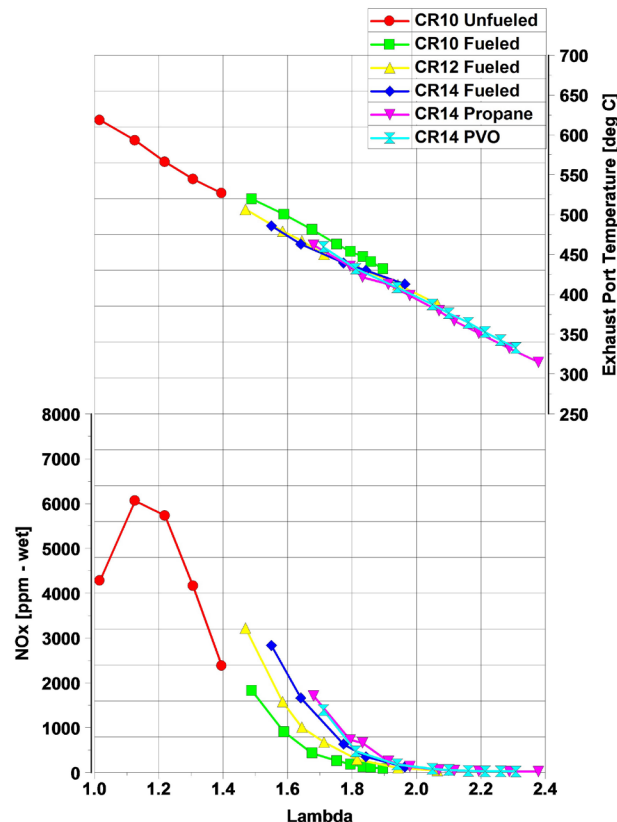


FIGURE 1. NTE and Combustion Efficiency vs. λ , 2,500 rpm , 47 kg/hr air flow – TJI Design 3

peak NTE achieved in this data is over 42%, competitive with previous research.

Figure 3 presents trends in NTE vs. main chamber lambda at a sample operating condition at a compression ratio of 10 (CR10). The three designs presented here utilize a common pre-chamber design with the following nozzle designs: Design 3, Design 4, and Design 5, providing nozzle orifice areas of 1X, 1.24X, and 2.48X that of the base area, respectively. At the tested operating condition (2,500 rpm, 47 kg/hr air flow), peak NTE is maximized with decreasing nozzle orifice area. Design 3 (with the smallest orifice area) achieves a peak NTE of approximately 41%, with Design 4 and Design 5 peaking at just over 40% and 39%, respectively.

Pre-chamber light-off, as characterized by CA0-10 duration in the pre-chamber, is displayed in Figure 4. This graph indicates that the larger nozzle orifice area results in superior pre-chamber ignition characteristics, i.e., CA0-10 is minimized. The largest orifice area nozzle consistently shows a 1.5 degree advantage over the smallest orifice area nozzle at this condition. This is believed to be due to superior mixing, i.e., a more favorable lambda in the spark plug region, superior

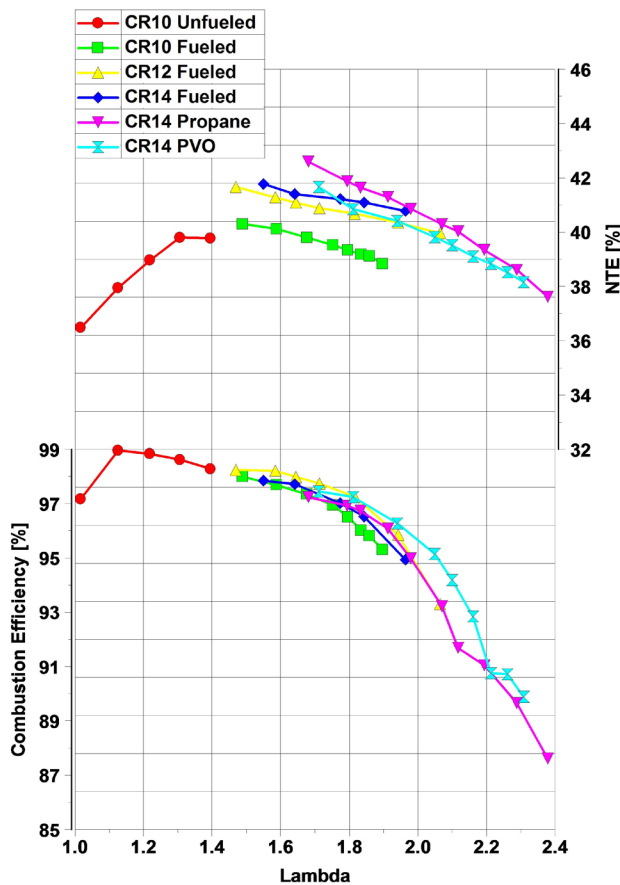


FIGURE 2. Main Chamber Exhaust Temperature and NO_x vs. λ , 2,500 rpm, 47 kg/hr air flow – TJI Design 3

scavenging of residual gases during the previous cycle's expansion stroke, or both.

The advantage in terms of quicker pre-chamber light-off of the larger orifice area nozzles is generally maintained when examining main chamber light-off as characterized by main chamber CA0-10 burn duration. Figure 4 demonstrates a shorter CA0-10 duration with Design 5 vs. Design 3, while Design 4 deviates from the trend, having the longest CA0-10 duration.

Figure 4 also shows a largely unchanged trend in CA0-50 duration from that of CA0-10 duration. However this trend essentially reverses, with Design 3 eliminating the gap in duration between it and Design 5, resulting in the consistently shortest CA10-90 duration of all the designs.

The overall faster combustion duration of the smaller nozzle orifice area designs corresponds to the higher peak NTE due to a higher proportion of the main chamber charge combusting closer to top-dead center.

Analyzing the optical engine data, jet velocity correlates well with jet penetration prior to ignition site

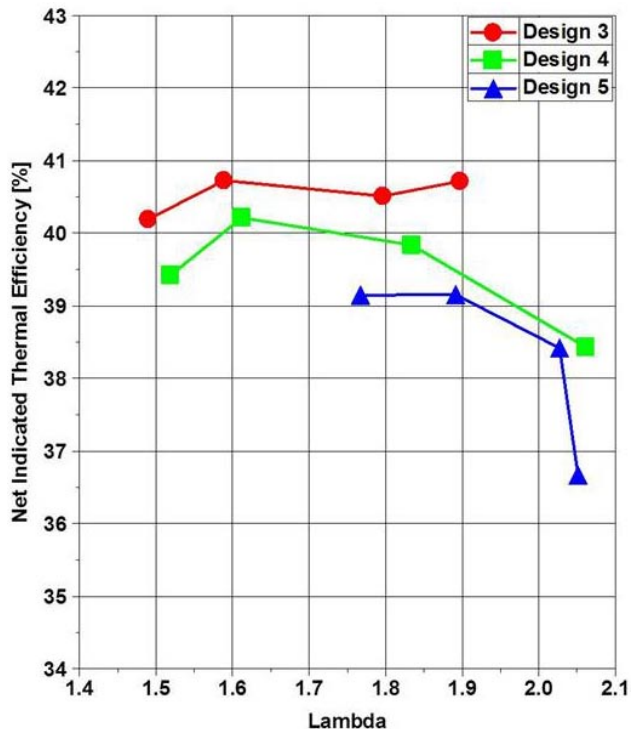


FIGURE 3. NTE vs. λ , 2,500 rpm , 47 kg/hr air flow – TJI Designs 3, 4, and 5

formation. Higher velocity jets are able to penetrate further into the main chamber prior to creating ignition sites. This degree of penetration, coupled with the ability of some or all of the jets to induce ignition sites, determine the distribution of ignition. As measured, jet velocity is largely driven by the peak pressure differential between pre-chamber and main chamber. This value is maximized with decreasing nozzle orifice area.

Figure 5 illustrates the site distribution differences among three designs. Jets emerging from Design 4 at high velocity penetrate deep into the main chamber before inducing ignition. Jets from Design 5 emerge at a significantly lower velocity and thus create ignition sites much closer to the nozzle. Jets from Design 3, with a velocity slightly below that of Design 4 penetrate into the main chamber creating ignition sites that occupy a space between those of the other designs. The distribution of these sites, however, is preferable for a more rapid main chamber combustion event. While Design 5 produces eight close-coupled ignition sites, the resulting flame fronts must travel out towards the walls to ignite the remainder of the charge. The four ignition sites created by Design 4 are closer to the chamber walls but are greatly separated from each other, requiring the flame fronts to travel great distances prior to convergence. Design 3 combines the close-coupling of Design 5 with the radial chamber coverage of Design 4, minimizing

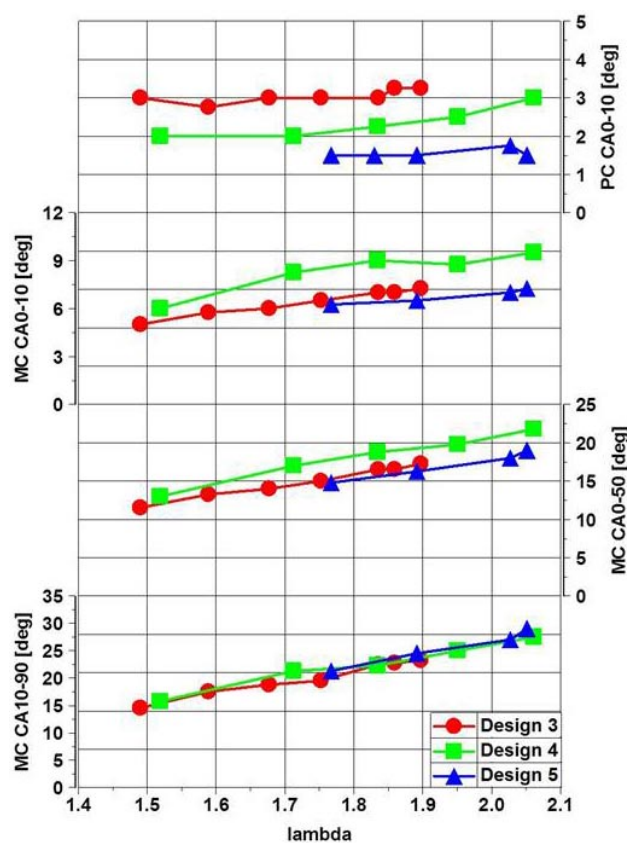


FIGURE 4. Pre-Chamber CA0-10, Main Chamber CA0-10, CA0-50, and CA10-90 vs. λ , 2,500 rpm , 47 kg/hr air flow – TJI Designs 3, 4, and 5

the distance each flame front is required to travel in order to consume a majority of the charge. This more rapid combustion event, illustrated in Figure 6, results in elevated NTE. NTE can thus be maximized by jet velocity targeting driven by nozzle design characteristics.

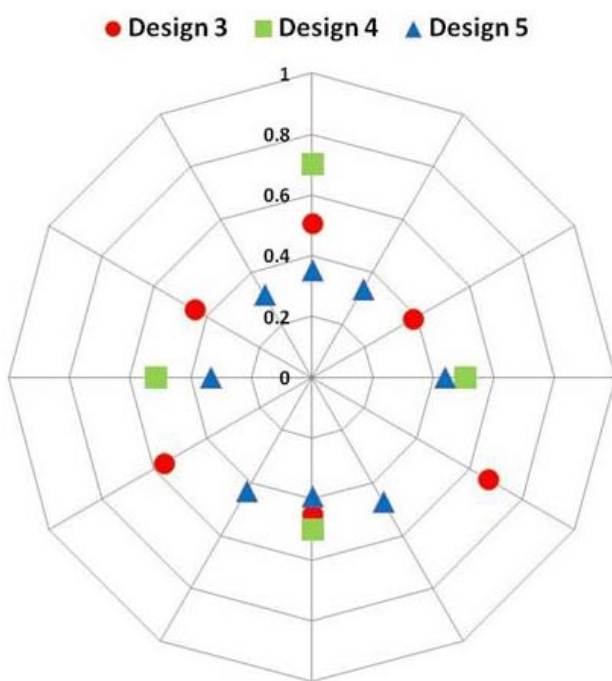


FIGURE 5. Ignition Sites – TJI Designs 3, 4, and 5.

CONCLUSIONS

Previous studies [2-5] have demonstrated the potential of TJI as an enabling technology for ultra-lean SI combustion to significantly increase NTE and reduce NO_x emissions. This project examines comparative performance of several TJI designs, specifically nozzle designs, in an effort to achieve the NTE, fuel economy, and emissions targets enumerated in the project objectives.

Jet velocity is shown to correlate well with degree of jet penetration into the main chamber prior to ignition site formation. Higher peak pre-chamber combustion

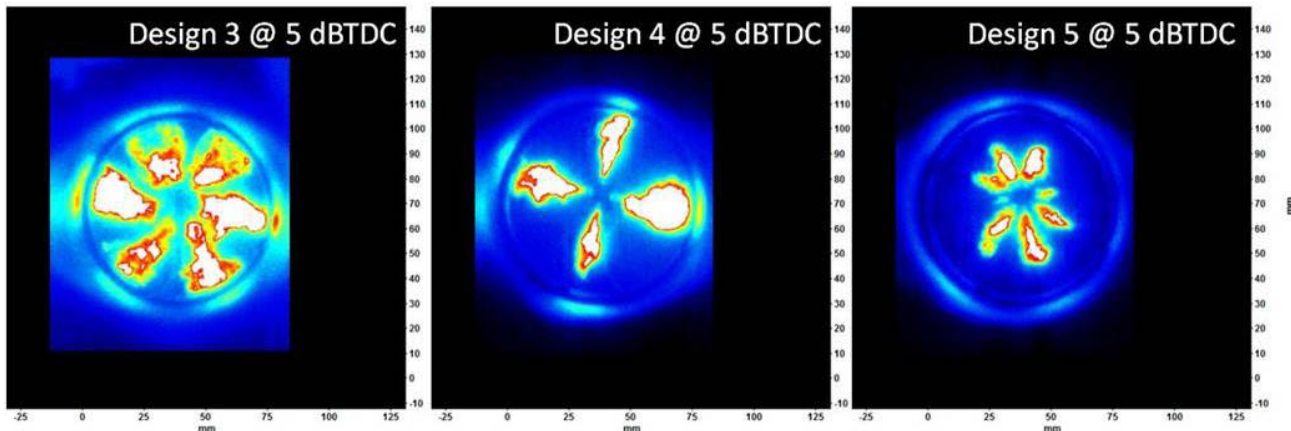


FIGURE 6. Optical Data @ 5 degrees before top-dead center (dBTD) – TJI Designs 3, 4, and 5

pressure, as induced by smaller overall nozzle orifice area, generally results in higher jet velocity and therefore more jet penetration. This degree of jet penetration coupled with the number of nozzle orifices determines the ignition site distribution in the main chamber. It is demonstrated that the design that has the most favorable distribution, i.e., large number of orifices with lowest overall orifice area results in the highest NTE. This is due to the flame front emanating from each of the ignition sites having less chamber volume to traverse, resulting in quicker main chamber combustion duration.

Proper targeting of nozzle characteristics such as orifice diameter, number of orifices, and overall orifice area can increase achievable NTE. These design features have significant bearing on physical jet properties such as velocity, penetration prior to ignition, and ignition site distribution.

Planned future work on this project will focus on confirming the empirical results obtained thus far using a correlated computational fluid dynamics model. This model will then be utilized as a quasi-predictive tool to further refine the TJI design. Future engine tests will focus on optimizing TJI engine operation to achieve the project targets.

FY 2013 PUBLICATIONS/PRESENTATIONS

1. Bunce, M., "Next Generation Ultra-Lean Burn Powertrain," 2013 DOE Vehicle Technologies Annual Merit Review, Washington, DC, May 2013.
2. Bunce, M., "Next Generation Ultra-Lean Burn Powertrain: DOE Project Phase 1 Summary," MAHLE North American Technical Exchange, Farmington Hills, MI, 6/4/2013.

REFERENCES

1. Germane, G., Wood, C., Hess, C., "Lean Combustion in Spark-Ignited Internal Combustion Engines – A Review," SAE Technical Paper 831694, 1983.
2. Attard, W., Toulson, E., Fraser, E., Parsons, P., "A Turbulent Jet Ignition Pre-Chamber Combustion System for Large Fuel Economy Improvements in a Modern Vehicle Powertrain," SAE Technical Paper 2010-01-1457, 2010, doi:[10.4271/2010-01-1457](https://doi.org/10.4271/2010-01-1457).
3. Attard, W., Kohn, J., Parsons, P., "Ignition Energy Development for a Spark Initiated Combustion System Capable of High Load, High Efficiency and Near Zero NO_x Emissions," SAE Journal Paper JSAE 20109088, 2010.
4. Attard, W., Blaxill, H., "A Gasoline Fueled Pre-Chamber Jet Ignition Combustion System at Unthrottled Conditions," SAE Technical Paper 2012-01-0386, 2012, doi:[10.4271/2012-01-0386](https://doi.org/10.4271/2012-01-0386).
5. Attard, W., Blaxill, H., "A Lean Burn Gasoline Fueled Pre-Chamber Jet Ignition Combustion System Achieving High Efficiency and Low NO_x at Part Load," SAE Technical Paper 2012-01-1146, 2012, doi:[10.4271/2012-01-1146](https://doi.org/10.4271/2012-01-1146).

IV.14 High Efficiency Variable Compression Ratio Engine with Variable Valve Actuation and New Supercharging Technology

Charles Mendler
ENVERA LLC
Los Angeles, CA 90068

DOE Technology Development Manager:
Roland Gravel

NETL Project Manager: Ralph Nine

Subcontractors:

- Eaton Corporation, Marshall, MI
- Roush Industries, Allen Park, MI

- VVA development and cylinder head installation
- Advanced supercharger integration into the engine



INTRODUCTION

This project is directed towards development of a high-efficiency VCR engine having VVA and new supercharging technology. Aggressive engine downsizing and the high-efficiency Atkinson cycle will be used during most driving conditions to attain large improvements in fuel economy. New supercharging technology will be used to provide V-8 like driving performance from the down-sized 4-cylinder VCR engine. Fleet operators are potential early adopters of the Envera VCR engine technology for use in light-duty delivery vans and pickup trucks. Replacing current V-8 engine offerings in these vehicles with a 4-cylinder VCR engine has potential for improving fuel economy by approximately 40% while retaining full engine power. The VCR engine can provide similar fuel economy benefits in other vehicle types such as passenger cars and sport utility vehicles.

Overall Objectives

The primary objective of this project is to develop a high-efficiency variable compression ratio (VCR) engine having variable valve actuation (VVA) and an advanced high-efficiency supercharger to obtain up to a 40% improvement in fuel economy when replacing current production V-8 engines with the new small displacement VCR engine.

- Target power range: 281 to 360 hp
- Target light and medium load efficiency: 230 g/kWh

Fiscal Year (FY) 2013 Objectives

- Confirm power and torque targets are feasible
- Capture interface and hard-point locations to support computer-aided design (CAD) design
- Initiate CAD design

Under the current project, Envera plans to demonstrate the benefits of the Envera VCR engine to prospective early adopters of the VCR technology while concurrently pursuing mass-market commercialization of the VCR engine, the Eaton VVA system, and the Eaton advanced supercharging technologies.

FY 2013 Accomplishments

- The VVA system was projected to attain cam lift and duration values needed for attaining engine power and efficiency targets
- The 4-cylinder VCR engine with advanced supercharging was projected to achieve power and torque targets
- CAD design of the VCR engine was initiated

APPROACH

The current project includes three phases. In Phase 1 the general feasibility of attaining performance goals was assessed. Durability of the VCR engine power take-off coupling will also be assessed. In Phase 2, the VCR engine will be designed and built, including the VCR crankcase, VVA-equipped cylinder head, and advanced supercharging installation. In Phase 3 the engine will receive baseline calibration and testing. Engine and chassis dynamometer testing will then be conducted to quantify baseline fuel economy improvements and performance. The current project builds on earlier development efforts, including a VCR crankcase and actuator development effort conducted with NETL/DOE, and a 1.8-L VCR engine built for Oak Ridge National Laboratory for combustion research.

Future Directions

During FY 2014 development work will be conducted in the following areas:

- VCR crankcase design and manufacture

RESULTS

Engine Performance Targets

Pickup trucks and utility vans have been identified as potential early adopter markets for the Envera 4-cylinder VCR engine. The market for utility vans is much larger in Europe. Because of these higher sales volumes, Europe needs to be included in the utility van commercialization game plan for the VCR engine. An initial finding was that European utility vans have very low power levels relative to U.S. vans. For example, the largest engine option for the Movano full-size van sold by Vauxhall (a General Motors subsidiary) is a 2.3-L 4-cylinder diesel that produces power and torque values of 107 kW (143 hp) at 3,500 rpm, and 350 Nm (258 ft-lb) at 1,500 rpm (see Figure 1). The 2.4-L Envera VCR engine can easily attain European performance targets.

Because the European vans have much smaller engines that are also diesel, fuel economy is exceptionally high by U.S. standards. The Envera VCR engine will attain high mileage through similar engine down-sizing plus use of the Atkinson cycle. The VCR engine will also be supercharged to provide high-power levels to meet U.S. commercial needs.

The power and torque needs are significantly higher for full-size U.S. pickup trucks. Baseline engine values are as follows: Ford F150 pickup truck with a 3.7-L Ti-VCT V-6 engine: 302 horsepower @ 6,500 rpm and 278 ft-lb torque @ 4,000 rpm. Chevrolet Silverado pickup truck with a 4.3-L V6 EcoTec3 engine: 285 hp @ 5,300 rpm and 305 ft-lb torque at 3,900 rpm. Dodge Ram 1500 pickup truck with 3.6-L Pentastar V-6: 305 hp at 6,350 rpm and 269 ft-lb torque at 4,800 rpm.

VCR Engine Power and Torque Assessment

The ability of the Eaton VVC mechanism (shown in Figure 2) to provide both Atkinson and high-power cam profiles was assessed. Envera generated baseline valve lift and valve timing values for attaining high efficiency using the Atkinson cycle and also for attaining high power levels with supercharging. Eaton then developed valve lift profiles to the specifications provided by Envera



FIGURE 1. The *Movano* is a Full-Size Van Sold by Vauxhall in England

to determine if the target values are attainable (see Figure 3). Kinematic calculations conclude that the Eaton VVA mechanism can be utilized for late intake valve closing to enable a switchable Atkinson cycle combustion strategy. The analysis indicates that the target values can be attained but may require about a three degree increase in the lob separation angle. A three degree increase in



FIGURE 2. Eaton VVA Mechanism

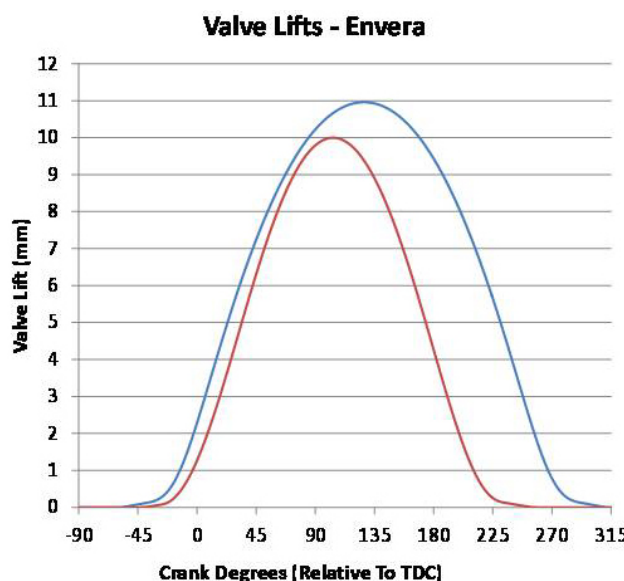


FIGURE 3. VVA Atkinson and Otto Cycle Cam Lift Profiles

lobe separation angle will not substantially change engine performance.

VCR engine performance targets were assessed with Eaton's advanced supercharger technology and VVA. The analysis included the performance and efficiency of the supercharger, and also its driveline losses. Engine power and torque were modeled knowing the supplied air boost pressure and mass flow. The analysis indicates that the performance targets for the current project are feasible. The supercharged VCR engine is projected to produce over 300 hp. In general, the larger the supercharger the larger the torque and power. Valve timing and duration events and sizing of the supercharger will be optimized during the project.

Engine Design

The General Motors 2.5-L model year 2014 Ecotec engine has been selected as the platform engine model for this project. A VCR crankcase will be developed that mates with the Ecotec cylinder head. Advanced supercharging and variable valve control will also be added to the engine.

Development work on the VCR crankcase is on schedule. General specifications and design have been completed for the piston, ring pack, cylinder liner, connecting rod, crankshaft, bearings, VCR cradle, cradle bearings, cradle links, and bedplate-to-crankcase design below the water jacket on the intake side of the engine (see Figures 4 and 5).

The VCR crankcase and cradle packaging design has exceeded expectations. Design upgrades from prior VCR engine builds include:

- Ring dowels used on all main fasteners for added stiffness
- Large clearances between the main bolt columns and cradle for lower-cost casting tolerances
- Raised cradle bearing race for easier and lower cost machining
- Off-set rails on the cradle bearing backs for easier assembly
- No cutout in the cradle for actuator space, to provide a stiffer cradle

CONCLUSIONS

Development of the ENVERA VCR engine is on schedule. Valve lift and duration values needed for Atkinson and Otto Cycle operation were projected to meet project needs. Power and torque values attainable with supercharging were also projected to meet

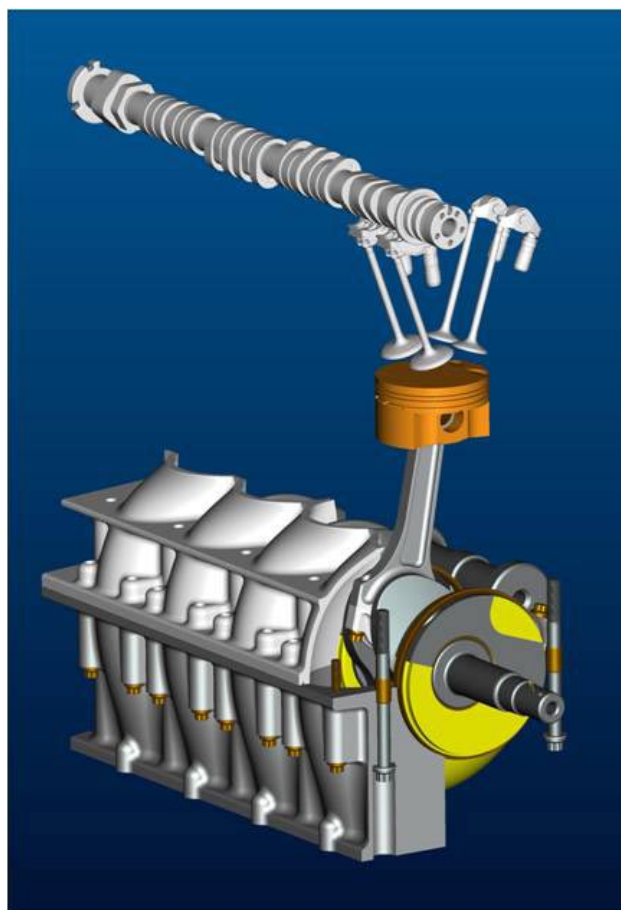


FIGURE 4. Envera VCR Engine Current Design Progress

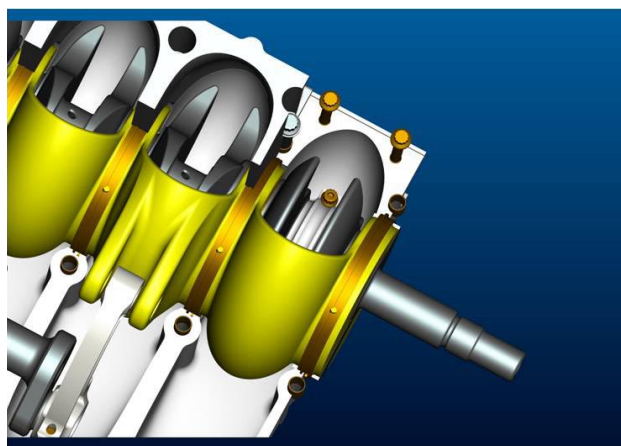


FIGURE 5. Envera VCR Engine Improvements

project targets. During FY 2014 and 2015 the VCR engine will be designed and built, including the VCR crankcase, VVA-equipped cylinder head, and advanced supercharging installation.

FY 2013 PUBLICATIONS/PRESENTATIONS

1. A press release for the NETL/DOE award was released on June 21, 2013, and also posted to the ENVERA website: VCREngine.com.

IV.15 Recirculated Exhaust Gas Intake Sensor (REGIS) Enabling Cost-Effective Fuel Efficiency Improvement

Claus Schnabel (Primary Contact),
Karen Carwile, Julia Miersch

Robert Bosch LLC
38000 Hills Tech Drive
Farmington Hills, MI 48331

DOE Technology Development Manager:
Roland Gravel

NETL Project Manager: Ralph Nine

Subcontractors:

- Clemson University, Greenville, SC
- Oakridge National Laboratory, Knoxville, TN

Overall Objectives

- The primary objective of this project is to develop an intake air oxygen (IAO2) sensor which directly and accurately measures the oxygen concentration in the intake manifold.
- This project will address the technical barriers in fundamental research, technology application, and system implementation to accelerate the development of an IAO2 sensor to directly and accurately measure the oxygen concentration in the intake manifold for gasoline engines using external exhaust gas recirculation (EGR).

Fiscal Year (FY) 2013 Objectives

- Evaluation of a baseline wideband exhaust oxygen sensor to determine required improvements to its thermal shock resistance, accuracy, response time, pressure dependency, and transient response
- System level cool EGR evaluation for sensor development and control development work
- Control concept with and without IAO2
- Requirements for sensor location
- Improvement of sensor housing and mounting design to meet performance targets
- Fabrication of prototype IAO2 sensor

FY 2013 Accomplishments

- Design concept for IAO2 was completed. Focus of component design and research was on the

subsystems sensor connector and housing as well as the protection tube.

- Development of protection tube led to benchmark functional performance in its design space.
- Bench testing and endurance tests to support development work throughout the project were developed and set up and used to steer design work.
- Testing of IAO2 baseline sensors was completed.
- Engine and simulation work for system evaluation and control development was conducted.

Future Directions

- Development of a control algorithm that uses the accurate IAO2 sensor oxygen concentration measurement to maximize combustion efficiency, and improve fuel economy.
- Fabrication of IAO2 sensors.
- Validation of 1st generation IAO2 sensor design (component and engine durability).
- Identification of further improvement potential on base of component validation and cool EGR system analysis.
- Set up and conduct design work to incorporate lessons learned from component validation and cool EGR system analysis.



INTRODUCTION

The primary objective of the REGIS project is to develop an IAO2 sensor which directly and accurately measures the oxygen concentration in the intake manifold. This capability affords vehicle manufacturers the ability to estimate the EGR percentage to a level of accuracy currently not possible. Accurate EGR estimation and resultant finer control improves engine efficiency, reduces fuel consumption, and maintains or improves exhaust emissions. More specifically, measurement of the actual EGR percentage enables a significant reduction in the calibrated safety margins required due to the inclusion of component tolerances in current EGR modeling approaches. Controlling EGR usage near optimized set points with improved combustion control is an enabler for gasoline engine fuel economy improvements in modern and advanced

engine concepts including conventional stoichiometric engines, advanced turbocharged and downsized engines, and Homogeneous Charge Compression Ignition (HCCI) engines.

APPROACH

The project will redesign the current generation of wideband exhaust gas oxygen sensors to meet the requirements of the intake manifold environment. The major challenges, as identified by Bosch internally and reported in the technical literature, of thermal shock, contamination, accuracy, pressure dependency, and response time will be addressed through design improvements. Clemson University, in collaboration with Bosch, will develop and validate robust control algorithms using IAO2-measured oxygen concentrations to improve combustion efficiency. Engine dynamometer tests will verify fuel economy improvements and sensor robustness to function and environment for gasoline engines with high concentrations of external EGR.

RESULTS

An exhaust oxygen sensor currently under development by Bosch is the basis for the IAO2 sensor design. The baseline sensor is a traditional threaded sensor with a wire harness. The IAO2 sensor has non-threaded mounting and a direct connection to the vehicle wire harness, thereby eliminating the pigtail attached to the sensor. Customer and internal Bosch specifications for both oxygen sensors and pressure sensors were compiled to create a list of requirements for the IAO2 design and used to establish testing procedures that support and validate design work.

The four main subsystems of the sensor were modified to take advantage of the application environment for the IAO2. Figure 1 displays the developed sensor design. The short sensor holds the sensing element in place and is the anchor for the other systems. The protection tube protects the sensing element from water, oil and the EGR particles in the intake air. It is further optimized to have a fast detection of change in oxygen level (response time) and influences the power consumption of the sensor.

The mounting components attach the sensor to the engine. The electrical connection provides power to the sensing element as well as conducting the signal to the vehicle's electronic control unit. The electrical connection also provides environmental sealing to the sensor from the under hood environment.

Two test stands were set up and validated to assess the impact of different design choices for the protection tube. A design of experiment was conducted to identify

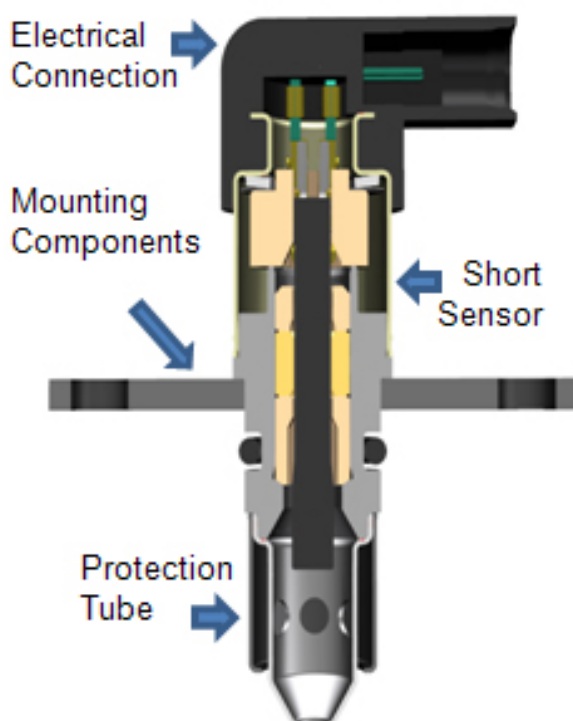


FIGURE 1. IAO2 Sensor Design

the design parameters ensuring optimal functional performance of the tube. Sensor testing on the high-volume flow bench was completed to evaluate the optimum tube for flow without a corresponding negative effect on current draw. It was used to document the sensor performance in response time and operation power. Various different protection tube designs capturing the design parameter space were compared.

Figure 2 shows the testing response time and the heater power demand of the different sensor designs when exposed to a flow velocity that is representative of engine part-load conditions. To evaluate thermal shock resistance a prototype test stand was designed and built.

The set-up parameters and the repeatability of the test bench to produce thermal shock are currently being validated. The thermal shock robustness of the IAO2 protection tubes is being compared against the baseline existing exhaust sensor protection tubes.

Procurement of the components needed for the initial prototype build is complete and build will be conducted in December 2013. Critical elements for prototype assembly have been identified and a prototype production process has been developed.

Engine work was started using the baseline part from current production. The Bosch partner, Clemson University began working in June of 2013 to begin data collection for simulations. Engine geometric data

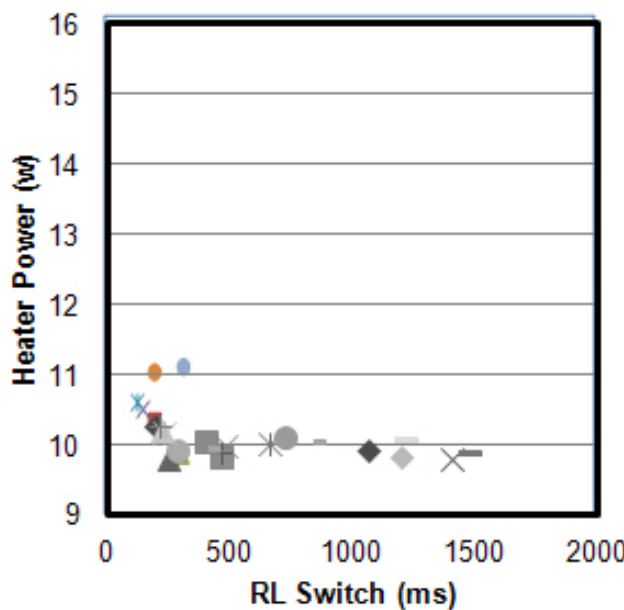


FIGURE 2. Design of Experiment: Impact of Protection Tube Design on its Performance at Part-Load Engine Condition, for References Competing Designs are Displayed

collection for implementation into the GT-POWER simulation is now complete. Information related to the fuel injectors, combustion chamber shape, valve lift profiles, and geometric parameters of the entire gas flow path have now been integrated. An engine has been selected and configured with a rapid-prototype engine controller that interfaces directly with the engine management program. A low-pressure ECR system and turbocharger have been incorporated into the engine along with a spare cylinder head for cylinder pressure transducers, engine mounts, a flywheel and a special turbo adapter flange, Figure 3.

A main objective of this project is to recognize the fuel economy benefits from knowing and accurately controlling the exact value of EGR dilution at all times. The process for determining fuel economy gain potential from the use of intake oxygen sensing was developed during Phase 1. Three engine configurations/calibrations will be compared: (1) best fuel economy calibration without EGR, (2) best fuel economy calibration with maximum EGR, and (3) best fuel economy calibration with slightly reduced EGR from maximum. Case 1 is being performed to demonstrate the importance of using EGR for fuel economy gains (against Cases 2 and 3). Case 2 is the best case calibration/EGR usage that is possible, up to the combustion stability limit,



FIGURE 3. Engine Installation on a Test Cell Cart at Clemson University

and is expected to represent and engine using an intake oxygen sensor for EGR valve control. Case 3 represents the current ‘state of the art’ in EGR control/calibration (without intake oxygen sensing) where a ‘safety-factor’ of several percent EGR is utilized to account for possible control uncertainty.

CONCLUSIONS

- Customer and internal Bosch specifications for both oxygen sensors and pressure sensors were compiled to create a list of design requirements for the IAO2 sensor. A wide range of conditions from customer to customer will need to be considered.
- Design parameters ensuring optimal functional performance of the prototype protective tube were defined. Testing identified that response time and the heater power demand of the different sensor designs could be used to distinguish and optimize the protective tubes.
- The IAO2 sensor design was finalized and prototypes will be built in December 2013.
- A Design for Six-Sigma study on the protection tube parameter space was conducted and will be completed in December 2013.
- Engine system and control related work was set up and is in progress at Bosch, Clemson and Oakridge National Laboratory. Objectives are to refine sensor requirements, to design control strategies and assess system-related benefits.

SPECIAL RECOGNITIONS & AWARDS/PATENTS ISSUED

| Title | Inventors | Institution | Date Invention Record Created | Institution Recording (Bosch, Clemson, ORNL) | IR Number |
|------------------------------|--------------------------|-------------|-------------------------------|--|-----------|
| Gas Sensor Protection Device | David Boyd, Craig Magera | Bosch | 3/27/2013 | Bosch | 2013/2095 |
| Mounting Flange Heat Shield | David Boyd, Craig Magera | Bosch | 3/18/2013 | Bosch | 2013/1803 |

IV.16 Robust Nitrogen Oxide/Ammonia Sensors for Vehicle Onboard Emissions Control

Rangachary Mukundan¹ (Primary Contact),
Eric L. Brosha¹, Courtney Kreller¹,
Vitaly Y. Prikhodko², Josh A. Pihl²,
and James E. Parks II², Wenzia Li³,
Ponnusamy Palanisamy³ and Fernando Garzon¹

¹Los Alamos National Laboratory (LANL)
MS D429, PO Box 1663
Los Alamos, NM 87544

DOE Technology Development Manager:
Roland Gravel

No Cost Partner:

²Oak Ridge National Laboratory (ORNL),
Oak Ridge, TN

Subcontractor:

³ESL ElectroScience, Inc. (ESL) King of Prussia, PA

Future Directions

- Demonstrate quantitative correlation of NO response of an optimized sensor to Fourier transform infrared (FTIR) response during engine testing.
- Demonstrate ammonia (NH₃) sensitivity of 10 ppm in an ESL-manufactured sensor.
- Report on nitrogen oxide/hydrocarbon sensor response optimization studies.
- Demonstrate >10 times NH₃ selectivity with respect to hydrocarbons.



INTRODUCTION

The 2010 Environmental Protection Agency (EPA) emissions regulation for NO_x is 0.2 g/bhr-hr, and they have started to certify diesel engines that can meet this regulation. Most manufacturers had initially opted instead to meet a Family Emission Limit around 1.2-1.5 g/bhp-hr NO_x with most of their engine emissions lying between the two standards [1]. Currently, the EPA has certified engines with both exhaust gas recirculation (EGR) and selective catalytic reduction (SCR) technologies to meet the strict 0.2 g/bhr-hr NO_x standard. While there is only one EGR system that has been certified by the EPA as meeting 2010 emissions regulations (Navistar, Inc.), there are several SCR systems that can meet this requirement (Cummins, Detroit Diesel, Volvo, etc.). Moreover, the SCR system, in addition to meeting emissions regulations, can result in a 3% to 5.5% increase in fuel efficiency [2].

The SCR system typically uses a zeolite NO_x adsorption catalyst that can selectively adsorb NO_x molecules during lean-burn operation and convert it to N₂ and H₂O with the injection of a urea-water solution called diesel exhaust fluid. It is the technology of choice for emissions control in Europe and several manufacturers have adopted it for the United States. SCR systems require tuning to work properly, and systems can be tuned with either pre-existing engine performance curves or with NO_x/NH₃ sensors. The use of NO_x/NH₃ sensors can provide closed-loop control of the SCR system that can optimize the system for improved NO_x reduction efficiencies and low NH₃ slip. According to a recent review by Docquier, et al., "Reliable and accurate NO_x sensors will be the key to the management of adsorption

Overall Objectives

- Develop a prototype NO_x sensor based on mixed-potential technology using a La_{1-x}Sr_xCrO_{3-dδ} (LSC) sensing electrode.
- Develop a prototype NH₃ sensor based on mixed-potential technology using an Au sensing electrode.

Fiscal Year (FY) 2013 Objectives

- Demonstrate sensor-to-sensor reproducibility in a commercially manufacturable sensor prototype.
- Demonstrate 1,000 hour durability in a commercially manufacturable sensor prototype.
- Demonstrate NO_x sensor performance in an engine dynamometer environment.

FY 2013 Accomplishments

- Qualitatively reproduced NO_x sensitivity and selectivity of a LANL bulk sensor in a commercially manufacturable device.
- Demonstrated sensor stability for 1,000 hours in both unbiased and biased mode with no systematic degradation in sensor sensitivity.
- Sensor tracks NO_x concentration in engine dynamometer testing performed at the National Transportation Research Center at ORNL.

catalysts” [3]. The optimized use of SCR systems can increase the value for the customer with fuel and diesel exhaust fluid savings (including reduced frequency and costs of the dealer servicing of the emissions system consumables) over the life of the vehicle helping defray the added cost of the system.

APPROACH

LANL has previously developed a new class of mixed-potential sensors that utilize dense electrodes partially covered with porous and/or thin film electrolytes [4-7]. This unique configuration stabilizes the 3-phase (gas/electrode/electrolyte) interface resulting in sensors with exceptional response stability and reproducibility. This configuration also minimizes heterogeneous catalysis resulting in high sensor sensitivity. Moreover, the electrode composition of these sensors can be varied to tune the selectivity relative to desired exhaust gas species. For example, a gold electrode has high NH_3 selectivity while an LSC electrode provides high hydrocarbon or NO_x selectivity. When the sensors using LSC electrodes are operated at open circuit, the voltage response is proportional to non-methane hydrocarbons and when they are operated under a current/voltage bias mode, the response is proportional to total NO_x .

The unique mixed-potential electrochemical sensors developed at LANL were experimental laboratory devices. Moreover, the sensors were bulky, hand-made devices that required a large external furnace for precise temperature control during operation. In this project LANL is working closely with ESL to apply commercial manufacturing methods to LANL laboratory NO_x sensor configurations. Through an iterative process of prototype preparation at ESL, laboratory testing and materials characterization at LANL, and a free exchange of performance and characterization data between LANL and ESL, the performance of the sensors will be reproduced in a commercially manufacturable device. These devices will be evaluated under realistic engine exhaust conditions at the National Transportation Research Center at ORNL. Commercial sensor manufacturing companies will be engaged if the project meets all its sensitivity, selectivity, and durability milestones.

RESULTS

In FY 2012, LANL worked with ESL to manufacture mixed-potential sensors using a commercial high-temperature co-fired ceramic process. The devices were initially prepared to LANL specifications; ESL optimized their manufacturing processes according to LANL feedback in order to provide us with devices that exhibited responses similar to the unique patented

tape cast LANL sensors [8]. The ESL-manufactured sensors showed NO_x sensitivity of ± 5 ppm and were self-heated devices with a heater circuit printed in the back of the sensor. Temperature control of these sensors was identified as critical and LANL worked closely with Custom Sensor Solutions, Inc., to manufacture heater control boards for heater feedback control.

The reproducibility of the sensors manufactured by ESL was evaluated at LANL. The response of three different devices from one batch of sensors is illustrated in Figure 1. The commercially manufactured sensors had a response behavior very similar to tape cast sensors when operated in both an unbiased (Figure 1a) and biased (Figure 1b) mode. When the sensors were operated in open-circuit mode they did not show NO_x selectivity and had significant interference from hydrocarbons and NH_3 . However, when the sensor was operated at a $0.2 \mu\text{A}$ bias, it exhibited excellent selectivity to NO_x . The average response of the three sensors to 100 ppm NO was 13.15 ± 3.5 mV under $0 \mu\text{A}$ bias and 165.58 ± 8.4 mV under $0.2 \mu\text{A}$ bias. This sensor-to-sensor reproducibility is comparable to that obtained with tape cast sensors and is a significant improvement over conventional mixed-potential sensors.

The long-term stability of ESL-manufactured sensors was also evaluated during FY 2013. Previous work at LANL had indicated that stable electrode and electrolyte morphology is critical for sensor stability. The current generation of LANL mixed-potential sensors utilize dense electrodes and porous electrolytes to impart stability to the electrode and electrolyte morphology. The result of this stable morphology is a stable sensor response as illustrated in Figure 2. The sensor response shows excellent stability when operated at $0 \mu\text{A}$ bias (Figure 2a) with the NO response drifting $\approx 1 \mu\text{V}$ per hour of operation during the 1,000 hours of testing. The response stability of the sensor when operated at $0.2 \mu\text{A}$ bias is controlled by the baseline stability that shows a drift of $\approx 18 \mu\text{V}$ per hour. The drift in NO and NO_2 responses when operated under bias are $\approx 15 \mu\text{V}$ per hour and $\approx 16 \mu\text{V}$ per hour, respectively. Further optimization is required to stabilize the baseline response under bias conditions. X-ray tomography and scanning electron microscope analysis of these sensors indicated that the Pt electrode still had some pores that change with time and are probably responsible for the sensor drift. The composition of the Pt paste used in the screen-printing process and the sensor-firing schedule will be optimized to further improve sensor stability.

LANL performed testing at ORNL's National Transportation Research Center on a 1.9-liter Opel (General Motors) turbocharged diesel engine equipped with EGR, a diesel particle filter and a diesel oxidation catalyst. This engine was also equipped with various

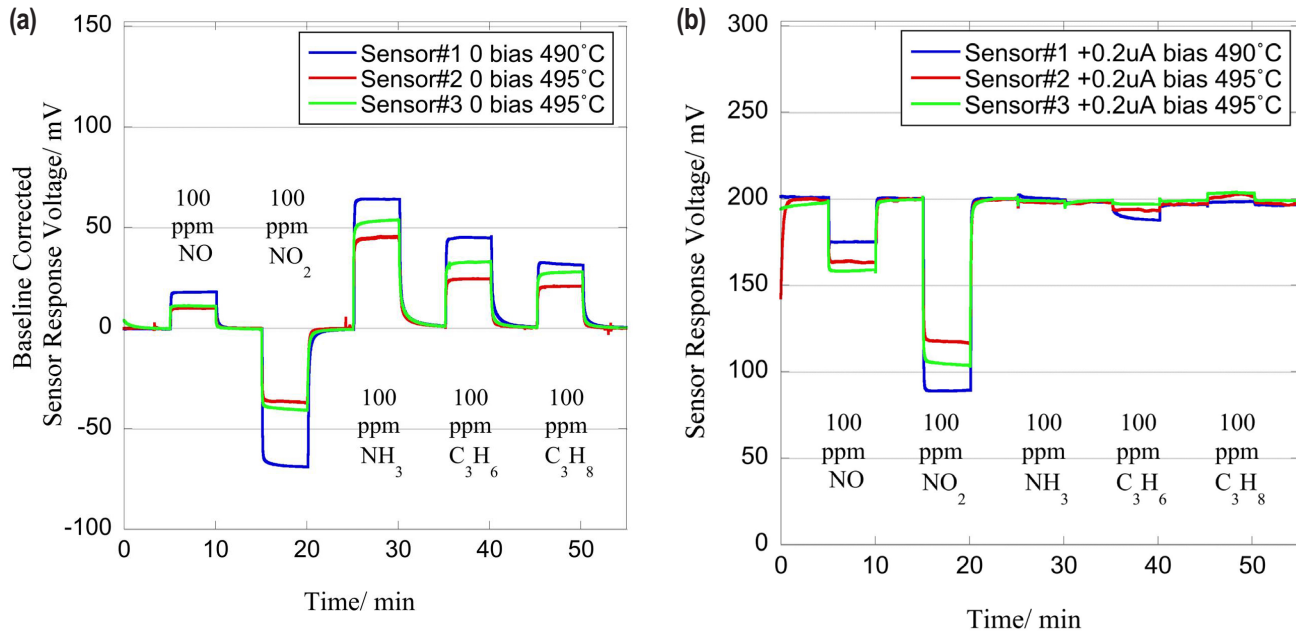


FIGURE 1. Comparison of the sensor response of three different mixed-potential sensors manufactured by ESL and operated under a) zero bias and b) 0.2 μ A bias.

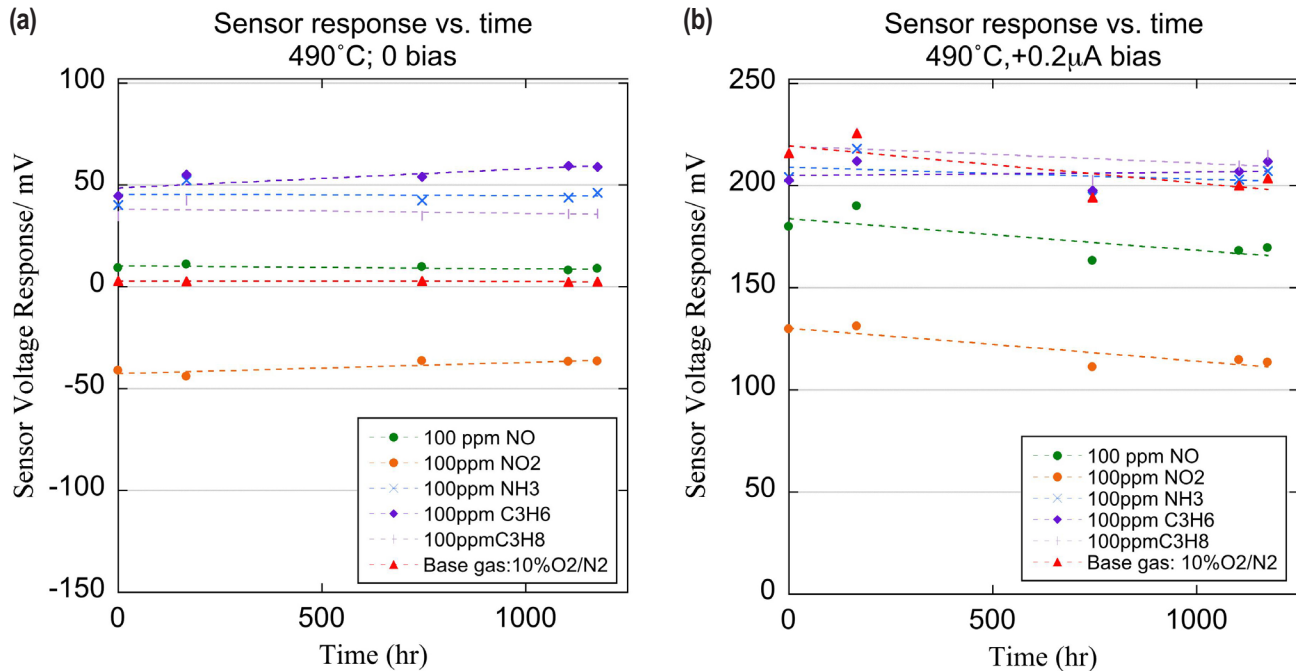


FIGURE 2. Stability of a mixed-potential sensor manufactured by ESL and operated E Inc.under a) 0.0 μ A bias and b) 0.2 μ A bias, for 1,000 hours.

instrumentation including a flame ionization detector (FID) to record total hydrocarbons (THCs), mounted close to the sensor, and an FTIR to monitor THCs and NO, mounted downstream of the sensor. The response of the LANL sensor when the EGR was turned off and on is shown in Figure 3 for a constant engine load at two

different engine speeds of 2,000 (Figure 3a) and 1,600 rpm (Figure 3b). The sensor response closely tracks the NO concentration in the engine exhaust with the sensor showing a marked decrease in voltage every time the EGR was turned off. The decrease in sensor voltage was 23 mV @ 2,000 rpm and 13 mV @ 1,600 rpm. The NO

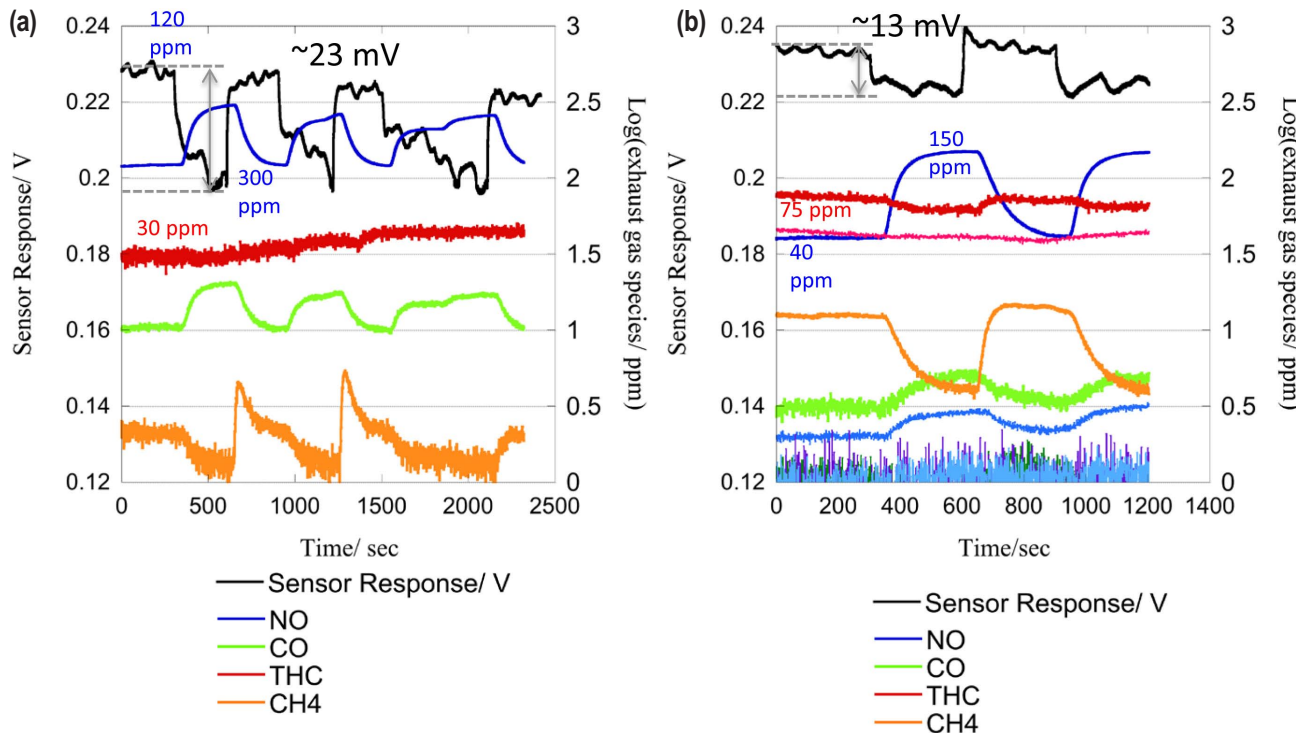


FIGURE 3. Sensor response at $0.2 \mu\text{A}$ bias to engine exhaust at a) 2,000 rpm and b) 1,600 rpm with EGR on and off. The NO, CO, THC and CH_4 concentration measured in the engine exhaust is also plotted.

concentration decreased from $\approx 300 \text{ ppm}$ to $\approx 120 \text{ ppm}$ @ 2,000 rpm and from $\approx 150 \text{ ppm}$ to $\approx 40 \text{ ppm}$ @ 1,600 rpm when the EGR was turned on. Independent sensor calibration at LANL on a different sensor showed a sensor response of 20 mV and 11 mV for these changes in NO concentration. These results demonstrate the ability of the LANL sensor to quantify NO concentration in a realistic engine exhaust environment.

The sensor response in Figure 3 illustrates fluctuations in sensor response while there is no corresponding change in the NO concentration monitored by the downstream FTIR. To further understand this discrepancy the THC concentration was also monitored close to the sensor using a FID. The sensor response under $0 \mu\text{A}$ bias is plotted along with the FID and FTIR response in Figure 4 where the engine was operated in the Premixed Charge Compression Ignition mode. The sensor operated at zero bias exhibits significant THC response that closely tracks the FID response. When the engine was operated under low-fuel conditions, the FID showed sharp fluctuations in the THC content which the sensor tracked. However the FTIR downstream of the sensor did not record these fluctuations, which were effectively smoothed by the orifice used to restrict the flow rate onto the sensor. These results illustrate the fast response of the LANL sensor and its ability to track changing gas concentrations in the engine exhaust.

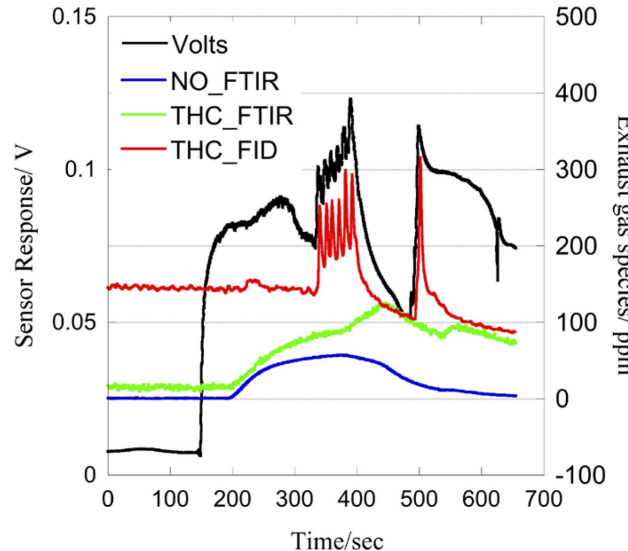


FIGURE 4. Sensor response at $0.0 \mu\text{A}$ bias to engine exhaust when operated in Premixed Charge Compression Ignition mode. The THC measured by an FID is plotted along with the THC and NO measured by a downstream FTIR.

CONCLUSIONS

- ESL utilized the high-temperature co-fired ceramic process to successfully manufacture mixed-potential sensors based on LANL sensor design.

- The performance of ESL sensors was comparable to previously reported LANL tape-cast sensors.
- ESL manufactured sensors exhibit good sensor-to-sensor reproducibility.
 - Further improvements in reproducibility possible with tighter control on heater resistance.
 - Further improvements in reproducibility possible with optimizing and improving performance of control electronics.
- ESL manufactured sensors show excellent long-term stability when operated in the zero bias mode.
 - The sensor response in the bias mode shows drift due to changes in the morphology of the Pt electrode. Elimination of porosity in this electrode should result in improvements in the sensor stability.
- LANL sensors can quantitatively track the NO and THC concentration in engine exhaust when operated in the unbiased and biased mode respectively.
 - Present sensors appear to exhibit sufficient response time to track real-time engine events.
- Optimization of sensor selectivity: selectivity through design changes and signal processing is being pursued.

REFERENCES

1. Diesel Power: Clean Vehicles for Tomorrow. Vehicle Technologies Program, U. S. Department of Energy, July 2010.
2. T.V. Johnson, “Review of Diesel Emissions and control”, International Journal of Engine Research, V10. No 5, 275 (2009).
3. N. Docquier, S. Candel, “Combustion control and sensors: a review”, Progress in Energy and Combustion Science, V 28, 107 (2002).
4. R. Mukundan, E.L. Brosha and F. H. Garzon. US Patent # 7,575,709 B2, “Tape Cast Sensors and Method of Making”; August 18, 2009.
5. F.H. Garzon, E.L. Brosha and R. Mukundan. US Patent #7,264,700, “Thin Film Mixed Potential Sensors”; Sept. 4, 2007.
6. R. Mukundan, K. Teranishi, E.L. Brosha, and F.H. Garzon, “Nitrogen oxide sensors based on Yttria-stabilized zirconia electrolyte and oxide electrodes”. *Electrochemical and Solid-State Letters*, **10(2)**, J26-J29 (2007).
7. F.H. Garzon, E.L. Brosha, and R. Mukundan, “Solid State Ionic Devices for Combustion Gas Sensing”. *Solid State Ionics*, **175(1-4)**, 487-490 (2004).

8. R. Mukundan, E.L. Brosha and F.H. Garzon. US Patent #7,575,709 B2, “Tape Cast Sensors and Method of Making”; August 18, 2009.

FY 2013 PUBLICATIONS/PRESENTATIONS

1. Julia Tsitron, Courtney R. Kreller, Praveen K. Sekhar, Rangachary Mukundan, Fernando H. Garzon, Alexandre V. Morosov, and Eric L. Brosha, “Bayesian decoding of the ammonia response of a zirconia-based mixed potential sensor in the presence of hydrocarbon interference,” submitted to Sensors and Actuators B, Summer 2103; accepted for publication, (November 2013).
2. C.R. Kreller, J. Tsitron, P.K. Sekhar, R. Mukundan, F.H. Garzon, A.V. Morozov, and E.L. Brosha, “Quantitative Decoding of Ammonia-Hydrocarbon Mixtures Using Zirconia-Based Mixed Potential Sensors,” 224th Meeting of the ECS, San Francisco, CA, October 2013.
3. C.R. Kreller, P.K. Sekhar, W. Li, P. Palanisamy, E.L. Brosha, R. Mukundan and F.H. Garzon, “Application of Commercial Manufacturing Methods to Mixed-Potential NO_x Sensors”, *ECS Trans.*, **50(12)**, 307-314 (2013).
4. P.K. Sekhar, H. Sarraf, H. Mekonen, R. Mukundan, E.L. Brosha, and F.H. Garzon, “Impedance spectroscopy based characterization of an electrochemical propylene sensor”, *Sensor and Actuators B*, **V177**, 111-115 (2013).
5. P.K. Sekhar, R. Mukundan, E.L. Brosha and F.H. Garzon, “Effect of perovskite electrode composition on mixed potential response”, *Sensors and Actuators B*, **V 183**, 20-24 (2013).
6. C.R. Kreller, P.K. Sekhar, W. Li, P. Palanisamy, D. Spernjak, E.L. Brosha, R. Mukundan and F.H. Garzon, “Impedance as a diagnostic tool to characterize mixed-potential sensor response”, 224th meeting of the Electrochemical Society, San Francisco (2013).

V. SOLID STATE ENERGY CONVERSION

V.1 Gentherm Thermoelectric Waste Heat Recovery Project for Passenger Vehicles

V. Jovovic¹, T. Barnhart (Primary Contact)¹,
J. LaGrandeur¹, C. Maranville², C. Haefele³,
M. Miersch⁴

¹Gentherm Inc.
5462 Irwindale Ave.
Irwindale, CA 91706

²Ford Motor Company
³BMW AG

⁴Tenneco GmbH

DOE Technology Development Manager:
Gurpreet Singh

NETL Project Manager: Carl Maronde

Subcontractors:

- BMW, Palo Alto, CA and Munich, Germany
- Ford Motor Company, Dearborn, MI
- Tenneco GmbH, Grass Lake, MI and Edenkoben, Germany

- Component, cartridge, and multi-cartridge-level testing to continue, both for performance and durability
- Vehicle and TEG system requirements to be completed, with significant input from new partner, Tenneco
- Further work on oxidation/sublimation suppression coating
- Further development of the TE material model for SKU from the California Institute of Technology (Caltech)
- Scale up TE material and cartridge fabrication methods, including tooling and process development, for commercialization quantities
- Deliver a functional cartridge to TARDEC for bench testing

FY 2013 Accomplishments

- Vehicle platforms/powertrains were re-evaluated and new vehicles were selected by BMW and Ford after further fuel efficiency improvement performance trade-off analysis. BMW will use a BMW X3 with a 4-cylinder gas engine. Ford will use a Ford F150 with a 3.5-L EcoBoost V-6. Both vehicles have had their exhaust streams mapped on the US06 Cycle.
- Developed TE cartridge assembly tooling, processes and fabrication methods. Assembly methods were validated through the production of 11 cartridges.
- Tenneco focused on the development of simulation tools that can be used to model TEG systems, design of electrical and coolant connection between cartridges and the development of mechanical connections between cartridges and TEG canning.
- Gentherm developed a novel process for manufacturing TE elements bonded to other cartridge components. A cost analysis shows the potential for a reduction in TE element manufacturing cost by a factor of 5-10.
- Gentherm's SKU material production capacity has been doubled with the purchase of an additional spark plasma sintering system. Today's press room capacities are at the level of one cartridge's worth of material per day.
- Caltech has developed a deeper understanding of the electronic structure of filled CoSb₃ (SKU). Experimental data has been used to successfully develop a model of the electronic structures of these materials.

Overall Objectives

- A detailed production cost analysis for thermoelectric (TE) generator (TEG) for passenger vehicle volumes of 100,000 units per year and a discussion of how costs will be reduced in manufacturing.
- A 5% fuel economy improvement by direct conversion of engine waste heat to useful electric power for light-duty vehicle application. For light-duty passenger vehicles, the fuel economy improvement must be measured over the US06 Cycle.
- Confirmatory testing of the hardware to verify its performance in terms of fuel economy improvement.
- Build scaled-up TEG for the Tank Automotive Research, Development and Engineering Center (TARDEC) Bradley Fighting Vehicle (BFV).

Fiscal Year (FY) 2013 Objectives

- Fabricate initial skutterudite (SKU) TE material cartridge for testing and evaluation
- Further modeling, including MATLAB®/Simulink® and computational fluid dynamics /finite element analysis, will continue to achieve a design freeze

- Testing of oxidation/sublimation suppression coating systems was completed with no acceptable coatings being found for this application.
- A TE cartridge assembly was provided to TARDEC for bench evaluation for heavy-duty application.

Future Directions

- Scale up TE engine subassembly (tooling and process development)
- TE engine scalability and power form
- TE engine durability
- Scale up TEG subsystem joining technologies
- Scale up TEG fabrication concept
- Complete assembly of light-duty vehicle TEGs
- Begin bench testing of light-duty vehicle TEGs
- Complete assembly and test of heavy-duty vehicle TEG and related system components
- Deliver heavy-duty vehicle TEG and cooling system to TARDEC



INTRODUCTION

Emission regulations continue to become more restrictive and fuel costs continue to rise. The need for vehicles with better fuel economy continues to be very important for vehicle manufacturers. With many fuel economy-saving technologies already implemented, vehicle manufacturers need to search for additional improvements. Waste heat recovery is one potential option with TE waste heat recovery being a leading candidate.

The objective of this project is to design and implement a 5% improvement in fuel economy for light-duty vehicles based on TE waste heat recovery while providing a path towards commercialization at passenger vehicle volumes of 100,000 units per year. Confirmatory testing of the hardware to verify its performance in terms of fuel economy improvement will be conducted.

In addition to building TEGs for passenger vehicles, an additional project component was added to build and test a TEG for a BFV for TARDEC. With a similar timeline to the passenger vehicle component, the TEG for TARDEC will be scaled up for the 15-L diesel engine of the BFV.

APPROACH

This project has a strong team that provides vital inputs at each stage of the project. The team includes two vehicle manufacturers: BMW and Ford to provide their needs for the TEG components. They will provide important information on the best platform and powertrain selection for successful commercial implementation. The Tier 1 exhaust supplier is Tenneco, who will translate the needs of the vehicle manufacturers into requirements for successful implementation into the exhaust system. Tenneco will also take the TEG subcomponents and package them (canning much like a catalytic converter) effectively into a TEG device that satisfies all of the vehicle and vehicle subsystem constraints. Gentherm, the overall lead of the project, will design, build, and test the TEG subcomponents for the project. These TEG subcomponents will be optimized based on the vehicle and vehicle subsystem requirements and the TE material performance. Extensive one-dimensional (1-D) and three-dimensional (3-D) modeling will be conducted by the team. 3-D models will be used to best understand the component details with the 1-D models being used for comprehensive design optimization and for integration into vehicle system level models. These models will be rigorously validated against targeted experiments.

Gentherm will also spend considerable effort to develop TE material scale up capabilities for the most cost effective designs at 100,000 units per year. Research to develop necessary oxidation and sublimation protection will also be conducted. The team also includes TE material improvement efforts from Caltech and third-party performance validation from the National Renewable Energy Laboratory.

RESULTS

The Gentherm-led TEG project including subcontractors Ford, BMW North America, Tenneco (starting in Phase 2), Caltech, and the National Renewable Energy Laboratory has progressed toward the project objectives. The cartridge design, shown in Figure 1, and manufacturing processes have continued to evolve, with 11 SKU-based cartridges having been produced. Bench testing of the cartridges has been used to validate the 1-D MATLAB®/Simulink® models and to create performance maps that are being used to design and develop the TEG assembly. The cartridge's performance is shown in Figures 2-4.

Final Vehicle platform/powertrain selections have been made by BMW and Ford after further trade-off analysis. BMW will use a BMW X3 with a 4-cylinder gas engine. Ford will use a Ford F150 with a 3.5-L

**FIGURE 1.** TEG Cartridge

EcoBoost V-6. Both vehicles have been evaluated on the US06 Cycle.

Integration of the cartridges into a TEG assemble, also known as canning, was started in this phase of the project. Tenneco, who is responsible for this activity, has developed simulation tools that can be used to model TEG systems. Initial assembly concepts, Figures 5 and 6, have been generated and are being evaluated for their impact on vehicle level packaging, and thermal stress mitigation. Tenneco has also begun to analyze the exhaust gas mass flows and temperatures provided by Ford and BMW to select the number of cartridges for the TEGs and the TEG's position in the exhaust system.

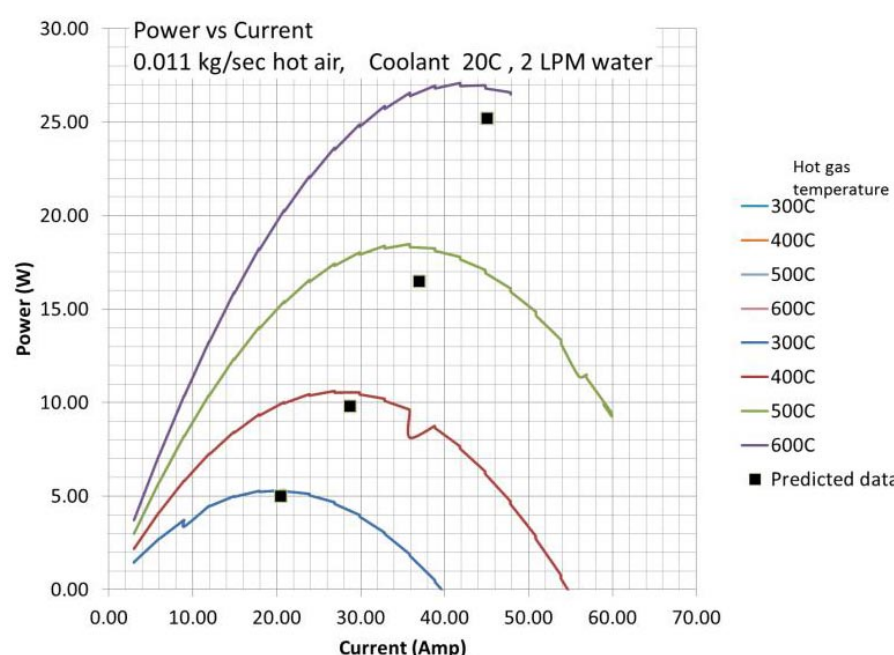
The teams also had success on developing advanced SKU materials and manufacturing processes. Gentherm

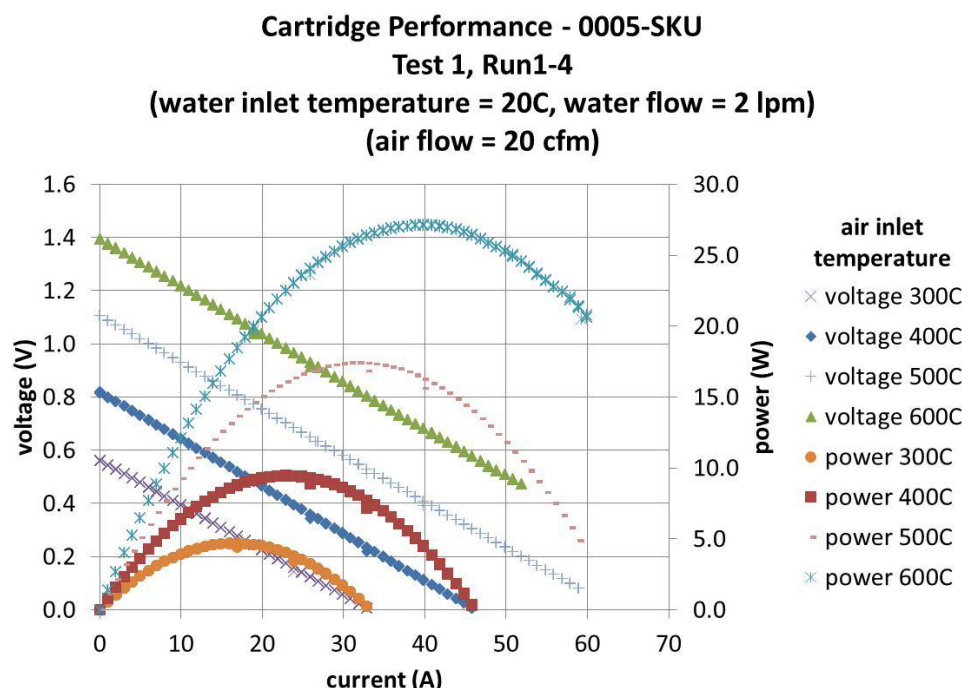
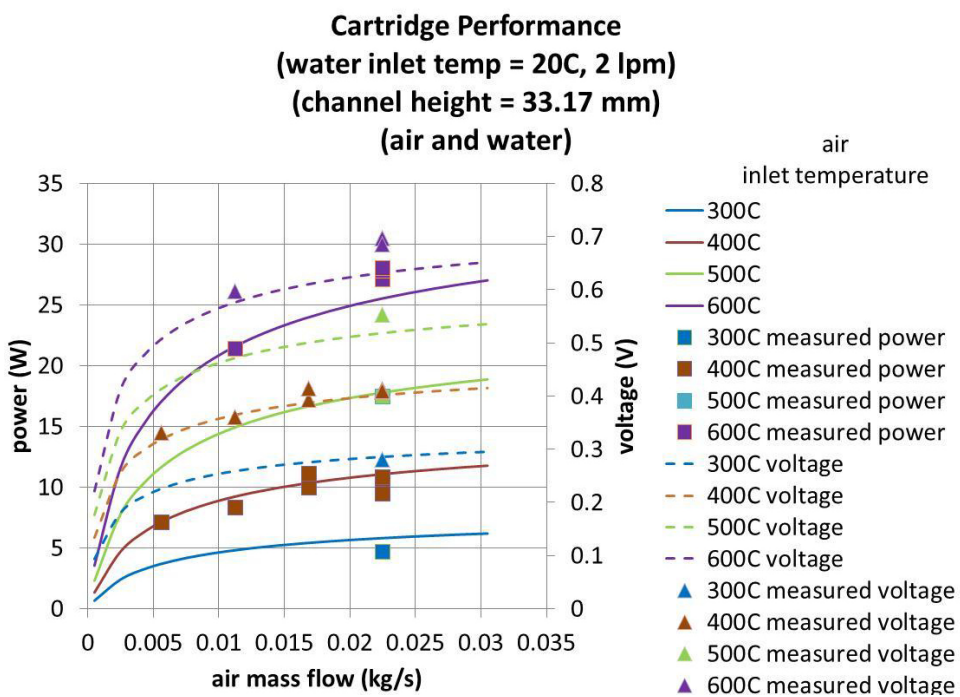
has developed a novel process for manufacturing TE elements bonded to other cartridge components. Caltech's work has yielded in a deeper understanding of the electronic structure of filled CoSb_3 . Experimental data has been used to successfully develop a model of the electronic structures of these materials. Based on these findings the group has demonstrated that by carefully controlling impurities it is possible to produce n-type materials with ZT values that are 15-20% higher than those used by Gentherm today.

CONCLUSIONS

The team's efforts continue to progress the designs and manufacturing processes towards a modular, scalable, and cost effective TEG design that is on a path to commercialization for the vehicle manufacturers.

- SKU materials and manufacturing processes have progressed and have shown significant potential for the needed cost reductions.
- The cartridge design has been advanced and validated with physical testing.
- Final vehicle platform/powertrain selections have been made by BMW and Ford after extensive trade-off analysis. The vehicles have been tested to measure the exhaust outputs over the US06 Cycle.
- Design of the TEG assemblies is advancing rapidly and the required design tools have been completed.

**FIGURE 2.** Cartridge Power vs. Current Curves

**FIGURE 3.** Cartridge Voltage vs. Current Curves**FIGURE 4.** Cartridge Voltage and Power vs. Air Mass Flow

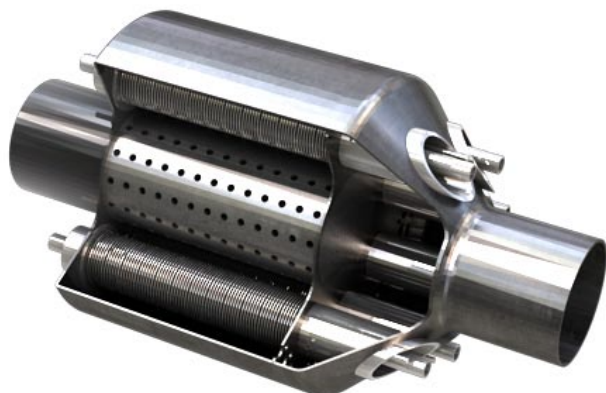


FIGURE 5. Initial TEG Assembly Concept

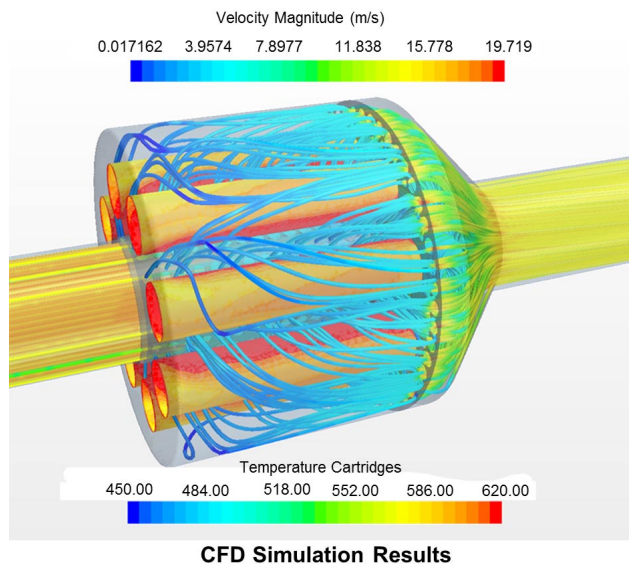


FIGURE 6. Initial TEG Assembly Computational Fluid Dynamics Simulation

FY 2013 PUBLICATIONS/PRESENTATIONS

1. “Cylindrical Cartridge as a Building Block for Thermoelectric Generator Applications”, Vladimir Jovovic, Doug Crane, John LaGrandeur, Marco Ranalli, Martin Adldinger, Eric Poliquin, Joe Dean, David Fang, Dmitri Kossakovski, ICT Kobe Japan, July 4th 2013.
2. “Automotive TEG Progress”, Dmitri Kossakovski, Exhibit at the Frankfurt IAA Show, September, 10–13, 2013.
3. “Exhaust Heat Recovery”, Michael Miersch, Adam Kotrba , presented at the Frankfurt IAA Show, September 10–13, 2013.

V.2 Improving Energy Efficiency by Developing Components for Distributed Cooling and Heating Based on Thermal Comfort Modeling

Jeffrey A. Bozeman (Primary Contact),
Kuo-Huey Chen
General Motors
30500 Mound Rd.
Warren, MI 48090

DOE Technology Development Manager:
Gurpreet Singh

NETL Project Manager: Carl Maronde

Subcontractors:

- Delphi Thermal Systems, Lockport, NY
- Faurecia Automotive Systems, Troy, MI
- Marlow Industries, Dallas, TX
- University of California, Berkeley, Berkeley, CA
- Oak Ridge National Laboratory, Oak Ridge, TN

Overall Objectives

- Develop a thermal comfort model and computer-aided engineering (CAE) tool to predict the occupant physiological response to localized heating and cooling through human subject testing—key to balance distributed heating, ventilation, and air conditioning (HVAC) components and to speed execution of stratified thermal systems.
- Reduce at least 30% of the fuel used to maintain occupant comfort through the localized use of thermoelectric (TE) technology while maintaining occupant comfort and safety.
- Develop TE HVAC components with a coefficient of performance (COP) >1.3 for cooling and >2.3 for heating, then integrate and test as a reliable system in an e-Assist Buick LaCrosse and an extended-range electric Chevrolet Volt.

Fiscal Year (FY) 2013 Objectives

- Deliver Buick LaCrosse demonstration vehicle with integrated TE components that provide 30% HVAC energy saving with baseline occupant thermal comfort.
- Deliver a TE coolant heater that can achieve a COP >2.3 during certain operation conditions for a Chevrolet Volt extended-range electric vehicle (EV).
- Deliver a thermal comfort CAE tool for quick thermal comfort evaluation of six representative

vehicles by using vehicle computer-aided design geometries and HVAC air data.

- Design face/chest TE devices, lap/foot TE devices, and new TE-equipped front seats for the Chevrolet Volt extended-range EV.

FY 2013 Accomplishments

- Delivered the completed Buick LaCrosse demonstration vehicle to the Department of Energy (DOE) and the California Energy Commission.
- Achieved estimated 30% HVAC energy saving with distributed TE components on the Buick LaCrosse demonstration vehicle.
- Maintained equivalent occupant thermal comfort in demonstration vehicle.
- Exceeded COP target of 1.3 in cooling and 2.3 in heating with prototype TE devices.

Future Directions

- Report detailed TE HVAC energy savings for the Buick LaCrosse demonstration vehicle.
- Install, calibrate and evaluate the TE system, including carry-over TE components (from the LaCrosse) and new seats with TE contact heating and cooling, in the Chevrolet Volt.
- Deliver the completed Chevrolet Volt demonstration vehicle to DOE by March 2014.



INTRODUCTION

The analysis of fuel consumption needed to provide vehicle air conditioning (A/C) in the United States on a state-by-state basis [1] shows an estimated 7 billion gallons of gasoline every year. This is equivalent to 6% of domestic petroleum consumption, or 10% of U.S. imported crude oil. The study further shows that vehicle A/C produces the most significant auxiliary load and outweighs other significant loads such as rolling resistance, aerodynamic drag, or driveline losses. Given this backdrop, energy-efficient HVAC systems deserve significant attention from the automotive industry in order to improve the fuel economy of their vehicles and to conform to heightened real world expectations and Corporate Average Fuel Economy standards. Traditional

comfort in a vehicle is achieved by either warming or cooling the vehicle from the ambient condition. When we acknowledge that a moving vehicle acts like a heat exchanger, we also recognize that energy is needed to maintain the vehicle climate when the vehicle interior is warmer or cooler than the ambient temperature. A larger temperature differential between the interior and the exterior requires more energy to maintain comfort. Our HVAC energy reduction strategy is to create a localized (micro) cooling/heating zone around individual vehicle occupants by supplementing a smaller central HVAC compressor with optimally placed distributed TE devices. The central HVAC compressor is still necessary for energy-efficient central humidity control and defogging. These passenger-directed microclimates reduce both the average temperature differential and the energy exchange between the vehicle interior and the external ambient environment.

The objective of this project is to develop distributed TE HVAC components to supplement the central HVAC system and then to integrate and evaluate the prototype system in a 5-passenger demonstration vehicle. The overall goal is to reduce the energy required by current compressed gas A/C systems by 30% and to develop supplemental TE HVAC components that have a COP greater than 1.3 for cooling and greater than 2.3 for heating. The final deliverable for the project is a demonstration vehicle with a functioning HVAC system that features TE-based distributed cooling and heating components. The first application is a Buick LaCrosse, a popular light-duty vehicle that utilizes a hybrid powertrain. The second application on a Chevrolet Volt extended-range EV is focused on the unique needs of EVs.

APPROACH

In FY 2013, the project team pursued the objective of maintaining equivalent thermal comfort while saving 30% of the HVAC energy usage by performing the following tasks: integrated the local TE HVAC components into two demonstration vehicles; configured HVAC and vehicle control systems to optimize system performance; and conducted evaluations to demonstrate the upper limits of cabin thermal stratification, to address the risk of window fogging and to reduce TE HVAC component nozzle condensation.

Our work included climatic wind tunnel evaluations that used a thermal manikin to establish an objective equivalent homogeneous temperature. The automatic climate control (ACC) settings for the TE-equipped vehicles were adjusted from the baseline to produce equivalent comfort. Human riders were also used for in-vehicle evaluations to confirm proper settings. The team

logged data for energy calculations during evaluations at ambient temperatures ranging from 32 to 100°F, relative humidity (RH) ranging from 40% to 80%, and solar loads up to 1,000 W/m².

RESULTS

Figure 1 shows the prototype TE HVAC components installed in the Buick LaCrosse, including the driver face/chest TE nozzles, front passenger face/chest TE nozzles, front passenger lap/foot TE slot nozzle, and rear passenger face/chest TE nozzle. The driver seat has TE devices (TEDs) installed in the cushion and both sides of the upper back. They are located internal to the seat and not visible. The front and rear passenger seats are equipped with resistive pads for heating and ventilated cushions for cooling, thus providing thermal comfort at a reduced system cost.

Figure 2 shows the thermal comfort CAE tool validation. The predicted overall and local thermal comfort levels for 16 body segments are shown for a spot cooling test configuration. The experimental test data is from human evaluations in the climatic wind tunnel. The test conditions are: vehicle speed of 50 km/h, solar load of 500 W/m², and climate settings to achieve an equivalent homogeneous temperature of 29°C. The total TE air discharging flow rate was 15 l/s (liter/second) for the face/chest, lap/foot nozzles and seat cooling. The TE discharge temperatures vary from 24 to 27°C. The comfort scale varies from -4 (very uncomfortable) to +4 (very comfortable) with 0 being neutral. The CAE predictions compare reasonably well for both the overall comfort and six key body segments data.

Figure 3 shows the comfort from human evaluations for both baseline and TE configurations. The test conditions are: 38°C (100°F), 40% RH, 1,000 W/m² solar load, and vehicle speed of 50 km/h. The baseline used an ACC set temperature of 21.5°C (71°F). Initially thermal comfort level was hot at -2.5 in the scale of -4 to +4. After 9 minutes, the comfort level crossed neutral and it reached steady-state comfort of 1.8 that is a clear indication of comfort. The TE configuration is shown at equivalent thermal comfort with an elevated ACC set point temperature of 24.5°C (76°F). Equivalent thermal comfort was maintained by adding TEDs for local spot cooling, while reducing energy from a higher ACC set point and a 25% lower flow of central air.

Figure 4 shows the HVAC power consumption curves over ambient temperatures ranging from 4 to 38°C (40 to 100°F) for the baseline and TE vehicles with three occupancy arrangements by the equivalent comfort ACC setting. The ambient conditions with humidity are 4°C x 90% RH, 10°C x 90% RH, 15°C x 80% RH, 21°C x 70% RH, 27°C x 60% RH, 32°C x 50% RH, 38°C x

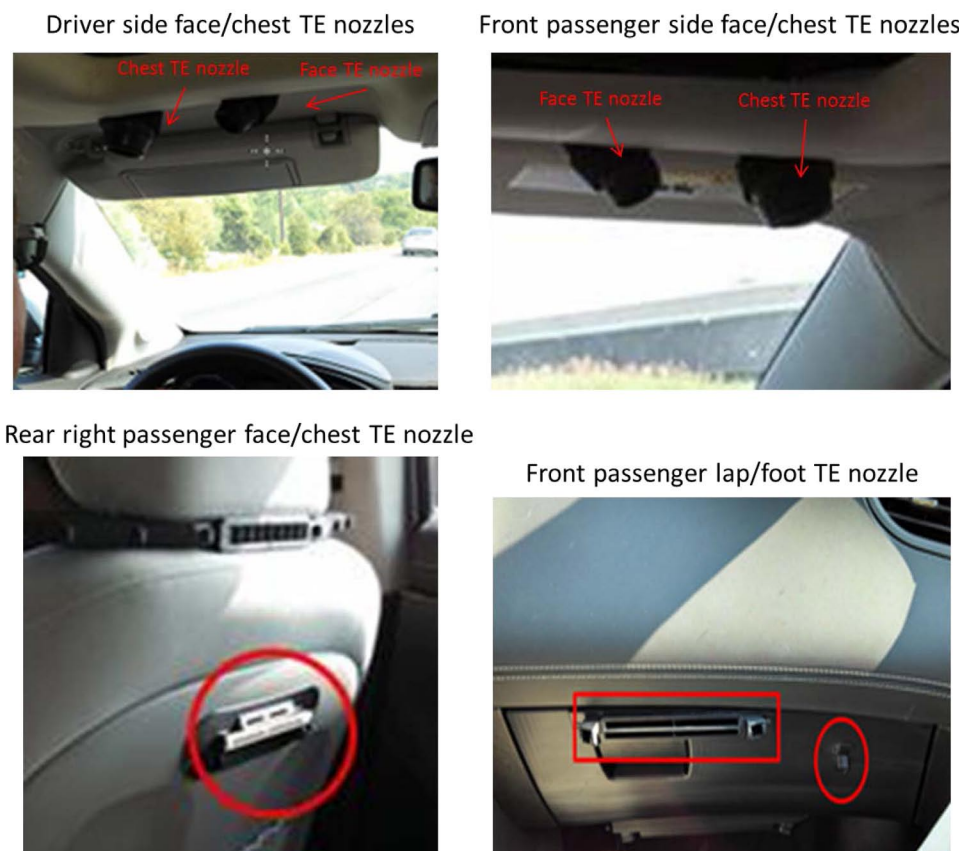


FIGURE 1. Nozzles for TE HVAC components in the Buick LaCrosse demonstration vehicle.

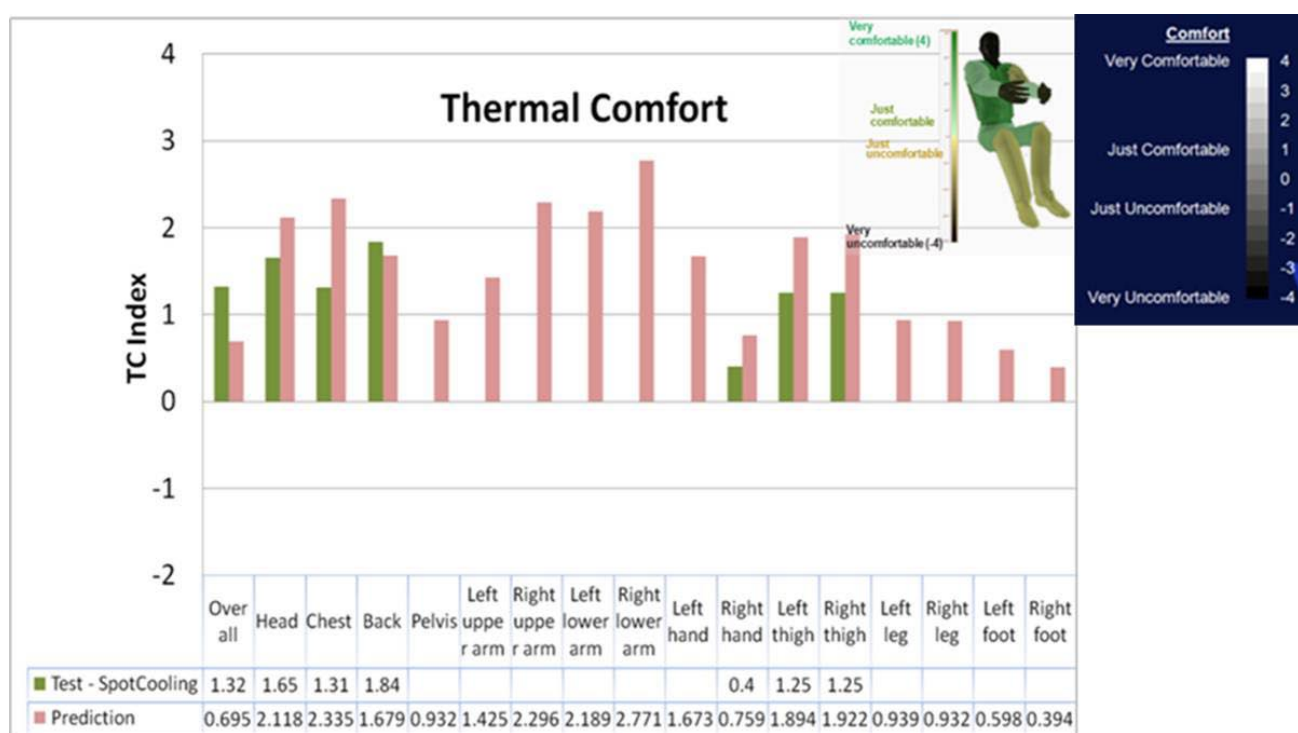


FIGURE 2. Thermal comfort CAE tool validation results for one of the spot cooling test conditions.

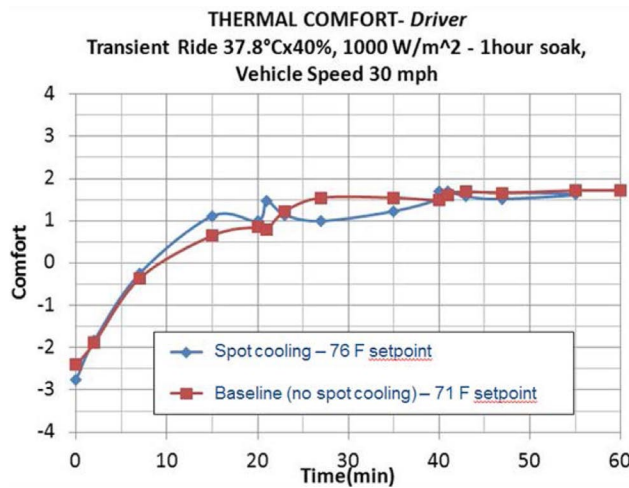


FIGURE 3. Equivalent thermal comfort comparison between TE-equipped vehicle and the baseline.

40% RH. The occupancy arrangements are shown. The TE-equipped LaCrosse demonstration vehicle clearly shows that over the entire ambient condition sweep it consumes less HVAC energy than the baseline vehicle for all occupancy arrangements.

In order to provide an energy savings estimate for all seasons of A/C operation in a single year, the A/C usage data in Figure 5(a) is used to generate a weighted average of the power use. This weighting was based on the Delphi-GM 1997 Buick LeSabre Usage Survey. Additional weighting of the power usage data was based on vehicle occupancy. Figure 5(b) shows the data based on a report submitted to the City of Lincoln, Nebraska by the Schemmer Associates. It shows that up to 83% of the

time a vehicle was observed to have only one occupant and only 2% of the vehicles travel with three or more passengers in the vehicle. For the TE HVAC weighted power usage calculation, the following formula was used:

$$p = \sum_t \left(\sum_j P_{ij} \mathbf{W}_a^j \right) W_o^t$$

where W_a^j represents the ambient weighting (% of occurrence) over a given set of ambient temperatures, W_o is the occupancy weightings, and P_{ij} represent the overall system power consumption under a given ambient and occupancy scenario. The TE vehicle achieved 51% direct central compressor power saving at 25% less central air flow rate. After subtracting the TE system related power consumption, an annualized HVAC energy savings estimate of 30.9% was calculated. The energy saving is most significant for milder ambient conditions between 10 and 24°C when the compressor was frequently shut off. Additionally, the Buick LaCrosse demonstration vehicle has the e-Assist feature that includes engine “idle off” technology. The engine “idle off” occurrence and duration is dependent on the climate control settings. The reduced differential between the exterior and cabin temperature enables more frequent and longer duration engine “idle off” time for the demonstration vehicle. A final energy savings estimate that incorporates the effect of increased engine “idle off” will be included in the final project report.

Table 1 shows the COP of the prototype TE HVAC components installed in the Buick LaCrosse demonstration vehicle for the cooling and heating operations. For cooling, it clearly shows the COPs >1.3 except for the seat bottom (with COP = 1.26), and for

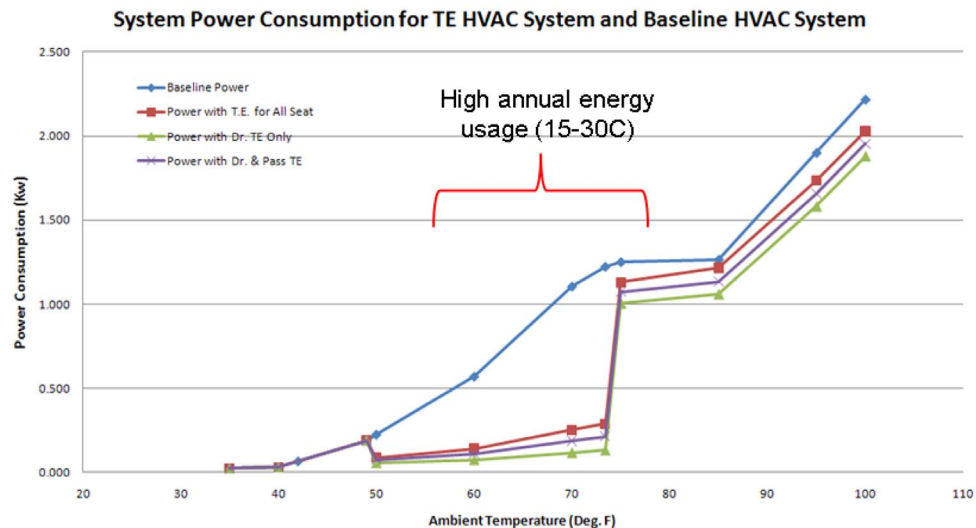


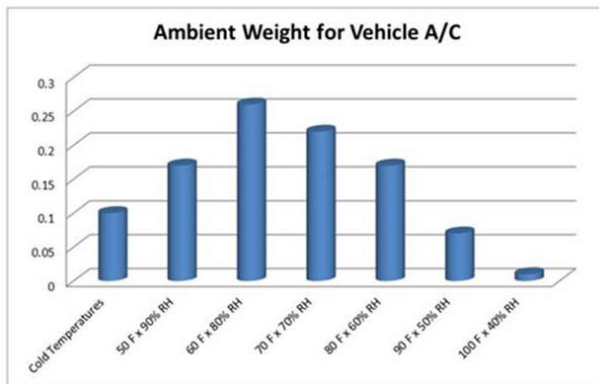
FIGURE 4. HVAC energy usage with equivalent thermal comfort for the baseline vehicle and for three occupancy scenarios in the TE-equipped vehicle under various ambient conditions.

TABLE 1. COP for Prototype TE HVAC Components

| | Cooling Requirements | | | Cooling Actual | | | |
|---------------------------|----------------------|---------|-----|----------------|---------|-----|------|
| | Airflow | Delta T | COP | Airflow | Delta T | PWM | COP |
| Chest/Face - 2 Lrg TEDs | 13 | 5 | 1.3 | 13 | 5.1 | 80% | 1.4 |
| Lap/Foot - 1Lgr/1Sm TED's | 15 | 2 | 1.3 | 15 | 5 | 60% | 1.7 |
| Seat-Upper - 1 Lrg TED | 4 | 2 | 1.3 | 4 | 7 | 60% | 1.89 |
| Seat-Lower- 1 Lrg TED | 4 | 2 | 1.3 | 4 | 5.7 | 60% | 1.26 |

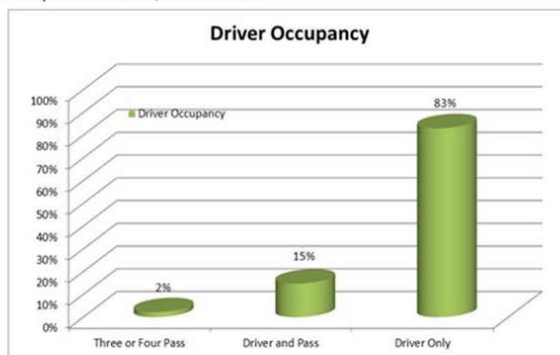
| | Heating Requirements | | | Heating Actual | | | |
|-------------------------|----------------------|---------|-----|----------------|---------|------|-----|
| | Airflow | Delta T | COP | Airflow | Delta T | PWM | COP |
| Chest/Face - 2 Lrg TEDs | 8 | 15 | 2.3 | 8 | 15.3 | 100% | 2.5 |
| Lap/Foot - 1 Lrg TED | 5 | 15 | 2.3 | 5 | 14 | 100% | 2.7 |
| Seat-Upper - 1 Lrg TED | 5 | 15 | 2.3 | 5 | 13 | 100% | 2.5 |
| Seat-Lower- 1 Lrg TED | 5 | 15 | 2.3 | 5 | 13.9 | 100% | 2.5 |

- Ambient Weighting of Vehicle A/C System Operation



(a). Ambient weighting

- Passenger Occupancy Weighting from Schemmer Associates (2005) for Lincoln, Nebraska



(b). Occupancy weighting

FIGURE 5. Weighting factors used to calculate annualized energy saving.

heating, they all exceeded the required COP of 2.3. Coolant-based waste heat management of the TEDs was essential for meeting the COP requirements. However, coolant-based waste heat management is more complex and costly than simpler (but less efficient) air-based waste heat components. For the minimal TED energy (40 watts

per occupant) requirements, which are very modest when compared to the central HVAC system (3,000 watts), the higher COPs of coolant-based waste heat TEDs do not appear to justify the added cost and complexity for a production applications.

CONCLUSIONS

- Distributed cooling and heating to create a microclimate is very efficient in terms of total required energy in vehicle climate control.
- Excellent synergy between the centralized HVAC system at a reduced output and the TEDs that provide small temperature adjustments to ensure vehicle occupant comfort.
- First TE distributed HVAC systems are expected to be executed on EVs (for energy savings and range enhancement) and on luxury vehicles (as a feature for enhanced comfort).
- Seldom occupied seating locations do not merit the cost of TEDs for energy savings (use pad heating and seat ventilation or fan only supplements)
- Air-based waste heat management is worthy of further study for reduced system complexity.

REFERENCES

1. Johnson, V.H. (2002), "Fuel Used for Vehicle Air-Conditioning: A State-by-State Thermal Comfort-Based Approach", SAE 2002-01-1957.

FY 2013 PUBLICATIONS/PRESENTATIONS

Publications

1. Y. Qui, L. Xi, X. Shi, P.F. Qiu, W.Q. Zhang, L.D. Chen, J.R. Salvador, J.Y. Cho, J. Yang, Y.-C. Chien, S.-W. Chen, Y Tang and G.J. Snyder: Charge-Compensated Compound

Defects in Ga-Containing Thermoelectric Skutterudites: *Adv. Func. Mater.* DOI: 10.1002/adfm.201202571.

2. J.Y. Cho, Z. Ye, M.M. Tessema, J.R. Salvador, J. Yang, W.Q. Zhang, J. Yang, W. Cai, and H. Wang: Thermoelectric Performance of $Yb_xFe_{4-y}PtSb12$ ($0.8 < x < 1$, $y = 1$ and 0.5) *J. Appl. Phys.* **113** 143708 (2013).

3. L. Guo X. Xu, J.R. Salvador, and G.P. Meisner: Coupled Vibrational Modes in Multiple-filled Skutterudites and the Effects on Thermal Conductivity Reduction, *Appl. Phys. Lett.* **102** 111905 (2013).

4. K.R. Saviers S.L. Hodson, T.S. Fisher, J.R. Salvador L.S. Kasten: Carbon Nanotube Arrays for Enhanced Thermal Interfaces to Thermoelectric Modules, *J. Thermophys. and Heat Transfer* DOI: 10.2514/1.T4026 (Award for best student paper by AIAA).

5. Z. Ye, J.Y. Cho M.M. Tessema, J.R. Salvador R.A. Waldo, H. Wang, W. Cai: The Effect of Structural Vacancies on the Thermoelectric Properties of $(Cu_2Te)_{1-x}(Ga_2Te)_x$, *J. Solid State Chem.* **201**, 262 (2013).

6. S. Kumar, S.D. Heister, X. Xu, J.R. Salvador, G.P. Mesiner: Thermoelectric Generators for Automotive Waste Heat Recovery Systems Part1: Numerical Modeling and Baseline Model Analysis, *J. Electronic Mater.* DOI: 10.1007/s11664-013-247-19.

7. J.R. Salvador, R.A. Waldo, C.A. Wong, M.M. Tessema, D.N. Brown, D. J. Miller H. Wang, A.A. Wereszczak, and W. Cai: Thermoelectric and Mechanical Properties of Melt Spun and Spark Plasma Sintered n-type Yb and Ba-filled Skutterudites, *Mater. Sci. and Eng. B* **178**, 1087 (2013).

8. J.R. Salvador, J.Y. Cho, Z. Ye, J.E. Moczygembba, A.J. Thompson, J.W. Sharp, J.D. Koenig, R. Maloney, T. Thompson, J. Sakamoto: Thermal to Electrical Energy Conversion of Skutterudite-Based Thermoelectric Modules, *J. Electronic Mater.* **42** 1389 (2013).

9. Z. Ye, J.Y. Cho, M.M. Tessema, J.R. Salvador, R.A. Waldo, J. Yang, H. Wang, W. Cai, M.J. Kirkham, J. Yang, and W.Q. Zhang: Thermoelectric Properties of Au-Containing Type-1 Clathrates $Ba_8Au_xGa_{16-3x}Ge_{30+2x}$, Accepted to *J. Alloys and Compds.*

Presentations

1. Energy Efficient HVAC system for Distributed Cooling/ Heating with Thermoelectric Devices: DOE Annual Merit Review Washington D.C., May 2013.

2. Energy Efficient HVAC system for TE Distributed Cooling and Heating: GM Warren Technical Center Warren, MI, September 2013.

3. Energy Efficient HVAC Final Meeting: Findings, Conclusions, Implications and Recommendations to the California Energy Commission Sacramento, CA, October 2013.

4. Energy Efficient HVAC Introduction to UC Davis Energy Sector Students and Faculty Sacramento, CA, October 2013.

5. Energy Efficient HVAC and TE Waste Heat Recovery Final Meeting: Findings, Conclusions, Implications and Recommendations to the Department of Energy Washington D.C. November 2013.

6. Materials, Modules and Systems: An Atoms to Autos Approach to Automotive Thermoelectric Systems Development: Contributed talk at Thermoelectrics goes automotive, Berlin, German, Nov. 2012.

7. Departmental Seminar University of Waterloo, March 20th 2013.

8. Skutterudite Based Thermoelectric Modules :Fabrication and Conversion Efficiency: Invited Talk PACRIM 2013 San Diego, CA.

9. Cost-Competitive Advanced Thermoelectric Generators for Direct Conversion of Vehicle Waste Heat into Useful Electrical Power: DOE Annual Merit Review Washington D.C., May 2013.

10. Materials, Modules and Systems: An Atoms to Autos Approach to Automotive Thermoelectric Systems Development: Invited Talk at the National Institute of Materials Science, Tskuba, Japan.

11. Challenges for Future Implementation of Thermoelectric Waste Heat Recovery: Invited Talk, International Conference on Thermoelectrics, Kobe, Japan.

SPECIAL RECOGNITIONS & AWARDS/ PATENTS ISSUED

1. K.R. Saviers S.L. Hodson, T.S. Fisher, J.R. Salvador L.S. Kasten: Carbon Nanotube Arrays for Enhanced Thermal Interfaces to Thermoelectric Modules, *J. Thermophys. and Heat Transfer* DOI: 10.2514/1.T4026 (Award for best student paper by AIAA).

V.3 Development of Cost-Competitive Advanced Thermoelectric Generators for Direct Conversion of Vehicle Waste Heat into Useful Electrical Power

Gregory P. Meisner (Primary Contact),

James R. Salvador

General Motors

30500 Mound Road

Warren, MI 48090

DOE Technology Development Manager:
Gurpreet Singh

NETL Project Manager: Carl Maronde

Subcontractors:

- Brookhaven National Lab, Upton, NY
- Dana Thermal Products, Oakville, Ontario, Canada
- Delphi Electronics & Safety, Kokomo, IN
- Eberspaecher North America, Inc., Novi, MI
- Jet Propulsion Laboratory, Pasadena, CA
- Marlow Industries, Inc., Dallas, TX
- Michigan State University, East Lansing, MI
- Molycorp, Inc., Singapore
- Oak Ridge National Lab, Oak Ridge, TN
- Purdue University, West Lafayette, IN
- University of Washington, Seattle, WA

- Determine TE leg dimensions and layout for the initial TEG subunit

FY 2013 Accomplishments

- Completed vehicle level analysis to determine electrical power requirement for the TEG system: estimated to be >1 kW average for a 5% FE gain over the US06 drive cycle
- Developed dual TEG subunit scheme to locate the TEG as close to the engine as possible
- Selected n-type and p-type skutterudite TE materials for the initial TEG subunit based on the most recent optimized material properties and processing parameters
- Established new formulations of p-type skutterudite with improved TE and mechanical properties and superior processing compatibility for the initial TEG prototype build
- Demonstrated that optimized n-type and p-type skutterudite materials without rare earth elements show little to no performance degradation
- Established the TE material quantity and the TE leg height required for the TE modules
- Fabricated kilogram quantities of skutterudite TE material and processed them into wafers with metallization and diffusion barriers
- Combined heat exchanger and TE module modeling and analysis into a combined transient thermal modeling tool for determining the optimized configuration of heat exchanger and TE module array for maximum heat conversion to useful electrical power
- Developed a Unified Model for vehicle level analysis that incorporates the combined thermal modeling of heat exchangers and TE modules with vehicle simulations for FE improvement estimation
- Established parameters and component choices for electrical circuit boards, connectors, and power conditioning components
- Constructed a bench test rig for data collection and testing of the initial TEG subunit under expected operating conditions

Overall Objectives

- Overcome major obstacles to the commercialization of automotive thermoelectric generator (TEG) systems
- Develop an overall TEG system including all necessary vehicle controls and electrical systems and fully integrate onto a light-duty vehicle
- Demonstrate fuel economy (FE) improvement of 5% over the US06 drive cycle

Fiscal Year (FY) 2013 Objectives

- Establish design targets for initial TEG system
- Establish design parameters for initial TEG components and subsystems
- Develop adequate modeling tools for a combined performance optimization of the heat exchangers, TE modules, TEG subassemblies, and vehicle
- Downselect TE material for TE module fabrication for the initial TEG subunit

- Conducted component testing including preliminary TE materials, TE modules, thermal interface materials, and materials compatibility for various key components of the TEG subunit

Future Directions

- Complete design and fabrication of initial TEG subunit for bench testing
- Analyze performance and durability of initial TEG subunit as input for redesign of the final TEG system
- Use vehicle level modeling to prioritize enhanced vehicle electrification schemes, such as electrification of belt-driven accessories, to ensure full use of the TEG electrical power delivered
- Complete vehicle level controls and integration to fully optimize vehicle performance with installed TEG
- Perform extensive testing and analysis of a demonstration vehicle with TEG installed, and deliver both the results and the demonstration vehicle to the U.S. Department of Energy
- Complete a study of cost and scale-up plans for TEG commercialization potential



INTRODUCTION

The goal of this project is to develop a low-cost and fully-integrated automotive TEG for recovering waste exhaust gas heat from production vehicles to improve FE. This effort will be a significant step forward in reducing energy consumption and emissions by the U.S. transportation sector. The twelve organizations partnering on the project team foresee a path to commercial viability for TEGs, especially for full-size trucks that face stringent future Corporate Average Fuel Economy mandates. Further innovation, however, is needed to overcome the major obstacles to successful automotive TEG commercialization. TE waste heat recovery is a new area of commercial technology that will be implemented without the added burden of displacing any existing technology. Moreover, this major effort to commercialize TE-based recovery of waste energy has significant potential beyond the automobile industry. The work from this project will culminate in the first application of high-temperature TE materials for high-volume use, and it will establish new industrial sectors with scaled-up production capability on all needed TEG materials and components. The team is creating a potential supply chain for automotive TEG technology and identifying manufacturing and assembly

processes for large-scale production of TE materials and components that include scale-up plans for the production of 100,000 TEG units per year.

APPROACH

The team is focused on several innovative paths for developing practical automotive TEGs: (1) enhanced TE material performance via band structure modification by doping and other compositional tuning; (2) optimized TE material fabrication and processing to reduce thermal conductivity and improve fracture strength; (3) unique and novel routes to high-volume production for successful skutterudite commercialization; (4) new materials, nanostructures, and nanoscale approaches to reduce thermal interface and electrical contact resistances; (5) innovative heat exchanger and TEG system design for high-efficiency heat flows and optimum temperature profiles despite the highly variable exhaust gas flows of typical automotive drive cycles; (6) a highly modular TEG design capable of being applied to a wide spectrum of vehicles; (7) new modeling and simulation capabilities; and (8) new highly thermal-insulating and coating substances for inexpensive insulation and encapsulation of materials for TEG technology.

The team's approach is to develop an initial TEG subunit design based on the results of the detailed thermal modeling of heat exchangers, TE modules, and the co-optimization of these combined subsystems. The initial TEG will be fully functional and instrumented for bench testing. The data collected, including the temperature profiles, heat flows, back pressure, current and voltage generated, and electrical power delivered, will inform a redesign of the TEG and completion of the vehicle integration and controls tasks for the final TEG system prototype. The final TEG system will include two TEG subunits, one for each side of the exhaust system of the V-8 engine, and it will be fully functional and subjected to a complete set of testing protocols to determine its performance and its impact on FE for a variety of driving conditions, including the US06 drive cycle.

RESULTS

The vehicle class selected for demonstration in this project, i.e., full-size light-duty pickup trucks and sport utility vehicles, represents a significant fraction of all domestic auto manufacturer fleets. A 5% FE improvement for these large vehicles equates to larger reductions in petroleum use and will shorten the technology investment payback schedule. The adequate underfloor space available and the dual exhaust manifold for the V-8 engine on the full-size truck are suitable for

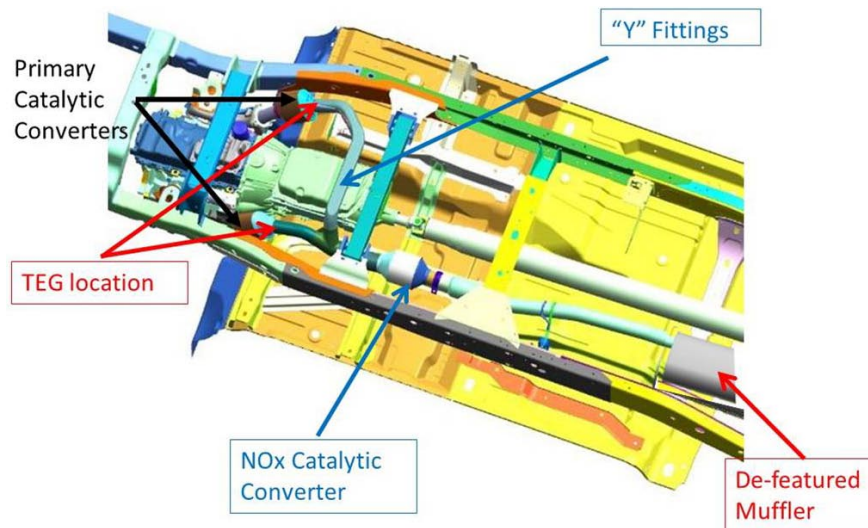


FIGURE 1. Schematic view of the underside of the full size pickup showing the proposed location of the dual TEG subunits and other features of the exhaust system.

two small, modular TEG subunits that will constitute the full TEG system. This modular TEG subunit approach should prove adaptable for practical exhaust gas waste heat recovery in smaller passenger vehicles. Figure 1 is a schematic view of the pickup truck exhaust system showing the proposed location of the two TEG subunits. Exhaust gas temperature and mass flow data were collected on a current production truck with this exhaust system to determine the expected operating conditions for the TEG when installed. Figure 2 shows the results measured at several locations in the exhaust system for the US06 drive cycle. The team integrated the TEG thermal model into a vehicle level Unified Model and estimated FE improvement for specific TEG output power levels in order to assess the impact of TEG power on FE over a variety of driving conditions. These data were used to establish performance specifications for the TEG system consistent with packaging space, backpressure limits, coolant system capacity, TEG output voltage and current limits, and maximum TE module (TEM) operating temperatures.

A transient thermal TEG system model was developed to simulate the heat flows and temperature profiles over the US06 drive cycle. These results were used together with the optimized TE material properties to determine the amount of TE material required for the initial TEG to deliver the electrical power needed to achieve the FE improvement goal. This kilogram quantity of n-type and p-type skutterudites were fabricated by the high-throughput technique of melt spinning and then processed into wafers with metallized diffusion barriers and electrical contacts. Further co-optimization of the heat exchanger and TE module subsystem has informed additional specifications for the TE leg cross-sectional

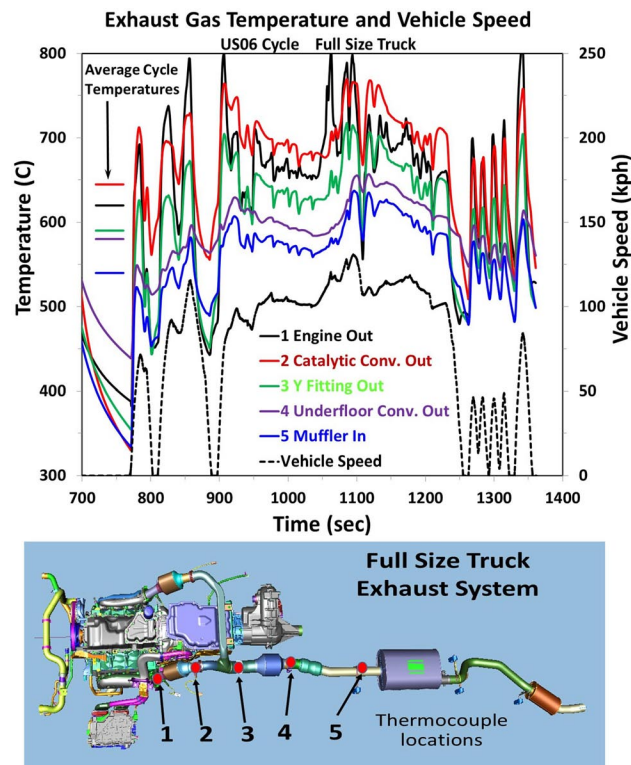


FIGURE 2. The exhaust gas temperatures and vehicle speed versus time for the US06 drive cycle (upper panel) and the thermocouple measurement locations along the exhaust system (lower panel) for a full size truck. The US06 drive cycle shown is the second of two sequential 600-second runs. The horizontal bars on the left of the upper panel are average cycle temperatures for each of the thermocouple locations as follows: Engine Out = 620°C, Catalytic Converter Out = 645°C, Y Fitting Out = 590°C, Underfloor Converter Out = 580°C, and Muffler In = 540°C.

area, TE module geometry and layout, hot and cold side heat exchanger area, circuit board configuration, electrical power conditioning requirements, and thermal and electrical interfaces. The electrical power output of test TEMs made from this material are 0.75 W/couple at anticipated operating conditions. The TEM output is expected to increase to >1 W/couple as the TEM fabrication and processing techniques improve. The team is finalizing the specifications of all of the individual components and subcomponents for the initial TEG subunit to be fabricated, assembled, and bench tested in 2014. The team estimates that >800 W averaged over the US06 drive cycle is possible based on the transient TEG model. Additional improvements in the TEG system design and components are being investigated and will be incorporated into the final TEG system prototype to be built and vehicle tested in the final year of this project.

CONCLUSIONS

- Design specifications for the initial TEG prototype are being completed based on extensive modeling of heat flows, thermoelectric performance, and vehicle operation
- Additional vehicle electrification will be necessary to fully utilize the electrical power delivered by the TEG for maximum FE improvement
- TE material has been fabricated and TE module fabrication is in progress
- Final design of the heat exchangers, subassembly clamping schemes, and other TEG components is underway for the initial TEG build
- Bench testing, data collection, and analysis of the initial TEG will inform a redesign for the final TEG system

FY 2013 PUBLICATIONS/PRESENTATIONS

1. J.R. Salvador, G.P. Meisner, M.G. Reynolds, J.E. Moczygemb, A.J. Thompson, R McCarty, D.N. Brown, D.J. Miller, "Materials, Modules and Systems: An Atoms to Autos Approach to Automotive Thermoelectric Systems Development," presented at the Thermoelectrics Goes Automotive Conference, Berlin, Germany, 23 November 2012.
2. J.R. Salvador, G.P. Meisner, H. Wang, "Thermoelectric Performance of Rare Earth-Free p-Type Skutterudite Materials," presented at the Fall 2012 Materials Research Society Meeting, Boston, MA, 27 November 2012.
3. J.R. Salvador, "Skutterudite Materials for Automotive Waste Heat Recovery Applications," invited seminar at the University of Waterloo Chemistry Department, 20 March 2013.
4. G.P. Meisner, "On the thermodynamics of waste heat recovery from internal combustion engine exhaust gas,"

presented at the American Physical Society (APS) March Meeting, Baltimore, MD, 20 March 2013.

5. J.R. Salvador, G.P. Meisner, "Cost-Competitive Advanced Thermoelectric Generators for Direct Conversion of Vehicle Waste Heat into Useful Electrical Power," presented at the DOE Annual Merit Review, Washington DC, 20 May 2013.
6. G.P. Meisner, "Advanced Thermoelectric Generators for Direct Conversion of Vehicle Waste Heat into Useful Electrical Power," invited presentation at the European Materials Research Society Meeting, Strasbourg, France, 30 May 2013.
7. J.R. Salvador, "Skutterudite Based Thermoelectric Modules: Fabrication and Conversion Efficiency," invited presentation at PACRIM 2013, San Diego CA, June 2013.
8. J.R. Salvador, "Materials, Modules and Systems: An Atoms to Autos Approach to Automotive Thermoelectric Systems Development," invited presentation at the National Institute of Materials Science, Tsukuba, Japan, 6 July 2013.
9. J.R. Salvador, "Challenges for Future Implementation of Thermoelectric Waste Heat Recovery," invited presentation at International Conference on Thermoelectrics, Kobe, Japan, 8 July 2013.
10. G.P. Meisner, "Thermoelectric Technology for Generating Useful Electrical Power from Automotive Waste Heat," invited presentation at IDTechEx 2013: Energy Harvesting & Storage USA Conference, Santa Clara, CA, 20 November 2013.
11. L. Guo, X. Xu, J.R. Salvador, G.P. Meisner, "Coupled Vibrational Modes in Multiple-filled Skutterudites and the Effects on Thermal Conductivity Reduction," Appl. Phys. Lett. **102** 111905 (2013).
12. K.R. Saviers, S.L. Hodson, T.S. Fisher, J.R. Salvador, L.S. Kasten, "Carbon Nanotube Arrays for Enhanced Thermal Interfaces to Thermoelectric Modules," J. Thermophysics and Heat Transfer **27** (3), July–September (2013) DOI: 10.2514/1. T4026 (Awarded the Best Aerospace Power Systems Student Paper at the 2012 AIAA International Energy Conversion Engineering Conference).
13. S. Kumar, S.D. Heister, X. Xu, J.R. Salvador, G.P. Meisner, "Thermoelectric Generators for Automotive Waste Heat Recovery Systems Part1: Numerical Modeling and Baseline Model Analysis," J. Electronic Mater. DOI: 10.1007/s11664-013-247-19.
14. J.R. Salvador, R.A. Waldo, C.A. Wong, M.M. Tessema, D.N. Brown, D.J. Miller, H. Wang, A.A. Wereszczak, W. Cai, "Thermoelectric and Mechanical Properties of Melt Spun and Spark Plasma Sintered n-type Yb and Ba-filled Skutterudites," Mater. Sci. and Eng. **B 178**, 1087 (2013).

SPECIAL RECOGNITIONS & AWARDS/ PATENTS ISSUED

1. Best Aerospace Power Systems Student Paper at the 2012 AIAA International Energy Conversion Engineering Conference: K.R. Saviers, S.L. Hodson, T.S. Fisher, J.R. Salvador, L.S. Kasten, "Carbon Nanotube Arrays for Enhanced Thermal Interfaces to Thermoelectric Modules,"

- J. Thermophysics and Heat Transfer 27 (3), July–September (2013) DOI: 10.2514/1.T4026.
- 2.** United States Patent US 8,309,839: “*Method of improving thermoelectric figure of merit of high efficiency thermoelectric materials*” issued 13 November 2012.
- 3.** United States Patent US 8,443,594: “*Method of controlling temperature of a thermoelectric generator in an exhaust system*” issued 21 May 2013.

4. United States Patent US 8,554,407: “*Bypass valve and coolant flow controls for optimum temperatures in waste heat recovery systems*” issued 8 October 2013.

United States Patent US 8,575,788: “*Method of operating a thermoelectric generator*” issued 5 November 2013.

5. Chinese Patent CN 102,235,212: “*Exhaust bypass control for exhaust heat recovery*” issued 16 October 2013; US patent pending.

V.4 Nanostructured High-Temperature Bulk Thermoelectric Energy Conversion for Efficient Automotive Waste Heat Recovery

Martin Cleary¹ (Primary Contact),
Xiaowei Wang¹, Boris Kozinsky², Li Jiang²,
Varun Mittal², Steve Gladstein², Zhifeng Ren³,
Jim Szybist⁴, Yanliang Zhang⁵

¹GMZ Energy
11 Wall St.
Waltham, MA 02453

DOE Technology Development Manager:
Gupreet Singh

NETL Project Manager: Carl Maronde

Subcontractors:

²Bosch of North America, Farmington Hills, MI
³University of Houston, Houston, TX
⁴Oak Ridge National Laboratory, Oak Ridge, TN
⁵Boise State University, Boise, Idaho

- Achieved the 2013 technical target of finalizing a detailed mechanical design of a 1-kW TEG for integration on to a BFV, within specified operating parameters.

Future Directions

- Thermoelectric modules will be subjected to extensive thermal and mechanical reliability testing. The module design is also being adapted for manufacturability.
- Fabricate the TEGs for the passenger vehicle and the BFV. Initial prototypes will be tested, which will influence the final design.
- TEGs will be integrated onboard a vehicle platform. The vehicle will be tested before and after TEG installation to demonstrate the improvement in fuel efficiency.



Overall Objectives

- Demonstrate a robust, thermally cyclable thermoelectric exhaust waste heat recovery system that will provide approximately a 5% fuel efficiency improvement for a light-duty vehicle platform.
- Develop an initial design/concept for a 1-kW thermoelectric generator (TEG) in the exhaust stream of a Bradley Fighting Vehicle (BFV).

Fiscal Year 2013 (FY) Objectives

- Finalize the mechanical design for the BFV TEG.
- Initiate thermoelectric module testing to establish efficiency improvements of initial devices.

FY 2013 Accomplishments

- A thermoelectric device has been subjected to 1,000 thermal cycles, between 600°C and 100°C, with <1% degradation in power output performance.
- High-temperature thermoelectric modules, which will be integrated into the passenger vehicle and BFV TEGs, were successfully fabricated and characterized.
- A new TEG design concept with a higher power output relative to the previous TEG design has been developed.

INTRODUCTION

The improvement of automotive vehicle efficiency is crucial to the conservation of petroleum and energy sustainability. Moreover, government regulations require increased vehicle fuel economy and reduced green house emissions. In order to meet these demands the use of a TEG in the engine exhaust to achieve a 5% fuel efficiency improvement for a light-duty vehicle platform is considered. Engine waste heat accounts for >30% of the total energy consumption in a vehicle. TEGs are robust solid-state devices that utilize the Peltier effect to directly convert heat into electrical power, which makes them ideal for waste heat recovery from engine exhaust.

APPROACH

This project is following a multi-tiered approach to achieve the outlined goals. At the materials level; theoretical simulations, composition optimization, and production scale up are being pursued to achieve high-efficiency thermoelectric materials with reduced cost. The half-Heusler thermoelectric materials are then integrated into high-temperature thermoelectric modules, which are designed to maximize power, efficiency and reliability. A TEG, consisting of an exhaust gas heat exchanger (HEX), modules and water-cooled cold plate, will be designed. The optimized TEG design will be

fabricated, characterized and installed on a vehicle platform. The vehicle platform will be tested on a chassis dynamometer to measure the improvement in fuel economy after the TEG installation

RESULTS

There are a number of steps in the materials fabrication process including melting, ball milling and hot pressing. Efforts have been ongoing at GMZ Energy to scale up the production by both increasing the batch size during melting and increasing the size of the hot-pressed disc. Over the last year the diameter of disc being hot pressed has increased from $\frac{1}{2}$ " to 2". The ZT, a thermoelectric figure-of-merit, was measured for the 2" disc at multiple locations and compared to the $\frac{1}{2}$ " baseline. It can be seen from Figure 1 that the 2" disc samples have a ZT similar to the $\frac{1}{2}$ " discs.

The vehicle exhaust stream is a very challenging environment, where components are subjected to repeated thermal cycling and peak temperatures in excess of 800°C. To assess the reliability of the thermoelectric devices, they were subjected to a cyclical temperature profile where the hot-side temperature peaked at 600°C while the cold-side was maintained at 100°C, which is representative of conditions in a TEG automobile application. The thermal cycling was performed on a custom-designed device characterization apparatus. It was found that there was <1% degradation in device power output after 1,000 thermal cycles, as shown in Figure 2, which indicates that the thermoelectric devices are robust and can operate under challenging thermal conditions.

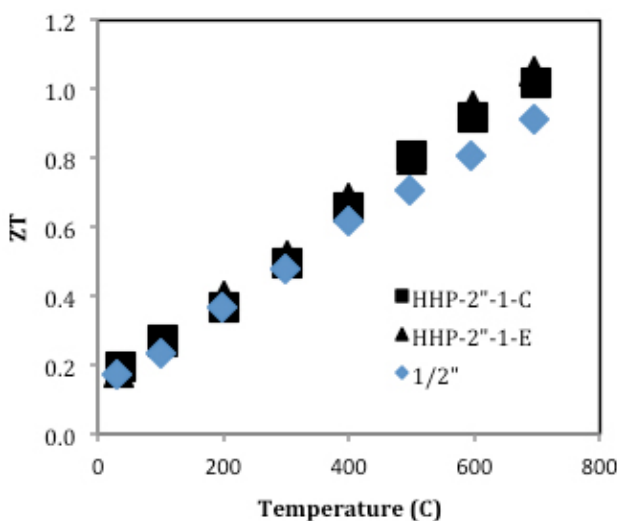


FIGURE 1. Comparison of ZT, a thermoelectric figure-of-merit, for a 2" hot-pressed disc sample of half-Heusler material with a $\frac{1}{2}$ " baseline sample.

A packaged high-temperature thermoelectric module, with the top casing removed, is shown in Figure 3. The module fabrication process has been refined such that this thermal resistance at the interface leads to <7% decrease in module power output. The casing is designed to maximize reliability while minimizing "heat leak" via the side of the casing. The manufacturing process for the modules has been refined such that they consistently demonstrate a power output of 7 W +/-10%. The production of repeatable thermoelectric modules is a significant milestone towards the task of fabricating a TEG with integrated modules for both the passenger vehicle and BFV applications.

A new TEG design concept was developed for the passenger vehicle application, as shown in Figure 4. The design is annular in nature, where the hot exhaust gas

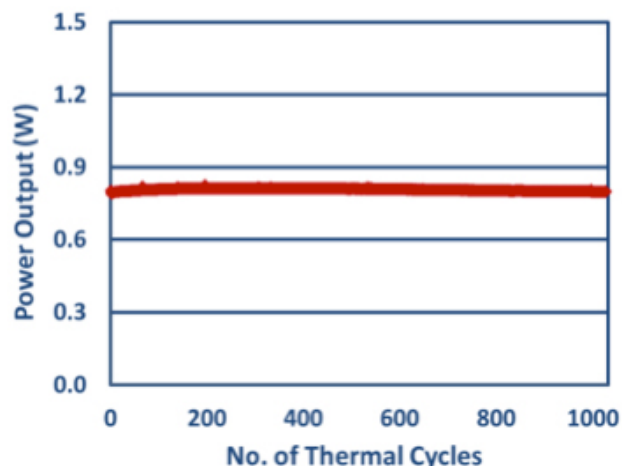


FIGURE 2. Power output of a thermoelectric device thermally cycled between 600°C and 100°C. The device shows <1% degradation in performance over 1,000 cycles.



FIGURE 3. High-temperature thermoelectric module with the hot-side casing removed.

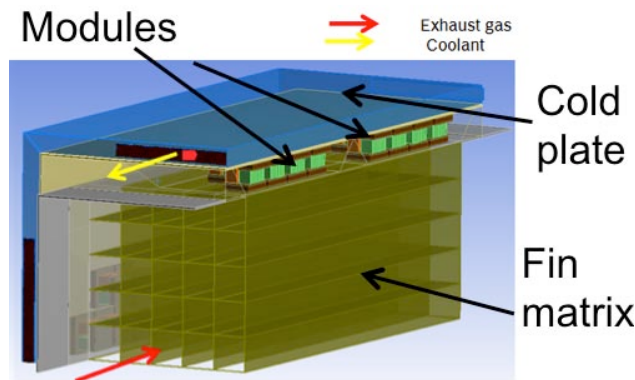


FIGURE 4. A cross-sectional view of the new TEG design concept for a passenger vehicle.

flows through a tube with an embedded fin structure. Modules surround the exhaust gas channel and an annular water jacket surrounds the modules. The design is modular, which allows the design to be deployed in parallel. Finite element flow and structural simulations were performed on the design. The design was compared with a previous, more conventional design, for similar conditions. This new design has a much higher power (30% improvement) with a similar backpressure loss. Therefore, the design represents a significant improvement over the previous design, which will enable a relatively higher fuel efficiency to be achieved.

An exploded view of the mechanical design of the TEG for the BFV is shown in Figure 5. Thermoelectric

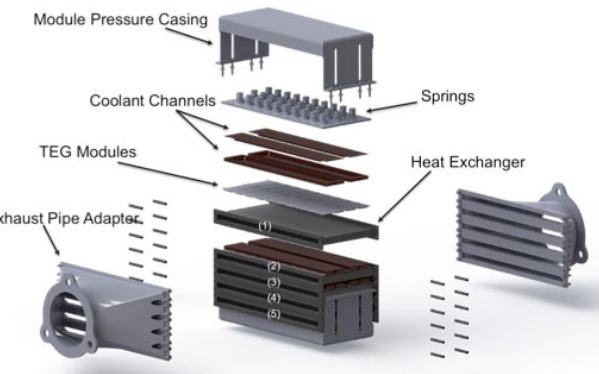


FIGURE 5. Exploded view of a detailed mechanical design of a TEG for a BFV.

modules are placed between the exhaust gas HEX and cold plates. Each layer contains 40 modules. In order to reduce thermal contact resistances between thermoelectric modules and heat exchanger, compression pressure is applied between two end cold plates through a pressure casing. This pressure casing is designed to provide good reliability after many thermal cycles due to the spring compliance. The power output and the pressure drop are shown as a function of fin packing fraction in Figure 6. Fins of 0.3-mm thickness and 25% packing fraction have an acceptable pressure drop and relatively higher output power, which are 2.9 kPa and 1.13 kW, respectively, that achieve the targets outlined for the BFV TEG.

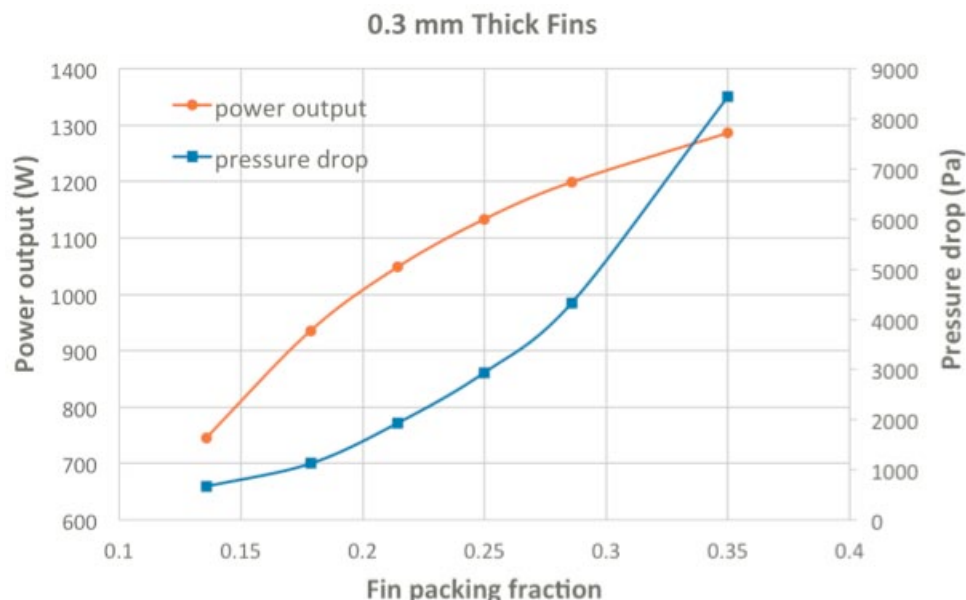


FIGURE 6. Electrical power output and pressure drop of the TEG shown in Figure 5 as a function of fin packing fraction for a fin thickness of 0.3 mm.

CONCLUSIONS

- A thermoelectric device has been subjected to 1,000 thermal cycles, between 600°C and 100°C, with <1% degradation in power output performance.
- High-temperature thermoelectric modules have been successfully fabricated. The modules consistently demonstrate a power output of 7 W +/-10%.
- A new TEG design concept has been developed. Simulations indicate that it has a much higher power output (30% improvement), with a similar backpressure loss due to the HEX, compared to the previous TEG design.
- A detailed mechanical design of the TEG for the BFV has been developed. Finite element simulations predict that this design will achieve the targets for the BFV TEG.

FY 2013 PUBLICATIONS/PRESENTATIONS

1. Giri Joshi, Tulashi Dahal, Shuo Chen, Hengzhi Wang, Junichiro Shiomi, Gang Chen, and Z. F. Ren, “Enhancement of thermoelectric figure-of-merit at low temperatures by titanium substitution of hafnium in n-type half-Heusler $Hf_{0.75-x}Ti_xZr_{0.25}NiSn_{0.99}Sb_{0.01}$,” *Nano Energy* 2, 82 (2013).
2. Shuo Chen, Kevin C. Lukas, Weishu Liu, Cyril P. Opeil, Gang Chen, and Zhifeng Ren, “Effect of Hf Concentration on Thermoelectric Properties of Nanostructured N-Type Half-Heusler Materials $Hf_xZr_{1-x}NiSn_{0.99}Sb_{0.01}$,” *Adv. Energy Mater.* 2013, 3, 1210–1214.
3. B. Yu, X. Wang, J. D’Angelo, J. Yang, Y. Zhang, G. Joshi, T. Pantha, and Y. Ma, “Development of High Temperature Power Generation Devices from Nanostructured Half-Heusler Materials,” Poster Presentation, The 32nd International Conference on Thermoelectrics, Kobe, Japan, June 30–July 4, 2013.

PATENTS ISSUED

1. Patent application number: 61/873,584, “Device for Exhaust Waste Heat Recovery,” V. Mittal, 2013.

V.5 NSF/DOE Thermoelectrics Partnership Project SEEBECK: Saving Energy Effectively By Engaging in Collaborative research and Sharing Knowledge

Joseph P. Heremans¹ (Primary Contact),
Guo-Quan Lu², Mercouri G. Kanatzidis³

¹The Ohio State University (OSU)
Department of Mechanical and Aerospace Engineering
Columbus, OH 43210

²Virginia Polytechnic Institute and State University (VT)
Department of Materials Science and Engineering
Blacksburg, VA 24061

³Northwestern University (NW)
Department of Chemistry
Evanston, IL 60208

NSF Manager: Sumanta Acharya

DOE Technology Development Manager:
Gurpreet Singh

Subcontractor:
Gentherm – ZT::Plus, Irwindale, CA

FY 2013 Accomplishments

- Demonstrated that strong reduction of the lattice thermal conductivity of Na-doped PbTe (over 60%) is achieved with CdS, ZnS, CaS and SrS.
- Demonstrated that the figure of merit ZT of *p*-type PbS can be increased to a record high value for this material of ~ 1.3 at 923 K by introducing CdS nanostructures, due to increased hole mobility.
- Demonstrated $ZT > 1.2$ near 300–350°C in PbSe doped with In or Al.
- Characterized ZnSb-based materials prepared at ZT::Plus and at OSU.
- Evaluated the adhesion quality of a Ti/Ag vacuum-deposited layer on TE materials by tape-peel test, which showed strong coating adhesion.
- Developed a diffusion-viscoelastic model on the evolution of internal stresses of a nanosilver bond-line upon drying, which illuminated the kinetics of defect formation in the bond-line and helped for designing ways to improve the bonding process.
- Achieved the 2010 technical target of developing an interface bonding metallurgy with an electrical contact resistance lower than $10^{-5} \Omega\cdot\text{cm}$ and an estimated thermal contact resistance close to $1.4 \times 10^{-3} \text{ K}\cdot\text{m}\cdot\text{W}^{-1}$ at high temperatures near 773 K or 500°C.
- Characterized the transient thermal impedance of power device packages interconnected by nanosilver sintering and correlated it with die-shear strength of sintered nanosilver joint.
- Attained the 2010 technical target of limiting interface bonding degradation to under 20% during temperature cycles.

Overall Objectives

- Develop non-toxic thermoelectric (TE) materials with high figure of merit ($ZT > 1$) using only earth-abundant elements.
- Develop an interface bonding metallurgy between the TE element and heat exchanger with an electrical contact resistance smaller than $10^{-5} \Omega\cdot\text{cm}$ and a thermal contact resistance smaller than $10^{-3} \text{ K}\cdot\text{m}\cdot\text{W}^{-1}$.
- Integrate and package TE devices with an overall performance that is not degraded by more than 20% over the theoretical performance of the material, with a 10-year lifetime, and the capability to withstand 10^6 thermal cycles from 773 K to 300 K.

Fiscal Year (FY) 2013 Objective

- Develop low-cost non-toxic high- ZT TE materials.
- Develop high- ZT TE materials suitable for use near and below 350°C, away from the 500°C range where today's high- ZT materials are optimized.
- Demonstrate a reliable metallization process for TE materials with diffusion barrier layers for nanosilver paste bonding.
- Evaluate the transient thermal impedance and bonding strength of sintered nanosilver joints.

Future Directions

Project terminating in 2013. VT and NW to request no-cost extensions 1) to finish remaining work on PbS aimed at understanding the thermal stability and further optimizing the ZT above 1.3; and 2) to finish reliability testing of nanosilver-bonded interface by temperature cycling.



INTRODUCTION AND MOTIVATION FOR THIS YEAR'S SPECIFIC RESEARCH DIRECTIONS

The goal of this research is to advance work in thermoelectricity for use in vehicular exhaust waste heat recovery systems, by focusing on (a) materials research (led by OSU and NU, with a subcontract to ZT::Plus) to develop advanced TE materials made from earth-abundant, geographically dispersed elements and compounds; (b) thermal management system design (Gentherm) to minimize losses by minimizing the number of interfaces, minimizing the amount of TE material used, and maximizing the durability of the product; and (c) interface quality control, led by VT and ZT::Plus, to 1) improve the metallization of the TE materials and device interconnection, and 2) increase the flexible bonding of the metallized elements to the heat spreaders so as to increase durability and reduce device level performance losses.

The team at NW has chosen to work on PbS because it is one of the most attractive candidate materials: it is the least expensive of all TE semiconductors, and, although it contains lead, it is a stable, naturally occurring, non-toxic mineral that is ubiquitous throughout the earth's crust.

The team at OSU has focused on addressing the latest challenge to automotive waste heat recovery, which stems from a change in engine operating temperatures. In general, average exhaust gas temperatures decrease with the increasing efficiency of automotive engines. Since the preferred location of a TE device is in the exhaust system downstream from the catalytic converter, the maximum temperature available for a waste heat recovery system in this configuration is currently around 500°C. Within the time frame that TE waste heat recovery systems will be available for fleet use, this maximum exhaust gas temperature will likely decrease to around 270–350°C due to the widespread use of more efficient engines. Since today's record ZTs are achieved near 500°C, OSU's goal this year was to develop materials with optimum ZT near about 300–350°C (around 600 K). To achieve this, OSU's research focused on PbSe, which avoids the use of tellurium, and ZnSb, that can be prepared by a method that requires only a short anneal. In the course of this research, OSU's project also addressed the issues of dopant distribution uniformity in PbTe.

The VT team focused on the low-temperature joining technique (LTJT) by silver sintering as a promising approach for mounting TE materials. LTJT is attractive because the silver joint has high thermal and electrical conductivities, high working temperature, and is highly reliable in thermal and power-cycling tests [1,2]. The VT team addressed problems with this approach that

are specific to TE energy converters. For example, silver diffuses quickly, and it is notoriously mobile as an ion in the presence of chalcogens. In addition, pressure is usually needed during the silver sintering process [3], which is a barrier for scaling conventional TE fabrication methods to industrial scales. This year, the metallization process of joining TE materials through coating and nanosilver-bonding was demonstrated. Through this, a model for better understanding the drying of nanosilver-enabled LTJT was developed, and the electrical/thermal resistivity and thermo-mechanical reliability of nanosilver-bonded interfaces were characterized.

APPROACH

Conventional solid-state chemistry techniques, such as ampouling and compounding, or ball-milling and spark plasma sintering, were used to synthesize the TE semiconductors; their properties were measured per long-established techniques in our laboratories [4,5]. Ag and Ti films were deposited on TE materials by physical vapor deposition, then bonded by nanosilver pressure-free joining techniques, then underwent shear testing. Interfacial electrical and thermal resistivity were measured, and the thermal performance of the interface was characterized by transient thermal impedance. A temperature cycling test between -40°C and 125°C was run on nanosilver-bonded parts.

RESULTS

Space limitations do not permit a detailed outline of all results; the conclusions are outlined in the following. Figure 1 (on PbTe) and Figure 2 (on PbSe) show that high values of $ZT > 1$ were obtained on several systems, in the case of PbSe at from 600 K on. This is especially favorable, as its performance peaked in a temperature regime that will better match future automotive exhaust. In Figure 3, the remarkable thermal performance of the nanosilver bonds is shown.

SUMMARY/CONCLUSION

- The TE performance of the PbS system can be enhanced by means of a closely coupled phonon-blocking/electron-transmitting approach that consists of embedding endotaxially nanostructured second phases. By extension, we anticipate that this approach can be successfully applied to other material systems as well. This work shows that the ZT of *p*-type PbS can be increased to the record high value of ~1.3 at 923 K with CdS nanostructures. Although the same strong reduction of the lattice thermal conductivity is achieved with ZnS, CaS and

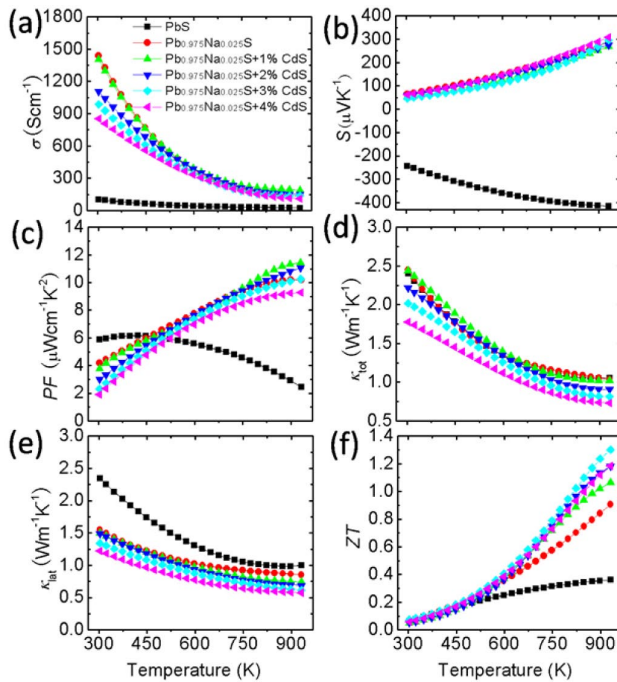


FIGURE 1. TE properties as a function of temperature for $\text{Pb}_{0.975}\text{Na}_{0.025}\text{S}$ with $x\%$ CdS: (a) electrical conductivity; (b) thermopower S ; (c) power factor; (d) total thermal conductivity; (e) lattice thermal conductivity; (f) ZT, the combined uncertainty for all measurements involved in the calculation of ZT is less than 15%. Similar results (not shown) were obtained using ZnS, CaS and SrS.

SrS, the enhanced ZT of the CdS system is unique and derives from better hole mobility.

- When optimally doped with Al and In then appropriately heat treated, PbSe can achieve a ZT value in excess of 1.2 over the temperature range of 600-700 K, even without the use of nanostructuring. This range is near where exhaust gas temperatures are projected to be in future high efficiency engines.
- An improved formulation of nanosilver paste was developed, which allows attaching by sintering at 250°C with no pressure. The electrical resistivity of the sintered nanosilver material was measured to be $2.63 \times 10^{-6} \Omega\cdot\text{cm}$, and the thermal resistivity was calculated to be $3.6 \times 10^{-3} \text{ K}\cdot\text{m}\cdot\text{W}^{-1}$ at 25°C and $1.4 \times 10^{-3} \text{ K}\cdot\text{m}\cdot\text{W}^{-1}$ at 500°C. A diffusion barrier metallization vapor-deposited on a Bi-Te material was studied and found to adhere strongly to sintered nanosilver.
- Transient thermal impedance of nanosilver-bonded power packages was measured and found to be about 20% lower than that of soldered joints. The relationship between thermal impedance and die-shear strength of nanosilver-bonded interface shows that a die-shear strength of at least 10 MPa is necessary for good thermal performance. Die-shear strength of nanosilver-bonded interface decreases

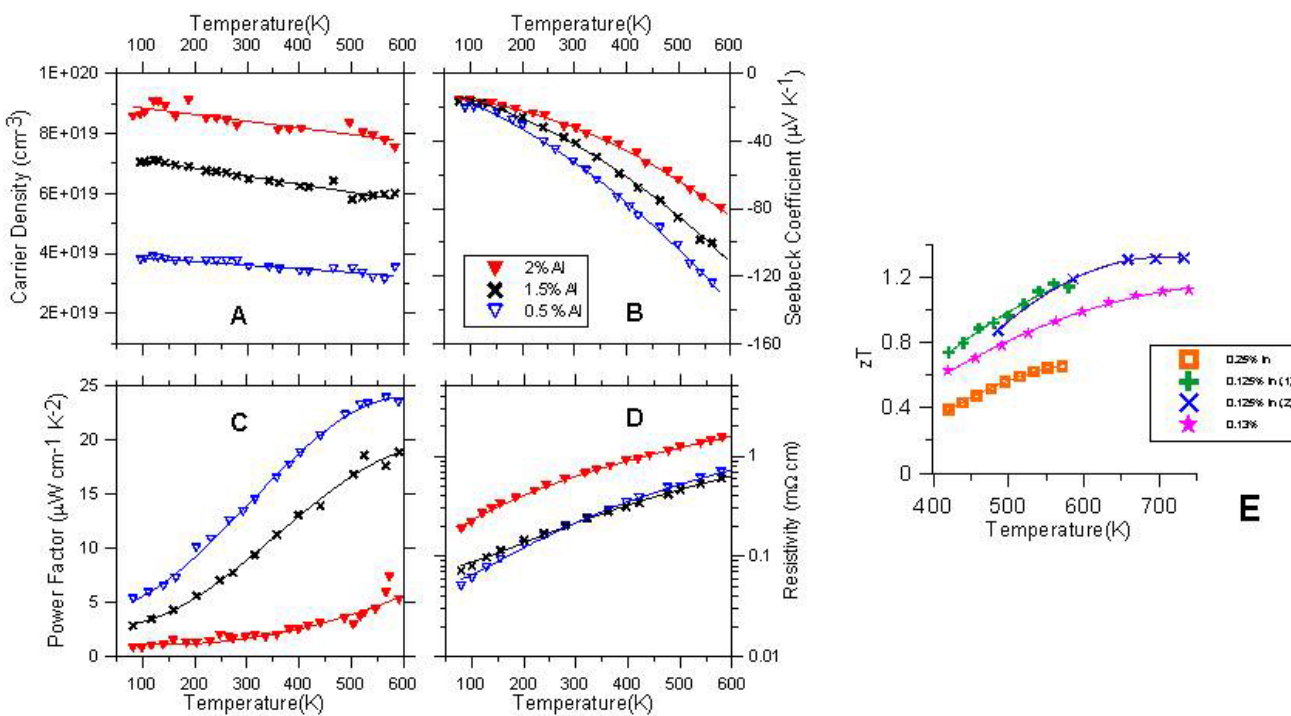


FIGURE 2. TE properties of $\text{Pb}_{1-x}\text{Al}_x\text{Se}$ with $0.5\% < x < 2\%$: carrier density (A), thermopower S ; (B), power factor (C) and electrical resistivity (D) vs. temperature (77-600 K). Similar data are obtained on $\text{Pb}_{1-x}\text{In}_x\text{Se}$ (E) the ZT for $\text{Pb}_{1-x}\text{In}_x\text{Se}$ reaches >1.2 and has a broad maximum at $T \geq 600$ K.

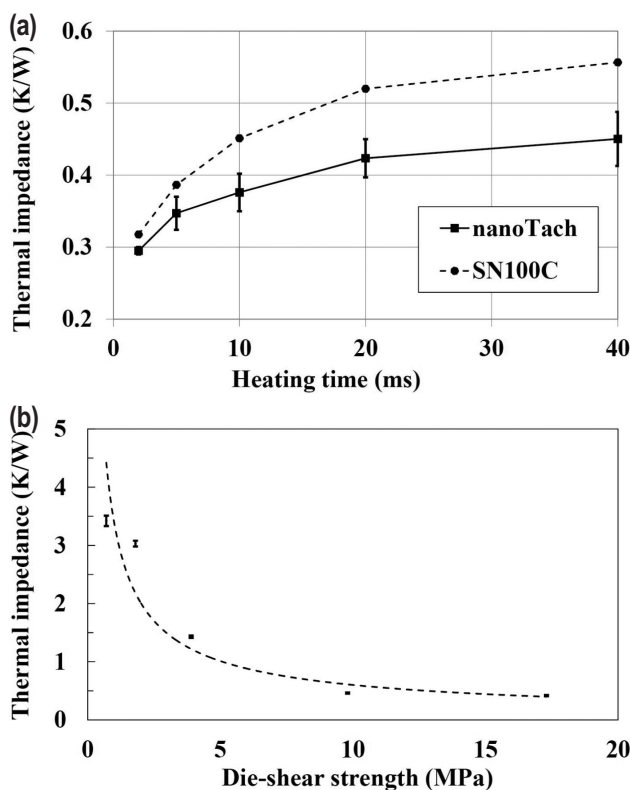


FIGURE 3. Plots of transient thermal impedance vs. (a) heating pulse width measured on power packages having chips bonded by nanosilver sintering (nanoTach) and lead-free soldering, and (b) die-shear strength with nanosilver-bonded joints showing that a minimum of 10 MPa bonding strength is necessary for high thermal performance of the sintered joint.

by less than 20% after 1,000 temperature cycles, indicating excellent thermo-mechanical reliability.

REFERENCES

- U. Scheuermann and P. Wiedl, Workshop on Metal Ceramic Composites for Functional Application, Vienna, Austria, p.181 (1997).
- H. Schwarzbauer and R. Kuhnert, IEEE Trans. Ind. Appl., 27 p.93 (1991).
- C. Göbl, P. Beckedahl and H. Braml, Automotive Power Electronics Paris, France, (2006).
- K. Biswas & al. *Nature*, 490, 414-418 (2012).
- J.P. Heremans & al., *Science* 321 554 -558 (2008).
- Christopher M. Jaworski, Michele D. Nielsen, Hsin Wang, Steven N. Girard, Wei Cai, Wally D. Porter, Mercouri G. Kanatzidis, and Joseph P. Heremans, Valence-band structure of highly efficient *p*-type thermoelectric PbTe-PbS alloys, *Physical Review B* 87, 045203 (2013)
- J.P. Heremans, Semiconductors for thermoelectric and spin-thermal solid-state energy conversion Joseph P. Heremans, AIP Conf. Proc. 1519, 43 (2013), DOI:10.1063/1.4794706
- J.P. Heremans, Resonant levels in bulk Semiconductors, Invited talk, E-MRS (European Materials Research Society), Strasbourg, France, May 26–30, 2013
- J.P. Heremans, Thermoelectric and spin caloritronics solid-state energy conversion, Plenary opening lecture, TEP-CH 2013 Synthesis and function of Thermoelectric Materials Conference, EMPA (Swiss Federal Laboratories for Materials Science and Technology), CH-8600 Dübendorf, Switzerland, Sept. 16-19 2013
- Lee, Y.; Lo, S.H.; Androulakis, J.; Wu, C.I.; Zhao, L.D.; Chung, D.Y.; Hogan, T.P.; Dravid, V.P.; Kanatzidis, M.G.: High-Performance Tellurium-Free Thermoelectrics: All-Scale Hierarchical Structuring of *p*-Type PbSe-MSe Systems (M = Ca, Sr, Ba). *Journal of the American Chemical Society* 135, 5152-5160 (2013)
- Zhao, L.D.; He, J.Q.; Hao, S.Q.; Wu, C.I.; Hogan, T.P.; Wolverton, C.; Dravid, V.P.; Kanatzidis, M.G.: Raising the Thermoelectric Performance of *p*-Type PbS with Endotaxial Nanostructuring and Valence-Band Offset Engineering Using CdS and ZnS. *Journal of the American Chemical Society* 134, 16327-16336 (2013)
- G-Q. Lu, “Nanosilver paste: its Sintering Behavior and Applications for Chip Interconnection”, 15th IEEE International Symposium on Advanced Packaging Materials (APM) 2013, Irvine, California, USA, (Feb 27 – Mar 1, 2013), invited presentation
- K. Xiao, S. Luo, K. Ngo, and G-Q Lu, “Low-temperature Sintering of a Nanosilver Paste for Attaching Large-area Power Chips”, 15th IEEE International Symposium on Advanced Packaging Materials (APM) 2013, Irvine, California, USA, (Feb 27 – Mar 1, 2013)
- Huang Zheng, Jesus N. Calata, David Berry, Khai D.T. Ngo, Susan Luo, and G-Q. Lu, “Low-Pressure Joining of Large Area Devices on Copper Using Nanosilver Paste,” in *IEEE Trans. on Components, Packaging and Manufacturing Technology* 3(6): 915-922, 2013.
- K. Xiao, J. Calata, H. Zheng, K. Ngo, and G-Q Lu, “Simplification of the Nanosilver Sintering Process for Large-Area Semiconductor Chip Bonding: Reduction of Hot-Pressing Temperature Below 200°C”, *IEEE Trans. on Components, Packaging and Manufacturing Technology*, 2013. 3(8): p. 1271-1278.
- K. Xiao, K. Ngo, and G-Q Lu, “A diffusion-viscoelastic analysis and experimental verification of defect formation in sintered silver bond-line,” submitted to *Journal of Materials Research* (2013)

FY 2013 PUBLICATIONS/PRESENTATIONS

- E.M. Levin, J.P. Heremans, M.G. Kanatzidis, and K. Schmidt-Rohr, Electronic inhomogeneity in *n*- and *p*-type PbTe detected by ¹²⁵Te NMR, *Physical Review B* 88 115211 (2013).

SPECIAL RECOGNITIONS & AWARDS

1. Joseph P. Heremans was elected to the National Academy of Engineering.
2. Mercouri Kanatzidis was elected Fellow of the American Association for the Advancement of Science.

V.6 NSF/DOE Thermoelectrics Partnership: Purdue – GM Partnership on Thermoelectrics for Automotive Waste Heat Recovery

Xianfan Xu (Primary Contact),
Timothy S. Fisher, Stephen D. Heister,
Timothy D. Sands, and Yue Wu
Purdue University
585 Purdue Mall
West Lafayette, IN 47907

NSF Manager: Sumanta Acharya

DOE Technology Development Manager:
Gurpreet Singh

NETL Project Manager: Carl Morande

- Scale up nanowire synthesis methods. Synthesize and evaluate telluride-based nanowire heterostructures. Further pursue scalable production and device demonstration.
- Characterize thermal transport in TiN/(Al,Sc)N metal/dielectric superlattice system, and developing models to understand the origin of high interface thermal conductance.
- Evaluate heat transfer concepts based on jet impingement to maximize TEG performance.
- For thermal interface material testing, design and fabrication of a thermal interface test rig, and generating initial high-temperature data from the test rig.

Overall Objectives

This project is in collaboration with the General Motors Global R&D (GM) to enable ultimately the broad adoption of thermoelectric (TE) waste heat recovery systems, or TE generators (TEGs), at a scale commensurate with the global vehicle manufacturing enterprise. We exploit the complementary missions of research/development at Purdue and deployment/commercialization at GM to develop the fundamental understanding and technology improvements needed to make viable the efficient conversion of waste heat in automotive exhaust systems to electricity. We address the key elements for the development and deployment of commercial automotive TEGs. The specific research tasks are:

- (1) Advancing the performance of skutterudites that are currently used as the TE material at GM through thermal conductivity reduction and phonon engineering
- (2) Development of nanowire TE materials
- (3) Development of metal-semiconductor laminate TE materials
- (4) Development of efficient heat exchanger and system level thermal modeling
- (5) Development of thermal interface materials

Fiscal Year (FY) 2013 Objectives

- Study the dynamics of energy-carriers in skutterudites using ultrafast laser spectroscopy to learn about the transport properties of carriers on different energy levels.

FY 2013 Accomplishments

- Investigated carrier relaxation rates for different filling ratio of filled-skutterudite. The study provided insight for the investigation of band structure and the manipulation of carrier transport properties of filled-skutterudites.
- Grew PbTe, Bi₂Te₃, and Ag₂Te nanowires in large quantities (>10 g/batch). Synthesized and evaluated PbTe-Bi₂Te₃ and PbTe-Ag₂Te nanowire heterostructures. Tested a thin-film TE device using p-type and n-type PbTe nanocrystals.
- Extraordinarily interface thermal conductance that exceeds any values in literature is achieved. Relationship between superlattice periodicity and thermal conductivity is established.
- Developed new TEG designs based on jet impingement mechanism and developed numerical models to evaluate such designs.
- Designed and assembled a test bench for experimental verification of system level performance with various configurations of hot- and cold-side heat exchangers and thermal interface materials and successfully characterized thermal interfaces.

Future Directions

- Find out how the filling ratio in skutterudite affects the electronic band structure and energy carriers in skutterudites. Obtain relaxation time of carriers in skutterudites.

- Dope nanowire materials to optimize the TE performance. Develop hydrazine-free telluride nanowire synthesis methods. Make a nanocrystal-coated fiber TE device.
- Develop a theoretical model to explain the origin of such high interface thermal conductance and measurement of cross-plane electrical properties of superlattices.
- Experimental assessment of impinging and longitudinal heat exchangers for analytical model verification, allowing system optimization and initial TEG performance estimates.
- Increase the maximum operating temperature of the test rig to at least 800°C. Use carbon nanotube (CNT)-based interface materials to address thermomechanical stress issues.



INTRODUCTION

The development of a TEG requires research and development in multiple areas, from TE materials to thermal management. The current project consists of five different tasks as indicated in the “Overall Objectives” section. The progresses on these five tasks are reported in the following:

1. Advance the Performance of Skutterudites That Are Currently Used as the TE Material at GM through Thermal Conductivity Reduction and Phonon Engineering

Skutterudites filled with heavier elements are found to have significantly reduced thermal conductivity, which can be candidates for efficient TE materials. Study of the

role of the energy carriers can help to optimize the design of TE materials and thus to make better use of the waste heat.

Approach: Femtosecond time-resolved spectroscopy measurement is performed to obtain the transient reflectance signals of skutterudites, which reflects the behavior of energy-carriers and the electronic structure. Skutterudite samples with varying filling ratios are compared to study the effect of doping ratio. Probe with varying wavelengths is used to detect relaxation process of different energy levels.

Results: The transient reflectance measurements of skutterudites indicate the dynamics of carrier relaxation and slower carrier-phonon relaxation. Figures 1a and 1b show the reflectance changes are different in the samples with different filling ratios, indicating the electronic structures are changed significantly by filling. Analysis of the reflectance evolution reveals the carrier relaxation time, carrier-lattice coupling time, and the lattice cooling time. The signal within 10 ps after the excitation mainly reflects the cooling of the carriers through carrier-carrier scattering and carrier-phonon scattering. Therefore the signal within this period is significantly dependent on the probe wavelength and the filling ratio, which modifies the band structure and is an indication of the transport properties of filled skutterudite.

Conclusions: Skutterudites have different electronic band structures caused by filling, which affects the behaviors of carriers in the material and the TE properties and can be probed using femtosecond laser spectroscopy by varying probe wavelength.

2. Development of Nanowire TE Materials

Many high-performance materials require expensive manufacturing techniques, which are not suitable for large-scale production. Meanwhile, solution-based

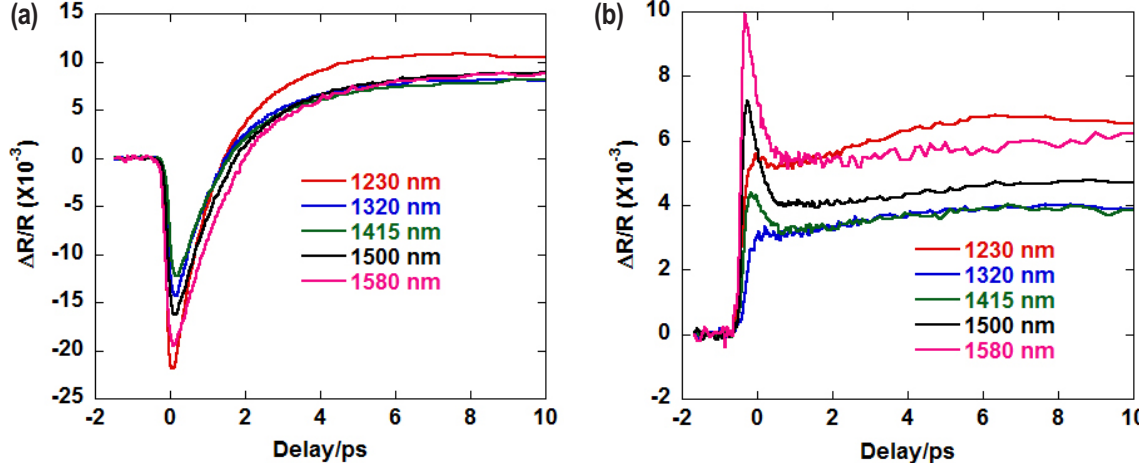


FIGURE 1. (a) Transient reflectance signal of $Mm_{0.07} Fe_{0.43} Co_{3.56} Sb_{12.12}$, (b) Transient reflectance signal of $Mm_{0.72} Fe_{3.43} Co_{0.57} Sb_{11.97}$.

syntheses can produce nanostructures at a high yield and low cost.

Approach: Solution-synthesis methods are developed for large-scale production of nanowires and nanowire heterostructures. These materials are purified, dried into powder, and hot pressed into discs for TE property measurements. Furthermore, colloidal PbTe nanocrystals are synthesized and coated onto glass fibers or glass substrates to demonstrate the potential for solution-based TE device manufacturing.

Results: Nanowires of PbTe, Bi₂Te₃ and Ag₂Te have been synthesized in large quantities (>10 g/batch) with PbTe and Bi₂Te₃ being produced at yields higher than 80%. PbTe-Bi₂Te₃ heterostructure nanowires were synthesized and hot pressed into nanocomposite discs. The thermal conductivity was reduced (0.30 to 0.55 W/m-K) compared to bulk values (around 1.40 W/m-K). Similarly, Ag₂Te nanowires and PbTe-Ag₂Te heterostructures were synthesized. Figure of merit, ZT, reached 0.48 and 0.58 in Ag₂Te and PbTe-Ag₂Te, respectively. Novel colloidal n-type PbTe nanocrystals

were synthesized in solution. Fibers with various nanocrystal coating thicknesses were tested using the 3ω method; the axial thermal conductivity was found to be ~0.9 W/mK near room temperature (see Figure 2).

Conclusions: The scalability of the solution synthesis of nanowire and nanowire heterostructures has been established with good TE performance shown for nanocomposite discs. TE devices and fiber-based materials made with solution processable nanocrystals continue to yield promising results.

3. Thermal Transport in TiN/(Al,Sc)N Metal/Dielectric Superlattices

Approach: Understanding the role of interfaces in thermal transport across nanoscale superlattices is important to the design of TE materials and devices with improved efficiency and for building efficient thermal management technologies for nano- and opto-electronic devices. Nitride metal/semiconductor superlattices are not only promising for achieving highly efficient TE devices, they also serve as a model

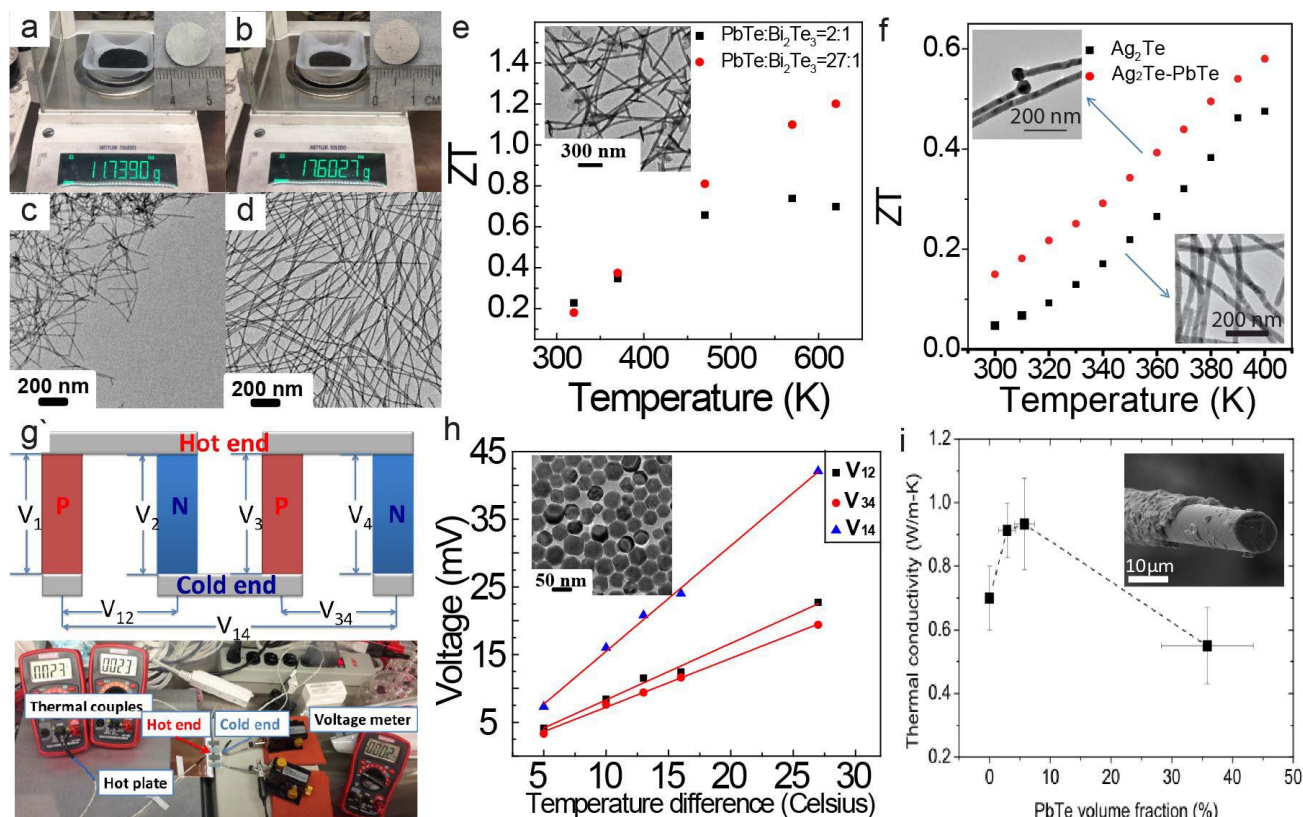


FIGURE 2. (a,b) One batch of PbTe (a) and Bi₂Te₃. (b) Nanowire powder (insets are hot-pressed discs of the respective materials). (c,d) Transmission electron microscope (TEM) images of nanowires of PbTe (c) and Bi₂Te₃ (d) synthesized at large-scale. (e) ZT of PbTe-Bi₂Te₃ heterostructures (inset is TEM image of the material with PbTe:Bi₂Te₃ ratio of 27:1). (f) ZT of Ag₂Te and PbTe-Ag₂Te heterostructures (insets are TEM images). (g) Schematic representation and digital photograph of four-leg nanocrystal film TE module. (h) Voltage generated by the nanocrystal film TE module (inset is TEM of n-type PbTe nanocrystals). (i) Thermal conductivity of PbTe nanocrystal-coated glass fibers of various compositions (inset is scanning electron microscope image of PbTe nanocrystal coated fiber).

system where fundamental physical processes involving thermal conduction can be tested and understood. Here in this report, we present our analysis on the role of the superlattice interfaces on the thermal transport in TiN/(Al,Sc)N superlattices. Details about the superlattice growth and microstructural characterization were presented in earlier reports.

Results: The time-domain thermo reflectance measurements are used to characterize thermal transport in the superlattices. Our results (see Figure 3) indicate that the thermal conductivity undergoes a minimum at a superlattice period thickness (a) of 4 nm corresponding to 4.5 W/m-K. The corresponding thermal interface conductance are extremely high with $G=2$ to 6 GW/m²-K

for $4 \text{ nm} \leq a \leq 30 \text{ nm}$. When the period thickness is smaller than 4 nm, the interface conductance increases even more possibly due to tunneling effects. Since these conductance values are higher than the prediction of perfect phonon transmission model, we suspect a strong electron-phonon coupling at the superlattice interfaces that increases thermal conductance.

Conclusions: TiN/(Al,Sc)N metal/dielectric superlattices show extremely high interface thermal conductance that exceeds the prediction of perfect phonon transmission model. Such high interface conductance can be engineered to develop efficient thermal management system for waste heat recovery and dissipation.

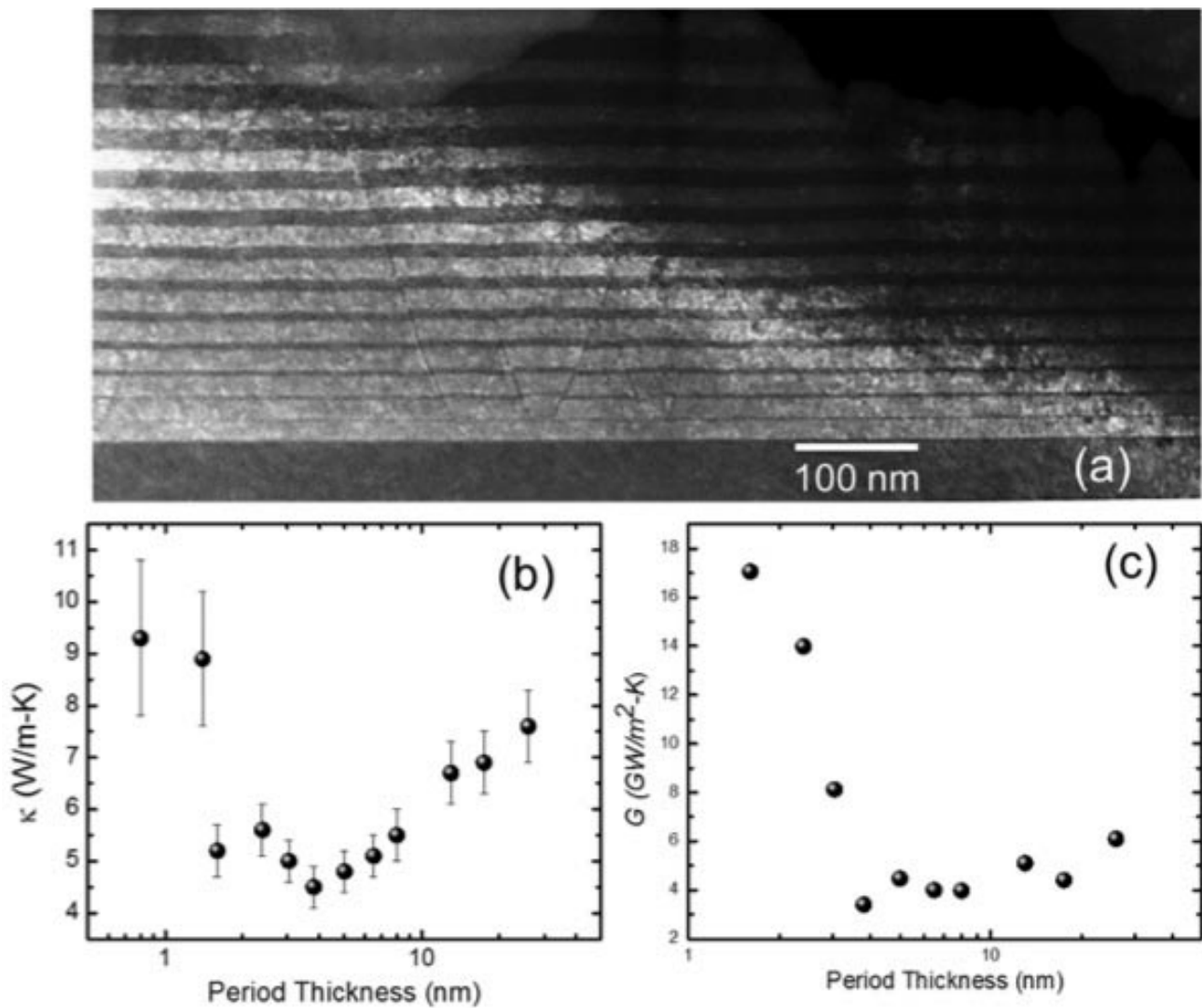


FIGURE 3. (a) High angle annular dark field scanning transmission electron microscopy image of a lattice matched, epitaxial, single crystalline TiN/(Al,Sc)N superlattice showing excellent interface quality. (b) Thermal conductivity as a function of the superlattice periodicity of the superlattice. Minimum in thermal conductivity is obtained at a period thickness of 4 nm. (c) Interface thermal conductance as a function of the superlattice periodicity is presented. For the period thickness great than 4-nm interface conductance have values between 2-6 GW/m²-K.

4. Development of Efficient Heat Exchanger and System Level Thermal Modeling

A comprehensive numerical model has been developed to examine plate fin-type heat exchanger-based TEG systems. System modeling and optimization of various TEG configurations have been reported previously [1,2]. The jet impingement method has been known to offer high thermal fluxes at the expense of high pressure drops. TEG system designs based on jet impingement heat transfer mechanism have been investigated.

Approach: To analyze an entire TEG system, representative modular shroud designs based on jet impingement concept have been formulated. These designs encase one TE module (TEM) with single or an array of impinging jets. The flexible design shown in Figure 4 allows varying the jet diameter, configuration, and height as well as interchanging enhanced impingement plates including flat plate, sparse pin fins, and dense pin fins, and a DANA turbulizer design. Heat transfer correlations presented in literature have been considered to calculate heat transfer at the impingement regions. The thermal resistance network method is used to compute heat and electrical fluxes through the components within the permissible pressure budget. Experimental verification of the analytical models will allow accurate TEG performance evaluation and optimization. Exhaust gas and coolant streams will be used as the temperature reservoirs to enable full system testing of hot- and cold-side heat exchangers, TEMs, and thermal interface materials at various scales. The

test setup will also be utilized to assess and optimize the novel impingement heat exchanger concept.

Results: An experimental test bed has been designed and assembled at Purdue University, with proven exhaust gas capabilities of flow rates up to 4g/s N_2 at 700°C and coolant from 10°C to 90°C , and includes a variable clamping load designed to reach 300 psi. Improvements including an inert gas environment for the TEM, digital data acquisition, and additional instrumentation for measuring heat fluxes, clamping load, pressure drop, and TEM temperatures are in progress to provide full-system performance data throughout the operational temperature range.

Conclusions: A prospective TEG system based on the jet impingement concept is being investigated. Various modular test shrouds have been fabricated for experimental evaluations.

5. Thermal Interface Materials Development

In this FY, a high-temperature one-dimensional reference bar test rig for measuring thermal contact resistance was built, and several thermal interfaces were characterized with the system.

Approach: The design and fabrication of a thermal interface test rig was a high priority in this FY. This rig was designed based on a one-dimensional reference bar technique to quantify the heat flux conducting through two copper bars that serve as reference calorimeters (see Figure 5). An interface material is placed between the copper bars, thus allowing extraction of the thermal

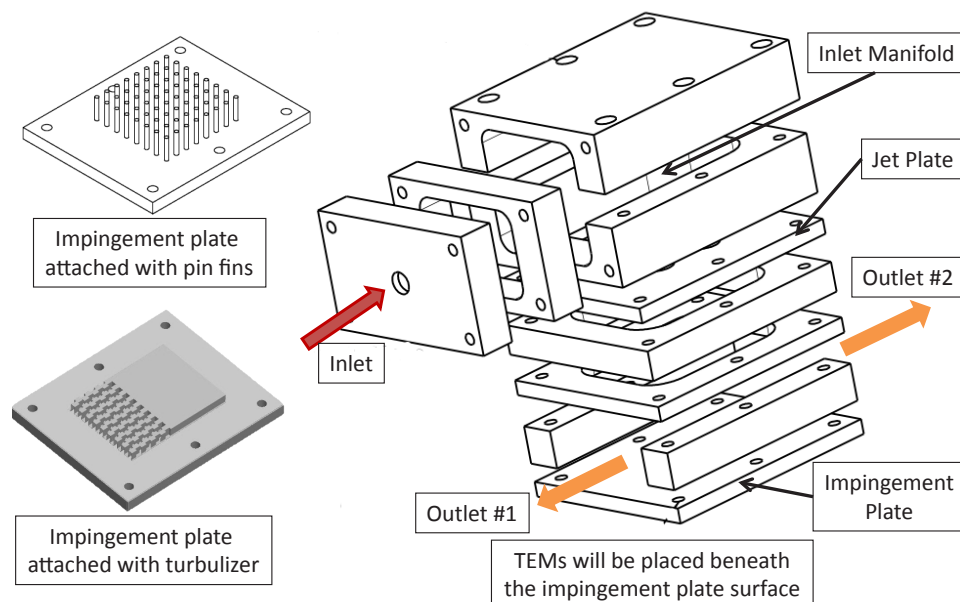


FIGURE 4. Schematic of test shroud based on jet impingement heat transfer mechanism. Flexible design enables evaluation of various surface enhancements such as pin fins and turbulizer.

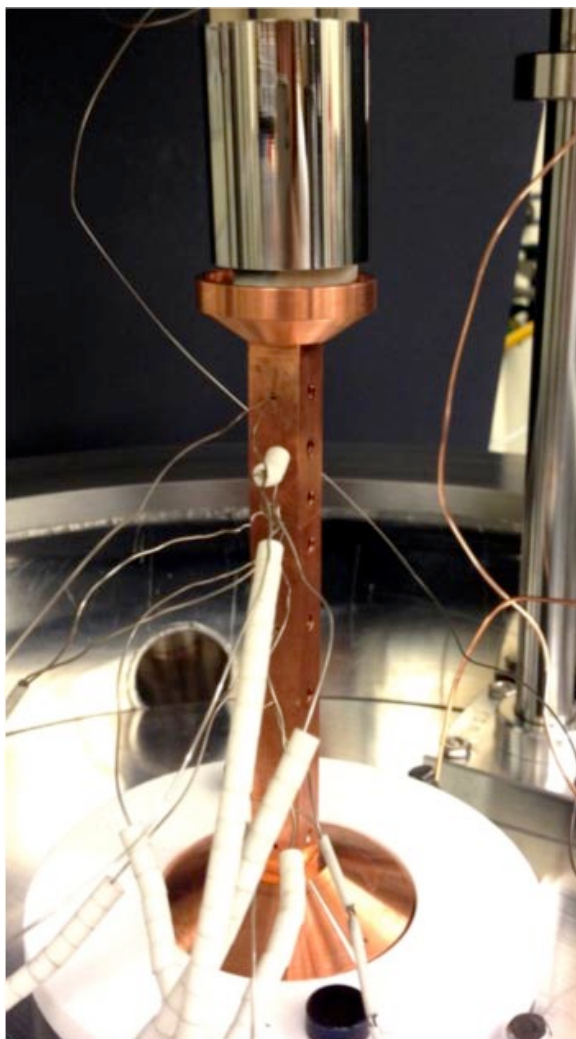


FIGURE 5. High-temperature one-dimensional reference bar thermal interface test rig.

interface resistance from the raw data. In order to achieve high-temperature capability, the rig is placed in a vacuum bell jar with radiation shielding around the copper bars to minimize convective and radiative heat losses as well as oxidation by ambient air. Along with the hardware, a LabVIEW program was created for data collection. For high-temperature thermal interface material development, a new concept of a modified CNT thermal interface material for high-temperature applications has been developed and is being tested. In order to maximize the actual number of individual CNTs in an array that are in contact with the opposing surface to reduce the thermal resistance, the free-tip end of the CNT array is brazed with filler metal to the opposing surface.

Results: Several thermal interfaces have been characterized with the test rig. As expected, CNTs grown on Gd foil have been shown to drastically reduce thermal

contact resistance from $1,230 \text{ mm}^2\text{K/W}$ to $143 \text{ mm}^2\text{K/W}$. A commercially available direct-bonded aluminum, that is AlN plate with an Al layer bonded to each side, and a promising candidate for the TE substrate as selected by industrial partners, was tested up to 500°C . The interface between AlN and Al had low resistance initially but deteriorated substantially during thermal cycling, with interfacial thermal resistance increasing up to five-fold. This degradation is presumably caused by the coefficient of thermal expansion mismatch between AlN and Al layers, resulting in large mechanical stress and associated micro-cracks during temperature change. For the brazed CNT concept, several alloys have been tested, and TiCuSil has been identified as a promising braze alloy for this application because of its good wetting behavior with CNTs and its suitable working temperature range.

Conclusions: A one-dimensional reference bar test rig for thermal interface characterization has been built and shown to operate at temperatures up to 800°C . Thermomechanical stress is a critical issue for TE modules in the current application, and CNT-based interface materials exhibit promising properties to address this issue in near-future work.

REFERENCES

1. Kumar S., Heister S.D., Xu X., Salvador J.R., and Meisner G.P., 2013a, "Thermoelectric Generators for Automotive Waste Heat Recovery Systems Part I: Numerical Modeling and Baseline Model Analysis," *J. Electron. Mater.*, **42**(4), pp. 665–674.
2. Kumar S., Heister S.D., Xu X., Salvador J.R., and Meisner G.P., 2013b, "Thermoelectric Generators for Automotive Waste Heat Recovery Systems Part II: Parametric Evaluation and Topological Studies," *J. Electron. Mater.*, **42**(6), pp. 944–955.

FY 2013 PUBLICATIONS/PRESENTATIONS

1. Guo, L., Xu, X., Salvador, J.R., and Meisner, G.P., 2013, "Resonant Oscillations in Multi-Filled Skutterudites", *J. of Electronic Materials*, Vol 42, pp. 1978.
2. Guo, L., Xu, X., Salvador, J.R., and Meisner, G.P., 2013, "Coupled vibrational modes in multiple-filled skutterudites and the effects on lattice thermal conductivity reduction", *Appl. Phys. Lett.*, Vol. 102, pp. 111905, 2012.
3. Guo, L., Xu, X., Carrier Dynamics in Skutterudites, ASME 2013 International Mechanical Engineering Congress & Exposition, IMECE2013-63667, November 2013, San Diego, CA.
4. Wang Y., Xu, X., Mode-wise Phonon Properties of Bismuth Telluride, ASME 2012 International Mechanical Engineering Congress & Exposition, IMECE2012-89666, November 2012, Houston, TX.

- 5.** Xu, X., Plenary lecture, “Thermoelectrics for Automobile Waste Heat Recovery – Challenges in Multi-scale Thermal Science” 8th International Symposium on Heat Transfer, October 2012, Beijing, China.
- 6.** Xu, X., invited talk, “Phonon Dynamics in Nano-structured Materials”, ASME 2013 Summer Heat Transfer Conference, July 2013, Minneapolis, MN.
- 7.** Qiu, Bo; Bao, Hua; Zhang, Gengqiang; Wu, Yue; Ruan, Xiulin. Molecular dynamics simulations of lattice thermal conductivity and spectral phonon mean free path of PbTe: Bulk and nanostructures. *Computational Materials Science*, 2012, 53, 278–285.
- 8.** Wu, Yue (Contribution talk) “Nanowire Heterostructures for Thermoelectric Energy Harvesting”, 2012 AIChE Meeting, October, 2012.
- 9.** Wu, Yue (Invited talk) “Advanced Nanostructures for Thermoelectric Energy Harvesting”, American Vacuum Society Annual Meeting, November, 2012.
- 10.** Fang, H.; Feng, T.; Yang, H.; Ruan, X.; Wu, Y. Synthesis and Thermoelectric Properties of Compositional-Modulated Lead Telluride-Bismuth Telluride Nanowire Heterostructures. *Nano Lett.* 2013, 13, 2058–2063.
- 11.** Finefrock, Scott W.; Wang, Y.; Ferguson, J.B.; Ward, J.V.; Fang, H.; Pfluger, J.E.; Dudis, D.S.; Ruan, X.; Wu, Y. Measurement of Thermal Conductivity of PbTe Nanocrystal Coated Glass Fibers by the 3ω Method. *Nano Letters Article ASAP*.
- 12.** Jha, P., T.D. Sands, L. Cassels, P. Jackson, T. Favaloro, B., Kirk, J. Zide, X. Xu, A. Shakouri, 2012, Cross-plane electronic and thermal transport properties of p-type La_{0.67}Sr_{0.33}MnO₃/LaMnO₃ perovskite oxide metal/semiconductor superlattices, *J. Appl. Phys.*, Vol. 112, p. 063714.
- 13.** Pankaj Jha, Timothy D. Sands, Cory Bomberger, Philip Jackson, Tela Favaloro, Xianfan Xu, Joshua Zide, and Ali Shakouri, Cross-plane thermoelectric transport in p-type La_{0.67}Sr_{0.33}MnO₃/LaMnO₃ oxide metal/semiconductor superlattices, 2012 MRS Meeting, November 2012, Boston, MA.
- 14.** Bivas Saha, Gururaj Naik, Vladimir Drachev, Alexandra Boltasseva, Ernesto E. Marinero, and Timothy D. Sands, Electrical and Optical Properties of ScN and Mn-doped ScN deposited by dc-magnetron sputtering. *Journal of Applied Physics*, 114, 063519 (2013).
- 15.** Polina V. Burmistrova, Jesse Maassen, Tela Favaloro, Bivas Saha, Shuaib Salamat, Yee Rui Koh, Mark S. Lundstrom, Ali Shakouri, and Timothy D. Sands, High mobility and high thermoelectric power factor in epitaxial ScN films deposited by reactive magnetron sputtering onto MgO(001) substrate. *Journal of Applied Physics* 113, 153704 (2013).
- 16.** Gururaj V. Naik, Bivas Saha, Jing Liu, Sammy M. Saber, Eric Stach, Joseph MK Irudayaraj, Timothy D. Sands, Vladimir M. Shalaev and Alexandra Boltasseva, Titanium nitride-based metamaterial for spontaneous emission rate engineering. (*Under Review*).
- 17.** Kumar S., Heister S.D., Xu X., Salvador J.R., and Meisner G.P., 2013, “Thermoelectric Generators for Automotive Waste Heat Recovery Systems Part I: Numerical Modeling and Baseline Model Analysis,” *Journal of Elec Materi*, 42(4), pp. 665–674.
- 18.** Kumar S., Heister S.D., Xu X., Salvador J. R., and Meisner G.P., 2013, “Thermoelectric Generators for Automotive Waste Heat Recovery Systems Part II: Parametric Evaluation and Topological Studies,” *Journal of Elec Materi*, 42(6), pp. 944–955.
- 19.** Kumar S., Heister S.D., Xu X., and Salvador J.R., 2013, “Numerical Analysis of Thermoelectric Modules for Automobile Waste Heat Recovery Systems.” ASME 2013 IMECE, San Diego, CA (*to be presented on 21st November, 2013*).

SPECIAL RECOGNITIONS & AWARDS/ PATENTS ISSUED

- 1.** K.R. Saviers, S.L. Hodson, J.R. Salvador, L.S. Kasten, T.S. Fisher, “Carbon nanotube arrays for enhanced thermal interfaces to thermoelectric modules,” 10th International Energy Conversion Engineering Conference, paper # AIAA-2012-4048, July 2012. This paper was awarded *2012 Best Aerospace Power Systems Student Paper* by the AIAA Aerospace Power Systems Technical Committee.
- 2.** US and International Full Patent application filed: TiN/(Al,Sc)N Metal/Dielectric Superlattices for Metamaterial Applications in the Visible Range. Gururaj Naik, Bivas Saha, Timothy D. Sands, and Alexandra Boltasseva.

V.7 Automotive Thermoelectric Modules with Scalable Thermomechanical and Electromechanical Interfaces

Kenneth E. Goodson (Primary Contact),
Mehdi Asheghi, Michael T. Barako,
Marc T. Dunham, Yoonjin Won
Department of Mechanical Engineering
Stanford University
Bldg. 530, Room 214
Stanford, CA 94305

George S. Nolas, Yongkwan Dong
Department of Physics
University of South Florida

Boris Kozinsky, Georgy Samsonidze
Robert Bosch LLC
Research and Technology Center North America

DOE Technology Development Manager:
Gurpreet Singh

NETL Project Manager: Carl Morande

Fiscal Year (FY) 2013 Objectives

- Measure thermal and mechanical properties of bonded and unbonded carbon nanotube arrays, including key performance and reliability metrics.
- Create and validate coarse-grained molecular simulation for prediction of thermal and mechanical properties of carbon nanotube (CNT) and metal nanowire (NW) arrays.
- Construct and test infrared microscopy apparatus up to 600°C.
- Develop apparatus for metal NW synthesis and grow repeatable, proof-of-concept copper NW arrays with tunable geometries.
- Establish high sensitivity thermal metrology based on the three-omega method using microfabricated electrothermal devices to characterize metal NW arrays.
- Synthesize and optimize high-temperature p- and n-type TE materials.
- Develop methodology for calculating the electronic relaxation time from first principles using codes developed in collaboration with university partners.
- Demonstrate the accuracy of electronic relaxation time calculations by computing the intrinsic electrical resistivity of well-characterized metals and doped semiconductors.

Overall Objectives

- Evaluate novel interface options, which can accommodate the massive fluctuations in thermomechanical strain in automotive systems while providing excellent thermal and electrical contact.
- Create and measure high-temperature p- and n-type thermoelectric (TE) materials that are both efficient and stable at high temperatures, and which can be reliably attached to heat sinks and electrodes.
- Develop practical metrology and metrics relevant for system development, which also can be used to assess performance and durability during thermal cycling of the TE energy generators over a wide range of temperatures.
- Optimize and investigate the TE properties of p-type skutterudites, fine grain half-Heusler alloys, and novel chalcogenides.
- Develop ab-initio methods and tools for computational modeling of the electronic transport in TE materials.
- Provide theoretical guidance towards optimization of material compositions to enhance the TE performance.

FY 2013 Accomplishments

- Constructed and validated a high-temperature apparatus for making infrared microscopy characterization of materials and interfaces over a temperature gradient from 0-600°C.
- Established a complete electrodeposition apparatus at Stanford for template-assisted fabrication of nanostructured metal thermal interface materials (TIMs).
- Designed, fabricated, and calibrated microfabricated heater/thermometer devices for thermal characterization of metal NW arrays using the three-omega method.
- Synthesized copper NW arrays with tunable properties, including lengths from 1-60 μm, diameters of 200 nm, and volume fractions from 10-50% over large areas.

- Validated coarse-grained molecular simulation tool for CNT arrays by comparing predicted modulus values to those obtained experimentally during FY 2011-2012.
- Synthesized and measured the transport properties of novel skutterudites and chalcopyrite related compounds as well as half-Heusler alloys for combustion exhaust applications.
- Performed ab initio calculations of the electronic relaxation times and the electronic transport coefficients.
- Demonstrated an excellent agreement with experimental data for the calculated doping and temperature dependence of the intrinsic electrical resistivity of graphene.
- Acquired a detailed microscopic understanding of the relative role of different phonon modes in electron scattering processes in doped graphene.

Future Directions

- Adapt the thermal and mechanical characterization metrology developed for CNT arrays during FY 2011 and FY 2012 to perform full characterization on metal NW arrays.
- Adapt coarse-grained molecular simulation tool to predict properties in nanostructured metal TIMs, including NW arrays, and compare to data obtained experimentally.
- Demonstrate matrix stabilization of metal NW arrays to lend mechanical integrity to metal NW arrays as freestanding TIMs.
- Utilize high-temperature infrared microscopy apparatus to make measurements on novel TE materials and nanostructured TIMs at temperatures comparable to combustion exhaust streams.
- Develop systems-level model for a complete TE generator system integrated into an automobile exhaust stream.
- Synthesize and characterize additional compositions of skutterudites and chalcogenides.
- Perform first principles calculations of the electronic transport coefficients and the figure of merit ZT for different compositions of skutterudites and half-Heusler compounds.
- Identify the optimal compositions and the optimal doping concentrations in the chemical space of skutterudites and half-Heusler compounds which give the maximum values of the figure of merit ZT.



INTRODUCTION

TE generators for automotive waste heat recovery are developed to convert thermal energy in hot post-combustion gases directly into electricity for use in automobiles. Automobile combustion produces exhaust gases at ~600°C which are currently expelled to the environment as waste heat. By recovering some of this energy via TE energy conversion, the exhaust stream can provide supplemental electricity to the vehicle to reduce the alternator load and eventually to eliminate the need for an alternator altogether. This directly improves engine performance and increases automobile fuel economy.

We have identified two critical areas for improving TE device performance for combustion systems: (1) the need for scalable TE materials optimized at high temperatures and (2) the development of thermomechanical interfaces to improve device performance and reliability. Through this project, we have developed and measured novel TE materials, including skutterudites and half-Heusler alloys.

This includes the development of first-principles computational tools to predict material properties and the relevant experimental metrology for characterizing these materials. We have also explored the use of nanostructured TIMs, which uniquely combine the properties of high thermal conductance and mechanical compliance, to improve conversion efficiency and device lifetime. Systems-level modeling and full device-scale characterization was also performed to construct a complete architecture for optimizing a TE generator system for recovering waste heat from automobile combustion.

TE materials require a low electrical resistivity, ρ , to lessen Joule heating, a low thermal conductivity, κ , to reduce thermal losses, and a high absolute Seebeck coefficient, S , to obtain high TE performance as defined by the dimensionless TE figure-of-merit ($ZT = S^2 T / \rho \kappa$, where T the absolute temperature) in the temperature range of interest. The three material properties that define ZT can be varied by doping; however, they are not independent of each other [1-4]. Beyond well-known TE materials such as Bi_2Te_3 , PbTe , and TAGS (AgGeTe_2 - GeTe_2), recently skutterudites, half-Heuslers, and Cu-based chalcogenides have attracted attention as TE materials because of low κ values attributed to their crystal structures. In addition, its constituents are made of earth-abundant non-toxic materials, and the electrical properties can be modified by appropriate doping and/or variations in stoichiometry.

The electronic transport coefficients of metals and doped semiconductors can be calculated by solving the Boltzmann transport equation (BTE) for electrons. These calculations require as input the electronic band

structure and the electron relaxation time, which is a central quantity in the BTE theory. The electronic band structure is easily computable using density functional theory (DFT) or higher level methods, while calculating the relaxation time from first principles poses a computational challenge. The relaxation time is often assumed to be a constant (independent of material composition, electron energy, doping level, and temperature). We have found that the constant relaxation time approximation works well for metals but it fails for doped semiconductors. Since most TE materials are heavily doped semiconductors, ab initio relaxation times are required for accurate modeling of electronic transport in these materials. We therefore develop a methodology for computing the relaxation time from first principles, and we validate our method for well-characterized materials such as aluminum and doped graphene. We then proceed to computing the electronic transport coefficients and the figure of merit ZT for half-Heusler compounds.

APPROACH

We use a variety of in-house thermal and mechanical characterization tools to investigate the performance of nanostructured metal TIMs, including arrays of CNTs and metal NWs. For measuring intrinsic thermal properties with high sensitivity, these include the time-domain thermoreflectance systems (both nano- and pico-second) as well as an electrothermal measurement technique (the three-omega method), which measure the spatial distribution of thermal properties on the micro- and nanometer length scales. At larger length scales ($>100 \mu\text{m}$) and larger temperature gradients, we employ cross-sectional infrared microscopy to measure thermal conductivities and thermal interface resistances. We also use two mechanical techniques to determine the compliance of the nanostructured TIMs. For the out of plane modulus measurement, we use a resonator technique which involves measurement of the resonant frequency of each microfabricated cantilever before and after CNT film growth. The elastic modulus is extracted by modeling the Si-CNT cantilevers as two-layer composite beams. We also extract the out-of-plane mechanical modulus of CNT films using a nanoindentation technique.

To design and synthesize TE materials, we propose fundamental research by means of experimental science and first principle calculations to enhance and fine tune transport properties of filled Skutterudites and half-Heusler intermetallic alloys. The previously mentioned TE materials are synthesized by high-temperature solid state reaction as well as arc-melting methods, followed by densification by hot-pressing or spark plasma sintering. The crystal structures and compositions were

examined by the combination of Rietveld refinement on powder X-ray diffraction and elemental analysis. Low- and high-temperature transport properties were investigated using various measurement systems. The Materials Computation group at Bosch NA, led by Dr. Kozinsky, will conduct state-of-art ab-initio simulations for TE materials design. A dedicated high-temperature facility will be constructed to perform measurements on high-temperature performance of TEs, which will be complemented by standard high-temperature TE property measurements at the National Institute of Standards and Technology. We provide a fully microscopic and first-principles characterization of the temperature- and doping-dependent phonon-limited electrical resistivity in metals and doped semiconductors. We first use DFT and density functional perturbation theory as implemented in the Quantum ESPRESSO distribution [5] within the local density approximation [6] to compute the electronic and vibrational properties including the electron-phonon coupling matrix elements. Next, we interpolate the electron-phonon matrix elements to an ultra-dense grid of points in the Brillouin zone using maximally located Wannier functions as implemented in the Wannier90 [7] and EPW [8] packages. Finally, we calculate the electrical resistivity within a Boltzmann transport framework by numerical integration over this ultra-dense grid of points.

RESULTS

The Stanford Nanoheat group has been collaborating with researchers at Northrop Grumman to develop and test reactive metal bonding (as demonstrated in FY 2012) using ultrahigh conductivity CNT arrays. This collaboration demonstrated the mechanical stability and integrity of electronic devices (thin-film resistors and GaN-based devices) bonded to a substrate using reactive metal-bonded CNT arrays as TIMs. The devices were subjected to thermal cycling (up to 150°C). The thermal performance of the devices was evaluated as a function of thermal cycling using two-dimensional infrared thermography to examine heat dissipation from the device into the substrate. The devices demonstrated successful heat dissipation through 100 cycles, which indicates stable thermal properties of the CNT TIM and the reactive metal bond. The mechanical integrity was evaluated via scanning electron micrography (see Figure 1, left). The CNTs maintain good structural integrity and mechanical compliance due to a novel polyurethane infusion technique implemented by Northrop Grumman. Previously, Won, et al. developed a coarse-grained molecular simulation to predict the mechanical properties of vertically aligned CNT films. In this coarse-grained model, each nanotube is represented by a set of nodes connected by many short, elastic nanotube segments, that behave as Euler-

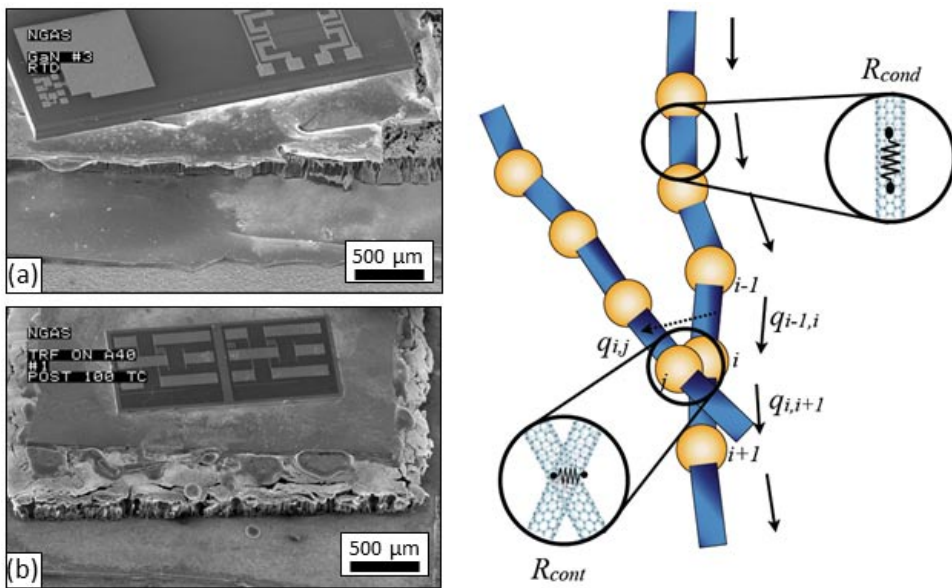


FIGURE 1. (left) Scanning electron micrographs of electronic test devices, including (a) a GaN-based device and (b) a thin-film resistor device. These devices are attached to substrates using reactive metal-bonded CNT TIMs. (right) Representative nodal network for CNT coarse-grained model.

Bernoulli beams. The simulation results are consistent with previous experimental measurements of the elastic modulus of CNT arrays using resonators and nanoindentation. In addition to accurately predicting the elastic modulus of CNT films, the simulation also defines the energetically-relaxed three-dimensional morphology of the CNT network. This geometry is then used to measure thermal transport across the array, including axial CNT conduction as well as CNT-CNT thermal contact resistances within the array (see Figure 1, right).

Metal NW arrays are expected to exhibit a lower modulus based on data available for CNTs owing to similar geometric arrangements. The Stanford Lab has been successful to date in developing the tools and techniques necessary to perform both the electrochemical synthesis and the thermal, electrical, and mechanical characterization of these types of materials. NW arrays of copper have been successfully synthesized in both anodic aluminum oxide and polycarbonate track-etched membranes with NWs ranging from 1-60 μm in length, diameters of 200 nm, and volume fractions from 10-50% (see Figure 2). There is substantially less entanglement and more homogeneity along the NW length with the metal NWs than there are for CNTs due to the template-assisted solution synthesis. Several new characterization techniques have been developed, including high-sensitivity microdevices for characterizing the effective thermal conductivity of the NW arrays based on the well-established three-omega method.

Efforts led by USF focused on investigating the fundamental properties and optimizing the TE properties of p-type CoSb_3 -based skutterudites as well as filled ternary skutterudites that are isoelectronic to this binary composition. We have successfully synthesized partially-filled p-type skutterudites with $ZT=0.85$ at 500°C as shown in Figure 3. In addition, we are investigating ternary modified skutterudites. These form by substitution at the anion site by elements from groups 14 and 16 (e.g., $\text{CoGe}_{1.5}\text{S}_{1.5}$) [9] or by isoelectronic substitution at the cation site by a pair of elements from groups 8 and 10 (e.g., $\text{Fe}_{0.5}\text{Ni}_{0.5}\text{Sb}_3$) [10]. Although a number of ternary skutterudites have been reported [9-13], there has been little work to date on the structural and physical properties of these materials. While ternary skutterudites formed by cation substitution appear to be isostructural to the binary skutterudites, structural studies carried out on materials prepared by anion substitution, such as $\text{CoSn}_{1.5}\text{S}_{1.5}$ and $\text{CoGe}_{1.5}\text{Te}_{1.5}$ [11,12] suggest that these compounds crystallize in a modification (Rhombohedral, $R-3$) of the skutterudite structure (Cubic, $I\bar{m}-3$). We recently demonstrated filled variants of these modified ternary skutterudites [14].

ZrNiSn and $\text{Zr}_{0.5}\text{Hf}_{0.5}\text{NiSn}$ have been prepared by arc-melting at University of South Florida and sent to Dr. James Salvador for melt-spinning at General Motors R&D. For ZrNiSn , melt-spinning was not successful due to the high melting temperature and fast solidification upon injection. On the other hand, $\text{Zr}_{0.5}\text{Hf}_{0.5}\text{NiSn}$ was successfully melt-spun and further investigations,

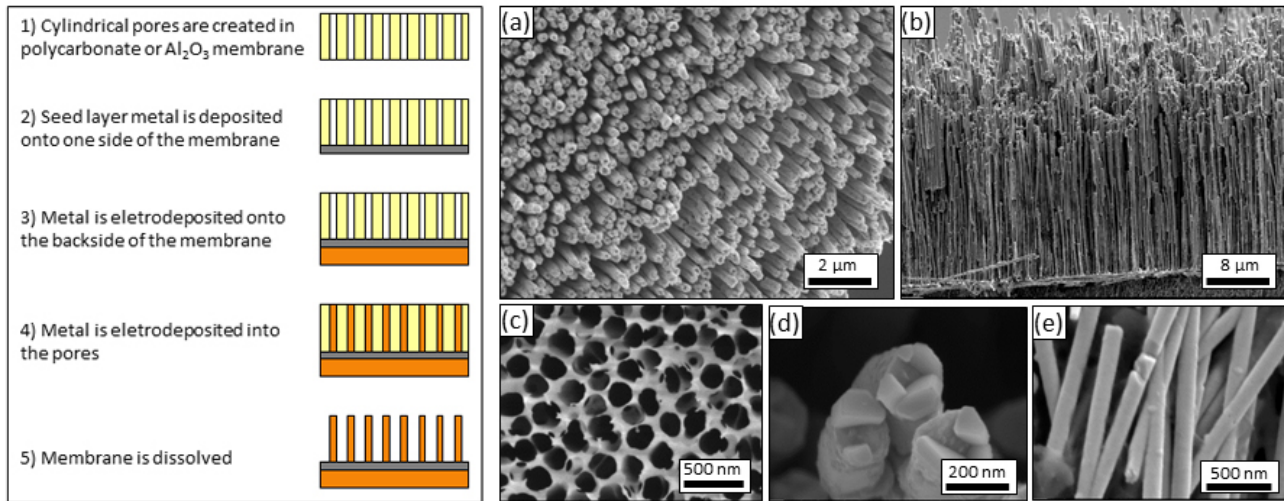


FIGURE 2. (left) Overview of fabrication process of freestanding metal NWs grown by sacrificial template-assisted electrodeposition. (right) Example of copper NW arrays. (a) NW arrays can be fabricated with extraordinarily high number densities with (b) nominally-vertical pores with minimal entanglement. (c) Anodic aluminum oxide membranes can be fabricated with diameters as small as ~ 15 nm and porosities up to 50%. (d) The grain size and crystal orientation of the NWs can be estimated by examining the exposed planar crystal faces at the growth surface (the tip) of each NW. (e) The NWs have very long, straight segments with smooth sidewalls that enhance conduction transport along the wires in the array.

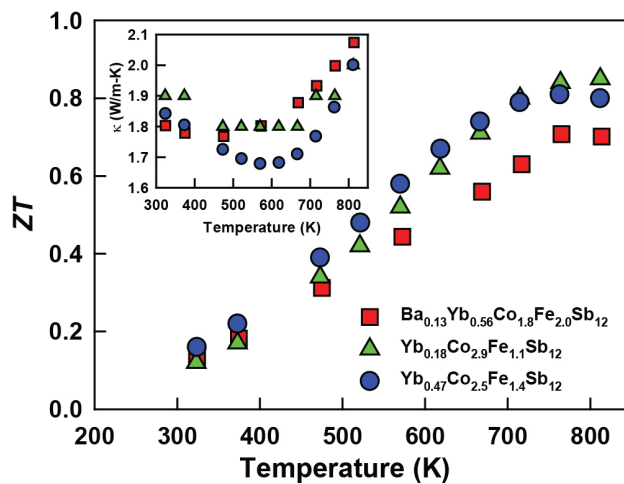


FIGURE 3. Temperature dependent ZT for double- or mono-filled Fe substituted skutterudites. Inset figure shows temperature dependent thermal conductivity, κ , for the three skutterudite specimens.

including crystallinity and transport properties has been taken. Quaternary stannites $\text{Cu}_{2+x}\text{Zn}_{1-x}\text{SnSe}_4$ ($x=0, 0.15, 0.2$) were prepared by melting, annealing, and hot pressing in order to investigate their high temperature TE properties. Rietveld refinement and elemental analysis results confirm the composition of each specimen to be close to that of their nominal composition. Our results indicate that the local structural disorder due to the partial substitution of Cu for Zn scatters phonons effectively while introducing conducting pathways that results in the reduction of κ_L and decrease in ρ

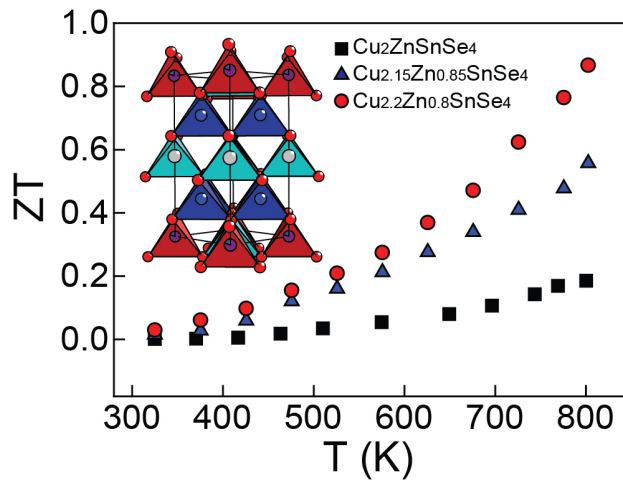


FIGURE 4. ZT vs. temperature for $\text{Cu}_{2+x}\text{Zn}_{1-x}\text{SnSe}_4$ ($0 \leq x \leq 0.2$) and crystal structure of stannite compositions $\text{Cu}_{2}\text{ZnSnSe}_4$.

simultaneously. Thus enhancement of the TE properties of these *p*-type stannites was achieved by increasing the Cu content, while the highest ZT value (0.86) was achieved from the specimens with the highest Cu content shown in Figure 4.

Figure 5 summarizes our final results for the electrical resistivity of graphene as a function of doping, temperature, and compares them with experimental data [15]. Our results reproduce well both the low- and high-temperature regimes observed in experiment [15], with theoretical data at most 30–40 % lower than

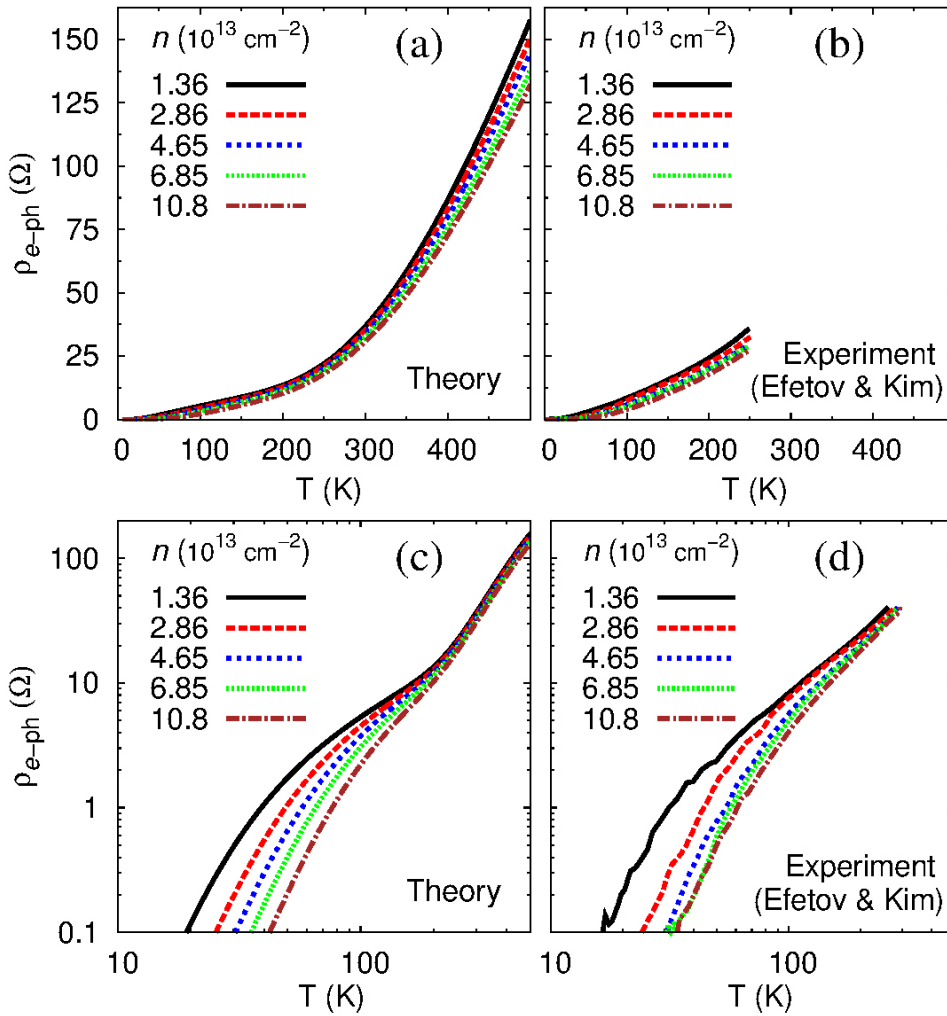


FIGURE 5. Electrical resistivity of n-doped graphene arising from electron-phonon interactions versus temperature incorporating electron-electron interaction effects [(a) and (c)] and the corresponding experimental data from Ref. [15] [(b) and (d)]. Quantities are plotted in linear scale in (a) and (b) and in logarithmic scale in (c) and (d).

measured values. Importantly, we predict a steep increase of the slope of the resistivity vs. temperature curve, as a result of the strong contribution of the optical phonon modes, at temperatures higher than those accessed in current experiments [15], suggesting the importance of higher temperature tests. Previous theoretical studies underestimated the electrical resistivity of graphene by 4–13 times. Based on our results, we can attribute these discrepancies partly to the difference in the calculated electron-phonon coupling matrix elements and partly to the incomplete inclusion of electron-electron interaction effects beyond the local density approximation. Although the velocity enhancement due to electron-electron interactions was considered, the enhancement of the electron-phonon coupling matrix elements and the renormalization of the phonon frequencies were not considered, leading to an underestimation of the resistivity. While intrinsic graphene is not an

attractive TE material, there have been ideas about its modifications using functionalization. We primarily use it to benchmark and validate our new methodology for computing electronic lifetimes before moving on to more complex materials.

The results of our calculations of the electronic transport coefficients and the figure of merit ZT for half-Heusler compound HfNiSn are summarized in Figure 6. The calculated temperature dependence of the electrical conductivity for lightly n-doped HfNiSn_{0.99}Sb_{0.01} shown in Figure 6(b) is in good agreement with the measured one for a similar composition Hf_{0.25}Zr_{0.25}NiSn_{0.99}Sb_{0.01} shown in Figure 6(a). The remaining differences between the two plots are attributed to electron scattering by dopant atoms, the mechanism which is missing in our calculations, and is prevalent at lower temperatures, where power conversion efficiency is, in any case, low. The figure of merit ZT is computed as a function

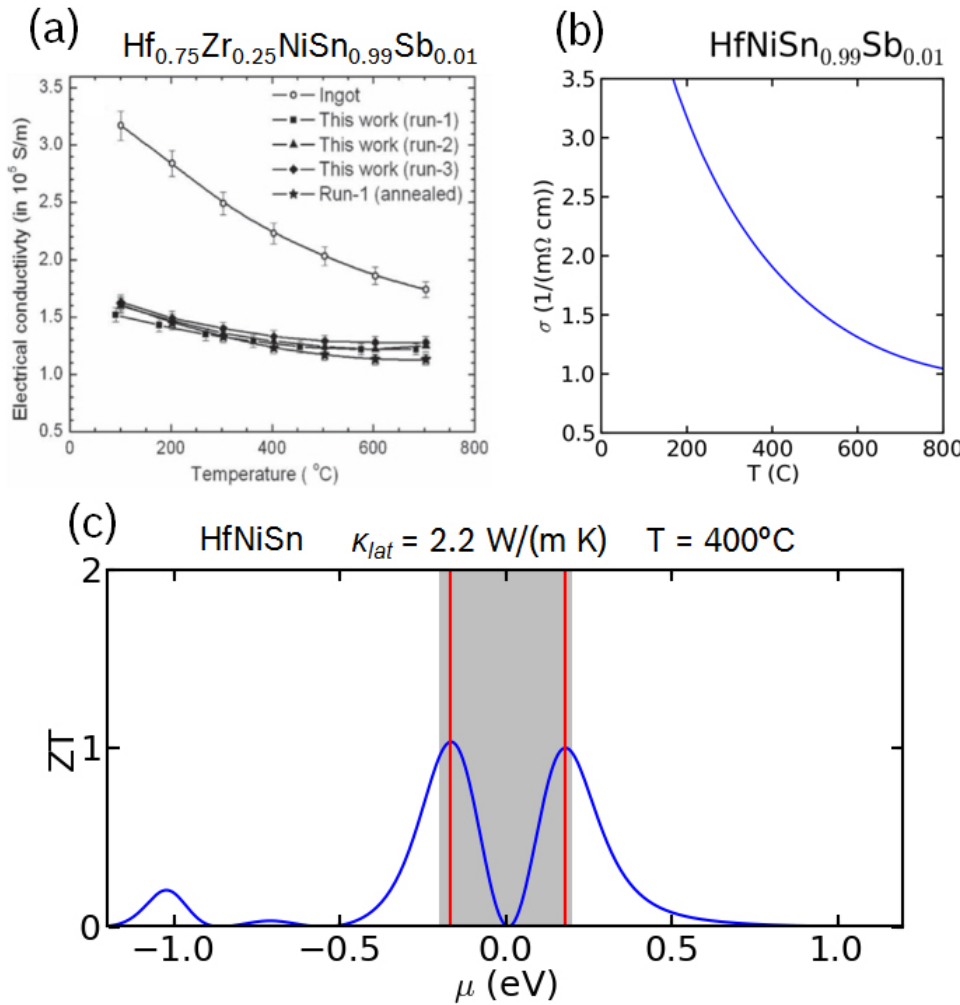


FIGURE 6. (a) The measured electrical conductivity vs. temperature for half-Heusler compound $\text{Hf}_{0.75}\text{Zr}_{0.25}\text{NiSn}_{0.99}\text{Sb}_{0.01}$ taken from Ref. [16]. (b) The calculated electrical conductivity vs. temperature for half-Heusler compound $\text{HfNiSn}_{0.99}\text{Sb}_{0.01}$. (c) The calculated figure of merit ZT vs. chemical potential μ for half-Heusler compound HfNiSn at temperature $T=400^{\circ}\text{C}$ using the experimental value for the lattice part of thermal conductivity $\kappa_{\text{lat}} = 2.2 \text{ W}/(\text{m K})$ taken from Ref. [16]. The band gap is shown in gray.

of chemical potential μ at the average operating temperature $T=400^{\circ}\text{C}$ as shown in Figure 6(c). This computation allows us to quantitatively predict the optimal doping levels, as a function of temperature, for any material. The values of μ that maximize ZT are indicated by the vertical red lines. The red line on the right side corresponds to the lightly n-doped material. The maximum $ZT=1.0$ and the corresponding doping level $x = 0.006$ electrons per unit cell are in good agreement with the experimental $ZT=0.7-0.9$ for $\text{Hf}_{0.25}\text{Zr}_{0.25}\text{NiSn}_{0.99}\text{Sb}_{0.01}$ (doping level $x=0.01$ electrons per unit cell) at $T=400^{\circ}\text{C}$ taken from Ref. [16]. This is the first time to our knowledge that fully first principles calculations of electronic properties have been performed on TE materials, going beyond constant relaxation time approximations. This complements our previous

efforts to compute lattice thermal conductivity from first principles, moving towards a fully ab-initio ZT .

CONCLUSIONS

The following achievements have been completed in FY 2013 under this project:

- We developed and characterized the performance and reliability of CNT-based TIMs bonded with reactive metal subjected to thermal cycling.
- We adapted a coarse-grained molecular simulation (developed and published in FY 2011-2012) to predict thermal transport properties of CNT and metal NW arrays.

- We developed and validated in situ thermal measurement techniques for characterization and reliability testing of TEG devices using high temperature infrared thermometry.
- We established a complete electrodeposition apparatus for template-assisted fabrication of nanostructured metal TIMs.
- We have synthesized copper NW arrays with tunable properties, including lengths from 1-60 μm , diameters of 200 nm, and volume fractions from 10-50% over large areas.
- We have designed, fabricated, and calibrated microfabricated heater/thermometer devices for thermal characterization of metal NW arrays using the three-omega method.
- The University of South Florida team has developed and produced various high-temperature TE materials such as filled variants with Fe substituted CoSb₃, skutterudites, half-Heusler, and Cu-doped stannites.
- New powerful methodology was developed to compute electron-phonon scattering effects and electronic lifetimes. These computations were integrated into Boltzmann transport theory to achieve a fully first principles prediction of electronic properties.
- The calculated electrical resistivity of doped graphene agrees well with the available experimental data. This comparison validates our computational methodology. Detailed analysis of the calculation provides useful insight into relative contributions of different phonon modes to the electrical resistivity of graphene.
- Good agreement between the calculated and measured values of the electronic transport coefficients and the figure of merit ZT for half-Heusler compounds.

REFERENCES

1. F.J. DiSalvo, *Science* **1999**, 285, 703.
2. G.S. Nolas, J.W. Sharp, H.J. Goldsmid, *Thermoelectrics: Basics Principles and New Materials Developments*; Springer-Verlag: 2001.
3. T.M. Tritt, *Ann. Rev. Mater. Res.* **2011**, 41, 433.
4. G.D. Mahan, *Solid State Phys.* **1998**, 51, 81.
5. G.S. Nolas, J. Yang, R.W. Ertenberg, *Phys. Rev. B*, **2003**, 68, 193206.
6. A. Kjeshus, D.G. Nicholson, T. Rakke, *Acta Chem. Scand.* **1973**, 27, 1315.
7. J. Navrátil, T. Plecháček, L. Beneš, Č. Drašar, F. Laufek, *J. Elec. Mater.* **2010**, 39, 1880.

8. P. Vaqueiro, G.G. Sobany, A.V. Powell, *Dalton Trans.* **2010**, 39, 1020.
9. F. Laufek, J. Navrátil, J. Plášil, T. Plecháček, Č. Drašar, *J. Alloys Compd.* **2009**, 479, 102.
10. Y. Dong, K. Wei, G.S. Nolas, *Phys. Rev. B* **2013**, 87, 195203.
11. P. Giannozzi et al. *J. Phys.: Condens. Matter* **21**, 395502 (2009).
12. J.P. Perdew and A. Zunger. *Phys. Rev. B* **23**, 5048 (1981).
13. A.A. Mostofi, J.R. Yates, Y.-S. Lee, I. Souza, D. Vanderbilt, and N. Marzari. *Comp. Phys. Commun.* **178**, 685 (2008).
14. J. Noffsinger, F. Giustino, B.D. Malone, C.-H. Park, S.G. Louie, and M.L. Cohen. *Comp. Phys. Commun.* **181**, 2140 (2010).
15. D.K. Efetov and P. Kim. *Phys. Rev. Lett.* **105**, 256805 (2010).
16. G. Joshi et al. *Adv. Energy Mater.* **1**, 643 (2011).

FY 2013 PUBLICATIONS/PRESENTATIONS

1. M.T. Barako, Y. Gao, Y. Won, A.M. Marconnet, M. Asheghi, and K.E. Goodson, “Reactive Metal Bonding of Carbon Nanotube Arrays for Thermal Interface Applications.” *Journal of Electronic Packaging*, *Submitted*.
2. M.T. Barako, W. Park, A.M. Marconnet, M. Asheghi, and K.E. Goodson, “Thermal Cycling, Mechanical Degradation, and the Effective Figure of Merit of a Thermoelectric Module,” *Journal of Electronic Materials*, vol. 42, pp. 372-381, 2013.
3. A.M. Marconnet, M.A. Panzer, and K.E. Goodson, “Thermal conduction phenomena in carbon nanotubes and related nanostructured materials,” *Reviews of Modern Physics*, vol. 85, pp. 1295-1326, 2013.
4. Y. Dong, K. Wei, G.S. Nolas, “Transport properties of partially filled skutterudite derivatives Ce_{0.13}Co₄Ge₆Se₆ and Yb_{0.14}Co₄Ge₆Se₆”, *Phys. Rev. B* **87** (2013) 195203.
5. Y. Dong, P. Puneet, T.M. Tritt, G.S. Nolas, “High temperature thermoelectric properties of p-type skutterudites Yb_xCo₃FeSb₁₂”, *Phys. Status Solidi RRL* **7** (2013) 418.
6. Y. Dong, P. Puneet, T.M. Tritt, G.S. Nolas, “Crystal structure and high temperature transport properties of Yb-filled p-type skutterudites, Yb_xCo_{2.5}Fe_{1.5}Sb₁₂”, *J. Solid State Chem.* accepted, *J. Solid State Chem.* **209**, (2014) 1.
7. Y. Dong, H. Wang, G.S. Nolas, “Synthesis and thermoelectric properties of Cu excess Cu_{2+x}Zn_{1-x}SnSe₄”, *Adv. Energy Mater.* under review.
8. Y. Dong, H. Wang, G.S. Nolas, “Synthesis, crystal structure, and high temperature transport properties of p-type Cu₂Zn_{1-x}Fe_xSnSe₄”, *Inorg. Chem.* under review.
9. G.S. Nolas, Y. Dong, K. Wei, P. Puneet, T.M. Tritt, J. Martin, “Synthesis and optimization of the thermoelectric properties of p-type skutterudites”, INVITED, the 10th Pacific Rim Conference on Ceramic and Glass Technology, San Diego, CA, USA, June 2, 2013.

- 10.** G.S. Nolas, Y. Dong, M. Barako, M. Asheghi, K.E. Goodson, G. Samsonidze, B. Kosinsky, “Thermoelectric research for automobile application: An experimental and computational approach to materials and interfaces”, INVITED, the European Materials Research Society Conference, Strasbourg, France, May 28, 2013.
- 11.** W. Hill, Y. Dong, G.S. Nolas, “Skutterudite $\text{YbCo}_4\text{Ge}_{6+x}\text{Se}_{6-x}$ ($x = 0.2, 0.4, 0.6, 0.8, 1.0$) for thermoelectric materials”, American Physical Society, Baltimore, Maryland, USA, March 18, 2013.
- 12.** Cheol-Hwan Park, Nicola Bonini, Thibault Sohier, Georgy Samsonidze, Boris Kozinsky, Matteo Calandra, Francesco Mauri, and Nicola Marzari. “Electron-phonon interactions and the intrinsic electrical resistivity of graphene.” Nano Lett. (submitted).
- 13.** “Path to predictive computations of thermoelectric effects: thermal and electronic transport”, TMS conference 2013, San Antonio TX, Symposium: Computational Modeling and Simulation of Advanced Materials for Energy Applications

V.8 NSF/DOE Thermoelectrics Partnership: Integrated Design and Manufacturing of Cost-Effective and Industrial-Scalable TEG for Vehicle Applications

Lei Zuo (Primary Contact), Jon Longin,
Sanjay Sampath, Qiang Li
Stony Brook University
Heavy Engineering Room 212
Stony Brook, NY 11794

DOE Technology Development Manager:
Gurpreet Singh

Overall Objectives

- Development of a scalable high-throughput, non-equilibrium synthesis process for high figure of merit (ZT) thermoelectric (TE) materials from abundant low-cost feedstock by using thermal spray technology.
- Development of an integrated manufacturing process to fabricate TE structures directly onto exhaust pipe components with enhanced performance, durability.

Fiscal Year (FY) 2013 Objectives

- Synthesis TE material magnesium silicide and optimize its ZT in terms of different thermal spray conditions.
- Investigate the phase composition and microstructure influence on thermal-sprayed magnesium silicide including thermal, electrical and Seebeck coefficient.
- Study the feasibility of preparing filled skutterudite TE material using thermal spray.
- Demonstrate the feasibility of fabrication of TE structure using thermal spray technology including insulation, conducting, and TE functional layers.

FY 2013 Accomplishments

- Vacuum plasma spray (VPS) has been successfully used to synthesize magnesium silicide by thick coatings and the maximum ZT achieved 30% by the traditional hot-press method using the same feedstock powder.
- VPS provides denser coating due to its high velocity and Hall Effect measurement showed carrier concentration and mobility enhanced the ZT of magnesium silicide coating for VPS compared with atmospheric plasma spray.

- High velocity atmospheric plasma spray for filled skutterudites as quench powder has been successfully deposited on an Al substrate without obvious oxidation or evaporation.
- TE functional layer as well as insulation and conducting layer have been thermal sprayed for TE device fabrication.

Future Directions

- Evaluate the TE properties of doped magnesium silicide using thermal spray.
- Anneal thermal sprayed as-quenched powder to get filled skutterudite phase.
- Try cold spray for filled skutterudite powder for better TE properties.
- Conduct a series of experiments on thermal spray conditions to optimize the electrical conduction while suppressing heat conduction.
- Fabricate a complete TE working device and test its efficiency.



INTRODUCTION

As a solid-state energy conversion device, thermoelectric generators (TEGs) have many benefits for converting automobile engine exhaust to electrical power. Recent research supported by the U.S. Department of Energy indicated that 350-390 watts of electricity recovery can increase fuel efficiency by 3% for a mid-size truck and 4% for a sedan [1]. Extensive interest and research over the past decade continues to explore new potential TE materials. Among these, Mg₂Si is of particular interest in applications for the recovery of automobile exhaust heat [2,3], since it has reasonable ZT in the exhaust temperature range and is abundant on earth, thus making it much less expensive than traditional TE materials such as bismuth telluride.

In this work, the properties for Mg₂Si deposited using thermal spray are reported. Thermal spray is a cost-effective, flexible and industry-scalable manufacturing process that has been widely used in the aerospace and automotive industries. In the past decade Sampath et al. [4] extended this technique to synthesize functional electronics and sensor materials.

Like melt spinning [5], thermal spray also has a very high quenching rate (10^6 – 10^7 K/sec). The use of thermal spray to fabricate integrated TE devices on automotive exhaust systems was proposed by Zuo et al. [6,7].

APPROACH

By investing the parameters that are used in thermal spray, each condition (for example, temperature, velocity, powder size, offset distance) can be optimized to give the best ZT. More importantly, understanding how phase, microstructure and carrier concentration are inter-connected with thermal, electrical and Seebeck coefficient will allow proper control of the whole ZT. Carrier mobility should also be measured to compare the thermal spray method with traditional hot press.

Demonstration of a three-dimensional prototype has been carried out in stages. First, the bonding between insulation, conducting and TE function layer was achieved. Then the mask was used for patterning alternating p and n typed of TE material. Lastly, the bridging between conducting layer has been fulfilled by using a sacrificial layer for supporting.

RESULTS

TE properties including thermal conductivity, electrical conductivity and Seebeck coefficient were characterized and compared between VPS and hot press samples. Figure 1 shows the thermal conductivity of Mg_2Si prepared by VPS and hot press. The thermal conductivity is measured from 300–700 K in a nitrogen environment. Thermal-sprayed samples V1 (18 kW, nominal ratio powder), V2 (18 kW, Mg 5% rich powder) and V3 (21 kW, nominal ratio powder) have a thermal

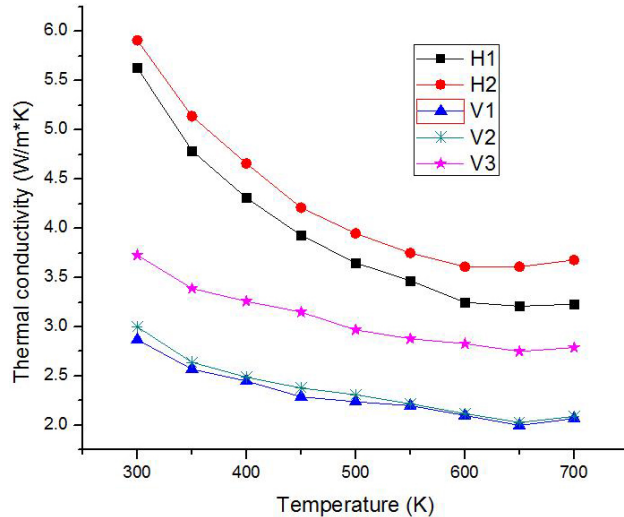


FIGURE 1. Thermal Conductivity of Mg_2Si and Hot Press

conductivity at least 40% lower than the hot-press samples H1 (nominal ratio powder) and H2 (Mg 5% rich powder). This is likely due to the large numbers of pores and cracks in the sample that enhance phonon scattering. Electrons also contribute to the thermal conductivity. The lower thermal conductivity of samples V1 and V2, both of which were sprayed at the lower power (18 kW), is likely due to the reduced electron concentration, as measured from the Hall measurements discussed in the following.

Electrical conductivity measurements were also made at 300–700 K. The measured electrical conductivity for both VPS and hot-press samples are shown in Figure 2. As can be seen, the variation in electrical conductivity is significant in the samples. Among the VPS samples, V2, which was made from the Mg-rich powder, has a slightly higher conductivity than V1 with nominal ratio powder, because the carrier concentration is higher, and this can be seen from Hall Effect measurements. For the hot-press samples, H2 has higher conductivity than H1, which is again likely due to the additional Mg present in the raw powder. In order to understand the mechanisms and key parameters that affect electrical conductivity, Hall Effect measurements at room temperature were made, with the results shown in Table 1.

Figure 3 shows the measured Seebeck coefficient for the VPS and hot-press samples. Seebeck coefficient was found to be comparable to those of the single-crystal samples, which shows that the Seebeck coefficient is relatively insensitive to microstructure. However, the Seebeck coefficient is very sensitive to carrier concentration and is inversely proportional to electrical conductivity due to the opposite dependence of carrier concentration. For the hot-press samples, the Mg-rich

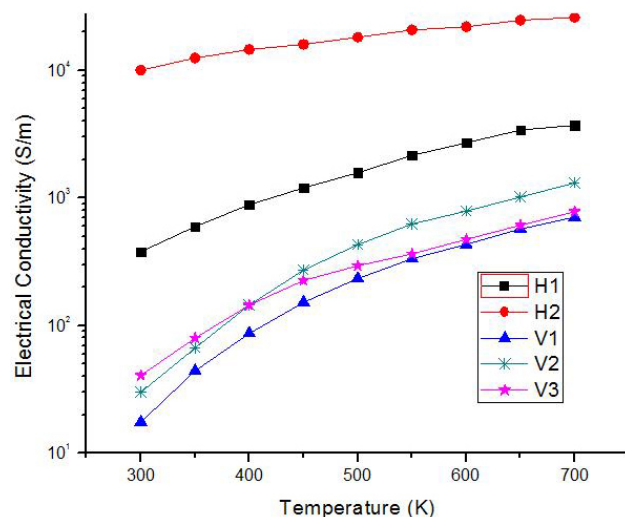
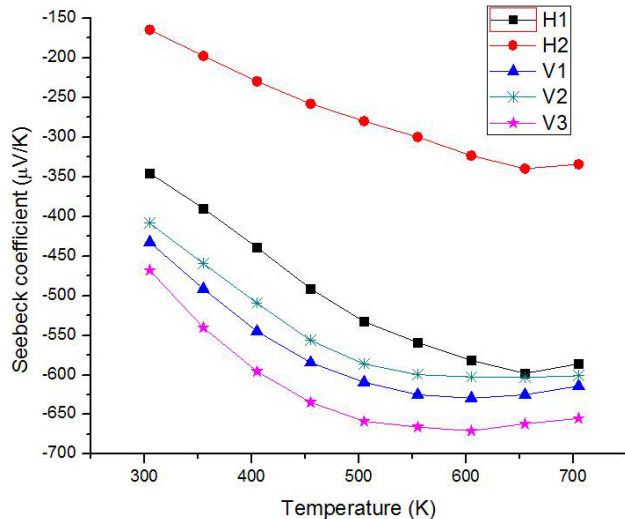


FIGURE 2. Electrical Conductivity of Mg_2Si by VPS and Hot Press

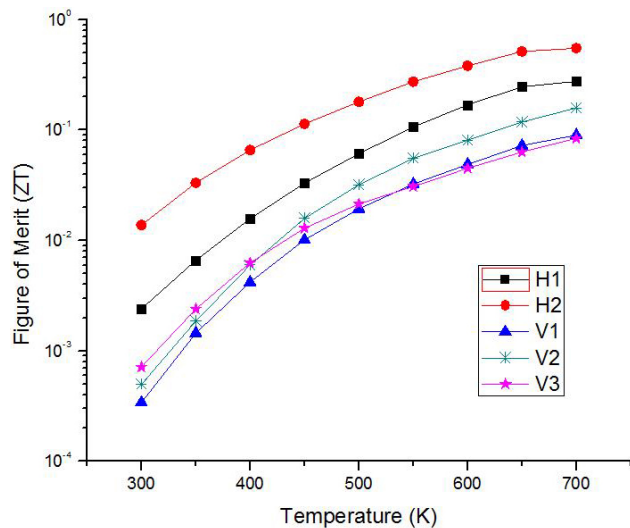
TABLE 1. Hall Effect Measurements of Hot Press and VPS Samples

| Sample | n ($10^{17}/\text{cm}^3$) | μ ($\text{cm}^2/\text{V}\cdot\text{s}$) | $\sigma = ne\mu$ (S/m) |
|--------|-------------------------------|---|-----------------------------------|
| H1 | 22.6 | 13.31 | 481 |
| H2 | 258 | 26.72 | 11,040 |
| V1 | 8.24 | 1.31 | 17.3 |
| V2 | 10.5 | 1.74 | 29.3 |
| V3 | 7.94 | 3.14 | 40 |
| Tani | 4.3 | 204 | 1,404 |

**FIGURE 3.** Seebeck of Mg_2Si by VPS and Hot Press

sample H2 had a lower Seebeck coefficient because of its larger carrier concentration. The hot-press samples had carrier concentrations larger than all of VPS samples V1, V2 and V3, resulting in a lower Seebeck coefficient, compared to the VPS samples.

Figure 4 shows ZT for the VPS and hot-press samples. Overall, the VPS samples have a lower ZT than the hot-press samples because of low carrier mobility, even though the VPS samples have a much lower thermal conductivity. VPS for sample V2 at 18 kW with Mg-rich powder has a higher ZT as compared with the Mg nominal sample V1. Even though V1 has a slightly higher Seebeck coefficient than V2, the electrical conductivity of V1 is nearly half that of V2. Also, the thermal conductivity of V2 is similar to the thermal conductivity of V1, which results in a higher ZT for V2. For sample V3, with Mg nominal ratio powder, and 21 kW, ZT is slightly higher than that of 18 kW sample (V1) at room temperature and nearly the same up to 700 K. For the hot-press samples, the nominal-ratio-powder sample H1 has a lower ZT than the Mg-rich sample H2. H2 has much higher electrical conductivity than H1, and, noting that the Seebeck and thermal conductivity between them does not differ significantly, H2 thus has a higher ZT

**FIGURE 4.** ZT of Mg_2Si by VPS Reached 30% of by Hot Press with Same Powder

than H1. VPS samples with Mg-rich powder at 18 kW has highest ZT at higher temperature, and should be able to be further increased by proper doping.

Figure 5 shows the three-dimensional fabrication of a functional TE device. The n, p type material has been deposited using thermal spray with self-designed masks. The bonding between insulation, conducting and TE functional layer is good and the bridging of the top electrical conducting strip was facilitated using sacrificial material shown at the bottom in the figure. To evaluate techniques for the gap-bridging required to deposit the top conducting layer, a 50 mm x 50 mm x 12 mm aluminum block was machined with grooves of different widths to simulate the TE elements. A mixture of fine white sand and water-soluble polyvinyl alcohol (PVA) was squeegeed into the grooves and allowed to dry overnight. Next a 0.7 mm top conducting NiCr layer was sprayed over the elements and the filled gaps. After the top layer was applied, the sacrificial sand/PVA material was removed by placing the sample in an oven at 400°C for 20 minutes. This burns out the PVA and loosens the sand, which is then removed from the grooves.

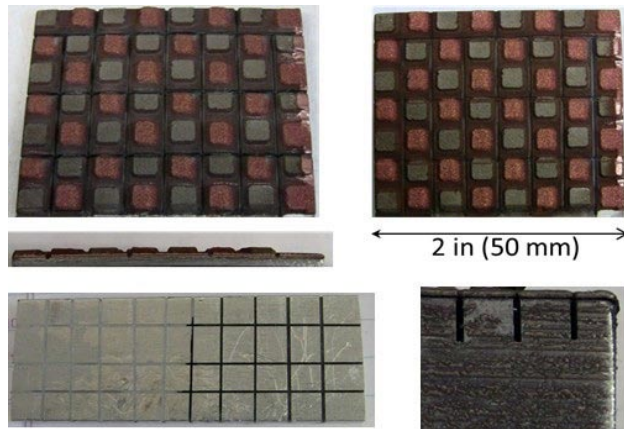


FIGURE 5. TEG Prototype Fabricated Using Thermal Spray

CONCLUSIONS

- Industrial scalable thermal spray method achieved 30% ZT compared with hot press using the same feedstock powder.
- VPS with the proper power Mg-rich powder optimized carrier concentration and increased carrier mobility.
- TE functional layers as well as insulation and conducting layers have been thermal sprayed for TE device fabrication.

REFERENCES

- Patel, P. *Powering Your Car with Waste Heat*. MIT Technology Review, 2011.
- Morris, R.G., R.D. Redin, and G.C. Danielson, *Semiconducting Properties of Mg₂Si Single Crystals*. Physical Review, 1958. **109**(6): p. 1909-1915.
- Labotz, R.J., D.R. Mason, and D.F. Okane, *The Thermoelectric Properties of Mixed Crystals of Mg₂Ge_xSi_{1-x}*. Journal of the Electrochemical Society, 1963. **110**(2): p. 127-134.
- Sampath, S., *Thermal Spray Applications in Electronics and Sensors: Past, Present, and Future*. Journal of Thermal Spray Technology, 2010. **19**(5): p. 921-949.
- Li, Q., Z.W. Lin, and J. Zhou, *Thermoelectric Materials with Potential High Power Factors for Electricity Generation*. Journal of Electronic Materials, 2009. **38**(7): p. 1268-1272.
- L. Zuo, J.L., S. Sampath, B. Li, Q. Li, *Integrated Design and Manufacturing of Cost-Effective and Industrial-Scalable TEG for Vehicle Applications*, in *DOE Thermoelectrics Workshop 2011*.
- J.P. Longtin, L.Z., D. Hwang, G. Fu, M. Tewolde, Y. Chen, S. Sampath, *Fabrication of Thermoelectric Devices Using Thermal Spray: Application to Vehicle Exhaust Systems to Improve Fuel Economy*. JTST, 2012.

FY 2013 PUBLICATIONS/PRESENTATIONS

- G. Fu, L. Zuo, J. Longtin, C. Nie, R. Gambino "Thermoelectric Properties of Magnesium Silicide Fabricated using Vacuum Plasma Thermal Spray", Journal of Applied Physics, (Vol.114, Issue 14) 144905, 2013.
- J. Longtin, L. Zuo, D. Hwang, G. Fu, M. Tewolde, Y. Chen and S. Sampath, Fabrication of Thermoelectric Devices Using Thermal Spray: Application to Vehicle Exhaust Systems, Journal of Thermal Spray Technology, Volume 22, Issue 5, pp 577-587, 2013.
- G. Fu, L. Zuo, J. Longtin, C. Nie, Y. Chen, M. Tewolde and S. Sampath, Thermoelectric Properties of Magnesium Silicide Deposited using Atmospheric Plasma Thermal Spray, accepted by the *Journal of Electronic Materials*.
- G. Fu, L. Zuo, J. Longtin, Y. Chen and S. Sampath, Progress on Searching Optimal Thermal Spray Parameters for Magnesium Silicide, accepted by *Material Research Society*, Vol 1490, 2013.

V.9 NSF/DOE Thermoelectrics Partnership: Inorganic-Organic Hybrid Thermoelectrics

Sreeram Vaddiraju

Department of Chemical Engineering
237 Jack E. Brown Bldg.
3122 TAMU
Texas A&M University
College Station, TX 77843

NSF Manager: Sumanta Acharya

DOE Technology Development Manager:
Gurpreet Singh

NETL Project Manager: Carl Maronde

- Deducing the microstructural composition-thermoelectric performance relationship in semiconductor nanowire-metal nanoparticle composites.

FY 2013 Accomplishments

- Fabricated bulk thermoelectric devices from mass-produced Zn_3P_2 and ZnO nanowire powders. Deduced that consolidation of the nanowires into highly dense pellets ($>98\%$ densities), without altering the morphologies of the nanowires, requires that the nanowires be mechanically flexible in nature. Established collaboration with Prof. Reza Yassar's group at Michigan Technological University to determine the effect of diameter on the mechanical behavior of Zn_3P_2 nanowires. Through this collaboration, it was deduced that nanowires with diameters less than 50 nm are highly flexible in nature, unlike thicker nanowires that are brittle by nature.
- Deduced that the thermoelectric performance of highly dense Zn_3P_2 nanowire pellets is very low. This was primarily attributed to their low electrical conductivities. To overcome this limitation, copper nanoparticles were added to Zn_3P_2 nanowires and the mixtures were pressed into dense pellets for the determination of their thermoelectric performance. These experiments indicated that composition at microscale plays a crucial role in their ultimate thermoelectric performance. Pellets composed of unfunctionalized Zn_3P_2 nanowires and copper nanoparticles were observed to be non-uniform in composition at microscale. These composites exhibited figure of merit (zT) values as high as 0.23 @ 770 K. Interface-engineered composites that are uniform in composition were obtained when 1,4-benzenedithiol (BDT) functionalized nanowires mixed with copper nanoparticles were pressed into pellets. These pellets exhibited low thermoelectric performance.
- Extended the nanowire composite fabrication strategy to obtain degenerately doped zinc oxide nanowire pellets. This method resulted in the lowest thermal conductivity reported for zinc oxide due to alloy scattering in conjunction with boundary scattering at the nanowire interfaces. A zT value of 0.65 was achieved in these pellets. This value is higher than that previously reported in the literature.

Overall Objectives

- Synthesis of inorganic nanowires and quantum wires of both $CoSb_3$ and $InSb$, and organic conducting polymer thin films, and assembling them into inorganic-organic hybrid thermoelectrics cells with sizes ranging from a few mm^2 to a few cm^2 , using conjugated linker molecules to tether the nanowires to each other or to conducting polymer thin films.
- Systematically studying the effect of inorganic nanowire size and organic conducting polymer thin film chemistry and thickness on their individual thermoelectric performance, and also on their performance when used in unison as 'molecular wired' inorganic-organic hybrids, in the temperature range of 300-1,100 K.
- Determine the type of the metal required for assembling individual thermoelectric devices into thermoelectric modules without lowering their performance, i.e., finding metals that have very low contact resistance with individual thermoelectric cells.

Fiscal Year (FY) 2013 Objectives

- Evaluation of the thermoelectric performance of highly dense nanowire pellets and nanowire-conjugated linker molecule hybrid pellets.
- Evaluation of the thermoelectric performance of highly dense semiconductor nanowire-metal nanoparticle composite pellets fabricated using both unfunctionalized and organic molecule functionalized nanowires.

- In addition, a phase transformation route was developed for converting single-crystalline silicon nanowires into polycrystalline/single-crystalline metal silicide nanowires. As silicon nanowire synthesis is currently a mature technology, this strategy is expected to lead to the mass production of metal silicide nanowires, which are highly useful for thermoelectric device fabrication.

Future Directions

Thermoelectric performance evaluation of Zn_4Sb_3 nanowire pellets and Zn_4Sb_3 nanowire-copper nanoparticle composite pellets. Deduction of the microstructural composition-thermoelectric performance relationships in both BDT functionalized Zn_4Sb_3 nanowire-copper nanoparticle composite and unfunctionalized Zn_4Sb_3 nanowire-copper nanoparticle composite. This system is expected to provide additional evidence that compositional disorder is useful for enhancing the efficiencies of thermoelectrics.



INTRODUCTION

The operational anatomy of a typical automobile engine shows that approximately 40% of the heat generated by gasoline combustion is lost through the exhaust gases [1]. Solid-state thermoelectric modules could convert this heat into electricity in a clean manner and increase the overall fuel efficiency.

The performance of thermoelectrics depends on a dimensionless number called zT , which is related to the Seebeck coefficient (s), electrical conductivity (σ), the thermal conductivity (κ) and the absolute temperature (T) according to the following relationship: $zT = s^2\sigma T/\kappa$ [2.3]. Therefore, the fabrication of highly efficient thermoelectrics requires a material that is a good electrical conductor, but a poor thermal conductor. Materials in nanostructured format are ideal for accomplishing this task [4]. In this context, the primary objective of this project is the development of simple strategies for the bulk synthesis, assembly, and thermoelectric performance evaluation of thin nanowires of two materials systems, Zn_3P_2 and ZnO .

APPROACH

All the nanowire synthesis experiments were performed using a typical hot-walled chemical vapor deposition chamber (CVD). For the synthesis of Zn_3P_2 nanowires, vapor transport of phosphorus (using red phosphorus in the presence of hydrogen as a source) onto coiled zinc foils was employed. The synthesis of

ZnO nanowires was accomplished using an atmospheric plasma jet in collaboration with Prof. Mahendra Sunkara at the University of Louisville. For the measurement of the thermoelectric performance of nanowires, the nanowire powders were pressed in a uniaxial hot-press at a temperature of 650°C and a pressure of 120 MPa for duration of 1 hour. After polishing the cylindrical nanowires pellets obtained had diameters of 12 mm and thickness of 2 mm. The density of the pellets (ρ) was confirmed to be greater than 98% of the theoretical density by both geometrical measurements and Archimedes principle. Seebeck coefficient was measured using the analogue subtraction method [5], while the electrical and thermal conductivities were measured, respectively, using the 4-point probe method and a combination of differential scanning calorimetry and the laser flash methods.

RESULTS

Zn_3P_2 Nanowires Production, their In Situ Functionalization and Diameter Reduction

The synthesis, in situ functionalization and diameter reduction of compound semiconductor nanowires was studied using Zn_3P_2 system as an example. These experiments indicated that gram quantities of nanowires can be produced by direct reaction of the component elements, as in Zn and P for Zn_3P_2 nanowires powder synthesis. In the interest of brevity, these results were not discussed in detail here. All the details pertaining to this work could be found in Brockway et al., [6]. Details of the experimental procedure and the mechanism underlying the decomposition of nanowires for uniformly reducing their diameter could be found in Brockway *et al.*, [7].

Thermoelectric Performance of Zn_3P_2 Nanowire Pellets

The measurement of the thermoelectric performance of Zn_3P_2 nanowires required pressing them into highly dense pellets. Monte Carlo simulations indicate that this is not possible if the nanowires are brittle in nature as they break into multiple pieces along their lengths during the consolidation process. It is however possible when the nanowires are flexible in nature. Mechanical testing of the nanowires performed in situ in a transmission electron microscope (TEM) indicated that Zn_3P_2 nanowires are flexible in nature, provided that their diameter is below 50 nm (Figure 1). The bending of the nanowires allowed them to maintain their morphology and still stay assembled as high density pellets. A high Seebeck coefficient of 260 $\mu V/K$ was observed in these pellets at a temperature of 510 K in the undoped non-degenerate samples (Figure 2a). In contrast, BDT functionalized Zn_3P_2 nanowire pellets exhibited a high

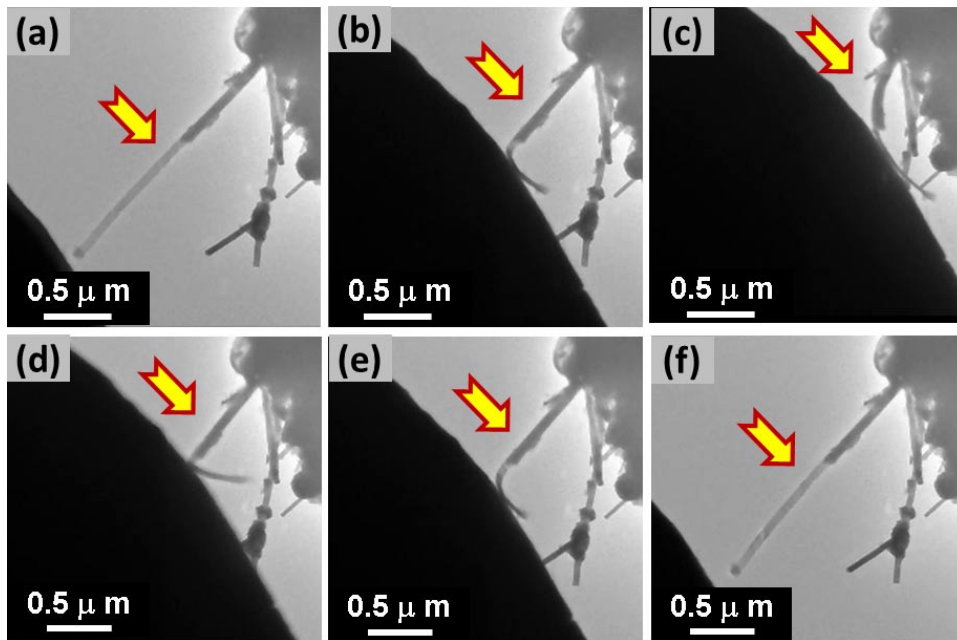


FIGURE 1. (a) to (c) TEM images of nanowire under various stages of compression. In the images, the nanowire is fixed to the grid (shown on the right side of the images), while an atomic force microscopy tip (shown at the bottom left) moves to the right to compress the nanowire. (d) to (f) TEM images of the nanowire under decompression. The nanowire reverts back to its original shape without breaking under stress. This elastic nature of the nanowires allowed for their consolidation into highly dense pellets.

Seebeck coefficient of $500 \mu\text{V/K}$ at 510 K (Figure 2a). The electrical conductivity of BDT functionalized Zn_3P_2 nanowires was also observed to be higher than that observed in unfunctionalized Zn_3P_2 nanowires (Figure 2b). The data is inconsistent with that predicted by single parabolic band model theory in that when the Seebeck coefficient increases, the electrical resistivity also increases. This result can be explained by considering that the interfaces are different in the samples. Low energy carrier filtering at the nanowire interfaces in the BDT functionalized nanowires is believed to be responsible for their enhanced Seebeck coefficients. The absence of insulating $\text{Zn}_3(\text{PO}_4)_2$ at the interfaces in the BDT functionalized nanowires, coupled with their single-crystalline nature, also explains their higher electrical conductivity. A manuscript describing these results and titled “Thermoelectric properties of Bulk Assembled Unfunctionalized and Functionalized Zn_3P_2 nanowire Powders” is currently under review for publication in the Journal *Nanotechnology*. This manuscript also describes the low thermal conductivity of the Zn_3P_2 nanowire pellet, ranging from 0.85 to $1.5 \text{ W m}^{-1}\text{K}^{-1}$ (Figure 2c). The thermal conductivity values obtained are smaller than those previously reported. Previous report by Nagamoto *et al.* [8] indicated the thermal conductivity of Zn_3P_2 is $1.5 \text{ W m}^{-1}\text{K}^{-1}$ at its lowest, higher than that obtained in pressed Zn_3P_2 nanowire pellets. This 30% decrease in thermal conductivity is expected to be due to the

enhanced scattering of phonons in nanowire form of Zn_3P_2 .

To overcome the low electrical conductivities of Zn_3P_2 pellets, mixtures of copper nanoparticles and Zn_3P_2 nanowires were pressed into pellets and their composites were tested for their thermoelectric performance. These studies indicated that compositional disorder (Figure 3a) found in pellets composed of unfunctionalized Zn_3P_2 nanowires greatly enhances their thermoelectric performance (Figure 4). A zT of 0.23 at 770 K was obtained in these composites. Compositional disorder enhanced the electrical conductivities of the pellets without significantly enhancing their thermal conductivities. Compositionally uniform composites were obtained when pellets composed of copper nanoparticles and BDT functionalized Zn_3P_2 nanowire were fabricated (Figure 3b). These pellets did not indicate any enhanced thermoelectric performance (Figure 4).

Thermoelectric Performance of Dually-Doped Zno Nanowires

ZnO nanowires used as a starting material for this study were synthesized using a microwave plasma jet reactor [9]. These nanowires were mixed with Al_2O_3 and Ga_2O_3 nanoparticles in various ratios in a high-energy ball mill for 15 minutes. The ceramic powders were then placed into a graphite die and consolidated using

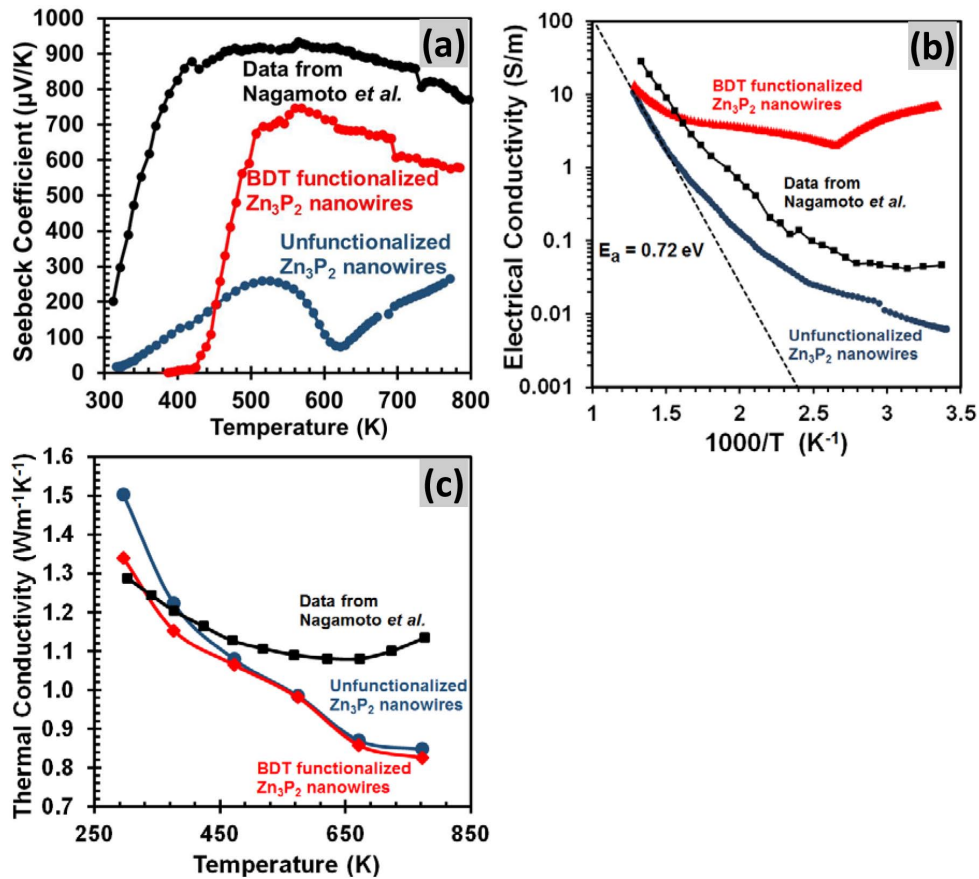


FIGURE 2. Plots showing the variation of (a) Seebeck coefficients, (b) electrical conductivities, and (c) thermal conductivities of both a functionalized and unfunctionalized Zn_3P_2 nanowire pellet with temperature. For comparison, thermoelectric properties of Zn_3P_2 microparticles previously reported by Nagamoto *et al.* are also included.

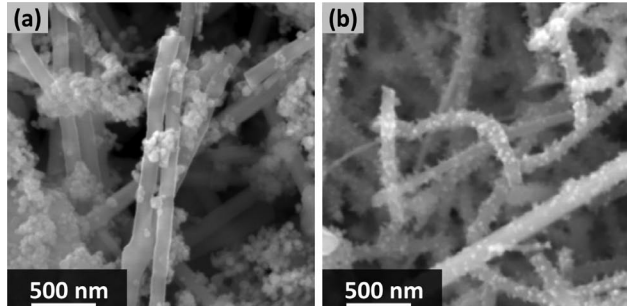


FIGURE 3. (a) Scanning electron micrograph of mixtures of unfunctionalized Zn_3P_2 nanowires and copper nanoparticles. Here, nanowires and nanoparticles remained as individual units. (b) Scanning electron micrograph of copper nanoparticle decorated Zn_3P_2 nanowires obtained by mixing BDT functionalized Zn_3P_2 nanowires and copper nanoparticles.

spark plasma sintering at 1,200 °C and 100 MPa for the determination of their thermoelectric performance. The consolidated resulted in $\text{Zn}_{1-x-y}\text{Al}_x\text{Ga}_y\text{O}$ ceramics. The

chemical composition of the ultimate ceramic pellets was varied by varying the ratios of various oxides employed in the preparation of the mixtures prior to consolidation.

The Seebeck coefficients, electrical resistivities and the thermal conductivities of various oxide samples are depicted in Figure 5. The variation of the carrier mobilities, carrier concentrations and zT values with temperature of the samples are presented in Figure 6. All samples have a Seebeck coefficient that is inversely proportional to their carrier concentration and follow normal band-behavior except $\text{Zn}_{98}\text{Al}_2\text{GaO}_{100}$ which seemingly violates the classical band transport theory (Figure 5a). Modeling work is currently underway to explain this phenomenon. Additionally, boundary scattering at the nanowire interfaces, coupled with phonon scattering at the boundaries of the spinel phases formed, led to a reduction in the thermal conductivities of the samples. Consequently, this strategy for making ZnO alloy nanostructured thermoelectrics results in the lowest thermal conductivity reported to date for ZnO -based systems. Overall, oxide sample with $\text{Zn}_{97}\text{Al}_2\text{GaO}_{100}$

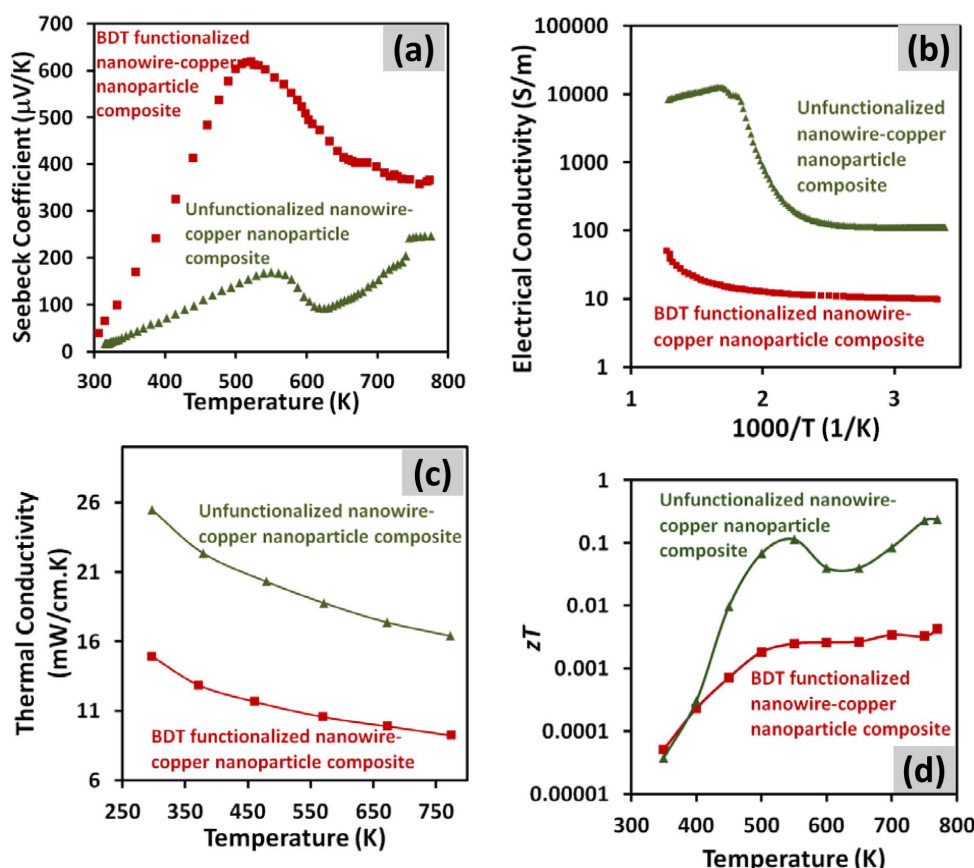


FIGURE 4. Plots showing the variation of (a) Seebeck coefficients, (b) electrical conductivities, (c) thermal conductivities, and (d) zT values of both BDT functionalized Zn_3P_2 nanowire-copper nanoparticle composite and unfunctionalized Zn_3P_2 nanowire-copper nanoparticle composite with temperature.

composition exhibited the maximum thermoelectric performance of the samples studied. This sample exhibited a peak zT of 0.65 at 1,273 K. Although oxide materials are still behind the state of the art in terms of thermoelectric performance, they can be synthesized into modules at a much lower cost per watt. Consequently, further research should be done to improve the zT to 1 to enable oxide thermoelectrics to be used for terrestrial applications. A manuscript describing these results is currently being prepared. It is anticipated that this manuscript will be submitted for publication in the next few weeks.

REFERENCES

- Yang, J.H.; Stabler, F.R., Automotive Applications of Thermoelectric Materials. *Journal of Electronic Materials* **2009**, *38*, 1245-1251.
- Snyder, G.J.; Toberer, E.S., Complex thermoelectric materials. *Nature Materials* **2008**, *7*, 105-114.
- Chen, G.; Shakouri, A., Heat transfer in nanostructures for solid-state energy conversion. *Journal of Heat Transfer-Transactions of the Asme* **2002**, *124*, 242-252.
- Chen, G.; Dames, C., Thermal Conductivity of Nanostructured Thermoelectric Materials. In *Thermoelectrics Handbook*, CRC Press 2005.
- Sumanasekera, G.U.; Grigorian, L.; Eklund, P.C., Low-temperature thermoelectrical power measurements using analogue subtraction. *Measurement Science & Technology* **2000**, *11*, 273-277.
- Brockway *et al.*, *Phys. Chem. Chem. Phys.*, 2013, *15*, 6260-6267.
- Brockway *et al.*, *Crystal Growth & Design*, **2013**, *11*, 4559-4564.
- Nagamoto, Y.; Hino, K.; Yoshitake, H.; Koyanagi, T.; Ieee, I., *Thermoelectric properties of alpha-Zn₃P₂*. IEEE: New York, 1998; p 354-357.
- Kumar, V.; Kim, J.H.; Pendyala, C.; Chernomordik, B.; Sunkara, M. K., Gas-Phase, Bulk Production of Metal Oxide Nanowires and Nanoparticles Using a Microwave Plasma Jet Reactor. *The Journal of Physical Chemistry C* **2008**, *112*, 17750-17754.

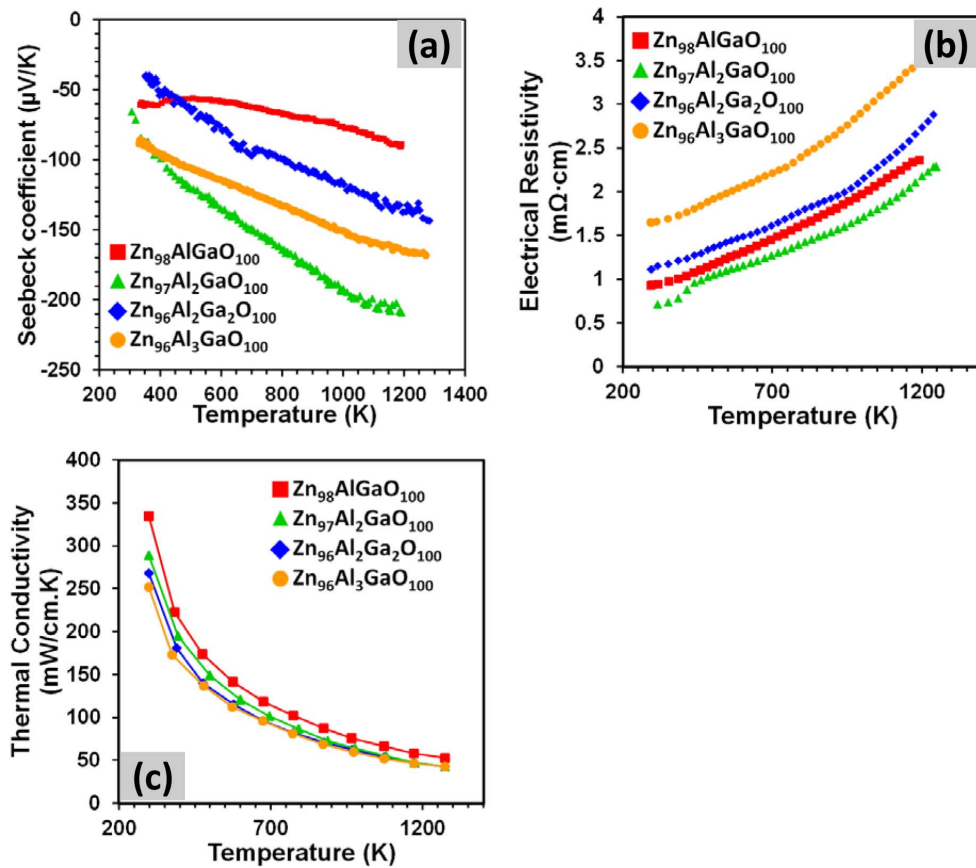


FIGURE 5. Plots showing the variation of (a) Seebeck coefficients, (b) electrical resistivities, and (c) thermal conductivities of dually-doped ZnO nanowire-bulk pellets of various compositions with temperature.

FY 2013 PUBLICATIONS/PRESENTATIONS

- Brockway, L.; Van Laer, M.; Kang, Y.; Vaddiraju, S. (2013) Large-scale synthesis and in situ functionalization of Zn_3P_2 and Zn_4Sb_3 nanowire powders. *Physical Chemistry Chemical Physics*, 15(17), 6260-7.
- Kang, Y.; Brockway, L.; Vaddiraju, S. (2013) A simple phase transformation strategy for converting silicon nanowires into metal silicide nanowires: Magnesium silicide. *Materials Letters*, 100, 106-110.
- Brockway, L.; Vasiraju, V.; Asayesh-Ardakani, H.; Shahbazian-Yassar, R.; Vaddiraju, S. (2013) Thermoelectric Properties of Bulk Zn_3P_2 Nanowire Assemblies, Manuscript under review, *Nanotechnology*.
- Brockway, L.; Vasiraju, V.; Vaddiraju, S. (2013) Compositional Disorder and its Effect on the Thermoelectric Performance of Zn_3P_2 Nanowire-Copper Nanoparticle Composites, Manuscript under review, *Nanotechnology*.

5. Vaddiraju, S.; Brockway, L.; Vasiraju, V., ‘Thermoelectric Properties of Bulk Pellets of Unfunctionalized and Functionalized Zn_3P_2 Nanowires’, Annual meeting of the American Institute of Chemical Engineers (AIChE), San Francisco, November 3-8, 2013.

6. Vaddiraju, S., Kang, Y., Brockway, L., ‘Phase Transformation of Silicon Nanowires As a Route for the Mass Production of Mg_2Si Nanowires’, Annual meeting of the American Institute of Chemical Engineers (AIChE), San Francisco, November 3-8, 2013.

SPECIAL RECOGNITIONS & AWARDS/ PATENTS ISSUED

- S. Vaddiraju, L. Brockway, M. Van Laer, Y. Kang, “Synthesis of Inorganic Nanowires and Organic Hybrids Thereof for Electronic Elements and Devices”, US Patent Application #61/800,384, 2013.

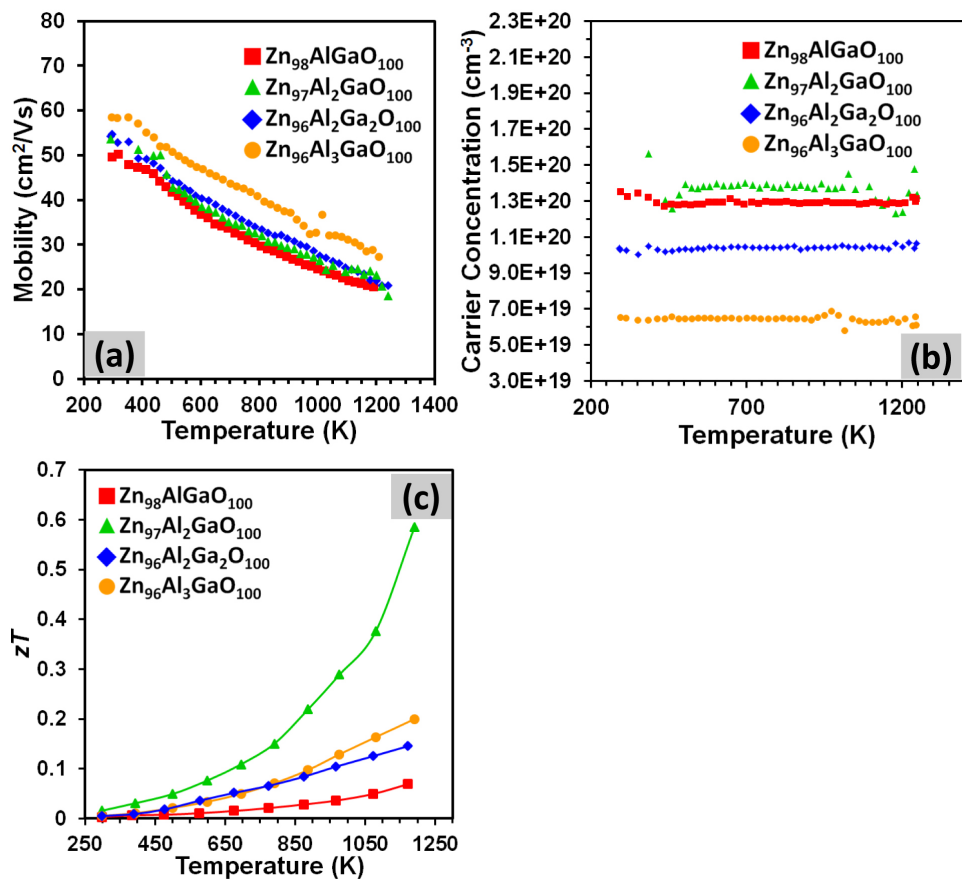


FIGURE 6. Plots showing the variation of (a) mobilities, (b) carrier concentrations, and (c) zT values of dually-doped ZnO nanowire-bulk pellets of various compositions with temperature.

V.10 Integration of Advanced Materials, Interfaces, and Heat Transfer Augmentation Methods for Affordable and Durable Thermoelectric Devices

Y. Sungtaek Ju (Primary Contact) and
Bruce Dunn
UCLA
420 Westwood Plaza
Los Angeles, CA 90095-1597

NSF Manager: Sumanta Acharya

DOE Technology Development Manager:
Gurpreet Singh

INTRODUCTION

When dealing with TE devices, a major issue is the reliability of the interfaces formed between the TE material and the structures into which they are integrated. Large mismatches in thermal expansion across such interfaces result in large thermomechanical stresses that are responsible for the devices' poor performance and even outright failures [1]. Magnesium silicide (Mg_2Si), which is one of the attractive economic TE materials, has a CTE of around 7.5 ppm/K [2,3]. This is much lower than that of Cu and other metals currently used as electrical leads.

Our approach involves the development of metal-matrix composites in which a negative thermal expansion oxide is embedded within a metal matrix: while the continuous metal matrix is responsible for achieving electrical contact with TE elements, the presence of the oxide allows the tailoring of the CTE in order to match the value of the TE elements. By adjusting the relative amount of the two components, the properties of the composite can be tailored in order to match specific requirements, which are otherwise impossible to obtain with one component alone.

APPROACH

We prepared metal-ceramic composites with Cu nanoparticles and a negative thermal expansion (NTE) oxide, ZrW_2O_8 , both of which were synthesized in our laboratory. ZrW_2O_8 was synthesized by the sol-gel method [4,5] and Cu nanoparticles (<10 nm) were synthesized using reduction of Cu^{+2} ions in the presence of polyvinylpyrrolidone (PVP) as a size-controlling agent [6]. Metal-ceramic composites containing varying compositions of Cu/ZrW_2O_8 were hot pressed at 500°C for 1 hour under forming gas atmosphere at 40 MPa. Under these conditions, relatively dense materials were obtained where the metallic Cu was not oxidized and the ZrW_2O_8 did not decompose, enabling the composites to perform as expected.

For the characterization of the composites, we measured the density of the pressed pellets using the Archimedes method. A Fei Nova NanoSEM 230 Scanning Electron Microscope (SEM) was used to characterize composite microstructures. A Netzsch DIL 402PC dilatometer was used to measure the CTE of the composites under inert argon atmosphere, and every



sample underwent at least three heating/cooling cycles between room temperature and 300°C. The CTE reported for every sample represents an average of at least five measurements. The electrical conductivity was measured by the four-point Van der Pauw method, and the thermal conductivity was measured with the laser-flash and hot-wire technique using a Netzsch LFA 447 Nanoflash instrument.

RESULTS

The microstructure of the composites was characterized using SEM cross sections of fractured surfaces. Pellets were fractured after cooling in liquid nitrogen, and representative results are shown in Figure 1. By using such fracture surfaces, we avoid polishing, that can be problematic as Cu is a ductile metal. SEM images of a hot-pressed pure Cu pellet (Figures 1a and 1b) show a homogeneous fracture surface over several tens of micrometers, without any change in morphology. The apparent roughness is possibly due to a transgranular fracture. SEM images of a Cu-ZrW₂O₈ composite pellet show that the zirconium tungstate microparticles are homogeneously dispersed within the copper matrix (Figure 1c). High magnification of the copper matrix of the composite pellet (Figure 1d) indicates that the metal

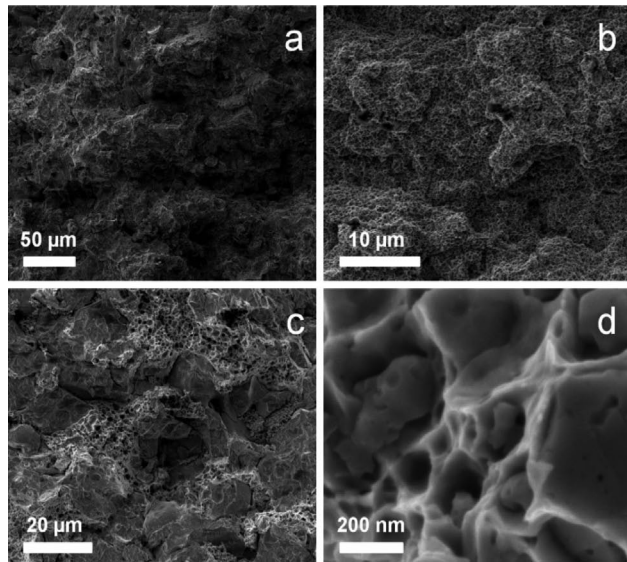
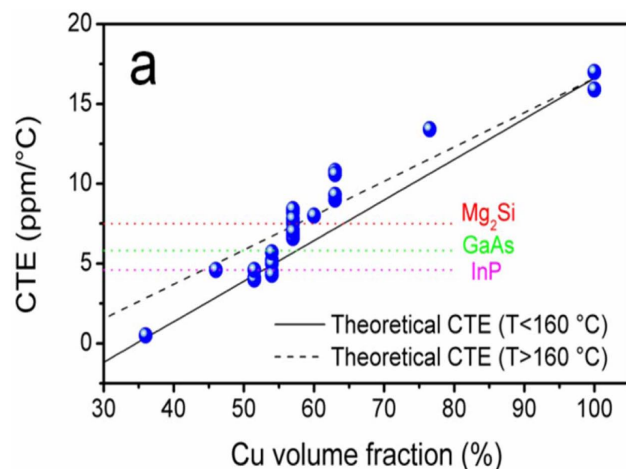


FIGURE 1. Cross-sectional SEM micrographs of a pure Cu pellet at different magnifications (1a, 1b), showing a homogeneous fracture surface over several tens of microns, without any change in morphology. Cross-sectional SEM micrographs of 57 vol% Cu/43 vol% ZrW₂O₈ at different magnifications (1c, 1d); the ZrW₂O₈ microparticles are homogeneously dispersed within the copper matrix (1c). High magnification of the copper matrix of the composite pellet (1d) indicates that the metal matrix is fully sintered.

matrix is fully sintered. These microstructures confirm the high quality of the prepared samples.

The Cu-ZrW₂O₈ composites were measured for CTE with good agreement between the experimental values and the theoretical values from the rule of mixtures. Different samples fabricated from the same metal-oxide composition show good reproducibility in measured CTE values. The experimental results are presented graphically in Figure 2, along with a table showing the actual values. The CTE for a pure Cu sample prepared by hot-pressing Cu nanoparticles was essentially the same as the CTE reported for pure bulk Cu (16.5 ppm/°C).

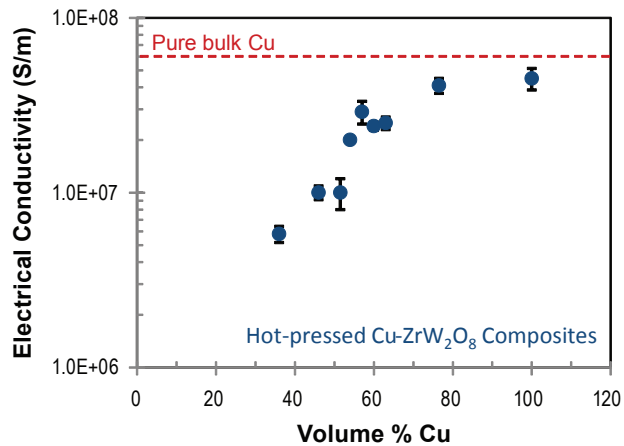


| Cu volume fraction (%) | Experimental Average CTE (ppm/°C) | Theoretical CTE using Rule of Mixtures (ppm/°C) |
|------------------------|--|---|
| 100 | 15.9 ± 1.8, 17.0 ± 1.6 | 16.5 |
| 76.5 | 13.4 ± 0.7 | 10.7 |
| 63 | 9.0 ± 0.9, 9.3 ± 0.9, 10.8 ± 1.0 | 7.2 |
| 60 | 8.0 ± 0.6 | 6.5 |
| 57 | 8.2 ± 0.9, 7.8 ± 1.0, 6.8 ± 1.1, 8.3 ± 0.7, 6.6 ± 0.4, 7.0 ± 0.5 | 5.7 |
| 54 | 5.0 ± 0.4, 4.5 ± 1.0 | 5.0 |
| 51.5 | 4.1 ± 0.9, 4.0 ± 0.5 | 4.3 |
| 46 | 4.6 ± 0.6 | 2.9 |
| 36 | 0.5 ± 1.3 | 0.4 |

FIGURE 2. Average CTE in the 80-300°C range as a function of the Cu volume fraction for the hot-pressed, metal-ceramic composites. The theoretical CTE values are calculated based on the rule of mixtures, using two different CTEs for ZrW₂O₈: -8.8 ppm/°C (CTE for ZrW₂O₈ <160°C) and -4.9 ppm/°C (CTE for ZrW₂O₈ >160°C). These are highlighted with straight and dashed lines, respectively. The CTE values for Mg₂Si, GaAs, and InP are also shown. A table with the experimental values for individual samples is also provided.

We measured the CTE between room temperature and 300°C. ZrW_2O_8 undergoes a reversible phase transition at ~160°C, where below 160°C, the α phase has a NTE of -8.8 ppm/°C, but above 160°C, the β -phase has a NTE of -4.9 ppm/°C. Our experimental CTE values are higher than the theoretical CTE predicted using a NTE of -8.8 ppm/°C but show good agreement with the theoretical CTE predicted by the rule of mixtures calculated using a NTE of -4.9 ppm/°C. Our results show that by tailoring the composition, we are able to achieve CTEs that match the CTE of metal silicides and semiconductors, and the composites show excellent stability as measurements of CTE using the same samples after weeks of storage in air did not change.

We also characterized the Cu-ZrW₂O₈ composites for their electrical and thermal conductivity. The electrical conductivity results are presented in Figure 3, along with a table showing the experimental values. The electrical



| Cu volume fraction (%) | Measured Conductivity (S/m) | % Cu bulk conductivity |
|------------------------|-------------------------------------|------------------------|
| 100 | $4.5 \cdot 10^7 \pm 6.3 \cdot 10^6$ | 76.0 ± 10.5 |
| 76.5 | $4.1 \cdot 10^7 \pm 4.0 \cdot 10^6$ | 69.1 ± 6.5 |
| 63 | $2.5 \cdot 10^7 \pm 2.1 \cdot 10^6$ | 42.6 ± 3.6 |
| 60 | $2.4 \cdot 10^7 \pm 1.3 \cdot 10^6$ | 40.3 ± 2.2 |
| 57 | $2.9 \cdot 10^7 \pm 4.3 \cdot 10^6$ | 45.0 ± 6.5 |
| 54 | $2.0 \cdot 10^7 \pm 6.4 \cdot 10^5$ | 34.2 ± 1.4 |
| 51.5 | $1.0 \cdot 10^7 \pm 2.0 \cdot 10^6$ | 17.2 ± 3.3 |
| 46 | $1.0 \cdot 10^7 \pm 9.0 \cdot 10^5$ | 17.1 ± 1.5 |
| 36 | $5.8 \cdot 10^6 \pm 6.2 \cdot 10^5$ | 9.8 ± 1.1 |

FIGURE 3. Average electrical conductivity as a function of Cu volume fraction for hot-pressed Cu-ZrW₂O₈ composites. The expected value for bulk, fully dense copper (6.0 S/m) is highlighted with a dashed line. The composites show good electrical conductivity, and as expected, the conductivity decreases as the volume fraction of ZrW₂O₈ increases. A table with the experimental values is also provided.

conductivity of pure Cu prepared by hot-pressing Cu nanopowders averaged about 75% of the conductivity of bulk copper, with the best samples reaching 85-90% of the bulk Cu conductivity (~ 6×10^7 S/m). These results indicate relatively high quality of the prepared materials and the ability to achieve bulk-like material properties at hot-pressing temperatures as low as 500°C. As expected, the electrical conductivity decreases steadily with increasing amount of ceramic oxide (ZrW₂O₈); however, the composite samples are still relatively conductive. For example, the electrical conductivity of samples containing 40+ vol% ZrW₂O₈ has conductivity >40% of bulk Cu, while samples containing 64% oxide exhibit a conductivity (5.8×10^6 S/m) higher than pure titanium (2.5×10^6 S/m). The high electrical conductivity, along with the tunability of the CTE, make the metal-ceramic composites suitable for a variety of applications in which the device has to be thermally cycled, good electrical contact must be maintained, and problems with thermomechanical stresses must be avoided.

Figure 4 shows the measured and predicted thermal conductivities of the composites at room temperature as a function of the volume fraction of Cu. Without the ceramic oxide, the measured thermal conductivity of a pure Cu pellet from hot-pressed Cu nanoparticles is 340 W/mK, which is about 85% of the expected value for bulk Cu (401 W/mK). The thermal conductivity decreases steadily with increasing ZrW₂O₈ loading, as expected. We compared the experimental data with predictions from two models. The Maxwell-Eucken model assumes that the dispersed component does not form continuous conduction pathways and therefore gives an upper or a lower bound. The effective medium model represents a heterogeneous material where the two components

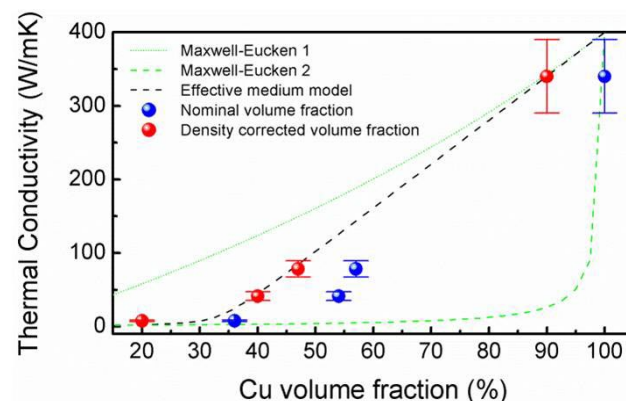


FIGURE 4. Thermal conductivity as a function of Cu volume fraction for hot-pressed Cu-ZrW₂O₈ composites. After correcting for porosity based on independent density measurements, the experimental data show excellent agreement with the effective medium model (dashed black line). The trends predicted by the Maxwell-Eucken model (dotted and dashed green lines for the upper and lower limit, respectively) are also shown for comparison.

are distributed randomly and either of them may form continuous conduction pathways. As shown in Figure 4, the experimental data (blue dots) follow the trend of effective medium model predictions although there is a horizontal shift compared to the model. The reason for this shift is that we calculated the Cu volume fraction as a nominal value obtained from the weight fraction when, in fact, the samples show a certain amount of porosity, as confirmed by the density measurements. By taking into account the porosity of the samples from the density measurements, we obtain good agreement between the measured thermal conductivity and the predicted conductivity based on the effective medium model (red dots in Figure 4).

CONCLUSIONS

- We successfully fabricated metal-ceramic composites over a wide range of compositions using Cu nanoparticles and ZrW₂O₈ powders, with CTEs that can be tuned from ~16 ppm/°C (100 vol% Cu) to <1 ppm/°C (36 vol% Cu/64 vol% ZrW₂O₈).
- CTE data show excellent reproducibility and shelf life.
- The Cu-ZrW₂O₈ composites possess high electrical and thermal conductivities, with both conductivities varying as a function of composition in an expected manner.
- Improved thermomechanical reliability from this unique combination of high electrical and thermal conductivities and relatively low thermal expansion enables these metal-ceramic composites to be used as electrical leads for a variety of TE elements.

REFERENCES

1. V. Ravi, S. Firdosy, T. Caillat, E. Brandon, K.V.D. Walde, L. Maricic, A. Sayir, *J. Electron. Mater.*, **2009**, *38*, 1433.
2. K. Kondoh, H. Oginuma, R. Tuzuki, T. Aizawa, *Mater. Trans.*, **2003**, *44*, 611-618.
3. S.K. Thakur, B.K. Dhindaw, N. Hort, K.U. Kainer, *Metall. Mater. Trans. A*, **2004**, *35*, 1167-1176.
4. K. De Buysser, P.F. Smet, B. Schoofs, E. Bruneel, D. Poelman, S. Hoste, I.V. Driessche, *J. Sol-Gel Sci. Technol.*, **2007**, *43*, 347-353.
5. J.E. Trujillo, J.W. Kim, E.H. Lan, S. Sharratt, Y.S. Ju, and B. Dunn, *J. Electron. Mater.*, **2012**, *41*, 1020-1023.
6. E. Hao, T. Lian, *Chem. Mater.*, **2000**, *12*, 3392-3396.

FY 2013 PUBLICATIONS/PRESENTATIONS

1. Enrico Della Gaspera, Ryan Tucker, Kurt Star, Esther H. Lan, Yongho Sungtaek Ju and Bruce Dunn, “Copper-based conductive composites with tailored thermal expansion,” to appear in *ACS Applied Materials and Interfaces*.

V.11 High-Performance Thermoelectric Waste Heat Recovery System Based on Zintl-Phase Materials with Embedded Nanoparticles

Ali Shakouri (UC Santa Cruz),
Zhixi Bian (UC Santa Cruz),
Susan M. Kauzlarich (UC Davis)
University of California, Santa Cruz
Electrical Engineering Department
1156 High Street
Santa Cruz, CA 95064

NSF Manager: Sumanta Acharya

DOE Technology Development Manager:
Gurpreet Singh

NETL Project Manager: Carl Morande

- Synthesis and SPS of n-type Mg_2Si with embedded WC nanoparticles—characterization and transport modeling.
- Identification of bipolar thermal conductivity as a key factor limiting thermodynamic figure of merit (ZT) of $Mg_2Si_{1-x}Sn_x$ at high temperatures. Proposed electron energy filtering to reduce bipolar thermal conductivity and achieve $ZT > 2$.

Future Directions

Finalize papers on the latest materials synthesized and summarize the key theoretical results including the calculation of the bipolar thermal conductivity.



Overall Objectives

- Develop novel thermoelectric materials based on abundant and non-toxic Zintl-phase magnesium silicide alloys.
- Demonstrate that with the use of embedded nanoparticles of appropriate concentration (0.01-5%) and diameter (2-15 nm), thermal conductivity will be reduced by scattering of mid to long wavelength phonons.
- Optimize the thermoelectric power factor and figure of merit by band engineering and electron filtering using Mg_2Si nanoparticles embedded in $Mg_2Si_xSn_{1-x}$ alloys.

Fiscal Year (FY) 2013 Objectives

- Synthesis of n-type Mg_2Si and study of particle size and grain boundaries and n-type Mg_2Si with tungsten carbide (WC) nanoparticles.
- Structural and thermoelectric characterizations.
- Comprehensive multiband thermoelectric transport modeling using Boltzmann equation.
- Optimization of thermal conductivity and thermoelectric power factor by modifying the alloy composition, doping, temperature and energy filtering.

FY 2013 Accomplishments

- Optimization of spark plasma sintering (SPS) of n-type Mg_2Si and effect on grain boundaries.

INTRODUCTION

We are developing novel thermoelectric materials based on abundant and non-toxic Zintl-phase magnesium silicide alloys. We have demonstrated a synthetic method that naturally provides embedded nanoparticles within a magnesium silicide alloy matrix, providing uniform mixing with minimal aggregation. With the use of embedded nanoparticles of appropriate concentration (0.01-5%) and diameter (2-15 nm), thermal conductivity will be reduced by scattering of mid to long wavelength phonons. Controlling the heterostructure band offset and the potential barrier of nanoparticles with respect to matrix, power factor will be increased by selective scattering of hot carriers. Electron energy filtering will also reduce bipolar thermal conductivity which is important for small bandgap $Mg_2Si_{1-x}Sn_x$ material at high temperatures. Detailed transport calculations show that $ZT > 2$ at 800 K can be achieved.

APPROACH

Mg_2Si can be synthesized with MgH_2 and Si powders as starting materials. By changing the ratio of the starting materials, a proper amount of Si nanocomposites can be easily cooperated with the matrix. N-type dopants are intentionally mixed with starting materials homogeneously in a ball mill to tune the carrier concentration. Either flow furnace and SPS in combination or SPS alone are employed to achieve the Mg_2Si product as well as dense pellets. Carrier concentration is adjusted using P, Sb, or Bi dopants and thermal conductivity is reduced using heavy

element dopants which isovalently replace elements in the structure or fill vacancies, or with the use nano-structuring or the use of nano-sized inclusions. Simply reducing crystallite size of Mg_2Si to the nano-size reduces thermal conductivity, but also raises electrical resistivity. We systematically investigated the influence of sample preparation and sintering conditions on the transport properties of Yb-doped Mg_2Si utilizing hydrides in an in situ reaction during SPS experiments.

We have shown that thermal conductivity of Mg_2Si can be reduced due to the additional interfaces and phonon scattering centers introduced by Si nanoinclusions [1] or doping of heavy Yb into Mg site. We have investigated the effect of Ge nanoparticles prepared by the solution-assisted method [2] on the thermal conductivity of pristine Mg_2Si and compare it with the thermal conductivity of the Ge-substituted Mg_2Si . However, the produced samples are poor electrical conductors with associated high values of electrical resistivity due to the scattering of electrons by the phase interfaces and boundaries. Optimization of the electrical properties of the Mg_2Si composites was performed by adding different concentrations of Group 15th elements as dopants and also by adding WC.

On the theory side, we have developed a multiband Boltzmann transport model for both n- and p-type $Mg_2Si_{1-x}Sn_x$ ($0 \leq x \leq 1$) solid solutions over a wide temperature range from 300 K to 900 K with the temperature-dependent band structure and the energy-dependent relaxation times (acoustic phonon deformation potential scattering, the polar optical phonon scattering and the ionized impurity scattering).

RESULTS

Grain Boundaries

Scanning electron microscopy (SEM) was used to determine the microstructure of the fracture faces of the samples prepared by the reaction of $MgH_2 + Si$. Looking at the three samples prepared by long ball milling and sintering at 500°C or 650°C, one can see that the sintering of the samples improves with increasing temperature. At 500°C (Figure 1, left) large grains with sizes up to about 10 μm are visible, but they are embedded in a matrix of smaller grains which exhibits a fairly large size distribution. With larger magnification it becomes clear that some of the smaller grains (sizes of about 0.5–1.5 μm) are also sintered well but again are embedded in a matrix of sub-micron sized particles. The same is true for the sample sintered at 650°C (Figure 1, right). Overall the crystalline size increases, which can be attributed to the higher sintering temperature used, but still these crystals are not well sintered. Besides the low degree of sintering some small voids are visible. It

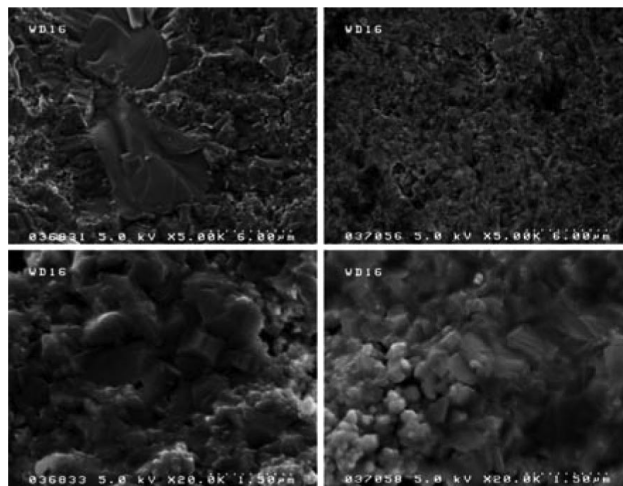


FIGURE 1. SEM images of the methanol-etched fracture faces of 1.0% Yb doped Mg_2Si . The two left images show the microstructure of a sample sintered at 500°C using 5k (top left) and 20k (bottom left) magnification. The images on the right were taken on a sample sintered at 650°C. The top right one at a magnification of 5k, the bottom right one at 20k.

cannot be clearly determined if these holes are due to the etching or are a feature created by the sintering; but, since the pellets show high density, it is more likely to be formed during the etching process. Figure 2 shows the images of samples prepared with Yb and Bi doped Mg_2Si sintered at 750°C. It is clear that both samples show better sintering than that shown in Figure 1, and the samples with Bi show larger grain size.

Transport Properties

The sintered and cut samples were mounted on a Linseis LRS3 instrument and electrical resistivity and Seebeck coefficient were measured from room temperature to 773 K and back (Figure 3). The measured electrical resistivity shows an interesting behavior, since the shape of the curve looks like what is expected for an undoped semiconductor. The resistivity has values of ~230 m Ω cm at 323 K of samples sintered at 500°C. It drops to ~22 m Ω cm at 773 K. When the sintering temperature is increased to 650°C the shape of the curve stays similar, but the resistivity drops to ~70 m Ω cm at 323 K and ~9 m Ω cm at 773 K. When sintered finally at 750°C, the resistivity is still above undoped Mg_2Si (~40 m Ω cm at 323 K; ~5 m Ω cm at 773 K) which can be attributed to the low degree of sintering of the samples.

Mg_2Si with Embedded WC

The p-doped Mg_2Si composites with WC inclusions were prepared by utilizing reaction of MgH_2 with Si/P/WC and densified by means of SPS. Electron probe micro-analysis shows that the distribution of Mg, Si, and P dopant in Mg_2Si /WC composite is homogeneous, while

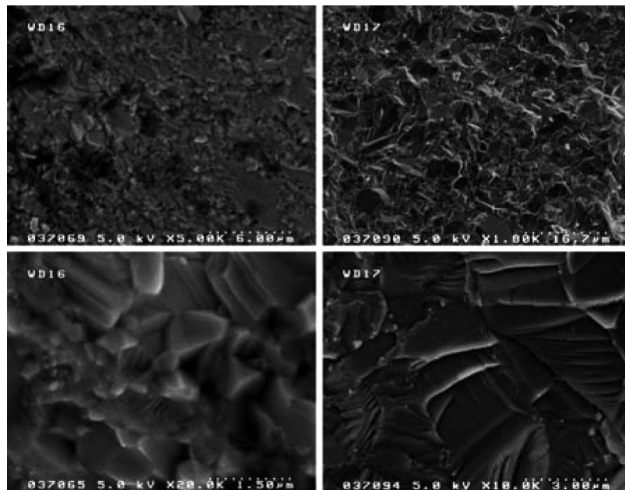


FIGURE 2. SEM images of the methanol-etched fracture faces of 1.0% Yb doped Mg₂Si (left) and 1.0% Bi doped Mg₂Si (right). The two left images show the microstructure of a sample sintered at 750°C using 5k (top left) and 20k (bottom left) magnification. The images on the right were taken on a sample sintered at 700°C but prepared by a short ball mill approach. The top right one was taken at a magnification of 1.8k, the bottom right one at 10k.

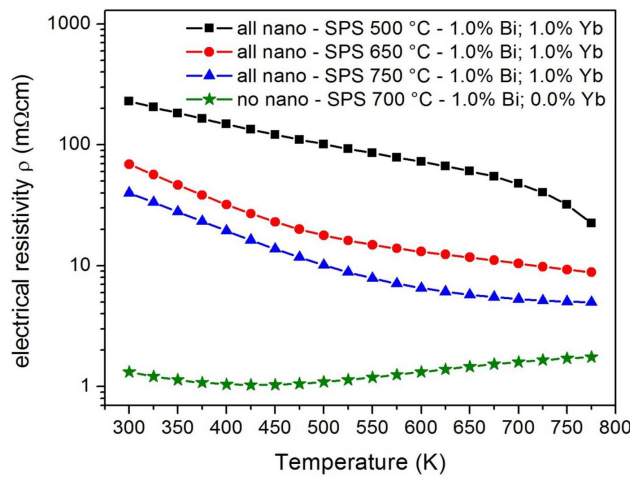


FIGURE 3. Electrical resistivity vs. temperature for Yb- and Bi-doped Mg₂Si and the effect of grain size.

WC forms inclusions and does not dissolve in the Mg₂Si matrix (Figure 4). Addition of WC into Mg₂Si drastically enhances electrical transport, while having only moderate impact on the thermal conductivity (Figure 5). The measured carrier concentration of $1.9 \times 10^{20} \text{ cm}^3$ is close the optimal and the low electrical resistivity and is attributed to the enhanced electron mobility ($68 \text{ cm}^2/\text{V}\cdot\text{s}$). However WC has a negative impact on the Seebeck coefficient. Overall, WC enhances ZT, which reaches a maximum of 0.52 at 770 K for Mg₂Si/1% P/3% WC as compared to ZT = 0.33 at 865 K for P-doped Mg₂Si [3].

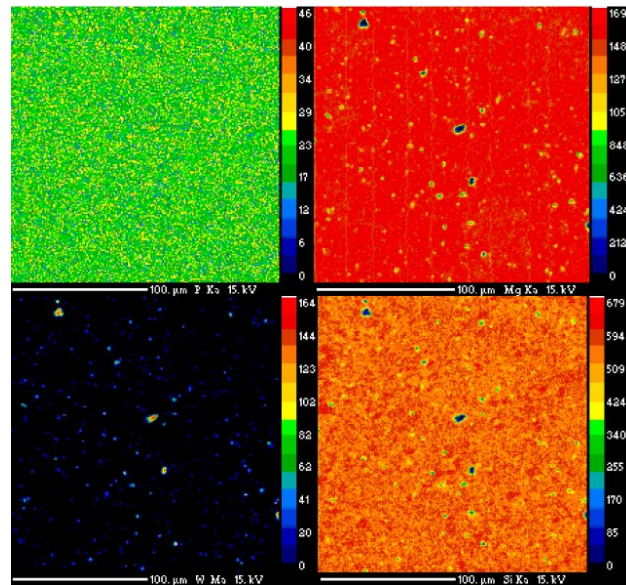


FIGURE 4. Electron probe microanalysis X-ray maps showing P, Mg, Si and W distribution in P-doped Mg₂Si/WC sample (from left to right).

We also notice the enhanced mechanical properties, e.g., less cracks, upon addition of WC into Mg₂Si.

Theoretical Modeling

A variety of experimental data from literature are fitted very well by this model and analyzed for further material optimization. Our analysis shows that the compositions of $x = 0.6$ to 0.7 exhibit the highest ZT among n-type Mg₂Si_{1-x}Sn_x in the mid-temperature range 600 K to 900 K due to both the high power factors achieved by the convergence of the two conduction bands and low electronic thermal conductivities (Figure 6). For the p-type materials, we find that the bipolar electronic thermal conductivity is a major factor limiting ZT. Low Sn content ($x < 0.4$) alloys show a larger figure of merit among the p-type materials due mainly to their lower bipolar thermal conductivities with larger bandgaps.

CONCLUSIONS

It has been shown that Bi and Sb are superior dopants for the Mg₂Si-based materials, since they are not only electron dopants, but also scatter phonon effectively, thus lowering thermal conductivity. The highest ZT of 0.86 at 862 K for Mg₂Si-based compounds was reported in the case of Bi-doped material [4]. Further work on the Bi- and Sb-doped Mg₂Si with various concentrations of WC is currently in progress. Finally, we propose that hot carrier energy filtering can be very useful for these alloys as it can simultaneously reduce the electronic thermal conductivity and enhance the power factor. A ZT greater than 3 is possible for n-type Mg₂Si_{0.4}Sn_{0.6} ($x = 0.6$) at

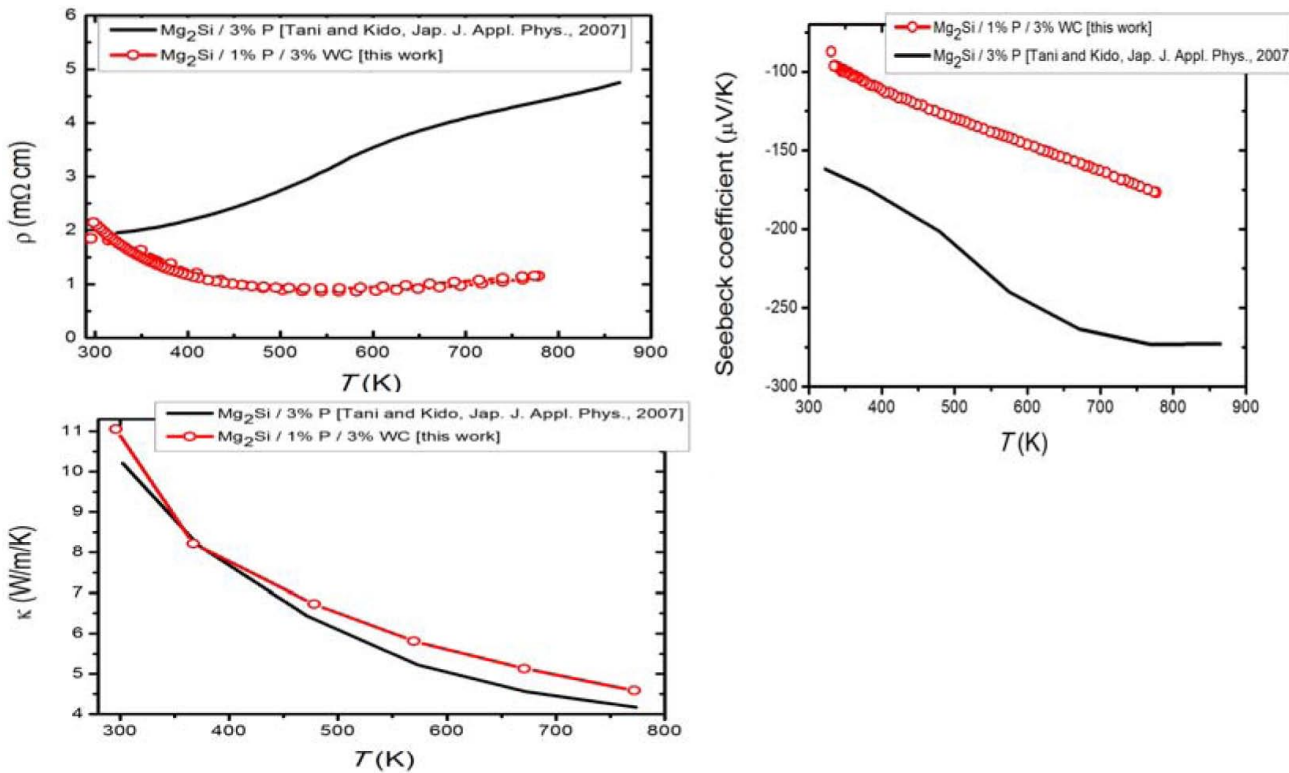


FIGURE 5. Thermoelectric properties of P-doped $\text{Mg}_2\text{Si}/\text{WC}$ composite are compared with that of P-doped Mg_2Si [3].

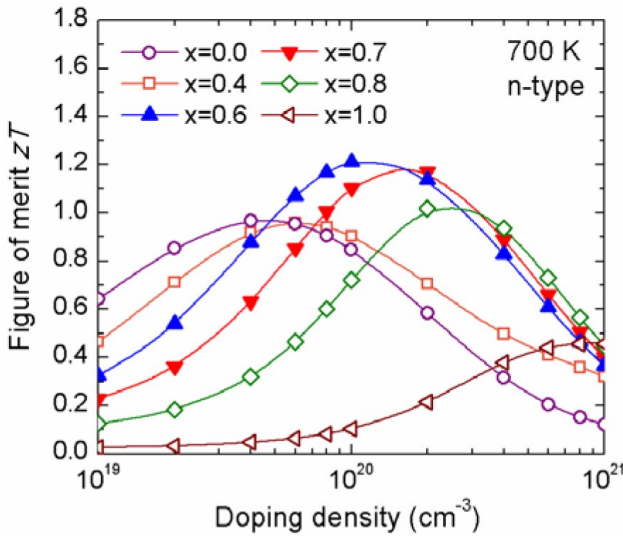


FIGURE 6. Calculated figure of merit ZT as a function of doping density for n-type $\text{Mg}_2\text{Si}_{1-x}\text{Sn}_x$ with varying $x=0\sim 1.0$ at 700 K. The lattice thermal conductivity is assumed to be 1.0 W/mK for all the compositions.

700 K if electrons with energies lower than 0.4 eV are effectively prevented from participating in transport (Figure 7).

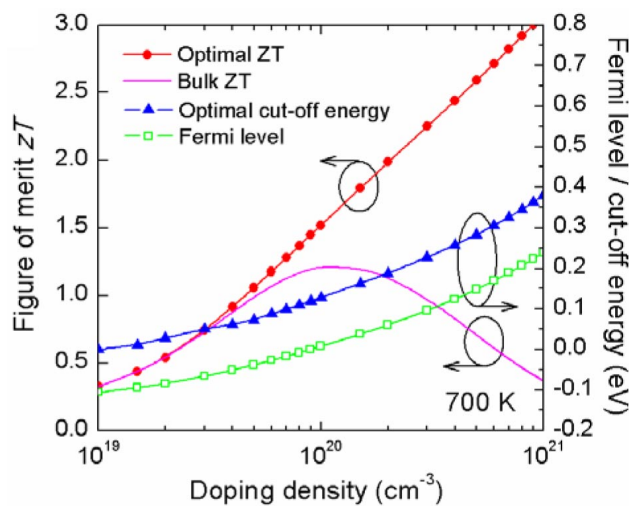


FIGURE 7. Calculated ZTs of n-type $\text{Mg}_2\text{Si}_{0.4}\text{Sn}_{0.6}$ as a function of doping density by the optimal electron energy filtering effect at 700 K. The Fermi level and the optimal cut-off energy level used at each doping density are shown on the right y-axis. The bulk property value is also shown for comparison.

REFERENCES

1. Yi, T.; Chen, S.; Li, S.; Yang, H.; Bux, S.; Bian, Z.; Katcho, N.A.; Shakouri, A.; Mingo, N.; Fleurial, J.-P.; Browning, N.D.; Kauzlarich, S.M., *J. Mater. Chem.* 2012, 22, 24805-2481.
2. Muthuswamy, E.; Iskandar, A.S.; Amador, M.M.; Kauzlarich, S.M., *Chem. Mater.* 2013, 25, 1416-1422.
3. J. Tani, H. Kido, *Jap. J.Appl. Phys.* 2007, 46, 3309.
4. Tani, J.-i.; Kido, H., *Physica B* 2005, 364 (1-4), 218-224.

FY 2013 PUBLICATIONS/PRESENTATIONS

1. Je-Hyeong Bahk, Zhixi Bian, Tela Favaloro, Ali Shakouri, Tanghong Yi, Oliver Janka and Susan Kauzlarich, Hydrogen and Fuel Cells Program and Vehicle Technologies Program Annual Merit Review and Peer Evaluation Meeting, Washington, D.C., May 13–17, 2013.
2. Je-Hyeong Bahk, Zhixi Bian and, Ali Shakouri, “Electron transport modeling and energy filtering for efficient thermoelectric Mg₂Si_{1-x}Sn_x solid solutions,” submitted for publication to *Physical Review B*, 2013.

V.12 An Integrated Approach Towards Efficient, Scalable, and Low-Cost Thermoelectric Waste Heat Recovery Devices for Vehicles

Scott Huxtable (Primary Contact),
Srinath Ekkad, and Shashank Priya
Virginia Tech
Center for Energy Harvesting Materials and Systems
Department of Mechanical Engineering
Blacksburg, VA 24061

DOE Technology Development Manager:
Gurpreet Singh

NSF Manager: Sumanta Acharya

Subcontractor:
Dr. Andrew Miner, Romny Scientific, San Bruno, CA

- Develop an experimental test facility to investigate the prototype heat exchanger module.
- Create a performance map of the heat exchanger module and the TE system over a range of operational parameters (engine speed, coolant pumping power, etc.).
- Create a model of the fluid flow and heat transfer behavior inside the exhaust pipe test section with internal fins using computational fluid dynamics.
- Scale the synthesis process for the previously developed N-type magnesium silicide materials to produce large volumes without loss in material performance.
- Examine the role of the fabrication process parameters on the micro/nano structure for further reduction of thermal conductivity in ZnO materials.
- Examine the doping mechanism(s) and influence of synthesis conditions on carrier concentration, and, ultimately, power factor of ZnO materials.

Overall Objectives

- Fabricate and characterize new thermoelectric (TE) materials grown with scalable techniques for production of large quantities of efficient, yet non-toxic and inexpensive elements capable of long-term operation at high temperatures over thousands of thermal cycles.
- Design, fabricate, and characterize heat sinks that include modifications such as jet impingement (coolant), pin-fins, louvers, etc. (exhaust gas) in order to enhance heat transfer with minimal rise in back pressure and without significant increases in cost, complexity, or weight.
- Characterize TE transport properties, species diffusion, and adhesion for interfaces to reveal the effects of material composition, microstructure, processing and assembly techniques on thermoelectric generator (TEG) performance and lifetime.
- Assemble a laboratory-scale test bed comprising of recirculating hot air flow through an automotive exhaust system that is fitted with a complete TEG system to evaluate system level models and to quantify individual component and overall system performance.

Fiscal Year (FY) 2013 Objectives

- Fabricate prototype heat exchanger modules for use in experiments to validate the computational models for heat transfer.

FY 2013 Accomplishments

- Manufactured several small-scale heat exchanger modules for use in experiments to validate the numerical models for heat transfer behavior characterization. The impinging geometry on the heat exchanger was shown to produce significant efficiency improvements (~15%) over the baseline case.
- Completed an experimental test facility to investigate heat exchanger modules previously designed and manufactured.
- Created a performance map of the heat exchanger module and the TE system over a range of operational parameters (engine speed, coolant pumping power, etc.).
- Modeled fluid flow and heat transfer behavior inside the exhaust pipe test section with internal fins (multi-louvered fins and wavy Herringbone fins) using computational fluid dynamics.
- Scaled the synthesis process for the previously developed n-type magnesium silicide materials to allow for production of over 3,000 elements/hr.
- Reduced the thermal conductivity of the ZnO materials through nanostructuring. Thermal conductivity is further reduced by 30-50% between

100 and 300°C by sintering the material in vacuum. These thermal conductivity values are 7-fold lower than that of non-network-grain and non-nanoprecipitate filled ZnO.

- Characterized the effect of synthesis and sintering conditions on the doping mechanisms on carrier concentration and power factor in the ZnO materials.

Future Directions

In the following year, the team plans to:

- Perform a sensitivity study on the performance of the system to various parameters including the number of TEG modules, engine power, vehicle speed, etc. and find the optimum operating conditions for the system.
- Modify design to perform optimally in the typical operating conditions.
- Develop a prototype of the TEG.
- For layered network-grain structure, work will continue regarding the critical growth mechanisms in ZnO in order to improve the material properties. Low-temperature oxygen annealing will be explored to improve the carrier density of ZnO with the layered network-grain structure.
- Methods to improve the electrical conductivity in the ZnO materials will also be explored. Specifically, the effect of chemical defects, such as vacancies, introduced by elevated temperatures will be examined in order to improve electrical conductivity with changes in sintering temperature and atmosphere.



INTRODUCTION

A significant amount of the energy input to a vehicle is wasted as heat in the exhaust. Capturing even a fraction of this wasted energy would translate into tremendous savings in fossil fuel usage as well as a reduction in vehicle emissions. TE devices that can directly convert the thermal energy lost in the hot exhaust gases into useful electrical power offer a possible method for partial recovery of this wasted energy. However, TE materials and devices suffer from several drawbacks including poor efficiency, high cost, manufacturability at the large volumes needed for automobiles, and durability to withstand rugged use on vehicles.

APPROACH

The overall approach is to focus on making fundamental, yet practical, industry relevant, advances in several key areas—materials, heat sinks, thermal management, interfaces, and durability—that are critical for the realization of widespread deployment of TE devices in vehicles. The principal investigators are examining several approaches for creating micro/nano structured bulk TE materials where the aim is to take advantage of nanoscale effects, yet rapidly fabricate materials at a bulk scale. These approaches include mechanical alloying and batch furnace pressing of TE powders, and solid-state reactions and chemical synthesis of nanostructured bulk materials from abundant and low-cost materials at appropriate sizes and shapes. The approach for heat sinks is employ jet impingement for the liquid side, and to use small pin-fins and/or louvered fins on the air side to enhance heat transfer while limiting back pressure and maintaining relatively simple, low-cost, and manufacturable designs. For thermal management, the team is taking an integrated approach where appropriately scaled heat sinks, TE elements, and packaging are examined individually and collectively for device performance and durability in models and laboratory-scale experiments. Interfaces are characterized thermally with optical techniques, and mechanically for adhesion and lifetime following thermal cycling.

RESULTS

This work can be organized into two broad categories: (1) thermal management, and (2) materials development and characterization. The results from the thermal management work are discussed first, followed by advances with the materials. The experimental test facility was completed this year, and it was used to verify the numerical simulations, and it conclusively showed that the impinging geometries for the heat exchangers gave efficiency improvements of up to 15% over baseline cases. The principal investigators also used the validated models to examine the efficiency of the TEG systems at realistic engine conditions and speeds, and found diminishing returns at high speeds. Building on previous work with pin-fins, the team examined the use of internal multi-louvered fins and Herringbone wavy fins to enhance heat transfer on the air-side heat exchangers (see Figure 1), and found that these structures can increase heat transfer to a similar extent as the pin-fins, however the pressure drop for the louvered fins was found to be considerably larger than for the Herringbone fins. For the louvered fins, the wall temperature increased with the angle of the louvers, and with the ratio of the louver pitch to fin pitch. With the Herringbone fins, the wall

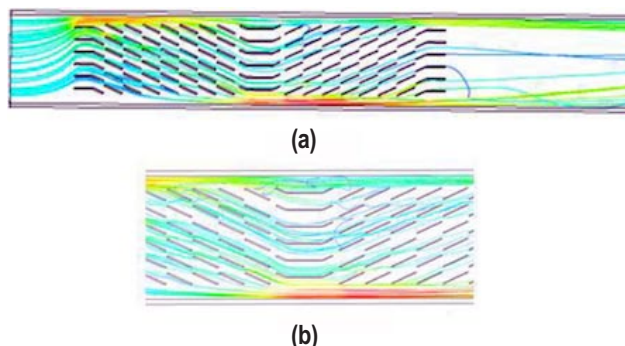


FIGURE 1. Representative plot of flow streamline visualization for louvered fins in exhaust gas heat exchanger.

temperature also increased with the angle of the fins, and with the height of the fins until the fins reached about 50% of the channel height.

On the materials side, the team has continued development on magnesium silicide and zinc oxide elements. Romny has developed a process using an electrically driven five-ton automated powder consolidation press to produce solid powder compacts with high density and good TE properties that are equivalent to, or surpass, those formed using a manual hydraulic press (see Figure 2 for representative samples). The automatic press system was characterized in great depth, including studies of the output sample consistency in terms of relative density. Batches with up to 25 samples each were found to have densities that varied less than 5% across months of production runs. Dimensionless figure of merit values for these n-type Mg-Si samples were measured to be ~0.25 at 150°C and ~0.5 at 300°C, as shown in Figure 3. High-temperature sintering processes were examined in order to understand the process sensitivities by varying temperature, pressure, and time for the sintering process. A summary of the results of this study is also shown in Figure 3. The process was quite consistent, other than the notable reduction in TE figure of merit for process runs for higher temperature and lower time. Production scaling capabilities were also improved this year, and the capability to produce consistent TE elements at rates of over 3,000 pieces per hour has been demonstrated.

The principal investigators have continued the development of bulk Al-doped ZnO with a novel self-assembled layered network-grain structure embedded with nano-scale precipitates (see Figure 4). The layered network grains display one preferential growth orientation, along with oriented anisotropic interspace and nano-precipitates. The mechanism of this layered network structure has been investigated to relate with vapor transport grain growth mechanisms, second phase separation, and density distribution with a spring-back effect after uniaxial pressing. The addition



FIGURE 2. Sample MgSi TE material created with cold pressing and sintering. Production of elements at a rate of 3,000 pieces per hour was demonstrated.

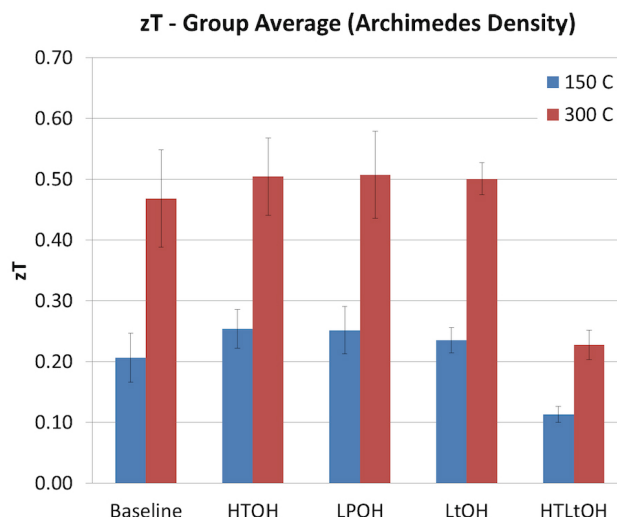


FIGURE 3. Measured ZT values for n-type Mg-Si elements from a sintering process study. Results were consistent for the high-temperature (HTOH), low-pressure (LPOH), and low-time (LtOH) cases, while the high-temperature, low-time case (HTLtoH) was comparatively poor.

of Al, atmospheric conditions during sintering, and powder compaction have been tuned to obtain the layered network grain structure. This structure creates ~50% decrease of the thermal conductivity at 300°C compared with dense ZnO with nano-precipitates. Further reductions in thermal conductivity are achieved by controlling the sintering environment (see Figure 5). These thermal conductivity values are 7-fold lower than that of non-network-grain and non-nanoprecipitate filled ZnO. The sintering atmosphere also plays a role with the Seebeck coefficient and the electrical conductivity. Electrical conductivity values of over 1,000 S/cm

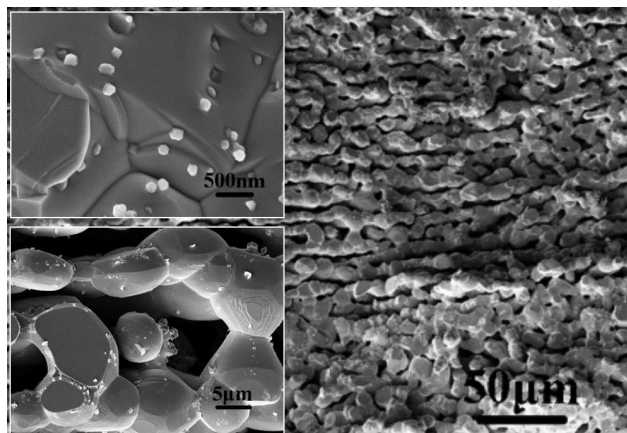


FIGURE 4. Scanning electron micrographs of the layered ZnO materials including the Al nanoprecipitates.

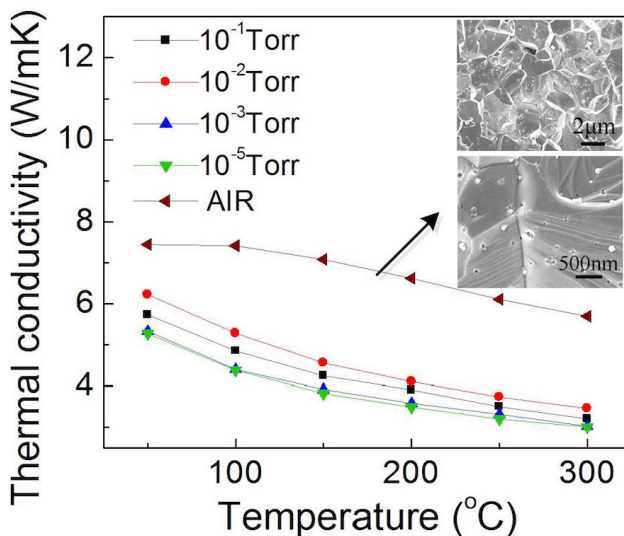


FIGURE 5. Thermal conductivity of layered ZnO materials sintered in vacuum compared with samples sintered in air. The layered structure strongly reduces thermal conductivity, while still allowing adequate electrical conductivity.

have been obtained for materials sintered in vacuum at 1,200°C, with corresponding Seebeck coefficients ~100 $\mu\text{V/K}$. The Seebeck coefficients varied strongly with sintering conditions, thus this is an area of ongoing work.

CONCLUSIONS

- Computational fluid dynamics models for hot- and cold-side heat exchangers were validated with an experimental test facility.
- Impinging geometry on the heat exchangers provides ~15% improvement in the system efficiency.
- Numerical results show that incorporating internal multi-louvered fins and Herringbone wavy fins in the exhaust pipe section increase the heat transfer coefficient. However, the pressure drop in the louvered fins is much higher than that for the Herringbone wavy fins.
- Mg-Si materials with ZT values of ~0.25 at 150°C and ~0.5 at 300°C were produced with an automated press capable of producing 3,000 pellets per hour.
- ZnO is a promising material for high-temperature TE power generation. Significant reductions in thermal conductivity have been achieved, yet further reductions with minimal losses in power factor are still required.

FY 2013 PUBLICATIONS/PRESENTATIONS

- Pandit, J., Thompson, M., Ekkad, S.V., Huxtable, S., "Experimental And Numerical Investigation of Heat Transfer Across A Thermoelectric Generator For Waste Heat Recovery From Automobile Exhaust Gases," HT2013-17438, Summer Heat Transfer Conference, American Society of Mechanical Engineers, Minneapolis, MN, July 2013.
- Athavale, J., Pandit, J., Ekkad, S.V., Huxtable, S.T., "Evaluation of Multi-Louvered Fin Based Heat Exchangers for use in Automobile Exhaust Energy Harvesting Systems," - accepted for AIAA conference in January 2014.
- Pandit, J., Thompson, M., Ekkad, S.V., Huxtable, S.T., "Effect of Pin Fin to Channel Height Ratio and Pin Fin Geometry on Heat Transfer Performance for Flow in Rectangular Channels," submitted to International Journal of Heat and Mass Transfer, 2013.
- Ekkad, S. V., "Thermal design for Thermoelectric Generators for Waste Heat Recovery from Automobile Exhaust," International Workshop on Heat Transfer Advances for Energy Conservation and Pollution Control (IWHT), Shaanxi, China, October 21–23, 2013 (Invited presentation).

V.13 High-Performance Thermoelectric Devices Based on Abundant Silicide Materials for Vehicle Waste Heat Recovery

Li Shi (Primary Contact), John B. Goodenough, Matthew J. Hall, Jianshi Zhou, Xi Chen, Libin Zhang, Haiyan Fateh, Annie Weathers
The University of Texas at Austin
Department of Mechanical Engineering
Austin, TX 78712

Song Jin, Steven Girard, Ankit Pokhrel
University of Wisconsin-Madison

DOE Technology Development Manager:
Gurpreet Singh

NETL Project Manager: Carl Morande

- Addressed the chemical instability problem of Mg_2Si -based compounds.
- Designed and fabricated the 1st generation and the improved 2nd generation TE devices, and measured contact resistance and power output to correlate to and validate the device model.

Future Directions

- Improve the TE properties of silicides by nanostructuring and modulation doping.
- Understand the crystal complexity on the phonon dispersion and transport in HMS.
- Test TE devices coupled with heat exchanger and validate the system level model.
- Incorporate thermal and electrical contact resistance in the system level model.



Overall Objectives

- Increase the figure of merit (ZT) of earth abundant and low-cost magnesium silicides (Mg_2Si) and higher manganese silicides ($MnSi_{1.73}$, or HMS) to the level found in state-of-the-art thermoelectric (TE) materials that contain scarce and expensive elements.
- Improve the chemical stability of TE silicides at high temperatures.
- Enhance thermal management performance for silicide TEs installed on a diesel engine.

Fiscal Year (FY) 2013 Objectives

- Synthesize and characterize HMS crystals by chemical vapor transport.
- Improve the ZT of HMS and $Mg_2Si_{1-x-y}Sn_xGe_y$ by chemical substitution, doping and nanostructuring.
- Fabricate and test thermoelectric generator (TEG) devices to validate the TE device model.

FY 2013 Accomplishments

- Obtained the TE and magnetic properties of high-purity HMS chemical vapor transport (CVT) crystals.
- Developed an approach to generate high yields of HMS nanowires (NWs).
- Revealed the effect of (Al,Ge) double doping on the TE properties of HMS.
- Understood the TE properties and chemistry of Ge substituted $Mg_2Si_{0.4}Sn_{0.6}$ compounds.

INTRODUCTION

The objective of this project is to achieve high-performance TE devices based on low-cost silicide materials that are earth-abundant, yet hold promise for achieving a ZT value comparable to or higher than state-of-the-art TEs over the temperature range from 300 K to 800 K. Based on this research team's prior research results, complex doping and nanostructuring are promising strategies to improve the TE performance of bulk silicides. The project includes four thrusts on TE materials, thermal management, interfaces, and metrology.

APPROACH

Our approach is to develop nanostructured bulk silicide materials exhibiting reduced thermal conductivity by incorporating nanostructures into silicides or discreetly fabricating nanostructured silicides. We are also working on investigating chemical substitutions and doping to improve the thermoelectric power factor in bulk silicides. System and device level computations are used to provide guidance on approaches to maximize the hot-side temperature and enhance heat transfer to the TE devices. TE elements (n-type and p-type) are fabricated by multiple steps including ball milling and the spark plasma sintering (SPS) technique that gives high-density bulk materials whereas the nanostructures

remain. The TE devices are tested in similar conditions as those in vehicles and the results are used to validate the computation models.

RESULTS

HMS Materials

It is difficult to synthesize pure HMS phase without significant MnSi or Si impurities [1]. In order to overcome the difficulty, we have established a new synthetic method of CVT. HMS crystals are grown in a home-built apparatus using differing metal halides as transport agents, including CuCl₂, FeCl₂, MnCl₂, ZnCl₂, AlCl₃, SnCl₂, CrCl₂, MnI₂, and FeI₂. Of the transport agents studied, we were able to grow the largest and most pure crystals of HMS by using FeCl₂ and CuCl₂. Scanning electron microscopy/energy-dispersive spectroscopy, high-resolution transmission electron microscopy, microprobe, inductively coupled plasma, and synchrotron powder X-ray diffraction analysis all confirm these HMS crystals to be extremely pure with little MnSi impurity present, as shown in Figure 1. We verified the anisotropic properties of HMS as measured along the different orientations (Figure 1). We also find that these crystals exhibit anomalous Hall effect at low magnetic fields (<2,000 Oe) from 20–400 K. A large collection of single crystals were sintered into a hard pellet by using SPS. The TE properties of the pellet were compared with regular samples containing MnSi impurity prepared via a conventional method. We have found that the elimination of the MnSi impurities have very little effect on the TE properties (Figure 1).

We demonstrated that Si NWs can be successfully converted to HMS NWs by reacting Si NWs and Mn vapor. We have investigated the role of the sintering temperature, precursor, and Si substrate on the conversion. Reactions were carried out at 850–950°C for 45 min and X-ray diffraction of the products show that single phase of HMS was formed only at 950°C or higher temperatures (Figure 2). Similarly, we have found that the precursor mass is a critical factor for growing HMS NWs. As the mass of precursor is over 15 mg, impurity MnSi and Mn₃Si₂ phases appeared. The in situ heating experiments by using a synchrotron source revealed that around 750°C, HMS and MnSi started to form. After annealing at 950°C for 45 min, MnSi and HMS were still observed, suggesting that excess Si from the silicon substrate is crucial in the formation of pure HMS.

We have investigated the effects of Al and (Al,Ge) doping on TE properties of polycrystalline HMS samples. The samples were prepared by solid-state reaction, ball milling, and followed by SPS. As shown in Figure 3, the Al doping effectively increases the hole concentration [2],

that leads to an increase in the electrical conductivity and power factor. By introducing the second dopant Ge into Al-doped HMS, the electrical conductivity is increased, and the Seebeck coefficient is decreased as a result of further increased hole concentration. The peak power factor is found to occur at a hole concentration between 1.8×10²¹ and 2.2×10²¹ cm⁻³ measured at room temperature. The (Al,Ge)-doped HMS samples show lower power factors owing to their higher hole concentrations. The maximum ZT of (Al,Ge)-doped HMS is 0.57 at 823 K, which is similar to the highest value found in the Al-doped HMS samples and about 25% higher than that of undoped HMS. The ZT values were reduced in the Mn(Al_{0.0035}Ge_ySi_{0.9965-y})_{1.8} samples with high Ge concentration of y = 0.025 and 0.035, because of reduced power factor.

Mg₂Si-Based N-Type Materials

In the Mg₂Si-based TE materials, the power factor at high temperatures could be further enhanced if the bipolar effect can be suppressed. We have attempted to increase the band gap by substituting Sn with Ge in Mg₂Si_{0.4}Sn_{0.6}. In this study, the carrier concentration of the Mg₂Si_{0.4}Sn_{0.6-y}Ge_y (y=0, 0.2, 0.4) solid solutions is controlled to be about (2.4±0.2)×10²⁰ cm⁻³ as confirmed by the Hall measurement. As shown in Figure 4(a), the thermopower decreases with increasing Ge substitution, which is accompanied by an increased electrical conductivity, Figure 4(b). In addition, the thermopower of Mg₂Si_{0.4}Sn_{0.6} appears to reach a maximum at 800 K while those of Mg₂Si_{0.4}Sn_{0.4}Ge_{0.2} and Mg₂Si_{0.4}Sn_{0.2}Ge_{0.4} continue to increase at higher temperatures. One possible cause of this difference is that the bipolar effect has been suppressed by substituting Sn with Ge in Mg₂Si_{0.4}Sn_{0.6}. The result suggests the possibility to obtain a higher power factor in Mg₂Si_{0.4}Sn_{0.4}Ge_{0.2} at temperature above 800 K. In addition, the Mg₂Si-based TE materials deteriorate quickly at high temperatures even in the inert atmosphere. This issue is a major hurdle for the application of these materials for vehicle waste heat recovery. In order to improve chemical stability, we have coated a thin oxide layer on the surface of pellets of Mg₂Si and Ge-substituted Mg₂Si. The oxide forms a dense, airtight protection layer on the surface of Mg₂Si, which effectively protects the Mg₂Si samples and eliminates the degradation at high temperatures.

Thermoelectric Device Design, Fabrication, and Testing

Two different TE devices, the 1st and 2nd generation, each composed of a pair of TE legs, were fabricated for the purpose of model validation and electrical contact resistance measurement (Figure 5). For both the 1st and 2nd generation TE devices, the TE legs were fabricated by

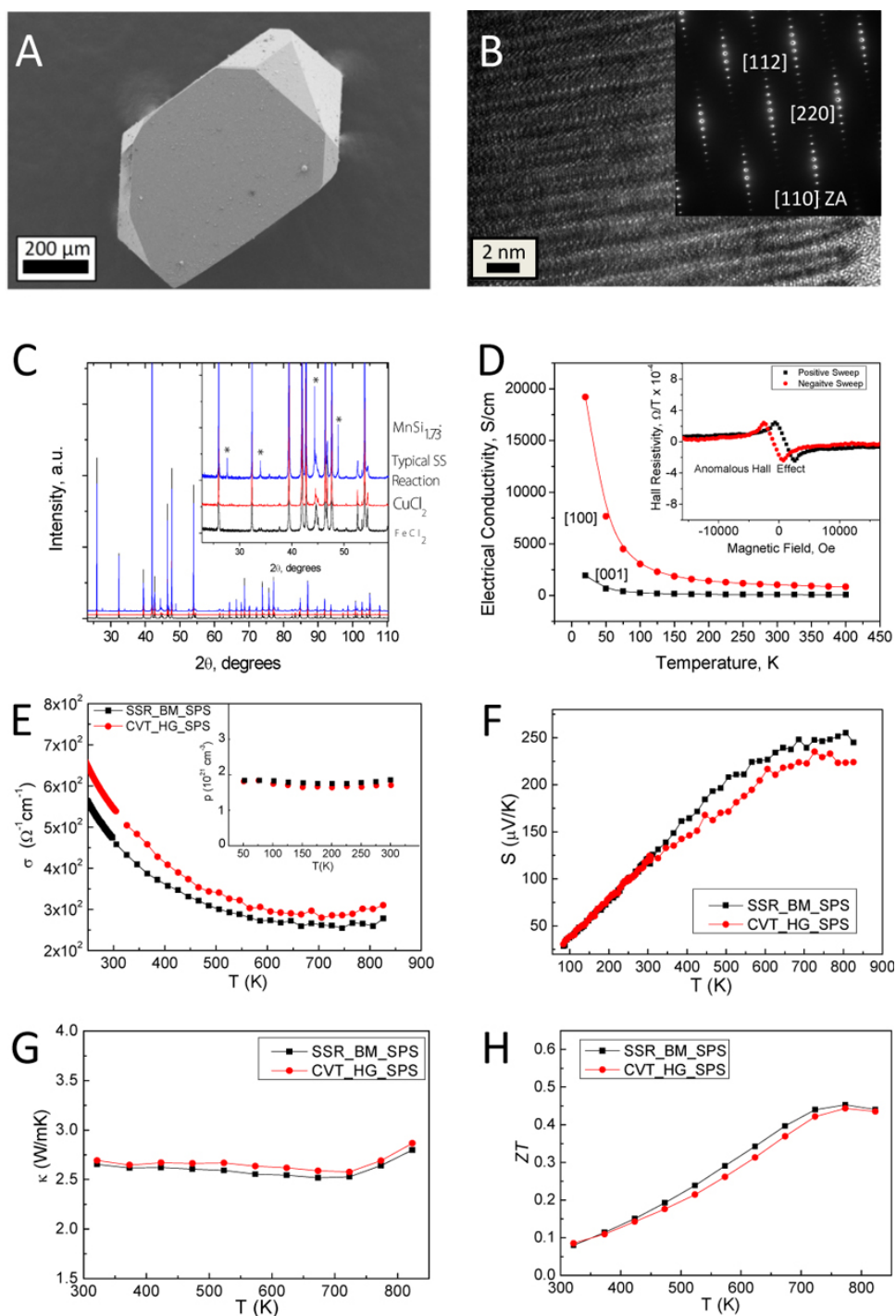


FIGURE 1. (a) Representative scanning electron microscope image of a crystal synthesized by CVT, (b) High-resolution transmission electron microscopy and selected area (electron) diffraction (inset) showing characteristic HMS superstructure along the [110] zone axis, (c) high-resolution powder X-ray diffraction data showing the extremely high purity of the CVT crystals by the lack of MnSi impurities indicated by asterisks, (d) measured electrical conductivity of a CVT crystal along the anisotropic [100] and [001] directions (inset shows the indication of the anomalous Hall effect). (e)–(h) Electrical conductivity, Seebeck coefficient, thermal conductivity, and ZT of SPSed CVT sample are directly compared to a sample with MnSi impurities present. Despite a slight difference in carrier concentration, the samples have virtually identical thermoelectric properties.

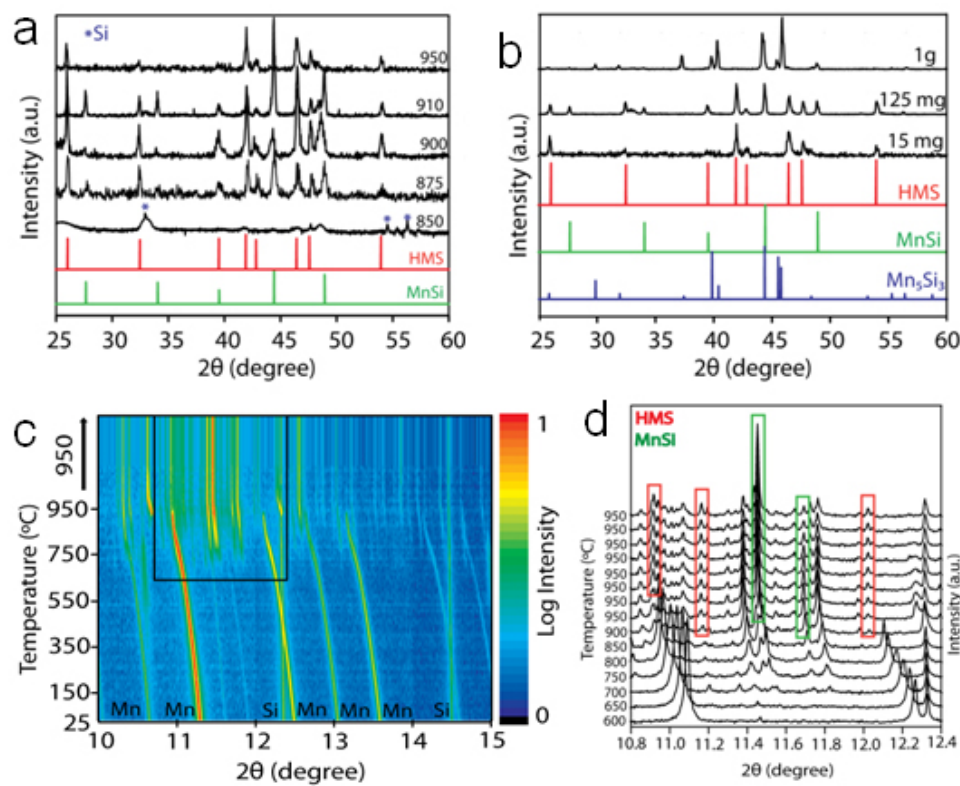


FIGURE 2. (a) Powder X-ray diffraction patterns of NW arrays converted at 850, 875, 900, 910, and 950°C,
(b) Powder X-ray diffraction patterns of converted NW arrays made with 15, 125, and 1,000 mg of Mn precursor,
(c) In situ high-resolution powder X-ray diffraction contour plots showing the silicidation process of Si NW,
(d) selected high-resolution powder X-ray diffraction patterns in the region highlighted in (c) showing the emergence of MnSi and HMS during the heating process.

the SPS. The 1st generation TE device was constructed using a one step SPS process. This TE device was then assembled by bonding copper interconnects directly to the TE elements by using a commercial silver paste with high thermal and electrical conductivity. An improved 2nd generation TE device was constructed using a two-step SPS process. First, the p-type and the n-type solid TE element samples were prepared using SPS. In the second step, thin copper electrodes (~1-mm thickness) were bonded to the TE elements directly by using a secondary SPS process. A test rig was designed and constructed with a heating and a cooling element. Power output from the device for a range of temperature differences was measured. The results were used to correlate to the results obtained from the numerical model. The electrical contact resistance for the 1st generation TE device was found to be 2.568 ohms, while the 2nd generation TE device showed a largely improved contact resistance of 0.0148 ohms only.

CONCLUSIONS

- Synthesis of the HMS without MnSi impurities by CVT has been demonstrated. Measurements on the pellet were compared with the regular HMS samples. This comparison indicates that the existence of MnSi phase has a negligible effect on the TE properties.
- The peak power factor of HMS was found to occur at a hole concentration in the range of $1.8\text{--}2.2 \times 10^{21} \text{ cm}^{-3}$. The maximum ZT of (Al,Ge)-doped HMS is 0.57 at 823 K, which is about the 25% higher than that of undoped HMS.
- The Ge substitution in $\text{Mg}_2\text{Si}_{0.4}\text{Sn}_{0.6}$ was found to increase the band gap. As a result, the bipolar effect is suppressed, which leads to a slightly higher power factor at $T > 800$ K. Coating a thin layer of Al_2O_3 on the surface of Mg₂Si based TE pellets significantly improves the chemical stability for the application at high temperatures.
- Numerical model for the TE device was validated for steady state performance and electrical contact

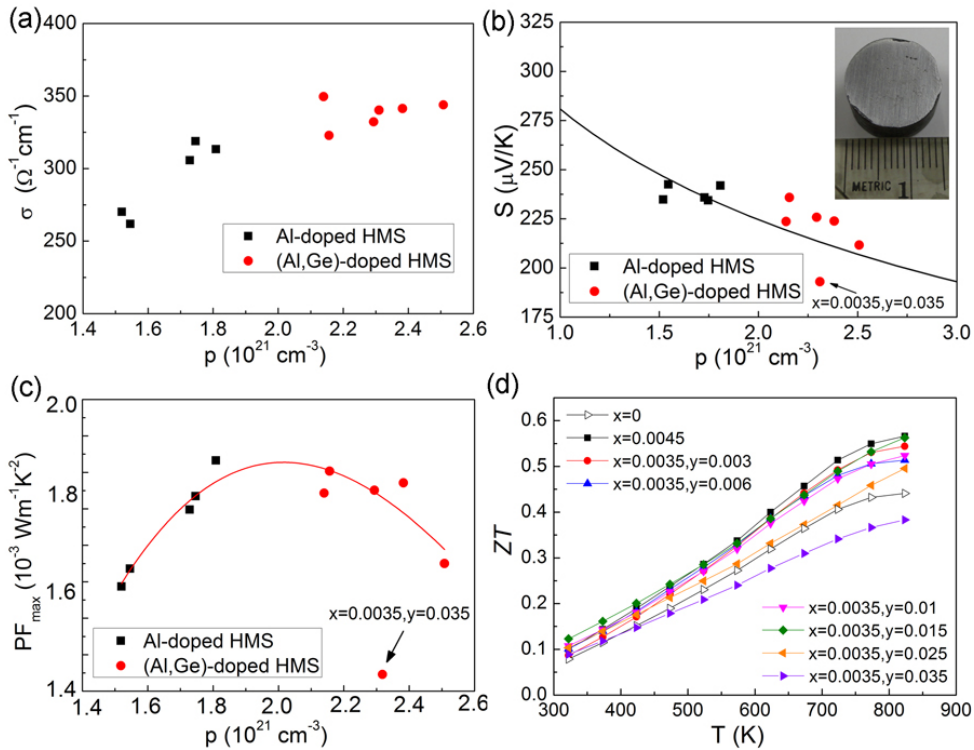


FIGURE 3. (a) Electrical conductivity at 800 K, (b) Seebeck coefficient at 800 K, and (c) Peak power factor as a function of the hole concentration at room temperature in $\text{Mn}(\text{Al}_x\text{Si}_{1-x})_{1.8}$ and $\text{Mn}(\text{Al}_{0.0035}\text{Ge}_y\text{Si}_{0.9965-y})_{1.8}$, (d) ZT values of $\text{Mn}(\text{Al}_x\text{Si}_{1-x})_{1.8}$ and $\text{Mn}(\text{Al}_{0.0035}\text{Ge}_y\text{Si}_{0.9965-y})_{1.8}$. Inset of (b) is a photograph of a 15-mm diameter, 8-mm thick disc made by SPS.

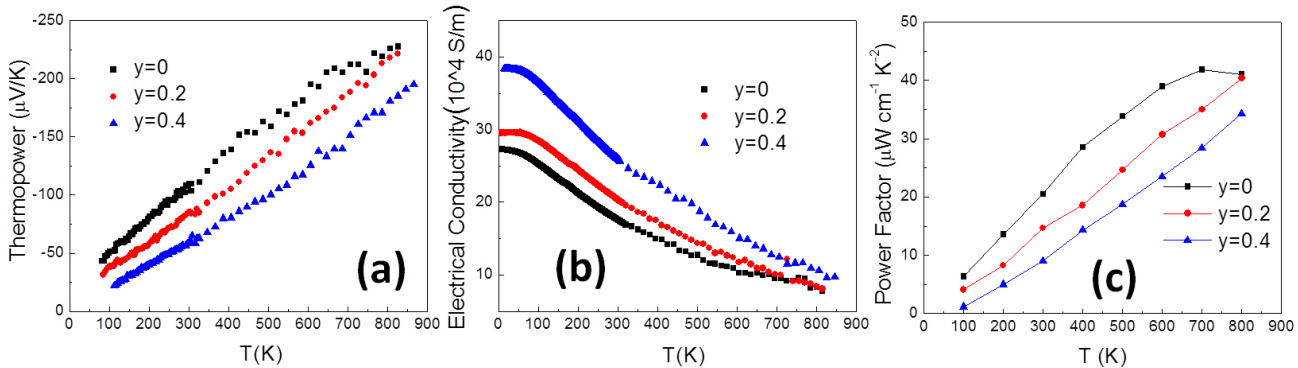


FIGURE 4. (a) Thermopower, (b) Electrical conductivity, and (c) Power factor of $\text{Mg}_2\text{Si}_{0.4}\text{Sn}_{0.6-y}\text{Ge}_y$ ($y=0, 0.2, 0.4$) solid solutions with carrier concentration of $(2.4 \pm 0.2) \times 10^{20} \text{ cm}^{-3}$.

resistance was measured and incorporated into the model.

- Two generations of silicide TE devices have been fabricated and tested. The results have been compared with the numerical models.

REFERENCES

- I. Kawasumi, M. Sakata, I. Nishida, and K. Masumoto, J. Mater. Sci. **16** (2), 355 (1981).
- W.H. Luo, H. Li, F. Fu, W. Hao, and X.F. Tang, J. Electron. Mater. **40** (5), 1233 (2011).

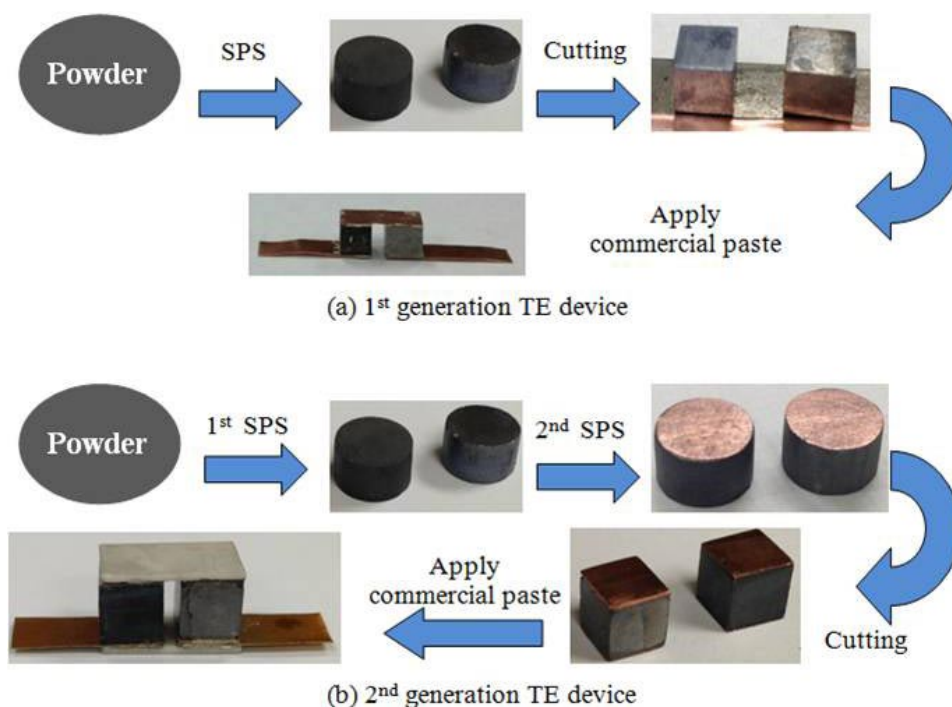


FIGURE 5. Fabrication of 1st and 2nd generation TE devices using SPS.

FY 2013 PUBLICATIONS/PRESENTATIONS

1. Ankit Pokhrel, Zachary Degregorio, Jeremy Higgins, Steven Girard, and Song Jin, *Vapor Phase Conversion Synthesis of Higher Manganese Silicide ($MnSi_{1.73}$) Nanowire Arrays for Thermoelectric Applications*, Chem. Mater. **2013**, 25 (4), pp 632–638.
2. Xi Chen, Annie Weathers, Daniel Salta, Libin Zhang, Jianshi Zhou, John B. Goodenough, Li Shi, *Effects of (Al,Ge) double doping on the thermoelectric properties of higher manganese silicides*, J. Appl. Phys., 2013, 114 173705.

3. “Nanostructured $MnSi_{1.73}$ Thermoelectric Composites Prepared by Matrix Encapsulation.” Steven Girard, oral presentation. Materials Research Society Symposium H, San Francisco, CA, April 2013.
4. “High Purity Crystals of Higher Manganese Silicides Grown by Chemical Vapor Transport.” Steven Girard, Poster presentation. Materials Research Society Symposium H, San Francisco, CA, April 2013.

V.14 Thermoelectric HVAC and Thermal Comfort Enablers for Light-Duty Vehicle Applications

Clay Maranville

Research & Advanced Engineering
Ford Motor Company
MD 3182/RIC Building
P.O. Box 2053
Dearborn, MI 48121-2053

DOE Technology Development Manager:
Gurpreet Singh

NETL Project Manager: Carl Maronde

Subcontractors:

- Halla-Visteon Climate Control Corporation, Van Buren Township, MI
- Gentherm Corporation, Northville, MI
- National Renewable Energy Laboratory, Golden, CO

Overall Objectives

- Develop a thermoelectric (TE) heating, ventilation, and air conditioning (HVAC) system to optimize occupant comfort and reduce fuel consumption
- Reduce energy required to operate the air conditioning compressor by one-third
- Demonstrate TE devices that achieve a coefficient of performance in cooling of better than 1.3 and a coefficient of performance in heating of better than 2.3
- Demonstrate the technical feasibility of a TE HVAC system for light-duty vehicles
- Develop a commercialization pathway for a TE HVAC system
- Integrate, test, and deliver a 5-passenger TE HVAC demonstration vehicle

Fiscal Year (FY) 2013 Objectives

- Complete fabrication and bench testing of zonal TE HVAC subsystems
- Conduct ancillary load analysis study to assess benefit of complimentary technology
- Complete commercialization and systems cost assessment studies
- Assess benefits and future research needs for TE materials and devices

- Integrate prototype TE HVAC system into demonstration vehicle and calibrate controls
- Complete system performance testing to determine reduction in air conditioning compressor and climate system energy consumption
- Finalize TE HVAC testing to assess occupant thermal comfort response compared to baseline test results
- Complete vehicle preparations to enable technology demonstrations at California Energy Commission and DOE performance sites

FY 2013 Accomplishments

- Completed all zonal TE HVAC system fabrication and bench testing.
- Completed TE HVAC system installation into Lincoln MKZ hybrid electric vehicle (HEV) demonstration vehicle.
- Completed ancillary loads analysis that indicated directions for future research to further reduce climate-control energy consumption.
- Completed zonal HVAC system calibration in preparation for wind tunnel confirmatory testing.
- Demonstrated a 33% reduction in air conditioning compressor power consumption in vehicle wind tunnel testing.
- Achieved equivalent occupant thermal comfort response, compared with baseline system performance, while delivering an annualized 12% reduction in climate system energy usage in vehicle wind tunnel testing.
- Demonstrated TE device coefficient of performance (COP) = 2.3 at 13.6°C temperature rise in heating mode and COP = 1.3 at 17.9°C temperature drop in cooling mode during calorimeter testing.
- Completed commercialization assessments that showed TE heated/cooled seats can be integrated into vehicle climate system designs to improve overall system efficiency. Specific cost and performance barriers were identified to address further market penetration.

Future Directions

- No additional work is planned for this project. Project completion is scheduled for November 2013.

- Additional (not funded) work, as an extension of this project's findings, may focus on development of TE materials that reduce tellurium usage, refining thermal comfort models for transient and asymmetric environments, studying methods to improve zonal controls for vehicle climate systems, or optimizing vehicle thermal environment.



INTRODUCTION

Current light-duty vehicles provide passenger thermal comfort primarily through the use of a centralized heating, ventilation, and air conditioning unit that distributes conditioned air to vent locations throughout the vehicle. Powertrain energy is used to generate hot or cold working fluids that are subsequently used to condition the entire cabin and certain surrounding structures. Because of this, the majority of the power expended by today's automotive HVAC systems does not directly contribute to occupant thermal comfort. This is an important consideration for overall vehicle efficiency, since the energy available to provide occupant comfort is becoming a larger fraction of the total energy budget in a vehicle. The climate energy usage is particularly significant for advanced technology powertrains, including HEVs and battery electric vehicles.

The zonal climate system design of this project, enabled by small TE heater/coolers, can target the conditioning of individual vehicle occupants. The project has progressed by developing new thermal comfort metrics and tools, studying and optimizing system design topologies for zonal cabin conditioning, and by conducting targeted research into methods to reduce the cost and commercialization barriers to introduction of TE devices.

APPROACH

A phased approach was used to quantify anticipated benefits through detailed design and modeling prior to building and testing subsystems. The first phase of the project progressed through the initiation of a system architecture study, modeling to predict fuel efficiency, and occupant thermal comfort modeling for baseline and distributed system options. Design requirements were developed to provide a starting point for detailed hardware design and build activities. Research efforts into more efficient TE materials and the design of liquid-to-air TE devices for distributed heating and cooling were refined and optimized. This design work and establishment of test metrics and methods were critical to setting guidelines that the team used to develop, design,

build, and validate the performance of the TE HVAC system.

In the second phase, key subsystems, including TE modules, the means for distribution of hot and cold working fluids, power management, and system controls, were modeled, designed, built, and tested. Engineering and systems specifications were developed to guide hardware design. The team also conducted a business cost analysis to understand barriers to commercialization. Work was conducted using advanced multi-domain computer-aided engineering (CAE) and thermal comfort models to perform CAE modeling of the TE HVAC architecture in both a test chamber environment and in the vehicle, and to develop recommendations for next-generation thermal comfort tools to assess transient spot conditioning of vehicle occupants. Finally, a significant amount of the project research into advanced TE materials was conducted.

In the third phase of the project, TE device characterization was conducted, and hardware prototypes for integration into the target vehicle were designed and fabricated. The vehicle-intent hardware prototypes were tested and results compared to initial prototypes to assist predictions of in-vehicle performance. Advanced TE p- and n-type materials were tested at the research device couple-level. The subsystem-level hardware was evaluated on a bench test stand to validate model-based performance predictions. A business cost analysis was conducted using low- and high-content assumptions.

In the final phase, the subsystem hardware fabrication was completed and the subsystems were packaged into the test vehicle. System tests, based on the developed test conditions, were performed to quantify system benefits and performance compared to the baseline system. Climactic wind tunnel tests were conducted to evaluate the performance of the TE HVAC system in a full range of operating conditions. Technical results and energy savings analysis were completed from this testing. Commercialization issues and future research focus areas were identified. Finally, the prototype vehicle was prepared for demonstration at California Energy Commission and DOE test sites.

RESULTS

1. Zonal TE HVAC System Integrated Successfully into Test Vehicle

The zonal TE HVAC components and subsystems were installed into the test vehicle, a 2011 Lincoln MKZ HEV. This required removal and modification of several base vehicle components to allow for installation of the new system. In addition, the installation of ~175 sensors and a full data acquisition system was

completed. Finally, the zonal TE HVAC systems and interior trim modifications were installed. The function and operation of the new HVAC system and its control system were verified. Calibration of all sensor channels was completed. Once the base system modifications were completed and the sensors were installed and validated, the installation of the zonal TE system components began. This required installation of several subsystems: an independent coolant loop for the TE subsystems; overhead ventilation and registers, auxiliary thermoelectric devices, blowers, and air-intake system; a set of liquid-to-air heated and cooled TE seats at four seating positions; power converters and regulation boards; hardware controls, relays, and wiring; a central control computer and remote network with dedicated software for controls and data logging; a power inverter, auxiliary battery, and 110-V alternating current power network. Once installation of the system was completed, over 100 hours of wind-tunnel and on-road tests were conducted in order to develop calibration routines to control the TE devices in unison with the central HVAC system. A photo of the control, data acquisition, and blower systems installed in the vehicle trunk is shown in Figure 1.

2. TE Device Efficiency Meets Project Objectives

A TE device, built in the same batch as the units installed into the test vehicle, was evaluated on a custom-designed calorimeter to assess its heating and cooling performance. The device weighed 1.85 kg. It had an overall length of 350 mm, width of 110 mm, and height of 49 mm. It contained approximately 600 TE pellets. A photograph of the tested device is shown in Figure 2. The TE HVAC device efficiency targets required a minimum COP of 1.3 in cooling mode and 2.3 in heating mode. The efficiency was calculated by measuring the air-side heat gain or loss in the device ($Q=m\times C_p \times \Delta T$) and dividing by input power to the device. The target COP was achieved during calorimetric testing of the TE modules, with a



FIGURE 1. Data Acquisition System, TE System Controls, and TE Devices Packaged into the Trunk of the Test Vehicle

temperature drop of 13.6°C measured in cooling mode and a temperature rise of 17.9°C measured in heating mode. Results of cooling performance measurements are shown in Figure 3. Results of heating performance measurements are shown in Figure 4.

3. Cost and Commercialization Analysis Shows TE System Potential

Trade studies were used to assess the component and investment cost impact of implementing zonal TE HVAC systems in a vehicle, and also to establish steps required for commercialization of the technology. Cost studies indicated a significant on-cost to incorporate a full zonal TE system. The commercialization assessment completed in Phase 4 suggested that TE heated/cooled seats and zonal climate system remain viable technologies to pursue in commercial application, but there continue to be significant issues around device performance capabilities and TE material costs.

Potential performance improvement and cost reduction actions that could help enable the further commercialization of TE HVAC devices were identified, including targeted utilization of TE devices, improved heat exchanger performance, and improvements in thermal interface resistances. Additionally, areas of interest for future research were identified, including efforts to substantially reduce or eliminate tellurium from TE materials operating in the mid-temperature range, efforts to improve TE material metallization methods, and efforts to improve TE element joining techniques to help reduce thermal contact resistance. All of these concepts could enable higher-performance and lower-cost TE HVAC devices in the future.

To improve the economic viability of TE devices for automotive applications, both the cost structure and power density of the designs were identified as needing improvement. Improvements in cost were considered achievable through traditional means of finding lower-cost design options that deliver equal performance or by finding design options that may have no cost advantage per unit measure, but improve performance by reducing the cost per watt of thermal output (\$/Q). For reference, the TE device developed for this project had a cost per watt of thermal output 5-10 times higher than the cost



FIGURE 2. TE Device Used in Zonal HVAC System

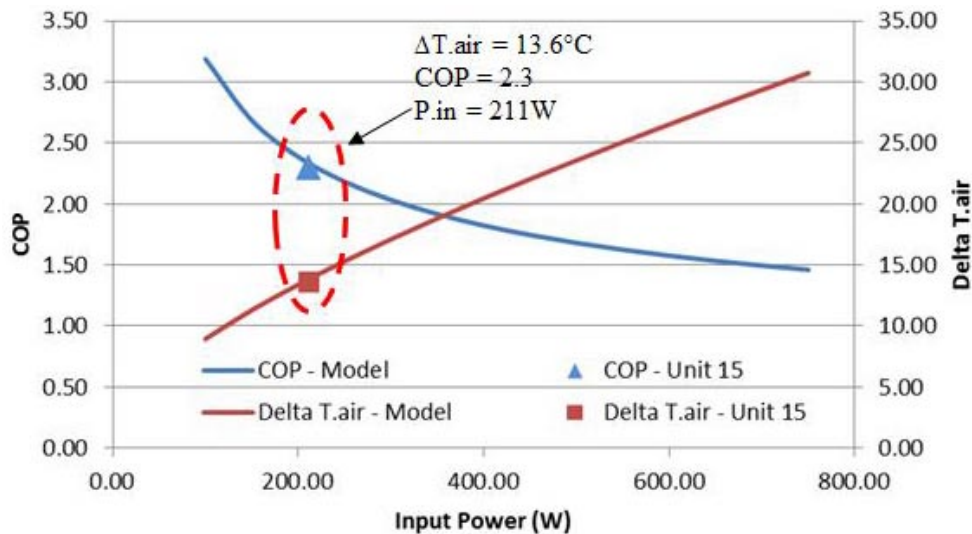


FIGURE 3. Calorimeter Performance and Efficiency of TE Device in Cooling Mode

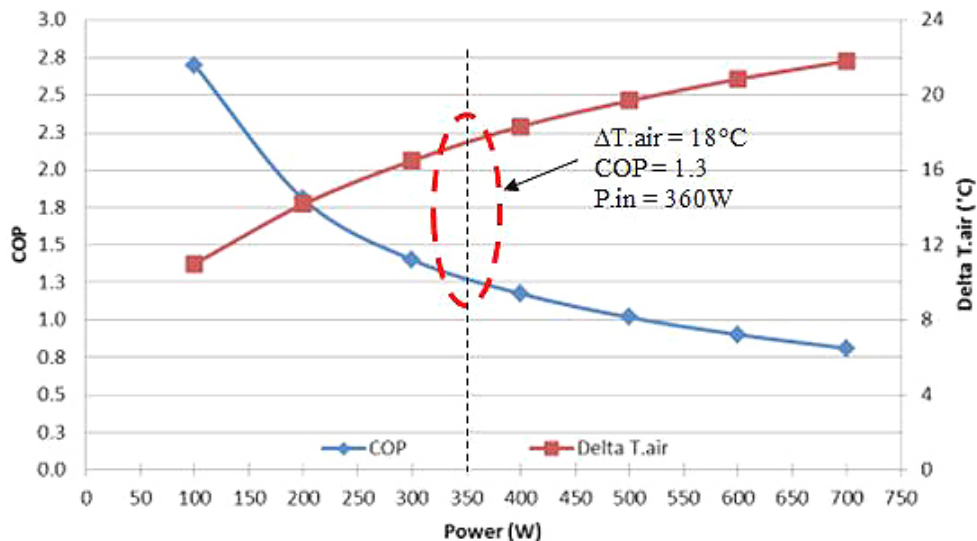


FIGURE 4. Calorimeter Performance and Efficiency of TE Device in Heating Mode

per watt of thermal output from a vapor compression air conditioning system. The wide range in the TE device's \$/Q ratio was due to the heating or cooling output dependence on the operating point. For example, in Figure 5, it can be seen that the cost/watt ratio generally tracks the COP.

4. TE HVAC System Shows Reduced Energy Consumption Compared with Baseline Vehicle Testing while Achieving Equivalent Occupant Thermal Comfort

Vehicle energy usage test methods were established to assess the energy consumption from the zonal

TE HVAC system, as well as for determining the energy consumption reduction of the air conditioning compressor. Results of testing showed that delivering targeted heating and cooling to the occupants via zonal TE devices in the headliner and seats, while reducing the cooling and heating from the central HVAC unit, could provide equivalent occupant comfort response from vehicle occupants. Results of zonal energy consumption testing compared to baseline system testing are shown in Figure 6, which indicate a 12% energy reduction overall.

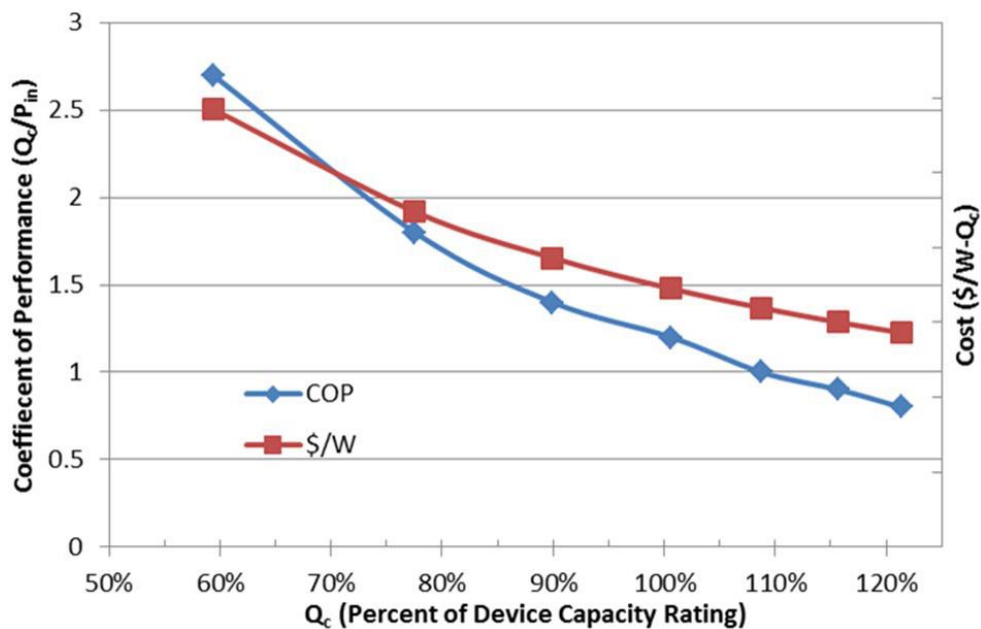


FIGURE 5. Correlation between Cost and Thermal Capacity of TE Devices for Heating and Cooling

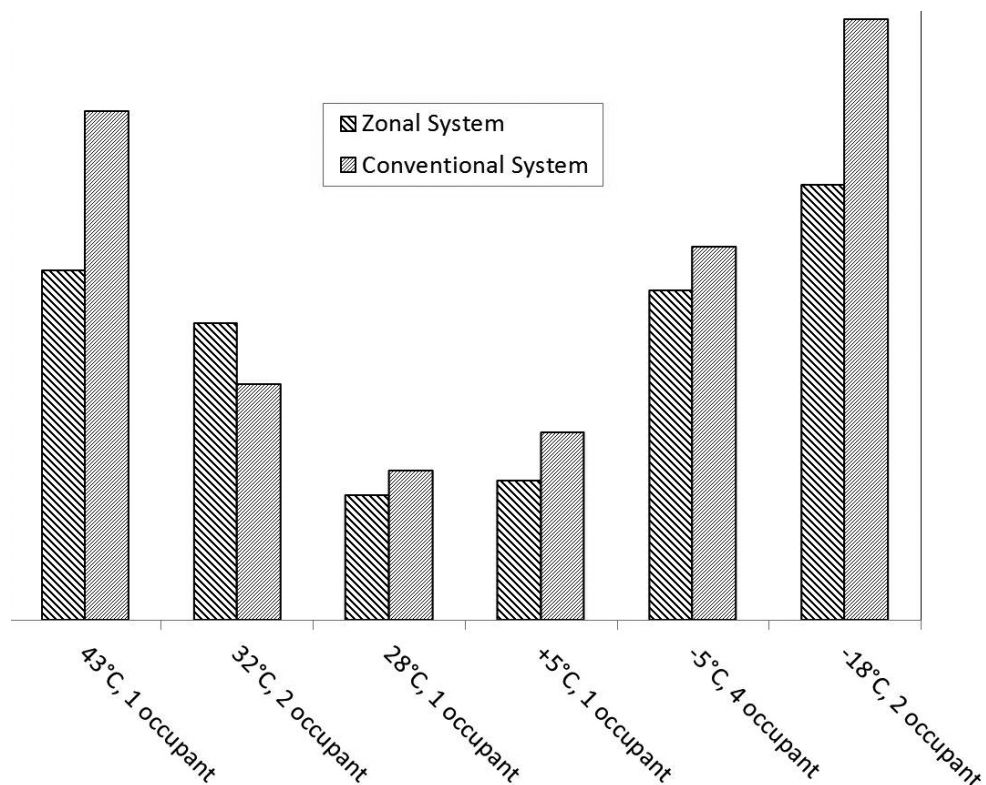


FIGURE 6. Relative Energy Consumption of HVAC System Measured during Wind Tunnel Evaluations

CONCLUSIONS

- Zonal HVAC system successfully packaged into test vehicle
- TE devices met project objectives of COP > 1.3 in cooling and COP > 2.3 in heating
- HVAC system annualized energy consumption was reduced by 12% compared to baseline vehicle
- Cost of TE devices tracks closely with performance and capacity requirements

FY 2013 PUBLICATIONS/PRESENTATIONS

1. C.W. Maranville, et al., "Improving the Efficiency of a Vehicle HVAC System with Comfort Modeling, Zonal Design, and Thermoelectric Devices", Proceedings of the 2012 DEER Conference, Dearborn, MI, October 18, 2012.
2. J.G. Gebbie & C.W. Maranville, "Zonal Climate System Test Conditions for Passenger Vehicles", Paper #12TMSS-0051, presented at the 2012 SAE TMSS Conference, Scottsdale, AZ, October 31, 2012.
3. C.W. Maranville, "Thermoelectric HVAC and Thermal Comfort Enablers for Light-Duty Vehicle Applications", presented at the 2013 DOE Merit Review Conference, Crystal City, VA, May 17, 2013.

VI. Acronyms, Abbreviations, and Definitions

| | | | |
|--------------|---|------------------|--|
| η_g | Gross indicated thermal efficiency | ASME | American Society of Mechanical Engineers |
| γ | Ratio of specific heats (c_p/c_v) | atdc, ATDC, aTDC | After top-dead center |
| κ | Thermal conductivity | atm | Atmosphere |
| λ | Stoichiometric ratio; air/fuel equivalence ratio | a.u. | Arbitrary units |
| ϕ | Fuel/air equivalence ratio | Au | Gold |
| σ | Electrical conductivity | Avg. | Average |
| μs | Micro-second | B | Boron |
| $^{\circ}C$ | Degrees Celsius | B10 | Blend of 10% biodiesel and 90% diesel fuel |
| $^{\circ}CA$ | Degrees crank angle, 0° = TDC | Ba | Barium |
| $^{\circ}F$ | Degrees Fahrenheit | $BaAl_2O_4$ | Barium aluminate |
| ΔP | Pressure change | $Ba(NO_3)_2$ | Barium nitrate |
| ΔT | Delta (change in) temperature | BaO | Barium oxide |
| 0-D | Zero-dimensional | bar | unit of pressure (14.5 psi or 100 kPa) |
| 1-D, 1D | One-dimensional | BBDC | Before bottom-dead center |
| 2-D, 2D | Two-dimensional | BDC | Bottom-dead center |
| 3-D, 3D | Three-dimensional | BES | Basic Energy Sciences |
| T_{90} | 90% volume recovered temperature | BET | Named after Brunauer, Emmett and Teller, this method for determining the surface area of a solid involves monitoring the adsorption of nitrogen gas onto the solid at low temperature and, from the isotherm generated, deriving the volume of gas required to form one monolayer adsorbed on the surface. This volume, which corresponds to a known number of moles of gas, is converted into a surface area though knowledge of area occupied by each molecule of adsorbate. |
| ABDC | After bottom-dead center | BFV | Bradley Fighting Vehicle |
| AC | Alternating current | bhp-hr | Brake horsepower hour |
| AC, A/C | Air conditioning | BiTe | Bismuth telluride |
| ACC | Automatic climate control | BMEP | Brake mean effective pressure |
| ACCESS | Advanced Combustion Controls—Enabling Systems and Solutions | Bsfc, BSFC | Brake specific fuel consumption |
| ACE | Advanced Combustion Engine | bsNOx, BSNOx | Brake specific NOx emissions |
| ACEC | Advanced Combustion and Emissions Control | BTDC, btdc | Before top-dead center |
| ACES | Advanced Collaborative Emissions Study | BTE | Brake thermal efficiency; Boltzmann transport equation |
| A/F, AFR | Air/fuel ratio | C_2H_4 | Ethene |
| Ag | Silver | C_2H_6 | Ethane |
| AGM | Absorbed glass mat | C_3H_6 | Propylene |
| AHR | Apparent heat release | ca. | About, approximately |
| AHRR | Apparent heat release rate | CA | Crank angle |
| a.k.a. | Also known as | | |
| AKI | Anti-knock index | | |
| Al | Aluminum | | |
| Al_2O_3 | Aluminum oxide | | |
| ALE | Arbitrary Lagrangian-Eulerian | | |
| ANL | Argonne National Laboratory | | |
| ANR | NH_3/NOx ratio | | |
| API | American Petroleum Institute | | |
| APS | Atmospheric plasma spray | | |
| APU | Auxiliary power unit | | |
| ASC | Ammonia slip catalyst | | |
| ASI | After start of injection | | |

VI. Acronyms, Abbreviations, and Definitions

| | | | |
|------------------|--|--------|---|
| CA10 | Crank angle at which 10% of the combustion heat release has occurred | CT | Computed tomography |
| CA50 | Crank angle at which 50% of the combustion heat release has occurred | CTC | Cummins Technical Center |
| CAC | Charge air cooler | CTE | Coefficient of thermal expansion |
| CAD | Crank angle degrees, computer-aided design | Cu | Copper |
| CAE | Computer-aided engineering | Cu-CTA | Copper chabazite zeolite |
| cc | Cubic centimeter | CVD | Chemical vapor deposition |
| CCD | Charge-coupled device | CVT | Chemical vapor transport |
| CDC | Conventional diesel combustion | DADS | Direct ammonia delivery system |
| CDI | Compression direct injection | DBI | Diffused back-illumination |
| CDPF | Catalyzed diesel particulate filter | DC, dc | Direct current; dynamic capacity |
| Ce | Cerium | DCN | Derived cetane number |
| CeO ₂ | Cerium oxide | dCSC™ | diesel Cold Start Concept |
| CFD | Computational fluid dynamics | deg | Degrees |
| CF-E0 | Certification gasoline with zero ethanol | D-EGR™ | Dedicated exhaust gas recirculation |
| CH ₄ | Methane | DEIS | Directed Energy Ignition System |
| CHA | Chabazite zeolite | °CA | Degrees crank angle, 0° = TDC |
| CI | Compression ignition | ΔT | Delta (change in) temperature |
| CIDI | Compression ignition direct injection | DFT | Density function theory |
| CLC | Chemical looping combustion | DI | Direct injection, direct-injected |
| CLCC | Closed-loop combustion control | DMP | Diesel micro pilot |
| CLEERS | Cross-Cut Lean Exhaust Emissions | DOC | Diesel oxidation catalyst |
| | Reduction Simulations | DOE | U.S. Department of Energy |
| cm | Centimeter | DOHC | Double overhead camshaft |
| cm ³ | Cubic centimeters | dP | Differential pressure |
| CMOS | Complementary metal oxide semiconductor | DPF | Diesel particulate filter |
| CN | Cetane number | DRIFTS | Diffuse reflectance infrared Fourier-transform spectroscopy |
| CNG | Compressed natural gas | DSC | Differential scanning calorimeter |
| CNL | Combustion noise level | E10 | 10% ethanol, 90% gasoline fuel blend |
| CNT | Carbon nanotube | E15 | 15% ethanol, 85% gasoline fuel blend |
| CO | Carbon monoxide | E20 | 20% ethanol, 80% gasoline fuel blend |
| CO ₂ | Carbon dioxide | E85 | 85% ethanol, 15% gasoline fuel blend |
| COP | Coefficient of performance | EC | Elemental carbon |
| COV | Coefficient of variation (variance) | ECM | Electronic (engine) control module |
| cP | Centipoise | ECN | Engine Combustion Network |
| CPF | Catalyzed particulate filter | ECU | Electronic (engine) control unit |
| cpsi | Cells per square inch | EDS | Energy-dispersive spectroscopy |
| CPU | Central processing unit | EDX | Energy dispersive X-ray |
| Cr | Chromium | EELS | Electron energy loss spectroscopy |
| CR | Compression ratio | EERE | Energy Efficiency and Renewable Energy |
| CRADA | Cooperative Research and Development Agreement | EEVO | Early exhaust valve opening |
| CRC | Coordinating Research Council | EFA | Exhaust Filtration Analysis |
| CRF | Combustion Research Facility | EGR | Exhaust gas recirculation |
| CSI | Convergent Science, Inc. | EHN | Ethyl hexyl nitrate |
| | | EHT | Equivalent homogenous temperature |
| | | ELOC | Extended-lift-off combustion |
| | | EMPA | Electron microprobe analysis |
| | | EOI | End of injection |

| | | | |
|-------------------|---|-------------------------------|---|
| EPA | U.S. Environmental Protection Agency | H ₂ O | Water |
| EPR | Electron paramagnetic resonance | H ₂ O ₂ | Hydrogen peroxide |
| ERC | Engine Research Center | HAADF STEM | High angle annular dark field scanning transmission electron microscopy |
| ESL | ElectroScience Inc. | | |
| et al. | Et Alii: and others | | |
| EV | Exhaust valve | HC | Hydrocarbons |
| EVC | Exhaust valve closing | HCCI | Homogeneous Charge Compression |
| EVO | Exhaust valve opening | | Ignition |
| EVVT | Electrical variable valve timing | HD | Heavy-duty |
| EXAFS | Extended X-ray absorption fine structure | He | Helium |
| Fe | Iron | HECC | High Efficiency Clean Combustion |
| FE | Fuel economy | HEI | Health Effects Institute |
| FEA | Finite-element analysis | HEV | Hybrid electric vehicle |
| FEM | Finite-element method | HEX | Heat exchanger |
| FFVA | Fully flexible valve actuation | HFIR | High Flux Isotope Reactor |
| FID | Flame ionization detector | HHV | Higher heating value |
| FMEA | Failure mode and effects analysis | HIL | Hardware in the loop |
| FMEP, fmep | Friction mean effective pressure | hp | Horsepower |
| FPEG | Free-piston electric generator | HPC | High-performance computing |
| FSN | Filter smoke number | HPL | High pressure loop |
| FTIR | Fourier transform infrared | HPLB | High-pressure, lean-burn |
| ft-lb | Foot-pound | hr | Hour |
| FTP | Federal Test Procedure | HR | Heat release |
| FTP-75 | Federal Test Procedure for light-duty vehicles | HRR | Heat release rate |
| FY | Fiscal year | HRTEM | High-resolution transmission electron microscopy (microscope) |
| g, G | Gram | HVA | Hydraulic valve actuation |
| g/bhp-hr | Grams per brake horsepower-hour | HVAC | Heating, ventilation and air conditioning |
| GC | Gas chromatography | HWFET | Highway Fuel Economy Test |
| GC-FID | Gas chromatograph combined with a flame ionization detector | HWG | Hollow waveguide |
| GCI | Gasoline compression ignition | Hz | Hertz |
| GC-MS | Gas chromatography – mass spectrometry | IAO2 | Intake air oxygen |
| GDCI, GDICI | Gasoline direct-injection compression ignition | IARC | International Agency for Research on Cancer |
| GDI | Gasoline direct injection | IC | Internal combustion |
| Ge | Germanium | ICCD | Intensified charged-coupled device |
| g/hphr | Grams per horsepower-hour | ICE | Internal combustion engine |
| GHSV | Gas hourly space velocity | ID | Internal diameter |
| gIMEP | Gross indicated mean effective pressure | IE | Ion exchange |
| GM | General Motors | IMEP | Indicated mean-effective pressure |
| g/mi | Grams per mile | IMEP _g | Indicated mean effective pressure, gross |
| GPF | Gasoline particulate filter | IMEP _{net} | Indicated mean effective pressure, net |
| GPU | Graphical processing unit | IR | Infrared |
| GTDI | Gasoline turbocharged direct injection | ISFC | Indicated specific fuel consumption |
| GTI | Gas Technology Institute | ISX | Cummins Inc. 15-liter displacement, inline, 6-cylinder heavy duty diesel engine |
| H ₂ | Diatom (molecular) hydrogen | ITE | Indicated thermal efficiency |
| H ₂ CO | Formaldehyde | | |

VI. Acronyms, Abbreviations, and Definitions

| | | | |
|-------------------|--|-------------------------|--|
| ITHR | Intermediate temperature heat release | m^2/gm | Square meters per gram |
| IV | Intake valve | m^3 | Cubic meters |
| IVC | Intake valve closing | mA | Millamps |
| IVO | Intake valve opening | MAP | Manifold air pressure |
| J | Joule | mbar | Millibar |
| k | thousand | MBT | Minimum (spark advance) for best torque; |
| K | Kelvin, potassium | | Maximum brake torque |
| kg | Kilogram | MCE | Multi-cylinder engine |
| kHz | Kilohertz | MD | Medium-duty |
| KIVA | Combustion analysis software developed by Los Alamos National Laboratory | MER | Molar expansion ratio |
| KIVA-CMFZ | KIVA Coherent Flamelet Multi-Zone | Mg | Magnesium |
| kJ | Kilojoules | mg/cm^2 | Milligrams per square centimeter |
| kJ/L | Kilojoules per liter | mg/mi | Milligram per mile |
| kJ/m ³ | Kilojoules per cubic meter | mg/mm^2 | Micrograms per square millimeter |
| KLSA | Knock-limited spark advance | mg/scf | Milligrams per standard cubic foot |
| KMC | Kinetic Monte Carlo | mi | Mile |
| kPa | Kilopascal | μs | Micro-second |
| kW | Kilowatt | min | Minute |
| L | Liter | MIR | Mid-infrared |
| La | Lanthanum | MIT | Massachusetts Institute of Technology |
| LANL | Los Alamos National Laboratory | MPRR | Maximum pressure rate rise |
| lb ft | Pound foot | μm | Micrometer |
| lb/min | Pounds per minute | mm | Millimeter |
| lbs | Pounds | mmols | Micro-moles |
| lbs/sec | Pounds per second | Mn | Manganese |
| LD | Light-duty | Mo | Molybdenum |
| LDB | Lean Downsize Boost | mol | Mole |
| LDT | Light-duty truck | mol/s | Moles per second |
| LED | Light-emitting diode | MOR | Morpholine |
| LES | Large-eddy simulation | MOU | Memorandum of understanding |
| LHV | Lower heating value | MPa | Megapascals |
| LIF | Laser-induced fluorescence | mpg | Miles per gallon |
| LII | Laser-induced incandescence | mph | Miles per hour |
| LLNL | Lawrence Livermore National Laboratory | MPICH | Portable Implementation of MPI |
| LMO | LaMnO_3 | MPT | MAHLE Powertrain |
| LNT | Lean-NOx trap | ms | Millisecond |
| LOL | Lift-off length | MS | Mass spectrometry |
| LP | Low pressure | MSU | Michigan State University |
| LPL | Low-pressure loop | MTU | Michigan Technological University |
| LRRI | Lovelace Respiratory Research Institute | MWASP | Microwave-assisted spark plug |
| LSC | $\text{La}_{1-x}\text{Sr}_x\text{O}_{3-\delta}$ | MZ | Multizone |
| LSCO | $(\text{La},\text{Sr})\text{CoO}_3$ | N_2 | Diatomeric nitrogen |
| LSMO | $(\text{La},\text{Sr})\text{MnO}_3$ | N_2O | Nitrous oxide |
| LTC | Low-temperature combustion | N_2O_3 | Nitrogen trioxide |
| LTGC | Low-Temperature Gasoline Combustion | Na | Sodium |
| LTJT | Low-temperature joining technique | NA | Naturally aspirated |
| m^2 | Square meters | NETL | National Energy Technology Laboratory |
| | | NH_3 | Ammonia |

| | | | |
|-----------------------------------|---|-------------------|---|
| NL | Natural luminosity | PMP | Particle Measurement Program |
| nm | Nanometer | PNA | Passive NOx adsorber |
| Nm | Newton meter | PNNL | Pacific Northwest National Laboratory |
| NMEP | Net mean effective pressure | ppb | Parts per billion |
| NMHC | Non-methane hydrocarbon | PPC | Partially premixed combustion |
| NMOG | Non-methane organic gases | PPCI | Partially premixed compression ignition |
| NO | Nitric oxide | ppi | Pores per square inch |
| NO ₂ | Nitrogen dioxide | ppm | Parts per million |
| NO _x , NO _x | Oxides of nitrogen | PRF | Primary reference fuel |
| NRE | NOx reduction efficiency | PRF80 | PRF mixture with an octane number of 80 (i.e., 80% iso-octane and 20% n-heptane) |
| ns | Nanosecond | PRR | Pressure rise rate |
| NSC | NOx storage capacity | PSAT | Powertrain Systems Analysis Toolkit |
| NSR | NOx storage and reduction | psi | Pounds per square inch |
| NTC | Negative temperature coefficient | psig | Pounds per square inch gauge |
| NTE | Negative thermal expansion | Pt | Platinum |
| NVH | Noise, vibration, and harshness | PTO | PbTiO ₃ |
| NVO | Negative valve overlap | PV, P-V | Pressure-volume |
| NW | Nanowire | PVA | Polyvinyl alcohol |
| O ₂ | Diatom (molecular) oxygen | PVP | Polyvinylpyrrolidone |
| O ₃ | Ozone | PVT | Pressure-volume-temperature |
| OBD | On-board diagnostics | Q | Heat |
| OC | Organic carbon | Q1, Q2, Q3, Q4 | First, second, third and fourth quarters |
| OCC | Output covariance constraint | R&D | Research and development |
| OD | Outside diameter | RANS | Reynolds Averaged Navier-Stokes |
| ODE | Ordinary differential equation | RCCI | Reactivity Controlled Compression Ignition |
| OEM | Original equipment manufacturer | RCF | Rapid compression facility |
| OH | Hydroxyl | RCM | Rapid compression machine |
| OH PLIF | Planar laser-induced fluorescence of OH | Re | Reynolds number; radius of gyration |
| ORC | Organic Rankine cycle | RF | Radio frequency |
| ORNL | Oak Ridge National Laboratory | Rh | Rhodium |
| OSC | Oxygen storage capacity | RI | Ringing intensity |
| P | Pressure | RoHR | Rate of heat release |
| PAH | Polycyclic aromatic hydrocarbon | RON | Research octane number |
| PCCI | Premixed Charge Compression Ignition | RPM, rpm | Revolutions per minute |
| PCI | Premixed compression ignition | S | Seebeck coefficient |
| PCS | Predictor-corrector split | S | Sulfur |
| PDF | Probability density function | SA | Spark assist(ed) |
| PDI | Port-assisted direction injection | SACI | Spark-Assisted Compression Ignition |
| PEDOT | poly(3,4-ethylenedioxythiophene) | SAE International | SAE International |
| PFI | Port fuel injected; Port fuel injection | | Technical association formerly known as the Society of Automotive Engineers |
| PFS | Partial fuel stratification | SA-HCCI | Spark-Assisted Homogeneous Charge Compression Ignition |
| P-G | Petrov-Galerkin | sccm | Standard cubic centimeters |
| PGM | Platinum-grade metal, platinum group metal | SCE | Single-cylinder engine |
| P _{in} | Intake pressure | SCF/min | Standard cubic feet per minute |
| PLIF | Planar laser-induced fluorescence | | |
| PLII | Planar laser-induced incandescence | | |
| PM | Particulate matter; premixed | | |

VI. Acronyms, Abbreviations, and Definitions

| | | | |
|-----------------|--|------------|--|
| SCR | Selective catalytic reduction | TE | Thermoelectric; Thermal efficiency |
| SCRF® | Selective catalytic reduction on filter; integrated DPF and SCR technologies | TED | Thermoelectric device |
| sec | Second | TEG | Thermoelectric generator |
| SEM | Scanning electron microscopy | TEM | Transmission electron spectroscopy; thermoelectric module |
| Si | Silicon | TGA | Thermal gravimetric analysis (analyzer) |
| SI | Spark ignition, Spark-ignited | THC | Total hydrocarbon |
| SIDI | Spark Ignition Direct Injection | TIM | Thermal interface material |
| SFC | Specific fuel consumption | T_{in} | Intake temperature |
| SG5 | Spray Guided Engine version 5 | TJI | MAHLE Powertrain's Turbulent Jet Ignition |
| SGS | Subgrid-scale | TPD | Temperature-programmed desorption |
| SKU | Skutterudite | TPO | Temperature-programmed oxidation |
| SLPM | Standard liters per minute | TPR | Temperature-programmed reduction or reaction |
| SMPS | Scanning mobility particle sizer | TRF | Toluene reference fuel |
| SNL | Sandia National Laboratories | TS | Thermal stratification |
| SO ₂ | Sulfur dioxide | T_{wall} | Temperature, wall |
| SOC | Start of combustion; soluble organic compound | TWC | Three-way catalyst |
| SOI | Start of injection | UC | Unused capacity |
| SOF | Soluble organic fraction | UCB | University of California, Berkeley |
| SOFC | Solid oxide fuel cell | UDDS | Urban Dynamometer Driving Schedule |
| SO _x | Oxides of sulfur | UEGO | Universal exhaust gas oxygen |
| SpaciIR | Spatially resolved capillary inlet Fourier transform infrared | UHCs | Unburned hydrocarbons |
| SpaciMS | Spatially resolved capillary inlet mass spectrometer | UHP | Ultra-high porosity |
| SPLAT II | Custom instrument that determines aerosol vacuum aerodynamic diameter and mass spectra of individual particles | ULSD | Ultra-low sulfur diesel |
| SPS | Spark plasma sintering | UM | University of Michigan |
| Sr | Strontium | US06 | Supplemental Federal Test Procedure (SFTP) drive cycle |
| SRM | Stochastic reactor model | U.S. DRIVE | United States Driving Research and Innovation for Vehicle efficiency and Energy sustainability |
| SSIE | Solid state ion exchange | USSET | U.S. Supplemental Emission Testing |
| SU | Stanford University | UV | Ultraviolet |
| SULEV | Super Ultra-Low Emissions Vehicle | UW | University of Wisconsin |
| SUV | Sport utility vehicle | UW-ERC | University of Wisconsin Engine Research Center |
| SwRI® | Southwest Research Institute® | UWS | Urea-water solution |
| T | Temperature | V | Volt |
| T2B2 | Tier 2 Bin 2 | VAC | Volts, alternating current |
| T2B5 | Tier 2 Bin 5 | VCR | Variable compression ratio |
| T ₉₀ | 90% volume recovered temperature | VDC | Volts – direct current |
| TAP | Temporal analysis of products | VEM | Vehicle Energy Model |
| TARDEC | Tank Automotive Research, Development and Engineering Center | VES | Vehicle Energy Simulator |
| TC | Turbocompound; total capacity | VGC | Variable geometry compressor |
| TCR | Thermochemical recuperation | VGT | Variable geometry turbocharger |
| TDC | Top-dead center | VNT | Variable nozzle turbine |
| TDL | Tunable diode laser | VOCs | Volatile organic compounds |

| | | | |
|------|-------------------------------------|-----|---|
| VOIS | Variable output ignition system | XPS | X-ray photoelectron spectroscopy |
| VPS | Vacuum plasma spray | XRD | X-ray diffraction |
| VTCE | Virtual Thermal Comfort Engineering | Y | Yttrium |
| VVA | Variable valve actuation | yr | Year |
| VVT | Variable valve timing | YSZ | Ytrria-stabilized zirconia |
| W | Watt | Zn | Zinc |
| WC | Tungsten carbide | Zr | Zirconium |
| W/F | Weight to flow | zT | Dimensionless thermoelectric figure of merit; equal to: (electrical conductivity) (Seebeck coefficient) ² (temperature)/(thermal conductivity) |
| WGS | Water-gas shift | ZTO | Zn_2SnO_4 |
| WHR | Waste heat recovery | | |
| WSR | Well-stirred reactor | | |
| wt% | Weight percent | | |
| WTT | Well-to-tank | | |
| XAFS | X-ray absorption fine structure | | |

VII. Index of Primary Contacts

A

Amar, Pascal IV-11

B

Barnhart, Todd V-3

Blaxill, Hugh IV-59

Bozeman, Jeffrey V-8

C

Carrington, David II-67

Ciatti, Steve II-90

Cleary, Martin V-19

Confer, Keith IV-15

Curran, Scott II-102

D

Daw, Stuart II-107, III-3, III-8

Dec, John II-19

Domingo, Norberto II-117

E

Edwards, Dean II-87

G

Goldsborough, Scott II-46

Goodson, Kenneth V-35

Greenbaum, Dan III-77

H

Harold, Mike III-53

Heremans, Joseph V-23

Huxtable, Scott V-64

J

Johnson, Terry II-112

Ju, Sungtaek V-55

K

Karim, Ayman III-28

Kaul, Brian II-98

Keating, Edward IV-48

Koeberlein, David IV-3

L

Lee, Kyeong III-66

M

Maranville, Clay V-74

McConnell, Steve II-122

McNenly, Matthew II-62

Meisner, Greg V-14

Mendler, Charles IV-64

Miles, Paul II-3

Mukundan, Rangachary IV-72

Muntean, George III-15

Musculos, Mark II-9

O

Ofelelein, Joe II-41

P

Parks, Jim III-43

Partridge, Bill II-124, III-48

Peden, Chuck III-21

Pickett, Lyle II-15

Pitz, Bill II-51

Powell, Chris II-36

R

Rappe, Ken III-32

Reese, Ron IV-38

Ruth, Michael IV-29

S

Sappok, Alexander IV-42

Schnabel, Claus IV-68

Shakouri, Ali V-59

Shi, Li V-68

Sisken, Kevin IV-8

Smith, Stuart IV-25

Som, Sibendu II-30

Steeper, Richard II-26

Stewart, Mark III-71

Subramanian, Swami IV-54

T

Toops, Todd III-37, III-60

V

Vaddiraju, Sreeram V-48

VII. Index of Primary Contacts

W

Wagner, Terry IV-19
Wallner, Thomas II-93
Whitesides, Russell II-55
Woolridge, Margaret II-72

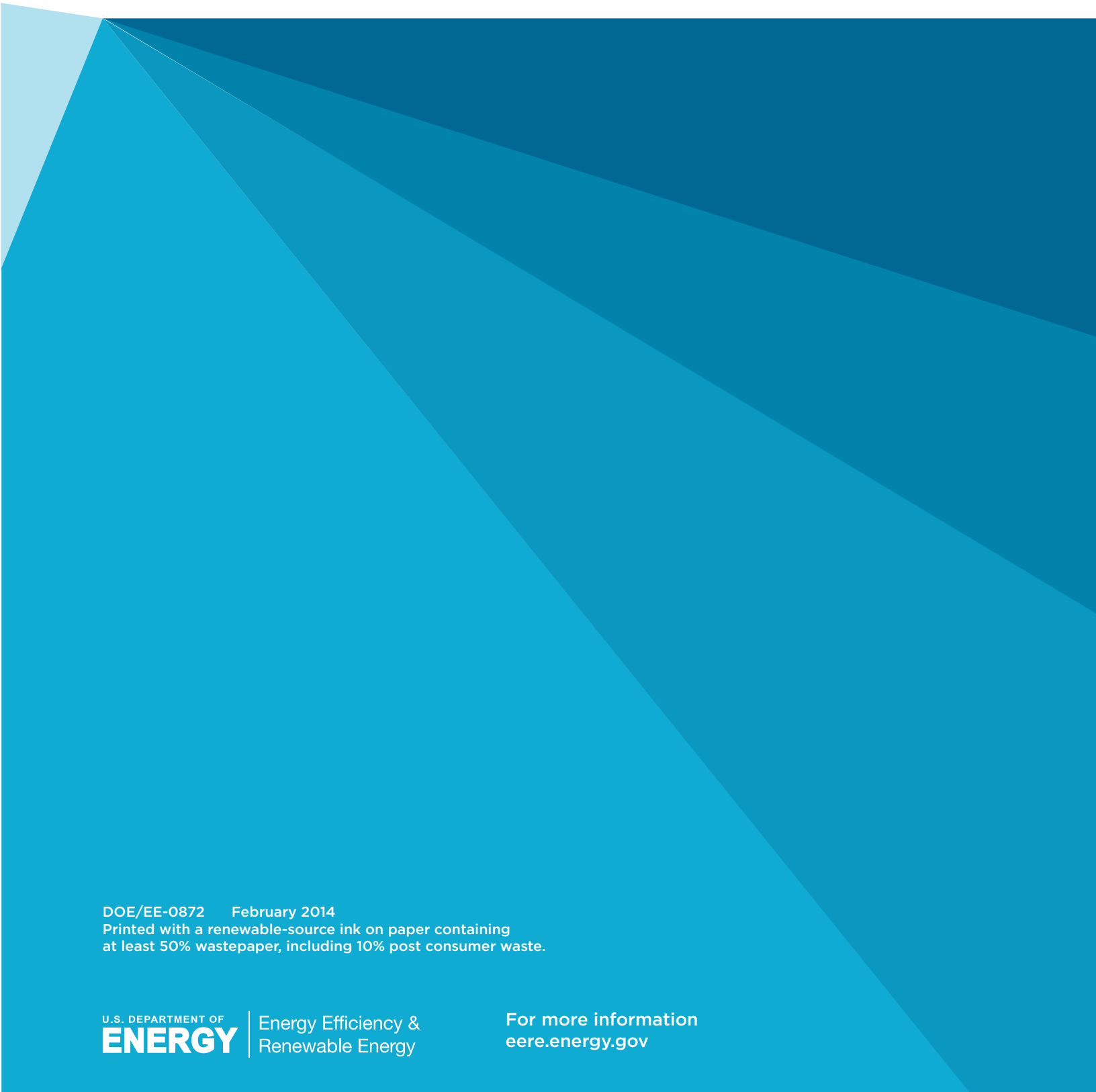
X

Xu, Xianfan V-28

Y

Yilmaz, Hakan IV-32
Z
Zhu, Gouming II-82
Zuo, Lei V-44

This document highlights work sponsored by agencies of the U.S. Government. Neither the U.S. Government nor any agency thereof, nor any of their employees, makes any warranty, express or implied, or assumes any legal liability or responsibility for the accuracy, completeness, or usefulness of any information, apparatus, product, or process disclosed, or represents that its use would not infringe privately owned rights. Reference herein to any specific commercial product, process, or service by trade name, trademark, manufacturer, or otherwise does not necessarily constitute or imply its endorsement, recommendation, or favoring by the U.S. Government or any agency thereof. The views and opinions of authors expressed herein do not necessarily state or reflect those of the U.S. Government or any agency thereof.



DOE/EE-0872 February 2014
Printed with a renewable-source ink on paper containing
at least 50% wastepaper, including 10% post consumer waste.



Energy Efficiency &
Renewable Energy

For more information
eere.energy.gov